ADVANCED STRUCTURAL MASS SPECTROMETRY FOR METABOLOMICS

By

Cody R. Goodwin

Dissertation

Submitted to the Faculty of the

Graduate School of Vanderbilt University

in partial fulfillment of the requirements

for the degree of

DOCTOR OF PHILOSOPHY

in

Chemistry

May, 2013

Nashville, Tennessee

Approved:

Prof. John A. McLean

Prof. Terry P. Lybrand

Prof. Brian O. Bachmann

Prof. John P. Wikswo

Prof. Kevin T. Seale

To the woods, the trails, and the unknown

and

To those I love and who generously love back

ACKNOWLEDGEMENTS

I would like to thank those that I have worked closely with to accomplish the following body of work. First and foremost, I must thank Professor John A. McLean, who has directed my research and provided valuable guidance and mentorship. From the beginning, Prof. McLean has helped to cultivate my scientific curiosity and refine me as a scientist, and for that, and so much more, I thank him. I would also like to give my gratitude and many thanks to my committee members, Prof. Brian O. Bachmann, Prof. Terry P. Lybrand, Prof. John P. Wikswo, and Prof. Kevin T. Seale, who have each helped to enhance and influence my scientific career, with valuable suggestions and guidance. Prof. Bachmann has provided a valuable collaboration that resulted in significant contributions to Chapters 2-4 of this dissertation, and has been an indispensable mentor from the beginning, and spurring countless scientific pontifications. Prof. Lybrand has influenced significantly the work described in Chapter 2, providing expertise in the implementation of molecular dynamics and the understanding of the applied methods, in addition to his unrelenting optimism and encouraging

reflections. Prof. Wikswo has provided valuable contributions to Chapter 4 of this work, suggesting the use of self-organizing maps for the analysis of metabolites, in addition to being an influential mentor throughout my studies at Vanderbilt, encouraging me to think outside convention. Prof. Seale has first and foremost encouraged me think critically, to challenge the norm, and influenced my own mentoring approach. He has endowed in me an outlook on life that breeds happiness.

Beyond my committee, there are countless individuals who have contributed to the following work. Dagmara "Kasia" Derewacz has applied her considerable expertise in biochemistry and NMR interpretation to solve the structures of the new compounds presented in Chapters 2 and 3, and for that I cannot thank her enough. Prof. Jody May has been both a friend and a source of thought provoking conversations, and his understanding of ion mobility is matched only by his willingness to help others. He also contributed significantly to Chapter 1. Dr. Michal Kliman and Dr. Larissa Spell-Fenn provided molecular modeling guidance and acquired collision cross sections used in Chapter 2, respectively. Dr. Christina Marasco helped with the sample processing in the work presented in Chapter 4, and has been a steadfast friend throughout my studies, providing valuable advice and an open ear. Prof. Nicole Schramm-Sapyta provided the biological samples for the study conducted in Chapter 4. Dr. Jeffrey Enders has been a great friend throughout my studies, and our many conversations have caused great reflection. I would also like to acknowledge Mr. Edward Hawkins, who left us far too soon, and always greeted me with a warm

smile and pleasant conversation. He will be missed. And finally, Prof. Darryl J. Bornhop, who has been a friend, climbing partner, and mentor to me from near the beginning. Without his perspective and advice, I could not have succeeded in my studies.

I could not have reached this point without the endless love and support of my family. From the beginning, they have provided me with the encouragement to pursue what I love in life, and have instilled the ethics that guide my decisions, and for this I am eternally grateful. Finally, I must thank the one who has endured my endless ups and downs that accompany graduate school, fact-checked me when I reached outside my realm of comfort, and has continued to love and support me in all aspects of life, Mary Ellen Koran. Without her, the following work would not exist.

TABLE OF CONTENTS

LIST OF TABLES

LIST OF FIGURES

LIST OF ABBREVIATIONS/NOMENCLATURE/SYMBOLS

φ	Peak capacity
Ω	Collision cross section
µs	microsecond
AC	Alternating current
ACN	Acetonitrile
ADEQUATE	Adequate double quantum transfer experiment
CCS	Collision cross section
CE	Capillary electrophoresis
COSY	Correlation spectroscopy
Da	Dalton
DMS	Differential mobility spectrometry
ESI	Electrospray ionization
FAIMS	High-field asymmetric waveform ion mobility spectrometry
GC	Gas chromatography
GEDI	Gene Expression Dynamic Investigator
GEMMA	Gas-phase electrophoretic molecular mobility analyzer
H_2O	Water
HMBC	Heteronuclear multiple-bond correlation spectroscopy
HSQC	Heteronuclear single-quantum correlation spectroscopy
IM	Ion mobility
MALDI	Matrix assisted laser desorption/ionization
MDa	Mega-Dalton

MEDI	Metabolite Expression Dynamics Investigator
MeOH	Methanol
MOE	Molecular Operating Environment
ms	Millisecond
MS	Mass spectrometry
MS^E	Untargeted tandem mass spectrum
MS^n	nth order mass spectrum
MVSA	Multivariate statistical analysis
m/z	mass-to-charge
NMR	Nuclear magnetic resonance
PCA	Principal component analysis
RMSD	Root-mean square distance
t_d	Drift time
Td	Townsend
TOF	Time-of-flight
TWIM	Traveling wave ion mobility
UPLC	Ultra-performance liquid chromatography
UV	Ultraviolet
Q	Quadrupole

CHAPTER 1[A]

ION MOBILITY-HIGH RESOLUTION MASS SPECTROMETRY BASED METABOLOMICS

1.1   Introduction

Metabolite analysis is a demanding initiative for analytical technologies. It is estimated that between 4,000 and 20,000 distinct metabolites are expressed in eukaryotic organisms, spanning between 7-9 orders of magnitude in concentration range,[1, 2] which necessitates highly sensitive and broad dynamic range analyses. This is particularly true when considering xenobiotic metabolites, in which all feasible biotransformations an administered drug may undergo must also be considered. These may occur over a large dynamic range of possible concentrations, and depending on the dose administered, may require highly sensitive analytical techniques.[3] Metabolism is a dynamic process, requiring measurement strategies that provide high sample throughput and instrument duty cycle. A further challenge is that metabolites represent a diverse set of chemical classes possessing disparate polarities, such that there is no single extraction or separation technique which can handle most, much less all, metabolites present. Because of the shortcoming of current technologies, contemporary profiling strategies are necessarily focused on a relatively small

number of known metabolites and thus are noncomprehensive. Nevertheless, targeted analysis and low complexity metabolite profiling approaches have been highly successful in drug discovery and development.[4, 5]

Established bioanalytical methods for studying metabolites are predominately based on nuclear magnetic resonance (NMR) and mass spectrometry (MS). MS methods are widely used and are routinely combined with additional separations (*e.g.*, gas and liquid chromatography prior to MS identification), to improve instrument sensitivity and dynamic range to detect lower abundance analytes. In parallel with advances in MS has been the development of post-ionization gas-phase separations based on ion mobility (IM).[6-8] IM is a compartmentalized technology which offers a combined separation and analysis that is *ca.* 4 to 6 orders of magnitude faster than gas chromatography (GC) and liquid chromatography (LC), respectively.[9] Since gas-phase ionization is a prerequisite for both IM and MS, the two methods are commonly coupled into a single analysis technique referred to as ion mobility-mass spectrometry (IM-MS), which allows separations on the basis of two physical properties: ion mobility (size) and ion mass (weight). IM-MS is still an emerging technology and one major challenge associated with using IM-MS for metabolite profiling is the limited amount of validation that can be drawn from the literature. Another challenge is the limited orthogonality between IM and MS separation dimensions, since analyte size and mass are two closely correlated physical properties.[10] Nevertheless, the extremely high speeds of the separation (micro- to milliseconds) and the potential for enhancing existing MS

methodologies offers great promise for IM-MS to become a complimentary bioanalytical technique for dynamic metabolic and metabolomics analyses.

This introductory chapter provides an overview of the ion mobility technique and a review of the various analytical approaches that utilize ion mobility for metabolomics. The coupling of IM and MS is discussed in light of the herein utilized analytical advantages and the additional information gained in these 2-dimensional analyses. In recent years, high resolution mass spectrometers have allowed for the determination of metabolite identity based upon high mass accuracy measurements which allow the determination of metabolic transformations based upon mass defect filtering, which is further enhanced in combination with IM. Tandem MS experiments (MS/MS) are important methods for elucidating analyte identity, and the common methods of operation will be outlined. The addition of IM capabilities to MS instrumentation permits several useful combinations of tandem experiments (e.g., IM-MS/MS, MS/IM-MS, MS-IM-MS/MS, etc.) which enhance the current commercial MS/MS capabilities, and these will be discussed in detail at the end of this chapter.

1.2   An Overview of Ion Mobility Techniques

1.2.1 Fundamental Aspects of Ion Mobility

Ion mobility can be broadly defined as the kinetic behavior (velocity) of ions in a neutral gas. Differences in the velocity of two ions, even those that are isobaric (*i.e.* same mass), can be used to differentiate the two ions experimentally. The analytical technique which utilizes the property of ion mobility to separate ions is often called ion mobility spectrometry, to draw parallels with mass spectrometry. Other names such as gas-phase electrophoresis[11] and plasma chromatography[12] have also been used. In terms of the technology, ion mobility spectrometry closely resembles mass spectrometry, however, the separation mechanism is very similar to chromatography, which can cause confusion if the fundamentals of the ion mobility method are described from either a spectrometric or chromatographic perspective.[13] Here, we will refer to the analytical technique simply as ion mobility (IM) and will make important distinctions where necessary.

From a pedagogical perspective, all IM techniques can be conceptualized as a series of opposing vector forces: (i) the electric field force which directs ions across a defined region and (ii) the opposing force of ion-neutral collisions which impedes this forward motion. In the simplest IM experiment, ions are pulled by an electric field through a chamber filled with a constant pressure of gas and disperse in time based on differences in their mobility. The number of ion-neutral collisions is related to the size of the ion. Thus, for two ions of equal mass but

different sizes, the smaller of the two will have a higher ionic mobility (velocity) and traverse the region the fastest, arriving on the other side of the region first. This kind of ion mobility experiment is known as the drift tube IM technique and is the most commonly encountered IM method in the literature.

The term ion mobility does not refer to any single experimental method but rather it encompasses a family of different analytical techniques, all of which utilize the same basic concept of an ion's gas-phase mobility to generate an analytically useful separation. As with mass spectrometry, ion mobility techniques can be broadly divided into two categories: (i) temporally dispersive methods which separate all ions in time but along the same spatial path, and (ii) spatially dispersive methods which separate ions along different trajectories. The conceptual differences between temporal and spatial dispersion are depicted in **Figure 1.1**. Temporally dispersive IM methods can obtain a complete IM spectrum in a single measurement cycle while spatially dispersive IM techniques are almost always configured to transmit only a narrow IM range of ions at a time. Members of the spatially dispersive IM category are considered scanning methods which filter ions based on their mobilities and require that a parameter (typically a voltage) be scanned in order to generate the broadband spectrum. **Table 1.1** contains a listing of several different ion mobility methods along with their defining attributes. The distinction between any two IM techniques can be most easily made by comparing the relative direction of the various field forces (electric field and gas flow) with respect to the motion of the ion. Note here that the ion motion will preferentially follow one of the forces such that the ion velocity

vector is aligned with one of the force vectors. A listing of the analogous MS method for each IM technique is also provided in **Table 1.1**.
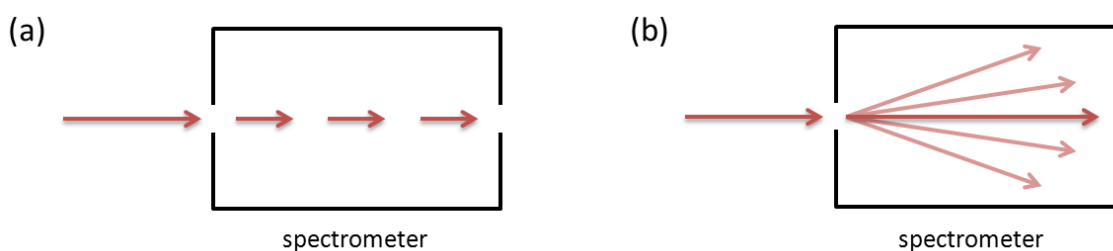
Figure 1.1. *Conceptual schematic of the two types of separation schemes for ion mobility techniques.* (A) Temporally dispersive separation methods partition a pulse of ions into different mobility values along the same spatial trajectory. Ions of different mobilities arrive at different times during each measurement pulse. (B) Spatially dispersive separation methods partition a continuous beam of ions into different mobility values along different spatial trajectories, with each trajectory representing ions possessing common gas-phase mobilities.

The following sections will describe each of the specific IM techniques in more detail. We will start with a qualitative description of the drift tube ion mobility method, and will use concepts discussed there as the foundation for understanding other IM techniques. These methods will initially be discussed in the absence of MS, however, the IM techniques will be framed as modular rather than stand-alone or end detection technologies. Governing equations, though important for each technique, will be avoided in this chapter in order to convey the qualitative operational principles clearly. The reader is directed towards specific references given in **Table 1.1** if a more thorough understanding of each technique is sought.

Table 1. 1. The different ion mobility techniques, defining features and currently achieved resolving powers reported in the literature. Also included are the analogous mass spectrometry methods for each ion mobility technique. References are provided directing the reader to comprehensive reviews on the separation described.

	Ion Mobility Technique	Vectors			Resolving Power* Achieved	MS Analogue	Ref
		ion motion	electric field	gas flow			
Temporally Dispersive	Drift Tube Ion Mobility Ion Mobility Spectrometry Plasma Chromatography Ion Chromatography	→	→	0	240[a]	Time-of-Flight	7, 9
	Traveling Wave IM	→	→→→	0	40[b]	"Solitron" (mass selective traveling wave[c])	14
Spatially Dispersive (scanning)	Differential High-Low Field IM High Field Asymmetric Waveform IMS (FAIMS) Differential Mobility Spectrometry (DMS)	→	→	↑	200[d]	Quadrupole	15, 16
	Differential Mobility Analyzer (DMA) Gas-phase Electrophoretic Molecular Mass Analyzer (GEMMA)	→	↑	→	50[e] to 80[f]	Magnetic Sector	17, 18

* It should be noted that resolving power does not adequately represent the separation efficiency of certain ion mobility methods, particularly the spatially dispersive IM techniques. For these methods, peak capacity is a more representative metric of separation ability (refer to Section 3.2).

a. [19]. A resolving power >300 has been observed for a special circular path drift tube which operates in a narrow bandpass mode. [20]

b. Experimentally observed on the Synapt Generation 2 (G2) for data obtained in the author's laboratory.

c. [21]

d. [22]

e. [23]

f. Performance specifications for the SEADM DMA interface.

1.2.2 Drift Tube Ion Mobility Spectrometry

The drift tube ion mobility technique is the most familiar IM method and has been a commercial technology since the 1970s, though it has primarily been used as a stand-alone technology for chemical screening in security applications.[24] Drift tube instruments can operate either at ambient pressure (*ca.* 760 Torr) or reduced pressure (*ca.* 1-10 Torr), the latter more amendable to coupling with vacuum MS techniques. Ambient pressure drift tubes do not need bulky vacuum systems and, owing to the high gas number densities, the IM separation occurs in a relatively short distance, so these instruments are often preferred as low-cost, portable chemical detectors. Reduced pressure drift tubes are more costly and technically complex due to the added vacuum hardware, but offer very high measurement precision and accuracy and are readily coupled to mass spectrometers. Complicating ion chemistry is often avoided at reduced pressures where ions experience fewer interactions with trace gas impurities inherently present in the drift gases used. Reduced pressure drift tubes are generally preferred in research applications where high quality ion measurements are desired, but one major disadvantage has traditionally been that these instruments were not readily available commercially. This situation has changed in the last five years or so as several commercial vendors have begun offering high performance drift tube ion mobility-mass spectrometers (IM-MS).
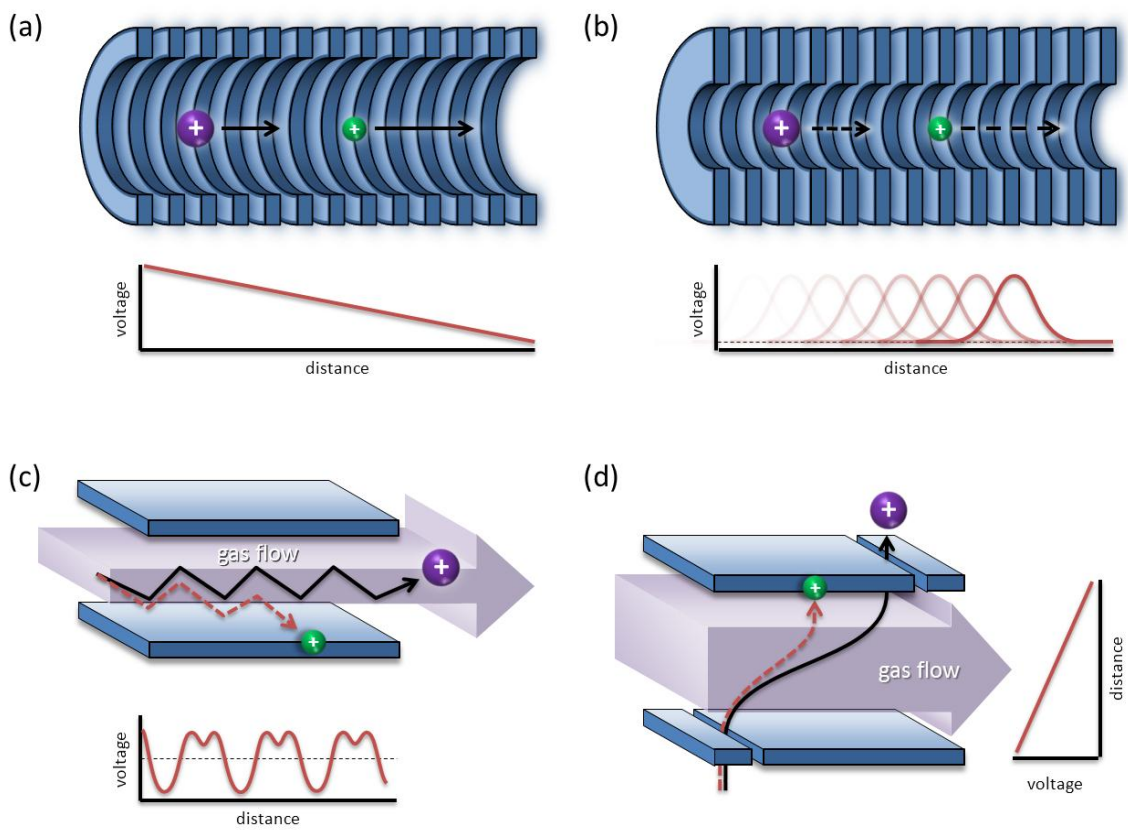
Figure 1.2. *The operation principles governing the four ion mobility techniques.*
(A) The drift tube ion mobility method disperses ions of differing mobilities
temporally along the same trajectory by utilizing a continuous declining potential
across a gas-filled region. (B) The traveling wave ion mobility method achieves
temporally dispersive mobility separations through the use of a traveling wave
potential across a gas-filled region. (C) The high field asymmetric waveform ion
mobility method disperses ions spatially along different trajectories through the
use of an orthogonally applied asymmetric waveform as ions are entrained in a
gas flow. (D) The differential mobility analyzer disperses ions spatially by mobility
through the use of a flow of gas and an orthogonally applied uniform electric field.

The basic components and operational principle of the drift tube IM technique is depicted in **Figure 1.2(A)**. A uniform electric field is defined along the length of a tube by a series of stacked ring electrodes. The tube is filled with an inert gas, usually helium or nitrogen, which is maintained at a constant pressure and low flow conditions. A pulse of ions is introduced at one end and allowed to drift down the length of the tube by the influence of the electric field *via* electrophoretic migration. During the ion's drift, it collides many times with the drift gas (greater than 10^4 collisions at 1 Torr) which slows the ion's forward motion. The amount of time any given ion spends in the drift tube is directly related to the number of collisions it experiences, which in turn depends on its collision cross section, or nominal gas-phase size and shape. This is analogous in principle to gas chromatography where the less volatile (lower vapor pressure) analyte will spend more time in the column. The measured drift times in the IM experiment are essentially the same in principle as retention times measured in chromatography, but it is important to note that IM is not chromatography in the strictest sense as there is no stationary phase (and thus no phase partitioning), but rather a constantly moving density of gas.

Because the electric field, gas pressure (number density), temperature and tube length are (ideally) all kept constant in the drift tube IM experiment, the relationship between the measured ion drift time and the collision cross section is direct and can be determined from first principle kinetic equations.[25] The measure of absolute gas-phase collision cross sections of ions is an important feature of the drift tube experiment. The interpretation of the collision cross

section value is, however, not straightforward since effects such as neutral gas polarization can contribute to nonideal (inelastic) ion-gas interactions.[26] This is particularly significant for small molecules such as metabolites, where the analyte polarity can contribute to a more attractive ion-gas interaction (a "sticky" collision) which will make the collision cross section appear larger than the physical size of the gas-phase analyte ion. Thus, it is difficult to assign any physical meaning to the collision cross sections measured for small molecules in the IM experiment. For larger analyte ions, greater than about 500 mass-to-charge, the size effects become the significant contributor to the measured drift times, and collision cross section in this case is a close representation of the physical size and shape of the gas-phase ion. The use of nonpolar drift gases also improves the accuracy of the collision cross section measurement, which is why helium is often preferred in research drift tube instruments. One prevailing advantage of drift tube instruments over the other IM techniques described in this chapter is the very high resolving powers which can be achieved (greater than 200) ,[19] which makes drift tubes the preferred IM instrumentation for core research and development.

1.2.3 Traveling Wave Ion Mobility Spectrometry

Traveling wave is a relatively new IM technique, but already has shown great promise to become a routine method for chemical analysis. This is largely due to the rapid commercialization of the technology, which is now widely available integrated into a high-end mass spectrometer platform.[14] The first commercial traveling wave instrument was released in 2006 (Synapt HDMS,

12

Waters) and has since seen a major revision (Synapt G2, 2009) which has improved the ion mobility resolving power by about a factor of four (currently *ca.* 40-50) and offers mass resolving powers up to *ca.* 50,000. The traveling wave concept itself can be traced back to early accelerator physics applications,[27] and early work with using RF fields to determine ionic mobilities,[28, 29] but until recently there have been no attempts made at translating this technology to separating ions by mobility on an analytical scale.

The basic components of the traveling wave IM device is shown in **Figure 1.2(B)** and are essentially the same as what can be found in a drift tube IM instrument. The drift region consists of a stacked ring ion guide and is filled with a low static pressure (1-5 Torr) of nitrogen. The rings serve two purposes: (i) a sinusoidal radio-frequency potential is applied to confine ions to the center axis of the device to improve instrument sensitivity, while (ii) a pulsed voltage is applied on sets of rings and rapidly switched from one end of the device to the other to generate the traveling wave potential for ion mobility separation. Ions which are introduced to the device in narrow pulses will be picked up by the wave and pushed down the length of the drift region where they experience many collisions with the nitrogen gas. Some ions experience more collisions with the drift gas and are pushed against the wave until they fall behind it and wait for the next wave to carry them forward again. The number of times any given ion will tumble behind the wave is directly related to its ionic mobility—larger ions are inherently more difficult to push forward than light ions. Thus, the device disperses ions based on their mobilities in much the same way as the drift tube experiment,

though fundamentally this is achieved in a very different manner. Because the wave travels at a fixed velocity, only ions which fall behind the wave will separate—those ions which are pushed along by a single wave will arrive at the same drift time and result in no useful mobility separation. Factors such as the wave velocity and voltage amplitude must be tuned in order to obtain a good mobility separation. The current second generation traveling wave instrument (Synapt G2) can achieve ion mobility resolving powers of *ca.* 45 (author's laboratory).

Because of the complex potentials utilized in the traveling wave IM instrument, there is no direct first principle correlation between measured drift times and collision cross sections. For those interested in obtaining structural information from the IM experiment, this is seen as a disadvantage when using the traveling wave IM technique, though methods have been proposed. By preparing a calibration curve with standards of known collision cross section, structural values have been extracted using traveling wave IM. This method is limited to the range of the calibration curve, which typically limits this method to the analysis of a particular biomolecular class. Additionally, methods of dynamically changing the traveling wave velocity for the determination of mobility have been presented as well, though this method is not commercially available and not particularly feasible for complex sample analysis. However, there are two distinct advantages that traveling wave IM offers over traditional drift tube IM. First, the axially confining electric fields results in very little ion loss and thus very good analyte sensitivity. Second, the traveling wave device is much easier to

couple to other instrumentation due to the fact that the potential at the start and exit of the device remains the same. In contrast, coupling instrumentation such as MS to a drift tube IM device requires either the front or back component be biased to a nonzero electric potential, increasing technical complexity. A third advantage might be that traveling wave instruments are becoming much more accessible to mainstream analytical research and will no doubt see some exciting applications in the near future, particularly in the area of drug research and discovery. Both the drift tube and traveling wave IM techniques disperse ions temporally along the same space, which permits an entire broadband mobility spectrum to be generated in each experimental measurement cycle. This has the obvious advantage of allowing one to obtain data on several analyte peaks at the same time. One limitation of temporally dispersive approaches is that ions are introduced in pulses, requiring that each measurement be complete before another pulse is admitted (a duty cycle) which reduces the overall sample throughput of the technique. In some cases, it is desirable to only monitor a few select analyte signals continuously, and so the next two IM techniques we will discuss act as narrow bandpass mobility filters and are particularly well suited for analyte monitoring applications.

1.2.4 High-Field Asymmetric Waveform Ion Mobility & Differential Mobility Spectrometry

Consider now a continuous stream of ions entrained in a gas flow that passes between two parallel plates as shown in **Figure 1.2(C)**. One plate is kept at a constant potential, usually ground, and on the other plate is applied an alternating (AC) voltage. This AC voltage is kept at the same average potential as the opposite plate but alternates between a short duration, high amplitude and a longer duration, low amplitude (an asymmetric waveform) as shown in Figure 1(c). The total magnitude of each push/pull potential is the same, such that the ions experience the same average electric field for each cycle, but in opposite directions. If the mobility of the ion during the push cycle is the same as during the pull cycle, then the ion's average displacement will be zero. However, the gas-phase mobility of an ion has an electric field dependence such that it changes between going from high field (*ca.* 20,000 V cm^{-1}) to low field (*ca.* 1000 V cm^{-1}).[30] This results in a different net displacement of the ion when subjected to the short duration, high field wave cycle than when it experiences the longer duration, lower field wave cycle. Ultimately this results in ions which are not balanced by the asymmetric waveform to be neutralized onto one of the plates. This device will transmit a narrow bandpass of ions whose high field and low field ion mobility is exactly matched by the waveform. An additional compensation voltage is applied to either plate to allow the device to be scanned, thus filtering ions possessing different changes in high/low field ion mobilities.

Devices which utilize this principle of ion mobility separation have been described by several names, the two most popular being high-field asymmetric waveform ion mobility spectrometry (FAIMS) and differential mobility spectrometry (DMS). In **Table 1.1**, we refer to both techniques as differential high-low field IM. Both terms describe the same general technique with defining differences being in the geometry of the electrodes used and how ions are detected in stand-alone applications. FAIMS and DMS devices do not separate purely by ion mobility, but rather separate by the difference in high/low field ion mobility (the first derivative) so the observed separations are often subtly different than those derived from the other IM methods. In many cases, these devices can resolve ion species which are difficult to separate by traditional IM, such as leucine and isoleucine.[31] Additionally, one can couple FAIMS or DMS with a temporally dispersive IM method (*i.e.*, drift tube or traveling wave IM spectrometry) and achieve excellent orthogonality between the two separations,[32] which is analogous in principle to 2-dimensional gas chromatography using polar and nonpolar columns. FAIMS and DMS have been successfully used to separate a variety of small molecules and both technologies are commercially available as front-end separators for mass spectrometers (FAIMS, Thermo Scientific, and DMS, Sionex). Because these devices operate at or near ambient pressure, they are readily compatible with atmospheric pressure ionization sources.

The high field/low field ion mobility behavior and transition between differential behaviors is still poorly understood. Because there is no first principle

correlation between the change in ion mobility and the low field collision cross section, analyte size information is difficult to obtain with any accuracy using the differential high-low field IM technique. Gas-phase collision cross sections can be determined in differential high-low field IM through special energy loss experiments using triple quadrupole mass spectrometry.[33]

1.2.5 Differential Mobility Analyzer

Differential mobility analyzers are a special class of ion mobility instruments used primarily for measuring the size of aerosol particles greater than 5 nm in diameter. These instruments are not commonly used for small molecules due to high diffusive ion losses; however, the method is included here to complete the discussion of IM technologies. The reader may skip to the next section if more relevant discussion regarding IM techniques for metabolite analysis is preferred.

Building on the differential high-low field IM technique described in the previous section, consider now a similar experimental setup whereby ions are entrained in a flowing gas and allowed to pass between two parallel plates as shown in **Figure 2(D)**. Instead of an alternating voltage, a direct voltage is applied across the two plates creating a uniform electric potential gradient perpendicular to the ion transit. This will cause ions to migrate from one plate to the other as they are being pulled along by the gas flow. All ions of the same charge will experience the same force of the electric field, but because of differences in their ion mobilities, smaller ions will be displaced a shorter distance

than larger ions. This results in a spatial dispersion of ions based on their ionic mobilities. Practical designs of this type of transverse field IM instrument utilize small apertures or slits on the parallel plates which are offset some defined distance from one another, as depicted in **Figure 1(D)**. Ions are introduced to the gas stream through one slit and the voltage is tuned to allow ions with different mobilities to pass through the second slit, in much the same way as tuning the m/z of a magnetic sector MS instrument. With the exit slit design, the instrument operates in a scanning mode. The exit slit can also be replaced by an array detector, which allows for broadband ion mobility spectrum to be measured,[34] however this design cannot be coupled as a front-end to MS (*e.g.*, IM-MS).

These instruments are sometimes called aspirator mobility analyzers due to the aspiration effect of introducing ions into the gas stream. More commonly they are referred to as differential mobility analyzer (DMA) and by the trade name gas-phase electrophoretic molecular mobility analyzer (GEMMA), the latter now referred to as *macro*IMS (TSI Incorporated). The DMA nomenclature is oftentimes confused with the DMS technique described in the previous section, but it should be noted that these two IM techniques separate ions by two very distinct mechanisms, specifically the DMA differentiates ions based on aerodynamic ionic mobility (IM in the presence of a gas flow) whereas DMS exploits ion mobility differences between high and low electric field conditions. DMA and GEMMA have been highly successful in measuring particle sizes down to the nanometer range.[17] Smaller ions are more difficult to transmit due to diffusive losses and the instrument performance is inherently tied to the size of

the slits used—larger slits improve sensitivity at a cost of resolution and vice versa. Recent technological improvements show promise for extending the usable size range down to small molecular ions with high sensitivity and ion mobility resolution.[23]

As with drift tube IM instruments, DMA measurements can be used to determine the ion's effective size since there is a direct relationship between the experimental conditions (transmission voltage and gas flow rate) and the experimentally measured gas-phase ion mobility. A hard sphere model is used to relate the measured ion mobility value to an effective size. As mentioned previously, DMA instruments are currently limited to the analysis of relatively large ions (10s of nanometers or greater in diameter), requiring that effects such as surface roughness be accounted for in the size calculation.[35] Nonetheless, because the DMA experimental separation parameters (voltage, drift length and gas flow) are well characterized, the resulting measurement precision of the DMA technique is high.

1.3   Integrated Ion Mobility-Mass Spectrometry

All of the IM methods described previously can operate as a stand-alone chemical analysis technology (*i.e.*, an ion mobility spectrometer). One shortcoming of ion mobility analysis alone is that the measured ionic mobility is a relative property of the analyte and will change with respect to different experimental conditions (*e.g.*, drift gas pressure, temperature and composition). Consequently, confident analyte identification using IM spectrometry information

20

alone (*via* the reduced mobility) relies on rigorous method validation and even then is subject to specific constraints on the system being studied.[36-38] In contrast, mass spectrometry measures an inherent physical property of the analyte (mass or more specifically, the mass-to-charge ratio) which can be used for analyte identification purposes, as the property of ion mass is readily comparable across instrument platforms. MS and tandem MS methods are the cornerstone technology of many analyte characterization initiatives, a fact which is reflected in the numerous contributions to this volume. Due to the requirement that the analyte be ionized, IM is particularly suited for coupling with mass spectrometry. The first IM-MS instruments appeared in the 1960s in response to the need to better characterize the ion chemistry observed in drift tubes.[39, 40] Bioanalytical drift tube mass spectrometers emerged in the 1990s owing to the development of soft ionization methods (MALDI and ESI which are discussed in other chapters).[6] Ion mobility-mass spectrometry (IM-MS) is now widely utilized and regarded as a technique in and of itself,[41] much like the integration of liquid chromatography to mass spectrometry (LC-MS). Most of the technical challenges associated with coupling the elevated pressure IM stage to a vacuum MS have been solved, largely due to parallel initiatives in improving the transfer efficiency of ions from atmospheric ionization sources to MS.[42] As mentioned previously, commercially available IM-MS instruments are now emerging and offer little to no compromise in performance as compared with the familiar MS platforms in which they are coupled. Thus, researchers familiar with existing commercial MS

technologies will find that IM capabilities enhance existing methodologies built upon MS analysis.

1.3.1 Ion Mobility-Mass Spectrometry Instrumentation

Figure 1.3(A) illustrates the basic components of an IM-MS instrument. Sample introduction can include direct infusion, GC or LC. Virtually every ionization source which has been used in MS has been coupled to an IM-MS instrument,[41] including all of the ionization techniques covered in this volume. Likewise, virtually every combination of IM and MS has been attempted. Temporally dispersive IM (drift tube and traveling wave) combined with temporally dispersive MS (time-of-flight) is a particularly useful combination since both techniques offer broadband analysis for each experimental cycle.[43] Another useful combination is coupling a scanning IM (*e.g.,* FAIMS or DMS) to a scanning MS (an ion trap), which allows selective monitoring and analysis experiments.[44] Instruments based on bracketing an IM between two mass spectrometer stages (MS-IM-MS) have also been developed,[45] allowing several useful stages of tandem ion experiment to be conducted.[46] We will discuss various combinations of tandem IM/MS in later sections. Commonality between all of these instrument configurations is the back-end mass analysis, which provides a comprehensive characterization of the sample by mass, or specifically, the mass-to-charge ratio. For the purposes of this chapter, we will focus primarily on IM-MS instruments which incorporate a first stage of mass selection and tandem capabilities with a high resolution mass spectrometer (so-called "high performance" IM-MS, **Figure 1.3(B)**). Though the literature defines high resolution mass spectrometers with a

degree of disparity, we will consider high resolution the ability to obtain part-per-million mass precision (*e.g.*, 1000 ± 0.015 Da, or 20,000 resolving power) within the mass-to-charge range of interest.

(a)

Sample Introduction → Ionization Source → IM → MS → Ion Detector

(b)

Sample Introduction → Ionization Source → MS → Ion Activation Region → IM → Ion Activation Region → MS → Ion Detector
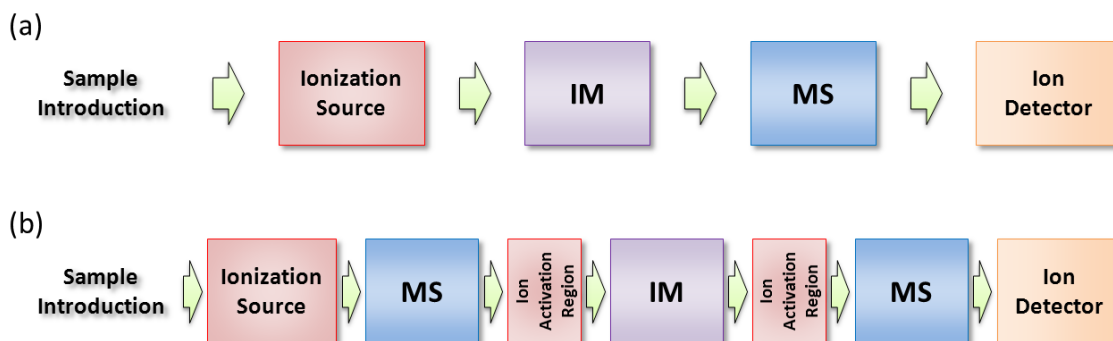
Figure 1.3. (A) A schematic of the basic components of an ion mobility-mass spectrometer. From left to right, sample is introduced, ionized, then separated first by ion mobility then by mass and finally detected. (B) A "high performance" ion mobility-mass spectrometer can include a mass spectrometer before the ion mobility spectrometer and several stages of ion activation located between each spectrometer component. Additionally, the spectrometers operate with high precision (resolving power) and sensitivity, enabling high quality measurements of mobility and mass to be made.

1.3.2 Orthogonality and Peak Capacity in Ion Mobility-Mass Spectrometry Analyses

The observed mobility-mass correlation in IM-MS data limits the orthogonality of the two separations. Completely orthogonal measurements would distribute data throughout two dimensional separation space with no correlation between the data sets, as each separation is contingent upon

chemical or physical properties that are independent of one another.[47] In other

words, data projected on a two-dimensional separation plot would occupy all of

separations space, as illustrated conceptually in **Figure 1.4(A)**, where analyte

signals distribute themselves across the full 2-dimensional area. This high

orthogonality is often observed, for example, in 2D gel electrophoresis [48, 49]

where the two dimensions of separation are analyte mass and isoelectric point—

two unrelated analyte parameters. The degree of orthogonality of IM-MS

separations is low due to the correlation of mass and size.[50] This is apparent

when considering an ion of increasing mass, which will inherently possess a

larger volume, and therefore occupy an established region of separations space,

a mobility-mass correlation termed "conformational space".[51] Low orthogonality

inherently limits the peak capacity (φ) of the IM separation, which is the

maximum number of resolvable peaks within the separation window, as

illustrated in **Figure 1.4(B**) for a hypothetical IM-MS spectrum.[52] Here, the narrow

distribution of data requires that the analysis window be narrowed accordingly,

depicted with the dotted lines in **Figure 4(B)**. Previous IM studies have reported

a peak capacity of approximately 5 for the IM dimension alone, which is low as

compared with other separation methods.[10] However, the strength of IM is that,

when combined with MS, the overall peak capacity of the MS dimension is

increased multiplicatively (specifically, five-fold). As there is virtually no

compromise in analytical performance when IM is added to MS, this represents a

significant improvement in analytical performance. For example, IM-MS has

recently demonstrated a peak capacity of 10^3 for metabolites in a single IM-MS

spectrum, which is comparable to that of highly orthogonal methods, such as reverse phase LC-MS (φ=1000-1500, *Shewanella oneidensis* lysate),[53] two dimensional gas chromatography-mass spectrometry (GCxGC-MS, φ=1200, lean C57BL/6 mice spleen extract, φ=1800 human serum),[54, 55] and capillary electrophoresis-mass spectrometry (CE-MS, φ=1692, *Bacillus subtilis* extract).[56] These examples represent general separation benchmarks for each analytical platform, and while useful for qualitative comparative purposes, it should be noted that the samples, conditions, and mass spectrometers are not consistent across each study.
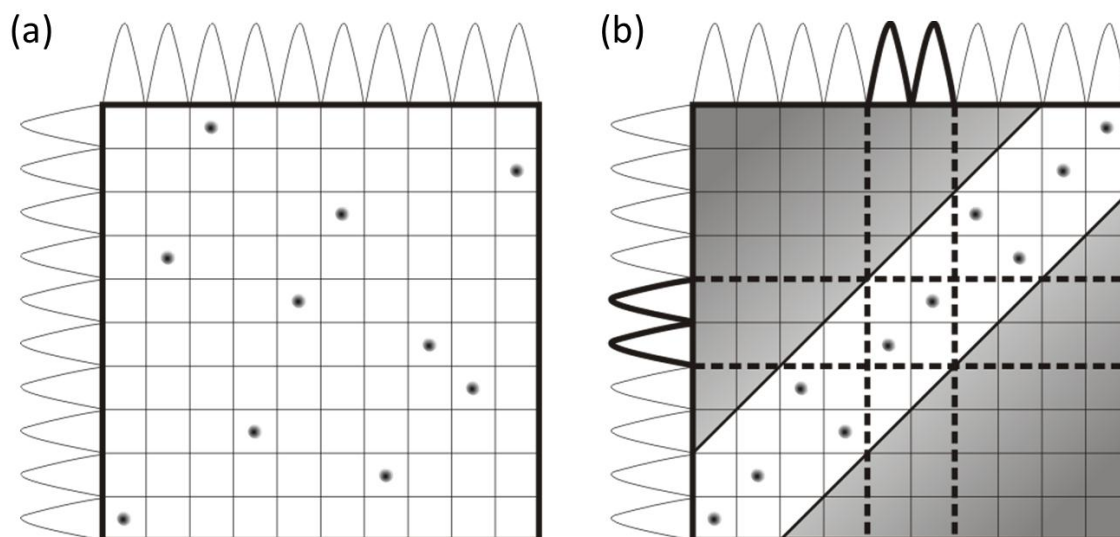
Figure 1.4. Shown in (A) is a theoretical distribution of peaks (represented in black in grid space) in two-dimensional space for completely orthogonal separations. Each axis corresponds to a theoretical separation parameter. The high orthogonality allows for the occupancy of all two dimensional space, thus having a peak capacity equivalent to the product of the two peak capacities. Illustrated in (B) are two separations with low orthogonality. The region of two-dimensional separations space that peaks occupy is limited to a fraction of all separations space. The region of analysis space is narrowed to that shown in the overlapping regions, for example. This limits peak capacity, as the total peak capacity is no longer the product of the two peak capacities, but a corrected value that is a fraction of the maximum. The grey areas are regions of separation space in which no signal appears.

1.3.3 Ion Mobility-Mass Spectrometry Analysis Speed

The main strength ion mobility holds over conventional separations techniques is that it occurs post ionization, which means separations are performed entirely in the gas phase. This results in a separation that occurs on the order of hundreds of microseconds to milliseconds. As a result, thousands of ion mobility spectra can be acquired each second. When compared with previously presented separation methods which are utilized prior to ionization (*e.g.*, LC, CE and GC), the time required for a mobility separation to occur is several orders of magnitude faster. An analysis speed comparison of several separation techniques is provided in **Figure 1.5**. For a typical metabolomics study, high performance liquid chromatography, two dimensional gas chromatography, and capillary electrophoresis separations occur on the order of minutes to hours. Additionally, gas chromatography separations often require analyte derivatization to promote volatility, which adds multiple hours in addition to the separation.[55, 57-61] While the orthogonality and peak capacity of IM-MS remains comparable to other 2-dimensional methods, it is the high speed of IM-MS which affords a great analytical advantage in terms of the peak production rate, as illustrated in **Table 1.2.**[9]

Table 1. 2. Several single dimensional separation methods and the parameter for separation, peak capacity (φ) and peak production rate (φ/s) associated with each.

Separation Method (Single Dimension)	Separation Parameter	Peak Capacity (φ)	Signal Peak Production Rate (φ/s)	Ref.
Capillary Electrophoresis (CE)	electrophoretic mobility	1000	0.5	62
Gas Chromatography (GC)	vapor pressure	75	6	63
Liquid Chromatography (LC) Ultrahigh Pressure LC	hydrophobicity	60 300	0.06 0.2	64, 65
1D Slab Gel Electrophoresis	isoelectric point, mass	100	0.03	66
Field Flow Fractionation (FFF)	hydrodynamic radius	10	0.005	66, 67
Ion Mobility (IM)	gas phase cross section	5	500	10
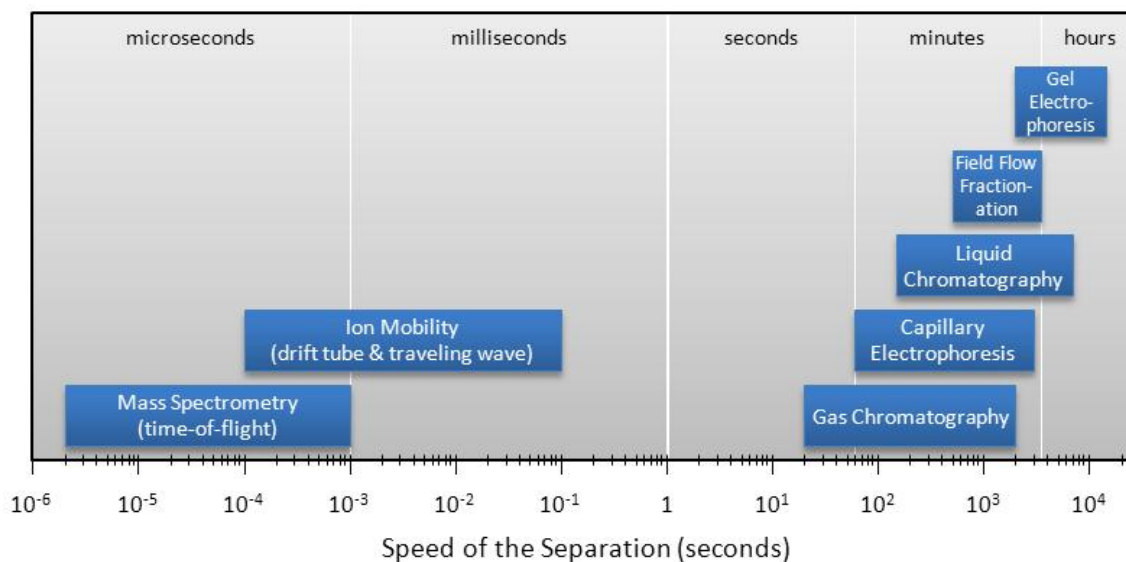
Figure 1.5. *Speeds for separation techniques commonly applied to metabolite analysis.* Note the logarithmic scaling on the abscissa.

In addition to the high data production rate of IM-MS, another key advantage of coupling time dispersive IM and MS is the complimentary nature of the timescales for each dimension of analysis. Because time dispersive IM separations (ms) occur 2-3 orders-of-magnitude slower than time dispersive MS (µs), hundreds of mass spectra can be acquired for each ion mobility spectrum, which benefits the sampling resolution across the IM dimension.[68] This temporal sampling benefit is commonly exploited in LC-MS where each LC trace is sampled numerous times by the MS. One criticism of LC-MS has been that the immensely disparate timescales (6 to 8 orders of magnitude) ineffectively utilizes the throughput of the mass spectrometer. IM readily bridges this time disparity

between LC and MS, which has been demonstrated for the three-dimensional analysis of complex biological samples.[69] CE-IM-MS has also been demonstrated to improve the sensitivity of the MS for low abundance analytes in complex biological samples.[70] Combining front end separation techniques with IM-MS is still an emerging area that holds great promise for improving the chemical analysis for both contemporary and future applications.

1.4 Information Content of Ion Mobility-Mass Spectrometry Analyses

One favorable consequence of the data correlation between ion mobility and mass is the potential for extracting additional information regarding specific analytes within the sample. This complimentary information can be used in a number of ways for more confident identification and characterization of analyte signals within the sample. **Figure 1.6(A)** contains a 2-dimensional projection of ion mobility-mass data for a nano-electrosprayed sample of a methanol extract of rat blood. This data was obtained in less than 1 minute in the author's laboratory using a traveling wave IM-MS instrument. The spectrum displays mass-to-charge (Da) on the abscissa and drift time (ms) on the ordinate. The spectrum is false colored (heat mapped) to represent relative signal abundances and is comprised of almost exclusively singly charged ions due to the nano-electrospray ionization conditions utilized. Immediately obvious is the close correlation between the mobility and mass, which manifests as a clustering of data along a mobility-mass correlation line.[71] This results from the intuitive scaling of the analyte size with its weight. **Figure 1.6(B)** illustrates the advantage of selective interrogation of data

corresponding to the mobility-mass correlation for lipids, peptides, and small molecules. The individual mass spectra are extracted directly from the combined mobility-mass spectrum (**Figure 1.6(A)**). The result is the extraction of relevant analyte signals, based upon the distillation of chemical noise, which greatly improves the amount of information which can be gleamed from the data. This strategy has recently been shown to be applicable to metabolite identification for the IM-MS analysis of human blood,[72] rat lymph fluid,[73] and *Escherichia coli* extracts.[74]
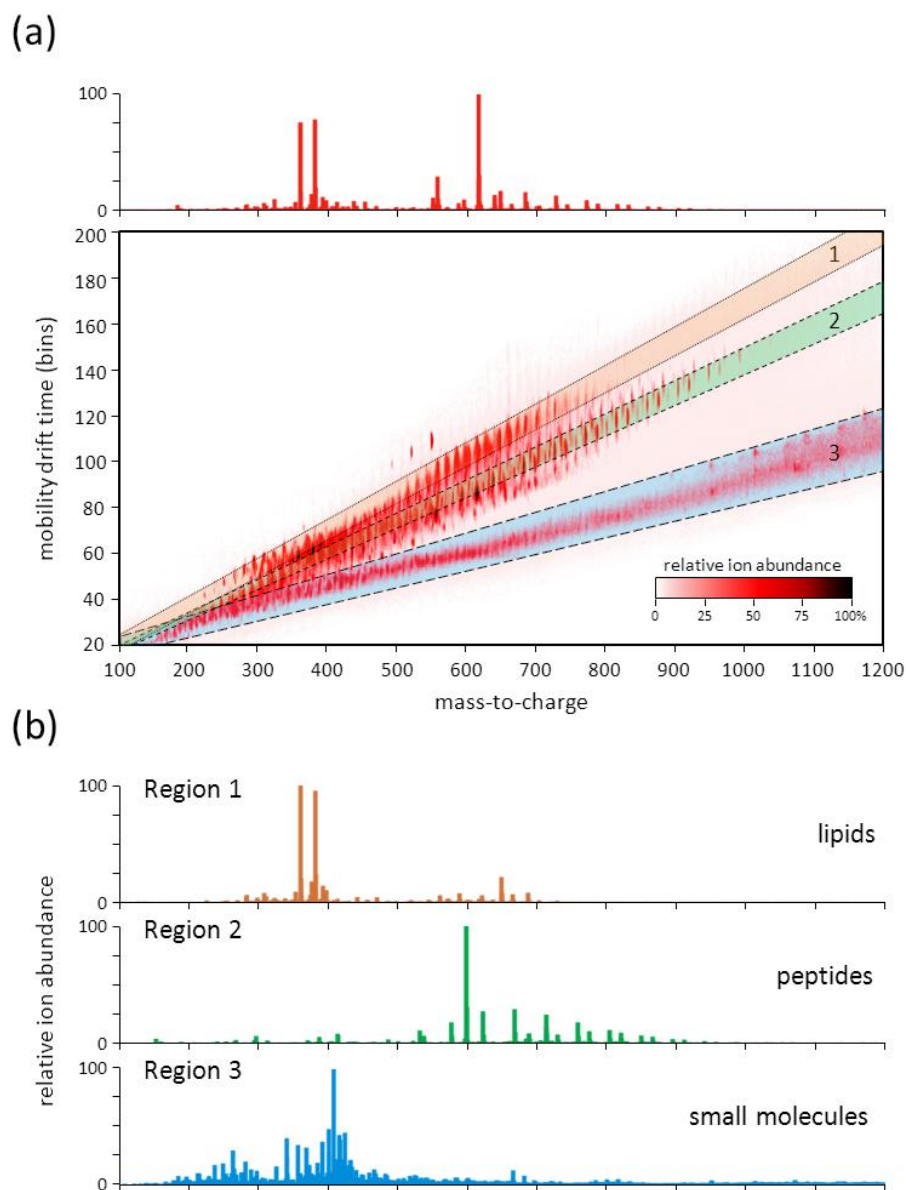
Figure 1.6. (A) Shown is a nano-electrospray ionization-ion mobility-mass spectrum of a methanol extract of rat blood. Mass-to-charge is depicted on the abscissa, with mobility drift time represented on the ordinate (ms). Peaks are false colored to illustrate relative abundance, with the scale displayed in the inset. Shown above the IM-MS plot is the corresponding mass spectrum for the entire sample. Regions corresponding to various mobility-mass correlation lines are highlighted and labeled, with the extracted mass spectra displayed in (B). Preliminary identifications are assigned based upon conformational space occupation.

One of the challenges of metabolite studies is the diverse representation of chemical species classified as metabolites. These include both large (*e.g.*, peptides, lipids and glycosides) and small (*e.g.*, alkaloids, terpenes and phenols) biomolecules, but traditionally focused on the latter due to available technologies for small molecule analysis (*e.g.*, GC-MS). As described previously, the IM-MS analysis provides an advantageous dimension of information in the form of molecular class-specific mobility-mass correlation lines which can be used for identification purposes, but also for isolation and extraction of certain chemical signals. From a global analysis perspective, this has the advantage of interrogating a large amount of chemical data simultaneously, which is particularly advantageous for whole systems approaches.[75] As an example of the utility of IM-MS for whole systems studies, **Figure 1.7(A)** depicts a mapping of ion collision cross section (ion mobility) versus ion mass for a large sample number (n=951) representing four biomolecular chemical classes: lipids, carbohydrates, peptides and nucleotides. **Figure 1.7(B)** contains logarithmic regression fits of the datasets in **Figure 7(A)** and illustrates the average mobility-mass correlation for each biomolecular class. Note that the ion mobility data normally projected as drift time has been converted to collision cross section (in square angstroms). What is immediately obvious is that the average mobility-mass correlation is different for each class, with notable disparity between peptides and carbohydrates. The data projections in Figure 6 represent an initial attempt at mapping mobility-mass data space for a large dataset representative of several molecular classes. The ultimate goal of such a project is to generate a

reliable "atlas" of conformational space of biologically relevant molecules and

apply this *a priori* knowledge towards an integrated "omics" approach.[76]
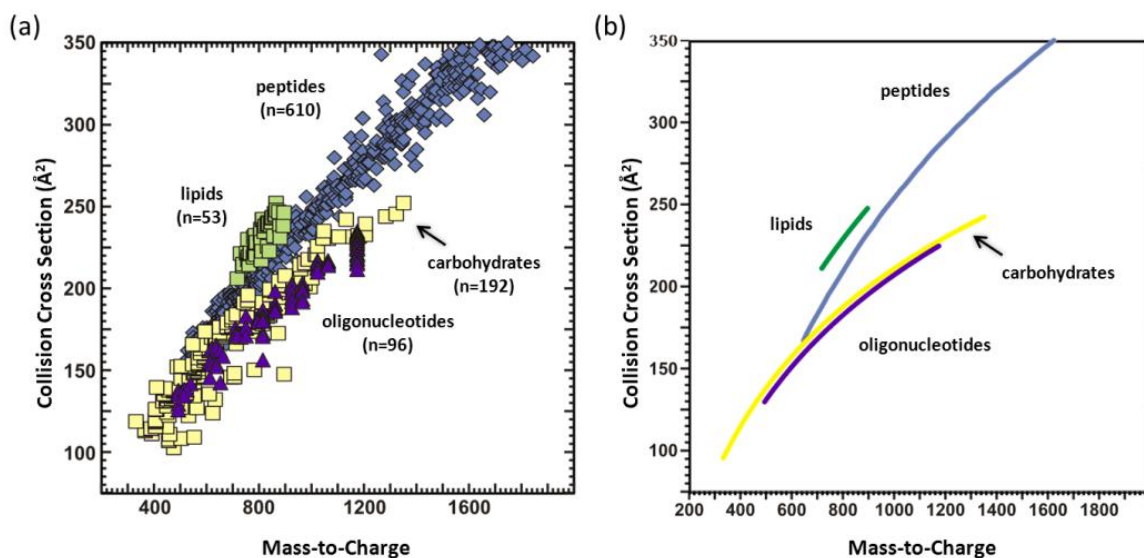
Figure 1.7. *Shown are the mass-to-charges and calculated collision cross sections (in Å^2) obtained using a drift tube ion mobility-mass spectrometer for 53 lipids, 610 peptides, 192 carbohydrates, and 96 oligonucleotides, illustrating the separation of biomolecular classes in two-dimensional space using IM-MS.* (B) Logarithmic regression fits applied to the biomolecular class distributions in (A). Adapted with permission from [77].

1.4.1 Tandem Methods for Ion Mobility-Mass Spectrometry

Ion mobility has so far been discussed with regards to the analytical merit of performing fast separation of mixtures and using the resulting separation to locate relevant chemical signals which may otherwise be disregarded in a single dimension of mass analysis, such as the case of structural isomers. While the identification of significant analyte signals (markers) in the spectrometric analysis is certainly important, it is more challenging to then assign these signals a chemical identity.[78] Tandem MS experiments (MS/MS) are a critical aspect of MS approaches to metabolite identification. MS/MS involves two mass separation steps with ion fragmentation occurring between. The first MS is used to isolate one mass-to-charge, which is then subjected to a fragmentation step (most commonly through energetic gas collisions in a pressurized chamber), causing decomposition of the selected precursor ion into fragments. The fragment ions are then analyzed in a second MS stage to generate a fragment ion mass spectrum. Fragmentation data is used to determine the precursor ion's identity based upon predicted fragmentation pathways.[79] Additionally, there are several useful "scans" which can be utilized with MS/MS in order to monitor, for example, specific product ions which are known metabolic markers for a particular drug. These tandem strategies will be briefly outlined later in the chapter. Tandem MS experiments are performed either using serial stages of MS instrumentation (tandem in space) or an ion trap instrument (tandem in time). When we discuss tandem experiments in IM-MS, we will only deal with tandem in space arrangements (primarily as a result of the lack of development of ion trapping

based IM technologies, though it is noted that such a device has been suggested theoretically).[80]

1.4.2 Scanning Modes for Tandem Mass Spectrometry

There are several "scan modes" which are useful in multi-stage tandem MS for metabolite screening applications. These modes differ only in whether each MS stage is operated in narrow (selected MS) or broadband (full MS) mode. With two MS stages (including a fragmentation stage in between), there are 4 possible combinations of scan modes which can be utilized. **Figure 1.8** illustrates these four scan modes, which are **(A)** precursor ion scan (full-selected), **(B)** neutral loss scan (full-full), **(C)** product ion scan (selected-full), and **(D)** selected reaction monitoring (selected-selected). Traditionally these modes were applied to triple quadrupole instruments, but the general methodology has since carried over to other MS/MS instrumentation, such as Q-TOF, TOF-TOF, and, to some extent, various ion trap platforms. The underlying difference in applying these scan modes to different instrument platforms is in the resulting performance: TOF instruments generally sacrifice sensitivity and broad range linear response (*e.g.*, quantitative ability) for high speed and high resolution/mass accuracy. Ion traps trade some degree of performance (speed and mass resolution) for experimental versatility, most notably the capability to do multiple stages of tandem experiments (MS^n, where n>2). Because TOF instruments obtain a broadband mass spectrum, the precursor and selective reaction monitoring experiments are performed post-data acquisition. What will follow is a

brief description of each scan mode as they are applied in tandem MS/MS experimentation.

The precursor ion scan (**Figure 1.8(A)**) and neutral loss scan (**Figure 1.8(B)**) modes are the first tandem MS experiments which are utilized in a metabolite study. These MS/MS experiments are considered reasonable preliminary methods since the information gained is broadly encompassing and requires very little *a priori* knowledge regarding the system under investigation. In a precursor ion scan, an expected product ion is selected with the second MS stage and the first MS stage is scanned through a range of m/z values until the expected product ion signal appears. The product ions of interest represent common metabolic alterations, such as glucuronidation (M+176). Additionally, the second MS stage can be set to monitor the m/z of the parent compound itself in order to discover metabolites which consist of an unaltered portion of the parent compound, such as oxidation (M+16). Because the fragmentation step in an MS/MS experiment results in both fragment ions and fragment neutrals, the mass spectrometer is blind to the latter. To overcome this fundamental limitation, the two MS stages can be set to transmit a fixed m/z difference from one another representing a characteristic neutral loss. For example, to locate an oxidation product metabolite, the first MS stage is scanned through a range of m/z values and the fragment ion, M-16, is monitored by the second MS stage. This will find all precursor ions which have been oxidized.
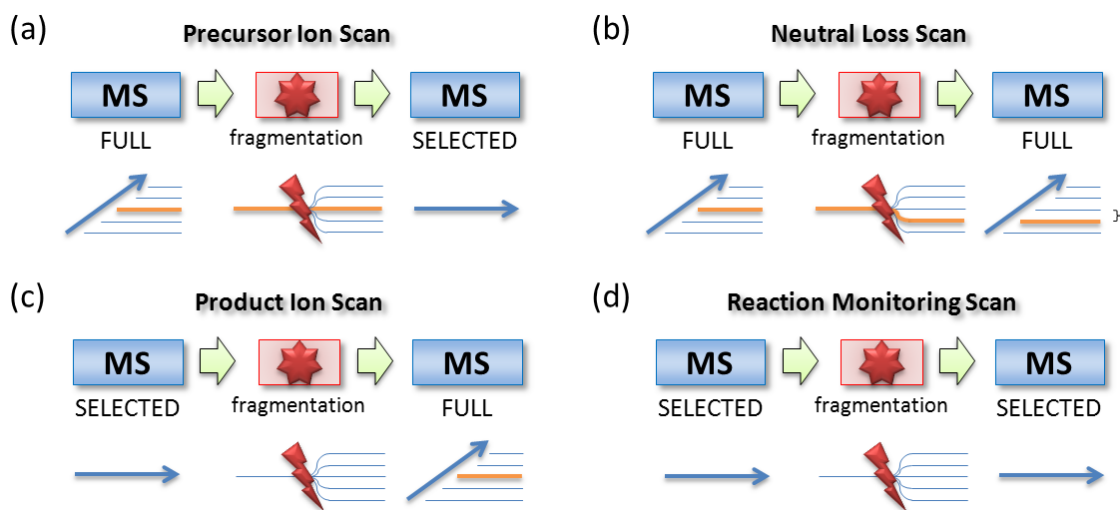
Figure 1.8. *Illustrations of the various MS/MS scanning methods for two tandem MS stages.* Fragmentation occurs between the two mass analyzers, as depicted. (A) A precursor ion scan, where the first mass analyzer performs a full scan, while the second mass analyzer is fixed to a given *m/z* that corresponds to an expected product ion. (B) A neutral loss scan, where both mass analyzers perform a full scan, with the second mass analyzer set to a fixed mass-to-charge difference from the first. Commonly, the analyzer offset corresponds to a known biotransformation. (D) A product ion scan in which the first mass analyzer isolates a particular mass-to-charge and the second mass analyzer performs a full scan to obtain all resulting fragments. (D) A reaction monitoring scan in which the first mass analyzer selects a specific mass-to-charge and the second mass analyzer is set to selectively monitor for the appearance of a particular product ion.

The product ion scan (**Figure 1.8(C)**) is the conventional mode for MS/MS experiments. In a product ion scan, a precursor ion m/z is isolated and transmitted by the first MS stage, fragmented and the entire fragment ion spectrum is obtained in the second MS stage. The product ion scan is useful for characterizing a precursor ion once it has been identified as being of interest. Finally, the reaction monitoring experiment (**Figure 1.8(D)**) is a powerful and

specific mode of MS/MS operation used primarily when quantitative information is sought. In this mode, an m/z of interest is selected by the first MS, fragmented, and a specific m/z is monitored by the second MS. Prior knowledge regarding the expected product ions is necessary. A single or multiple set of fragment ion m/z values can be monitored for each precursor ion transmitted by the first MS.

As mentioned previously, these scanning modes were originally developed for triple quadrupole instrumentation, but recent advances in hybrid MS instrumentation has expanded their usage to other platforms. The Q-TOF configuration is a particularly important instrument platform which replaces the final MS stage of a triple quadrupole with a broadband time-of-flight MS. This has the significant advantage that TOF MS performs with greater analyte sensitivity in its conventional broadband MS mode than a quadrupole operating in a full scan MS mode. The other important analytical advantage that Q-TOF instruments hold over a triple quadrupole platform is higher speed and consequently, higher sample throughput. Finally, the high mass resolving power capabilities of TOF greatly improve the mass measurement accuracy. Contemporary Q-TOF instruments are capable of resolving powers in excess of 40,000 with a theoretically unlimited mass range. Macromolecules in the MDa (10^6 mass units) range have recently been studied using QTOF instruments.[81]

1.5   High-Performance Tandem Ion Mobility-Mass Spectrometry Modes

The addition of ion mobility to multi-stage MS instruments offers greater experimental flexibility with regards to tandem experiments. For example, the use

of a FAIMS device at the front-end of an MS instrument introduces an added dimension of chemical noise discrimination which serves to enhance important ion signals which appear at low abundance [82]. A more versatile example is the addition of an IM dispersive stage into a hybrid quadrupole time-of-flight instrument (Q-TOF), which creates the useful MS-IM-MS configuration (specifically, a Q-IM-TOF). Because of the necessary transition between the two vacuum MS stages into the pressurized IM, elevated pressure ion guides are utilized between each stage to efficiently transfer ions into and out of the IM device, which creates an advantageous addition of two collision cells in the MS-IM-MS instrument configuration. Thus, collisional activation of ions can be accomplished before or after the IM separation, which creates a number of useful tandem arrangements. The next section will deal with the various tandem configurations afforded by the MS-IM-MS configuration and we will consider some of the added information which can be gleamed from each stage of tandem analysis. Regarding nomenclature, the hyphen designates two coupled analyzers (*e.g.*, IM-MS) while the forward slash designation (*e.g.*, MS/MS) denotes tandem capabilities (*i.e.*, a collision cell between the two components).

When considering an analytical configuration which brackets a mobility separation between two mass analyzers (MS-IM-MS), the first possibility is to select an m/z window with the first MS stage and immediately induce fragmentation prior to the IM-MS analysis (*i.e.*, MS/IM-MS). This will generate a comprehensive 2D IM-MS spectrum of resulting fragment ions, as illustrated in **Figure 1.9(A)**. This strategy is identical to performing a product ion scan but with

40

the added dimensionality of the ion mobility separation, resulting in separation of product peaks based upon both mobility and mass-to-charge. The practical benefit is the separation of product ions in chemical space, allowing for the distillation of the fragmentation spectrum. However, isobaric species will not be separated prior to fragmentation, and the resulting product ion spectrum may reflect multiple isobaric species not easily differentiated.

An alternative mode of operation is to first select a mass-to-charge of interest, mobility separate and then fragment the ions following the IM region (*i.e.*, MS-IM/MS). As a result, a particular mass of interest is dispersed based upon mobility prior to fragmentation and secondary mass analysis. An example spectrum is contained in **Figure 1.9(B)**. Because ion fragmentation follows the IM separation, resulting fragment ions will have mobility drift times correlated to their precursor ion signal. Thus, this method allows for the initial separation of isobaric ions based upon their different mobilities, while simultaneously correlating the product ions to their precursors. Thus, both chemical noise and isobaric signal overlap are attenuated through this fragmentation method. The MS-IM/MS method can greatly simplify analyte identification based upon the removal of contaminating product peaks contributed by isobaric ions.
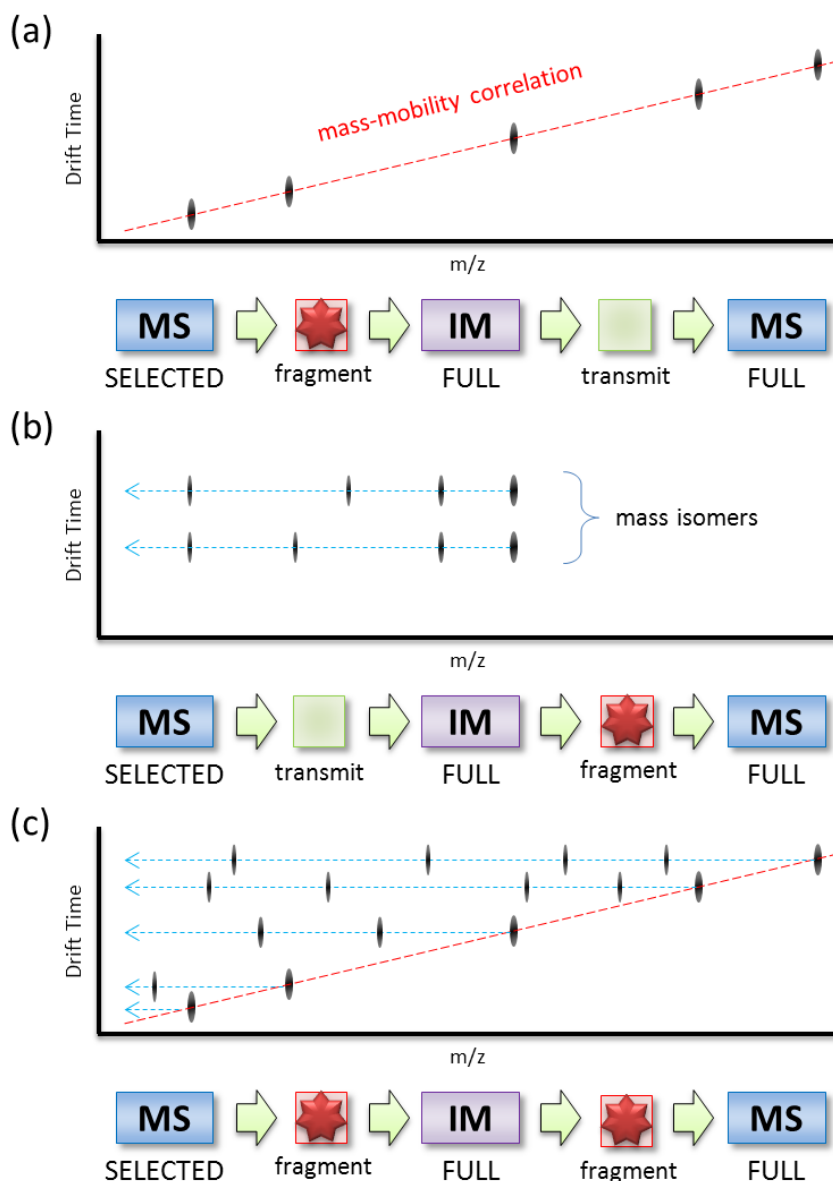
Figure 1.9. *Three different tandem modes for MS-IM-MS instrumentation.* Each 2-dimensional spectrum corresponds to a single m/z value isolated by the first MS stage. (A) MS/IM-MS mode in which fragmentation precedes the IM-MS analysis. (B) MS-IM/MS mode in which the mobility spectrum is generated prior to ion fragmentation, resulting in alignment of the fragment ions to respective precursor ion measured mobility value. As illustrated, this tandem mode is particularly useful for isobaric ions which cannot be differentiated by MS alone. (C) MS/IM/MS mode in which an isolated m/z value is fragmented both before and after the ion mobility analysis, resulting in parallel fragment ion alignment correlating to their respective precursor ion signals. In these examples, only singly charged ions are considered.

A third mode of operation which can be utilized in the MS-IM-MS configuration is to isolate a mass-to-charge in the first MS stage, induce dissociation and mobility separate the resulting fragments, and finally fragmented once again prior to the secondary mass analysis (*e.g.*, MS/IM/MS). This mode of operation (illustrated in **Figure 1.9(C)**) results in mobility correlated secondary product ions in a quasi- MS^3 experiment. **Figure 1.10** contains tandem data for the IM-MS analysis of the small carbohydrate, lacto-N-fucopentaose 1 and illustrates two modes of tandem IM-MS. In **Figure 1.10(A)** the ion fragmentation occurs before the IM-MS analysis which results in a 2-dimensional spectrum of fragment ions separated in both mobility and mass space. In **Figure 1.10(B)**, ions are induced to fragment both before and immediately following the IM analysis, resulting in a second stage of fragmentation (a pseudo MS^3 experiment). In this latter example, the secondary fragments align themselves to the precursor ion signals in which they originated since the ion mobility separation occurs prior to their formation. The novel aspect of this mode of tandem experimentation (MS/IM/MS) is that simultaneous ion activation can be achieved, generating a complete precursor and fragment ion spectrum during each experimental measurement cycle.
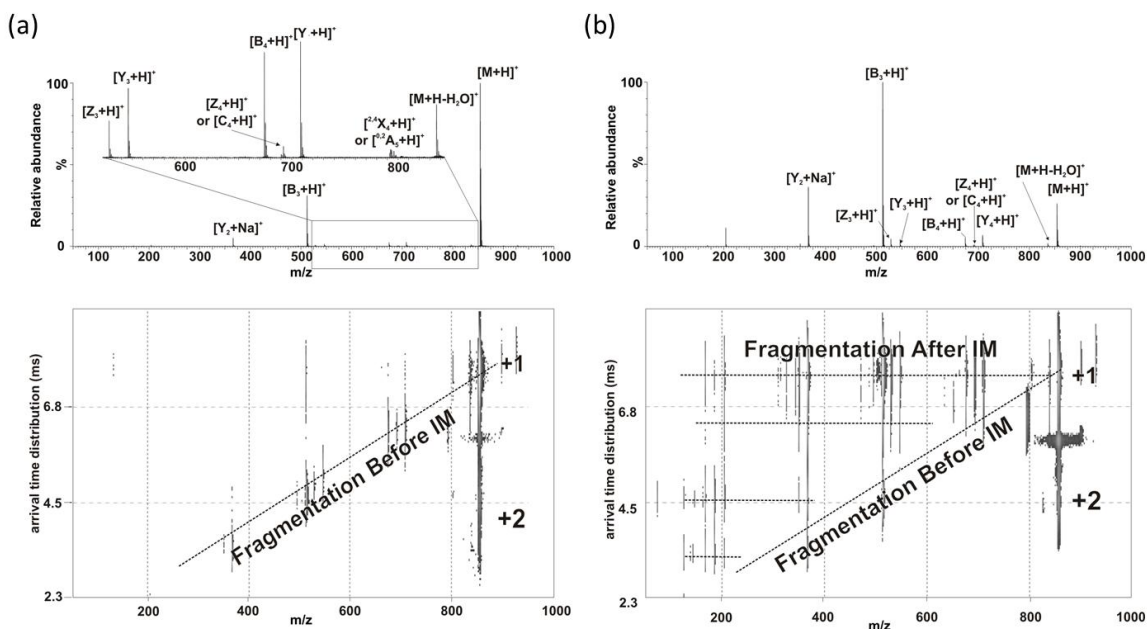
Figure 1.10. *Ion mobility-mass spectra of the small carbohydrate, lacto-N-fucopentaose 1, illustrating two tandem IM-MS modes.* (A) Spectra from fragmentation prior to IM-MS analysis, which results in dispersion of fragment ion signal across both dimensions of data analysis. (B) Spectra resulting from two stages of fragmentation, one before the IM analysis and one immediately following the IM. In this latter case, fragment ion signal is dispersed across the mobility dimension and secondary fragment ion signals align isobaric in mobility, resulting in simultaneous fragmentation of all ions resulting from the first stage of activation. For the mass spectra (above in both panels), the carbohydrate nomenclature used is from Domon and Costello.[83] Adapted with permission from [84].

1.5.1 Advantages of High Mass Accuracy and High Resolution in Metabolite Identification

In drug metabolism studies, the molecular formula of a metabolite of interest is a key piece of information. This information is most easily obtained by measuring the exact mass of the ion to high accuracy. High resolution MS can obtain a mass measurement with high precision which factors directly into the accuracy of the mass measurement. By obtaining an accurate mass measurement with high confidence, one can narrow down the number of possible molecular formulas pertaining to the measured mass. In many cases, sufficiently high mass accuracy can narrow down the possibilities to a single molecular formula and provide an unambiguous result.

When utilizing high resolution MS, an approach has been applied to metabolite identification that relies primarily on high mass accuracy to query the entire sample, post separation.[85] This method is termed MS^E, and functions by initially acquiring data over a large mass range (*ca.* 100-1000 Da). Subsequently, collision energy is imparted to the same range of ions in a ramped method from low to high energy. This results in data that combines both a full scan with corresponding fragments. Using the high mass accuracy of the instrument, product ions can be correlated back to their respective precursor ions based upon mass defect. This resolves the issue of discarding ions based upon selective fragmentation, as this method allows for the fragmentation of all ions within a time given range. High mass accuracy is maintained through the use of an internal standard for proper calibration. What results is the ability to perform

broadband fragmentation and monitor product ion transitions, as commonly done in scanning experiments, over an entire mass range. A fundamental limitation lies in the fragmentation of isobaric species which are inherently present in complex samples, as product ions for both isobars will be present in the fragmentation spectrum, resulting in convoluted data sets. This is commonly addressed by performing a pre-ionization separation. Fortunately, the IM separation can distinguish isobars in the mobility dimension. As a result, an additional degree of discrimination is present for compiling a list of product ions for a given precursor. Currently IM information is not used to deconvolute MS^E data, though the only apparent limitation is the potential to generate extremely large data files, which is becoming increasingly trivial with current data storage.

Tandem mass spectrometry inherently has limitations. Most notably, this method is insensitive to low intensity precursor ions, as these are often overlooked by automated systems if a particular peak is transient in nature. Selected precursor ions must be well above the limits of detection for a given tandem platform in order to generate meaningful tandem spectra. Isobaric species which would commonly convolute tandem spectra may be separated using IM post ionization separations to resolve isobars. While IM-MS enhances tandem experiments, currently IM separations are insufficient for the routine resolution of structurally similar isobars, *e.g.* compounds that differ by a single chiral center. This is where high resolution structural measurements, such as NMR, are required. However, these methods allow for the relatively rapid

interrogation of complex samples, allowing distillation of robust data sets to significant analytes.

We began this chapter by stating the technological challenges of metabolite analysis are substantial. While this is accurate, the number of metabolites expressed by eukaryotes is small in comparison to the number of proteins, which is estimated somewhere at *ca.* 200,000 for humans. If IM-MS and related technologies are to be commissioned into the global "omics" initiatives, then there is perhaps no greater potential for impact than in metabolite analysis. Future work should seek to implement the real time acquisition of metabolic information to better represent the dynamic nature of the metabolome. The temporal resolution necessary to understand transient biological responses will likely require the ability to acquire spectra at a rate that exceeds our current analytical capacity using pre-ionization separations. This conundrum lends itself strongly to the case for ion mobility-mass spectrometry as a means of rapid analysis of drug metabolism. By coupling ion mobility-mass spectrometry with microfluidics that allow for the trapping and maintenance of cell colonies, a global profile of a microenvironment can be acquired with high temporal resolution. This permits a more complete understanding of the underlying metabolic processes that preclude particular metabolites, while potentially circumventing the dilution issue commonly associated with bulk cultures. Though many technical issues exist with coupling microfluidic environments directly to ion mobility-mass spectrometers (*e.g.* ion suppression by non-informative, high abundance

metabolites and salts), these are surmountable, and have been addressed in a modular fashion.

1.6   Summary and Perspectives

Ion mobility spectrometry is the separation of gas phase ions based upon differential velocities through an inert buffer gas under the influence of an electric field, this rate being termed mobility. Four main ion mobility separations methods exist (drift tube ion mobility spectrometry, traveling wave ion mobility spectrometry, high-field asymmetric waveform ion mobility or differential mobility spectrometry, and differential mobility analyzer), each utilizing a different approach for separations of gas phase ions. These methods, though present in various geometries and grounded in disparate physical principles, have the common thread of performing a post-ionization separation based upon mobility. Drift tube and traveling wave ion mobility temporally separate ions along the same space, which has the advantage of generating a broadband spectrum for each measurement cycle, while limited to separating discontinuous ion pulses. High-field asymmetric waveform ion mobility and differential mobility analyzers separate ions along different spatial trajectories, allowing for a continuous beam of ions to be transmitted which possess a narrow band of mobilities. The latter techniques must be scanned across an instrument parameter (a voltage) to generate a broadband ion mobility spectrum.

Each ion mobility separation method has been integrated with mass spectrometry for two dimensional separations based upon both mobility and

mass-to-charge. These two analytical methods are readily coupled (IM-MS), as both separations occur post ionization, and result in rapid separations occurring on the order of milliseconds and microseconds, respectively. This temporal disparity allows for hundreds of mass spectra to be obtained for each mobility spectrum. For high performance mass spectrometry applications, broadband dispersion mobility separations are commonly implemented, which allow for global metabolome profiles to be obtained. Because the ionic mobility is a function of gas phase size and size a function of mass, a 2-dimensional IM-MS analysis results in a clustering of data along a narrow region of mobility and mass separation space. Thus, the degree of orthogonality between ion mobility and mass spectrometry is low, however the rate at which information is generated is very high, with signal peak production rates ca. 2 orders of magnitude greater than other analytical separations. The correlation between mobility and mass data exhibits a dependence upon intramolecular forces, monomer subunit composition, and degree of branching, which allows for the preliminary determination of biomolecular and metabolite class based upon mobility. Ion mobility-mass spectrometry allows spectra acquisition temporal resolution on the order of milliseconds, dispersion of chemical noise in two dimensions, separation of isobaric species based upon structural differences, and preliminary determination of molecular class based upon mobility. Ion mobility-mass spectrometry is also readily coupled to any liquid phase pre-ionization separation through electrospray ionization.

The ability to perform fragmentation between separations in an ion mobility-mass spectrometer allows for identification studies (tandem experiments) that enhance precursor ion identification confidence. Fragmentation is commonly prefaced with a mass selection step using a scanning mass analyzer (*e.g. a* quadrupole MS) in order to isolate a single mass-to-charge window. Fragmentation can occur either before (MS/IM-MS) or after (MS-IM/MS) the ion mobility separation, resulting in product ions or isobaric precursor ions separated in mobility space, respectively. Fragmentation prior to mobility separation results in mobility-resolved product ions, and these product ions can be further fragmented after mobility separation (MS/IM/MS), resulting in secondary product ions that can be correlated to primary product ions based upon the congruent mobilities. Broadband fragmentation can also be performed on relatively simple samples using a large mass window (*ca.* 100-1000 Da), a ramped fragmentation energy profile, and a high performance mass spectrometer. In this latter example, product ions are correlated to precursor ions based upon mass defect. Increased confidence is obtained through the use of mobility correlation to this broadband fragmentation method, as isobaric ions will convolute data otherwise.

Processing and prioritizing the extensive data that acquired during a typical high resolution mass spectrometry based metabolomics experiment is nontrivial. The focus of the work described herein seeks to utilize these multidimensional separations in conjunction with statistical workflows to prioritize

and identify meaningful analytes, assigning biological significance to features and

extending the utility of ion mobility measurements.

CONFORMATION BASED PRIORITIZATION OF SECONDARY MICROBIAL
METABOLITES

2.1 Introduction

A significant challenge in natural product discovery is the initial

discrimination of discrete secondary metabolites alongside functionally similar

primary metabolic cellular components within complex biological samples. A

property that has yet to be fully exploited for natural product identification and

characterization is the gas phase collision cross section, or, more generally, the

mobility-mass correlation. Peptide natural products possess many of the

properties that distinguish natural products, as they are frequently characterized

by a high degree of intramolecular bonding, and possess extended and compact

conformations among other structural modifications. Herein, a rapid structural

mass spectrometry technique based on ion mobility-mass spectrometry for the

comparison of cyclic peptide natural products to their primary metabolic

congeners using mobility-mass correlation is described. This property is

empirically determined using ion mobility-mass spectrometry, applied to the

[B]This work appears in:

C. R. Goodwin, L. S. Fenn, Dagmara K. Derewacz, B. O. Bachmann, J. A. McLean. Structural Mass Spectrometry: Rapid Methods for Separation and Analysis of Peptide Natural Products. *Journal of Natural Products.* **2012**, *67* (*35*): 48-53

D. K. Derewacz, **C. R. Goodwin**, J. A. McLean, H. A. Barton, B. O. Bachmann. Lechacyclines, new angucyclines and their mycothiol adducts from a deep hypogean Streptomycete. *In preparation for Organic Letters.*

analysis of linear versus cyclic peptides, and used to discriminate cyclic peptides in a crude microbial extract. Complementary computational approaches are utilized to understand the structural basis for the separation of primary metabolite linear peptides from secondary metabolite cyclic and modified cyclic species. These findings provide a platform for enhancing the identification of secondary metabolic peptides with distinct mobility-mass ratios within complex biological samples.

Further, this method was extended to commercially available traveling wave ion mobility instruments through the conceptualization of the "inherent trendline", which represents the common mobility-mass correlation for a given microbial extract. For this study, an actinomycete was isolated from Lechugilla cave in New Mexico at a depth of 1250 feet by dilution plating of pulverized wall rock sample. This organism, designated *Streptomyces cunninghamii*, was screened for secondary metabolic potential by chemical screening under multiple growth conditions, and features were prioritized for isolation by structural mass spectrometry using ion mobility-mass spectrometry. A new series of *C*-glycosylangucyclines designated Lechacyclines A–C were isolated from *Streptomyces cunninghamii* and the structures of these compounds were determined by a series of 1D and 2D NMR experiments and mass spectrometry fragmentation analysis.

2.2   A Basis for Peptide Natural Product Discrimination

The diverse activities of peptide natural products are partially a function of their unique structural attributes, which are defined by incorporation of nonproteinogenic amino acids and by extensive 'post-translational' modifications including macrocyclization, heterocyclization, and oxidation/elimination reactions. These modifications are responsible for the diversity of reported cyclic and heterocyclic scaffolds. Additionally, conformational restraints introduced through these modifications have been implicated in the biological activity of these secondary metabolites, as the entropic loss is less significant upon active site binding compared to non-constrained analogues.[86] Some microbial peptide secondary metabolites with medical relevance include cyclosporin (immunosuppressive), bialaphos (herbicide), vancomycin and penicillin (antibiotic), to name a few, and their activities have inspired the continuing search for new peptide natural products from microbial sources. This search has been reinvigorated in recent years by the discovery of a large reservoir of cryptic peptide gene clusters, both ribosomally encoded and nonribosomally encoded, in microbial genomes, potentially expressing new peptide natural products.[87, 88] Correspondingly, the conditions under which these gene clusters are expressed as well as the identity of their products are a matter of significant interest to the natural product biosynthesis and discovery communities, respectively. However, these discovery endeavors are challenged by low secondary metabolite abundance and the peptide rich background of biological extracts from which

they must be isolated. In this report we describe a structural mass spectrometry technique, ion mobility-mass spectrometry (IM-MS), to rapidly distinguish cyclic peptides from other species present in complex mixtures. This method of discrimination is then applied to a crude extract for cyclic peptide prioritization. Additionally, a simulated annealing computational approach provides a model to understand the structural differences characteristic of linear and cyclic peptides in the gas phase.

Briefly, IM-MS is a two-dimensional separation technique that first separates ions in a dimension related to structure (charge-to-surface area ratio) based on their collision cross section (CCS), which represents the area of the ion available for collisions with neutral molecules in the gas phase, and in a second dimension by mass-to-charge. Many forms of ion mobility exist: high-field asymmetric waveform ion mobility (FAIMS), differential mobility, traveling wave ion mobility (TWIM) and uniform field ion mobility (IM). However, for CCS measurements uniform field ion mobility is the only of these methods that presently allows for calculation of absolute CCS using the kinetic theory of gases.[89] For that reason, we choose to focus on this instrument as the foundation of this study.

Importantly, by using IM-MS, biomolecular classes can be separated in a complex mixture by their structure due to their different gas phase packing efficiencies dictated by the prevailing intermolecular folding forces.[77, 90] The average correlation for each biomolecular class is referred to as a mobility-mass correlation, or trendline , and significant deviation, *i.e.*, > 7% in CCS for linear

peptides (as it has been shown that ~94% of linear peptides fall within this range), from this correlation are observed for modifications and conserved secondary structure in the gas phase.[77, 90] A previous study found that the cyclic peptide gramicidin S (cyclo-VOLFPVOLFP) adopted a more compact structure than linear analogs.[9, 91] To understand the full potential for IM-MS to distinguish cyclic from linear peptides in complex samples, we have evaluated the general utility of structural separations for a suite of microbially produced cyclic peptide natural products in comparison to linear peptide congeners. Moreover, we have applied this method to the detection of the known macrocyclic peptide siamycin II, expressed in an extract from a recently isolated cave actinomycete, demonstrating the potential of IM-MS for distinguishing modified peptides in crude extracts.

2.3   Materials and Methods

2.3.1   MALDI sample preparation and analysis

The cyclic peptides, thiostrepton, vancomycin, ampicillin, valinomycin, phleomycin, cyclosporine A, polymyxin B, actinomycin D, and bacitracin, were obtained from Sigma and used without further purification. Crude extract was reconstituted in 50:50 MeOH:H_2O at a concentration of ~5mg/mL. To determine collision cross sections, MALDI ionization was performed by mixing analytes in a 200:1 molar ratio of saturated 2,5-dihydroxybenzoic acid in 20% methanol or 25 mg/mL α-cyano-4-hydroxycinnamic acid in 50% methanol with analyte. Samples were spotted onto a stainless steel plate, and allowed to dry before IM-MS

analysis. The MALDI-IM-TOFMS is equipped with a 13.9 cm ion mobility drift cell that is maintained at a pressure of *ca.* 3 Torr helium and an orthogonal reflectron TOFMS with a 1 m flight path maintained at 5 x 10^{-8} Torr. Further instrumental details have been published previously.[92]

2.3.2 Collision cross section calculations

The ion-neutral collision cross section (CCS, Ω) was calculated by determining the drift time (t_d) of the ions across the cell under low-field conditions. Drift time values were obtained at multiple field strengths of between 69 and 91 Townsend (Td), to ensure that measurements were performed under the low-field limit. Collision cross sections were calculated by the following:

$$\Omega = \frac{(18\pi)^{\frac{1}{2}}}{16} \frac{ze}{(k_B T)^{\frac{1}{2}}} \left[\frac{1}{m_i} + \frac{1}{m_n} \right]^{\frac{1}{2}} \frac{t_d E}{L} \frac{760}{p} \frac{T}{273} \frac{1}{N_0}$$

where L is the length of the drift cell, E is the electrostatic-field strength (~90-120 V cm^{-1}), z is the charge state of the ion, e is elementary charge, m_i and m_n are the masses of the ion and the neutral drift gas, respectively, N_0 is the gas number density at standard temperature and pressure, k_B is the Boltzmann constant, and p and T are the pressure (~3 Torr) and temperature (~293 K), respectively.[89]

2.3.3 Computational modeling charge derivation protocol

All molecules were first built in ChemBioDraw Ultra. Molecules were broken into fragments for charge derivation of feasible size for quantum based energy minimization and charge calculations (*i.e.* ~120 atoms or less). An initial energy minimization was performed using a B3LYP/HF 6-31G* level of quantum theory in Gaussian03.[93] After determining the calculation had converged upon a local minimum, the frequency values were interrogated to ensure the calculation had not rested upon a saddle point. These energy minimized structures were then subjected to further *ab initio* optimization and electrostatic potential calculations using Gaussian03, mimicking the protocol derived for the general Amber force field, applying a HF/6-31G* basis set and the Merz-Singh-Kollman scheme for charge parameterization.

2.3.4 Computational modeling molecular dynamics protocol

All molecular dynamics simulations were generated using the Amber 11 Molecular Dynamics Package.[94] Charge densities were converted to restrained electrostatic potential (RESP) values and prep files using antechamber.

Intact molecules were assembled and coordinated with sodium in LeAP using prep files. GAFF [95](general AMBER force field) was used for atom type descriptions. To define the sodium cation, AMBER99SB force field was used.[96, 97] Topology and coordinate files were generated for molecular dynamic simulations in sander. Initially, restraint files were generated for the sodium cation such that full exploration of the assembled molecule was possible, but if the cation began

to leave the molecule, a force would be applied to return the sodium within reasonable distance constraints of sodium-peptide interaction. Upon inspection of trajectory files, this restraint was not necessary, as the cation remained proximal to the molecule, yet was still able to fully explore all regions of the molecule. Prior to simulation, an energy minimization was performed using sander to ensure a stable starting structure. The simulated annealing protocol was carried out in three steps. First, the structure was heated to ~1200-1500K over 10 picoseconds using 0.25 femtosecond time steps. The structure was then held at this temperature for 9 nanoseconds using 0.25 femtosecond time steps, extracting a conformation every 3 picoseconds, resulting in 3000 conformational snapshots. These snapshots were cooled to ~320K over 15 picoseconds to allow the conformation to find a local minima. To generate the desired 24,000 conformations, this protocol was performed 8 times, using unique starting conformations for each to promote enhanced sampling of conformational space. Each conformation was then converted to a collision cross section using MOBCAL.[26, 98] The collision cross section and potential energy for each conformation was then extracted and visualized using a scatter plot. Data were then discriminated using the measured collision cross sections, with the sampling window ± 2 sigma of the IM CCS measurement.

2.3.5 Computational modeling clustering protocol

The extracted conformations were then aligned using super-positioning software, suppose, written by Jarrod Smith (Vanderbilt Center for Structural

Biology). These structures were then clustered based upon their root mean square distance (RMSD) over all atoms. A cutoff was then determined based upon the RMSD which resulted in approximately 19-21 conformations. This value was then imposed, and the most representative conformation from each branch of the cluster was extracted. This in effect distilled the data from ~400-2000 conformations to 20 which could be interrogated (see Supplementary Material). PDB files for each were generated and interrogated using Molecular Operating Environment (MOE).[99]

2.3.6 Fermentation and extraction conditions

BBBLUE19 was cultivated in a 1-L Erlenmeyer flask containing 500 mL of medium EA (5% lactose, 0.5% corn steep solids, 0.5% glucose, 1.5% glycerol, 1% soybean flour, 0.5% bacto-peptone, 0.3% $CaCO_3$, 0.2% $(NH_4)_2 SO_4$, 0.01% $FeSO_4 \cdot 7H_2O$, 0.01% $ZnCl_2$, 0.01% $MnCl_2$, 0.05% $MgSO_4 \cdot 7H_2O$) for 7 days at 30 °C on rotary shaker 170 rpm. The 25 g of Diaion HP-20 resin was added to the 500 mL culture and resin/culture mixture was agitated on a rotary shaker at 170 rpm for 1 hour. The mixture was separated by centrifugation and resin/cells layer was extracted separately with 300 mL of methanol and 300 mL of acetone. Combined organic fractions were evaporated to dryness to produce crude extracts. The closest relative by 16S RNA sequencing was *Streptomyces mirabilis* NBRC 13450 (99.9 % identity).

2.4   Results and Discussion

2.4.1 Measurements of Collision Cross Sections of Peptide Secondary Metabolites

Collision cross sections for a series of cyclic peptides including thiostrepton, vancomycin, ampicillin, valinomycin, phleomycin, cyclosporin A, polymyxin B, actinomycin D, bacitracin, and siamycin, are determined and compared to the values for a large suite of collision cross sections for linear peptides. Cyclic peptide CCS measurements are reported in **Table 2.1**. The cyclic peptides are prepared and analyzed using a MALDI-IM-MS instrument which is described previously,[92] and further information about the sample preparation and collision cross section calculations can be found in the experimental section above and in Appendix 1. The collision cross sections for all of the quasimolecular ions present (*i.e.*, [M+H]$^+$, [M+Na]$^+$, [M+K]$^+$, and [M+Cu]$^+$) in the IM-MS plot are compared to the mobility-mass correlation for the relevant 280 of 607 reported linear peptides which occur within the *m/z* range reported (see **Table 2.1, Figure 2.1**).[90] A power-fit line of regression is used to best describe the linear peptide data over this region (y=2.8269x$^{0.6475}$ R^2=0.8926). Notably, 76% of cyclic peptide signals fall below the peptide trendline consistent with cyclic peptide compact structure.

Table 2. 1. Cyclic peptides analysed in the present studies. Quasi-molecular ion types are shown with their associated CCS values. Ion deviation from expected linear peptide conformation is depicted in Figure 2.1. Number of measurements for each CCS is shown in parentheses.

Cyclic Peptide	Ion Adduct	*m/z* (Da)	Ω (Å^2)
ampicillin	[M+Na]$^+$	372.1	110.1±1.3(20)
valinomycin	[M+H]$^+$	1111.6	271.9±1.4(19)
valinomycin	[M+Na]$^+$	1133.6	269.7±0.8(19)
valinomycin	[M+K]$^+$	1149.6	274.5±0.6(19)
cyclosporine	[M+H]$^+$	1202.8	296.6±1.2(19)
polymyxin	[M+H]$^+$	1203.8	285.6±1.0(19)
cyclosporine	[M+Na]$^+$	1224.8	289.9±1.2(19)
polymyxin	[M+Na]$^+$	1225.7	279.4±0.9(19)
polymyxin	[M+K]$^+$	1241.7	284.4±4.9(19)
actinomycin	[M+H]$^+$	1255.6	280.1±1.9(18)
actinomycin	[M+Na]$^+$	1277.6	284.2±0.7(19)
actinomycin	[M+K]$^+$	1293.6	280.8±4.1(17)
bacitracin	[M+H]$^+$	1422.8	301.2±0.8(19)
phleomycin	[M+H]$^+$	1427.7	275.7±1.3(13)
bacitracin	[M+Na]$^+$	1444.7	305.3±1.0(19)
phleomycin	[M+Na]$^+$	1448.4	276.7±1.2(19)
vancomycin	[M+H]$^+$	1448.4	299.4±0.9(20)
bacitracin	[M+K]$^+$	1460.7	303.6±2.3(10)
vancomycin	[M+Na]$^+$	1470.4	296.0±3.7(20)
vancomycin	[M+K]$^+$	1486.4	299.4±3.8(15)
phleomycin	[M+Cu]$^+$	1489.5	276.8±2.7(19)
thiostrepton	[M+H]$^+$	1664.5	310.0±1.6(20)
thiostrepton	[M+Na]$^+$	1686.5	315.5±1.0(20)
thiostrepton	[M+K]$^+$	1702.5	314.8±3.0(10)
siamycin I	[M+Na]$^+$	2185.8	373.2±0.8(15)
siamycin I	[M+K]$^+$	2201.8	375.2±1.7(14)
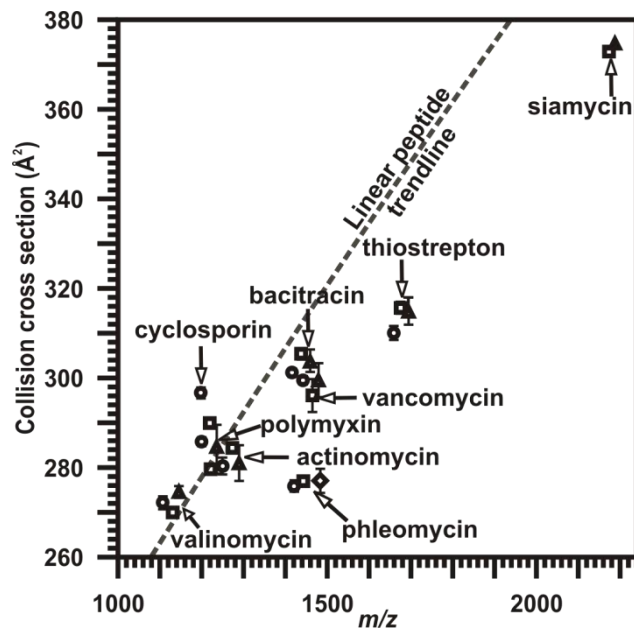
Figure 2.1. *Conformational space plot depicting the relative increased gas-phase density of cyclic peptides when compared to linear peptides.* IM-MS plot comparison of the collision cross sections of cyclic peptides compared to a trendline best representative of linear peptides for the mass range of 1100-2300 Da ($y=2.8269x^{0.6475}$ $R^2=0.8926$). The collision cross section values and associated error of measurements can be found in Table 2.1. Symbols are as follows: ●-$[M+H]^+$; ■-$[M+Na]^+$; ▲-$[M+K]^+$; and ◆-$[M+Cu]^+$.

2.4.2 Computational Modeling of Peptide Natural Products in the Gas Phase

To interpret the theoretical basis of these results, a molecular dynamics model was developed. For conformational analysis, a protocol analogous to simulated annealing was used in which snapshots of conformations were taken periodically during the heating procedure and these conformations were subsequently cooled to allow for energy minimization, generating 24,000 unique low-energy conformations. This method was performed for representative cyclic peptides based upon their chemical and structural diversity, as illustrated in **Figure 2.2**.[100] Further details regarding the modeling protocol can be found in the experimental section and in APPENDIX 2. Valinomycin is a macrocyclic depsipeptide comprised of a mixture of D- and L-Val. Vancomycin is a highly cross-linked tricyclic peptide compacted and rigidified by aromatic C-C and C-O (ether) cross links. Cyclosporin A is a nonribosomally synthesized macrocyclic molecule containing D-Ala along with a butenyl-N-methyl-L-threonine residue. Finally, polymyxin B is a lariat macrolactam with a hydrophobic tail and hydrophilic macrocyclic core. Shown in **Figure 2.2** are the most representative conformations describing the data discriminated using experimentally derived CCS values, which were extracted from the aforementioned 24,000 unique structures generated for each modeled structure. For structural analyses, larger sets (*ca.* 18-22 representative conformations) were generated using clustering analyses and interrogated to determine prevalent structural motifs (see APPENDIX 2).
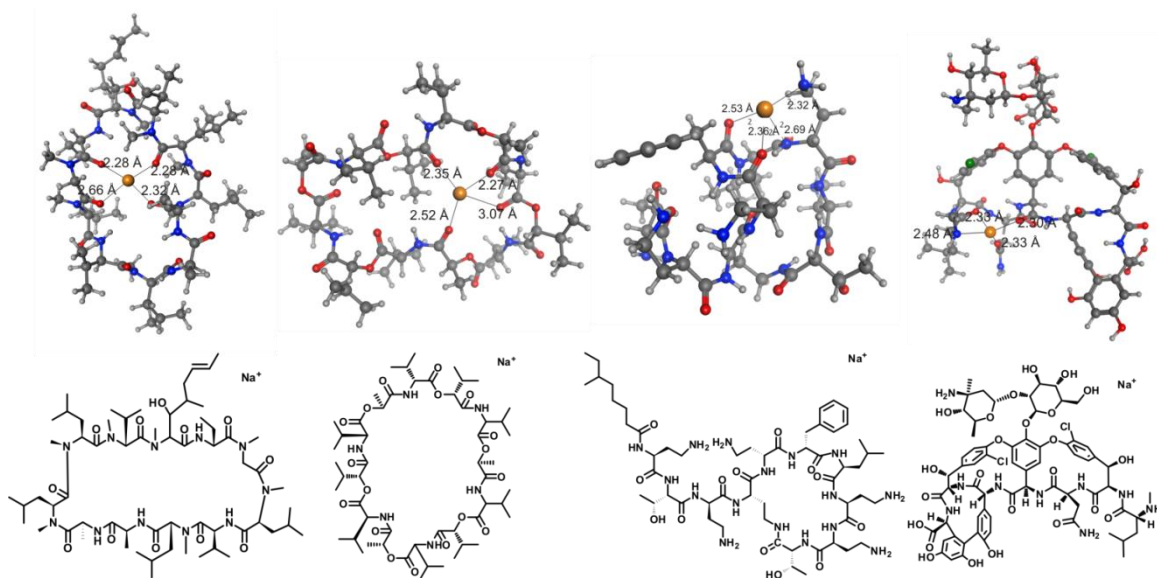
Figure 2.2. *Representative structures for cyclic peptides*. From left to right: sodiated cyclosporin A (24000 , 807), valinomycin (24000, 302), polymyxin B (24000, 891), and vancomycin (24000, 2010) conformations which are most representative (top row) of the extracted conformers discriminated based upon experimentally derived CCS values. The number of unique structures initially calculated and the number that correspond with the IM-MS empirical collision cross section are shown in parenthesis, respectively. The percent deviation of each calculated CCS value from predicted CCS values for isobaric linear peptides are 2.69%±0.43%, 0.43%±0.30%, -1.08%±0.32%, -6.88%±1.16%, respectively. Sodium coordination distances are labeled. Carbon atoms are shown in grey, hydrogen white, nitrogen blue, oxygen red, chlorine green, and sodium yellow. Shown below are the associated chemical structures.

These molecular dynamics calculations provide a model for rationalizing conformational differences for cyclic versus linear peptides. The primary features that influence gas phase conformational density are: (1) the loss of degrees of freedom due to macrocyclization, (2) the presence of highly coordinated metal atoms, and (3) the presence of atoms with intrinsically higher density, such as halides.[101] While it is expected that torsional freedom is significantly reduced for

cyclic peptides compared to linear peptides, this effect was visualized in these models. Notably, the degree of cyclization and the number of residues per ring has a large influence on trendline deviation. For example, valinomycin (a 12 residue macrocycle) and cyclosporin (an 11 residue macrocycle), each adopt CCS values greater than that predicted by the linear peptide trendline, while polymyxin B (a lariat compound with 7 residues present in the macrocycle) falls below the trendline. However, vancomycin (a tricyclic peptide with 3 - 4 amino acids per ring) falls significantly below the linear peptide trendline. Modeling indicates extensive coordination of sodium within the ring of cyclosporin and valinomycin, likely resulting in the less dense conformations, as this extends the ring. This is supported by the increased collision cross section of valinomycin when coordinated to potassium, which likely results in an extended ring conformation, as reported in the literature (as valinomycin is a potassium specific ionophore). Sodium coordination distances and proximities in cyclic peptides are consistent with those from quantum mechanical calculations previously reported for gas phase linear peptides.[102, 103] The observed high degree of coordination to sodium appears to be facilitated by the more constrained orientation of carbonyls, esters, ethers, amines, and other functional groups (*e.g.*, chlorine), but should not be considered an exclusive product of cyclization. It should be noted that post-translational modifications and the addition of atoms such as chlorine increase the density of the compounds, resulting in further deviation from the linear peptide trendline. Therefore, although cyclization provides increased

density, glycosylation and halide inclusion can further enhance the deviation from linear peptides in ion mobility based separations.

In individual cases, these models aid in rationalizing deviations. For example, the relatively low collision cross section deviation of polymyxin B is attributed to coordinating sodium by both the ring and tail portions of the lariat peptide. The small number of residues present in the ring allows for increased density due to this constraint, as well. The extended butenyl-methyl-L-threonine group of cyclosporin A likely expands its conformation relative to other peptides, while the large number of residues present in the ring structure preclude adopting a dense gas phase conformation. Vancomycin is an example of a molecule possessing both deoxysugars and halides present in addition to three small macrocyclic structures, factors that apparently contribute to the higher gas-phase packing efficiency.

2.4.3 Discriminating Cyclic from Linear Peptides

Intuitively, the apparent decreased mobility-mass correlation of structurally constrained peptides relative to linear peptides can potentially aid in discriminating peptide natural products from linear peptide ions. As previously noted, a line of regression best describing the mobility-mass correlation for a large number of linear peptides was generated. This creates a baseline of comparison, in which we explored the utility of analyzing percent deviation from this line of regression as a discriminator for cyclic peptides, termed the threshold. **Figure 2.3** displays the percentage of cyclic peptides (white fill) versus linear peptides (black fill) that fall beyond the applied threshold (*i.e.*, have a CCS value

smaller than the applied threshold). Using this threshold analysis, the enrichment of cyclic peptides is evident. For instance, 80% of peptide natural products possess CSS-mass ratios beneath a -3% deviation, whereas only 20% of linear peptides are observed. Using a more stringent analysis, beneath a 6.0% deviation threshold, 95% of linear peptides are excluded from analysis, while 40% of the cyclic peptides in the dataset remain. Beyond an -8% deviation threshold, ~99% of linear peptides are removed from analysis, at the expense of excluding ~2/3 of cyclic peptides. Therefore, while not an absolute discriminator of cyclic from linear peptides; we propose that the deviation of observed mobility-mass measurements from the linear trendline is a useful metric for enhancing the identification of peptide natural products in extracts containing competitive background levels of linear peptide signals.
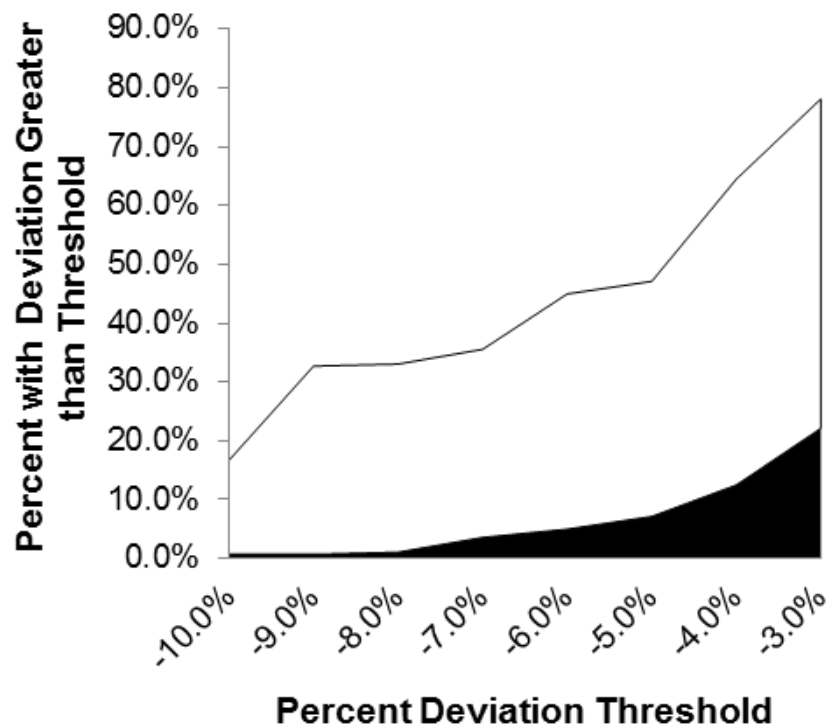
Figure 2.3. *Percentage of analyzed linear (black fill) and cyclic (white fill) peptides that deviate from the linear peptide mobility-mass correlation greater than an applied threshold.* As a function of percent deviation from the linear peptide trendline, the percentages of analyzed species that occupy a more dense CCS value are indicated. Notably, with a threshold of -6.0%, 95% of linear peptides are excluded from analysis, while 40% of cyclic peptides have more dense CCS values.

2.4.4 Cyclic Peptide Discrimination in a Crude Extract

To demonstrate the potential of IM-MS to discriminate peptide natural products within a crude microbial extract, we analyzed an extract derived from actinomycete "BBBLUE19", an organism recently isolated from a hypogean ecosystem (Blue Springs Cave, Sparta, TN). This organism was fermented and extracted under conditions typical for natural product discovery and a total hydrophobic extract of BBBLUE19 was analyzed using the aforementioned MALDI-IM-MS methodology. Correspondingly, the linear peptide mobility-mass correlation was superimposed on the IM-MS snapshot of the crude extract (**Figure 2.4(A)**). A threshold of -6.0% was applied to enrich for potential peptide natural products, and peaks were prioritized upon this basis. A series of high abundance peaks with significant trendline deviation were thus selected for further identification, one of which (accurate mass = 2175.88Da, CCS value 360.8±4.5Å^2) possessed > 11% deviation (predicted linear peptide CCS at this mass = 409.7Å^2, **Figure 2.4(B)**), which corresponds to a <1% probability of being a linear peptide. The observed mass was most consistent with Siamycin II (within 5 ppm mass error), previously isolated from *Streptomyces sp.* AA3891.[104-106] Subsequently, the isolated compound was dereplicatively identified and validated as siamycin II by comparison to the reported ^{1}H NMR spectrum. As a result, the tricyclic peptide natural product siamycin II was successfully prioritized from a crude extract using the unique CCS value adopted in gas phase.
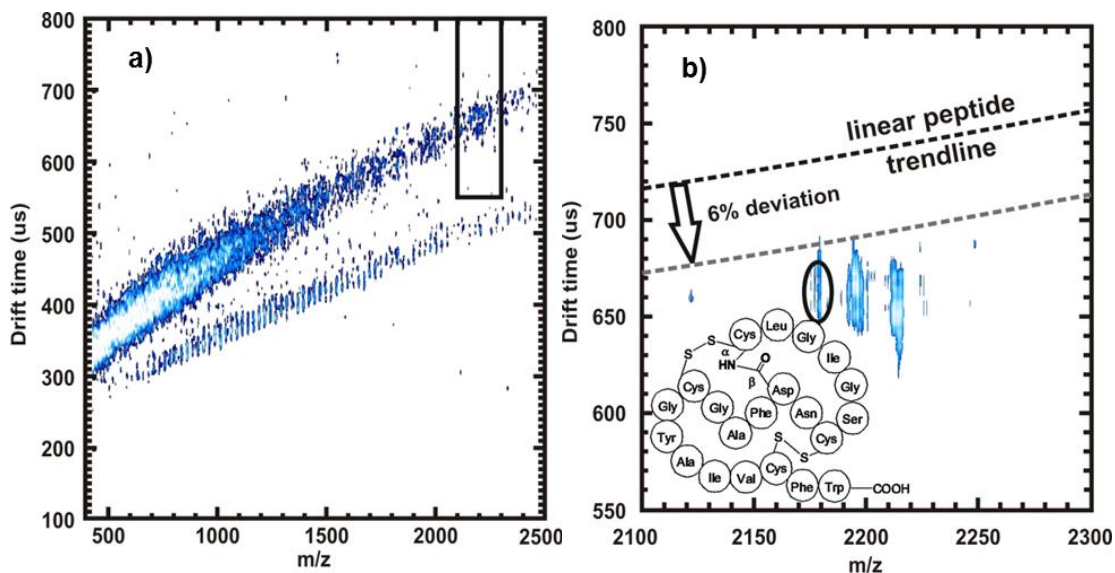
Figure 2.4. *Shown are the analyses of crude BBBLUE19 streptomycete extract using IM-MS methodologies for the determination of cyclic peptide compound presence.* (A) 2-dimensional MALDI-IM-MS spectrum of crude extract using drift tube mobility separations. The red-boxed in region is expanded in (B). In (B), the red-circled region annotates a peak that, upon initial inspection, has dense gas phase packing efficiency. Collision cross section measurements were performed, resulting in a CCS value of 360.8 ± 4.5 Å^2, a deviation of 11.9% below the linear peptide trendline for this m/z (predicted CCS value of 409.7Å^2). The sample was then analyzed using ESI-IM-high resolution MS (not shown). This compound was identified to be siamycin II, a cyclic peptide, using high mass accuracy measurements obtained from an IM-high resolution MS. The structure is shown as an inset in (B).

2.5   Uniform Field Perspectives

Uniform field IM-MS instruments as described herein remain an uncommon instrument in drug discovery laboratories. Commercially available IM-MS instruments typically use an alternative mobility separation paradigm termed a traveling wave, which is distinct from uniform field instruments and not amenable to absolute CSS determination using the kinetic theory of gases.[89] As

such, the utility of using the mobility-mass correlation as a means for discrimination of natural products using the commercially available traveling wave IM-MS were explored. The primary difficulty in comparing the two separations is the inability to extract CCS values from first principles using travelling wave IM separations, as the electric field gradient experienced by ions is time dependent, although CCS calibrants can be used to obtain relative CCS measurements.[14, 107] To address this, and extend the utility of ion mobility measurements beyond uniform field instruments, we have devised a method of assigning a "structural uniqueness" attribute to compounds through ion mobility measurements on a commercially available traveling wave instrument. This method utilizes the background signals present in crude extracts as a comparison.

2.6   Extension of Mobility Based Discrimination to Traveling Wave Ion Mobility

2.6.1 Overview of Biological Source

The organism interrogated for this study was again of hypogean origin. Caves possess properties favorable for microbial growth including extensive oxygen and water saturated aerobic surface areas supporting biofilm formation, in addition to a relatively constant temperature and humidity. However, the nutrient deprived nature of caves, with a common total organic content of less than 0.5mg per liter, results in the adaptation of cave microorganisms to these hypercompetitive environments.[108] Previously surveys of cave microbiotica have

72

revealed the presence of genera known to produce secondary metabolites including actinomycetes and myxobacteria.[109] Herein we describe the isolation of a cave actinomycete from a remote and deep cave system and the isolation and structural elucidation of a secondary metabolite from this strain using mobility guided prioritization. To facilitate identification of secondary metabolites within crude extracts we describe a new method using structural mass spectrometry to identify conformationally divergent mass features in order to prioritize compound discovery.

The strain LC30 was isolated from one of the most remote locations within Lechuguilla Cave, approximately 400m underground. The Lechuguilla cave is a deep and isolated cave found within Carlsbad Caverns National Park (USA). The cave was formed by hypogenic (ascending) sulfuric acid-rich water throughout the last 7 million years.[110-112] Due to the lack of surface inorganic flux and absence of sunlight, microbial community subsistence in this cave system is likely driven by chemolithotrophic activity.[116, 117] Visitation records available from Carlsbad Caverns National Park demonstrated that the sample site had only been visited once before, while the absence of scuff marks and boot prints indicated that no humans had accessed the actual sample site. The site itself was a wall without obvious signs of organic input, such as dripping water or condensation. It was also away from main airflow routes, limiting the likelihood that airflow had transported microorganisms from the surface to this location.

73

2.6.2 Interrogation of Hypogean Streptomycete Secondary Metabolites

Cultivation from the site sample on HC media revealed the presence of over 100 colonies, a number of which had the characteristic powdery appearance of *Actinomycetes.* Purification of these colonies revealed the presence of a number of *Streptomycetes,* including strain LC30, which demonstrated 100% identity with *Streptomyces anulatus* by comparative BLAST alignment. Strain LC30 was subsequently selected for secondary metabolome analysis, cultured in various fermentation media, and analyzed by liquid chromatography-mass spectrometry (LC-MS) and ion mobility-mass spectrometry (IM-MS).

In this chapter, we have demonstrated the ability to prioritize secondary metabolites in crude extracts using deviations from predicted mobility values.[119] Significantly, this study focused on analyte deviation from predicted peptide ion mobilities obtained on a drift tube style instrument.[120] However, to provide applicability of these methods across mobility platforms, ion mobility analysis was performed on a commercially available travelling wave instrument (SYNAPT G2 HDMS, Waters, Milford, MA). To determine unique mobility values, and thus prioritize metabolites accordingly, we devised the concept of the 'inherent trendline'. Essentially, this concept relies on the correlated nature of mass and size, and uses an empirically derived line of regression to determine what an expected mobility is for a given mass, as only singly charged species are considered.[9] In this regard, all extracted species are used to establish a common mobility value trend. Natural products commonly possess cyclization, rigid scaffolds, halogens, sugar moieties, or chelated metals, for example, all of which will produce a deviation from the predicted mobility.[90, 91, 121-124]

2.6.3 Inherent Trendline Analysis

Crude LC30 extracts were analyzed using IM-MS and revealed the presence of abundant features with high deviation from inherent trendline (**Figure 2.5**).To establish perspective, a deviation of greater than 17.3% was observed in 8.8% (141 of 1601) detected features with *m/z* values greater than 400Da. When the additional criterion of intensity is applied, Lechacycline C is prioritized in the top 5 compounds of 1601. When the structural deviation criterion is relaxed to 10.3%, 36% of detected features are prioritized, and when further relaxed to 5.5%, nearly two-thirds of all features possess this deviation. However, as abundance is critical to isolation, when intensity is factored as a secondary filtering variable, Lechacycline A-C are all found in the top 20 prioritized compounds, even at 5.5% deviation, with Lechacycline A and C found in the top 5 (top 0.31%). When based upon intensity alone, this falls to the top 30 compounds.

We consider the Lechacycline family an exemplary example of the added benefit provided by ion mobility. The rigid angucycline scaffold provides a basis for separation, as the planar structure results in inherently extended gas phase packing efficiency, as demonstrated by the large positive deviation of Lechacycline C. The addition of the **A2** group likely provides a mechanism for Lechacycline B to self-solvate in the gas phase, resulting in increased packing efficiency. The addition of the mycothiol moiety found in Lechacycline A

represents a bulky substituent that is demonstrated by the positive deviation from the inherent trendline.
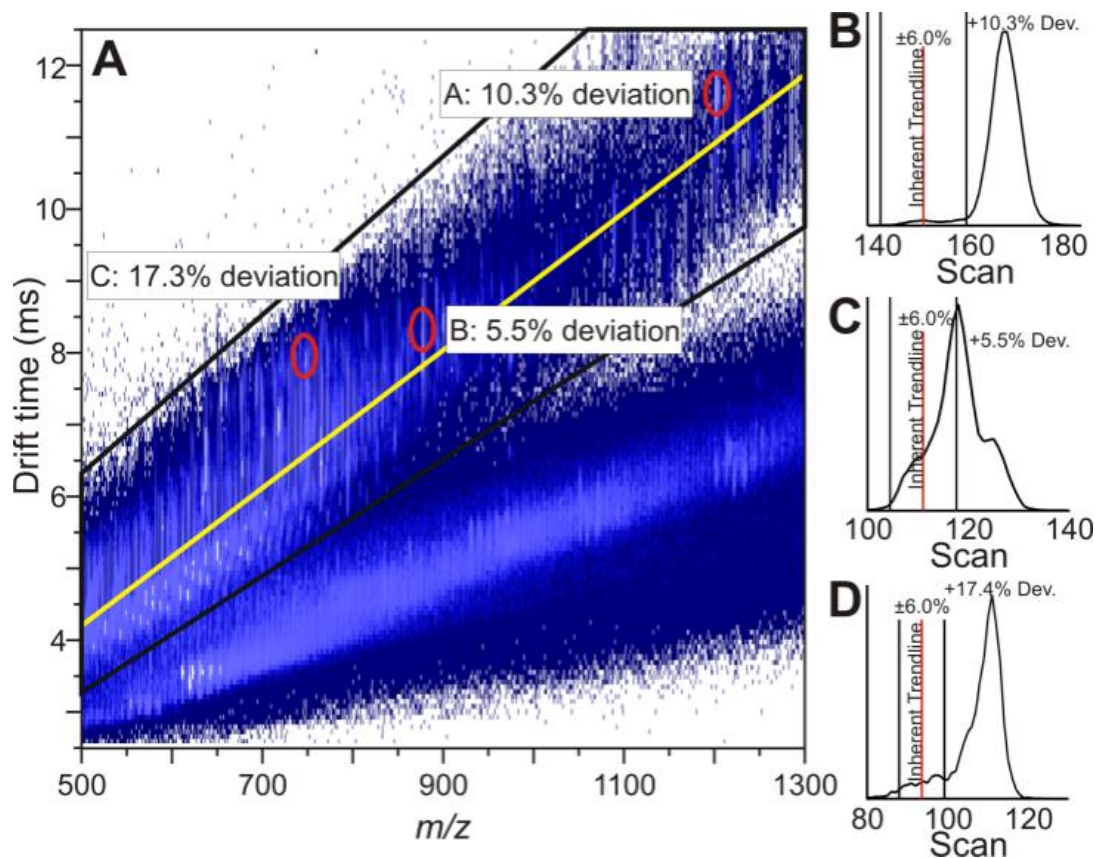
Figure 2.5. (A) Ion mobility-mass spectrum of crude LC30 extract. Singly charged species analyzed are indicated by inset black region. Lechacyclines A-C are annotated and percent deviation from the inherent trendline, indicated by yellow line, is reported. (B-D) depict drift time chromatograms for Lechacyclines A-C, respectively, with the inherent trendline and 6% deviation labeled for comparative purposes.

1 R = A1
2 R = A2
3 R = OH

A2

A1
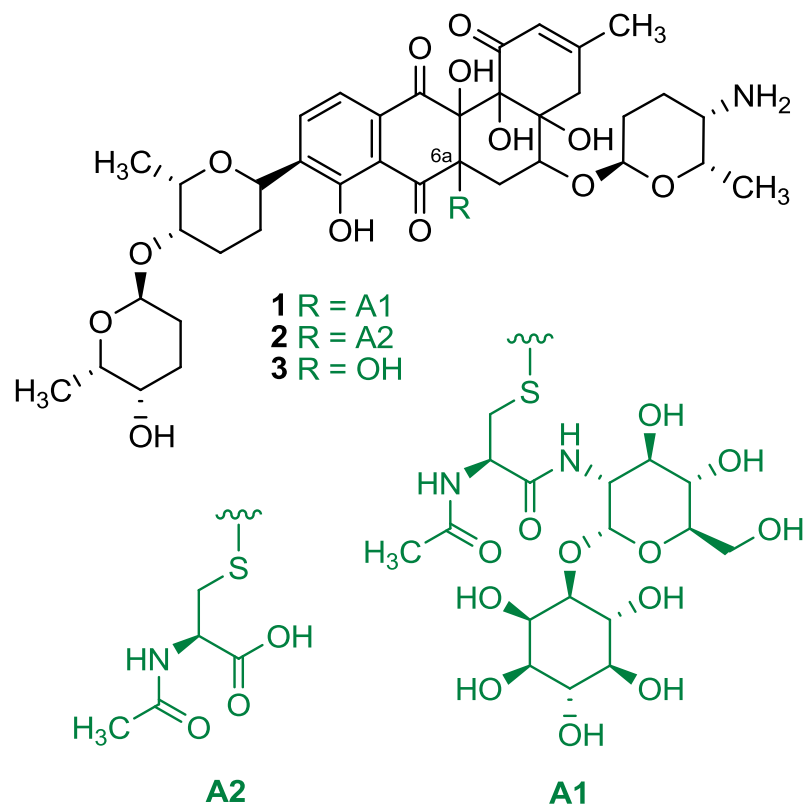
Figure 2.6. *Structures of Lechacyclines A-C.*

2.6.4 Isolation and Identification of Lechacyclines

Medium BA was selected for production scale up based on the highest abundance of compounds of interest. Solid phase extraction of broth and mycelium with Diaion HP-20 resin followed by extraction of mycelium and resin with methanol and acetone captured the targeted compounds. Prefractionation on LH20 size exclusion column followed by purification with reversed phase HPLC yielded three pure compounds of interest (**Figure 2.6**). Compound **1** was isolated with a high resolution mass spectrum yielding an m/z of 1200.46. $[M+H]^+$ and combined with UV and NMR data indicated a chemical formula of $C_{54}H_{77}N_3O_{25}S$, that does not correlate with known entries in natural product databases (Dictionary of Natural Products, PubChem).
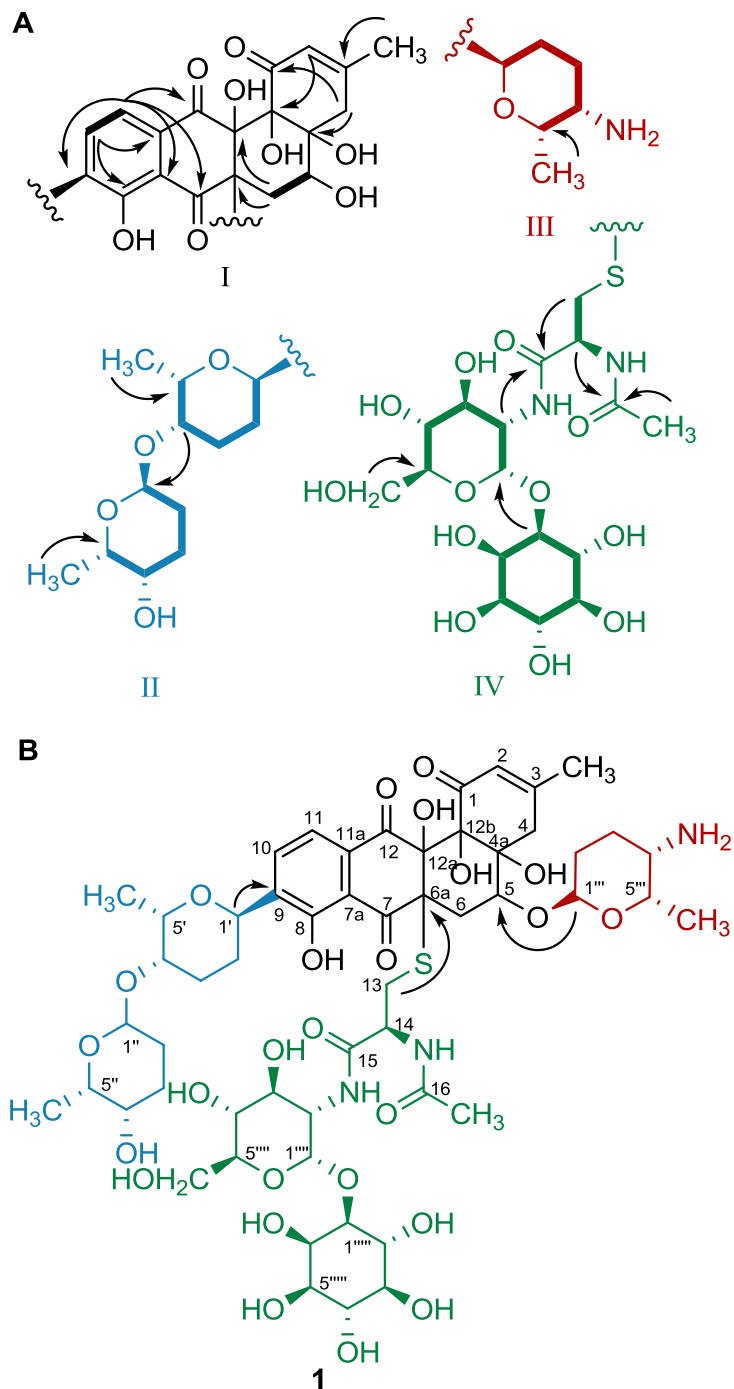
Figure 2.7. (A) Major substructures of Lechacycline A (1) assembled from COSY, HSQC and HMBC spectral data. (B) Substructures were linked via HMBC correlations.

Briefly, four partial structures (**I-IV**) (**Figure 2.7(A)**) were proposed based on COSY, HSQC and HMBC spectral data (**Table A2.3-5**) with ring assembly of tetracyclic aglycone core (**I**) closely resembling Aquayamycin-Type angucycline natural products.[125] HMBC correlations from H1' proton to C9 quaternary carbon determined the connectivity of disaccharide fragment **II** and aglycone **I** (**Figure 2.7(B)**). The chemical shifts of carbons C1' and C9 were characteristic to C-glycosidic linkage. We were able to assign relative stereochemistry of **II** based on coupling constants present in ^{1}H NMR experiment. HMBC from H1''' anomeric proton to C5 carbon established the relationship between fragments **III** and **I** (**Figure 2.7(B)**). Again we were able to assign relative stereochemistry of **III**, that turned out to be an unusual amino sugar, based on coupling constants present in ^{1}H NMR. Finally, we were able to link partial structures **IV** and **I** based on HMBC correlation from H13 methylene protons to C6a quaternary carbon. The chemical shift of carbon C6a indicates sulfur substituent in this position.This compound, that we named Lechacycline A (**1**) was isolated along with two analogs, Lechacyclines B (**2**) and C (**3**) that differ in substitution in position C6a (**Figure 2.6**).

A particularly interesting substituent in this position was fragment **IV** of Lechacycline A (**1**) called mycothiol, that has been previously reported in the literature.[126-128] We were able to assign relative stereochemistry of this moiety based on coupling constants of ^{1}H NMR but its absolute stereochemistry was established by Bewley and coworkers as 1-D-*myo*-inosityl2-deoxy-2(*N*-acetamido-L-cysteinamido)-α-D-glucopyranoside and was in agreement with our

assignment.[129] It has been reported that mycothiol in bacterial cells of actinomycetes is involved in detoxification pathway where it forms *S*-conjugate with alkylating agent, which is then cleaved to release mercapturic acid that is excreted outside the cell.[130] We can speculate that compounds **1** and **2**, that we captured are as well the products of detoxification pathway performed by our bacteria.

2.7   Conclusions and Perspectives

Herein we describe the application of ion mobility as an additional attribute for secondary metabolite prioritization. Through a suite of standards, a motif was established to prioritize cyclized and decorated natural products peptidic in nature. Additionally, this method was extended beyond a uniform field ion mobility instrument to the commercially available traveling wave ion mobility instrument. This extension considers structural uniqueness as a means of prioritization, as compared to the extract background. These methods resulted in the prioritization and isolation of the tricyclic peptide Siamycin II and a new class of molecules, termed Lechacyclines. The addition of ion mobility exhibits little to no negative consequences in extract interrogation, as the minor decrease in sensitivity is negligible, as analytes in abundance near the limits of detection are not optimal for natural product discovery. This provides an attribute orthogonal to conventional lead compound prioritization criteria.

In addition to prioritizing lead compounds, ion mobility allows comprehensive analysis of microbial extracts in one pass through the expansion

of peak capacity. Coupling this technique to liquid chromatography allows the acquisition of fragmentation spectra in a non-discriminant manner, as shown in the following chapter.

2.8   Supporting Information

Structures, clustering trees and representative structures from computational studies are available in APPENDIX 2. Additionally, all procedures for both studies and NMR assignments can be found in APPENDIX 2.

CHAPTER 3[C]

MULTIVARIATE STATISTICAL ANALYSIS METHODS FOR MICROBIAL EXTRACT INTERROGATION

3.1   Introduction

Bacteria develop resistance to many classes of antibiotics vertically, by engendering mutations in genes encoding transcriptional and translational apparatus. These severe adaptations affect global transcription, translation, and the correspondingly effected metabolism. Here we characterize metabolome scale changes in transcriptional and translational mutants in a genomically characterized Nocardiopsis in stationary phase. Analysis of UPLC-IM-MS metabolomic features from a cohort of streptomycin and rifampicin resistant mutants grown in the absence of antibiotics exhibit clear metabolomic speciation and loadings analysis catalog a marked change in metabolic phenotype. Consistent with derepression, up to 311 new features are observed in antibiotic resistant mutants that are not present in their progenitors. Mutants demonstrate changes in primary metabolism, such as modulation of fatty acid composition, and the increased production of the osmoprotectant ectoine, in addition to the presence of abundant emergent potential secondary metabolites. Isolation of three of these metabolites followed by structure elucidation demonstrates them to

be an unusual polyketide family with a previously uncharacterized xanthene framework resulting from sequential oxidative carbon skeletal rearrangements. Designated as 'mutaxanthenes', this family can be correlated to a type-II polyketide gene cluster in the producing organism. Taken together, these data suggest that biosynthetic pathway derepression is a general consequence of some antibiotic resistance mutations.

Increasing evidence is accumulating that a large fraction of antibiotic resistance may be elicited via horizontal transfer of resistance elements from the reservoir of microbial diversity found in soil. [131, 132] Additionally, bacterial resistance towards a significant subset of antibiotics is rapidly generated vertically by mutations in central housekeeping genes encoding polymerases and ribosomal subunits. For example, bacterial resistance to rifampicin is afforded by mutations in the RNA polymerase β-subunit, encoded by *rpoB*, while resistance to streptomycin results from mutations in the ribosomal 30S subunit and/or ribosomal methyltransferases. [133-135] Notably in these adaptive strategies, a small number of mutations ultimately result in complex and significant global changes in gene expression and protein synthesis. For instance, *rpoB* mutations foster the up-regulation of proteins involved in central metabolism (including nucleoside and nucleotide, amino acid, carbohydrate, lipid and phospholipid biosynthesis), detoxification, signal transduction, protein synthesis, and cell envelope processes, to name a few, while cell division proteins are generally down-regulated. [136, 137] Streptomycin resistance, via *rpsL* mutation (encoding for ribosomal protein S12, a subunit of the 30S ribosome), leads to increased

translational accuracy, slower overall translation and has demonstrated late growth phase protein synthesis increases in comparison to the wild type.[138] It follows causally that these changes are predicted to result in wholesale alterations in metabolism. Indeed, recent studies describe an apparent connection between vertically acquired antibiotic resistance and secondary metabolic fecundity in antibiotic producing soil organisms such as the actinomycetes. The acquisition of resistance to antibiotics in these strains results in enhanced levels of antibiotic production for both known [138-140] and previously unknown [141, 142] compounds. These data suggest that vertically selected antibiotic resistance may be a general strategy for eliciting secondary metabolism, but the scope of metabolic changes resulting from these mutations remains to be systematically described.

Herein we describe an assessment of the consequences of antibiotic resistance mutations on a comprehensive metabolome scale. Comparative analysis of metabolomic data is greatly facilitated by employing multivariate statistical analysis methods (*e.g.* principal component analysis, orthogonal projection to latent structures-discriminant analysis), which convert multidimensional microbial extract UPLC-MS data into lower-dimensional plots of maximally distinguishing eigenvectors.[143] Critical loadings evaluation [144] efficiently validates the observed changes and identifies subsets of metabolites that are unique or shared within the data sets of a given antibiotic-resistant mutant and its progenitor strain. With these tools, we endeavor to describe and discriminate how antibiotic induced mutations affect global metabolite pools and

how PCA-based comparative analysis can identify secondary metabolite derepression in an unbiased fashion. Using a genomically characterized soil actinomycete of the Nocardiopsis genus as an example, we demonstrate the degree of metabolomic speciation afforded by antibiotic resistance mutations in the RNA polymerase β-subunit and the ribosome. Additionally, this analysis facilitates the rapid identification of upregulated secondary metabolites. Isolations of several upregulated features, followed by structure elucidation by 2D-NMR and isotopic incorporation experiments, reveal a new polyketide carbon framework that may be correlated to a formerly unexpressed type-II polyketide gene cluster present in the producing strain. Methods described herein will enable future studies to determine if this derepression is an adaptive or coincidental trait, in the context of the evolutionary benefits of antibiotic resistance.

3.2   Materials and Methods

3.2.1 General Experimental

All reagents were purchased from Sigma/Aldrich Inc. Strains and primers used are listed in APPENDIX 2. NMR analyses were performed using a Bruker 600 MHz instrument equipped with 5mm Z-gradient TCI Cryo-probe. All strains were maintained on GYM agar (0.4% glucose, 0.4% yeast extract, 1% malt extract, 0.1% peptone NZ amine, 0.2% NaCl, 2% agar) containing 50 ug/ml apramycin. Seed cultures were generated by transferring a loop full of inoculum

into GYM broth and incubating for 7 days at 30°C. Fermentation cultures of strains were performed for 7 days at 30°C in R4 medium (1% glucose, 0.1% yeast extract, 0.01% casamino acids, 0.3% proline, 1% $MgCl_2 \cdot 6H_2O$, 0.4% $CaCl_2 \cdot 2H_2O$, 0.02% K_2SO_4, 0.56 TES, 0.2% (v/v) trace elements.

3.2.2 Preparation of Antibiotic Resistant Mutants

Spore suspensions of *Nocardiopsis sp. FU40 ΔApoS8* were inoculated onto GYM agar plates containing 50 ug/ml apramycin,400 ug/ml streptomycin and 50 ug/ml apramycin, 100 ug/ml rifampicin.. Agar plates were incubated for 10 – 14 days at 30 °C to select for antibiotic resistant colonies. Individual streptomycin and rifampicin resistant colonies were selected and inoculated onto GYM agar containing the appropriate antibiotic for validation of resistance phenotype and to prepare of glycerol stock solution for cryopreservation.

3.2.3 General Extraction Procedure and Analysis

Polystyrene solid phase extraction resin (HP-20, Diaion Inc) was added to 500 mL seven day fermentation cultures. Cells and resin were separated from the broth by centrifugation and extracted sequentially 250 mL with methanol and acetone. Combined extracts were dried *in vacuo* and analyzed by HPLC-IM-MS using a SYNAPT G2 HDMS (Waters, Milford, MA) as described in Appendix II.

3.2.4 Mass Spectrometry based Feature Identification

Features prioritized using the methods described herein were subjected to putative identification using both accurate mass (<10ppm) and fragmentation spectra (accurate mass < 20ppm). Liquid chromatography and ion mobility retention times were used to isolate features in separations space. This provided enhanced subtraction of concomitant peaks present in the analyzed fragmentation spectra. These spectra were then subjected to manual interpretation to determine the type of parent ion (*e.g.* protonated, sodiated, in-source fragment, etc.). In source fragmentation can be determined by determining if the ion in question occurs at multiple drift times. After determination of ion type, and isolation of fragmentation spectra, accurate mass was used for database searching from multiple sources. Databases queried include KEGG, Metlin, ChemSpider, PubChem, Human Metabolome Database, Dictionary of Natural Products, and MetaCyc. These databases were searched with a mass tolerance of 0.01Da. If the accurate mass deviated by more than 20ppm, the compound was excluded from further investigation from the database. Fragmentation spectra were subjected to both manual interpretation, and MetFrag evaluation, an *in silico* interpreter. High energy peak lists were imported into MetFrag using centroided data with an intensity cutoff of ~1%. To utilize MetFrag with the Dictionary of Natural Products and MetaCyc, .sdf files were prepared with all matching compounds within a tolerance of 0.01Da and scored accordingly. Congruency between retention time and ClogP was also considered when assigning identifications.

3.2.5 Mutaxanthene Purification

Crude extract, generated as above, was dissolved in water, acidified to pH 3 with trifluoroacetic acid and extracted with chloroform. The chloroform fraction was dried *in vacuo*, resuspended in methanol, and applied on a Sephadex LH20 size exclusion column (100 cm). The LH20 fraction containing mutaxanthenes was purified by RP-HPLC using a linear gradient of water/acetonitrile containing 0.1% trifluoroacetic acid.

3.2.6 Isotopic Incorporation Experiment

Modified media R4 was used to optimize compound production with variable pH (6, 7.2 or 8.2), glucose concentration (1% or 2%) and $MgCl_2 \cdot 6H_2O$ concentration (1% or 2%). Fermentation cultures were extracted following method described above and analyzed with HPLC/MS for the most improved production. A seed culture of R4 mutant was inoculated into 500 ml Erlenmeyer flask containing modified mediumR4 with pH 6 and incubated at 30°C in rotary shaker. After 36h the pulse feeding of $[1, 2-^{13}C]$sodium acetate was started and continued for a total of four 1 ml feedings and 0.5 g of labeled sodium acetate in 12h intervals. Culture was then incubated for another 72 h. Extraction and compound purification methods were as described above (General extraction procedure and analysis), yielding 7 mg of pure compound.

3.2.7 Data Processing and Multivariate Statistical Analysis

Data were centroided post-acquisition. Peaks were deisotoped, peak picked, and normalized using MarkerLynx data processing software (Waters, Milford, MA). Peak detection was performed on low energy data across the mass range of 100-2000 Da with retention times between 0.0 and 20.0 min, peak widths automatically detected, an intensity threshold of 2000, mass window of 0.08, retention time window of 0.60, noise elimination of 4.00. Multivariate statistical analyses were performed using Umetrics extended statistics software EZinfo version 2.0.0.0. (Umetrics AB, Umeå, Sweden). All data were pareto scaled.

3.3   Results and Discussion

3.3.1 Generation of a Cohort of Antibiotic-Resistance Mutants.

Nocardiopsis sp. FU40 ΔApoS8 was selected as a case study as it has been sequenced to high coverage, contains at least 19 identified secondary metabolic gene clusters, including several putative polyketides, and because the only secondary metabolite family identified from this organism to date are the pro-apoptotic macrolide polyketide apoptolidins A – H.[145] We have previously disabled the biosynthetic genes for the production of apoptolidins via gene replacement of the terminal polyketide synthase *ApoS8* with an apramycin resistance cassette, yielding a clean background for secondary metabolite analysis.[146] Antibiotic resistant mutants of this strain, *Nocardiopsis sp. FU40*

ΔApoS8, were generated by dilution plating of spore preparations on antibiotic containing media followed by selection of several rifampicin (R1 – R5) or streptomycin (S1 – S6) resistant colonies with and without obvious morphological phenotypic differences.

Resistant and progenitor strains were then grown in an antibiotic free vegetative medium and in production cultures from which total culture metabolite extracts were generated. Solid phase extraction of combined broth and mycelium with Diaion HP-20 resin followed by extraction of mycelium and resin with increasingly nonpolar solvents captured a wide subset of moderate to highly hydrophobic excreted and cell-associated components. Genetic analyses of *rpoB* and ribosomal mutations were performed by PCR amplification and re-sequencing of the corresponding genes (summarized in **Table A3.1(B)**). Sequencing of *rpoB* in resistant colonies demonstrated that all genes possessed a single G↔A transition at position 3280, a mutation not previously reported in antibiotic resistant *Streptomyces*.[139] Similarly, among streptomycin resistant clones, a handful of new resistance mutations were observed in S3,4,6 whereas in S1,2,5 no mutations were present in the amplified *rpsL* gene, suggesting that resistance to streptomycin in Nocardiopsis may occur outside of previously reported regions.

3.3.2 Analysis of Changes in Extracted Metabolomes in Antibiotic Resistant Mutants

The challenges to identifying mutation-induced changes in metabolism include detection/identification of discrete metabolites and ascertaining changes in generated metabolomes. We utilized unsupervised PCA of UPLC-IM-MS data followed by loadings-plot evaluation, reasoning that linking metabolomics changes to a biological phenomenon would be facilitated by identifying metabolic species that are unique and/or shared to mutational phenotype. UPLC-MS data were peak deconvoluted and deisotoped to provide discrete features corresponding to a specific retention time and *m/z* pair. These data were normalized to total ion count, and each feature was used as a dimension for subsequent PCA. This results in relatively smaller changes being attenuated less than large-fold changes. [147] Data compression occurs through the determination of the highest eigenvalue eigenvectors of the covariance matrix. The largest eigenvalue eigenvector is considered the principal component and describes the greatest variation in the data, with each subsequent eigenvector being orthogonal and describing progressively less variation. This provides sample grouping and separation based on patterns in the most significant detected features.
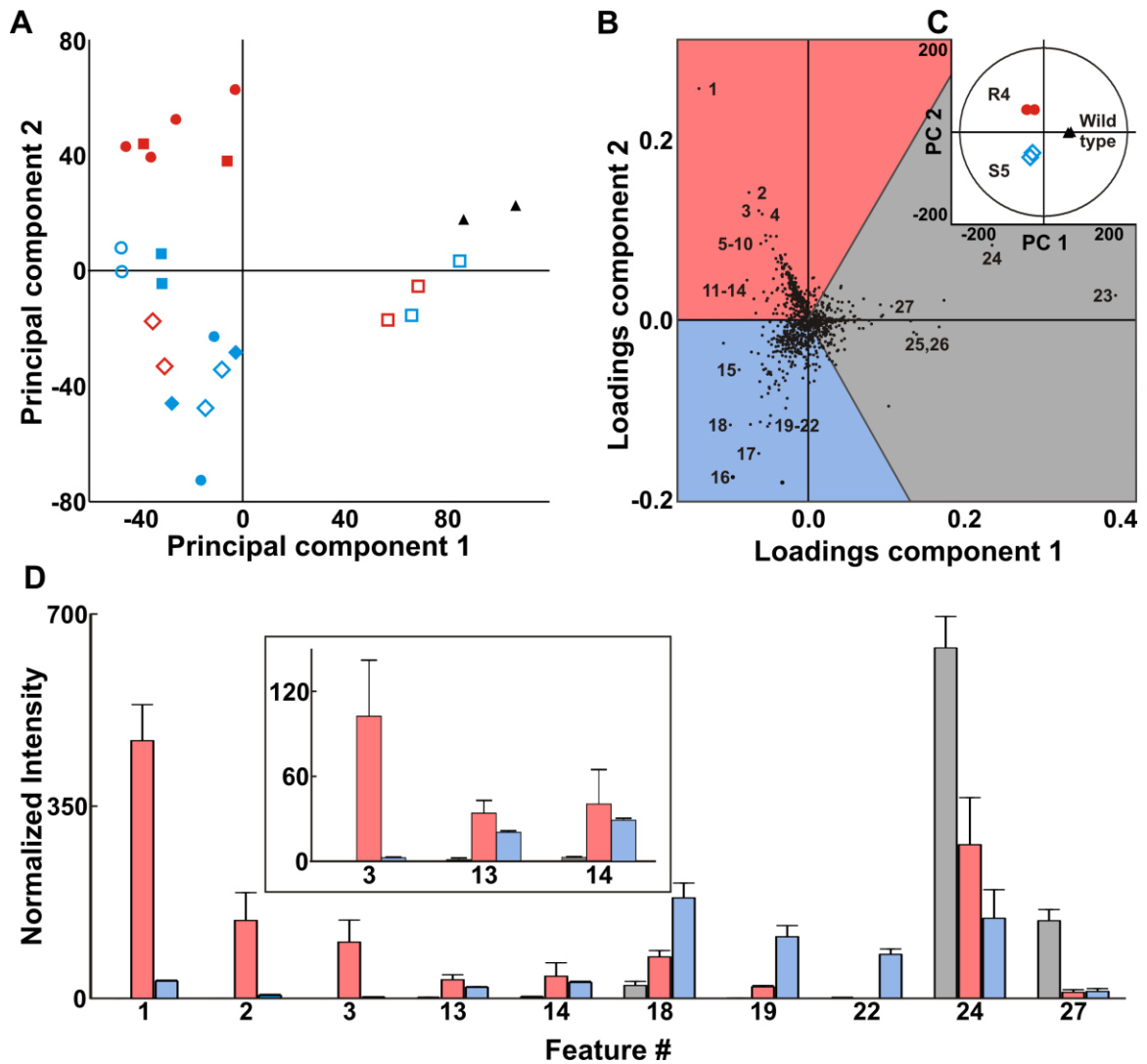
Figure 3.1. (A) Global PCA of five induced rifampicin (R1 – R5, red) and six streptomycin (S1 – S6, blue) mutants compared to the wild type *Nocardiopsis sp. FU40 ΔApoS8* (black). Technical replicates are represented with the same symbols. (B) A loadings plot indicating features which contribute to group separation for a comparison of select mutants. Features upregulated in R4, for example, fall in the center of the red shaded region, while the features that fall near region boundaries are shared. Labeled metabolites correspond to **Table 3.1**. (C) The inset PCA scores plot demonstrates mutant separations and indicates sample specificity of feature loadings. (D) Bar graph depicting normalized intensity of features as labeled in loadings plot for select rifampicin induced mutant (red), streptomycin induced mutant (blue), and wild type (black). Error bars include 1 standard deviation.

As shown in **Figure 3.1(A)**, PCA effectively clusters technical replicates of UPLC-MS analyzed metabolomes from various antibiotic-resistance mutants selected by streptomycin and rifampicin plating. Each data point represents 1065 feature/intensities, generated by UPLC-IM-MS and peak identification using MarkerLynx (Waters, Milford, MA). Plotting selected mutants in this manner reveals, without manual analysis of chromatograms or other visual phenotypic bias, which members are the most metabolically distinct from the progenitor strain. Interestingly, there is a marked metabolomic differentiation between antibiotic resistant clones selected using the same antibiotic. In the case of rifampicin induced mutations for example, which possess identical mutations in *rpoB,* these data suggest that additional mutations are responsible for transcriptional variation. This likelihood is in accordance with observations from compensatory mutations found in streptomycin and rifampicin resistant organisms [148, 149], which have been demonstrated to reverse the fitness costs of ribosomal and polymerase mutations. The PCA plots also demonstrate that different antibiotic induced mutations inducing transcriptional or translational variation can result in apparently similar global changes in metabolism.

3.3.3 Analysis of Metabolic Features

Interpretation of the significance of groupings determined via PCA require that the individual variance components be identified and, if possible, validated. Correspondingly, we endeavored to identify strain-specific metabolic features to develop an understanding of the lasting metabolic perturbations resulting from

the acquisition of antibiotic resistance. Aiding in these identifications, the addition of ion mobility [150] provided sufficient analyte separation to acquire untargeted fragmentation data of all detected species. Using both chromatography and mobility dimensions, high energy fragmentation data for analytes of interest were extracted by correlating both retention and drift times of product ions to precursors. This depletion of coeluting species and chemical noise increases the confidence of identification. In-source fragmentation can be discerned from retention and drift time correlations.

Loadings analysis is a tool used for identifying the contribution of individual peaks to the PCA dispersion. The cosine of the angle between a component and a feature describes the weight of that particular feature for that component. For example, **Figure 3.1(B)** shows three-way loadings analysis for selected strains shown in **Figure 3.1(C)**. To interpret these plots, the features in **Figure 3.1(B)** aligned along the vector of the strains in the inset PCA plot in **Figure 3.1(C)** represent those species that contribute most to the dispersion in the PCA analysis. Features with greater magnitudes describe more group variation, through both uniqueness and intensity in the UPLC-MS. The three-way loadings analysis is useful for illuminating clone-specific biosynthesis shared amongst cohorts. An analogous pairwise comparison (**Figure A3.2**) of a mutant to its progenitor stain is also useful for identifying new features in a single mutant.[144] **Figure 3.1(D)** demonstrates how loadings analysis successfully identifies and deconvolutes clone-specific metabolites from UPLC-IM-MS data without manual chromatrogram analysis. **Table 3.1** summizes a selection of the

most abundant metabolites unique to R4, S5 and the progenitor strains, respectively. A complete list of the 280 mutation upregulated metabolites in this pair, along with extracted ion chromatograms and MS/MS analyses, is found in APPENDIX 3 (**Figures A3.37-99**).

Table 3. 1. Putative identities of metabolites identified for strains

ID	m/z*	Mass error**	Putative Identification***
1	443.101	8.35	Mutaxanthene A
2	457.115	4.38	Mutaxanthene C
3	429.085	7.92	Mutaxanthene B
4	454.085	-6.61	Mutaxanthene A [2M+H+Na]$^{+2}$
5	465.081	4.30	Mutaxanthene A [M+Na]$^{+1}$
6	462.071	-8.66	Mutaxanthene A [2M+H+K]$^{+2}$
7	683.120	0.00	Mutaxanthene A [3M+H+K]$^{+2}$
8	360.217	0.00	$C_{21}H_{29}O_4N_1$
9	387.324	5.16	$C_{21}H_{42}O_4N_2$
10	296.222	-	No match in DNP, KEGG, METLIN
11	261.144	-3.82	Glu-Leu/Ile
12	297.169	-3.37	$C_{16}H_{24}O_5$
13	298.097	0.00	5'-deoxy-5'-(methylthio)adenosine
14	143.084	13.98	Ectoine
15	162.094	18.51	Salsolinol Variant (Water loss)
16	191.158	20.9	$C_{12}H_{18}N_2$
17	1161.159	-	5796.72 MW Peptide/Protein
18	230.113	-4.35	N-(5-Iminoprolyl)threonine
19	515.275	0.00	$C_{28}H_{38}N_2O_7$
20	384.217	0.00	$C_5H_9NO_3$ loss of 19
21	203.180	4.92	1,4(15),5,10(14)-germacratetraene
22	205.195	0.00	1(10),4(15),5-germacratriene
23	415.358	2.41	$C_{28}H_{46}O_2$
24	401.340	-4.98	$C_{27}H_{44}O_2$
25	399.324	-	[M+2H]$^{+2}$
26	407.314	-	[M+2H]$^{+2}$
27	443.388	-2.26	$C_{30}H_{50}O_2$

* Measured mass

** Mass error represents ppm deviation from the theoretical mass of the putative identification

***[M+H]$^+$ species are presented unless otherwise indicated

B

	WT	R1	R2	R3	R4	R5	S1	S2	S3	S4	S5
R1	53										
R2	82	157									
R3	100	166	132								
R4	99	151	173	85							
R5	90	129	203	118	172						
S1	56	134	331	226	236	251					
S2	99	146	221	120	158	168	166				
S3	103	152	215	110	177	152	154	122			
S4	65	142	286	177	213	146	130	179	195		
S5	57	111	94	159	181	143	118	143	183	44	
S6	81	115	237	145	164	77	118	103	150	45	91

A

R4: 164 — Wild Type: 56 — R4 ∩ Wild Type: 1 — center (R4 ∩ WT ∩ S5): 641 — R4 ∩ S5: 36 — Wild Type ∩ S5: 15 — S5: 80

C

	S5	S4	S3	S2	S1	R5	R4	R3	R2	R1	WT	
											188	R1
										302	366	R2
									83	77	141	R3
								110	112	213	281	R4
							165	172	180	208	244	R5
						160	157	178	151	104	184	S1
					270	124	133	145	174	208	301	S2
				162	313	104	157	151	168	252	311	S3
			101	75	85	89	79	82	94	77	103	S4
		86	171	143	234	98	175	211	192	169	236	S5
	135	121	154	170	228	76	161	174	170	187	247	S6

Figure 3.2. *Feature production comparison for mutants and wild type as generated through binary comparisons using OPLS-DA.* (A) A standard Venn-diagram depicting the number of unique and shared features for select mutants and wild type via the 3-way comparison. (B) Comparison of unique features specific to bottom-row organism when compared to left-column organism. (C) Features unique to right-column organism when compared to bottom-row organism. Values from tables in (B) and (C) were generated via pairwise comparison and hence cannot be compared to those of the tripartite comparison in (A).

Figure 3.2(A) depicts a summary of the global effects of acquiring antibiotic resistance on the metabolomes for R4, S5 mutants and WT via the tripartite analysis of **Figure 3.2(B)**. These values were obtained by permuting the three groups in binary comparisons using orthogonal projections to latent structures-discriminate analysis, a supervised multivariate statistical method that defines the first component (abscissa) as the eigenvector describing the greatest inter-group variation, with the second component (ordinate) defined as the

eigenvector describing the greatest intra-group separation.[151] A large portion of the features are present in all groups. In addition to new metabolites specific to a clonal metabolome, this also includes unmetabolized media components and other sample background peaks. Of the 993 total features identified as exclusive to S5 and R4 mutants, and the wild type *Nocardiopsis sp. FU40 ΔApoS8*, 56 features are exclusively expressed in the wild type *Nocardiopsis sp. FU40 ΔApoS8,* 641 are shared between the wild type and at least one mutant, and 280 of all features are produced as a result of *rpoB* or *rpsL* mutation. The resulting model was used to generate a plot of loadings contribution vs. correlation value. To generate group specific features, a correlation threshold of ≥ 0.9 was applied.

Half-matrix representations of these comparisons are displayed in **Figure 3.2(B)** and **Figure 3.2(C)**. **Figure 3.2(B)** can be interpreted as the number of unique features specific to the metabolomic extract of the organism indicated on the bottom row when compared specifically to the organism on the left column. Conversely, the half-matrix in **Figure 3.2(C)** represents the number of unique features specific to the organisms indicated on the right column, when compared specifically to the organisms on the bottom row. For perspective, a similar comparison of *Escherichia coli*, *Micrococcus luteus*, and *Bacillus subtilis* yield feature differences on the order of as little as 13 specific features, and a maximum of 166 unique features, when compared in a binary fashion (**Figure A3.1**). This suggests that the metabolic phenotypes of the mutant organisms are on the scale of inter-phylogenic differences. Of note, the biosynthesis of new features not detected, or at low levels, in the progenitor strain is often found to be

increased in multiple distinct mutants. The number of new features found in the resistant mutants range from 100 to over 300 (237 on average) in comparison to the nonresistant Nocardopsis progenitor, whereas the number of features unique to the progenitor strain in comparison to the mutants average 80. For example, an increase in feature 14, putatively identified as ectoine, is observed in multiple antibiotic resistance mutants. Likewise, features 11-15, in addition to many others, are shared by mutant groups. This includes the upregulation of the putatively identified quorum-sensing molecule (feature 13), dipeptides (feature 11) and features with no known match (feature 10, for example). Interestingly, lipid-like features in the progenitor Nocardopsis (*e.g.* 23, 24, and 27) appear attenuated in all antibiotic resistant strains. Together, these trends and specific analyses are consistent with generalized gene derepression as a consequence of mutations in the *rpsL* and *rpoB* genes. Normalized heat maps of features described as unique in **Figure 3.2(A-C)** are found in APPENDIX 2, **Tables A3.10-23).**
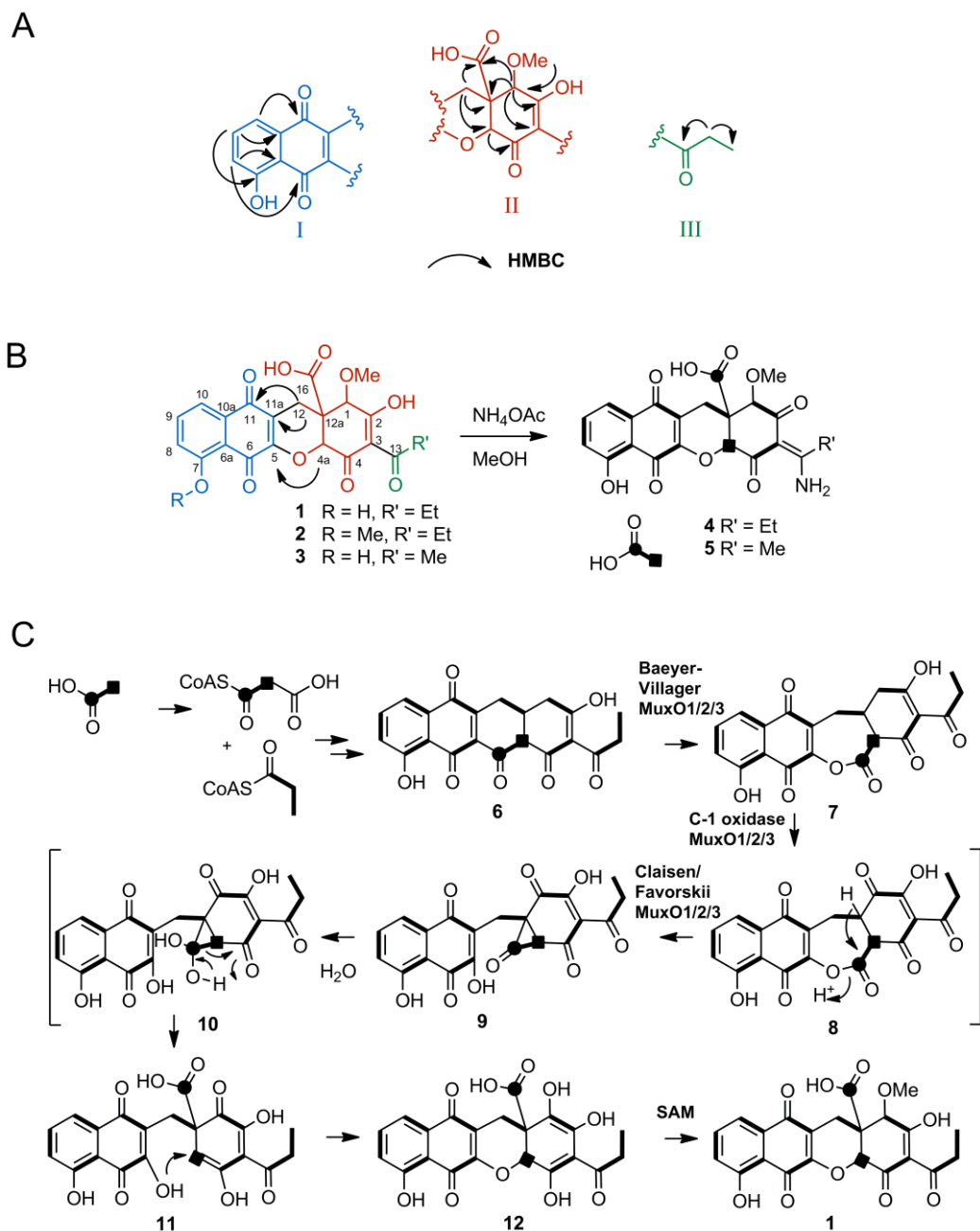
Figure 3.3. (A) Major substructures I – III were inferred from COSY, HSQC, HMBC, and ADEQUATE experiments. (B) Substructures were putatively linked via HMBC and ADEQUATE correlations. The xanthene frame work was confirmed by ^{13}C J-coupling measurements in the amino congeners of mutaxathenes (D 4, E 5), generated serendipitously by treatment with ammonium acetate, which were sharper than the A – C and afforded confirmation of the complete carbon framework of mutaxathenes. (C) Proposed biosynthesis of mutaxanthenes.

3.3.4 Isolation and Identification of Selected Secondary Metabolic Features

Many of the metabolic features corresponding to upregulated species in antibiotic resistant mutants (207 of ca. 650) possess high molecular weights (>400 Da), and are found to be upregulated in more than one mutant. To investigate whether these species correspond to secondary metabolites we isolated a subset of the most abundant features in rifampicin resistant mutant R4.

Feature 1 (**Figure 3.1(B)**, **Table 3.1**) was isolated with UV spectrum showing absorption maxima at 225, 252, 279 and 409 nm. The high resolution mass spectrum yields an apparent m/z of 443.101 $[M+H]^+$ and, along with a UV and NMR data, yields a chemical formula of $C_{22}H_{18}O_{10}$ that does not correlate with known entries in the aforementioned chemical databases. Challenges to structural elucidation of feature 1 include the large number of quaternary carbons, a high degree of unsaturation, and rapid dynamic chemical exchange properties of several resonances over the timescale of the NMR experiments. Briefly, three partial structures (**I** - **III**, **Figure 3.3(A)**) were proposed on the basis COSY, HSQC, HMBC and ADEQUATE NMR correlations. HMBC correlations from C14 methylene protons to C3 quaternary carbon determine the relationship of fragment **II** with fragment **III** and crucial HMBC and 1,1-ADEQUATE correlations from protons H12 to carbon C11a and from proton C4a to carbon C5 determine the connectivity between fragments **I** and **II** and permit the closure of the last ring, which revealed that the compound contains an unusual xanthene scaffold (Fig. 17B). This compound, which we named mutaxanthene A **1,** contained two minor variants, mutaxanthenes B **2** and C **3**, which correlate to

features 2 and 3 from the loadings analysis in **Figure 3.1(B)**. The remaining 4 most abundant features in this plot correspond to adducts of the mutaxanthenes. As less abundant features, they further validate the utility of loadings analysis in comparing metabolomic perturbations in antibiotic resistant mutants.

A notable property of mutaxanthenes A – C, is their ready conversion in pH ~ 6.6 ammonium acetate buffer into mutaxanthenes D (**4**) and E (**5**), which are tautomeric eneamine congeners of their parent compounds (Fig 17B). Notably, substantial line broadening of ^{13}C resonances of C1, C2 and C4 in mutaxanthenes A – C, ostensibly due to dynamic chemical exchange of the enol tautomers, appear as sharp singlets in D and E (**Figure A3.35**). This line width improvement in the amino congeners permits J-coupling values to be obtained for these atoms from 1,2-^{13}C sodium acetate incorporation experiments (**Figure A3.36**). Correspondingly, the structures of mutaxthenes A – E are supported by these incorporation experiments, which confirm the substructures and correct assembly of the xanthene scaffold and support the likely type II polyketide synthase origins of this family of compounds. A detailed description of NMR studies can be found in **Appendix 3**.

3.3.5 Analysis of Biosynthetic Gene Cluster and Proposed Biosynthetic Pathway

The 12,12a-dihydro-1H-benzo[b]xanth-ene-based carbon framework of the mutaxathenes has, to our knowledge, never before been reported in polyketide natural products. This unusual scaffold requires multiple skeletal rearrangements of an unreduced decaketide precursor. While the process for

generating the xanthene scaffold remains highly speculative, we can propose a pathway (**Figure 3.3(C)**) consistent with the following features: (a) acetate incorporation reveals that the two carbons at positions C-16 and C4a are uncoupled, suggesting that these carbons were once an intact acetate unit in the decaketide chain; (b) the ether and carboxylate moieties together with the position of the uncoupled acetate-derived carbons formally imply oxidative cleavage, but not cleavage between the aforementioned acetate unit; (c) the position of the acetate derived carboxylate in the middle of the polyketide chain suggests an additional carbon skeletal rearrangement involving a ring contraction. In the proposed pathway, the intermediate precursor **6** is common to several polyketide families including polyketomycin [152], and mithramycin [153]. The first oxidative cleavage resulting in **7** is a regiochemical variant of the Baeyer-Villiger oxidation found in mithramycin biosynthesis [154]. The ring contraction rearrangement may occur in analogy to the Favorskii-like reaction proven in the biosynthesis of the enterocins [155] and implied in okadaic acids [156], in which an oxidative carbonylation sequence via **8** precedes the formation of a cylopropanone intermediate **9,** which upon hydration may rearrange to the internally situated carboxylate **11**. An intramolecular Michael addition may be proposed to complete the xanthene framework. The previously reported genome sequence of *Nocardiopsis sp. FU 40 ΔApoS8* contains one typical type II polyketide gene cluster. Analysis of this gene cluster (**Table A3.7**) reveals hypothetical polyketide synthase proteins consistent with the generation of the common precursor **6** and genes encoding translated sequence similarity to flavin-

dependent oxidases (*Mtx O1, O2 O3*) consistent with the proposed oxidative rearrangement biotransformations. Future studies will define the relationship of these oxidases to the skeletal rearrangements implied in the proposed biosynthesis mutaxanthenes A -C.

3.4   Conclusions and Perspectives

We are broadly interested in detecting and identifying metabolome-scale changes in microorganisms and understanding their roles in cellular processes. As the end-product of the central dogma, metabolites and their dynamics may be used to complete our understanding of the molecular basis for biological phenomenon such as cell signaling, antibiotic resistance, pathogenicity, and metabolic fitness. The subject of this work, antibiotic resistance-induced changes in the transcriptional and translational apparatus of bacteria, has multiple aspects of interest. Investigating metabolome scale changes resulting from these adaptations may provide insight into these widespread modes of vertically acquired bacterial resistance in the clinic. Additionally, due to the established connection between acquired resistance adaptations and secondary metabolism, unbiased analytical methods to assess new features engendered by resistance can potentially accelerate natural product discovery.

To address these subjects, we describe here metabolome scale changes from resistance mutations in a secondary metabolite producing nonpathogenic soil organism. Notably, similarly drastic regulatory adaptations, engendered by

mutations in the S12 ribosomal subunit and *rpoB* polymerase, are stably maintained in some, but not all clinically resistance strains (e.g. *Mycobacterium tuberculosis, Streptococcus pyogenes, Staphylococcus aureus, Neisseria gonorrhoeae*). [157-159] However, despite the importance of antibiotic-selected mutations in both pathogenic and antibiotic-producing microorganisms, the downstream effects of a modified transcriptome and/or proteome on global metabolism have not been broadly investigated in a systematic manner. Here we quantify the metabolic feature differences in stationary phase between cohorts of mutants revealing the scope of changes in metabolomic phenotype. Notably, the number of new features found in resistant mutants is, on average, three-fold greater than the number of features identified as unique to wild-type using the same comparison. Together with the results that these new features number in the hundreds and that the majority of the new features are not found in the progenitor Nocardiopsis are shared throughout the diverse mutant cohort, suggest that one means by which S12/*rpoB* mutations affect survival may be by a strategy of general derepression of biosynthetic processes.

In the case of secondary metabolite producing actinomycetes, antibiotic induced S12 ribosomal subunit and *rpoB* polymerase mutants have been demonstrated to modulate the production of specific secondary metabolites resulting in increased production of poorly expressed or 'silent' gene clusters. [135, 138] However, it is not known if secondary metabolite production is simply a symptom of broader transcriptional and translational derepression, or a specific adaptive response to antibiotic challenge. The results described here measure

metabolomic changes in bacteria in the contexts of the phenomenon of vertically acquired antibiotic resistance and secondary metabolism. The observation that a large fraction of accumulated metabolites are of high molecular weight, are not identifiable in primary metabolism databases, and are demonstrated to be secondary metabolites, corroborates the hypothesis that generalized secondary metabolic derepression may be an important byproduct of antibiotic resistance to transcription/translation targeting antibiotics. It is conceivable that metabolic plasticity may be an evolutionary 'save all ships' response to antibiotic challenge. However, whether or not general metabolic derepression is an adaptive or coincident trait is unknown at this time. Future studies linking the quantification of identified accumulated metabolites to gene transcription and translation quantification data will define the relationship between primary and secondary metabolism, derepression, survival, and the mechanism of resistance in microorganisms.

3.5 Supporting Information

Supporting information, including metabolic heat maps, extracted ion chromatograms, fragmentation spectra, and all NMR spectra, can be found in APPENDIX 3.

DEVELOPMENT OF A SELF-ORGANIZED MAP DRIVEN WORKFLOW FOR METABOLOMIC DATA PROCESSING AND INTERROGATION

4.1   Introduction

Currently, we seek to enhance the interpretation of metabolomics data through the application of self-organizing maps to provide an additional dimension of data analysis: feature intensity profile correlation. The generation of these "metabolic profiles" allows for Gestalt comparison of samples, providing a global snapshot of metabolite production.

Metabolomics endeavors to interrogate the global metabolite profile of a particular biological system of interest, with the intent of gaining insight into the system phenotype or endotype, or how the system is interacting with the surrounding environment.[160] In metabolomics studies, the complexity of metabolic profiles is often distilled to a fundamental comparison of small molecule inventories derived from differing physiological states of interest at a single time point (*e.g.* "normal" vs. "diseased"). Up- and downregulated metabolites are then used to infer metabolic perturbations. Multivariate statistical methods are used frequently to distill the large dimensional datasets which commonly result from mass spectrometry based metabolomics experiments into

relevant features (*i.e.,* up- and downregulated metabolites),[161] with a feature defined as any detected molecular species, metabolite or other.[162] The wide-spread application of principal component analysis (PCA) to metabolomic studies has provided a means of visualizing sample groupings, and determining significant metabolite contributions through loadings plot interpretation. Other metabolomic based workflows utilize a univariate statistical approach and consider fold change differences in features.[163] Unfortunately, the interrelated nature of the metabolic fluctuations and underlying feature patterns through biological variation are often ignored in conventional feature prioritization workflows.

We have implemented a self-organizing map algorithm to visualize metabolic phenotype and feature patterns that is complimentary to traditional metabolomics approaches. Gene Expression Dynamics Investigator (GEDI) utilizes an algorithm intended for the organization of genes based upon underlying patterns in static or dynamic expression profiles using a self-organizing map based approach.[164] This has been applied to the visualization of metabolic profiles in a handful of studies, but never as a metabolite prioritization method.[165, 166] In this study, self-organizing maps group discrete features, which are defined by both retention time and mass-to-charge ratio, based upon similarities in signal intensity profiles across biological sample sets. In-other-words, features that change in similar trends across sample sets are grouped, whereas those that change differently group into separate neighborhoods, in an iterative fashion. As a result, metabolites cluster based upon underlying trends in

the biological samples. These maps may then be averaged across experimental groups and compared to provide a heat map of up-regulated and down-regulated metabolites as a function of experimental group. This added dimension of feature-feature correlation provides valuable insight into recognizing experimental subpopulations and relevant biomolecules, as well as allowing for the removal of biologically insignificant background features.

We have termed this workflow, which consists of studying MS based metabolic profiles using self-organizing maps, Metabolic Expression Dynamics Investigator (MEDI). Though we apply this method to static samples, this method is also well-suited for comparison of temporal dynamic samples, as the name implies. For the purpose of this work, however, we endeavor to describe this method on temporally pooled samples. Specifically, the MEDI workflow begins with data acquisition and ends with the identification of biologically significant up- and down-regulated mass spectrometry signals. To the authors' knowledge, no instructive tutorial on the use of self-organizing map algorithms for analyzing metabolomics based data exists. This manuscript describes the MEDI workflow method in detail, and subsequently applies MEDI to determine the metabolic effects of long term cocaine exposure upon rat populations. Currently, we display the application of self-organizing maps to a mass spectrometry based metabolomic analysis of static sera samples from cocaine-naïve rats and behaviorally distinct cocaine-exposed rat models (behaviorally addicted and non-addicted).[167] Though these sera samples were taken two weeks after the last administration of cocaine, clear distinction between cocaine naïve and

experienced sera profiles are distinguished using MEDI. This work describes an alternative and complimentary method for metabolomic data processing and visualization.

4.2   Materials and Methods

4.2.1   Rat Cocaine Addiction Behavioral Model

Addiction models were prepared using a long-term exposure self-administration protocol.[167] Briefly, rats were conditioned to become addicted to cocaine injections administered upon the completion of a task (i.e. depression of a stimulus specific paddle). This behavior was subsequently extinguished through the replacement of cocaine injections with saline injections upon task completion. For addiction class determination, a reinstatement injection was administered to rats that contained cocaine, and the rats were again given access to cocaine injections upon task completion. Based upon the recurrence and magnitude of cocaine seeking behavior, rats were classified as addicted or recreational drug users. Two weeks following the completion of the behavioral study, rats were sacrificed and their blood used for analyses.

4.2.2   Rat Serum Sample Preparation for UPLC-IM-MS Analysis

Frozen whole blood samples from "addicted", "non-addicted" and naïve rats were thawed at 4°C, and then centrifuged at 14k rpm for two minutes. 60µL of serum was removed and metabolites isolated by precipitating the proteins with

3:1 v:v cold methanol kept on dry ice. Samples were vortexed for 10 seconds and centrifuged at 14k rpm for 10 minutes at 4°C. 150uL of supernatant was extracted and dried down in a SpeedVac, after which the samples was reconstituted in 100uL of solvent A.

4.2.3 Liquid Chromatography-Ion Mobility-Mass Spectrometry Conditions

UPLC-IMS-MS and UPLC-IMS-MS^E analyses were performed on a SYNAPT G2 HDMS (Waters, Milford, MA) mass spectrometer equipped with a nanoAcquity UPLC and autosampler (Waters, Milford, MA). Metabolites were separated on a 75 µm x 100 mm HSS C_{18} (1.7 µm particle size) column and 180 µm x 20 mm HSS C_{18} (5µm particle size) trap column. Column temperature was maintained at 45°C to minimize chromatographic drift, and the auto-injector sample tray held at 4°C to minimize sample degradation. A double-loop injection volume of 10 µL was injected in a 5 µL loop. Chromatographic separations were performed by using a 20 min method at a flow rate of 450 nL/min using a gradient mixer of 0.1% formic acid in H_2O (mobile phase A) and 0.1% formic acid in ACN (mobile phase B). Briefly, a 3 min wash period at a flow rate of 15 µL/min, during which the eluent was diverted to waste prior to analytical separation. Following removal of residual salts and trapping of analytes on the trap column, flow was redirected to flow through the analytical column with an initial 99% mobile phase A for 0.5 min. Mobile phase B was increased to 60% over 6.5 mins and up to 99% in 4 min, and then held at 99% for 3 minutes. The column was re-equilibrated to 99% mobile phase A over 0.5 minutes and held for 5.5 min after

each run. All analytes were analyzed using positive mode nanoelectrospray ionization. Typical parameters include a capillary voltage of 3.5kV, sampling cone setting of 25.0 and extraction cone setting of 4.0, source temperature of 80°C, desolvation gas (N_2) flow of 600 L/hr, and a cone gas flow of 20 L/hr. Data were acquired in MS^E mode, which acquires both a low energy spectrum and a high energy spectrum. Collision induced dissociation (CID) was performed post mobility separation with a ramped energy profile from 20-60 V in the high CID acquisition. Traveling wave velocity was held constant at 550 m/s and a height of 40.0 V. Data was acquired at a sampling rate of 2 Hz over the mass range 50-1400 *m/z.* Sodium formate (10 µg/mL) in 90:10 propan-2-ol:water (v:v) was used to calibrate over this range with < 1 ppm mass accuracy. Leucine enkephalin in 50:50 H_2O:ACN with 0.1% formic acid (v:v) was used as a lock mass compound (accurate mass 556.2771 Da) at a flow rate of 0.6 µL/min and a concentration of 2 ng/mL every 10 seconds. Data acquisition was performed from 0 to 20 minutes of the liquid chromatography separation. Triplicate technical analysis was performed in a randomized fashion; with quality control samples analyzed every 5 injections. Quality control samples contained equal volume aliquots of each sample mixed together.

4.2.4 Data Processing and Multivariate Statistical Analysis

Data were mass corrected post-acquisition and centroided. Peaks were deisotoped and normalized using MarkerLynx data processing software (Waters, Milford, MA). Peak-picking using chromatographic profiles were also performed

using MarkerLynx. Peak detection was performed on low energy data across the mass range of 50-2000 Da with retention times between 1-20 min with peak widths ≤ 30 seconds (no applied smoothing), intensity threshold of 1000, mass window of 0.03 Da and retention time window of 0.1 min. Data were deisotoped and areas normalized to 10,000/sample.

Multivariate statistical analyses were performed using Umetrics extended statistics software EZinfo version 2.0.0.0 (Waters, Milford, MA). Principal component analysis (PCA) and orthogonal partial least squares-discriminate analysis (OPLS-DA) were performed on all data acquired and pareto scaled.

4.2.5 GEDI Parameters

A grid of 50X51 was defined and trained using 80 first phase and 160 second phase iterations. A neighborhood radius of 4.0 was used during the first phase, and 1.0 during the second. The first phase learning factor was 0.5 and 0.05 for the second phase. The neighborhood block size applied for the first and second phases were 4 and 2, respectively. A conscience of 3.0 was used for both phases. A random seed value of 1 was used, and Euclidean distance was applied for the distance metric. A linear initialization method was applied. Samples were average across technical and biological replicates, and subtracted across experimental groups within the GEDI software. GEDI maps were exported through the software, in addition to "Gene Assignment Lists", which indicate node location of features, and "Map Centroids" which were used for the generation of intensity values for regions of interest.

4.2.6 Statistical Analysis of Regions in MEDI heat maps

The cocaine-experienced MEDI self-organized heat map (**Figure 4.4(C)** shows the summed ion signal intensities for specific regions across sample types (cocaine-naïve, cocaine-addicted and cocaine-non-addicted)). This MEDI heat map has allowed us to quantify and determine the statistical significant regions, labeled A-F, using a one-way ANOVA test among sample types. A one-way ANOVA compares the effect of cocaine use using the grouped 'neighborhoods' of signal ion intensities for non-addicted, addicted, experienced (average of non-addicted and addicted samples) and naïve rats (see **Figure 4.6**). We observed a significant effect ($p<0.01$) based on cocaine exposure for all regions, and for those regions with unequal variance between groups, a Kruskal Wallis one-way ANOVA was conducted (regions a, d, e, and f). [a: $H(3,37)=22.03$, $p<0.0001$; b: $F(3,37)=4.99$, $p=0.0052$; c: $H(3,37)=21.83$, $p<0.0001$; d: $F(3, 37)=7.24$, $p=0.0006$; e: $H(3,37)=18.9$, $p=0.0003$; f: $H(3,37)=25.6$, $p<0.0001$], indicating that *post hoc* comparisons were appropriate. *Post hoc* comparisons using a Bonferroni-Holm's test show statistical significant differences ($p≤0.01$) for all regions (A-F) when comparing cocaine experienced, addicted, non-addicted and cocaine-naïve sample types. Additionally, region F showed a statistically significantly difference ($p<0.01$) between addicted and non-addicted rat models (see F in Figure 4). Region C, however, does not show a statistically significant difference ($p=0.06$) between non-addicted and addicted sample groups, which indicates that there are 'neighborhoods' that further discriminate cocaine non-addicted and addicted models.

4.2.7 Feature Identification

Putative identifications were performed using the monoisotopic accurate mass and raw data to determine molecular ion type. Monoisotopic masses were searched against the Human Metabolome Database (HMDB)[168, 169], METLIN[170], and LIPID MAPS[171] databases for putative identifications. When possible, fragmentation data were used to support identifications, utilizing mobility separation prior to fragmentation to isolate parent ions in separations space.

4.3 Overview of the Data Analysis Approach, Metabolite Expression Dynamics Inspection (MEDI)

For mass spectrometry based metabolomic data analysis, our Metabolite Expression Dynamics Inspection (MEDI) adapts the Gene Expression Dynamics Inspector (GEDI) software. **Figure 4.1** outlines the general workflow for the analysis of metabolomics data using a self-organizing map algorithm to sort detected features in an unsupervised, data-driven manner. This workflow facilitates the identification of unique expression profiles across samples based on feature patterns detected in the metabolomic analysis. Briefly, this workflow consist of six steps: (1) initial data acquisition, (2) data preprocessing which incorporates peak detection, alignment, and normalization, (3) the use of GEDI software to generate self-organizing maps, (4) differential analysis in GEDI of sample intensity maps generated in step (3) to determine relevant feature clusters, (5) interrogation of metabolite feature assignment maps to determine

unique features/analytes of interest, and lastly (6) identification of peaks of interest. The MEDI workflow is applicable across platforms, with the exception of peak identification, which will be technique/detector dependent. The generalized MEDI workflow is now described in greater detail.

4.3.1 Data Acquisition and Preprocessing (MEDI workflow – steps 1 and 2)

The first step in the proposed workflow is the initial data acquisition. It is important to note that no one sample preparation or mass spectrometry analysis technique will give a global metabolomic view, simply based on the chemical diversity associated with metabolites. It is therefore important to plan experiments, extractions, and analysis techniques accordingly. It is beyond the scope of this article to discuss all metabolite extraction and analysis protocols, but it is important to understand the limitations of each sample preparation and analytical method. We suggest a few relevant reviews.[161, 172, 173]

After data acquisition, raw data must be described as discrete features. This involves centroiding and aligning retention time and mass spectral profiles, in addition to deisotoping data to ensure monoisotopic peak comparison. Subsequent normalization scales data to reduce the impact of technical variation. Publically available software (*e.g.,* XCMS) can be used to filter, detect and align peaks; therefore this workflow is compatible across numerous mass spectrometry platforms (*e.g.,* LC-MS/MS, LC-IM-MS/MS, GC-MS) and vendors, in addition to 1-D data (*e.g.,* direct infusion, matrix assisted laser desorption/ionization MS), assuming relative quantitation applies.[163] After initial

peak filtering, detecting, aligning, and normalization, features are exported in a tab-delimited file congruent with GEDI (found at http://www.childrenshospital.org/ research/ingber/GEDI/GEDI_InputDataFormat.pdf).   Normalized   metabolomics data is then appropriate for feature organization through the self-organizing map algorithm.
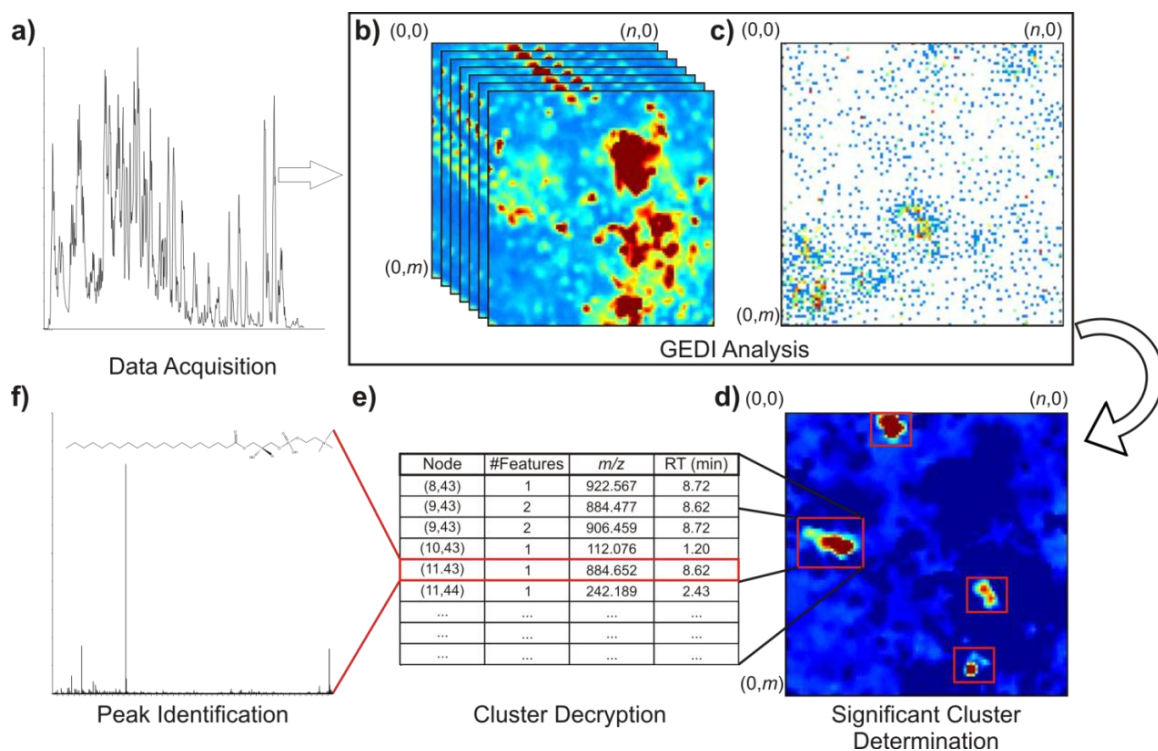
Figure 4.1. *Data processing workflow for metabolomics based analyses.* The generic process of data mining using self-organizing maps to sort data is shown. This begins with experimental data acquisition (A), and subsequent processing and formatting (not shown). Features are then used to generate heat maps for each sample, using the GEDI self-organizing map algorithm (B). The relative density of features per node can be seen in (C), with white indicating no features, blue indicating one features, scaling to red, indicating many features. Differential analyses of samples generates feature clusters of varied intensity (D). The feature assignment map is then used to determine the retention time and *m/z* identity of the features of interest (E). This prioritizes analytes for further identification (F).

4.3.2 Feature Organization and Analysis (MEDI workflow – steps 3 and 4)

In these MEDI workflow steps, a self-organizing map algorithm is used to assign detected features to a grid of user-defined dimensions. Specifically, the algorithm arranges features in an iterative manner based upon similarity in intensity profiles across samples. Initially, the grid is populated with randomly generated intensity profiles. Randomly selected features from the input data are placed in the grid location, or node, which best matches the intensity profile of that feature. This profile of this node is then adjusted to more closely resemble the profile of the matched feature. Surrounding nodes are also adjusted to more closely resemble the matched feature, but to a lesser extent. This process is then performed iteratively with a different, randomly selected input feature. Features that behave similarly across samples are assigned to a particular "neighborhood", or in nodes adjacent to like-features, as seen in the trend plots in **Figure 4.2**. The assignment of features to specific nodes is then iterated as node profiles evolve. After features are assigned to specific node coordinates, intensity maps are generated for each sample using the summed intensity for each node. These profile the metabolic phenotype for each sample (see **Figure 4.1(B))**, displaying all detected features in a heat map fashion. The relative number of features that contribute to a neighborhood is shown in the feature density map (**Figure 4.1(C))**. Subsequently, samples can be averaged and subtracted based on sample group and experimental specifics, as seen in **Figure 4.1(D)**. Differential profile maps show clusters/regions of up- or downregulated features, which are potential metabolites of interest. This specific analysis reveals regions

(red-boxed areas), which should be prioritized and compared across samples. Importantly, the feature density map indicates that many of these regions of interest are resultant of a small number of metabolites.
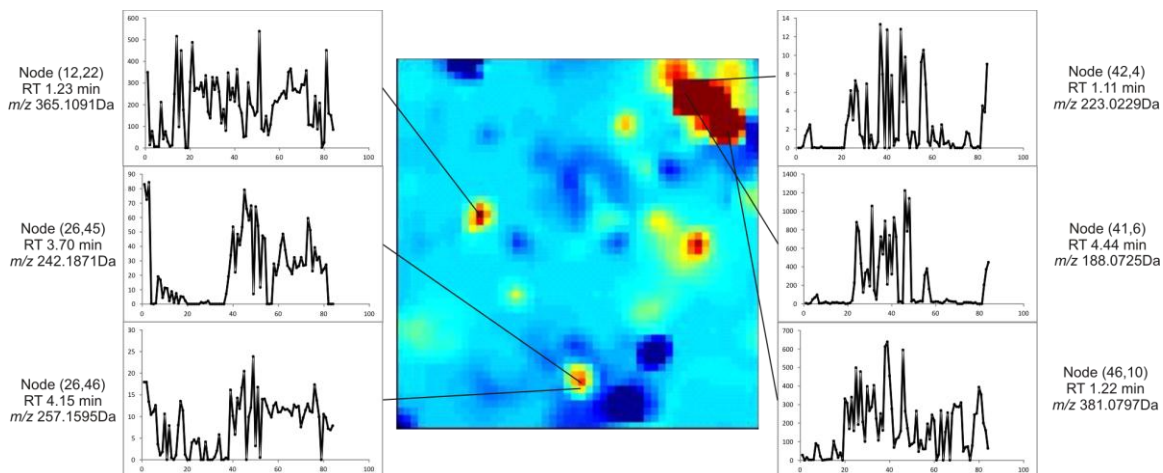
Figure 4.2. *Illustrative MEDI heat map indicating trend plots that correspond to seeded features.* Features that behave similarly across the samples or experimental conditions (81 total samples), which are depicted on the x-axis of the bracketing trend plots, are grouped into close regions. This results in the organization of features based upon similarities in relative intensity profiles.

4.3.3 Cluster Decryption (MEDI workflow step 5)

To extract which metabolomic features contribute to neighborhoods of interest, clusters must be decrypted into constituent features. Each node has a finite number of features associated **(Figure 4.1(C) and 4.1(E)**), which determine the images shown in **Figure 4.1(B) and 4.1(D)**. Multiple features can contribute to a single coordinate intensity, thus images need to be 'decrypted' by determining which features contribute to specific 'neighborhoods'. The descriptive data for a feature indicates the chemical properties of the feature and the location in the raw data.

4.3.4 Feature Identification (MEDI workflow step 6)

The final step in the proposed workflow includes the identification of significant features described in **Figure 4.1(E)**. These identifications will be platform specific, thus the tools used for analyte identification will also be platform specific. There are a number of tools available for fragmentation prediction and matching of spectra for metabolomic based studies, as well as databases (*e.g.,* Human Metabolome Database, Lipid Maps Structure Database, METLIN, Kyto Encyclopedia of Genes and Genomes).[168-171, 174, 175] The metabolites detected provide the basis for inferences on metabolic perturbations between sample groups. **Figure 4.1(F)** depicts a fragmentation spectrum used to identify a metabolite of interest. Guidelines for metabolite identification confidence have been outlined by the Metabolomics Standards Initiative.
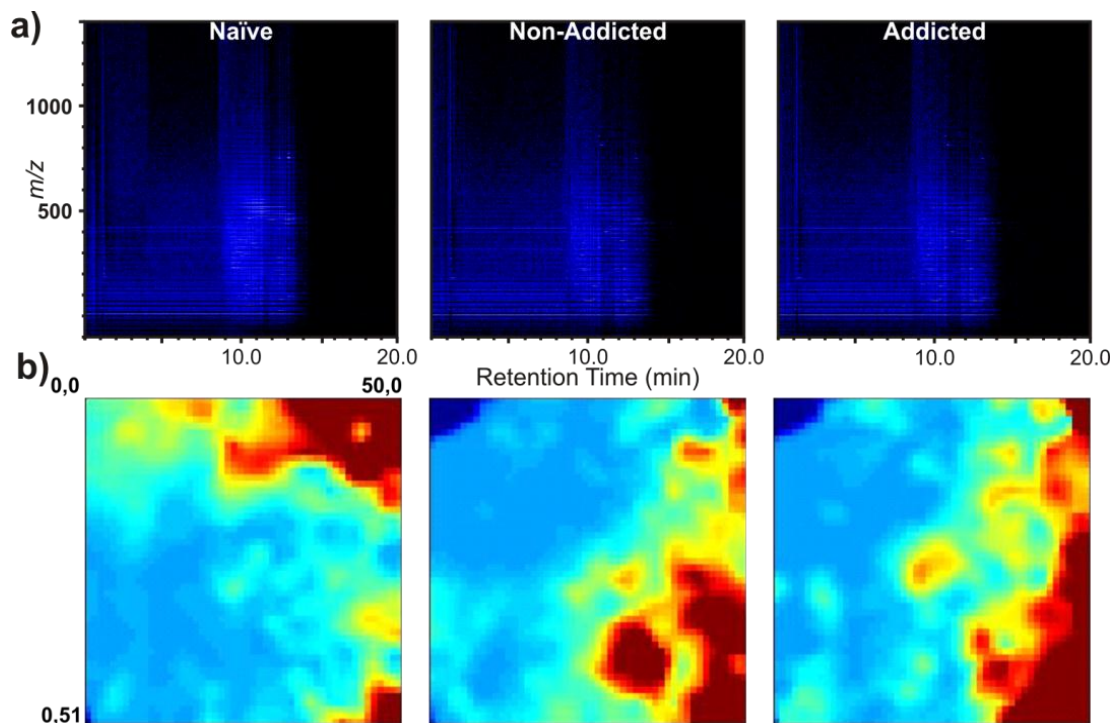
Figure 4.3. *Representative UPLC-MS and MEDI heat maps indicating relative analyte intensity.* For each of the two behavioral groups of cocaine use (addicted and non-addicted) and cocaine naïve rat sera metabolomes, corresponding heat maps for single UPLC-MS analyses (A) and average MEDI heat maps (B) are presented. Though differences may be seen in the UPLC-MS profiles, the static metabolite phenotypes displayed through self-organizing maps indicate gross differences between each group.

4.4   MEDI Analysis of Rat Sera Samples

4.4.1   Applying MEDI to Explore the Effects of Long-Term Cocaine Exposure

To display the utility of this workflow, we applied the MEDI process to liquid chromatography-mass spectral (LC-MS) sera profiles from cocaine-naïve rats and behaviorally distinct cocaine-addicted and non-addicted rats. **Figure 4.3(A)** illustrates a 2D retention time (RT) vs. mass-to-charge ratio heat maps for each sample type (cocaine-naïve, behaviorally non-addicted, and addicted rats). This is representative of raw data from selected samples from each group. In these 2D heat maps, we observed ~2266 unique features (RT – *m/z* pairs) across all samples after peak picking, alignment, and normalization using MarkerLynx software (Waters Corporation, Milford, MA). A visual investigation reveals that little, if any, information is gleaned from a casual viewing of these metabolic profiles. These same features were formatted for further analysis in the MEDI workflow.

Detected features were self-organized using the GEDI software, and average group heat maps are seen in **Figure 4.3(B)**. This function simply averages node intensities across a selected group of samples, which, in this case, is determined by behavioral class. For comparison of the generalized effects of cocaine exposure, the two behavioral classes were pooled and are classified "cocaine-experienced". These individual self-organizing heat maps clearly show distinct differences among groups. The density of metabolites for given nodes can be seen in **Figure A3.1**.

Visual inspection of the metabolite heat maps demonstrates that the sera profiles for the three groups have both shared and distinct characteristics. This displays a significant advantage to using GEDI for metabolic phenotype investigation. By virtue of the feature organization process, the groupings that result from the self-organizing algorithm are driven by hierarchical specificity. As a result, if experimental groups have significant differences, groups will emerge that concentrate these differences. Additionally, background, or ubiquitous, signals will be organized together and essentially eliminated from the analysis. Features that are specific to a particular sample will then occupy separate regions. To gain perspective on how the MEDI process compares to multivariate statistical analysis methods, we performed principal component analysis and orthogonal projection to latent structures-discriminant analysis on detected features.

4.4.2   Multivariate Statistical Analyses

The use of multivariate statistical analysis methods is a common informatics approach for metabolomics data. This enables researchers to determine significant features in complex datasets, interrogate sample grouping, investigate data acquisition reproducibility, and classify unknown samples based on example training sets. **Figure 4.4(A)** is a principal component analysis (PCA) of the three sample groups analyzed. In PCA, the intensity of each feature (considered a dimension) is used to describe a given sample. Briefly, PCA determines the largest eigenvalue eigenvector of the covariance matrix of the

data, which is principal component one. This eigenvector describes the largest differences in the samples, by definition. The second principal component is orthogonal to the first principal component and describes the next largest differences in the data. The result is sample grouping based upon similarity, and separation based upon the largest global feature differences in principal component one, and the next largest differences in principal component two. Principal components one and two are plotted in **Figure 4.4(A)** as the abscissa and ordinate, respectively. This displays the samples in maximally distinguishing 2-dimensional space, based upon feature intensity. Subsequent principal components are all orthogonal and describe progressively less variation *(i.e.* lower eigenvalue eigenvectors of the covariance matrix). The PCA plot in **Figure 4.4(A)** illustrates the ability for MS based metabolic profiles from cocaine-naïve and experienced rat sera to separate in the first principal component (see x-axis **Figure 4.4(A)**). This also shows a separation in the second principal component (see y-axis); cocaine-experienced rats further separate into two main groups. The top group (quadrant I) consist of data from both behaviorally addicted (black) and non-addicted rats (red), while the other group (quadrant IV) were data generated from biological duplicates of a behaviorally non-addicted rat (multiple points due to technical replicates). The grouping consistency in the biological duplicates indicates biological variation from the other cocaine exposed rats. It is unclear if this secondary separation is a result of behavioral class, or simply specific to the rat. Importantly, principal component one separates metabolomic profiles based upon cocaine history, independent of behavioral class. In these

experiments, rat serum was obtained 2 weeks after cocaine administration, therefore cocaine and its metabolites were not detected in these analyses. Though the PCA plot indicates separation based upon exposure, it describes only 24% of the variation with the first two principal components. For the purposes of subsequent binary comparisons, the samples are grouped as either cocaine- naïve or cocaine-experienced.
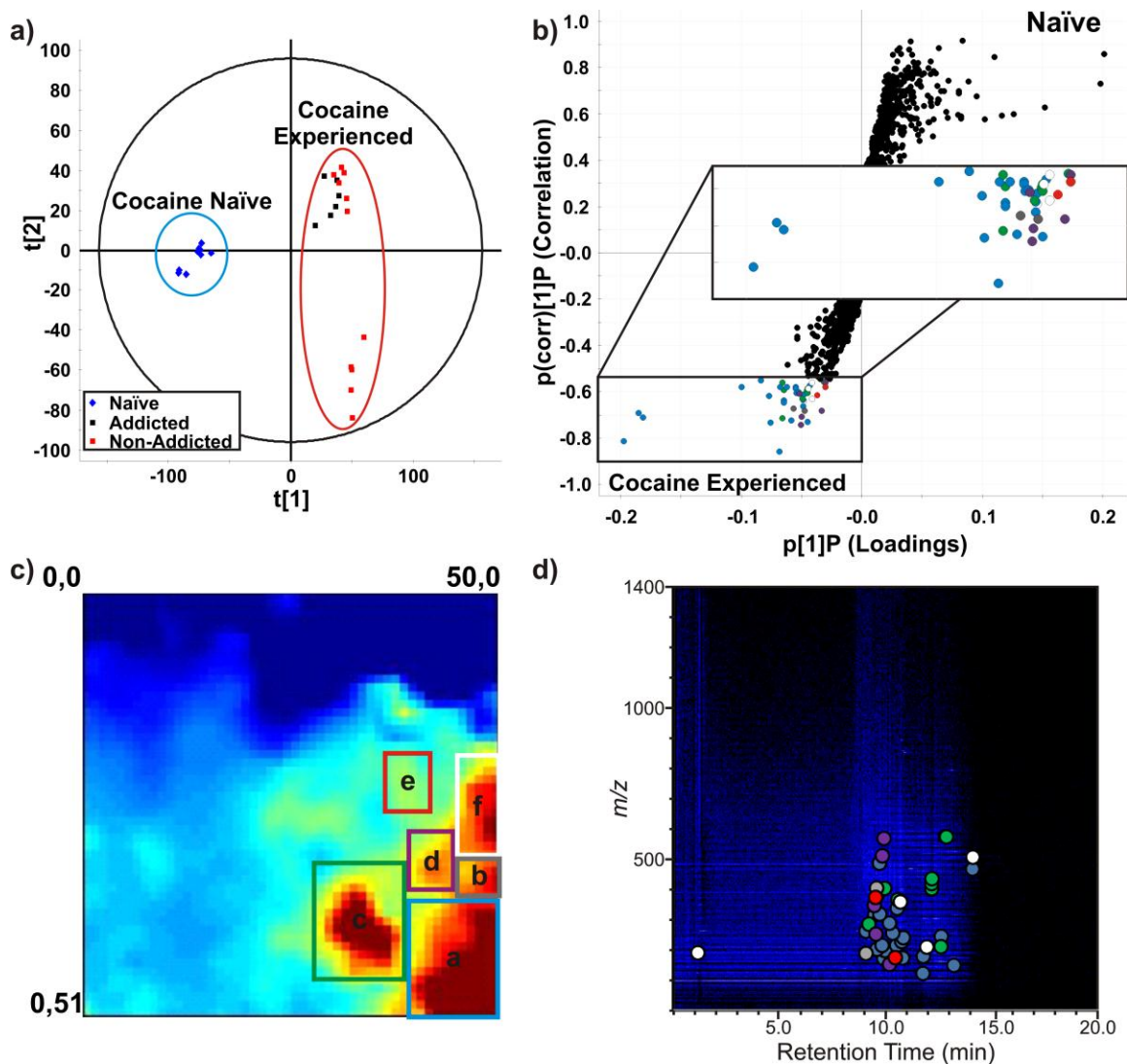
Figure 4. 4. *Rat sera metabolome depictions for cocaine-experienced versus naïve classes.* (A) Principal component analysis (PCA) of cocaine experienced (block markers) rat sera metabolomes plotted with cocaine-naïve (diamond markers). Behavioral sub-classes are indicated by color. (B) S-plot comparing cocaine-experienced (-) to cocaine-naïve (+) metabolomes. Marker color corresponds to the boxes in (C) (inset shows a magnified sub-image). (C) Differential MEDI heat map of average cocaine-experienced metabolic profiles with average cocaine-naïve profiles subtracted. Boxed in regions are then delineated in (D), which is an annotated representative UPLC-MS heat map marking feature location on the cocaine-experienced UPLC-MS plot. The colored dots correspond to the different feature islands in (C). [Box dimensions: a(39,38:50,51); b(46,33:50,37); c(28,34:38,46); d (39,28:45,36); e (36,20:42,27); f (46,20:50,32)]

Orthogonal partial least squares-discriminant analysis (OPLS-DA) can also be used to compare cocaine-naïve to cocaine-experienced rat sera profiles (**Figure A3.2**).[176] OPLS-DA is similar to partial least squares to latent structures (PLS), which, in this case, finds the relationship between the UPLC-MS data and cocaine history, and is a supervised method. However, OPLS-DA orients the model such that the abscissa is the predictive component, or between-group variation. The orthogonal ordinate then describes intragroup variation. Specifically, this model explains 98% of the data variation between groups. **Figure 4.4(B)** shows a corresponding S-plot used to determine metabolites of significance. This S-plot graphs features based upon group specificity or correlation (ordinate) and covariance (abscissa). Features with a high group correlation, or specific to either cocaine-exposed or naïve, in this case, have a large magnitude in the y-dimension. Features with a large loadings contribution to the predictive component possess large magnitudes in the x-dimension. Those features of interest have been colored in **Figure 4.4(B)**, which will subsequently be explained. In this manner, we are able to determine the features that are specific to long term cocaine exposure.

4.4.3 MEDI Heat Map Interpretation

The self-organizing map approach to feature organization places features with similar sample intensity profiles proximal in the coordinate grid, as afore mentioned. This generates regions of features that are up- and downregulated (*e.g.* **Figure 4.4(C)**, red and blue, respectively) consistently across samples, in

addition to regions that are specific to a subset of samples. This provides additional flexibility to data organization beyond the convention dimensions of loadings analyses of MVSA methods. Shown in **Figure 4.4(C)** is an average GEDI heat map of cocaine-experienced serum profiles (*i.e.* both behavioral classes) with the average naïve heat map subtracted to display metabolites that are either upregulated (yellow to red), or downregulated (blue to dark blue) as a general result of prolonged cocaine exposure. This differential analysis subtracts the average node intensities of cocaine-naïve rat sera profiles from the averaged experimental group. Though many islands exist, the more intense regions of upregulation are outlined for comparative purposes. These regions are both annotated and outlined with a colored box in **Figures 4.4(C)**. The colored boxes are for comparative purposes, which indicate the feature location in other data representations (**Figure 4.4(B) and 4.4(C)**) [Box coordinates: a(39,38:50,51); b(46,33:50,37); c(28,34:38,46); d(39,28:45,36); e(36,20:42,27); f(46,20:50,32)]. It should be noted that these boxes are consistent across sample groups and determined by group perimeter. Thresholding and image recognition software is being implemented for future applications.

Correlating the regions of interest in **Figure 4.4(C)** with a raw LC-MS plot (**Figure 4.4(D)**) illustrates the concept that grouped features display a large range of chemical properties, as they occupy different regions of separations space. The marker color in **Figure 4.4(D)** corresponds to the location in the heat map in **Figure 4.4(C)**. The S-plot in **Figure 4.4(B)**, described above as a common method to extract meaningful features from OPLS-DA binary analyses,

has been modified so the color of the markers correspond to the regions of interest in **Figure 4.3(C)**. All the features that would be prioritized through OPLS-DA are encapsulated in the regions of interest. These features occupy disperse regions of the S-plot.
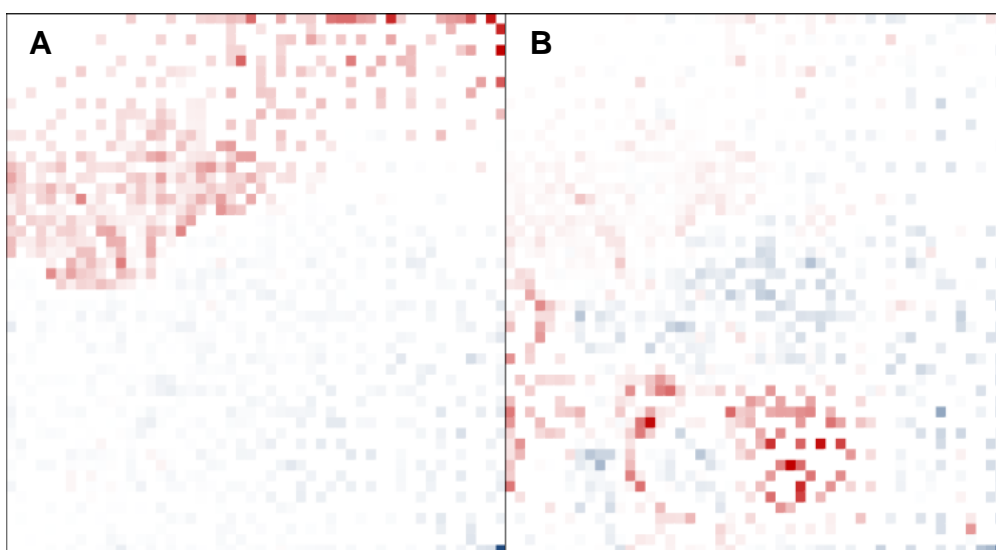
Figure 4.5. *Loadings contribution of nodes to PCA.* The contributions of each node to (A) principal component 1 and (B) principal component 2 are indicated by color intensity. Red indicates a negative contribution and blue indicates a positive contribution.

4.4.4 Loadings Contributions of MEDI Coordinates

Correlations between the MEDI feature assignment location and the loadings contributions to PCA are seen in **Figures 4.5(A) and 4.5(B)**. The loadings contribution of a feature to a particular principal component indicates the weight of that feature regarding sample magnitude in that dimension. In other words, a feature with a large negative loadings value in principal component one will influence a sample containing that feature to have a negative value in that component. Representing the loadings in this medium provides insight into neighborhood formation. The static nature of these samples means any clustering that occurs is sample-group-specific, assuming technical reproducibility. As such, what occurs in all cocaine-experienced sera profiles will group, and subsequent neighborhoods will form based upon sample specificity. **Figures 4.5(A) and 4.5(B)** should be considered with both **Figures 4.4(A) and 4.4(C)**, as the loadings contributions link the MEDI heat map to the PCA scores plot. The largest trends are resultant of cocaine experience, and have been organized into two main regions of the map accordingly. The upper portion of the map corresponds to features that are down-regulated, generally, in the cocaine-experienced. This is indicated by the dominantly blue upper portion. Features are initially partitioning based upon the global group differences. Considering the second principal component loadings, there is very little contribution from the features that are found in elevated intensities in the cocaine-naïve samples, which is seen by the relatively small contribution of the red region in **Figure 4.5(A)**. The second principal component loadings map offers more insight into

the formation of feature islands in the cocaine-experienced group. The significant feature loadings are those describing intra-experienced separations, which as indicated by the scores plot. The nodes that contribute greatly to principal component 2 form regions in the MEDI plot. This demonstrates the finer clustering effects of the feature sorting algorithm. Subpopulations of samples, such as the biologically distinct cocaine exposed rat, produce regions representing features that are unique to that subgroup. The grouping in principal component analysis, in addition to individual sample MEDI heat map investigation, provides insight into the interpretation of these underlying features.

Specifically, coordinate (50,51), or the extreme bottom right node, has the greatest contribution to a positive loading in principal component 1 and 2. This feature group, consisting of putatively identified 6-methyltetrahydopterin, deoxyuridine, and two other features, contains the most distinguishing features to cocaine experience in PCA. This group is also prioritized during the MEDI process. Other contributing signals are listed based upon their group occupation, feature descriptors, and, when applicable, a putative identification in **Table 4.1**. The greatest negative contributors to principal component 2 are found within region "c", in addition to more peripheral regions. These are features are upregulated in the distinct cocaine-exposed rat sera. As a result, these features provide insight into the difference between this rat and other cocaine-exposed models, whether biological or other. Additionally, region "f" has a positive contribution to principal component 2, and thus is upregulated in most cocaine

exposed rats. As a result, this region may provide alternative insight into the intra-group separation.

Table 4. 1. *Putative metabolite identification.* Metabolites were given preliminary identifications based upon accurate mass, ion type, and database searching.

Retention Time (min)	m/z	MEDI Region	Putative Identification
11.76	130.066	a	1: 3-Methylene-indolenine
12.83	616.179	a	2
13.22	158.154	a	3
9.92	182.192	a	4: 6-Methyltetrahydropterin
10.82	185.116	a	5: (3-Methoxy-4-hydroxyphenyl) ethylene glycol
11.78	190.086	a	6: Kynurenic acid
9.98	211.143	a	7
9.60	215.125	a	8
9.85	229.069	a	9: Deoxyuridine
10.53	229.142	a	10: Protein degradation dipeptide
10.77	243.104	a	11: Thymidine
10.85	257.136	a	12
12.63	261.109	a	13
10.34	273.168	a	14: Estradiol
9.09	279.688	a	15
10.19	308.091	a	16: Glutathione
9.49	338.087	a	17: 3-Indole carboxylic acid glucuronide
9.74	340.104	a	18: 5-Hydroxy-6-methoxyindole glucuronide
10.55	361.138	a	19: Dityrosine
14.09	500.277	a	20: LPE
9.72	520.313	a	21: LPC
9.58	432.280	b	31
9.09	201.072	b	32: Bilirubin oxidation product
12.87	614.174	c	22
12.62	225.110	c	23: 3-Hydroxykynurenine
9.22	305.159	c	24: Steroid-like molecule
10.58	392.138	c	25
9.60	406.164	c	26
12.18	430.296	c	27: Met 30-2H_2O
9.96	431.090	c	28
12.18	448.306	c	29: Met 30 –H_2O
12.19	466.318	c	30
10.19	162.056	d	33: 4,6-Dihydroxyquinoline
9.55	269.129	d	34: 3-Carboxy-4-methyl-5-pentyl-2-furanpropionic acid
9.48	371.227	d	35: 6-Keto-prostaglandin F1a
9.86	547.334	d	36
9.93	608.387	d	37
10.46	186.223	e	38
9.54	399.625	e	39: $[M+2H]^{2+}$
1.20	203.054	f	40: Succinylacetoacetate
11.94	223.066	f	41: Salsolinol 1-carboxylate
10.71	383.113	f	42
14.11	542.327	f	43: LPC

4.4.5 Region Interpretation and Comparison

Further heat map interpretation prioritizes regions of interest, which consist of grouped features. **Figure 4.6** compares the summed node intensities for outlined regions of the MEDI heat map. This provides insight into the significance of regions, in addition to the intragroup differences that occur. The summed intensities corroborate the loadings analysis, as the regions selected have significant differences in intensities between cocaine-experienced and naïve groups, and each have positive contributions to principal component 1. The regions that show differences within the experienced group (*i.e.* regions c and f) have varied intensities between behavioral classes, and also hold negative and positive contributions to principal component 2, respectively. The significance of the displayed differences was subsequently determined.

4.4.6 Determination of Contributing Features

Extracting relevant biological information is paramount in metabolomic experiments. Following regional analysis of MEDI heat maps, the extraction of contributing features is performed through the interface of GEDI by selecting a node, or through an exported "Gene Assignments List" (Metabolite Assignment List, in MEDI). **Table 4.1** lists relevant feature identifiers, region located, and, when available, putative identifications. The organization of features is a function of whether the feature is present in the same permutation of samples at relatively similar intensities. As a result, the subpopulations that arise indicate biological

subtleties that exist among groups. The putatively identified features in disparate

regions provide insight into these biological differences.
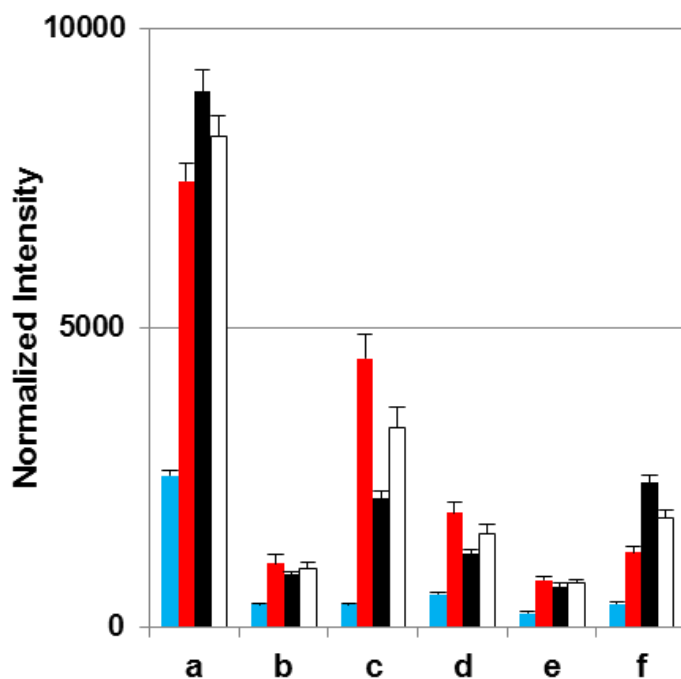
Figure 4.6. *Histogram depicting total area in enclosed regions of MEDI heat map, as indicated in Figure 4.3(C).* Rats with a history of cocaine exposure (white fill) had mean intensities significantly higher than cocaine-naïve rats (blue fill) in all regions tested ($p < 0.05$). Additionally, the mean intensity of region "f" was significantly higher in cocaine-addicted rats (black) than non-addicted (red) ($p < 0.01$).

Regions a-f all show distinct upregulation as a result of prolonged cocaine exposure, as seen in both **Figure 4.6** and the loadings representation in **Figure 4.5(A)**. Region "a" contains metabolites that occur in a majority of the cocaine exposed group. These include metabolite indicative of compensatory mechanisms of the biochemical effects of prolonged cocaine exposure. The most significant metabolite that is upregulated is 6-methyltetrahydropterin, which is a cofactor for tyrosine hydroxylase in the pathway to dopamine synthesis.[177] Elevated (3-methoxy-4-hydroxyphenyl)ethylene glycol, which is the primary serum metabolite of norepinephrine, has been found to be dysregulated following cocaine withdrawal.[178] Kynurenic acid is a naturally occurring metabolite resulting from tryptophan metabolism and has displayed protective effects against cocaine toxicity.[179] The inhibitory effects of cocaine exposure on glial cell growth have also been shown, significantly decreasing incorporation of thymidine in DNA synthesis, inhibiting growth.[180] The marked increase in serum thymidine concentrations is perhaps a compensatory result of cocaine exposure, or perhaps a result of metabolite pooling resulting from lack of incorporation. This could be the reason for upregulation of deoxyuridine as well. Alterations in estradiol concentrations have been seen in response to cocaine exposure, though why upregulation occurs in male rats following cocaine extinction is unclear. The presence of 3-Carboxy-4-methyl-5-pentyl-2-furanpropionic acid could speak to renal health as a result of the prolonged cocaine exposure.[181, 182]

Region "c" concentrates the biological differences that exist within the cocaine exposed group. The increased 3-hydroxykynurenine that appears to

exist implicates further tryptophan perturbations.[183] This metabolite has been associated with oxidative stress and neuronal cell death. Unidentified features that exist in this region may ultimately provide more insight into the biological variation that exists.

The other distinct region of difference within the cocaine-experienced group is region "f". The presence of succinylacetoacetate is a unique metabolite resulting from tyrosinemia, which has been shown to result from long term cocaine exposure.[184] Additionally, the presence of salsolinol 1-carboxylate, an intermediate toward the production of the endogenous neurotoxin salsolinol, is upregulated in region "f", which has been linked to stimulated dopamine production.[185, 186]

The current study focuses entirely on the upregulated features found in the cocaine-experienced group. There is a wealth of information that is present in the regions of down-regulation. However, considering the pedagogical nature of this dataset, we have chosen to demonstrate the relevance of the MEDI method using a subset of the prioritized features.

4.7   Conclusion and Perspectives

We have proposed and described the MEDI workflow, in detail, and applied this method to a static set of samples. We have demonstrated the utility of self-organizing maps to distinguish underlying feature motifs. Features that contributed to these regions were putatively identified and metabolic connections

that have been well described as consequential of cocaine exposure were established.

Though this method was applied to data acquired using mass spectrometry based detection, it is easily be applied to other metabolomics platforms (i.e., NMR), in addition to further degrees of separation. We have also only indicated the application of the MEDI workflow on s:-tatic samples, though the GEDI core software is ideal to determine underlying temporal dynamics. MEDI is a method that provides a medium to express metabolic phenotype and prioritize features based upon underlying sample patterns.

4.8   Supporting Information

Supporting information, including statistical summaries, can be found in APPENDIX 4.

Chapter 5

PERSPECTIVES AND PROPOSED IMPROVEMENTS ON THE APPLICATION OF MVSA AND MEDI WORKFLOWS TO MULTIDIMENSIONAL SEPARATION METABOLOMICS

5.1   Introduction

In this work, we sought to expand and apply the capabilities of multi-dimensional data collection and analysis to relevant systems, focusing on the interrogation of metabolites. This regards not only multi-dimensional separations, but also temporally defined data, which should be expanded upon in future work. A multitude of advancing integrations, applications, and modifications to enhance the applicability and functionality of these methods exist. Presented are meaningful endeavors that will advance metabolomic studies, and ameliorate the data processing bottleneck.

A large portion of the presented research advances the field of natural product discovery and the interrogation of metabolite profiles of microbial systems (**Chapters 2 & 3**). The structural properties of natural products allow ion mobility to be considered an attribute for lead prioritization. Additionally, the presented methods allow the organization of the large data associated with microbial extracts in an unbiased manner, providing a method for rapidly discriminating distinct features from a large cohort of extracts. Further development of these methods will only serve to expedite discovery methods.

It should not be overlooked that recent scientific momentum has mounted for the integration of other broad-scope, hypothesis generating studies, such as genomics, transcriptomics, proteomics, and lipidomics.[187] The integration of all these data into analyses provides connectivity in often isolated areas of research. This work has established a means for the comprehensive analysis of metabolites, a necessary framework for the establishment of more holistic studies.

5.2 Microbial Metabolite Interrogation

5.2.1 Extract Prioritization

The pursuit of new therapeutics from natural sources may require researchers to either approach discovery from the standpoint of analyzing extracts from many organisms in a high throughput fashion, screening for compounds based upon attributes (*i.e.* bioassay guided fractionation)[188], or comprehensively mining a single organism.[189] The implementation of the data acquisition and analysis methods described herein to either drug discovery approach allows unbiased prioritization of compounds, comparison of many extracts simultaneously, organization of analytes into unique feature regions using the MEDI process, and the addition of a structural attribute to detected analytes.

For the initial comparison of many extracts to determine unique metabolic profiles, such as that described in **Chapter 3**, principal component analysis or

other multivariate statistical analysis methods are appropriate. Applying multivariate statistical analysis methods provides a global perspective of sample clustering, and can be used to prioritize extracts and lead compounds for further analysis through loadings interrogation.
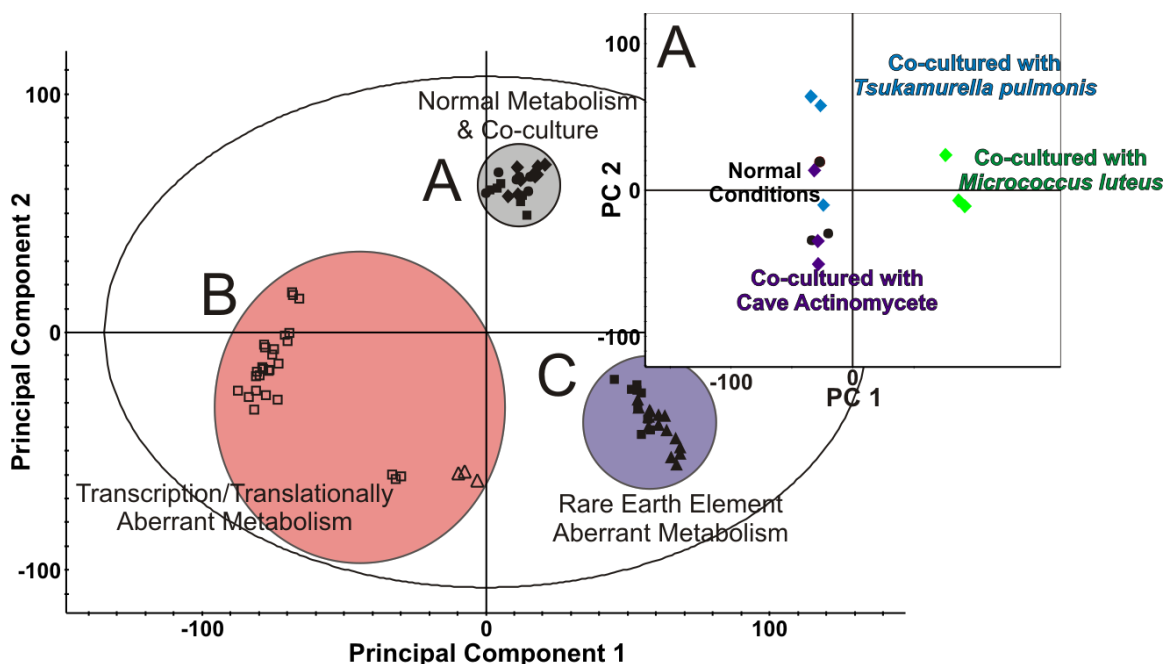
Figure 5.1. *Principal component analysis of* Streptomyces coelicolor *extracts from various growth conditions.* A global analysis of metabolic profiles reveals that the various methods for altering secondary metabolite production yield distinct differences. Region A is expanded in the callout, and principal components recalculated considering only mixed fermentation data. Regions B and C correspond to altered metabolism based upon transcription/translational mutations (as described in **Chapter 3**) and exposure to rare earth elements, respectively.

Figures **5.1** and **5.2** demonstrate the approach of growing an organism under a larger array of conditions to change metabolic expression.[189] The included data represent *Streptomyces coelicolor* extracts grown in the presence of the rare earth elements scandium and lanthanum (in varied concentrations), grown in mixed fermentation conditions with *Micrococcus luteus, Bacillus subtilis*, *Escherichia coli*, and *Tsukamurella pulmonis*, and mutated through conferring resistance to streptomycin and rifampicin (as described in **Chapter 3**). In **Figure 5.1**, distinct metabolic differences exist dependent upon the growth conditions. The density of the data is observed in the expansion of the compressed region A, which, when isolated and principal components are recalculated, reveals metabolic profile differences amongst mixed fermentation conditions.

The selected heat map in **Figure 5.2** corresponds to a mixed fermentation condition with *Tsukamurella pulmonis*, a mycolic acid-containing organism that has been demonstrated to change *Streptomycete* secondary metabolism expression.[190] The heat map represents features organized based upon all growth conditions with monoclonal cultures subtracted, leaving persisting regions of increased abundance representative of aberrant metabolism. This prioritized two regions of interest that corresponded to increased production of geosmin and 3,8-dihydroxy-1-methylanthraquinone-2-carboxylic acid (DMAC), known secondary metabolites of *Streptomyces coelicolor*.[191] This proof-of-principal demonstrates the application of the MEDI workflow to natural product discovery and, more generally, the interrogation of microbial extracts. However, this does not address the true bottleneck.
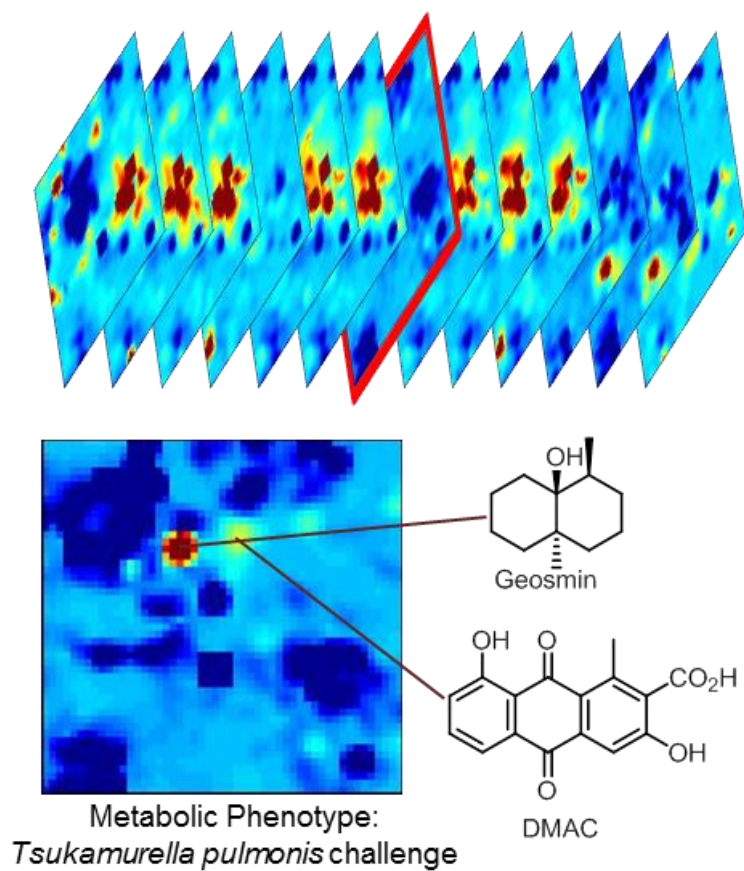
Figure 5.2. *MEDI heat map of a select* Streptomyces coelicolor *extract grown in competition with* Tsukamurella pulmonis. Using the MEDI process, one of a number of potential growth conditions (shown above) is selected and analyzed to determine compounds specific to the growth condition. The highlighted metabolites are upregulated in mixed fermentation conditions, and are known *Streptomycete coelicolor* secondary metabolites.

5.2.2 Feature Dereplication

An automated means of interrogating the acquired fragmentation data for a prioritized lead would aid in dereplication. The presented study in **Chapter 3** was performed on a single, untargeted analysis, demonstrating the density of data acquired using multi-dimensional separations. Through the addition of ion mobility, high energy data were acquired for essentially all analytes of moderately high abundance that were isolated in separations space. Through commonly occurring in-source fragmentation of certain analytes, often labile molecular decorations such as glycosylation or phosphorylation, higher order fragmentation data can be acquired. These data can be confidently correlated through drift time chromatogram consistencies. For example, if a particular mass possesses two distinct drift times in a high energy spectrum, one corresponding to a longer drift time, and the other a shorter, and this peak is the precursor ion for the shorter drift time, it follows that insource fragmentation has likely occurred, and tandem information found corresponding to the shorter drift time is exclusive to the insource fragment ion. By extracting drift time specific fragmentation information, and subsequently performing accurate mass discriminated *in silico* comparisons of compounds present in the Dictionary of Natural Products, LIPID MAPS[171], MetaCyc[192, 193], the Human Metabolome Database[168, 169], and METLIN[170] using MetFrag[194] or MassFragment (Waters, Milford, MA), confident dereplication can be automated. Additionally, a feature flagged as an insource fragment can be searched against a database of biotransformations. This higher order fragmentation data acquired from insource fragmentation can be used to

disambiguate structure. Additionally, analogous peak assignments for new compounds can be performed, providing insight into the moieties present.

Features prioritized using initial filtering criteria, whether through multivariate statistical analysis and MEDI methods, or attribute analysis, such as molecular weight, relative elution time, and structural uniqueness, would be dereplicated through retention time and drift time correlated high energy data extraction and comparison to the aforementioned database *in silico* predictions. A modified threshold would be empirically established corresponding to the number of matched fragment peaks, fragmentation feasibility, and mass accuracy of matching peaks. The incorporation of higher order fragmentation, which is available through insource fragmentation, can be incorporated to increase peak assignment and overall molecule matching confidence.

5.2.3 Lead Compound Mechanism of Action Determination

A final addition to the proposed drug discovery pipeline is the ability to determine an unknown compounds mechanism of action through the metabolomic analysis of a bioactivity assay. Preliminary data, shown in **Figure 5.3**, suggest metabolic indicators of mechanism of action exist which may be used to predict the mode of action for unknown compounds. The data shown represent biological duplicates of *Escherichia coli* cultures grown for 12 hours in the presence of lethal doses of apramycin, kanamycin, ampicillin, and vancomycin. These extracts were generated and analyzed in a similar fashion to

those described in **Chapter 3**. Global analysis reveals biologically reproducible

clustering based upon metabolic profiles, and warrant further investigation.
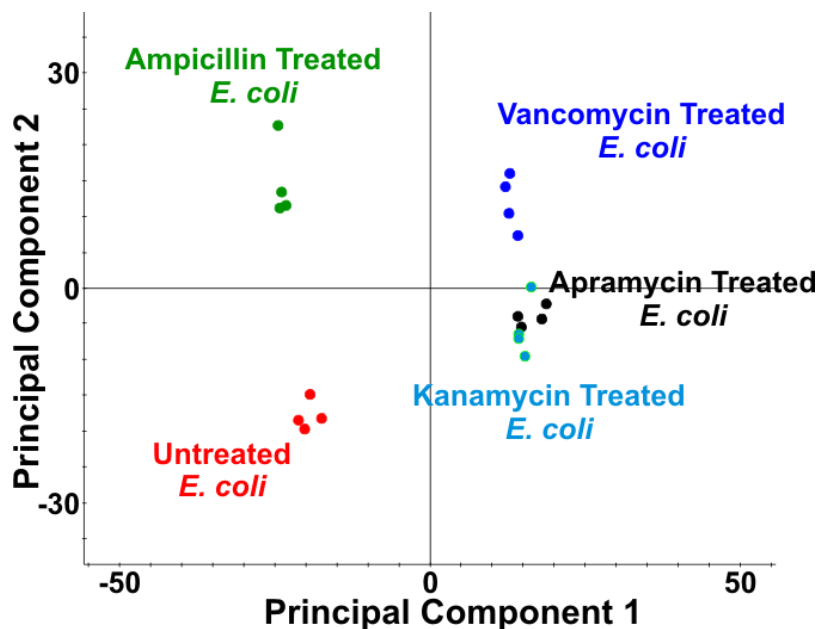
Figure 5.3. *Principal component analysis of* Escherichia coli *extracts after 12 hours of treatment with various antibiotics with known mechanisms of action.* Biological replicates indicate a reproducible clustering of extracts based upon treatment. Through analyzing antibiotics with known mechanisms of action, diagnostic metabolites can be determined to discern the mechanism of action of an unknown compound.

Initially, the metabolic ramifications treating a model organism (such as

Escherichia coli) with a library of antibiotics with known mechanisms of action will

be analyzed to determine metabolic indicators. In this manner, a forensic

approach can be taken to determine the mechanism of action for an unknown

bioactive compound. The biological insight gained through comprehensive

analyses of metabolic perturbations resultant from antibiotic treatments should not be overlooked, which expands beyond target prediction of an unknown compound. Conceptually, bioactive fractions from extracts collected through split-flow following LC can be extracted and analyzed for metabolic indicators of mechanism of action. Predictions of biological targets of bioactive fractions can be determined through comparisons to the training set.

5.3   Metabolite Organization Enhancement

The use of self-organizing map based analysis of metabolic profiles has been demonstrated in **Chapter 4**. There exist a number of additions and modifications to the MEDI workflow that would aid in ease-of-use, and enhance the utility and comprehensiveness of analysis. Through adding additional functionality, modifying the MEDI interface, and expanding analysis beyond feature prioritization, the cumbersome nature of the current implementation will be ameliorated, in addition to providing significance to features and aiding in feature identification.

5.3.1 MEDI Interface and Extension Modifications

The current MEDI process requires a significant amount of external processing and formatting. This generates a bottleneck at the manual stages of data analysis. Through interfacing peak-picking software and an mzXML viewer with the self-organizing map software, raw data can be accessed that

corresponds to a particular feature located at a node of interest. As mobility data becomes more ubiquitous amongst mass spectrometry laboratories, three-dimensional peak picking software will allow for the full utilization of the acquired data. As a result, peaks with isobaric retention and mobility times found in high energy data, as routinely acquired in the MS^E function (**Chapter 1.5.1**), can be called upon as well, providing automated return of fragmentation data for a particular node. It follows that these data be compared to publically available databases corresponding to the biological system in question, as described in **Chapter 5.2.3**.

Additionally, the ability to group samples prior to analysis, and later compare automatically detected regions of interest using univariate statistical methods, such as Welch's t test (which accounts for unequal variances), ANOVA testing and subsequent *post hoc* analyses would provide significance to selected regions and prioritize groups of features. Selecting specific features from a region and performing these analyses is also useful for obtaining the significance of a specific feature, though multiple hypothesis testing correction, such as Bonferroni correction, may be necessary. Regions detection should be automated through a thresholding method[195], which will first a region of interest, allowing the extraction of the features within, the statistics of the region across groups, and the contribution of features to the overall region intensity.

5.3.2 Inverse Feature Organization

Currently, MEDI processing occurs through a self-organizing map algorithm that arranges features based upon relative similarities in intensity profiles across a time series or samples using Pearson's correlation as the comparison metric.[164] As a result, intensity profiles of features that are similar are grouped. However, there is utility in analyzing inverse correlations amongst features. When considering a dynamic profile, it is extremely useful to monitor and group features that behave in a relatively inverse fashion. It should be noted, however, that this method is not relevant when considering binary comparisons, as all discriminating features will be grouped into one region.

5.3.3 High-Energy Data Comparison

A final proposed addition is the ability to compare high energy data within regions of interest. Transitions found within high energy data for selected features would first be compared for descriptive fragmentation, such as the loss of a lipid head group, phosphorylation, or glycosylation, as well as common transitions such as *b* and *y* ions in peptides. This provides an initial discrimination of the broad biomolecular class the feature occupies in an automated manner. A second layer of comparison would investigate similarities amongst features within a region, to determine chemical relation between features. Existing high energy transitions for a feature would be compared to those present in grouped features. When considering features that demonstrate inverse intensity profiles, it is feasible that the depletion of one feature supplies the generation of another.

Feature correlations can be surmised with increased confidence through comparison of high energy data, and the assumption that similar transitions will exist between related but biotransformed molecules. Additionally, a filter for common biotransformations and adducts would allow for the distillation of features, and would require simple comparison of mass differences in features with similar retention time and mobility values. These methods would be particularly valuable for metabonomics experiments in the identification of drug metabolites.

5.4. Integration into Trans-omics Studies

The described work fits neatly into a larger agenda, which aligns with a recent thrust in the scientific community approach biological problems from a holistic standpoint.[187] The visualization of metabolic profiles has significantly lagged behind the development of analysis methods.[196] As a result, the MEDI process provides a means for visualizing metabolomic data, though advancements in the interface and functionalities are necessary, as aforementioned. Additionally, ion mobility separations were used in this work for both structural discrimination and as a means of analyte isolation in separation space, but the full capabilities of these measurements should be utilized for metabolite identification.

Briefly, with advancements to MEDI, as described in the previous section, comparative metabolomics visualization and feature identification will be

enhanced to provide increased fragmentation confidence through the additional dimension of mobility separation in an untargeted manner, database searching using accurate masses and fragmentation spectra to discriminate matches, and correlation of features based upon up- or down-regulation trends. Through the addition of a mobility measurement discriminator, such as defined in previous works demonstrating biomolecular class separation in ion mobility[76], additional scores can be incorporated into feature identification. With the extraction of absolute collision cross sections, which may be done using a uniform field instrument[89] or through calibration profiles in traveling wave ion mobility[107, 197] (as described in **Chapter 1)**, assumptions of biomolecule class can be made, and through the development of a database with collision cross section values for metabolites, an additional parameter is available for metabolite identification. By enhancing the accessibility of metabolomics data through a more integrated interface, the potential of multi-dimensional separations data can be accessed. It should be noted, as well, that simultaneous metabolomics and lipidomics may be performed through the parsing of features based upon mobility-mass correlation, or predicted biomolecular class.

When considering the integration of metabolomics data into a systems biology approach, the correlation of regions of interest to metabolic pathways is necessary. The ability to assign identifications to features and map regions of interest within MEDI to KEGG pathways[174] allows for a direct comparison of metabolic ramifications. Furthermore, clustering of metabolic pathways based

upon self-organizing maps allows for organization of subgroups arising from potential biological variation.

5.4   Conclusions and Perspectives

This work has significantly advanced the fields of metabolite analysis by applying established multivariate statistical analysis methods to microbial metabolome analysis, developing a metric utilizing gas phase structure for lead compound prioritization, and integrating self-organizing map based algorithms for metabolite analysis. As a result, new advancements are present that build upon the herein-established framework. By integrating the necessary components for a metabolomics study into a central interface, feature determination, prioritization, and identification can be performed in the same suite, with the subsequent options of retrieving higher order data and performing automated analyses of experimental groups based upon regions of interest. Additionally, mobility correlation can be further implemented as a metric for lead compound prioritization, and established as an attribute for feature scoring in drug discovery endeavors. The interrogation of many growth conditions or strains can be performed through combining multivariate statistical analysis methods with the MEDI approach, with subsequent dereplication aided by automated database searching and fragmentation analysis.

The utility of the methods described herein is dependent upon the modification of the interface to incorporate feature detection, self-organizing map analysis along with multivariate statistical analysis methods, mobility and retention time

correlated feature high energy extraction, database searching using accurate mass and predicted fragmentation profiles in a central location. This package would provide a tool for secondary metabolite prioritization and dereplication for natural product discovery, along with primary metabolism insight and correlation to metabolic pathways.

APPENDIX 1

Chapter Reprint Permissions

The work in Chapter 1 is found in:

J. May, **C. R. Goodwin**, J. A. McLean. "Gas-Phase Ion Mobility-Mass Spectrometry and Tandem IM-MS Strategies for Metabolism Studies and Metabolomics," in the *Encyclopedia of Drug Metabolism & Drug Interactions,* D. C. Muddiman, Ed., J. Wiley & Sons (to be published **2012**) In press.

The works in Chapter 2 is found in:

C. R. Goodwin, L. S. Fenn, Dagmara K. Derewacz, B. O. Bachmann, J. A. McLean. Structural Mass Spectrometry: Rapid Methods for Separation and Analysis of Peptide Natural Products. *Journal of Natural Products.* **2012**, *67* (*35*): 48-53

D. K. Derewacz, **C. R. Goodwin**, J. A. McLean, H. A. Barton, B. O. Bachmann. Lechacyclines, new angucyclines and their mycothiol adducts from a deep hypogean Streptomycete. *In preparation for Organic Letters.*

The work in Chapter 3 is found in:

D. K. Derewacz*, **C. R. Goodwin***, C. R. McNees, J. A. McLean, B. O. Bachmann. Antimicrobial drug resistance affects broad changes in metabolomic phenotype in addition to secondary metabolism. *Submitted to the Proceedings of the National Academy of Sciences* (IN PRESS)

The work in Chapter 4 is found in:

C. R. Goodwin, S. Sherrod, C. C. Marasco, N. M. Smith, B. O. Bachmann, N. Schramm-Sapyta, J. P. Wikswo, J. A. McLean. Phenotypic mapping of metabolic profiles using self-organizing maps. *For s ubmission to PLOS ONE.*

APPENDIX 2

Supporting Information for Chapter 2

Table A2.1. Cyclic peptide collision cross sections reported in **Chapter 2**.

Cyclic Peptide Name	Species	*m/z* (Da)	Ω (Å²)	σ (# of measurements)
ampicillin	[M+Na]⁺	373.6	110.1	1.3(20)
valinomycin	[M+H]⁺	1110.5	271.9	1.4(19)
valinomycin	[M+Na]⁺	1133.3	269.7	0.8(19)
valinomycin	[M+K]⁺	1149.5	274.5	0.6(19)
cyclosporin	[M+H]⁺	1202.6	296.6	1.2(19)
polymyxin	[M+H]⁺	1203.6	285.6	1.0(19)
cyclosporin	[M+Na]⁺	1224.4	289.9	1.2(19)
polymyxin	[M+Na]⁺	1225.3	279.4	0.9(19)
polymyxin	[M+K]⁺	1240.2	284.4	4.9(19)
actinomycin	[M+H]⁺	1255.9	280.1	1.9(18)
actinomycin	[M+Na]⁺	1277.9	284.2	0.7(19)
actinomycin	[M+K]⁺	1293.8	280.8	4.1(17)
bacitracin	[M+H]⁺	1421.6	301.2	0.8(19)
phleomycin	[M+H]⁺	1427.7	275.7	1.3(13)
bacitracin	[M+Na]⁺	1444.6	305.3	1.0(19)
phleomycin	[M+Na]⁺	1448.4	276.7	1.2(19)
vancomycin	[M+H]⁺	1449.2	299.4	0.9(20)
bacitracin	[M+K]⁺	1466.6	303.6	2.3(10)
vancomycin	[M+Na]⁺	1470.6	296.0	3.7(20)
vancomycin	[M+K]⁺	1485.3	299.4	3.8(15)
phleomycin	[M+Cu]⁺	1489.5	276.8	2.7(19)
thiostrepton	[M+H]⁺	1668.6	310.0	1.6(20)
thiostrepton	[M+Na]⁺	1686.1	315.5	1.0(20)
thiostrepton	[M+K]⁺	1702.6	314.8	3.0(10)

Procedures used in Chapter 2.3.

Charge Derivation Protocol

All molecules were first build in ChemBioDraw Ultra. Molecules were broken into fragments for charge derivation of feasible size for quantum based energy minimization and charge calculations (*i.e.* ~120 atoms or less). An initial energy minimization was performed using a B3LYP/HF 6-31G* level of quantum theory in Gaussian03.[198] After determining the calculation had converged upon a local minimum, the frequency values were interrogated to ensure the calculation had not rested upon a saddle point. These energy minimized structures were then subjected to further *ab initio* optimization and electrostatic potential calculations using Gaussian03, mimicking the protocol derived for the general Amber force field, applying a HF/6-31G* basis set and the Merz-Singh-Kollman scheme for charge parameterization.

Molecular Dynamics Protocol

All molecular dynamics simulations were generated using the Amber 11 Molecular Dynamics Package.[199] Charge densities were converted to restrained electrostatic potential (RESP) values and prep files using antechamber.

Intact molecules were assembled and sodiated in LeAP using prep files. GAFF[95] (general AMBER force field) was used for atom type descriptions. To define the sodium cation, AMBER99SB[97, 200] force field was used. Topology and coordinate files were generated for molecular dynamic simulations in sander.

Restraint files were generated for the sodium cation such that full exploration of the assembled molecule was possible, but if the cation began to stray into space, a force would be applied to facilitate return. Upon inspection of trajectory files, this restraint was not necessary, as the cation remained proximal to the molecule, yet was still able to fully explore all regions of the molecule. Prior to simulation, an energy minimization was performed using sander to ensure a stable starting structure. The simulated annealing protocol was carried out in three steps. First, the structure was heated to ~1200-1500K over 10 picoseconds using 0.25 femtosecond time steps. The structure was then held at this temperature for 9 nanoseconds using 0.25 femtosecond time steps, extracting a conformation every 3 picoseconds, resulting in 3000 conformational snapshots. These snapshots were cooled to ~320K over 15 picoseconds to allow the conformation to find a local minima. To generate the desired 24,000 conformations, this protocol was performed 8 times, using unique starting conformations for each to promote enhanced sampling of conformational space. Each conformation was then converted to a collision cross section using MOBCAL.[26, 98] The collision cross section and potential energy for each conformation was then extracted and visualized using a scatter plot. Data were then discriminated using the measured collision cross sections, with the sampling window ± 2 times the error of the measurement.

Clustering Protocol

      The extracted conformations were then aligned using superpositioning software, suppose, written by Jarrod Smith (Vanderbilt Center for Structural Biology). These structures were then clustered based upon their root mean square distance (RMSD) over all atoms. A cutoff was then determined based upon the RMSD which resulted in approximately 19-21 conformations. This value was then imposed, and the most representative conformation from each branch of the cluster was extracted. This in effect distilled the data from ~400-2000 conformations to 20 which could be interrogated. PDB files for each were generated and interrogated using Molecular Operating Environment (MOE).[201]
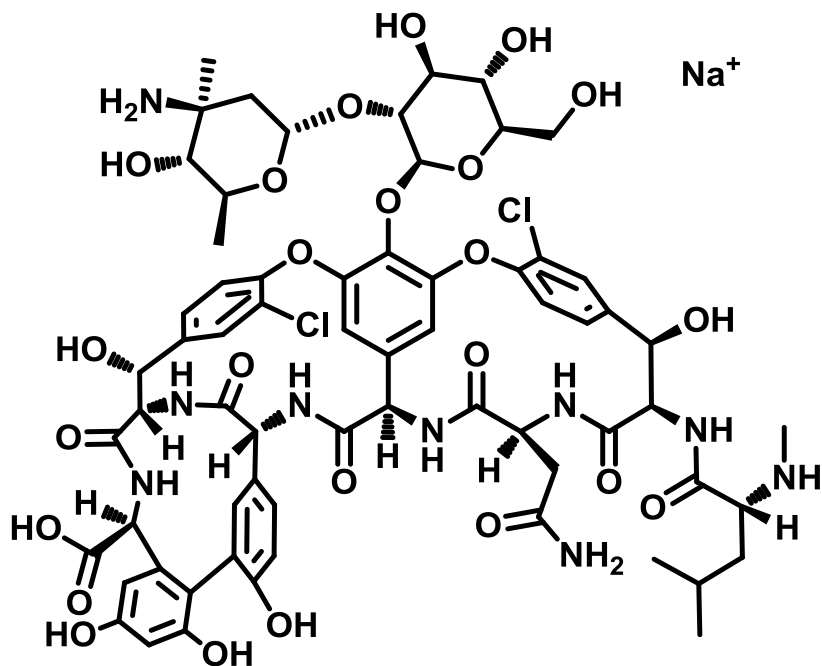
Figure A2.1. Chemical structure of sodiated vancomycin. Monoisotopic mass was measured to be 1470.42 Da. The calculated collision cross section used for conformation discrimination is 293.41 ± 7.22 Å^2, which is a window two times the error of the measurement.
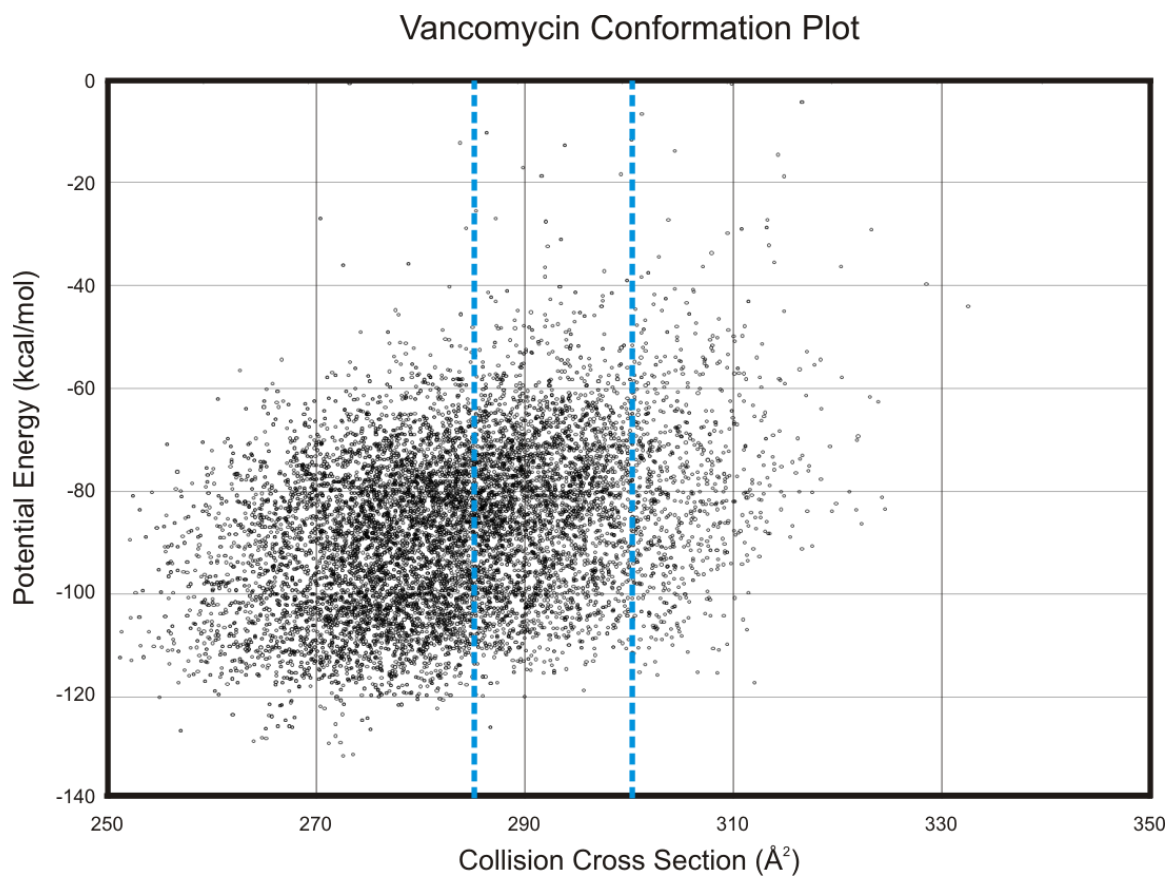
Figure A2.2. Scatter plot representative of 24,000 sodiated vancomycin conformations. Plotted on the abscissa is collision cross section in $\mathring{A}^2$, while the ordinate displays the relative potential energy of the conformation in kcal/mol. Each circle is representative of a unique conformation. The dashed blue lines indicate the region corresponding to experimentally measured CCS values. The width of the window corresponds to two times the standard deviation of the measurement. The data falling within the defined region were extracted for clustering analysis. Similar scatter plots were generated for all data to ensure proper sampling (not shown). It should be noted that this method of data projection does not express the data density with respect to conformational space occupation.

7.3

0.4845

RMSD (Å)
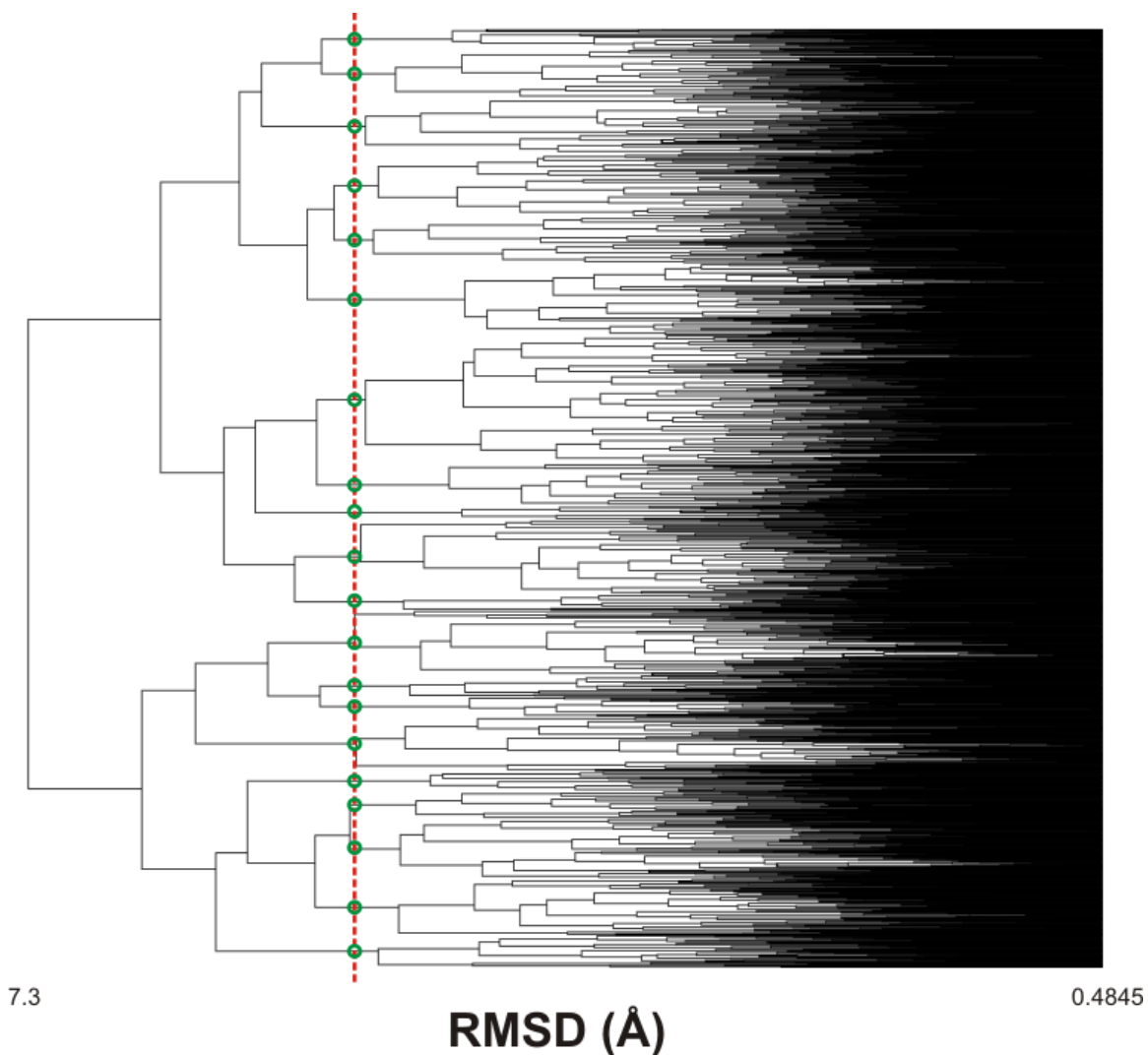
Figure A2.3. Clustering analysis of 2010 sodiated vancomycin conformations extracted from a set of 24,000 based upon collision cross section correlation. As the tree progresses from right to left, the clustering tolerance is increased. Clustering was done on the basis of root mean square distance of atoms after superimposing structures. The red dashed line indicates the cutoff for the generation of representative conformations. The green circles correspond to each branch that represents the entire dataset. In the end, all conformations were distilled into 20 representative structures. A clustering cutoff of 5.23 Angstroms was implemented.
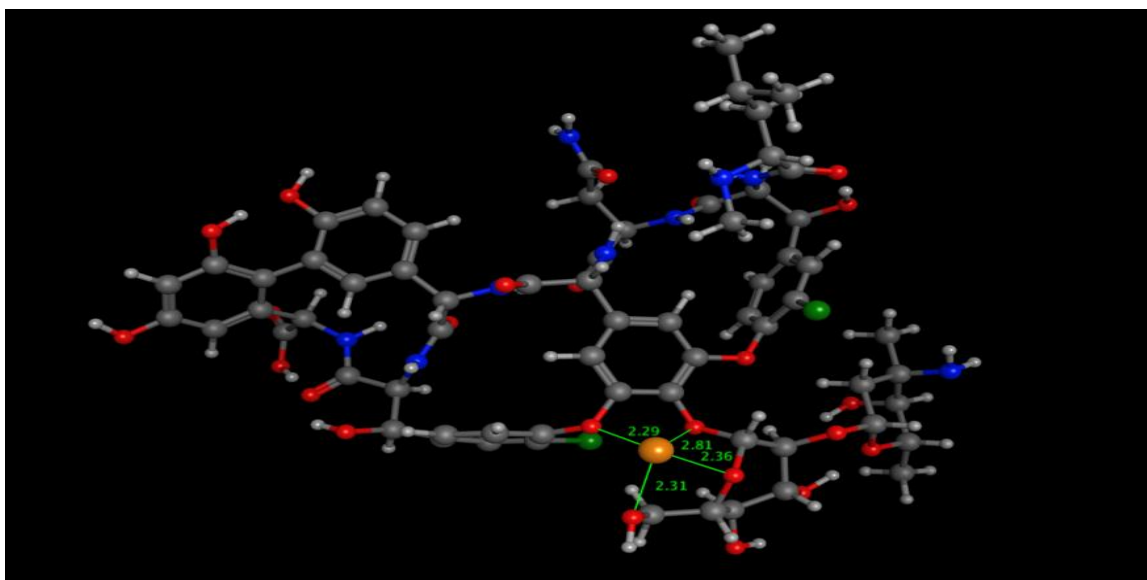
Vancomycin Conformation 1. *n*=140
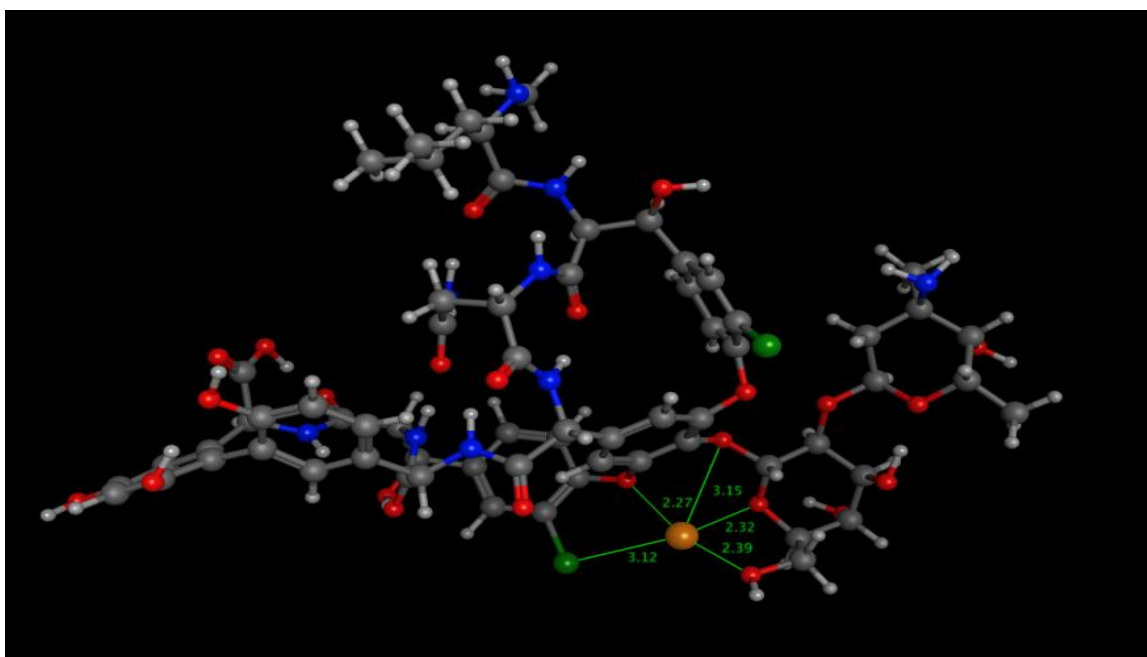
Vancomycin Conformation 2. *n*=116
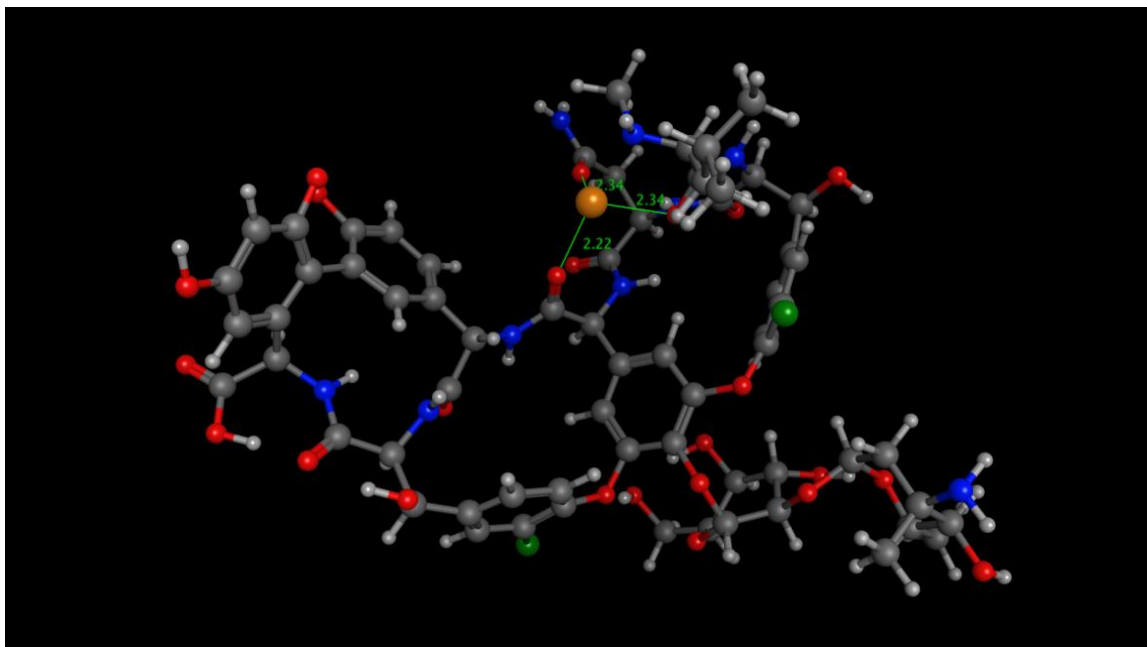
Vancomycin Conformation 3. *n*=159
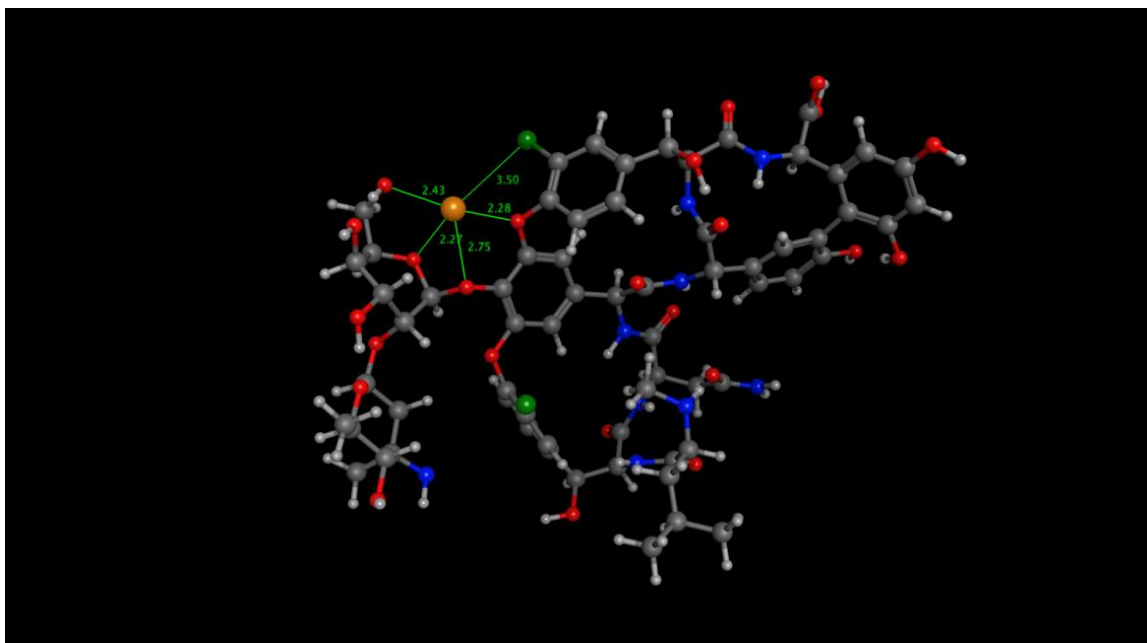
Vancomycin Conformation 4. *n*=275
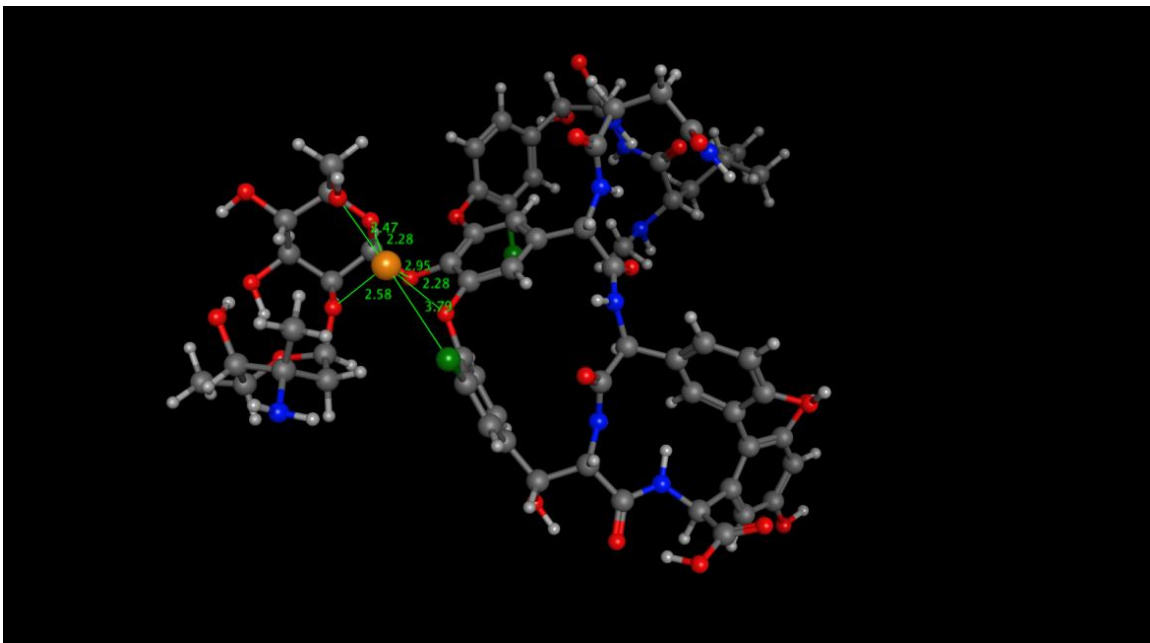
Vancomycin Conformation 5. *n*=122
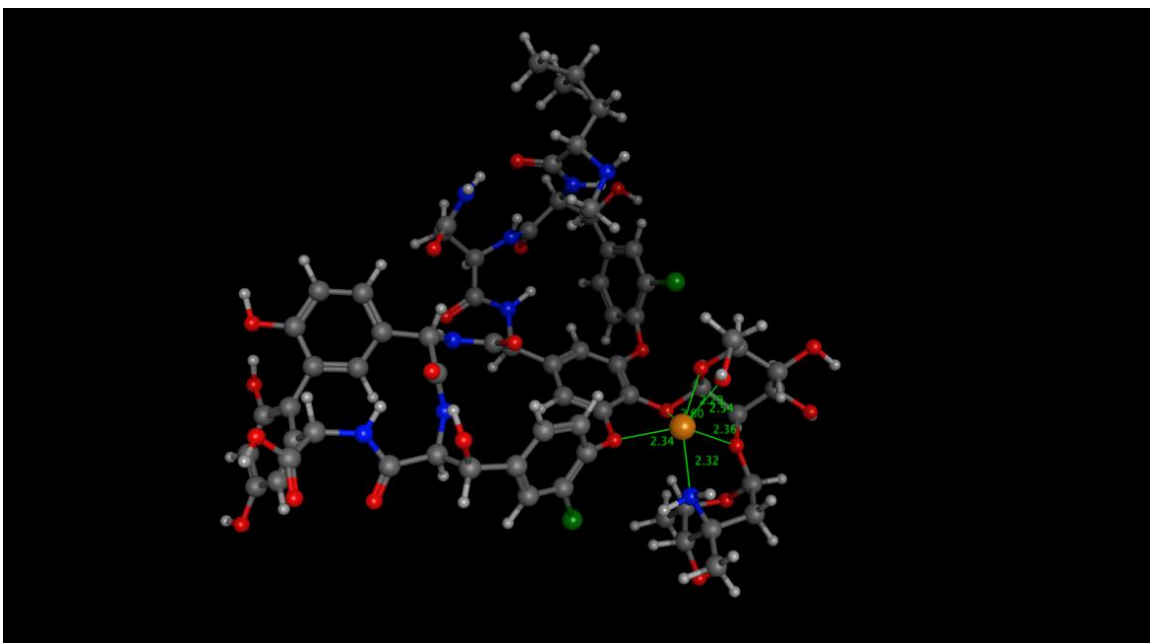
Vancomycin Conformation 6. *n*=101
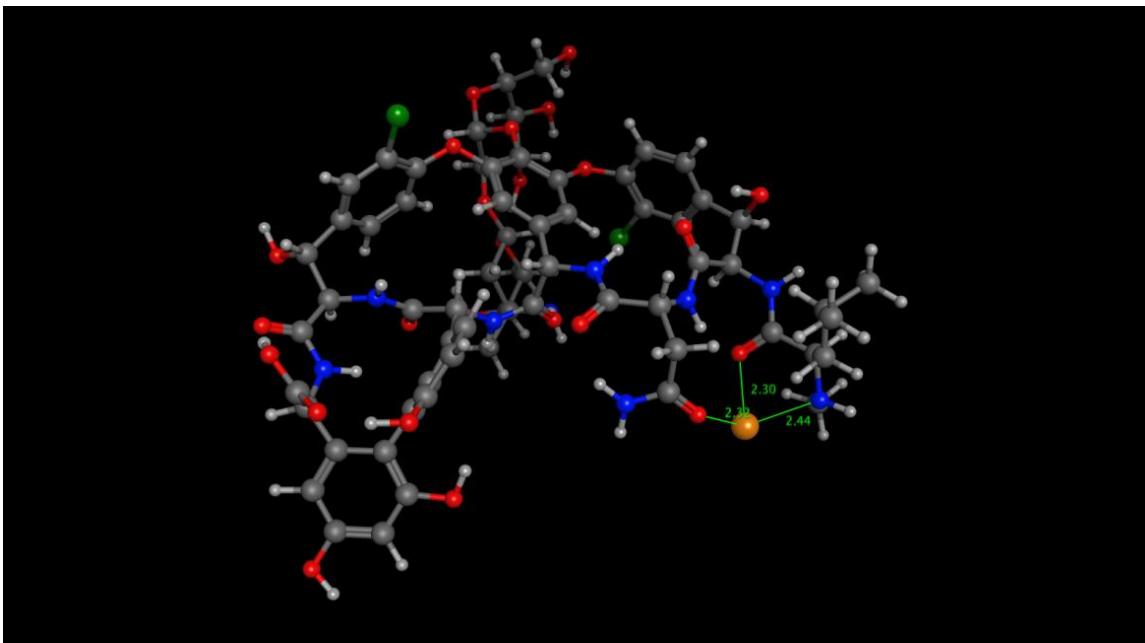
Vancomycin Conformation 7. *n*=69
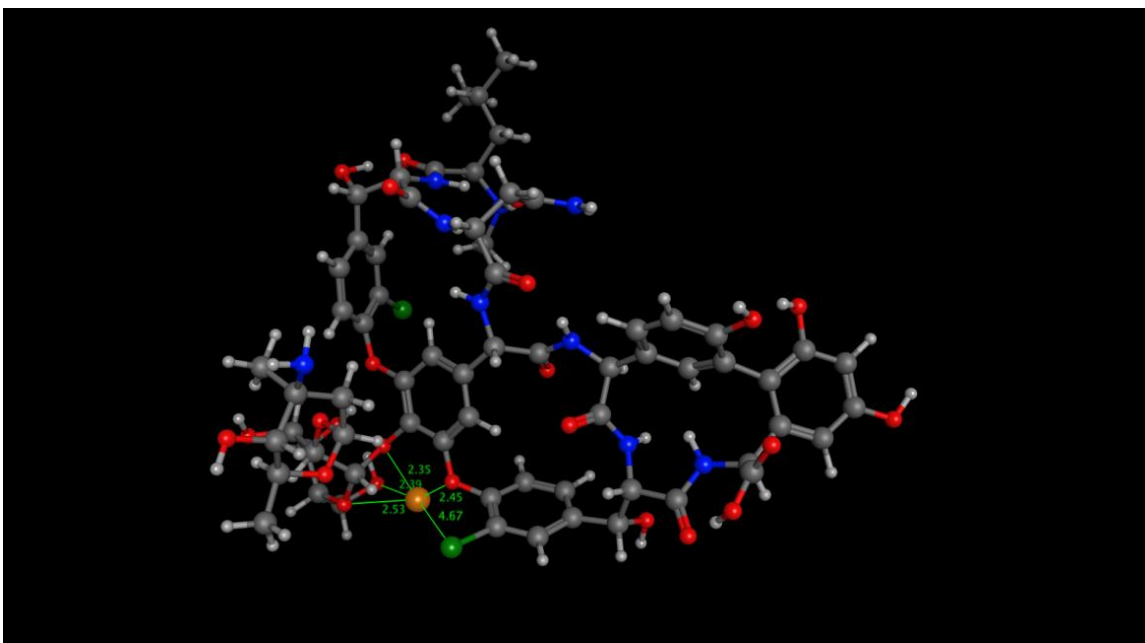
Vancomycin Conformation 8. *n*=132
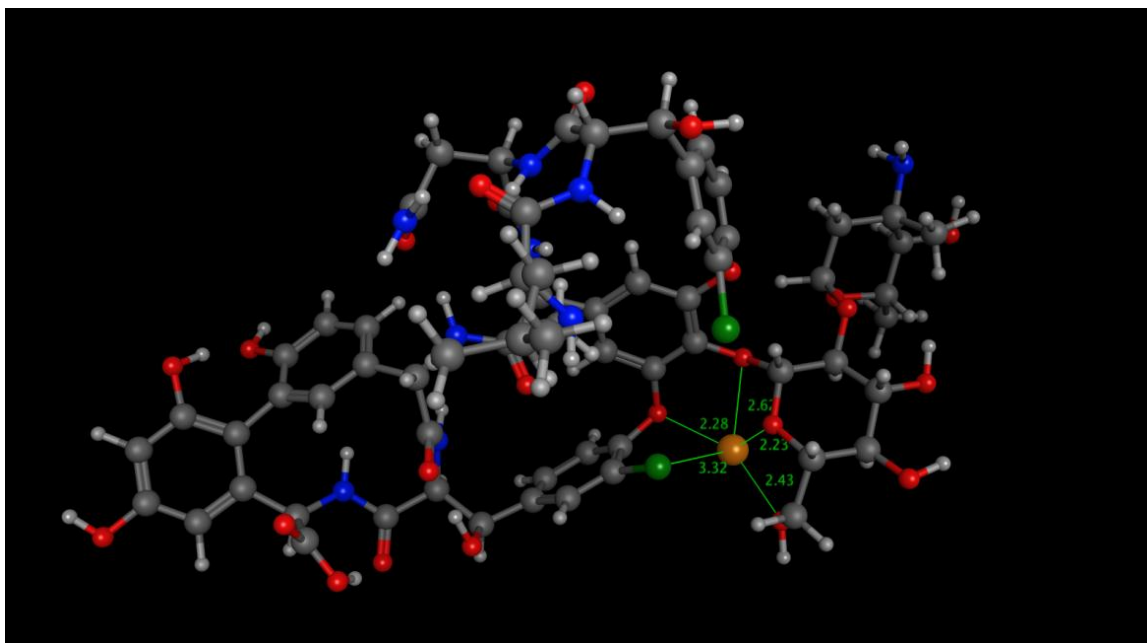
Vancomycin Conformation 9. *n*=103
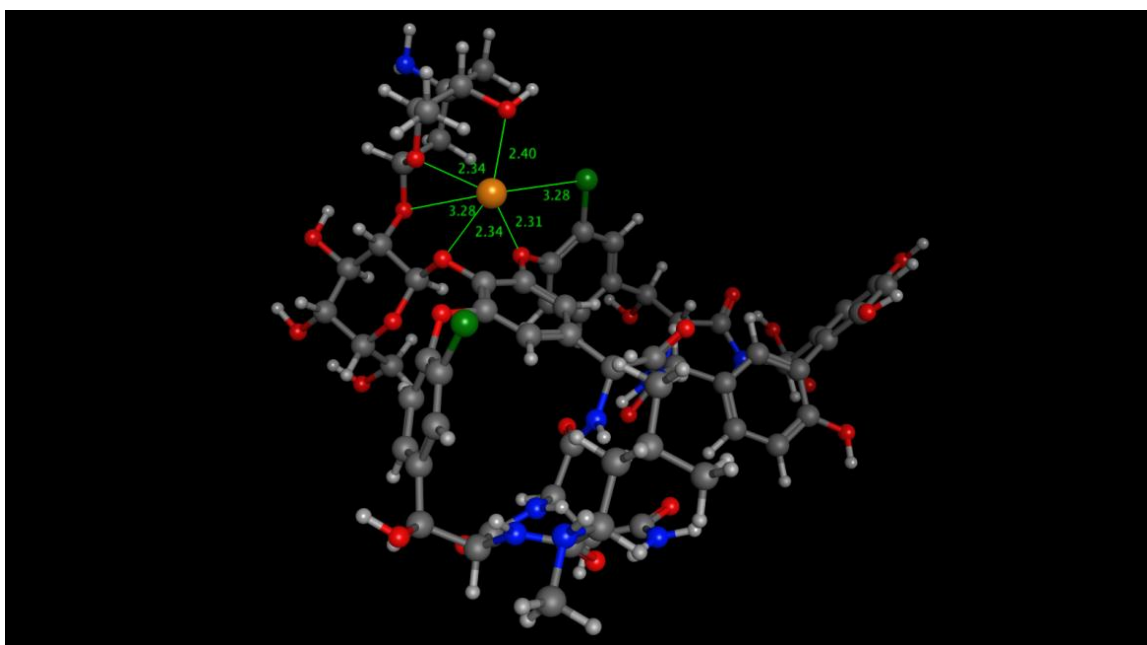
Vancomycin Conformation 10. *n*=119
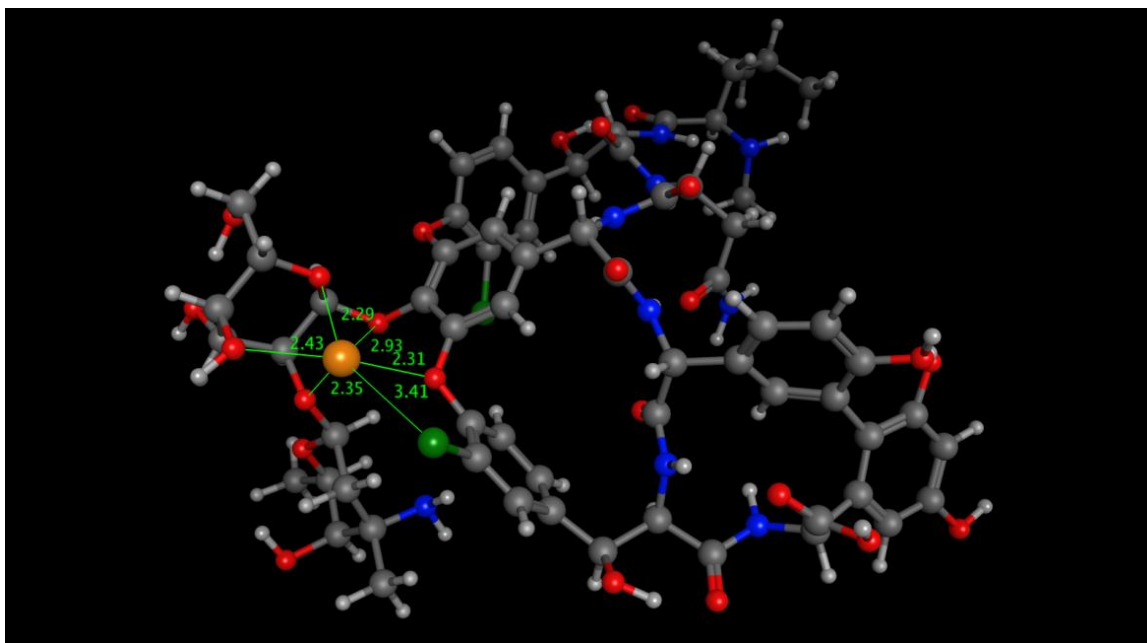
Vancomycin Conformation 11. *n*=131
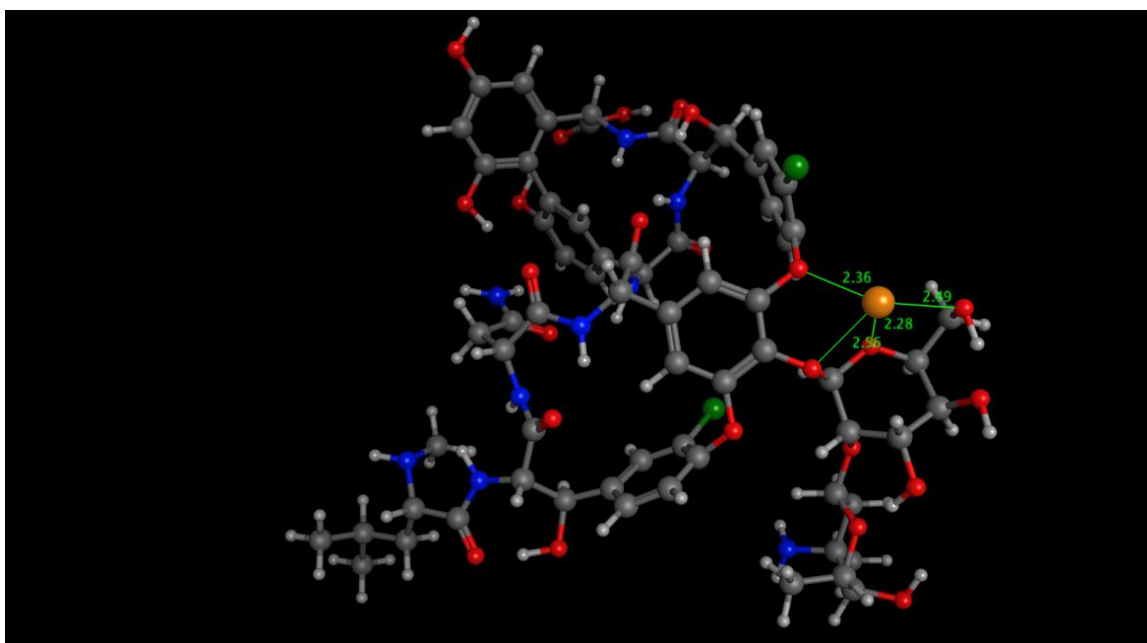
Vancomycin Conformation 12. *n*=35
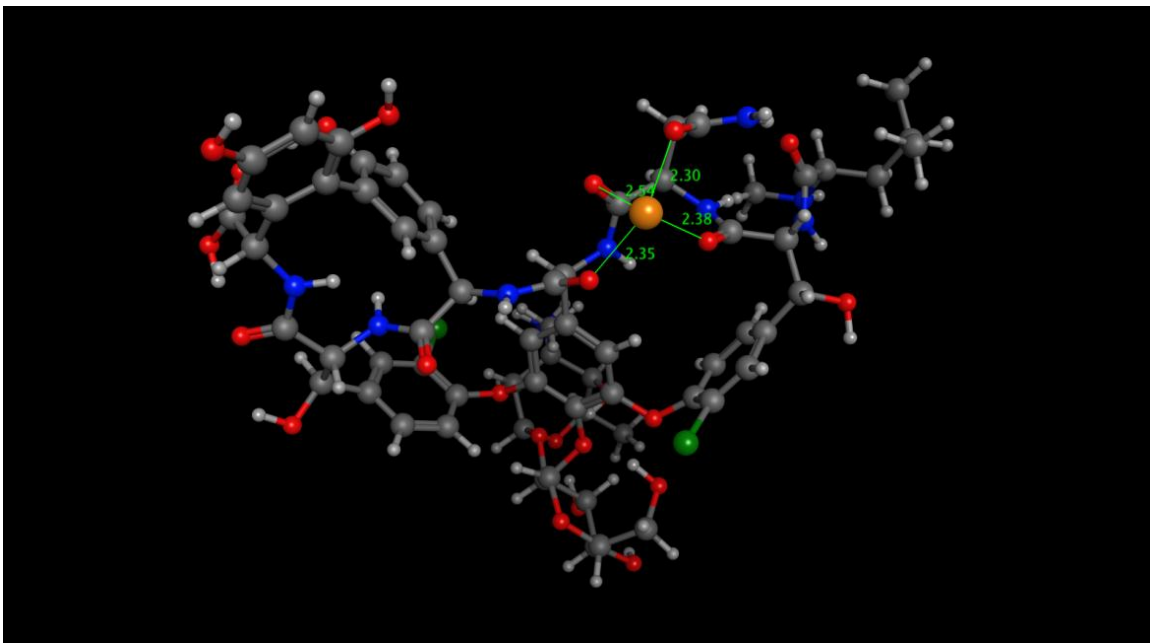
Vancomycin Conformation 13. *n*=45
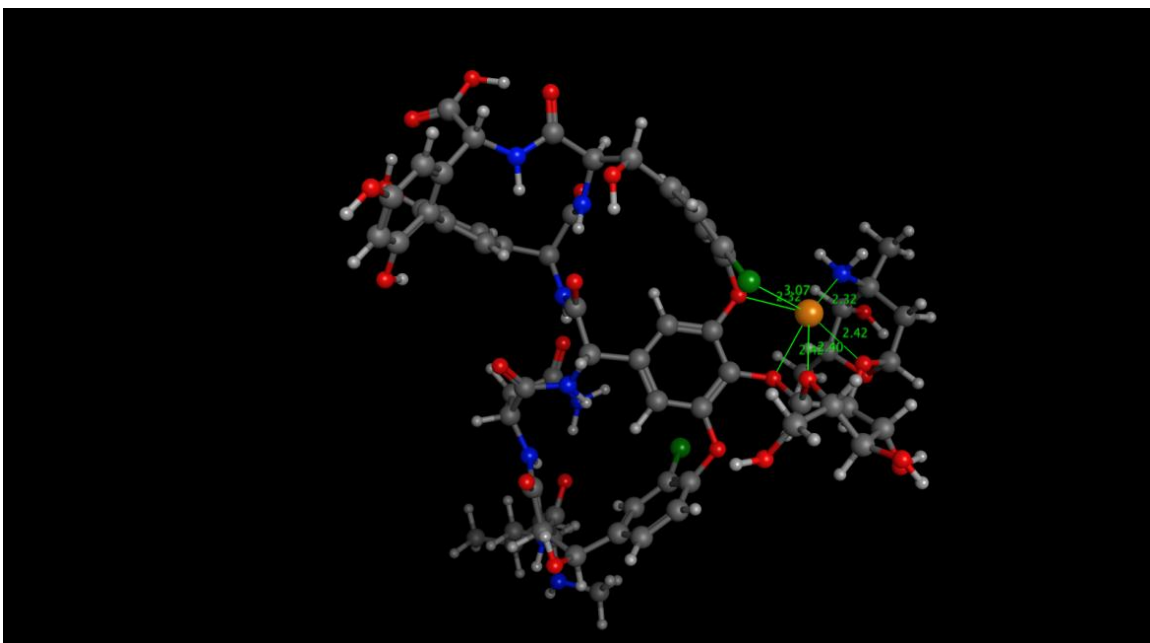
Vancomycin Conformation 14. *n*=58
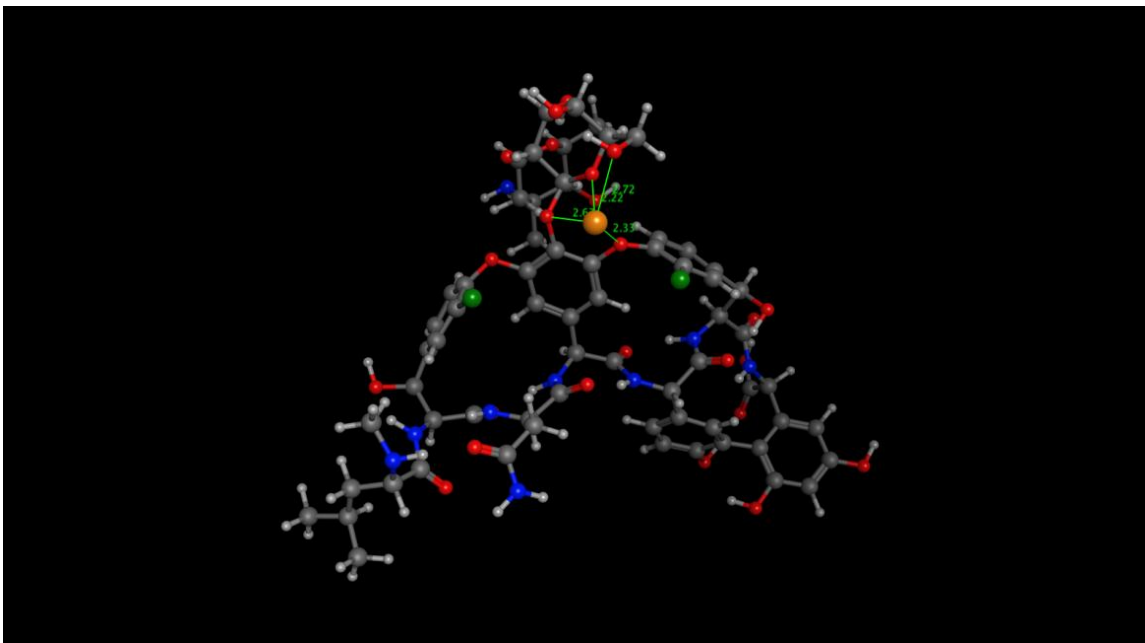
Vancomycin Conformation 15. *n*=44
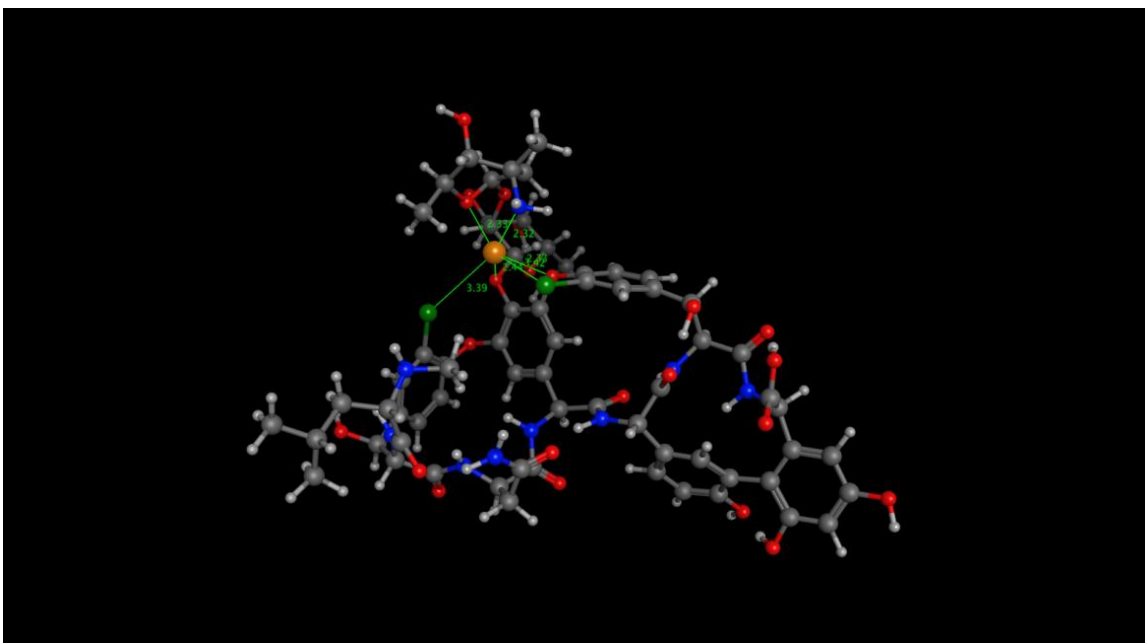
Vancomycin Conformation 16. *n*=90
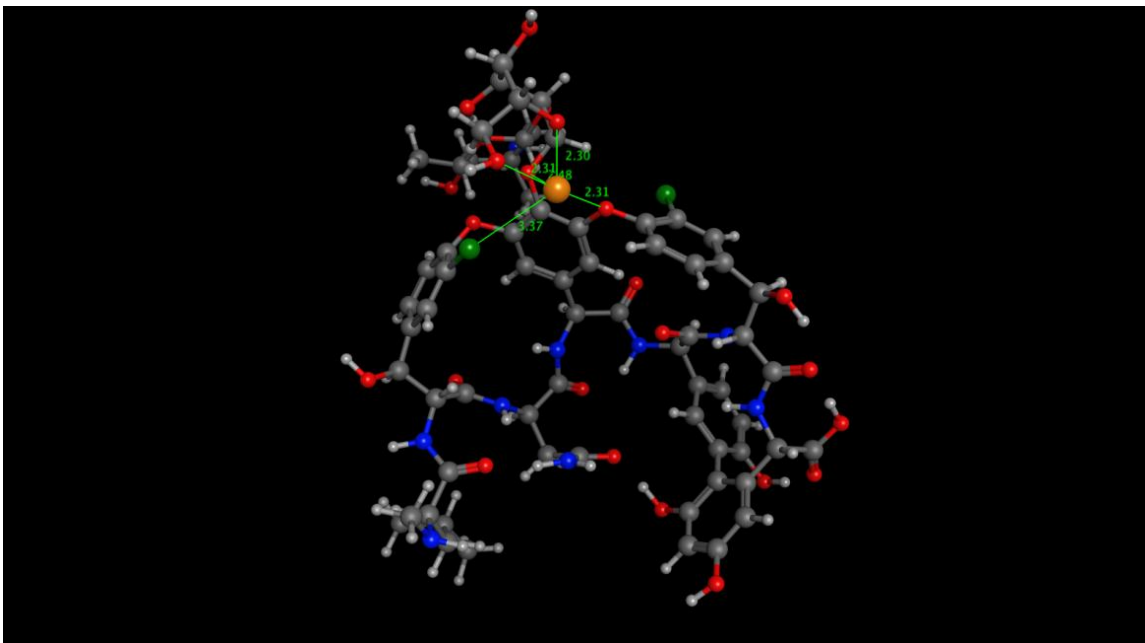
Vancomycin Conformation 17. *n*=45
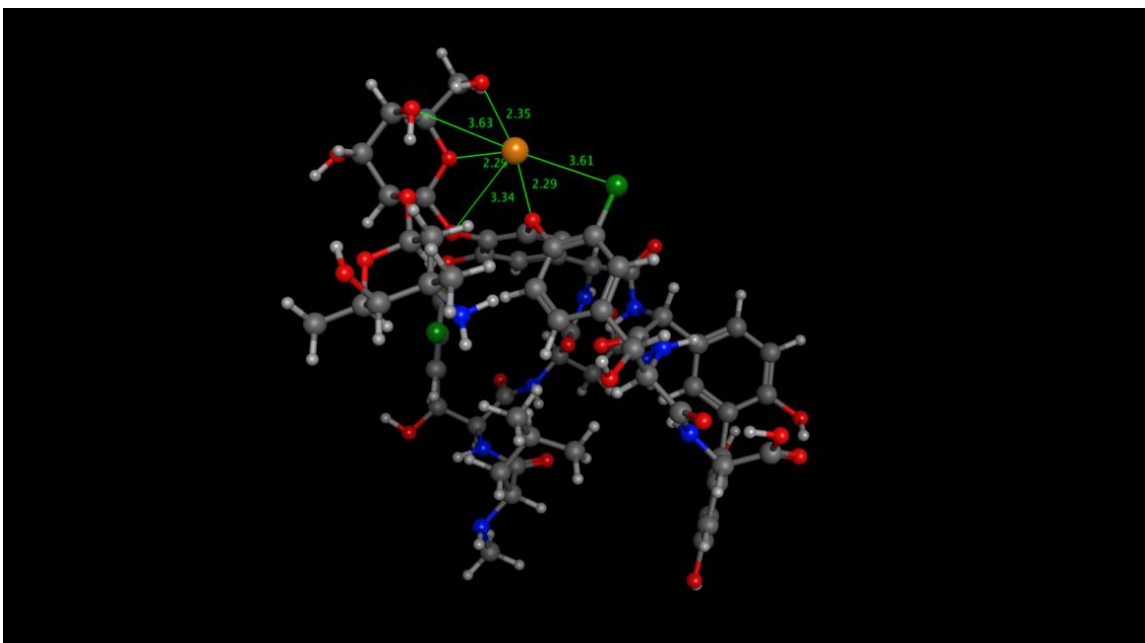
Vancomycin Conformation 18. *n*=29
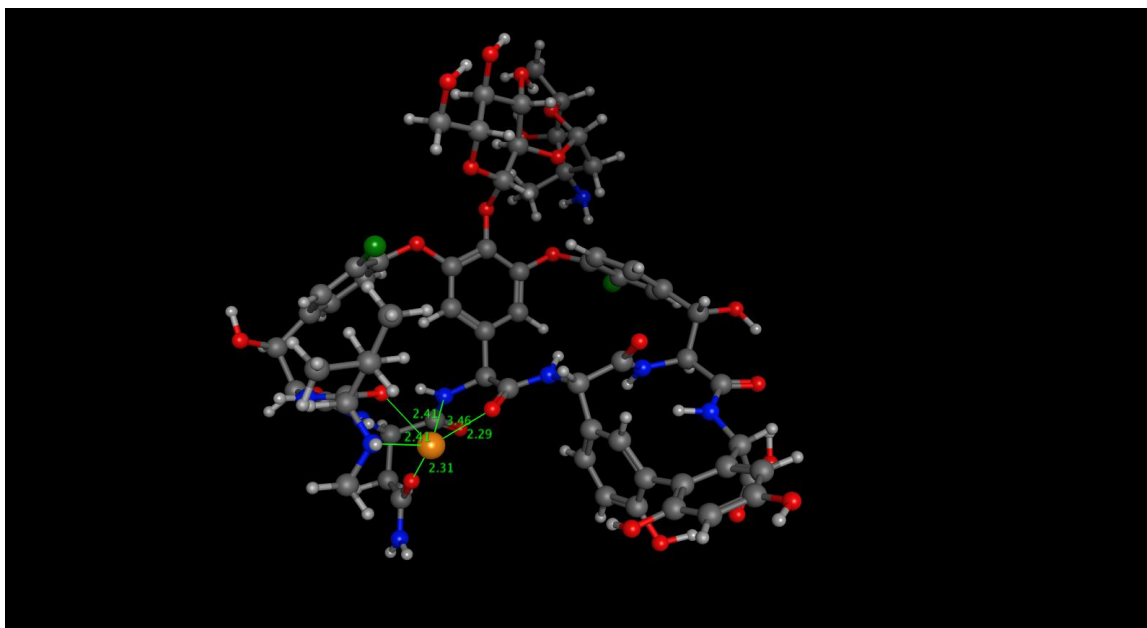
Vancomycin Conformation 19. *n*=154
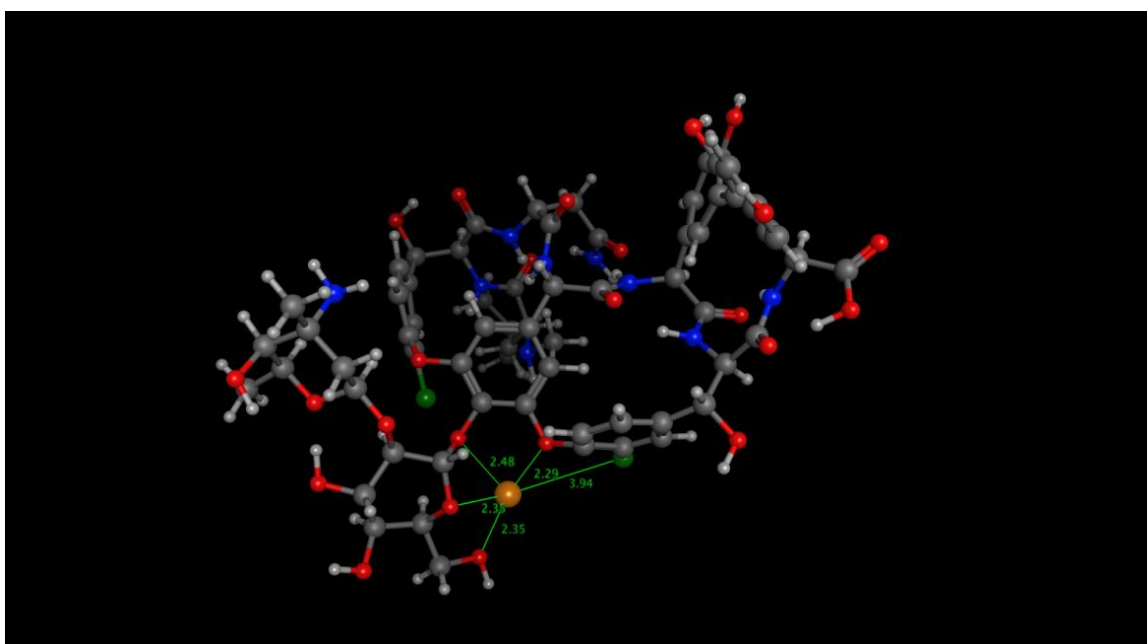
Vancomycin Conformation 20. *n*=43

Figure A2.4. Shown above are the 20 representative conformations of sodiated vancomycin generated from the simulated annealing molecular dynamics protocol. Each conformation represents between 30 and 300 structures, as indicated by *n.* Distances in Angstroms are annotated to indicate proximity of sodium cation. Carbon atoms are shown in grey, hydrogen in white, nitrogen in blue, oxygen in red, chlorine in green, and sodium in yellow.
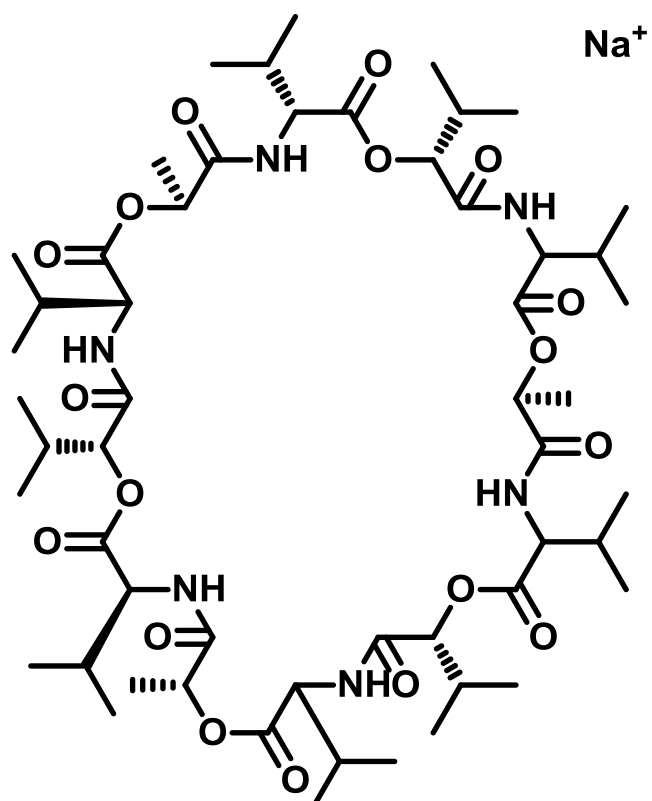
Figure A2.5. Chemical structure of sodiated valinomycin. Monoisotopic mass was measured to be 1133.34Da. The calculated collision cross section used for conformation discrimination is 269.72 ± 1.65 $Å^2$, which is a window two times the error of the measurement.

7.3

RMSD (Å)

0.4845
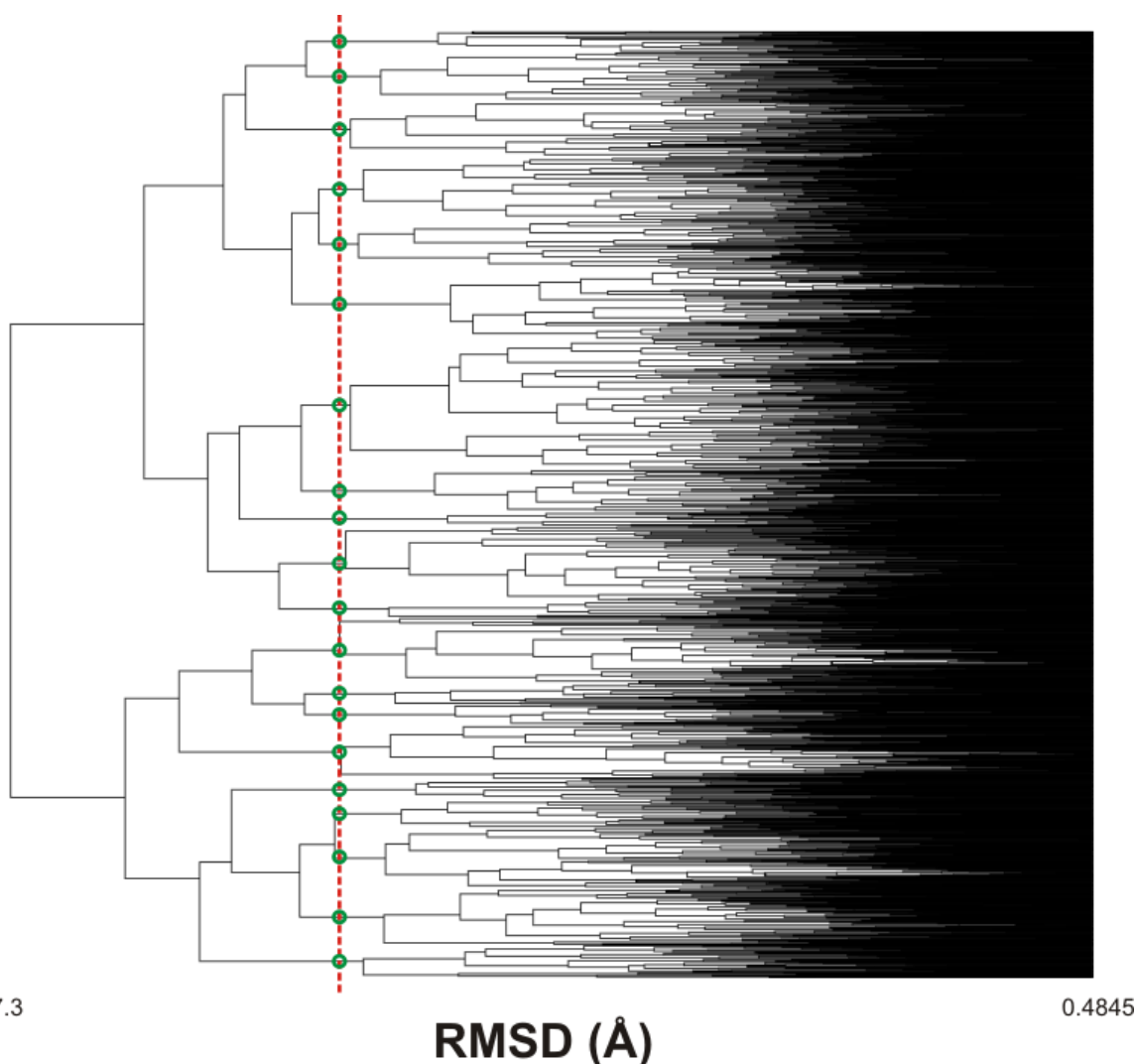
Figure A2.6. Clustering analysis of 302 sodiated valinomycin conformations extracted from a set of 24,000 based upon collision cross section correlation. As the tree progresses from right to left, the clustering tolerance is increased. Clustering was done on the basis of root mean square distance of atoms after superimposing structures. The red dashed line indicates the cutoff for the generation of representative conformations. The green circles correspond to each branch that represents the entire dataset. In the end, all conformations were distilled into 21 representative structures. A clustering cutoff of 5.09 Angstroms was implemented.
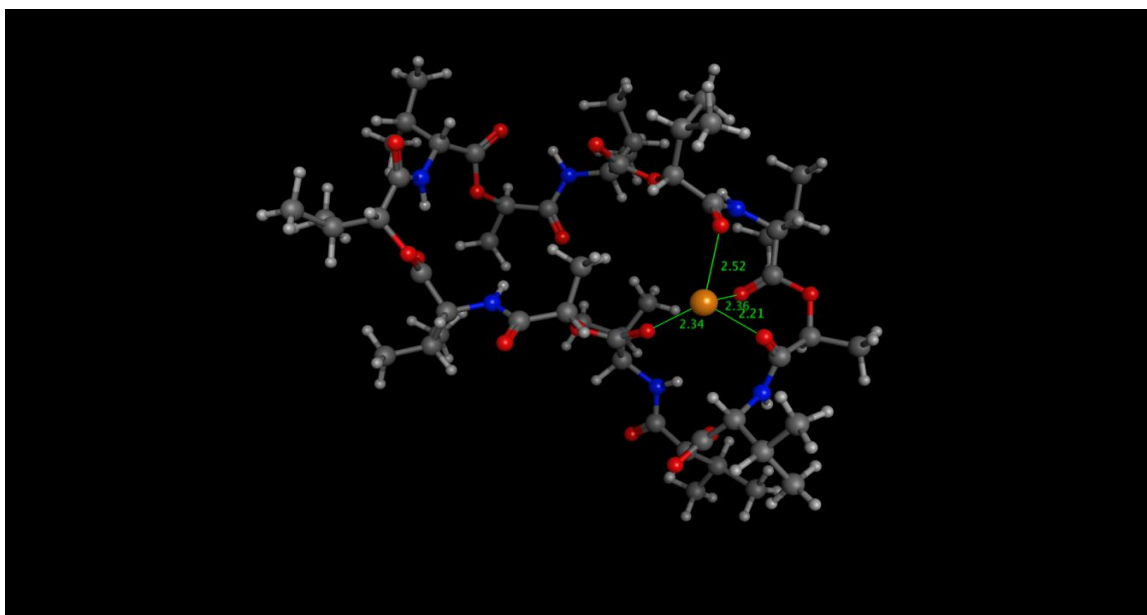
Valinomycin Conformation 1. *n=7*
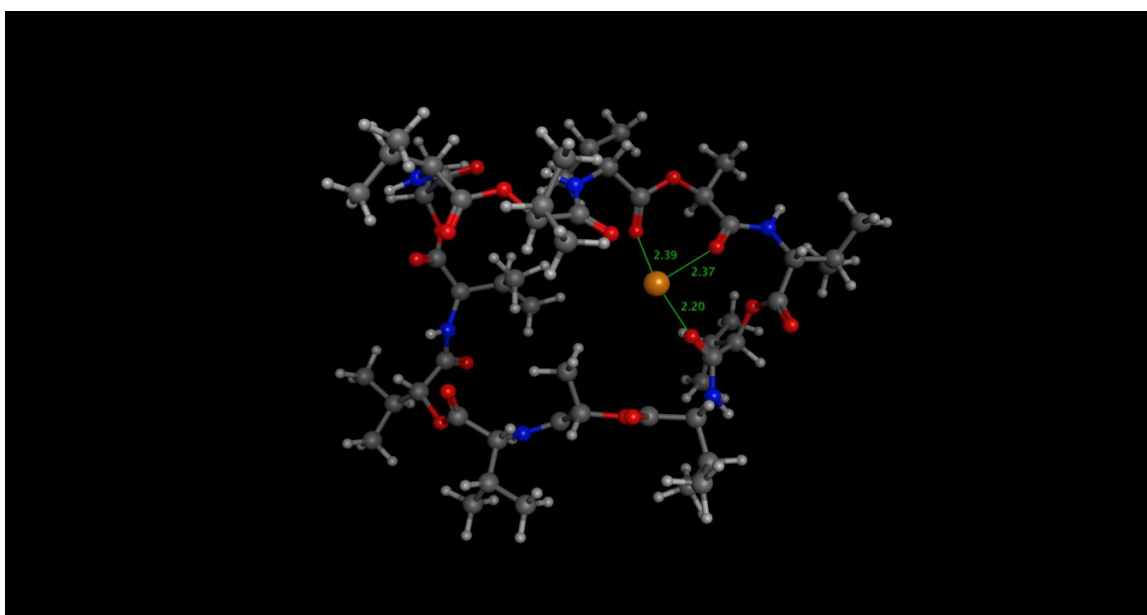
Valinomycin Conformation 2. *n=6*
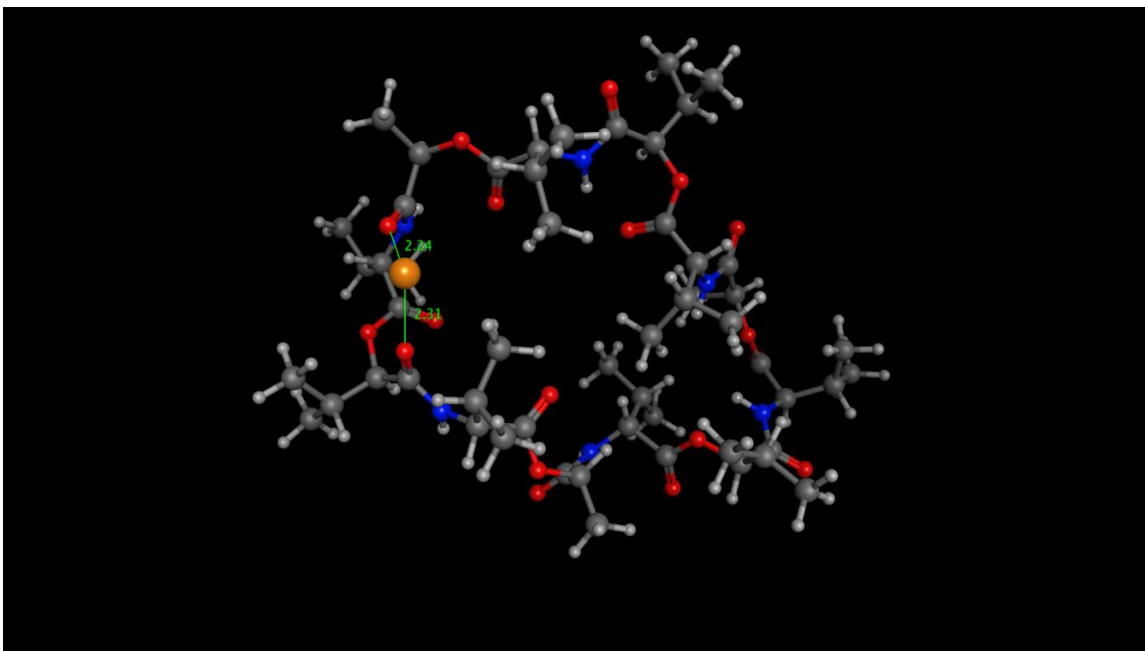
Valinomycin Conformation 3. *n*=12
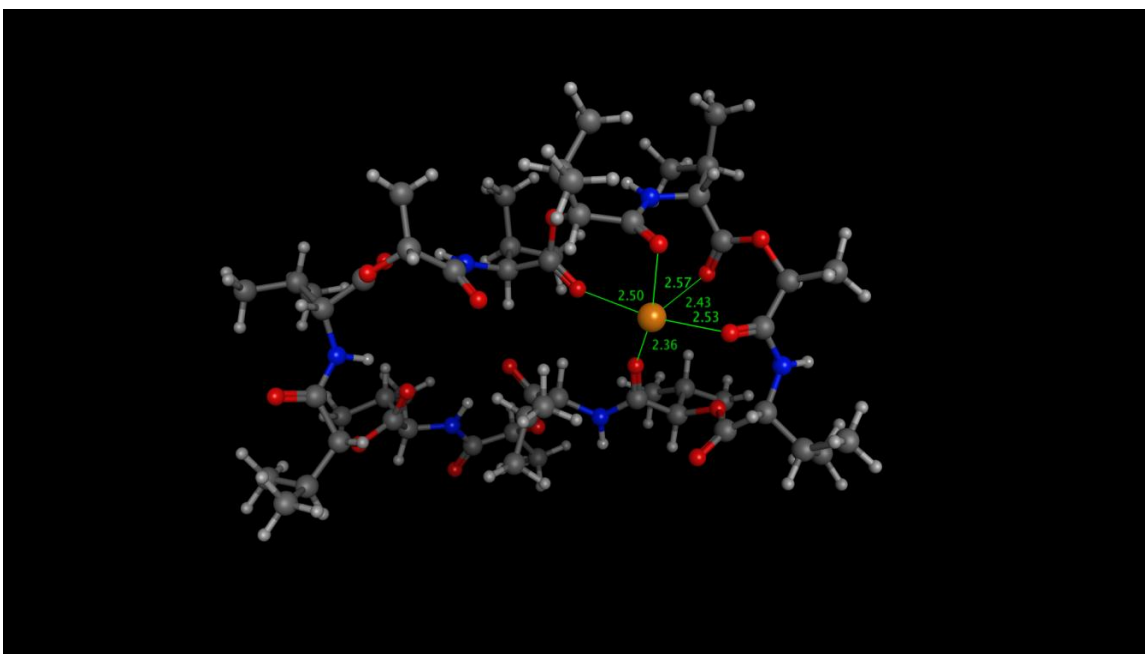
Valinomycin Conformation 4. *n*=6
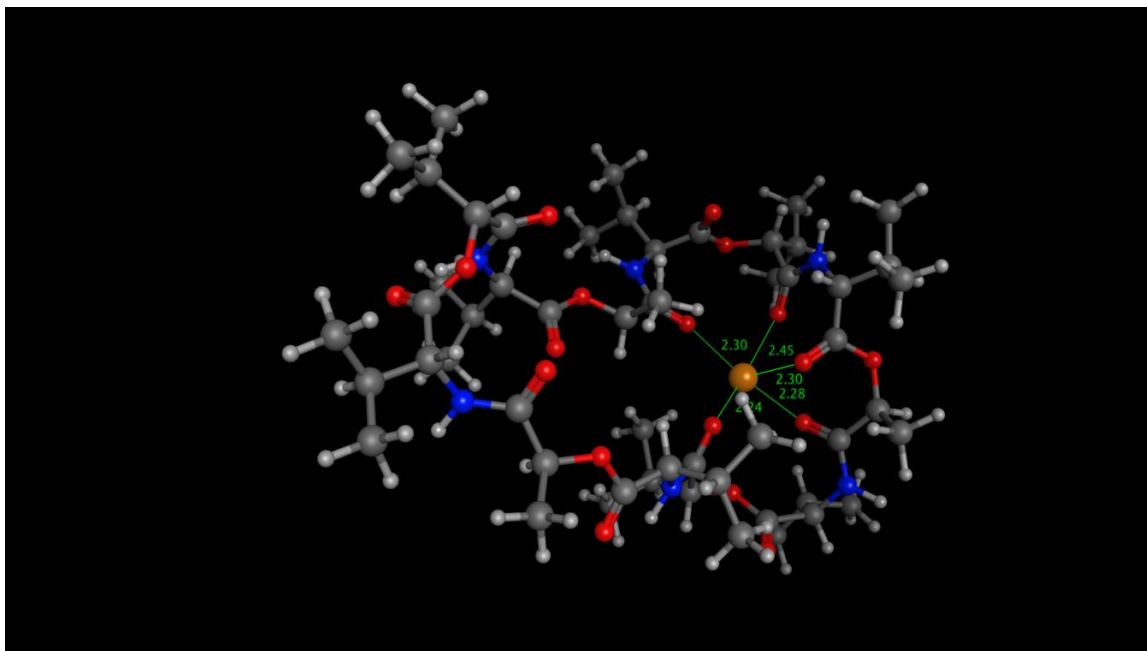
Valinomycin Conformation 5. *n*=12
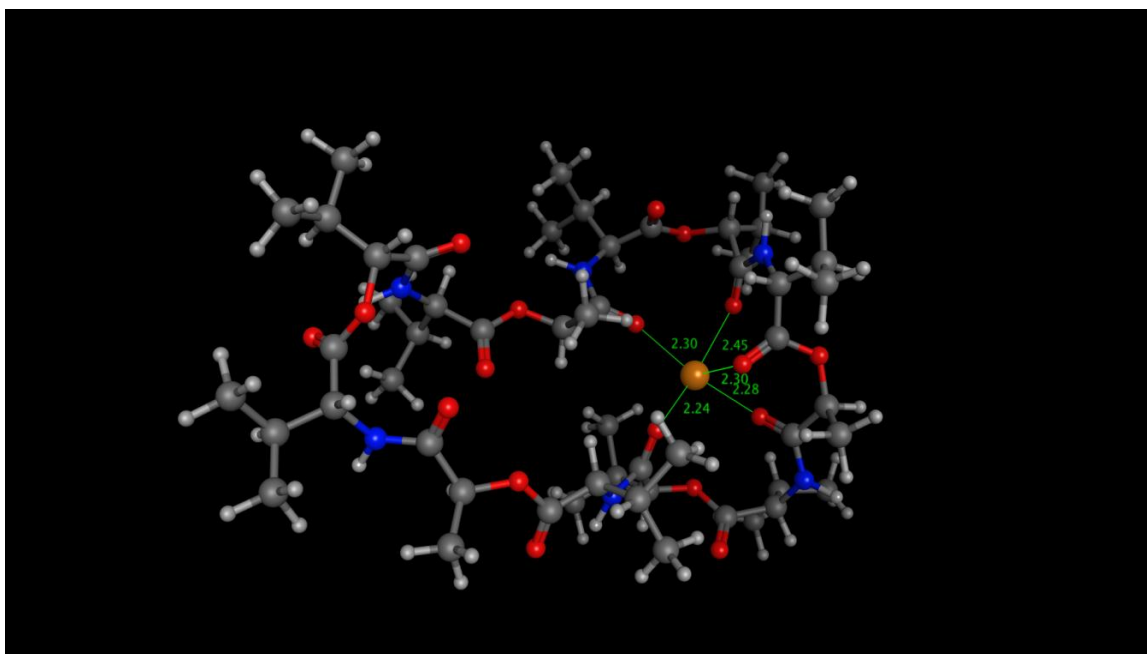
Valinomycin Conformation 6. *n*=14
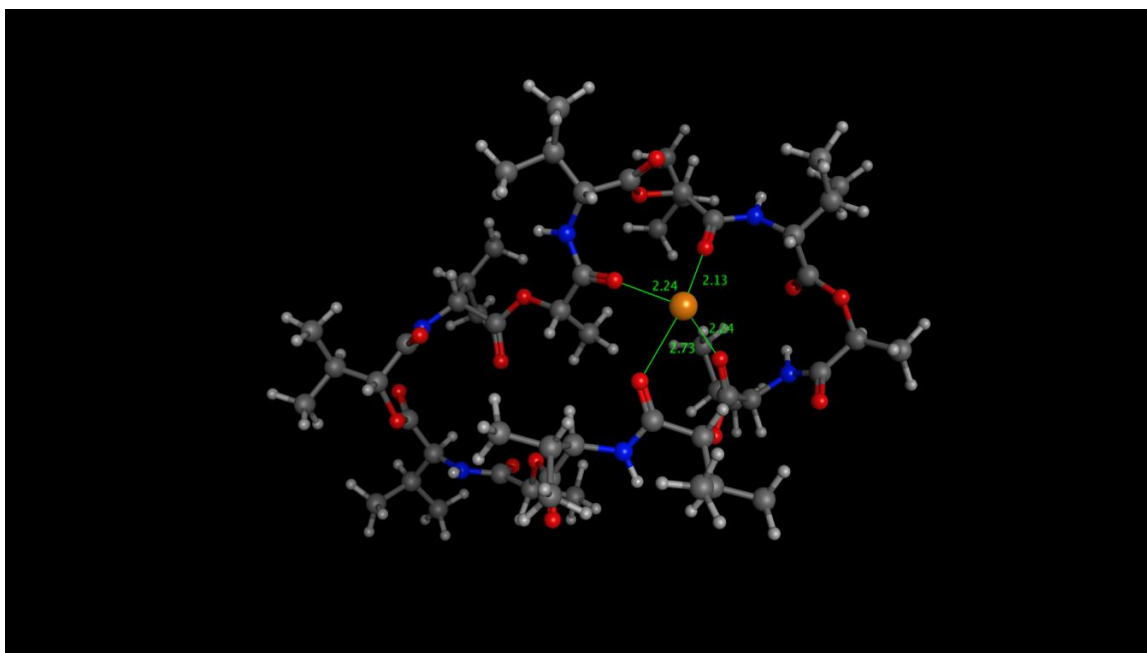
Valinomycin Conformation 7. *n*=7
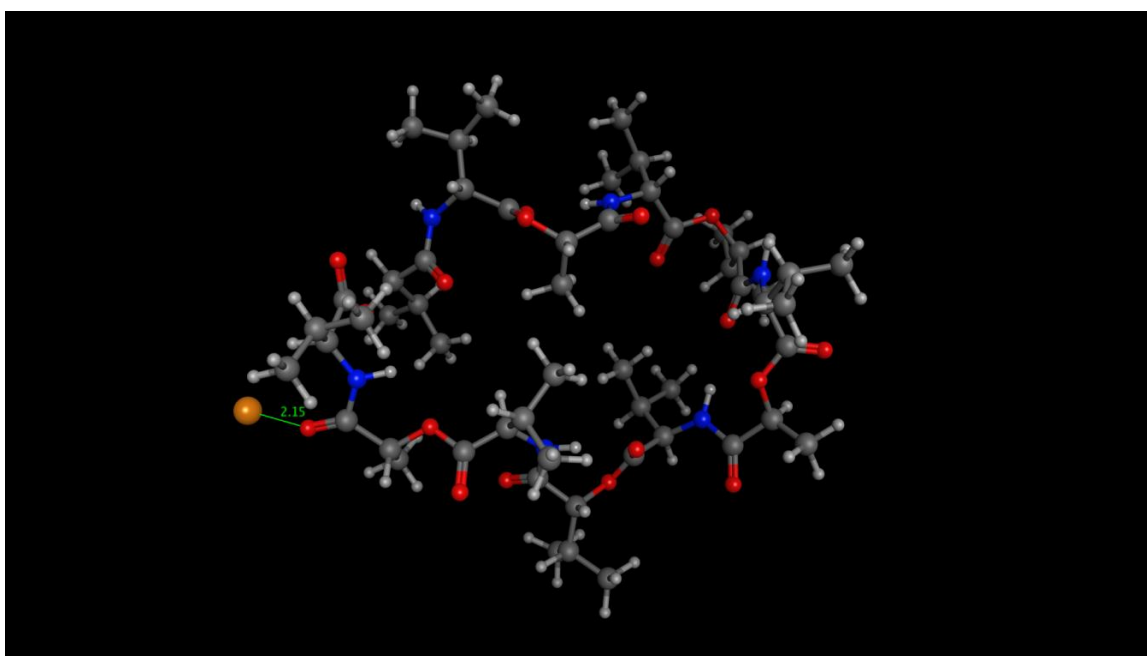
Valinomycin Conformation 8. *n*=5
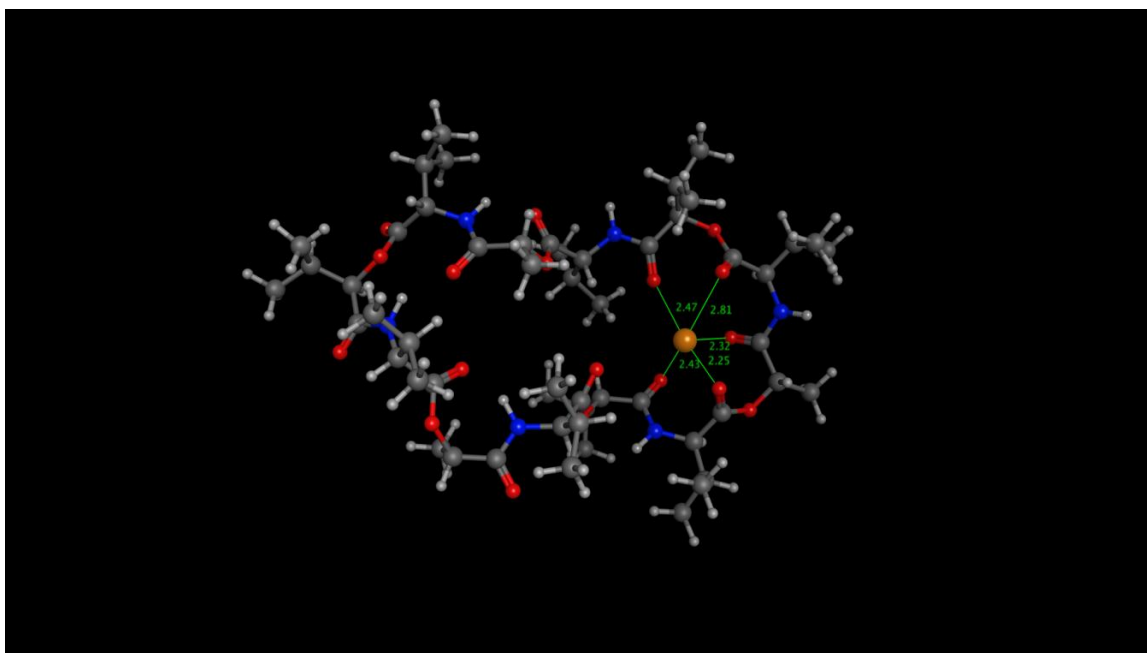
Valinomycin Conformation 9. *n*=14
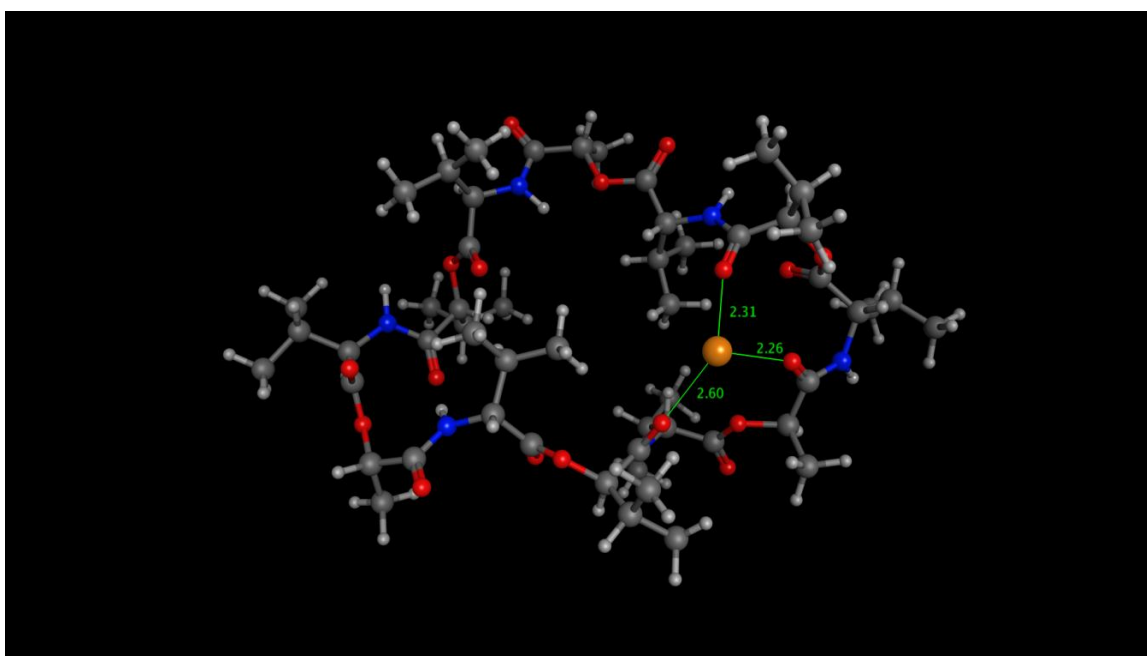
Valinomycin Conformation 10. *n*=25
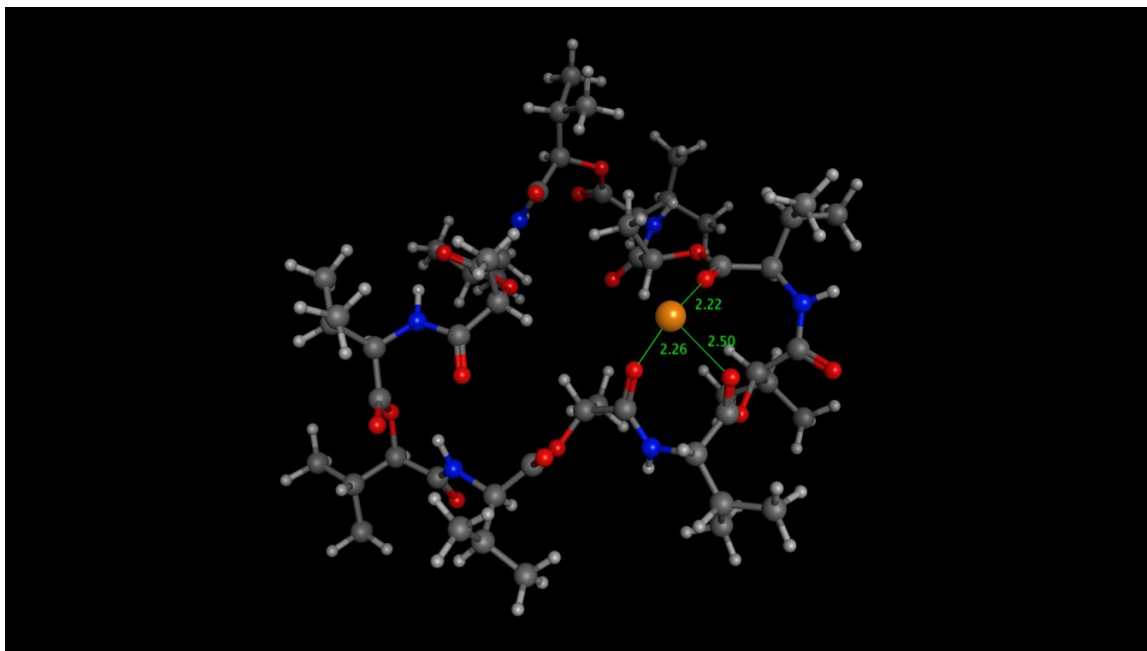
Valinomycin Conformation 11. *n*=15
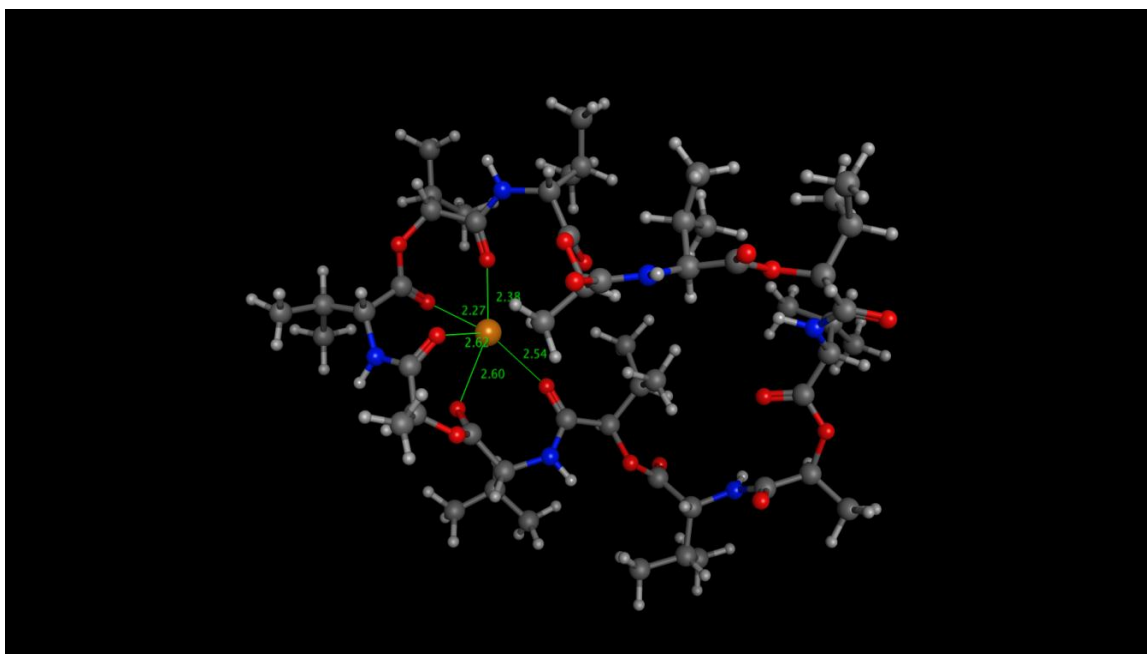
Valinomycin Conformation 12. *n*=21
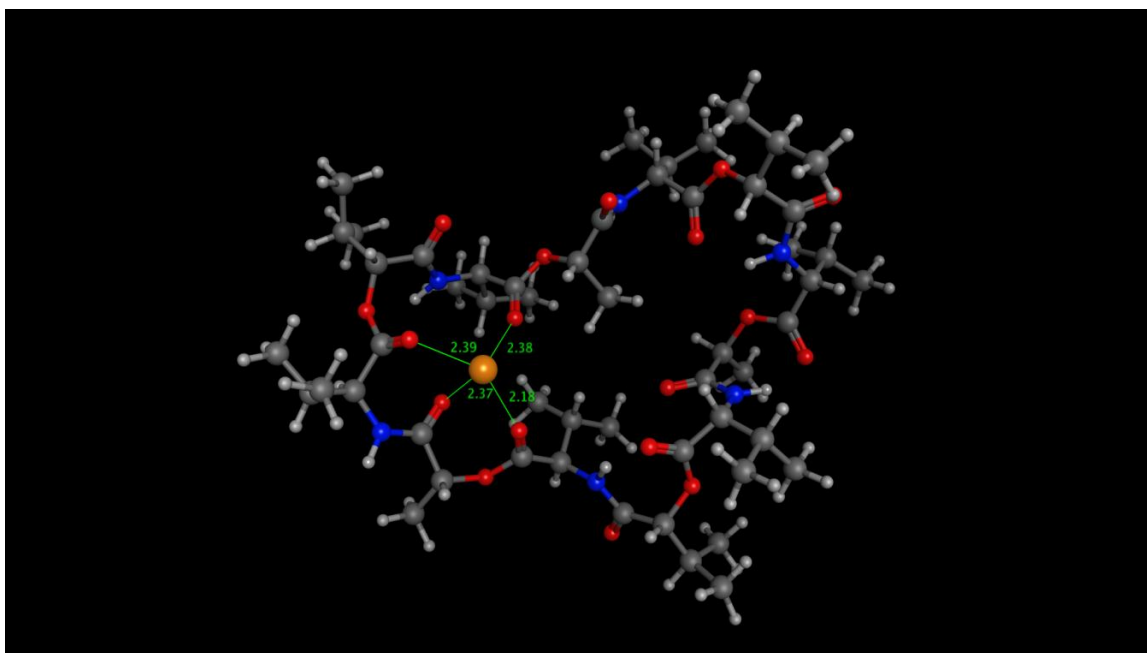
Valinomycin Conformation 13. *n*=18
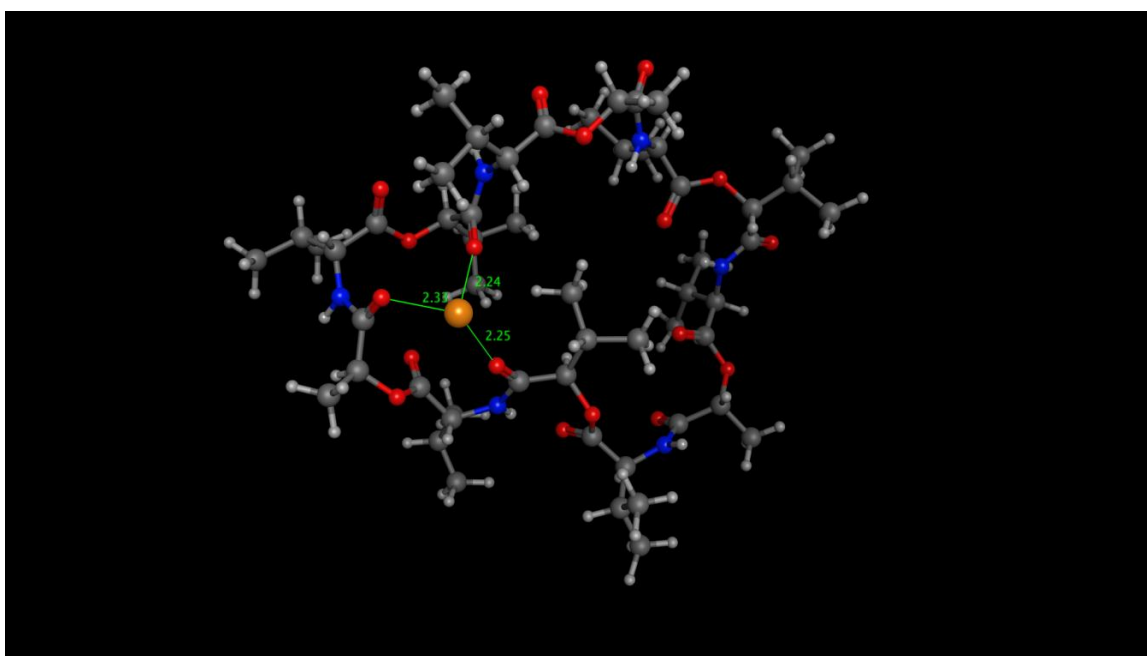
Valinomycin Conformation 14. *n*=9
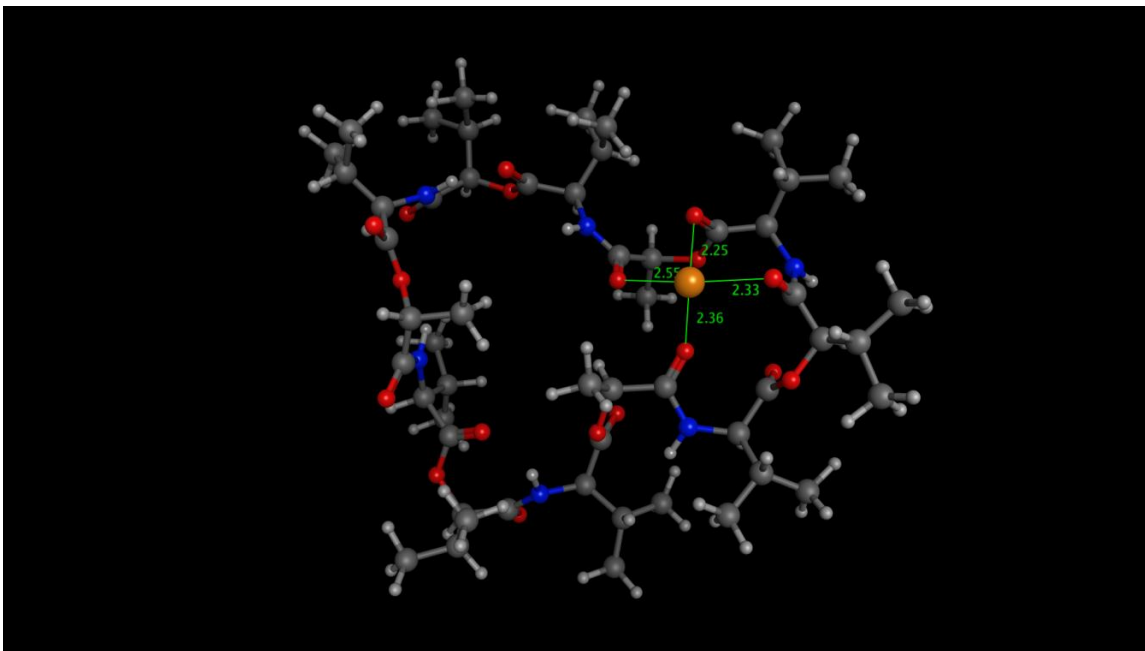
Valinomycin Conformation 15. *n*=20
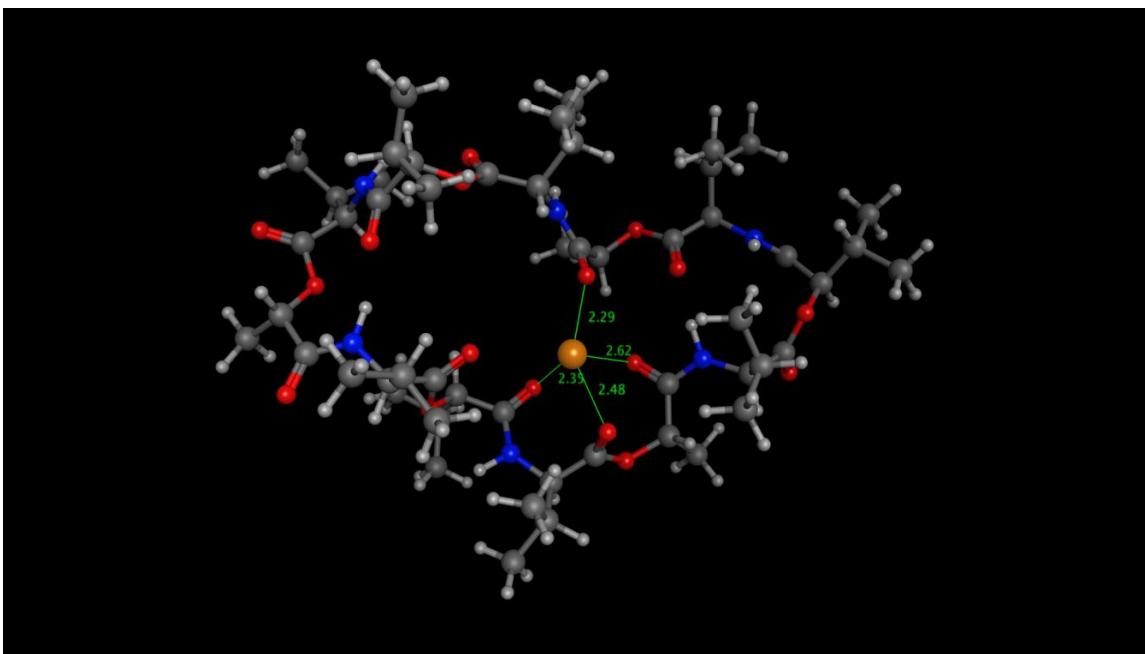
Valinomycin Conformation 16. *n*=18
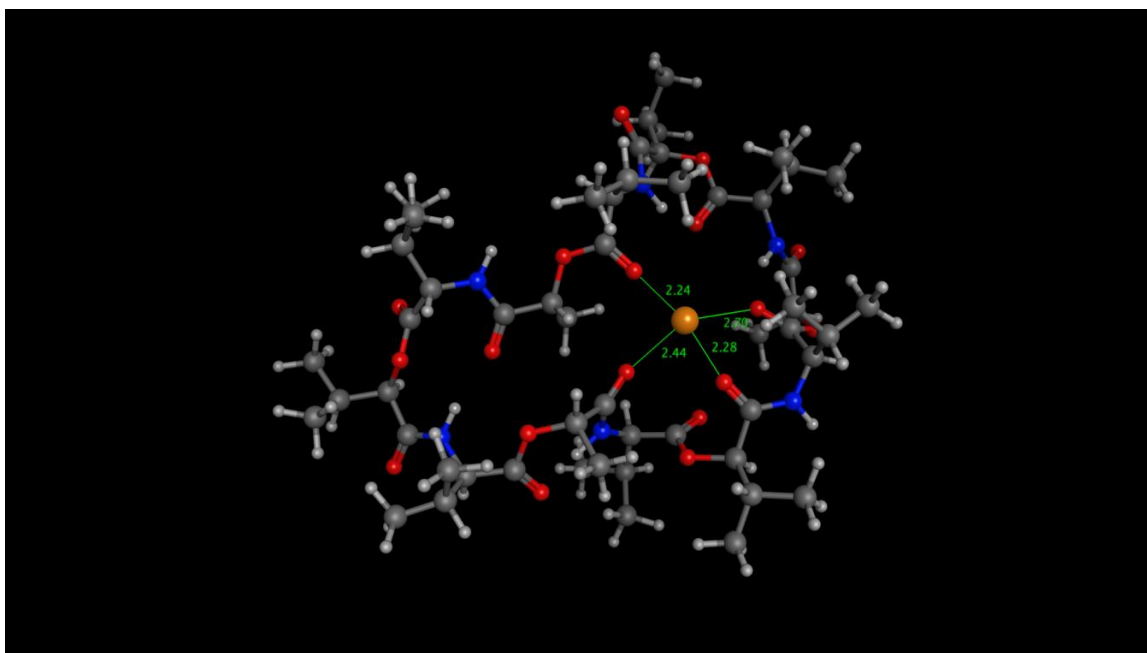
Valinomycin Conformation 17. *n*=11
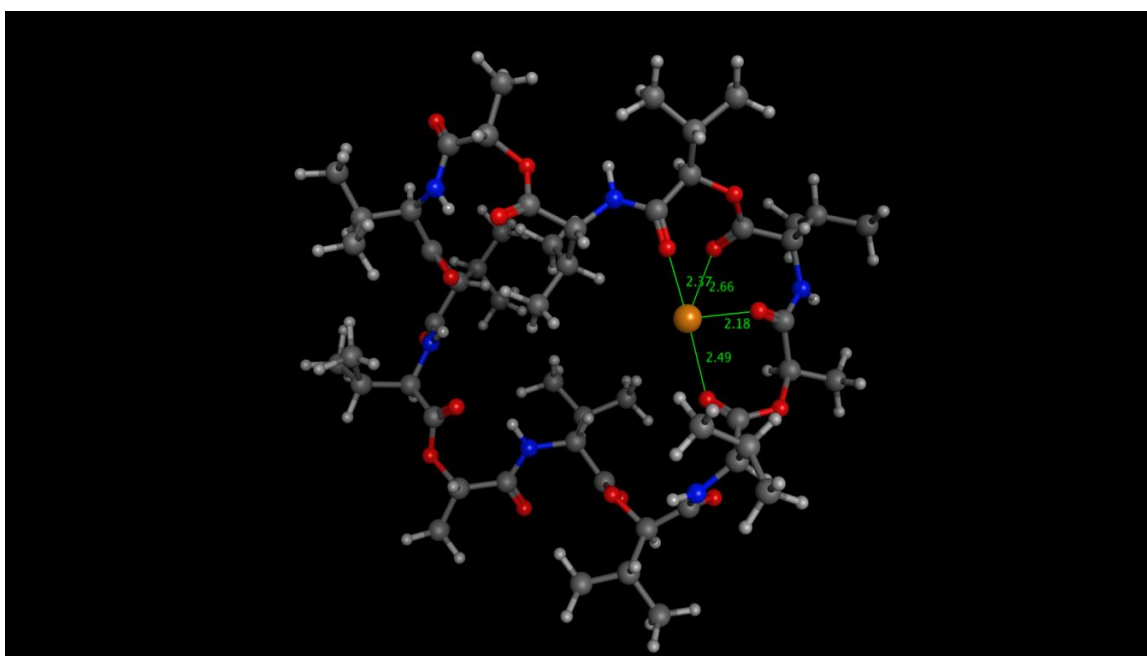
Valinomycin Conformation 18. *n*=10
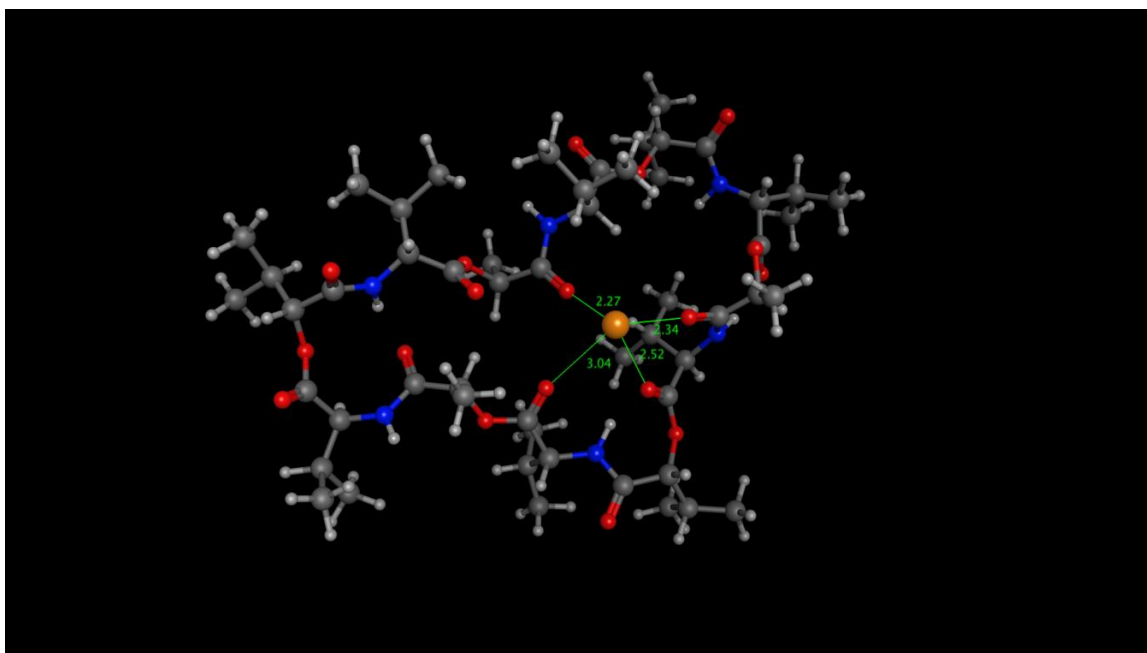
Valinomycin Conformation 19. *n*=30
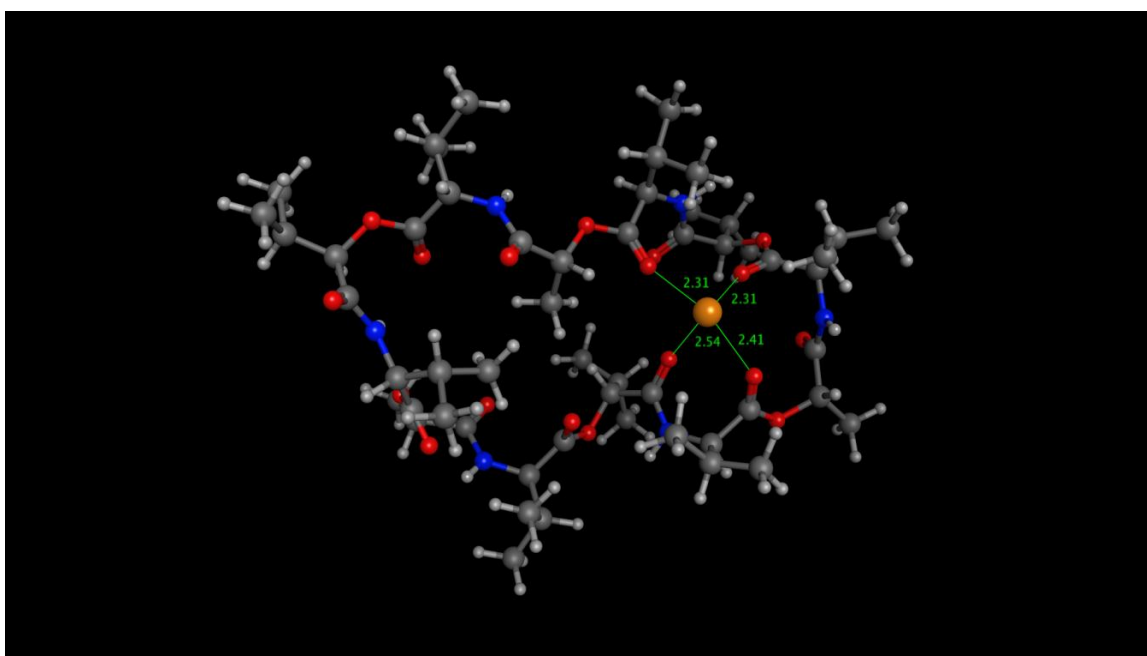
Valinomycin Conformation 20. *n*=16
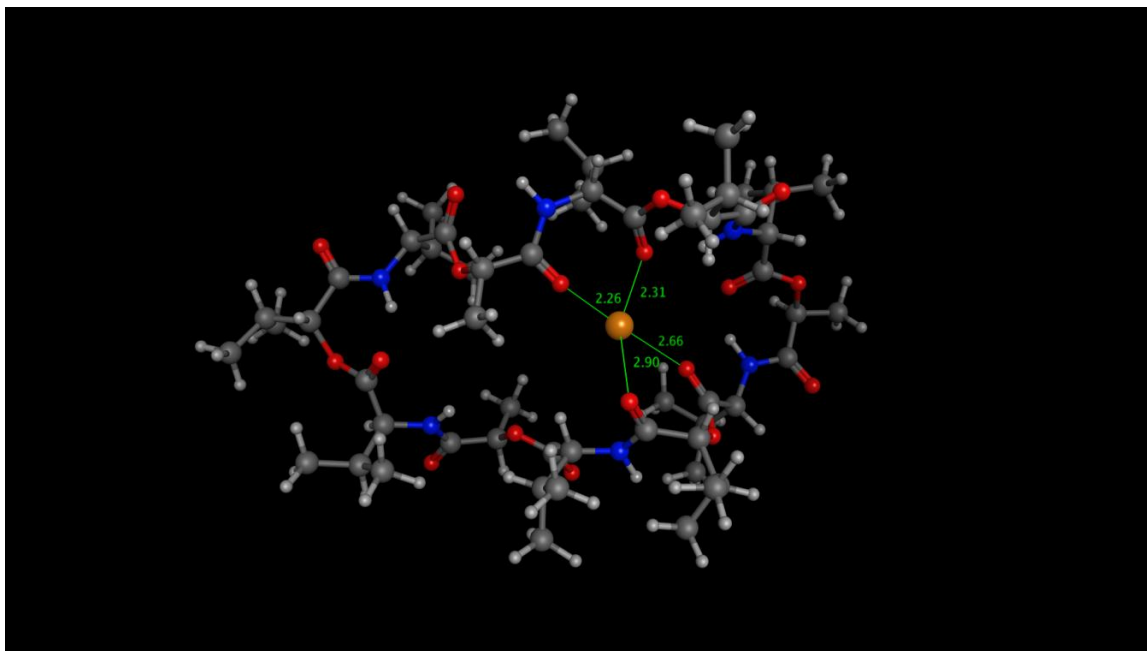
Valinomycin Conformation 21. *n*=26

Figure A2.7. Shown above are the 21 representative conformations of sodiated valinomycin generated from the simulated annealing molecular dynamics protocol. Each conformation represents between 5 and 30 structures, as indicated by *n.* Distances in Angstroms are annotated to indicate proximity of sodium cation. Carbon atoms are shown in grey, hydrogen in white, nitrogen in blue, oxygen in red, and sodium in yellow.
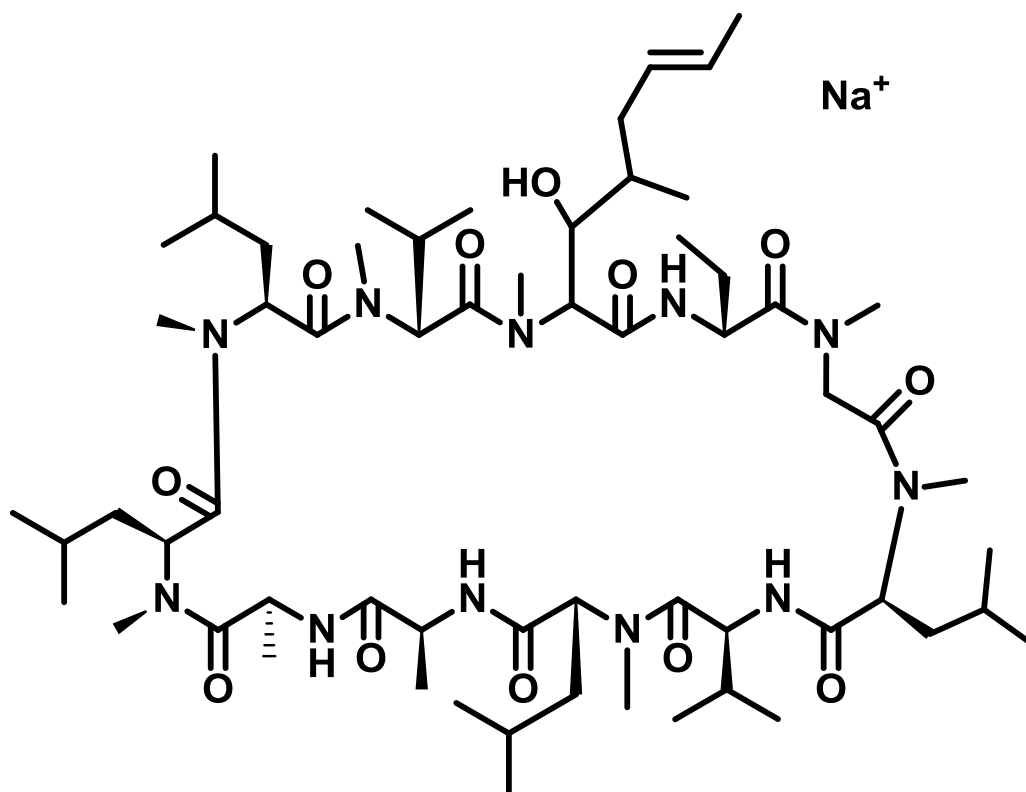
Figure A2.8. Chemical structure of sodiated cyclosporin A. Monoisotopic mass was measured to be 1224.40 Da. The calculated collision cross section used for conformation discrimination is 289.87 ± 2.37 $Å^2$, which is a window two times the error of the measurement.

7.49

1.843

RMSD (Å)
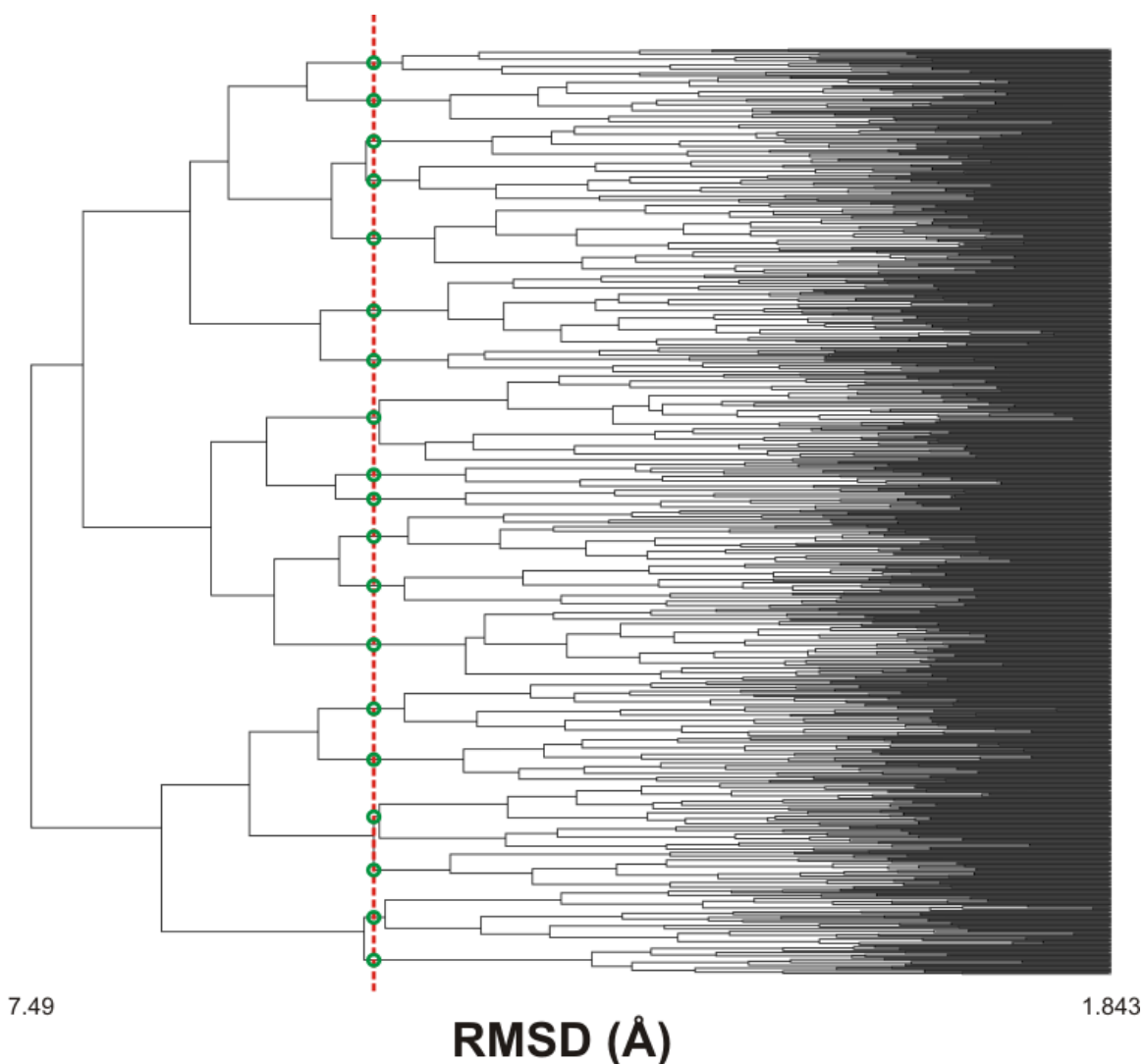
Figure A2.9. Clustering analysis of 807 sodiated cyclosporin A conformations extracted from a set of 24,000 based upon collision cross section correlation. As the tree progresses from right to left, the clustering tolerance is increased. Clustering was done on the basis of root mean square distance of atoms after superimposing structures. The red dashed line indicates the cutoff for the generation of representative conformations. The green circles correspond to each branch that represents the entire dataset. In the end, all conformations were distilled into 19 representative structures. A clustering cutoff of 5.67 Angstroms was implemented.
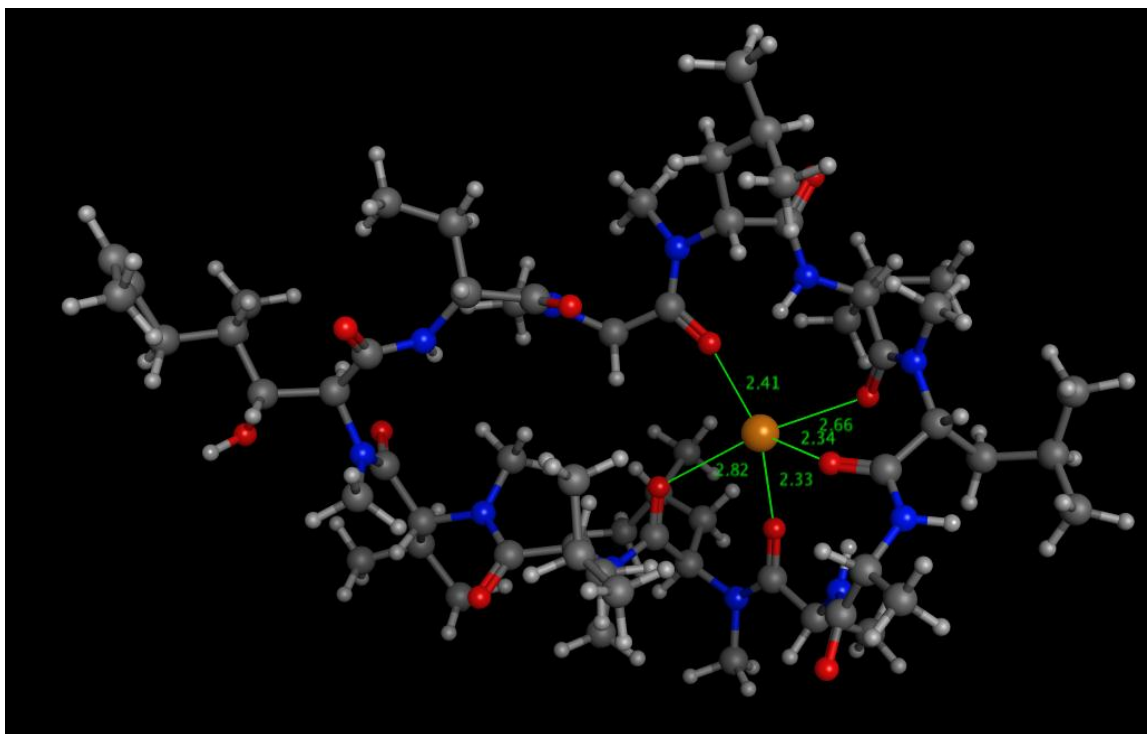
Cyclosporin A Structure 1. *n*=76
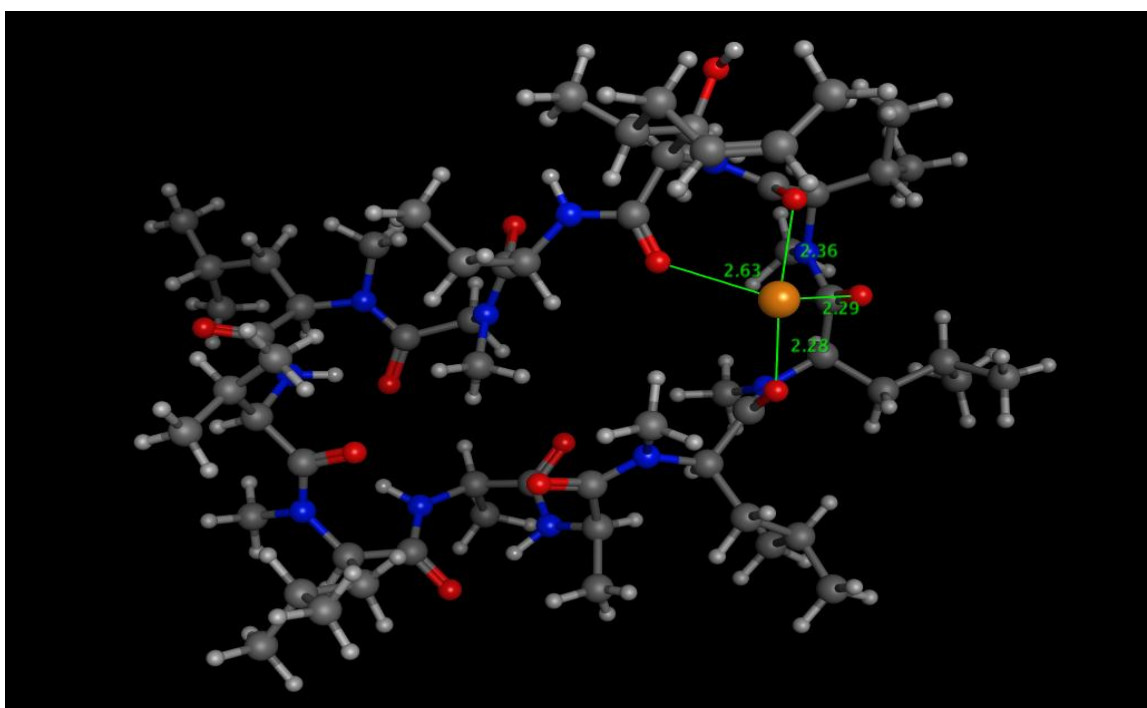
Cyclosporin A Structure 2. *n*=59
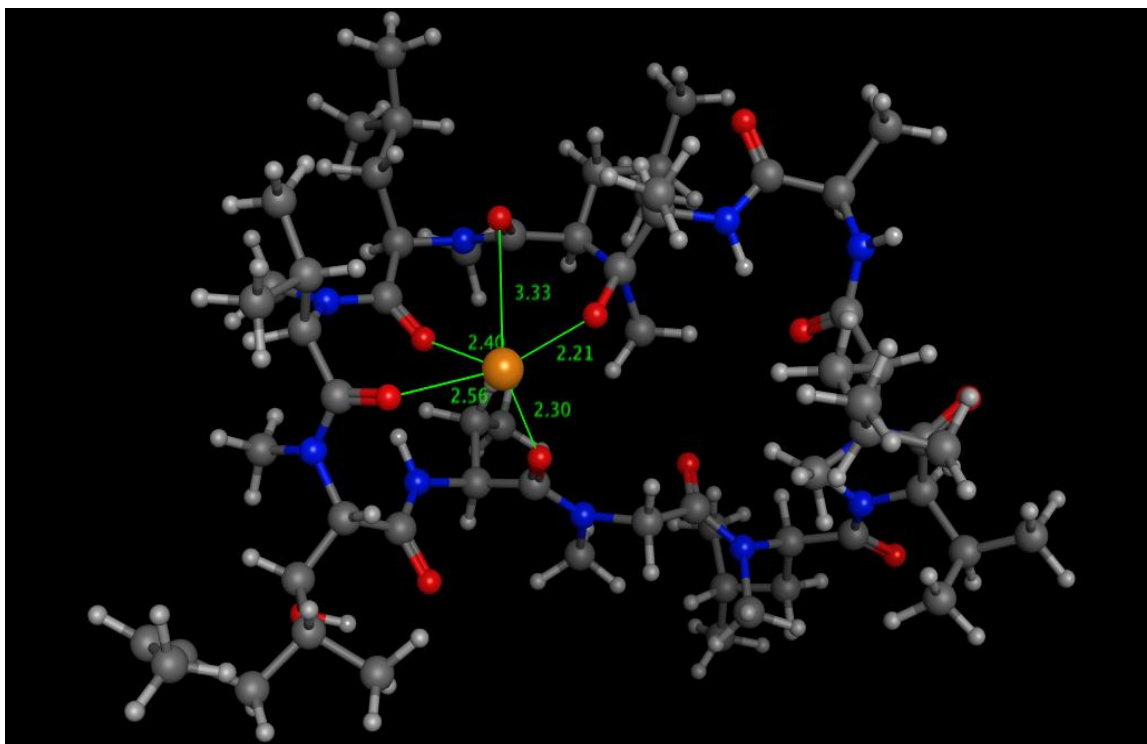
Cyclosporin A Structure 3. *n*=49
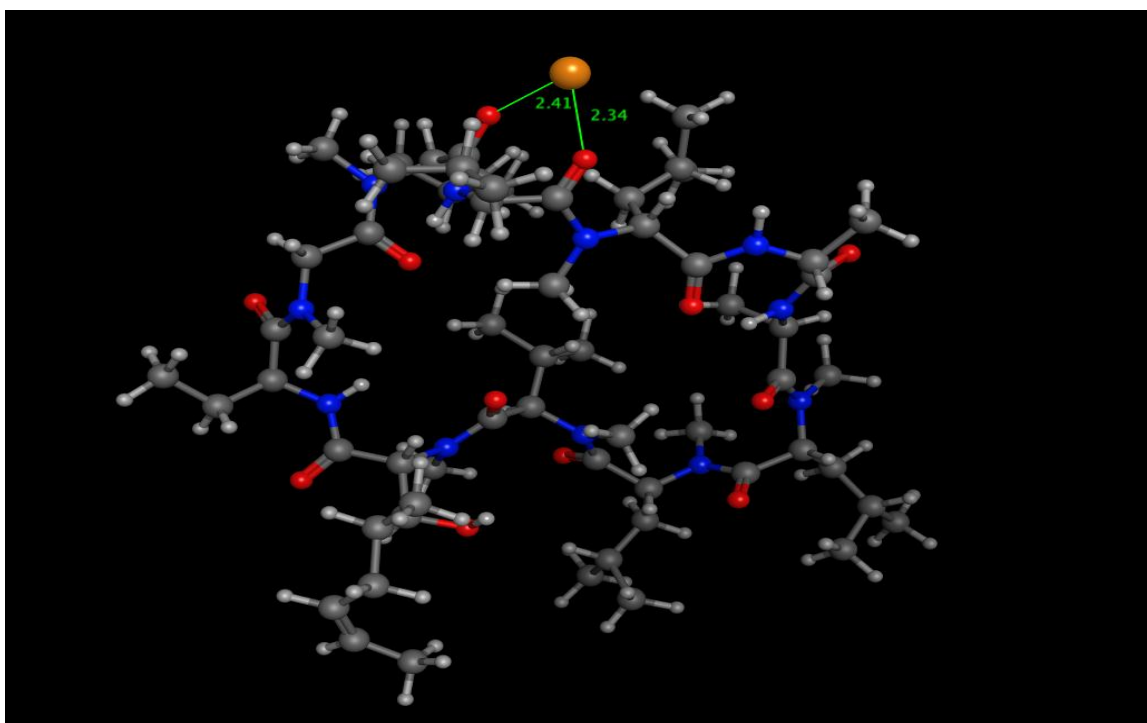
Cyclosporin A Structure 4. *n*=24
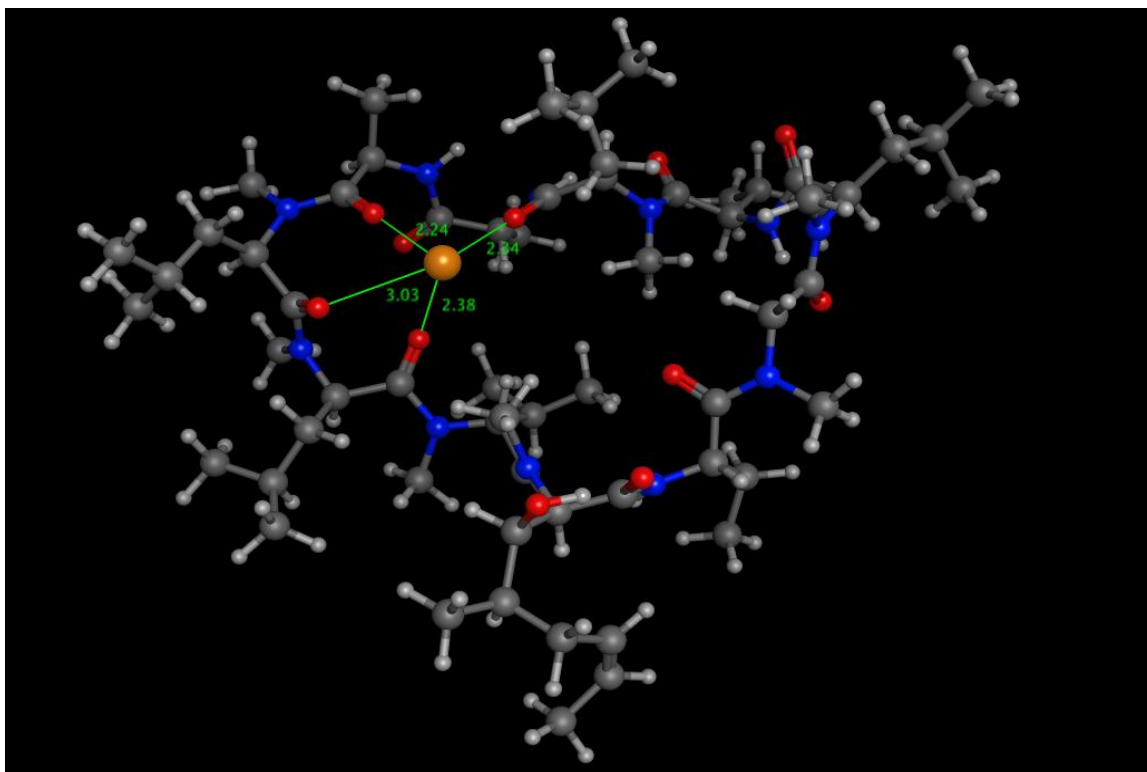
Cyclosporin A Structure 5. *n*=48
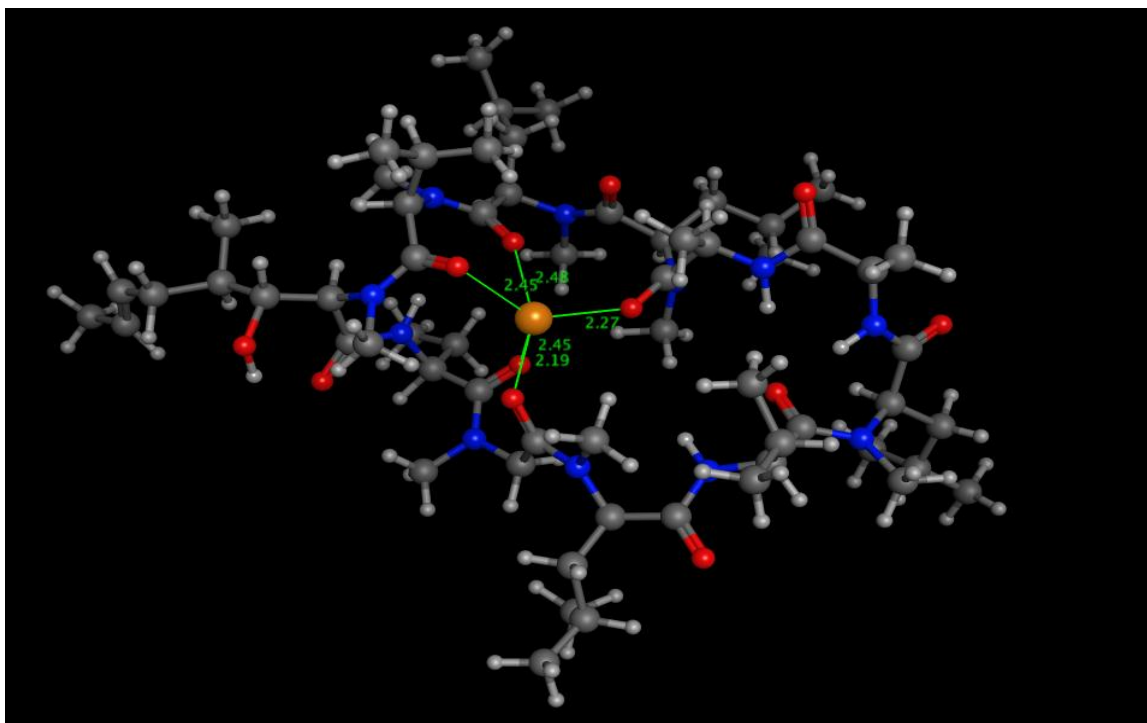
Cyclosporin A Structure 6. *n*=39
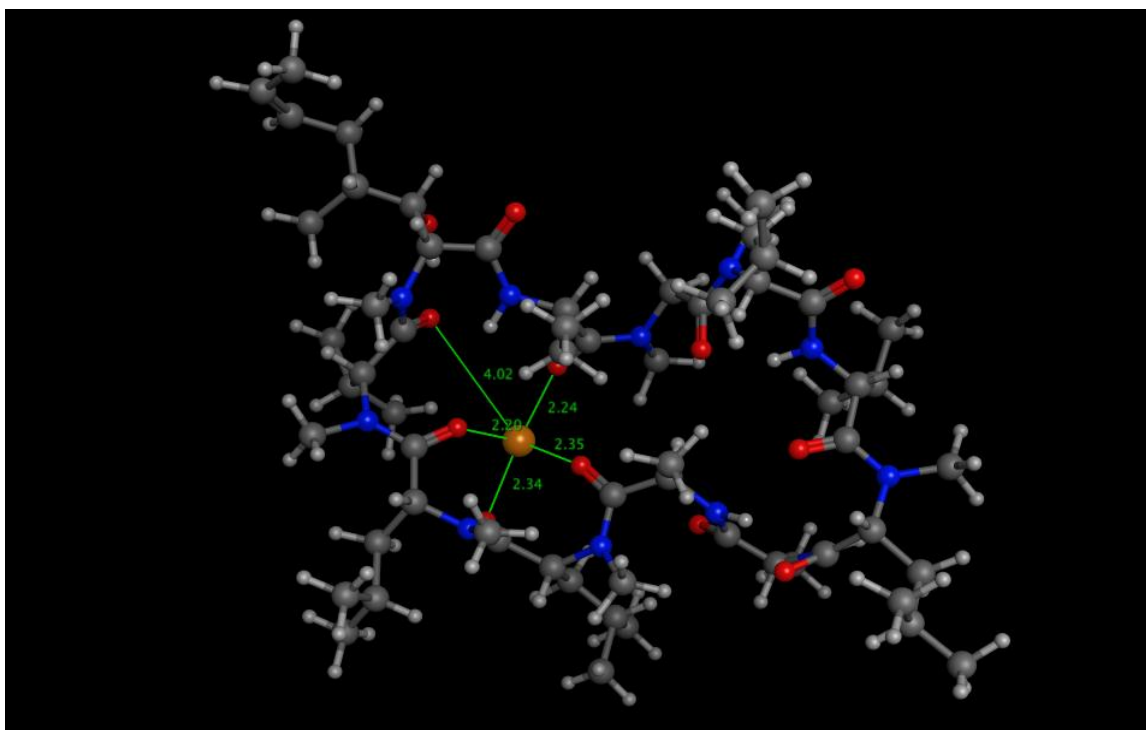
Cyclosporin A Structure 7. *n*=46
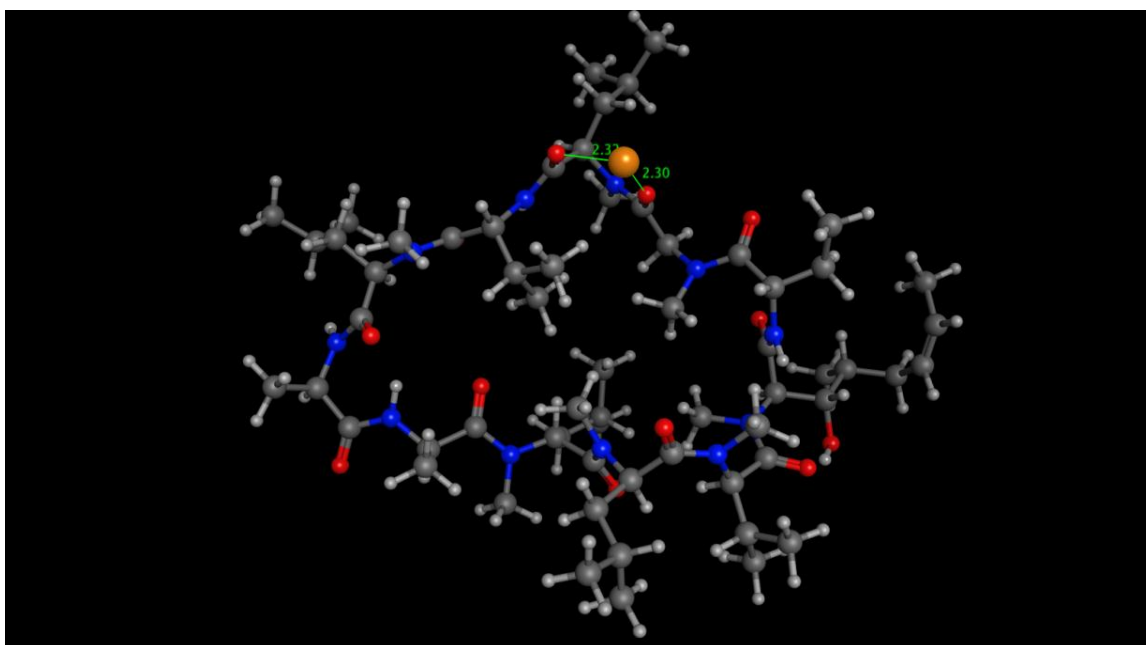
Cyclosporin A Structure 8. *n*=38
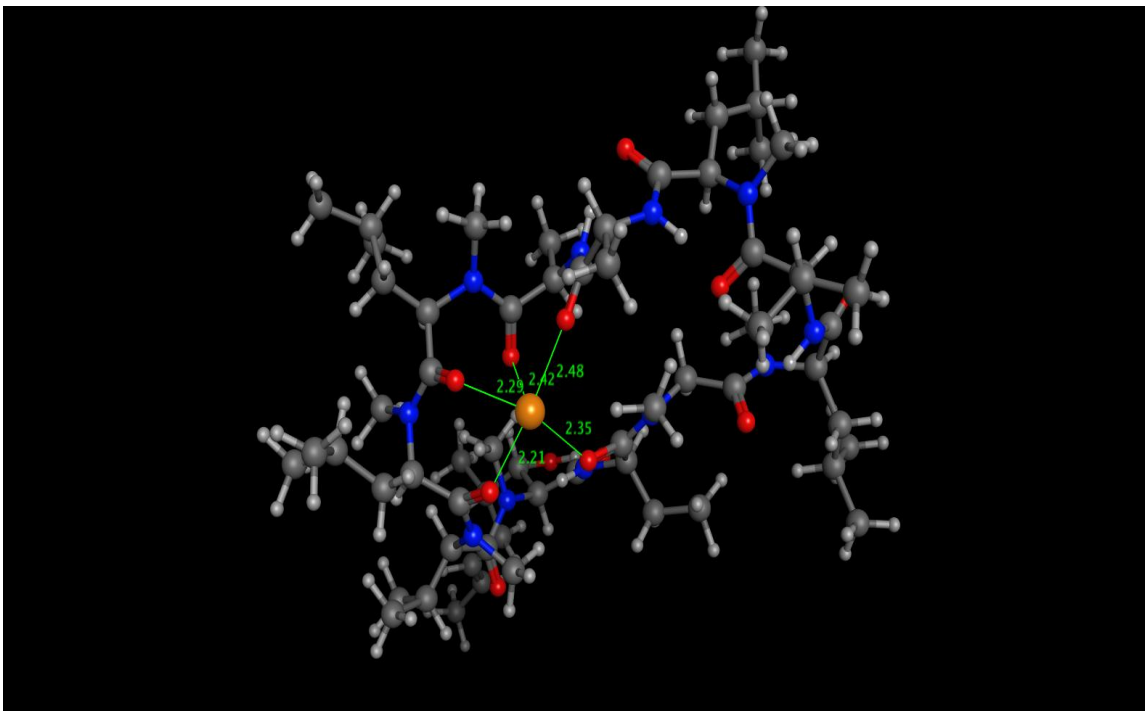
Cyclosporin A Structure 9. *n*=62
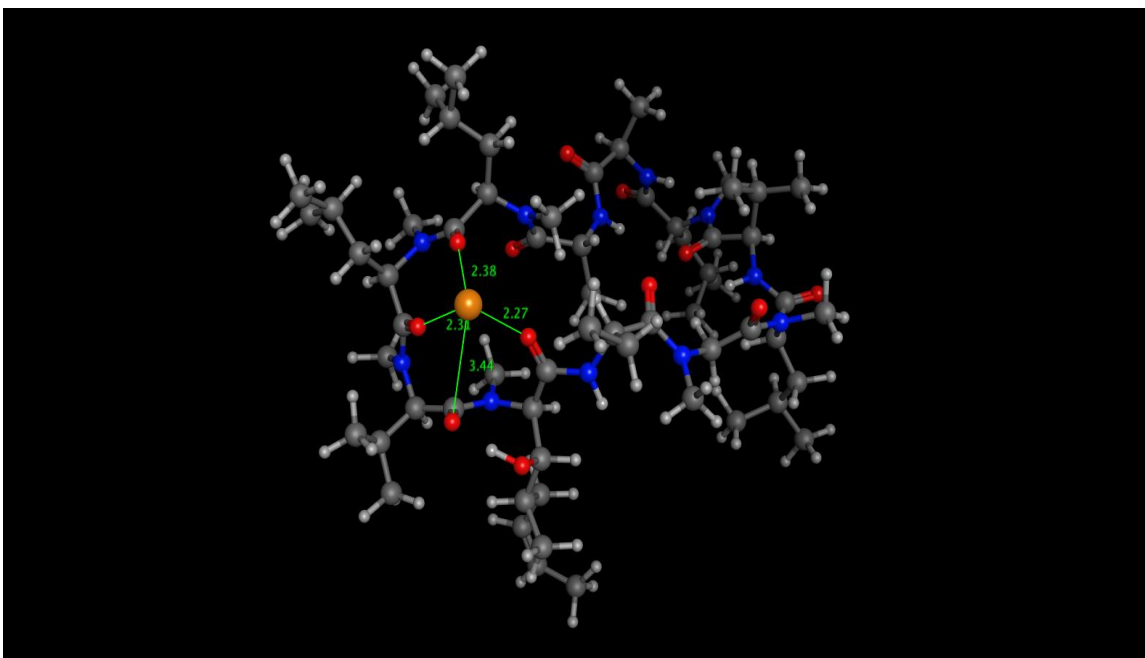
Cyclosporin A Structure 10. *n*=23
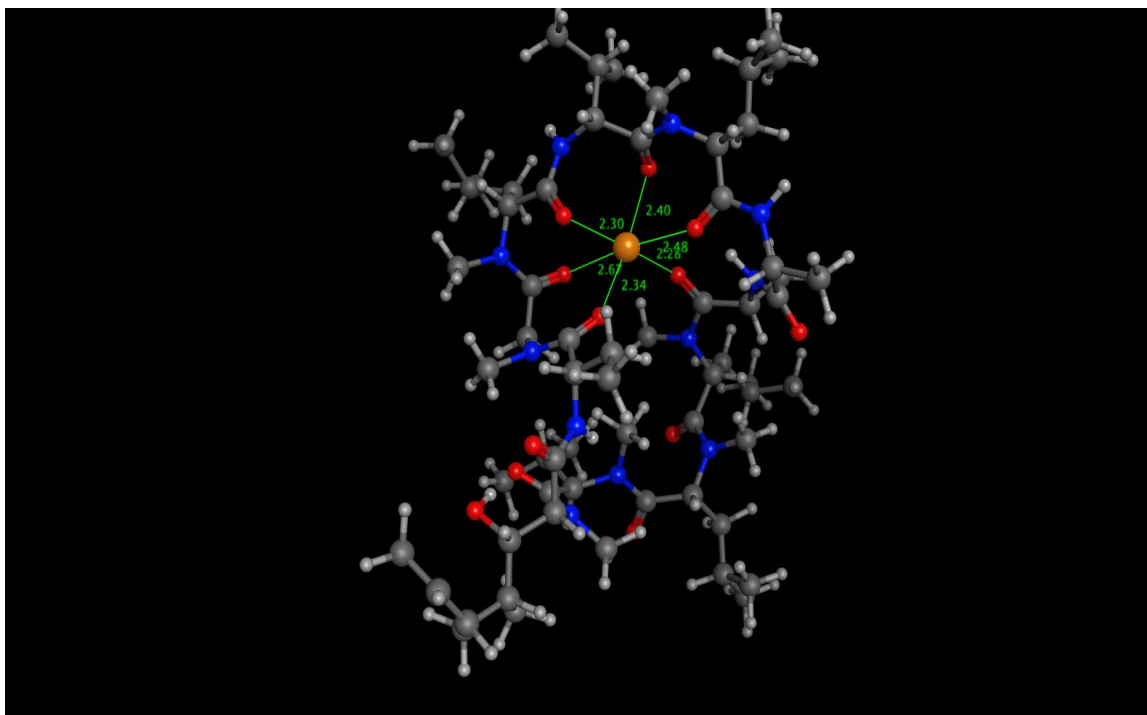
Cyclosporin A Structure 11. *n*=63
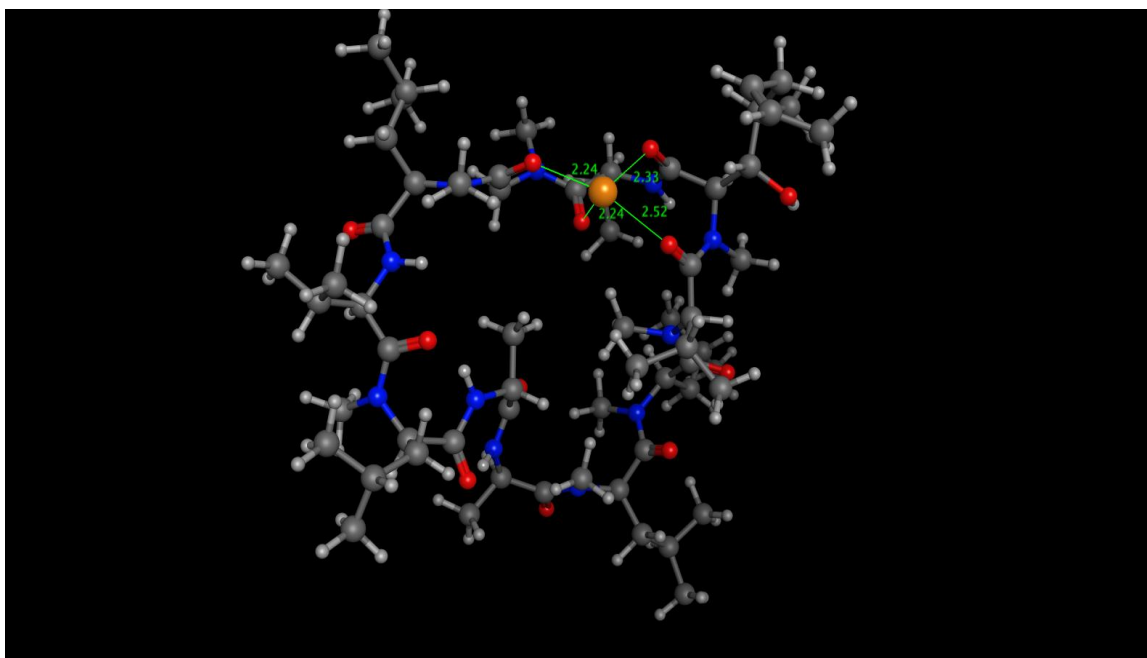
Cyclosporin A Structure 12. *n*=33
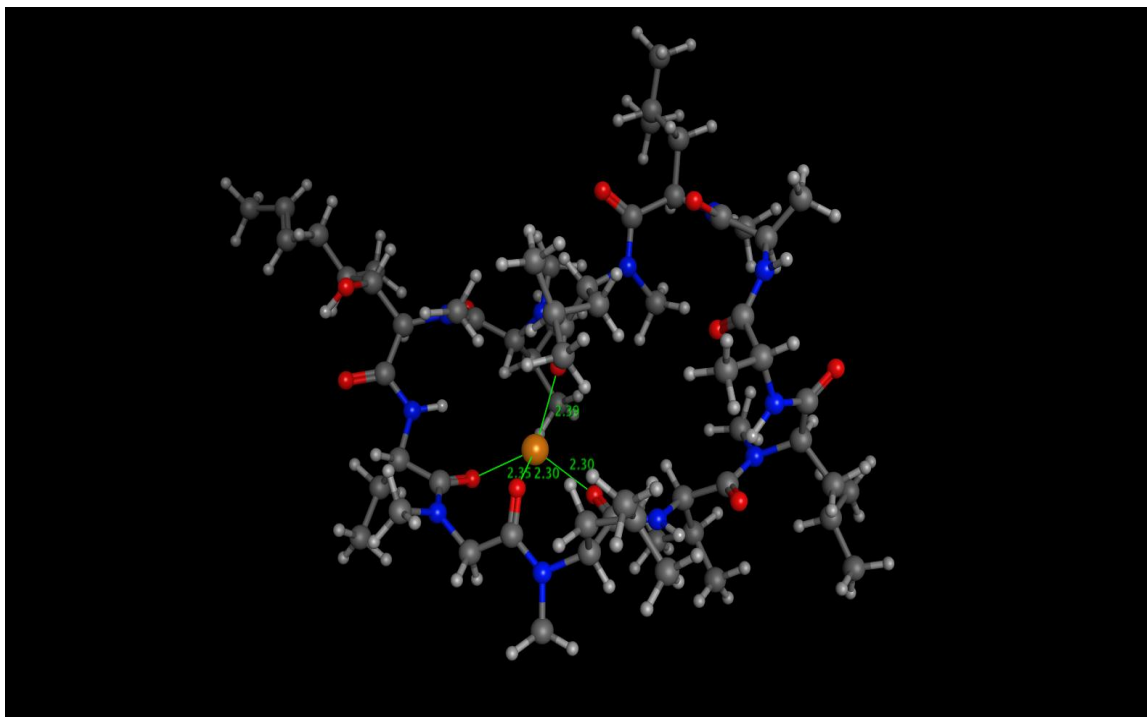
Cyclosporin A Structure 13. *n*=41
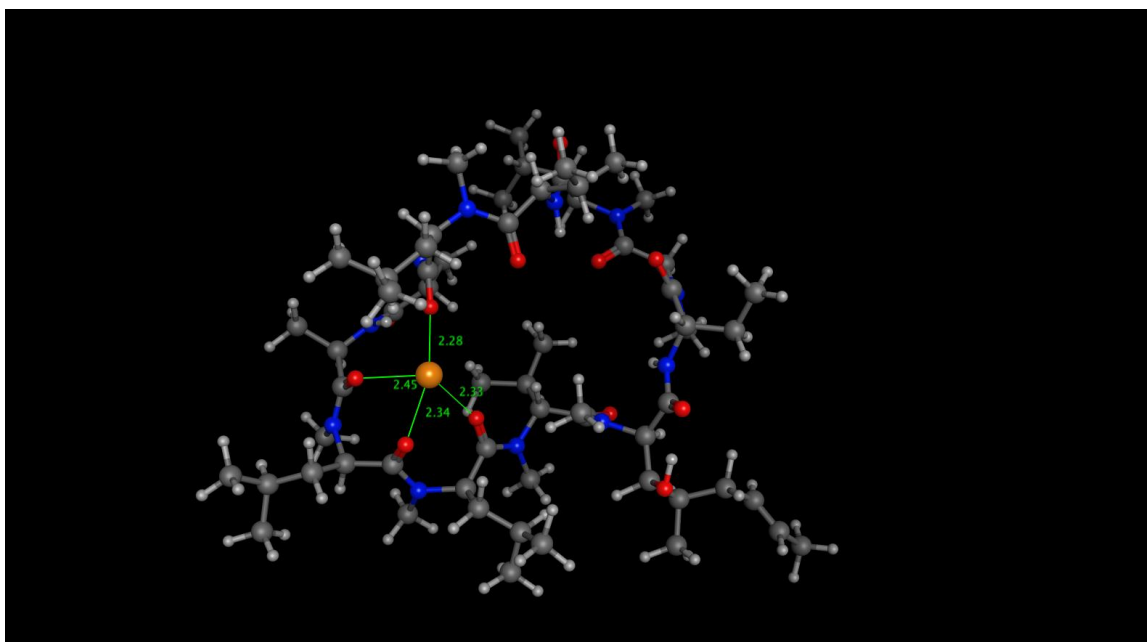
Cyclosporin A Structure 14. *n*=46
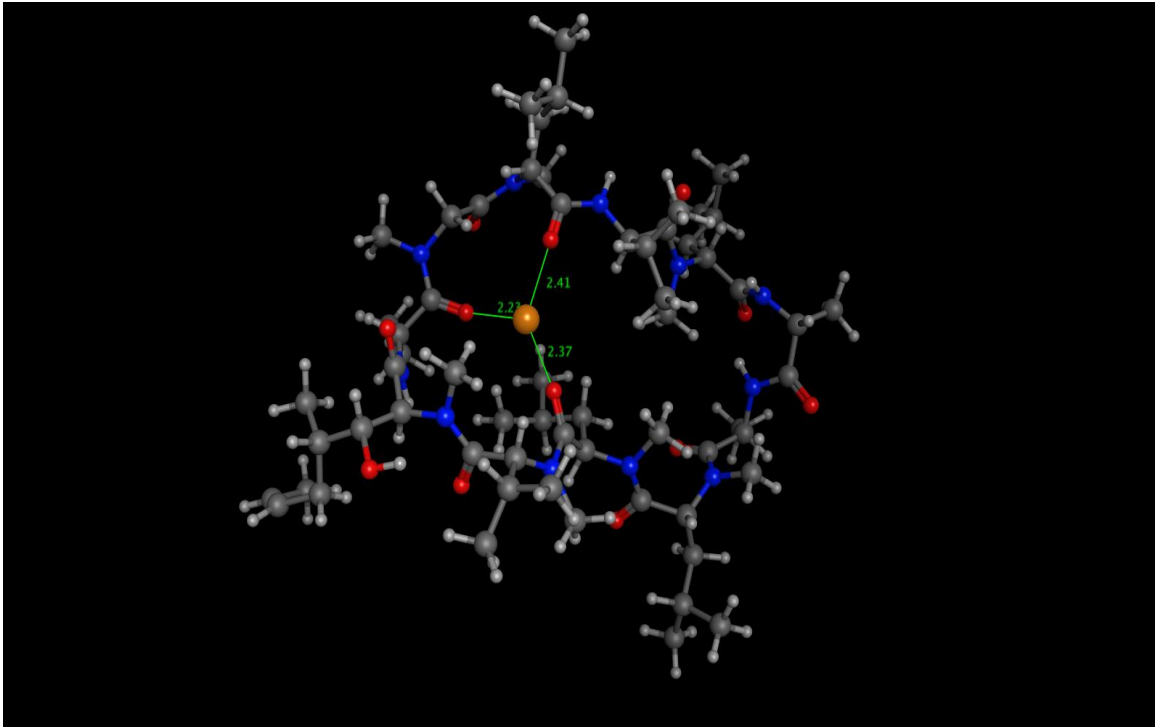
Cyclosporin A Structure 15. *n*=19
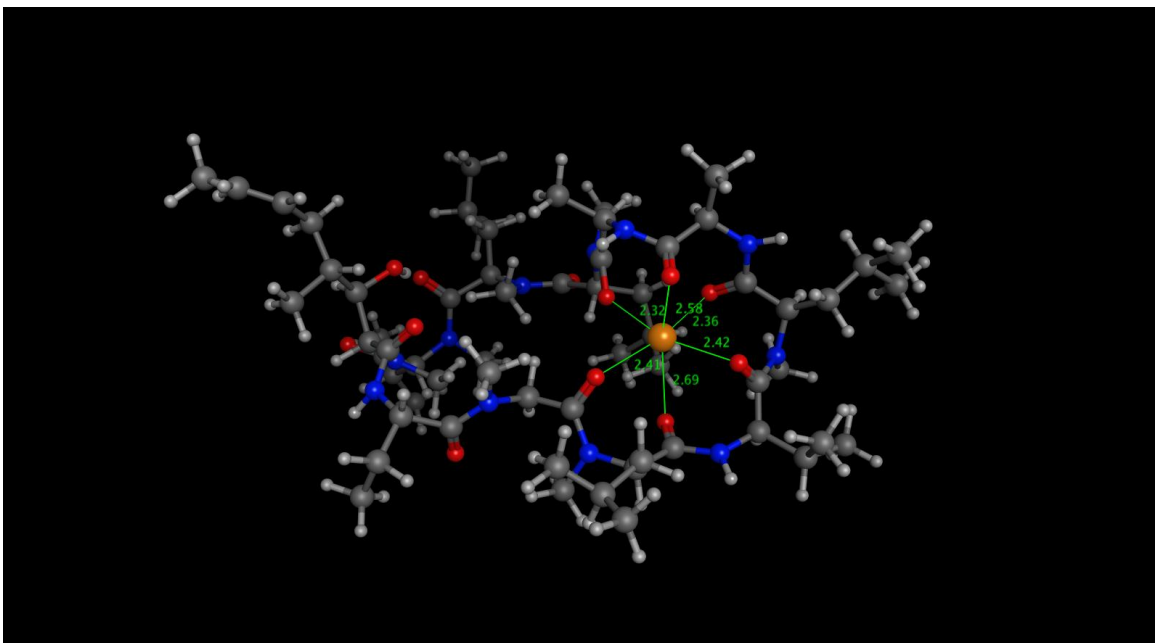
Cyclosporin A Structure 16. *n*=23
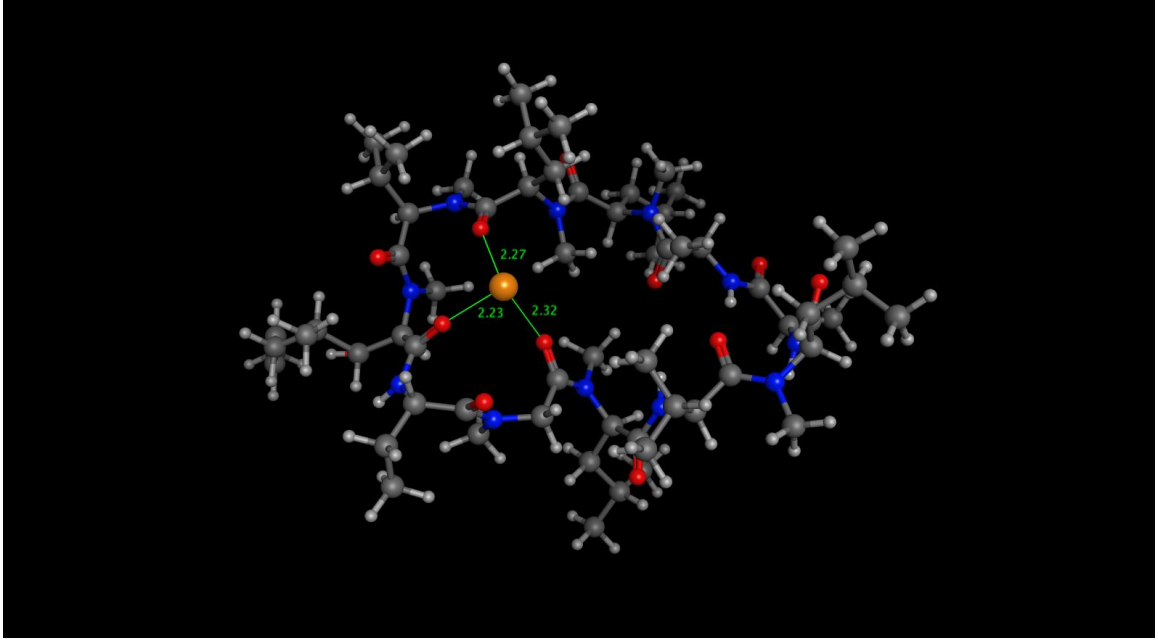
Cyclosporin A Structure 17. *n=63*
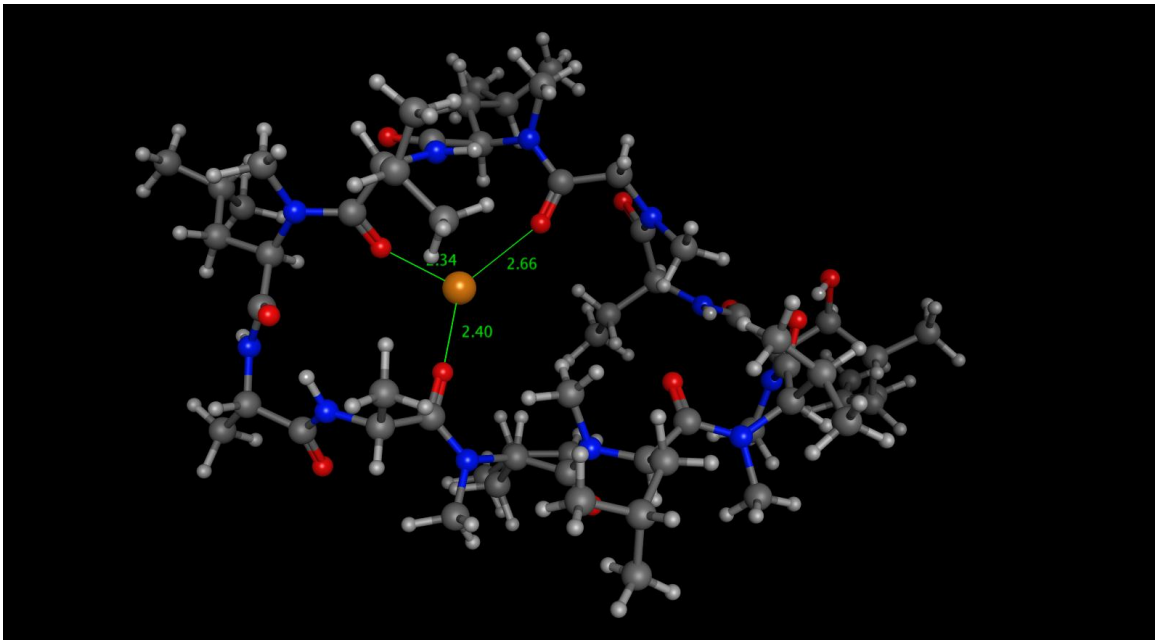
Cyclosporin A Structure 18. *n=30*
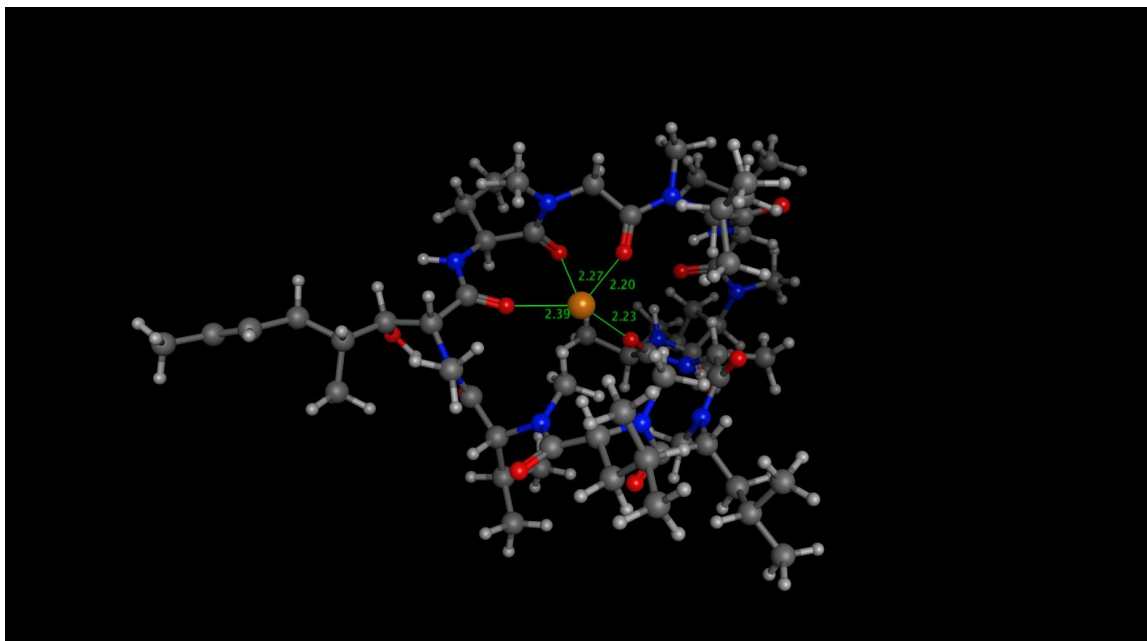
Cyclosporin A Structure 19. *n*=25

Figure A2.10. Shown above are the 21 representative conformations of sodiated cyclosporin A generated from the simulated annealing molecular dynamics protocol. Each conformation represents between 10 and 80 structures, as indicated by *n.* Distances in Angstroms are annotated to indicate proximity of sodium cation. Carbon atoms are shown in grey, hydrogen in white, nitrogen in blue, oxygen in red, and sodium in yellow.
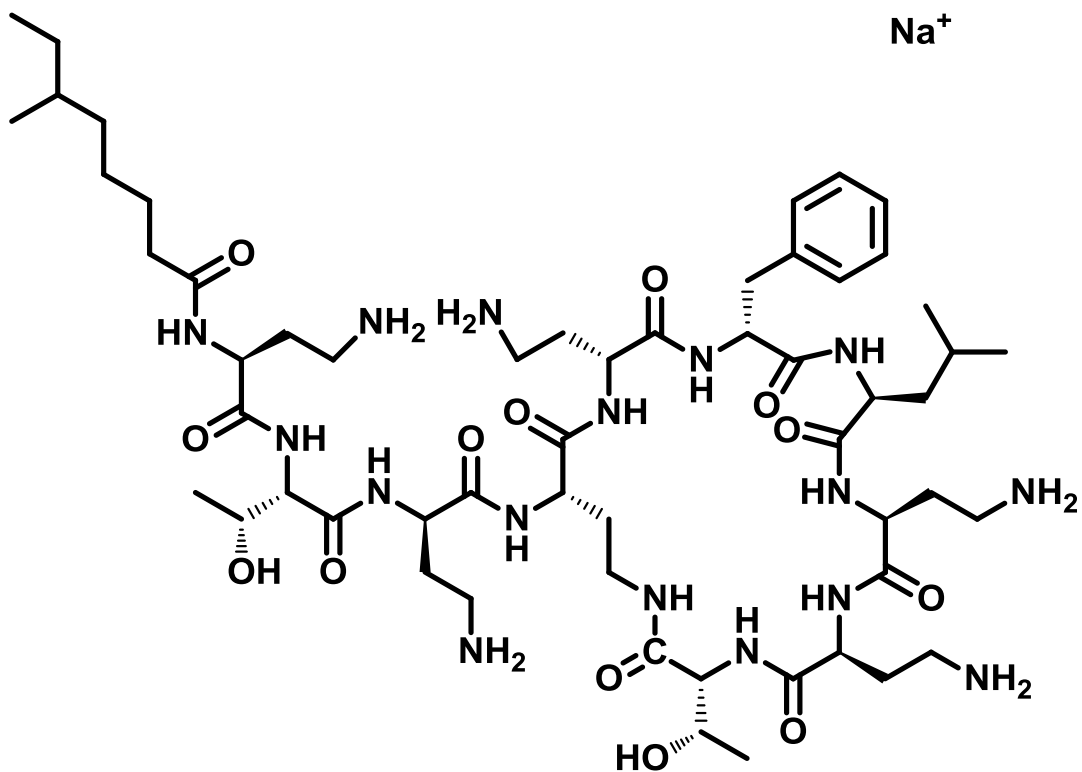
Figure A2.11. Chemical structure of sodiated polymyxin B. Monoisotopic mass was measured to be 1225.74 Da. The calculated collision cross section used for conformation discrimination is $275.65 \pm 4.03\text{Å}^2$, which is a window two times the error of the measurement.

6.88

1.159

RMSD (Å)
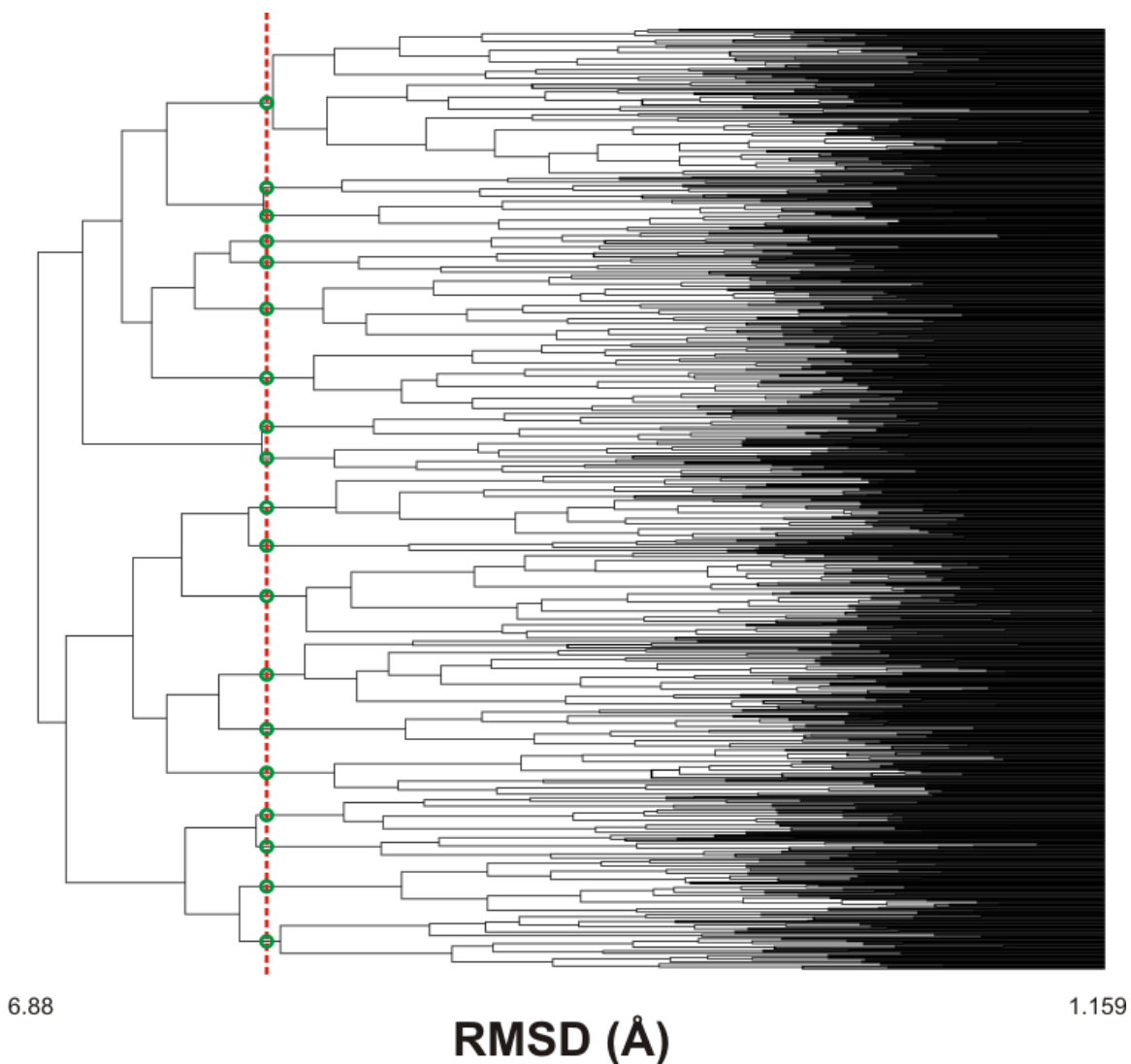
Figure A2.12. Clustering analysis of 891 sodiated polymyxin B conformations extracted from a set of 24,000 based upon collision cross section correlation. As the tree progresses from right to left, the clustering tolerance is increased. Clustering was done on the basis of root mean square distance of atoms after superimposing structures. The red dashed line indicates the cutoff for the generation of representative conformations. The green circles correspond to each branch that represents the entire dataset. In the end, all conformations were distilled into 20 representative structures. A clustering cutoff of 5.45 Angstroms was implemented.
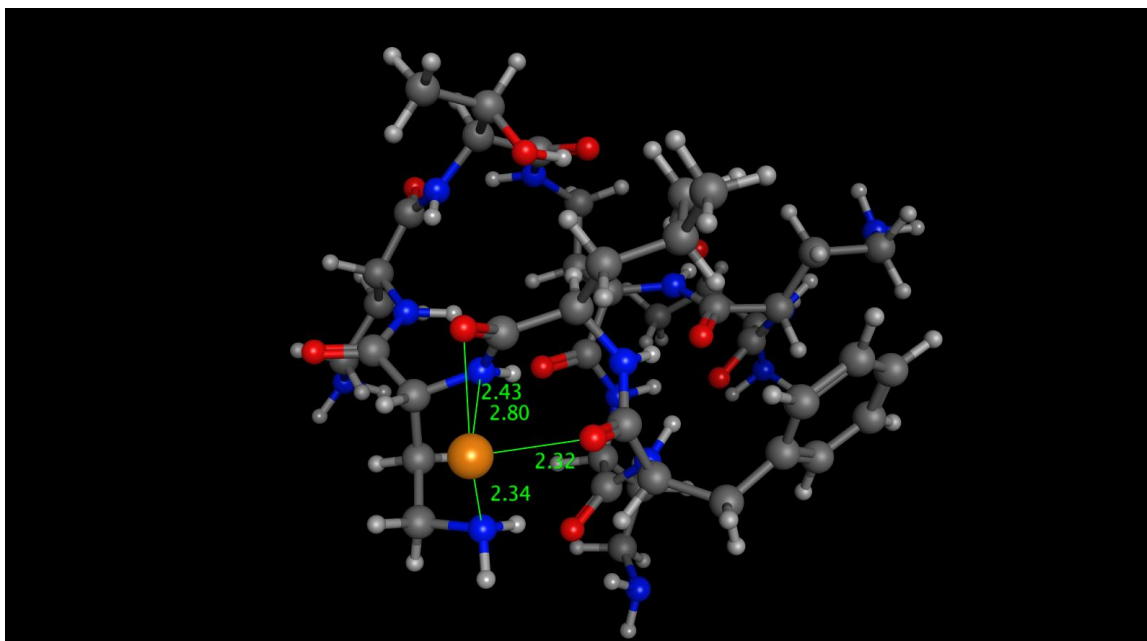
Polymyxin B Conformation 1. *n*= 66
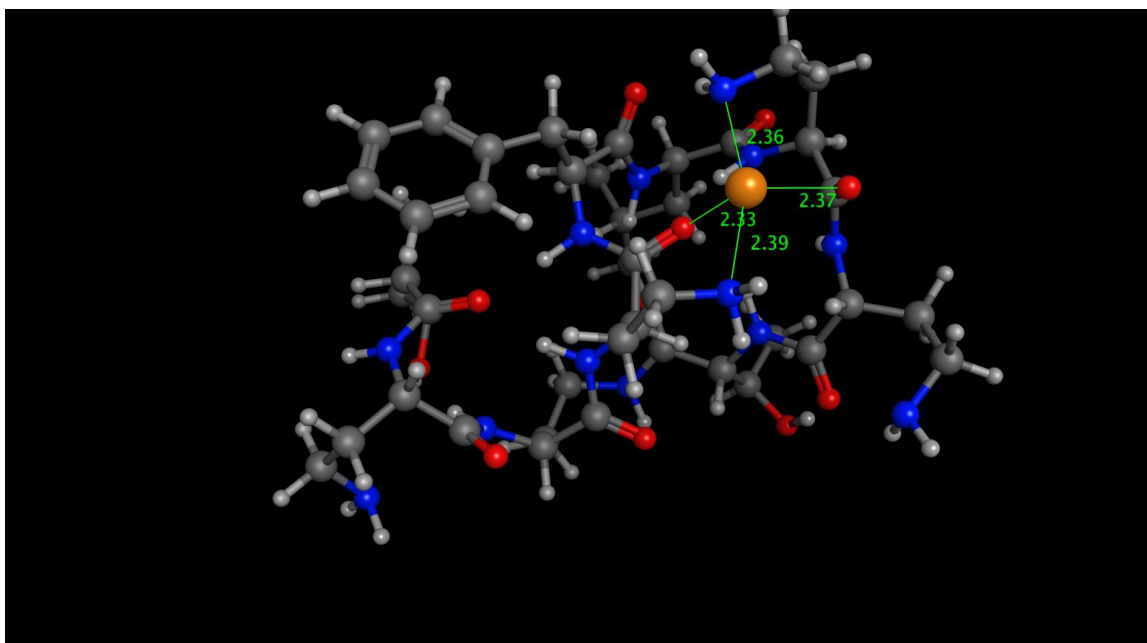
Polymyxin B Conformation 2. *n*= 84
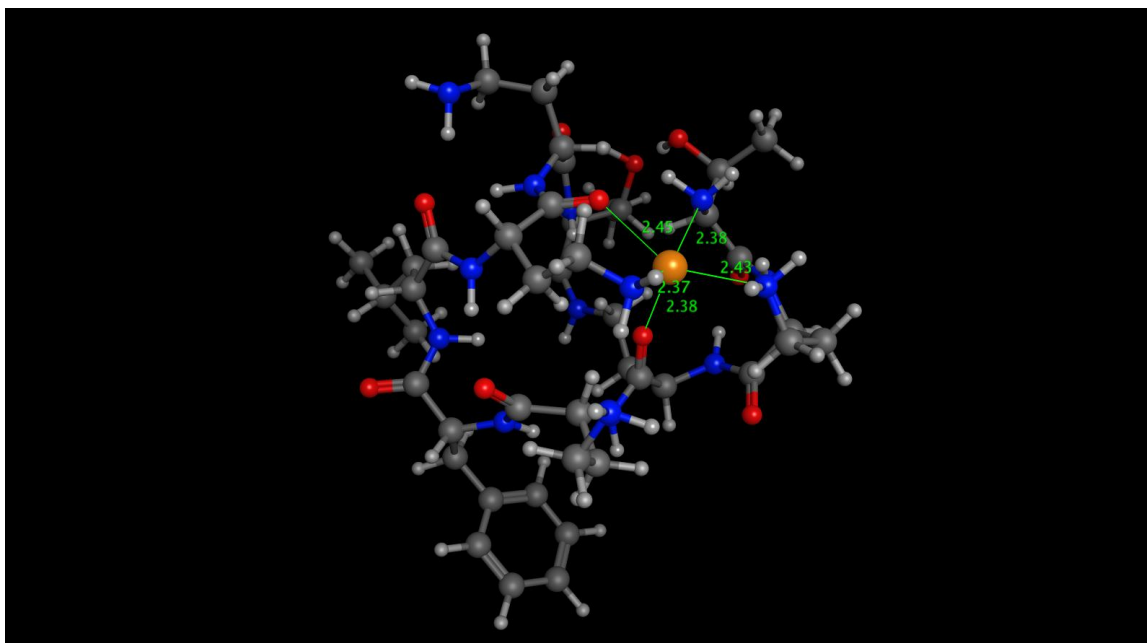
Polymyxin B Conformation 3. *n* = 66
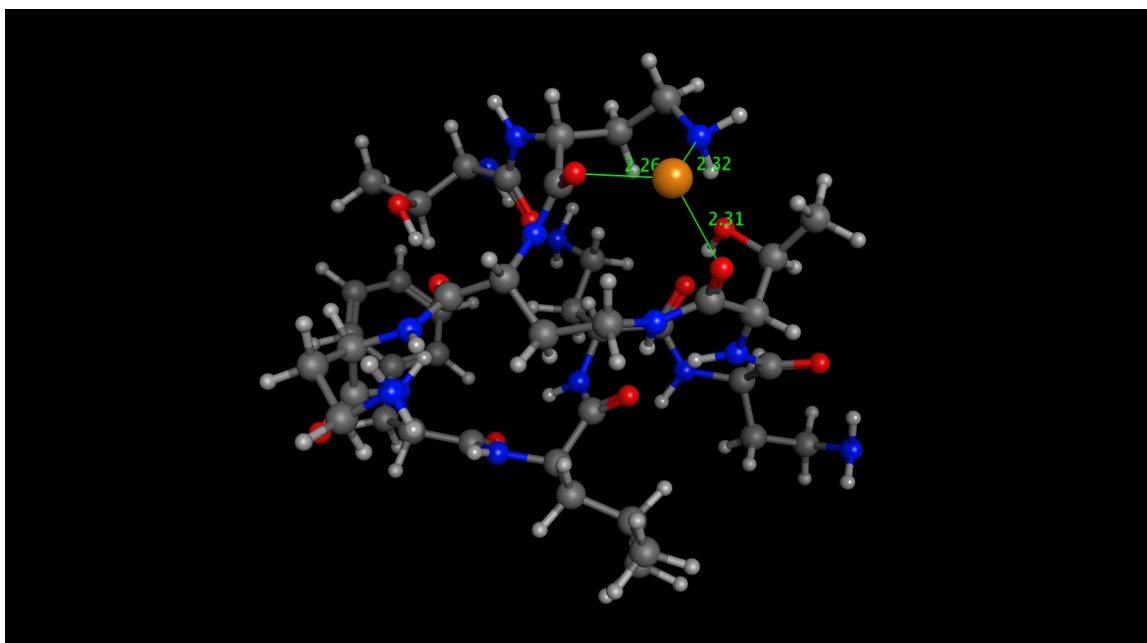
Polymyxin B Conformation 4. *n* = 66
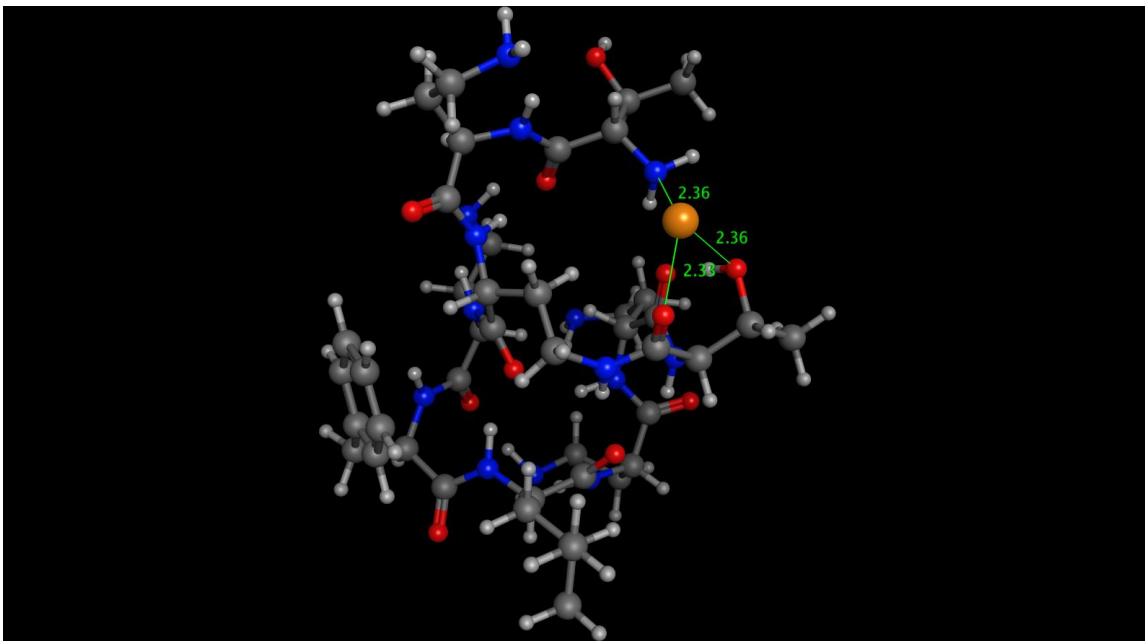
Polymyxin B Conformation 5. *n*= 91
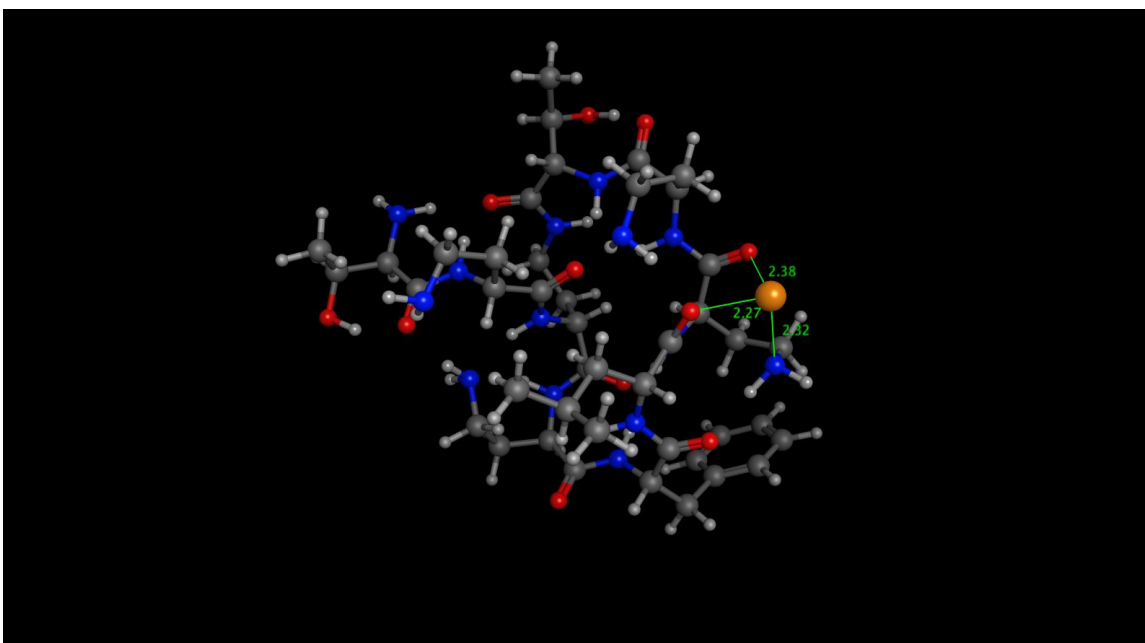
Polymyxin B Conformation 6. *n*= 45
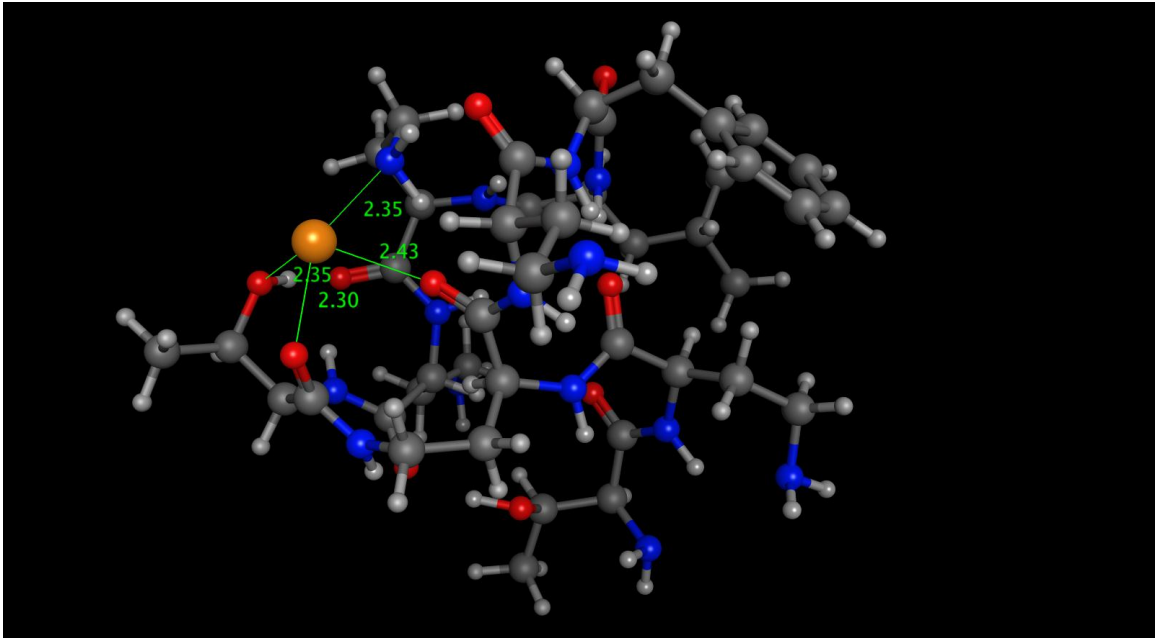
Polymyxin B Conformation 7. *n* = 33
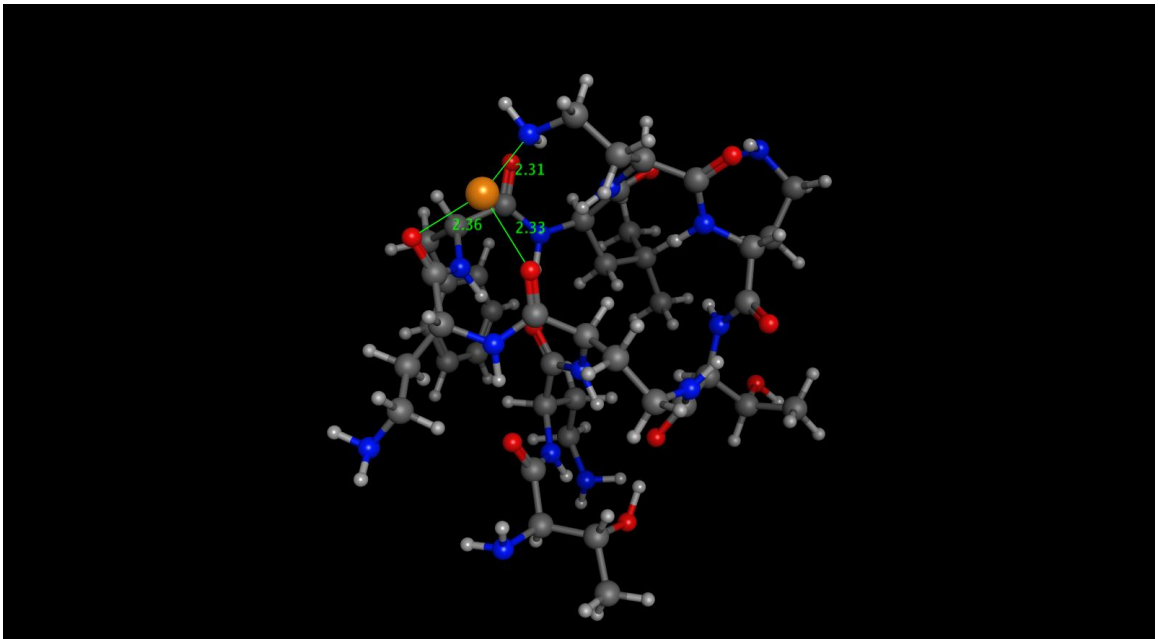
Polymyxin B Conformation 8. *n* = 50
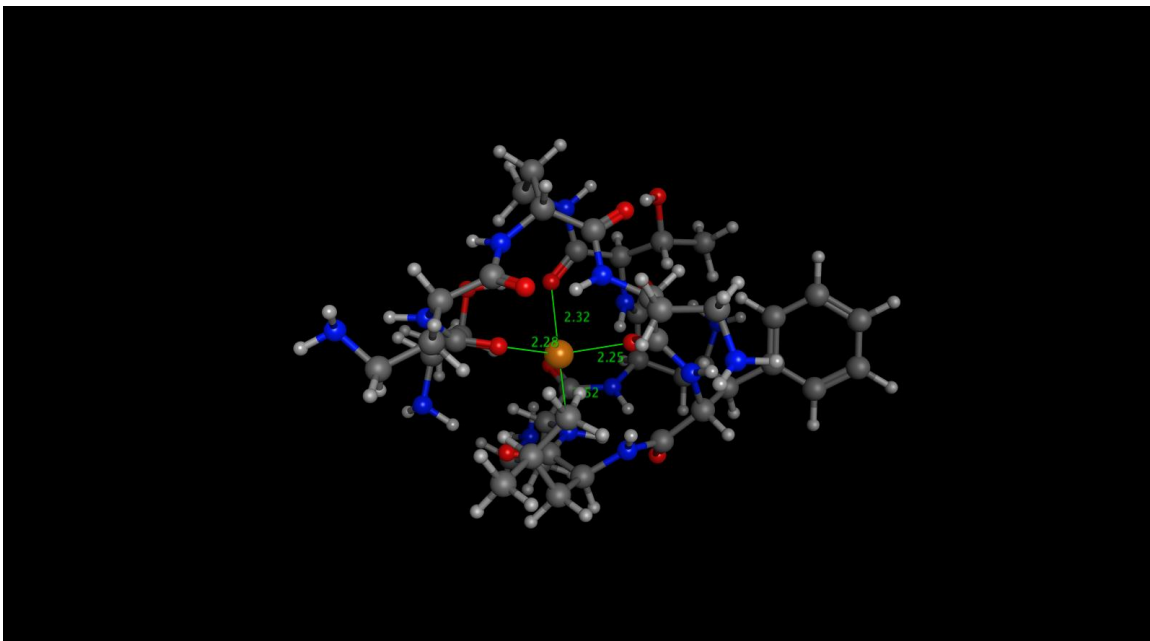
Polymyxin B Conformation 9. *n* = 61
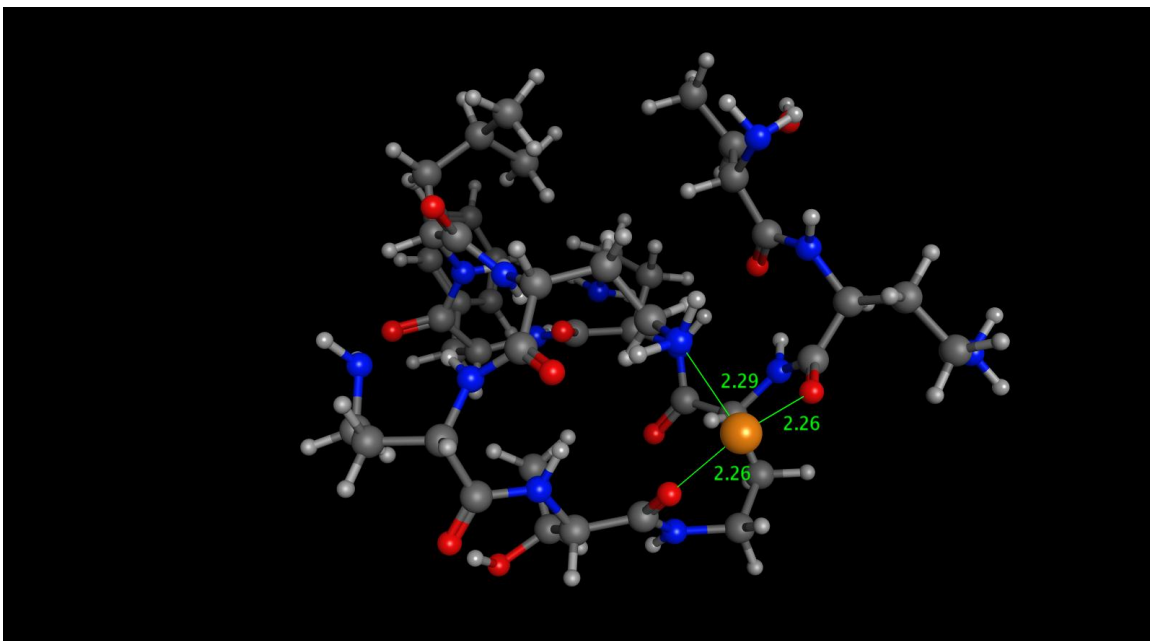
Polymyxin B Conformation 10. *n* = 21
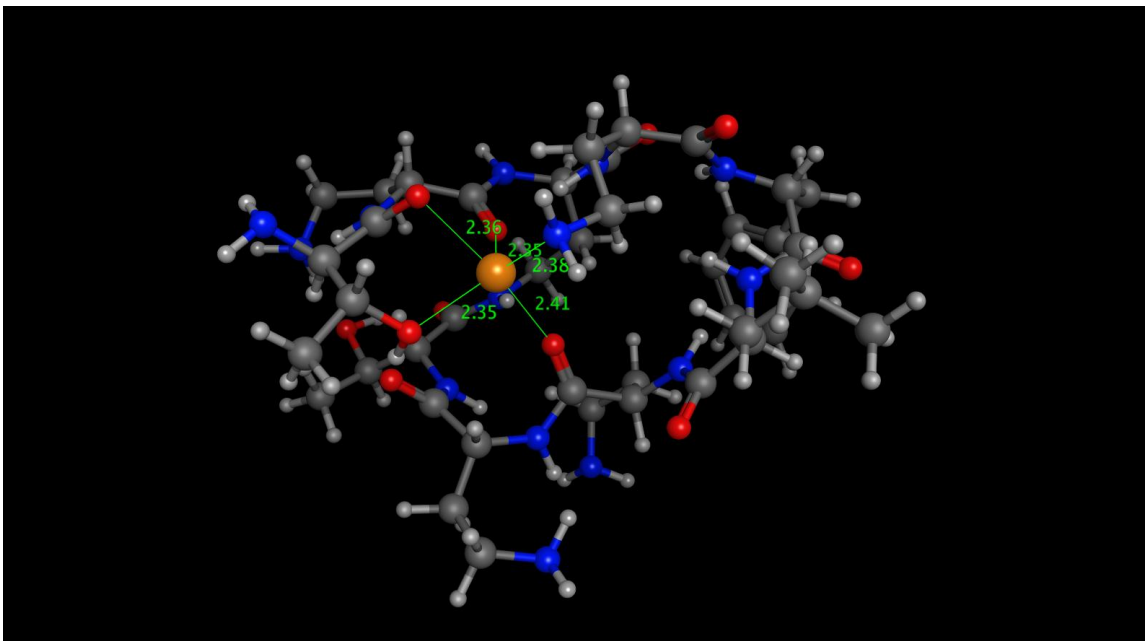
Polymyxin B Conformation 11. *n*= 36
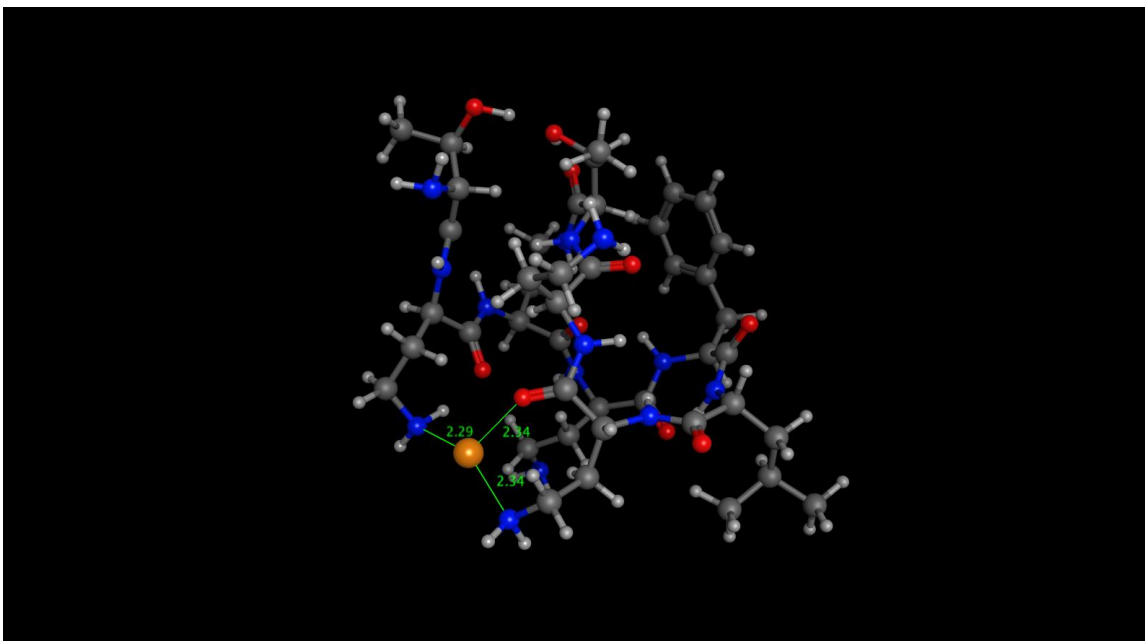
Polymyxin B Conformation 12. *n*= 23
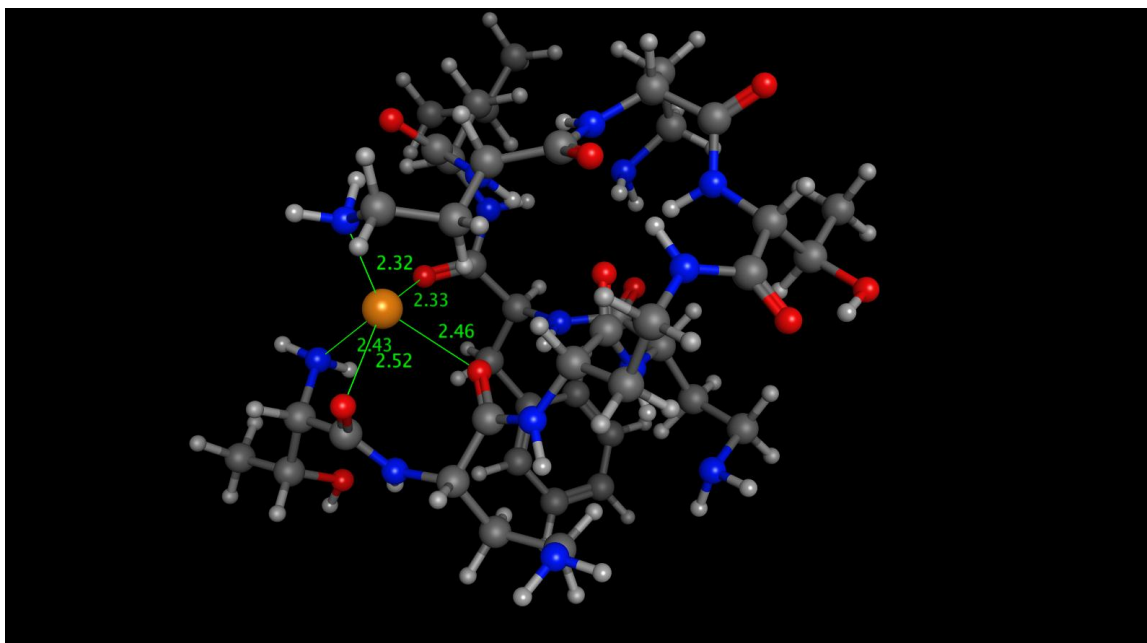
Polymyxin B Conformation 13. *n*= 27
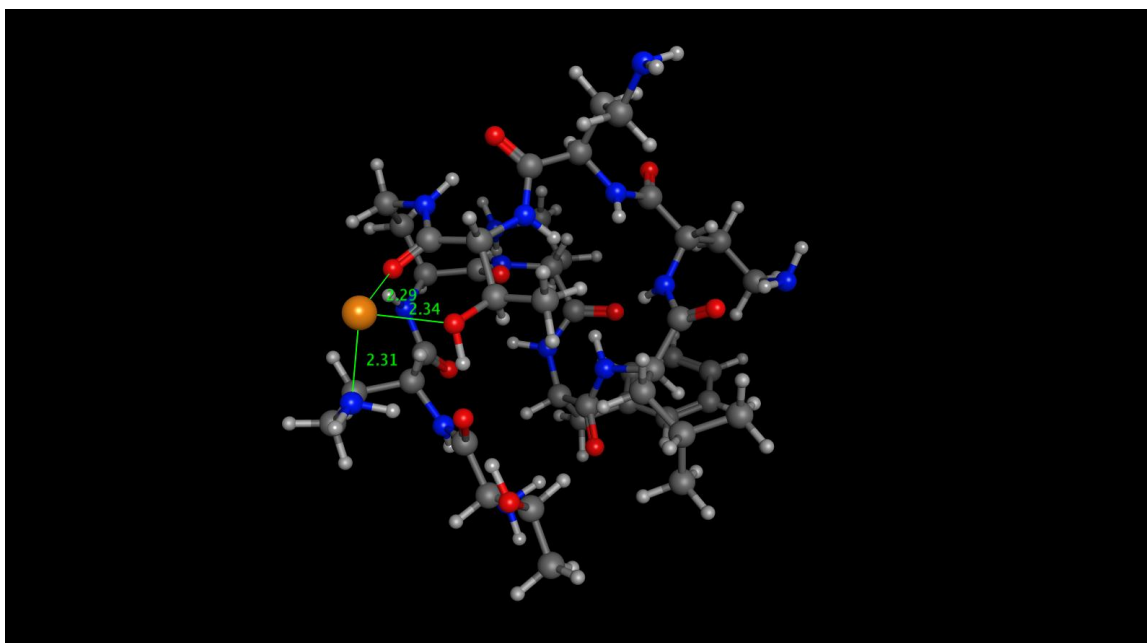
Polymyxin B Conformation 14. *n*=32
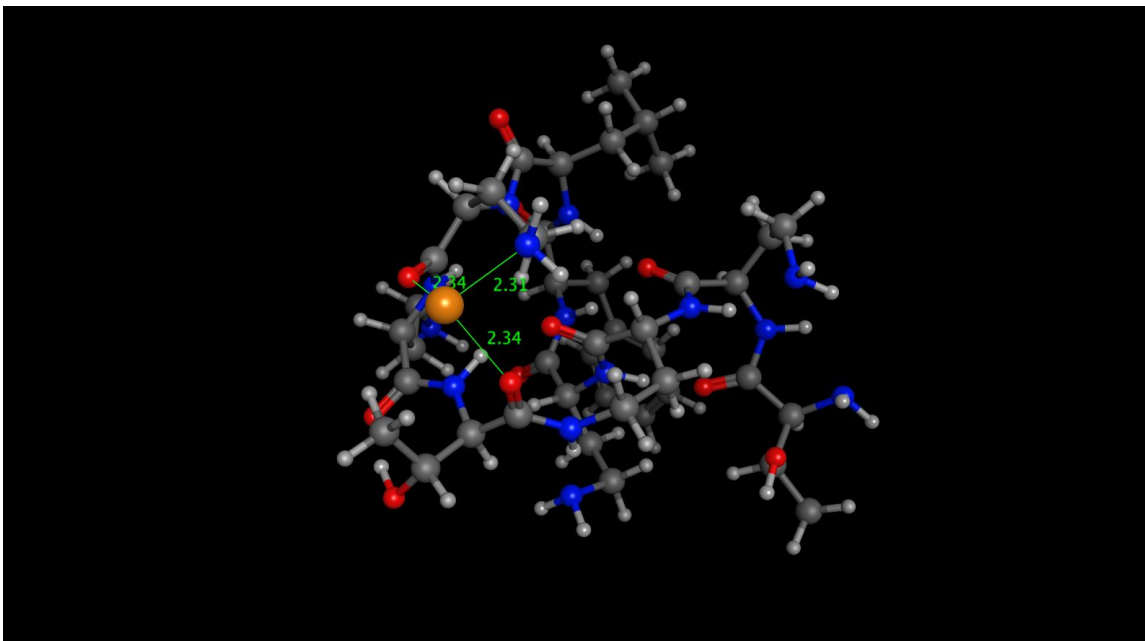
Polymyxin B Conformation 15. *n*= 24
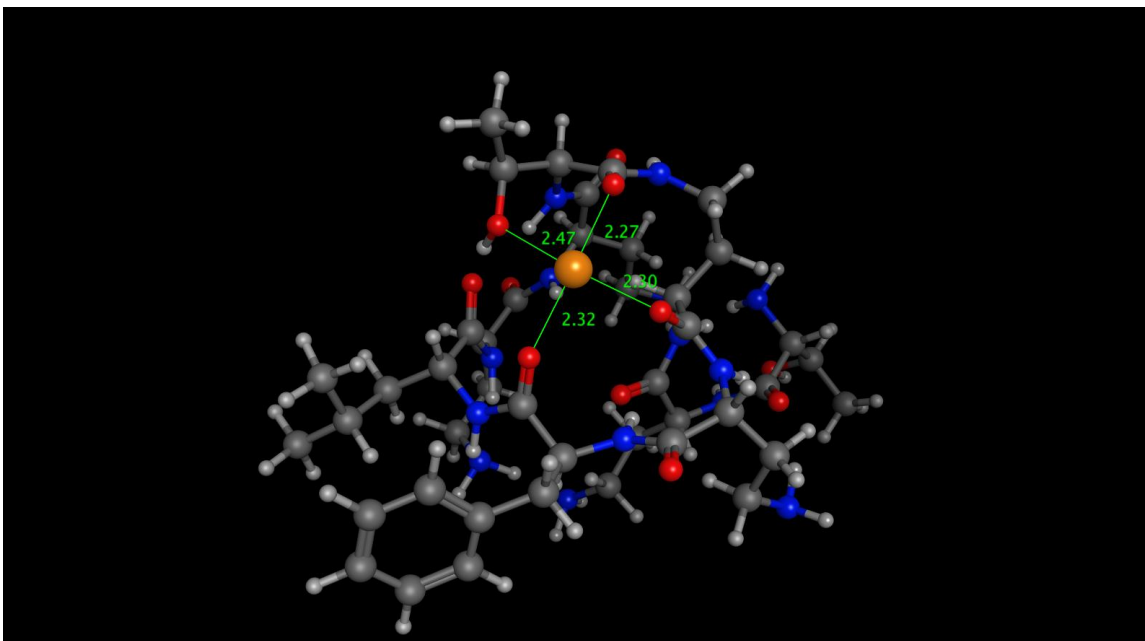
Polymyxin B Conformation 16. *n*= 52
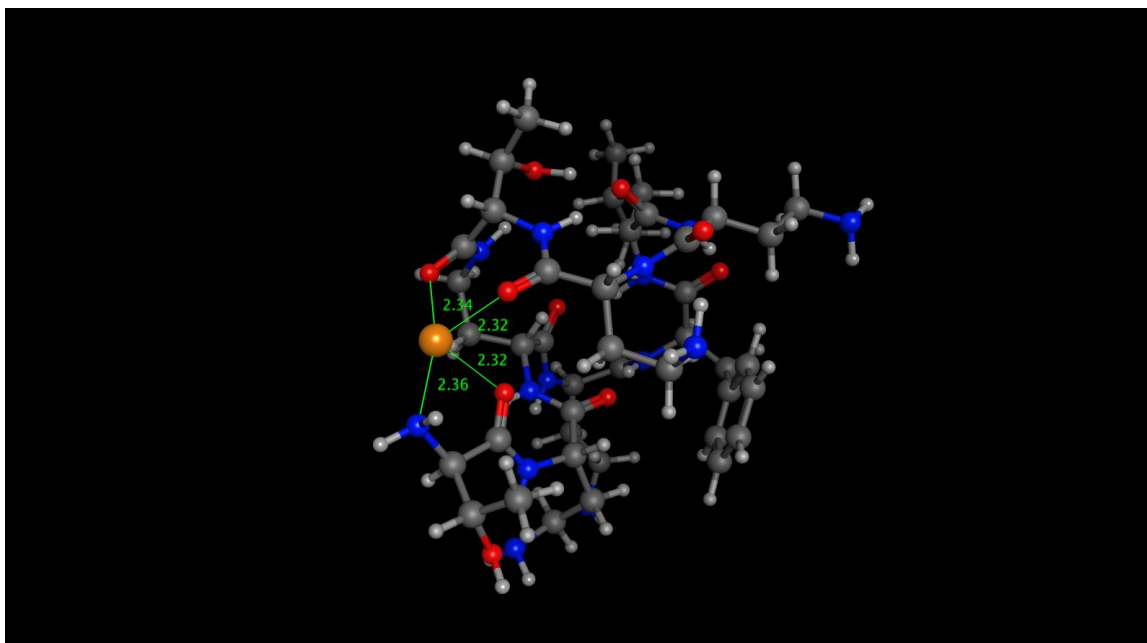
Polymyxin B Conformation 17. *n* = 38
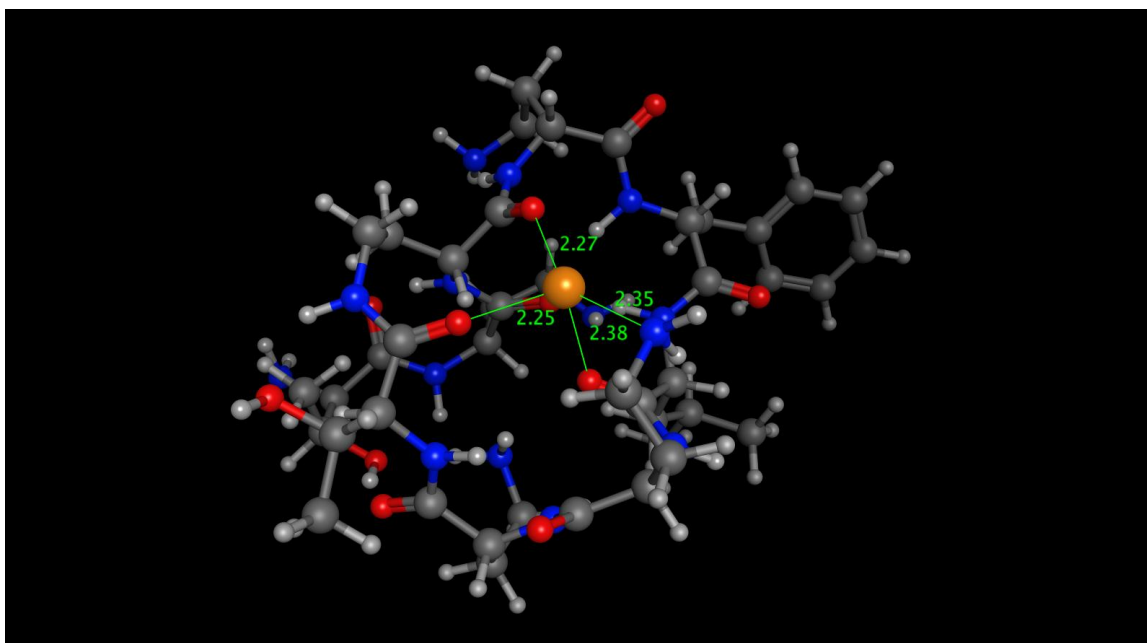
Polymyxin B Conformation 18. *n* = 12
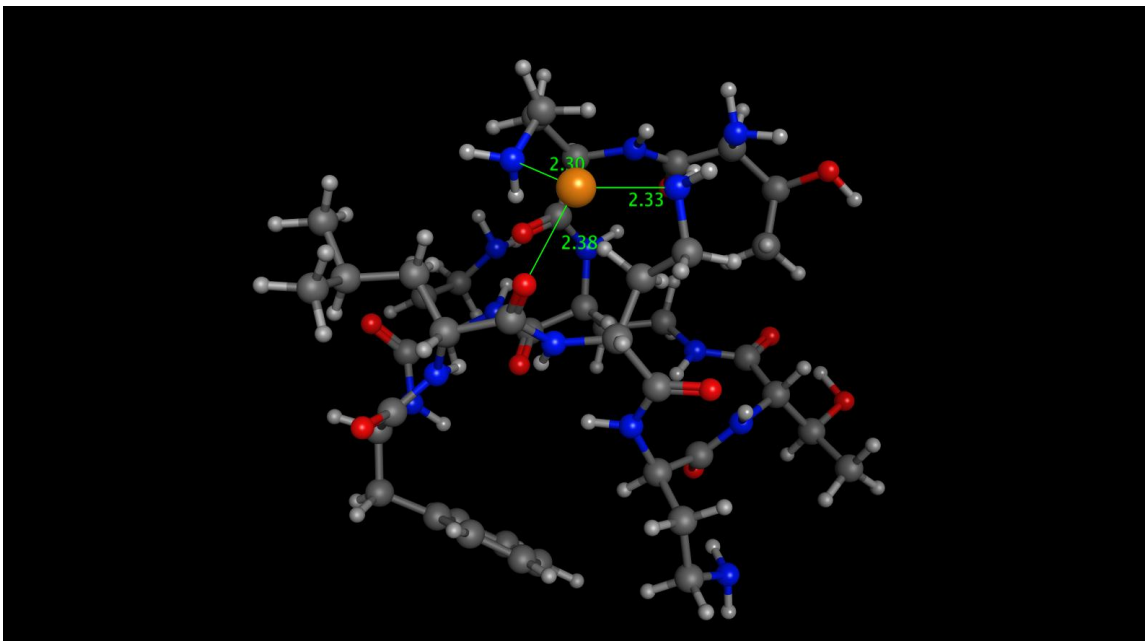
Polymyxin B Conformation 19. *n*= 30
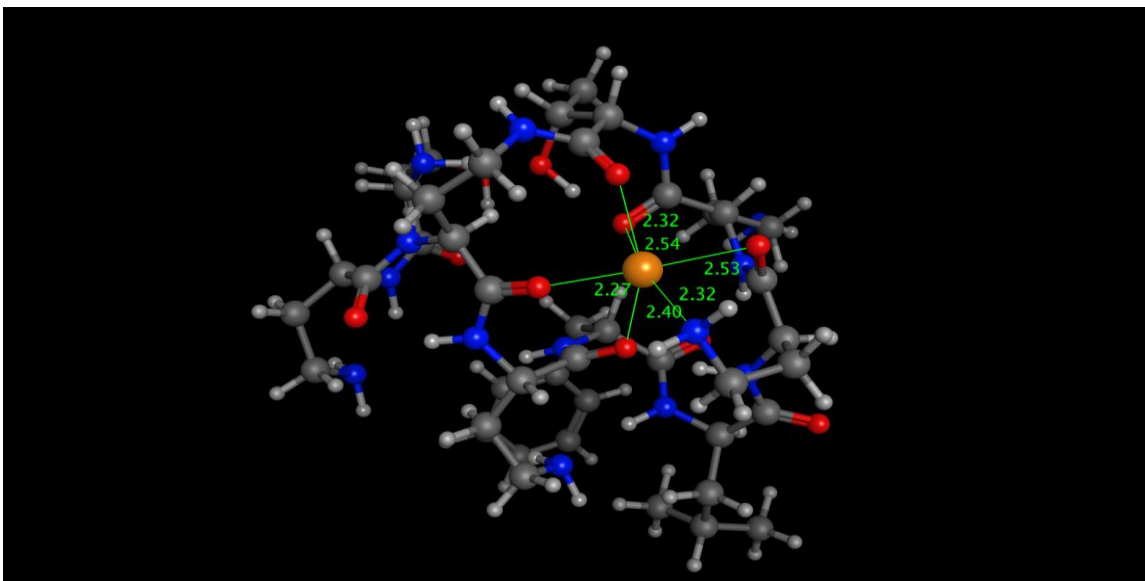
Polymyxin B Conformation 20. *n*=17

Figure A2.13. Shown above are the 20 representative conformations of sodiated polymyxin B generated from the simulated annealing molecular dynamics protocol. Each conformation represents between 10 and 100 structures, as indicated by *n.* Distances in Angstroms are annotated to indicate proximity of sodium cation. Carbon atoms are shown in grey, hydrogen in white, nitrogen in blue, oxygen in red, and sodium in yellow.

Procedures used in Chapter 2.6

General experimental procedures

All chemicals and drugs were purchased from Sigma manufacturer. All strains and primers used are listed in Table S1. ^{1}H, ^{13}C and 2D NMR spectra of pure compounds were recorded with a Bruker 600 MHz instrument equipped with 5mm Z-gradient TCI Cryo-probe. IMMS were performed on a SYNAPT G2 HDMS (Waters, Milford, MA) mass spectrometer equipped with a nanoAcquity UPLC and autosampler (Waters, Milford, MA).

Cultivation

Water was collected from a pool within travel distance of the sample site and filter-sterilized using a 0.22 mm nitrocellulose filter. A sterile Dremel tool was used to cut ~ 5 g piece of wall rock at each sample site, which was crushed *in situ* using a sterile steel pestle and mortar. Approximately 1 g of this material was then placed in 2 ml of the sterile cave water and mixed by shaking. The supernatant was used to inoculate the culture media. An uninoculated plate was used as a sampling control, to confirm that any growth was not the result of human contamination (either through preparation or during sample collection). The culture was carried out of the cave and shipped to the laboratory at 4°C (2 days), before incubating in the dark at 21°C (the temperature of Lechuguilla Cave) for approximately 4 weeks. All unique colonies were isolated in pure

culture and transferred to a 50% concentration of trypticase soy agar (TSA; (Difco™, Becton Dickinson, Franklin Lakes, NJ).

Strain Identification

To identify all the isolates, genomic DNA was extracted from each colony using a ZR Fungal/Bacterial DNA Kit (Zymo Research, Orange, CA) and the 16S ribosomal RNA gene sequences isolated as via PCR as previously described (Banks et al., 2010). Sequencing was carried out at the University of Kentucky Advanced Genetic Technologies Center (http://www.uky.edu/Centers/AGTC) and each species was identified by comparison with the NCBI Genbank database, with phylogenetic placement was confirmed via maximum likelihood analyses as described (Bhullar et al., 2012). 16S sequence of LC30 was deposited in Genbank database under accession number JN863449.

Growth and production conditions

The growth media contained a soil-extract of 40 mg/L humic acids, 4 g/L $CaCO_3$ light-powder (Sigma Chemical) and 1.5 g/L agarose (Difco™, Becton Dickinson, Franklin Lakes, NJ). The humic acids were extracted from commercially available potting soil as follows: 100 g of soil was mixed with 400 ml of water and the pH was adjusted to 7.0 using 1 M NaOH, this slurry was allowed to stir for 4 hours, after which the supernatant was collected by settling of the particulate matter followed by decanting of the supernatant. This supernatant was then successively filtered, first through cheesecloth and then through

increasingly fine Whatman (grade 6) filter papers. The pH of the clarified supernatant was dropped to 1.0 using 1 M HCl and stirred gently for 4 hours, allowing the humic acids to precipitate. Centrifugation at 10,000 x g was then used to separate the humic acid pellet, which was resuspended in approximately 100 mL of dH2O and adjusted to pH 7.0 using NaOH. The total organic carbon (TOC) content of the humic acid solution was measured as 2 mg/mL using the persulfate-ultraviolet method on a Shimadzu TOC analyzer by WATERS testing services, KY (waters.waterky.org).LC30 spore suspension was inoculated on ISP2 agar (0.4% glucose, 0.4% yeast extract, 1% malt extract, 2% agar) and incubated for 7 days at 30°C.A loop full spore sample was transferred into seed culture (0.4% glucose, 0.4% yeast extract, 1% malt extract) for another 7 days of incubation at 30°C. For fermentation, four 500 mL flask containing BA medium (1.5% soybean powder, 1% glucose, 1% soluble starch, 0.3% NaCl, 0.1% $MgSO_4 \cdot 7H_2O$, 0.1% K_2HPO_4) were inoculated with 25 mL of seed culture each and incubated at 30°C for 7 days.

Extraction and compound purification

HP-20 Diaion resin was added into 7 days fermentation cultures. Cells and resin were separated from the broth and extracted with methanol and acetone. Extracts were dried and analyzed by HPLC/MS with TSQ Triple quantum mass spectrometer equipped with ESI and Surveyor PDA detector with a linear gradient of water/acetonitrile containing 10 mM ammonium acetate using Thermo Fisher Xcalibur 2.1.0 as data analysis software and IMMS on a SYNAPT G2

HDMS (Waters, Milford, MA) mass spectrometer equipped with a nanoAcquity UPLC and autosampler(Waters, Milford, MA). For compound purification, crude extract was dissolved in methanol and applied on Sephadex LH20 size exclusion column for prefractionation. LH20 fraction was injected into RP-HPLC and separated with linear gradient of water/acetonitrile containing 10mM ammonium acetate. Finally, the HPLC fraction containing mixture of lechamycins was applied on Sephadex LH20 size exclusion column yielding X mg of Lechamycin A, X mg of Lechamycin B and X mg of Lechamycin C.

Ion mobility-mass spectrometry

MeOH extracts were diluted in 100% H_2O w/ 0.1% formic acid at a concentration of 10µg/mL and infused at a constant flow of 7.0 µL/min for 3 min. Ion mobility-mass spectrometry analysis was performed on a Synapt G2 HDMS (Waters, Milford, MA). Calibration was performed on date of acquisition with sodium formate clusters with a range of 50-1400 Da with a tolerance of 1ppm. Data were acquired at 2 Hz in resolution continuum mode. The capillary voltage was set at 4.00 kV, source temperature held constant at 80°C, the sampling cone was held at a setting of 40, with the extraction cone at a setting of 3.0. The nitrogen desolvation gas flow was held at a temperature of 150°C and a flow rate of 600.0 L/hr. The nitrogen cone gas flow was set to 20.0 L/hr. The helium cell prior to the mobility chamber had a gas flow setting of 180.0, and the ion mobility nitrogen gas flow was set to 90.0 mL/min. The ion mobility wave velocity was held constant at 550 m/s at a wave height of 40.0V. Data were peak-picked

within DriftScope (Waters, Milford, MA) with a threshold of 500 counts, a TOF resolution parameter of 10,000, and a mobility peak width parameter of 14 scans. These data were exported for further analysis in Excel (Microsoft, Redmond, WA).

Exported peaks were used to generate a mobility-mass correlation using regression analysis. The subsequent line of regression was used to predict the mobility for a given mass, and the percent deviation for detected peaks was generated for prioritization.

Structure elucidation of Lechacyclines

Lechacycline A (**1**) was isolated as pale yellow solid with the UV spectrum showing absorption maxima at 205, 238 and 359 nm. The HR-MS of m/z 1200.4713 $[M+H]^+$ combined with ^1H and ^{13}C NMR spectral data (**Table S1**) determined the molecular formula of $C_{54}H_{77}N_3O_{25}S$. The 13C NMR and HMBC spectra indicated the presence of 54 carbons including 5 methyl groups, 10 methylenes, 25 methines and 14 quaternary carbons. The 2D NMR signals allowed establishing partial structures (**I-IV**) with **I** being aglycone fragment, **II** and **III** being disaccharide and monosaccharide respectively and **IV** being an unusual mycothiol moiety. The HSQC data suggested the presence of four monosaccharide fragments within the molecule, including three O-glycosides and one C-glycoside. The COSY, HSQC and HMBC correlations indicated that the aromatic ring of aglycone (**I**) is tetrasubstituted with the hydroxyl group in C-8 position and C-glycoside in C-9 position. The HMBC correlations from proton H-

11 to carbons C-12 and C-7 suggested the presence of another ring adjacent to the aromatic ring with two carbonyls in positions C-12 (δ=191.8) and C-7 (δ=197.9) with ^{13}C NMR chemical shifts typical for a quinone-type ring that lacks double bonds. The COSY correlations between protons H-6 and H-5 and the HMBC correlations from methylene protons H-6 to carbons C4a, C-6a and C-12a allowed assembling another ring of aglycone fragment (**I**). The chemical shifts of carbons C-12a, C-12b and C-4a suggested that they all have hydroxyl groups attached, whereas quaternary carbon C-6a was shifted significantly upfield with chemical shift (δ= 60.5) typical for sulfur substituent. This was supported by chemical formula of **1**. The last ring was assembled based on ^{1}H proton and ^{13}C carbon chemical shifts and HMBC correlations from proton H-2 to carbon C-12b, from methyl protons to carbon C-3 and from methylene protons H-4 to carbons C-4a and C-12b. The partial structure **I** turned out to be tetracyclic aglycone with ring assembly characteristic for angucycline family compounds. The COSY and TOCSY NMR spectral data allowed establishing carbon backbone of two monosaccharide fragments of partial structure **II**. The HMBC correlation from proton H-4' to carbon C-1'' allowed assembling two monosaccharide fragments into disaccharide. Finally we were able to assign relative stereochemistry of partial structure **II** based on coupling constants present in ^{1}H NMR spectrum and comparison of ^{13}C NMR chemical shifts of fragment **II** and monosaccharides present in other, known anucyclines. The partial structure **III** was established based on ^{1}H proton and ^{13}C carbon chemical shifts and also COSY and HMBC spectral data. The presence of anomeric proton (δ = 5.25) attached to anomeric

carbon (δ= 94.9) in HSQC spectrum indicated that fragment **III** is a monosaccharide. The carbon C-4''' was shifted upfield significantly (δ = 50.0) suggesting the presence of amine in this position. The coupling constants present in ^{1}H proton spectrum allowed assigning the relative stereochemistry of partial structure **III** which turned out to be unusual amino sugar tolyposamin that was previously observed for some angucyclines. The last partial structure (**IV**) was assembled based on ^{1}H proton and ^{13}C carbon chemical shifts and HMBC spectral data. HMBC correlations from proton H-14 to carbons C-15 and C-16 and from methyl protons H-16 to carbon C-16 allowed toassemble the first component of **IV** that turned out to be acetylcysteine. COSY and HMBC correlations allowed assembling two other components: monosaccharide glucosamine and another 6-membered ring that turned out to be inositol. The HMBC correlation from proton H-1'''' to carbon C-1''''' established the connectivity between glucosamine and inositol moieties and HMBC from proton H-2'''' to carbon C-15 suggested that the glucosamine-inositol fragment and acetylcysteine moiety are connected through N-glycoside bond. Finally, the coupling constants present in proton spectrum of **1** indicated the relative stereochemistry of 6-membered rings in partial structure **IV**. The whole fragment consisted of glucosamine, inositol and acetylcysteine called mycothiol was previously reported in literature (citation) as bacterial analog of glutathione. The absolute stereochemistry of mycothiol was established as 1-D-*myo*-inosityl 2-deoxy-2-(*N*-acetamido-L-cystein-α-D-glucopyranoside (citation) which further supported our assignment of relative stereochemistry.

The key HMBC correlations allowed assembling all partial structures (**Figure A2.3**). The HMBC from proton H-1' to carbon C-9 established connectivity between fragments **I** and **II**. The chemical shift of carbon C-1' was characteristic to C-glycoside bond connection. Fragment **III** was connected to aglycone (**I**) based on HMBC from proton H-1''' to carbon C-6 and the attachment of fragment **IV** was established based on HMBC correlation from methylene protons H-13 to carbon C-6a.

Lechacycline B (**2**) was isolated as a pale yellow solid with the UV spectrum showing absorption maxima at 205, 238 and 359 nm. The HR-MS of m/z 877.3457 [M+H] combined with ^{1}H and ^{13}C NMR spectral data (**Table A2.4**) determined the molecular formula of $C_{42}H_{56}N_2O_{16}S$. The ^{13}C NMR and HMBC spectral data indicated the presence of 42 carbons including 5 methyl groups, 9 methylenes, 14 methines and 14 quaternary carbons. The 2D NMR signals allowed establishing partial structures (**I-IV**) with **I** being aglycone fragment, **II** and **III** being disaccharide and monosaccharide respectively and **IV** being acetylcysteine moiety. Comparative analysis of NMR data suggested that fragments **I**, **II** and **III** of **2** are the same as corresponding fragments of **1** but fragment **IV** lacked two 6-membered ring components and ^{13}C NMR chamical shift of carbon C-15 (δ=175.6) of **2** was shifted downfield suggesting hydroxyl group in this position. The whole fragment turned out to be acetylcysteine. Again, the key HMBC correlations allowed establishing connectivity between fragments (**Figure 2.7**).

Lechacycline C (**3**) was isolated as pale yellow solid with UV spectrum showing absorption maxima at 199, 238 and 360 nm. The HR-MS of m/z 732.3223 [M+H]$^+$ combined with ^{1}H and ^{13}C NMR spectral data (**Table A2.5**) determined the molecular formula of $C_{37}H_{49}NO_{14}$. The 13C NMR and HMBC spectra indicated the presence 37 carbons including 4 methyl groups, 8 methylenes, 13 methines and 12 quaternary carbons. The 2D NMR signals allowed assembling partial structures (**I-III**) and the comparative analysis of NMR data of Lechacycline C (**3**) and Lechacycline A (**1**) and B (**2**) indicated that fragments **II** and **III** of **3** are identical as corresponding fragments of **1** and **2**, however the aglycone partial structure **I** was modified in **3**. The downfield shift of carbon C-6a (δ= 78) suggested the replacement of acetylcysteine with hydroxyl group in **3**. This was supported by molecular formula that is missing sulfur element.

Table A2.2. Regression statistics used for the generation of the inherent trendline in **Figure 2.5.** Percent deviations for lechamycin compounds are reported.

	Coefficients	Standard Error
Intercept	2.105241	0.289343
X Variable 1	0.124053	0.000547

Regression Statistics		Compound	m/z	Measured Mobility	Predicted Mobility	Percent Deviation
Multiple R	0.972964	Lechamycin C	733.322	109.01	93.11	17.08%
R Square	0.946659	Lechamycin B	877.346	117.10	110.99	5.51%
Adjusted R Square	0.94664	Lechamycin A	1200.470	166.68	151.10	10.31%
Standard Error	7.026161					
Observations	2902					

Table A2.3. NMR spectroscopic data for compound lechamycin A in CD$_3$OD.
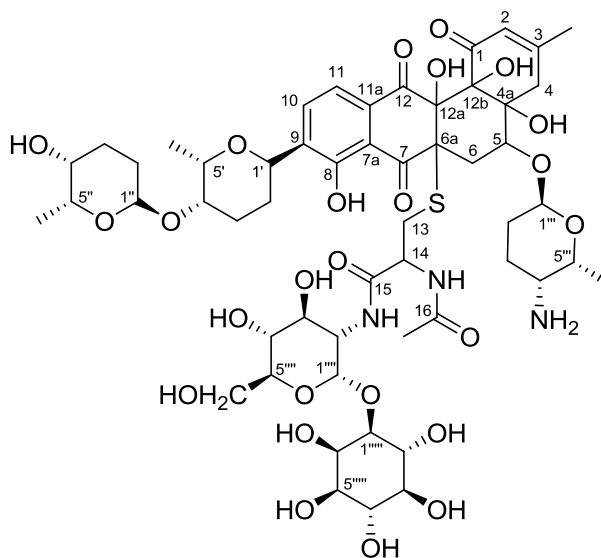
Pos.	^{13}C	^{1}H	HMBC
1	195.4		
2	125	5.92, 1H, br s	3-Me, 12b
3	160.8		
3-Me	24	2.04, 3H, br s	2, 3, 4
4	37.1	2.90, 2H, br s, 13 Hz	2, 3, 3-Me, 4a, 5, 12b
4a	80.3		
5	71.4	4.16, 1H, dd, 4 Hz, 12 Hz	1'''
6	24.6	2.40, 1H, dd, 4 Hz, 13 Hz, 2.47, 1H, dd, 4 Hz, 13 Hz	4a, 5, 6a, 12a
6a	60.7		
7	197.9		
7a	115.8		
8	159		
9	140.2		
10	133.9	7.84, 1H, d, 8 Hz	8, 11, 11a, 1'
11	120.5	7.66, 1H, d, 8 Hz	7, 7a, 9, 10, 12
11a	131.6		
12	191.8		
12a	79.9		
12b	77.7		
13	33.6	2.56, 1H, dd, 6 Hz, 13 Hz 2.77, 1H, dd, 6 Hz, 13 Hz	6a, 14, 15
14	54.3	4.36, 1H, dd, 6 Hz, 13 Hz	13, 15, 16
15	171.8		
16	173.7		
16-Me	22.9	1.92, 3H, s	16
1'	65.9	5.08, 1H, br d 11 Hz	2', 3', 8, 9, 10
2'	32.4	1.53, 1H, 2.19, 1H, m	1', 4'
3'	26.4	1.94, 2H	1', 2', 4', 5'
4'	74.1	3.95, 1H	1'', 5'-Me
5'	72.3	4.37, 1H	3', 4', 5'-Me
5'-Me	11.7	1.33, 3H, d, 7 Hz	4', 5'
1''	97.6	4.94, 1H, br d	3'', 4', 4''
2''	24.9	1.43, 1H, 2.01, 1H, br dd, 11 Hz	1'', 4''
3''	26.4	1.68, 1H, 2.02, 1H, br dd, 12 Hz	1'', 5''
4''	67.9	3.54, 1H, br	2''
5''	68	3.99, 1H,	
5''-Me	17.9	1.15, 3H, d, 7 Hz	5''
1'''	94.9	5.25, 1H, d, 3.5 Hz	5, 3''', 5'''
2'''	24.2	1.69, 1H, m, 2.24, 1H, m	4'''
3'''	24.5	1.84, 1H, 1.99, 1H	1'''
4'''	50	3.18, 1H	2'''
5'''	66.2	3.97, 1H, dq, 7 Hz	5'''-Me
5'''-Me	17.5	1.15, 3H, d, 7 Hz	4''', 5'''

1''''	100.3	4.96, 1H, d, 4 Hz	1''''',
2''''	55.7	3.82, 1H, dd, 4 Hz, 11 Hz	15, 4''''
3''''	72.9	3.68, 1H, dd, 10 Hz, 11 Hz	2'''', 4''''
4''''	72.3	3.25, 1H, t, 10 Hz	3'''', 5'''', 5''''-CH$_2$OH
5''''	74.4	3.82, 1H, m	3''''
5''''-CH$_2$OH	62.8	3.62, 1H, dd, 6 Hz, 12 Hz, 3.85, 1H, dd, 2 Hz, 12 Hz	5''''
1'''''	81	3.46, 1H, dd, 3 Hz, 10 Hz	1'''', 2'''''
2'''''	74	3.72, 1H, t, 10 Hz	1''''', 3'''''
3'''''	76.4	3.17, 1H, t, 10 Hz	4'''''
4'''''	74.1	3.58, 1H, t, 10 Hz	3''''', 5'''''
5'''''	73.1	3.36, 1H, dd, 3 Hz, 10 Hz	4'''''
6'''''	73.3	4.13, 1H, t, 3 Hz	1''''', 4'''''

Table A2.4. NMR spectroscopic data for lechamycin B in CD₃OD.
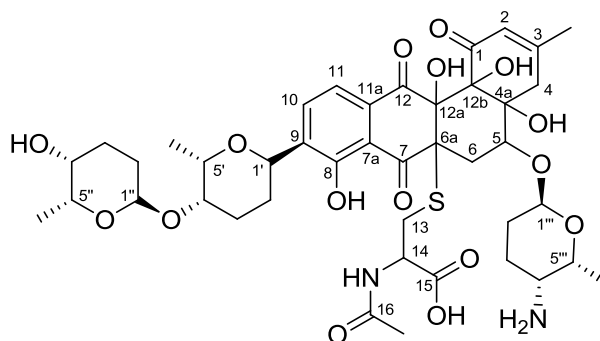
Pos.	^{13}C	^{1}H	HMBC
1	194.9		
2	125.1	5.87, 1H, br s	3-Me, 4, 12b
3	160.1		
3-Me	24.1	2.00, 3H, br s	2, 3, 4
4	37	2.86, 2H, br	3, 4a, 12b
4a	80.2		
5	71.3	4.21, 1H, dd, 2 Hz	6, 1'''
6	24.9	2.44, 1H, br dd 2 Hz, 2.47, 1H, brdd 2 Hz	5, 6a, 7, 12a
6a	60.5		
7	197.8		
7a	115.9		
8	158.9		
9	140		
10	133.7	7.82, 1H, d, 8 Hz	8, 11, 11a, 1'
11	120.2	7.65, 1H, d, 8 Hz	7a, 9, 12
11a	131.7		
12	192.4		
12a	79.6		
12b	77.8		
13	35.2	2.67, 1H, dd, 6 Hz, 12 Hz, 2.79, 1H, dd, 6 Hz, 12 Hz	14, 15
14	55.2	4.22, 1H, dd, 6 Hz	15, 16
15	175.6		
16	172.4		
16-Me	22.8	1.83, 3H, s	16
1'	65.8	5.09, 1H, dd, 2 Hz, 12 Hz	8, 9, 10
2'	32.4	1.54, 1H, ddd, 2 Hz, 9 Hz, 12 Hz, 2.19, 1H, ddd, 2 Hz, 9 Hz, 12 Hz	1', 4'
3'	26.4	1.94, 2H, dd, 9 Hz	2', 4'
4'	74.1	3.95, 1H, dd, 6.5 Hz	3', 5', 5'-Me, 1''
5'	72.3	4.37, 1H, dq, 6.5 Hz	
5'-Me	11.7	1.32, 3H, d, 6.5 Hz	4', 5'
1''	97.2	4.93, 1H, br	4', 3'', 4''
2''	25.1	1.45, 1H, m, 2.01, 1H, m	1'', 4''
3''	26.7	1.67, 1H, m, 2.02, 1H, m	1'', 4''
4''	67.9	3.54, 1H, br	2''
5''	68	3.99, 1H, dq, 6.8 Hz	4'', 5''-Me
5''-Me	17.7	1.13, 3H, d, 6.8 Hz	5''
1'''	95.6	5.22, 1H, d, 3 Hz	5, 3''', 5'''
2'''	24.8	1.78, 1H, m, 2.19, 1H, m	
3'''	24.5	1.68, 1H, m, 1.97, 1H, m	4'''
4'''	50	3.08, 1H, br	3'''
5'''	66.5	3.97, 1H, dq, 5.7 Hz	4'''
5'''-Me	17.5	1.13, 3H, d, 5.7 Hz	4''', 5'''

Table A2.5. NMR spectroscopic data for lechamycin A in CD$_3$OD.
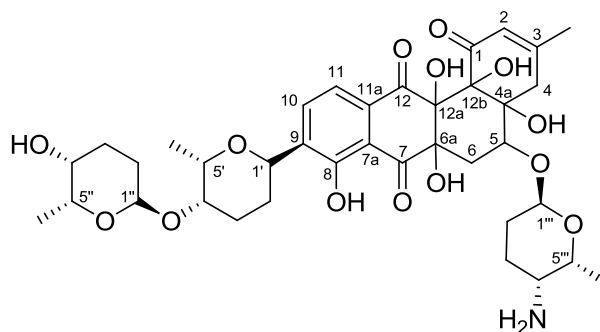
Pos.	^{13}C	^{1}H	HMBC
1	196		
2	125.1	5.88, 1H, br	3-Me, 4, 12b
3	160		
3-Me	24	2.00, 3H, br s	3, 4
4	37	2.86, 2H, br	4a, 5, 12b
4a	80.1		
5	70.1	4.06, 1H, dd 4.5 Hz, 12 Hz	
6	27.3	2.30, 1H, br, 2.42, 1H, br	6a
6a	78.5		
7	201.3		
7a	116.1		
8	159		
9	139.8		
10	134.1	7.88, 1H, d, 8 Hz	8, 11, 11a, 1'
11	120.5	7.72, 1H, d, 8 Hz	7, 7a, 9, 10, 12
11a	132.7		
12	194.5		
12a	78.4		
12b	78.2		
1'	65.9	5.09, 1H, d, 2 Hz	9, 10, 2'
2'	32.4	1.46, 1H, 2.14, 1H, ddd, 2.5 Hz, 13 Hz	
3'	26.4	1.91, 2H, br	2', 4', 5'
4'	74.1	3.94, 1H, m	5'-Me, 1''
5'	72.2	4.37, 1H, dq, 6.7 Hz	1', 3', 4', 5'-Me
5'-Me	11.7	1.33, 3H, d, 6.7 Hz	4', 5'
1''	97.6	4.93, 1H	4', 3'', 5''
2''	25.5	1.43, 1H, br, 2.00, 1H, br	1'', 3'', 4''
3''	26.7	1.67, 1H, br, 2.01, 1H, br	1'', 4''
4''	67.9	3.53, 1H, br	2''
5''	68	3.97, 1H, dq, 6.7 Hz	4'', 5''-Me
5''-Me	17.5	1.13, 3H, d, 6.7 Hz	5''
1'''	94.5	5.12, 1H, br	2''', 5'''
2'''	23.5	1.89, 1H, 2.30, 1H, m	
3'''	24.3	1.72, 1H, br, 1.95, 1H, br	
4'''	50.2	3.33, 1H, br	2'''
5'''	65.4	4.01, 1H, br	4''', 5'''-Me
5'''-Me	17.4	1.13, 3H, d, 6.7 Hz	4''', 5'''

APPENDIX 3

SUPPORTING INFORMATION FOR CHAPTER 3

Metabolomic analysis of microbial extracts

Mutational analysis of antibiotic resistant mutants

PCR of antibiotic resistance genes was performed using Taq DNA polymerase (Roche) and the primers listed in table A3.1. PCR products were purified and sequenced using BigDye Terminator chemistry and resolved on the ABI 3730xl or 3730 DNA analyzers.

Table A3.1. Primers used in this study.

Gene	Primer name	Sequence
rpsL	rpslf	5'-rtgccwacsatycagcag-3'
	rpslr	5'-yccytcttvgcgccgtar-3'
rpoB	rpobb1f	5'-ttggcagtctctcccgcgaa-3'
	rpobb1r	5'-gacacgtccatgtagtcg-3'
	rpobb2f	5'-ccgttcggcttcatcgag-3'
	rpobb2r	5'-tgcacgacgtcgtccaccga-3'

Table A3.1(B). Mutations in rifampicin (R1-R5) and streptomycin (S1-S6) cohort

Organism	gene	mutation
R1	*rpoB*	G3280A
R2	*rpoB*	G3280A
R3	*rpoB*	G3280A
R4	*rpoB*	G3280A
R5	*rpoB*	G3280A
S1	*rpsl*	No mutation
S2	*rpsl*	No mutation
S3	*rpsl*	A43G, C9G, G10C
S4	*rpsl*	C9G, G10C, G129C
S5	*rpsl*	No mutation
S6	*rpsl*	C9G, G10C

Liquid chromatography-ion mobility-mass spectrometry conditions

LC-IM-MS and LC-IM-MS^E analyses were performed on a SYNAPT G2 HDMS (Waters, Milford, MA) mass spectrometer equipped with a nanoAcquity UPLC and autosampler (Waters, Milford, MA). Metabolites were separated on a 1 mm X 100 mm HSS C18 (1.8μm particle size) column and 1 mm X 20 mm HSS C18 (5μm particle size) guard column. Column temperature was maintained at 40°C to minimize chromatographic drift, and the auto-injector sample tray held at 4°C to minimize sample degradation. A double-loop injection volume of 10μL was injected in a 5μL loop. Chromatographic separations were performed by using a 20 min gradient at a flow rate of 60 uL/min using a gradient mixer of 0.1% formic acid in H2O (mobile phase A) and 0.1% formic acid in ACN (mobile phase B). Briefly, the mobile phase was held constant at 100% A for 1 min, then ramped linearly to 100% B over 11 minutes, held for 2 minutes at 100%B, then returned to 100%A over 0.1min for a 5.9 min reequilibration period. All analytes were analyzed using positive mode electrospray ionization. Typical parameters include a capillary voltage of 3.0kV, sampling cone setting of 30.0 and extraction cone setting of 2.0, source temperature of 110°C, desolvation gas (N2) flow of 700 L/hr, and a cone gas flow of 10 L/hr. Data were acquired in MS^E mode, which acquires both a low energy spectrum and a high energy spectrum. Collision induced dissociation (CID) was performed post mobility separation with a ramped energy profile from 15-40 V in the high CID acquisition. Traveling wave velocity was held constant at 550 m/s and a height of 40.0 V. Data was acquired at a sampling rate of 2 Hz over the mass range 50-2000 m/z. Sodium formate (10

µg/mL) in 90:10 propan-2-ol:water (v:v) was used to calibrate over this range with < 1 ppm mass accuracy. Leucine enkephalin in 50:50 H2O:ACN with 0.1% formic acid (v:v) was used as a lock mass compound (accurate mass 278.1141, 556.2771 Da) at a flow rate of 7.0 µL/min and a concentration of 2 ng/mL every 10 seconds, with data corrected during acquisition. Data acquisition was performed from 0 to 20 minutes of the liquid chromatography separation. Duplicate technical analysis was performed in a randomized fashion; with quality control samples analyzed every 5 injections. Quality control samples contained equal volume aliquots of each sample mixed together.

Multivariate statistical analysis of microbial extracts from *Micrococcus luteus, Escherichia coli*, and *Bacillus subtilis.*

EZinfo 2 - 2012_05_17_cgsnai05 coculture3 (M2: PCA-X) - 2012-07-30 11:37:53 (UTC-6)
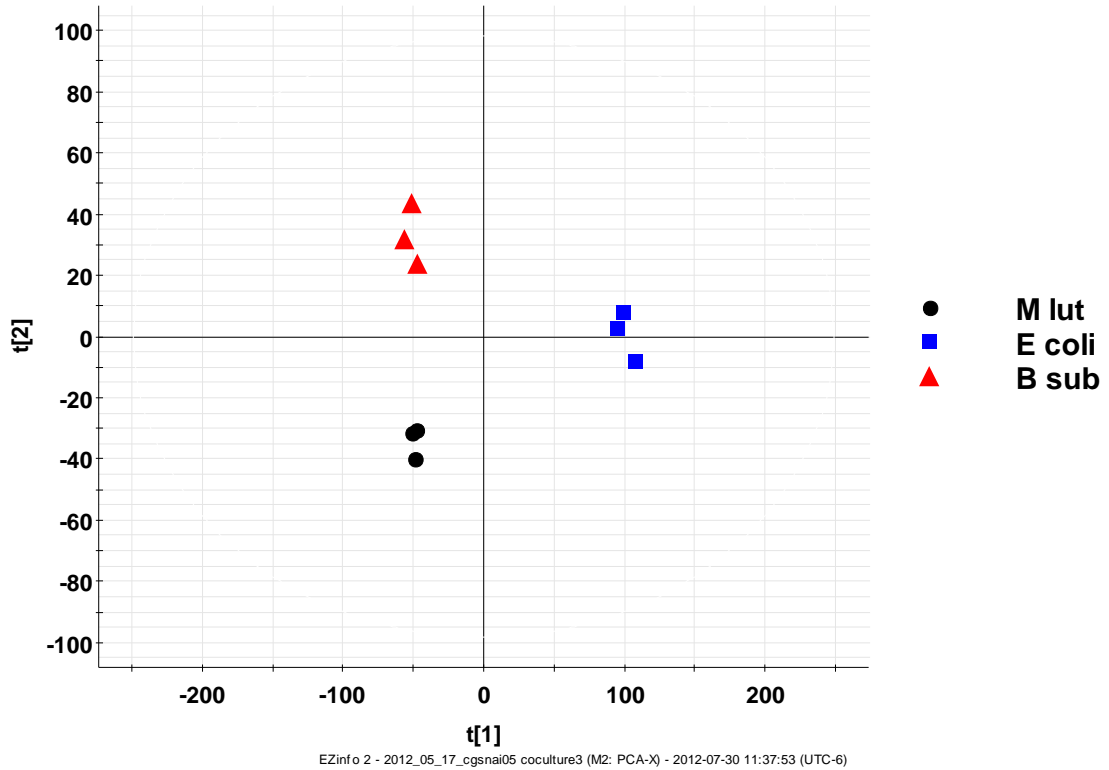
Figure A3.1. Principal component analysis of microbial extracts from *Micrococcus luteus, Escherichia coli*, and *Bacillus subtilis.* Symbols represent technical replicates. The clustering of technical replicates indicates instrument stability. The separation of groups indicates that the three organisms have sufficiently different metabolic profiles that the first two principal components are defined by these differences.

EZinfo 2 - 2012_07_03_ALL RIBO ENG (M5: OPLS-DA) - 2012-07-30 11:49:39 (UTC-6)
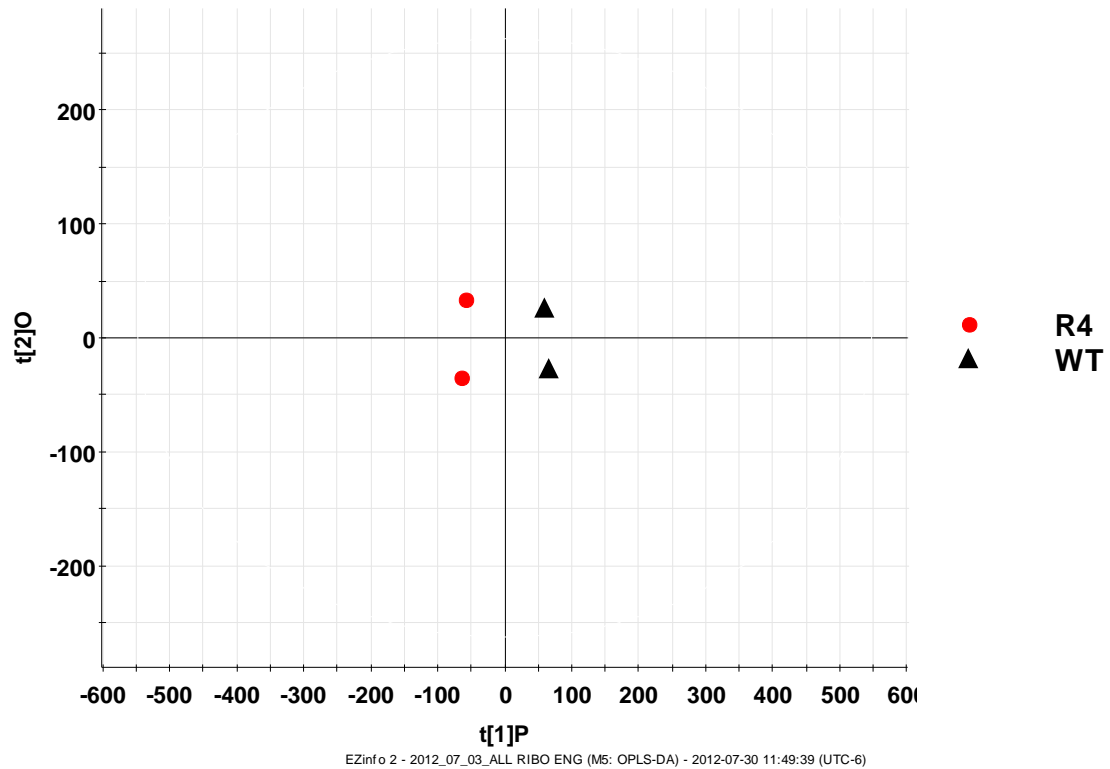
Figure A2.2. Orthogonal projection to latent structures-discriminant analysis (OPLS-DA) scores plot depicting R4 mutant vs. wild type in a binary fashion. OPLS-DA defines the first principal component as the eigenvector that with maximum eigenvalue of the covariance matrix between the two defined groups (R4 and wild type). The orthogonal vector describes the greatest intragroup differences.

232
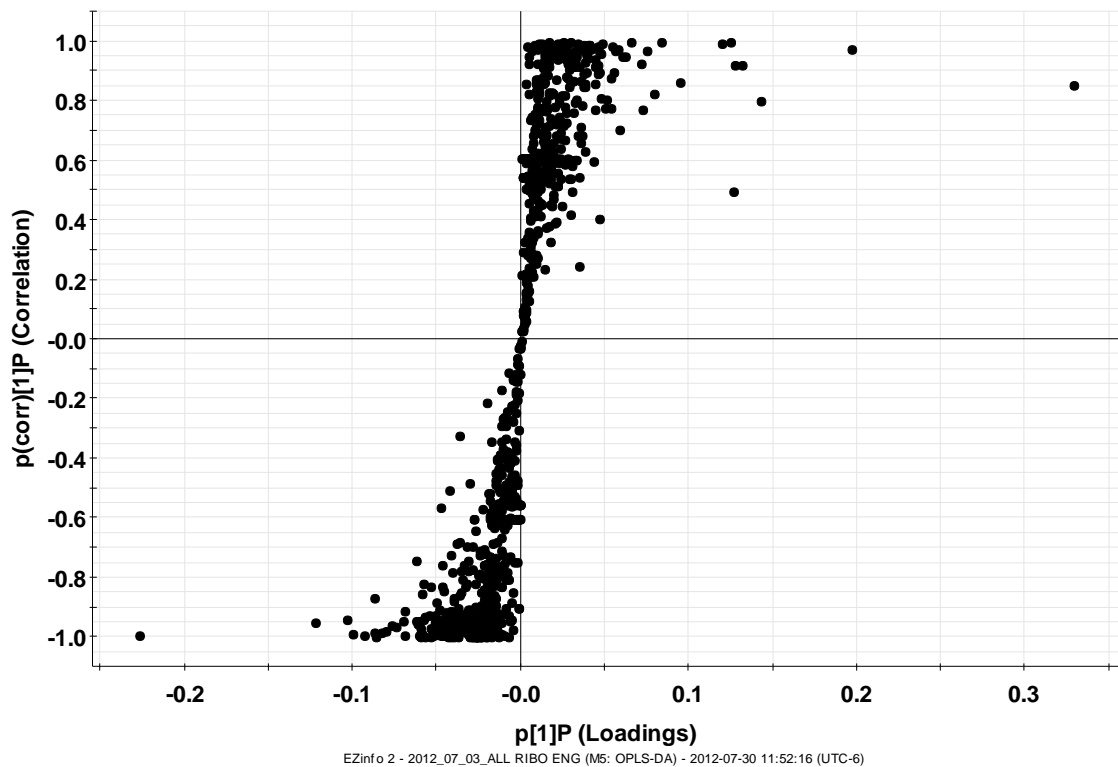
Figure A2.3. Representative S-plot of R4 mutant (-1) vs. wild type (+1). This S-plot corresponds to Figure A3.2, and is a visualization of loadings contribution. The correlation describes how specific to a particular group in the OPLS-DA a feature is (represented by a black dot). A correlation of 1 is perfect group correlation. The loadings correspond to the contribution of that feature to the first principal component of the OPLS-DA. As a result, outliers in quadrant I and III correspond to high abundance and exclusive features in the wild type and R4 mutant extracts, respectively. For all analyses, a correlation cutoff of ≥0.9 was used.

	E. coli	B. sub	M. lut.
E. coli	0	46	42
B. sub	126	0	40
M. lut.	166	13	0
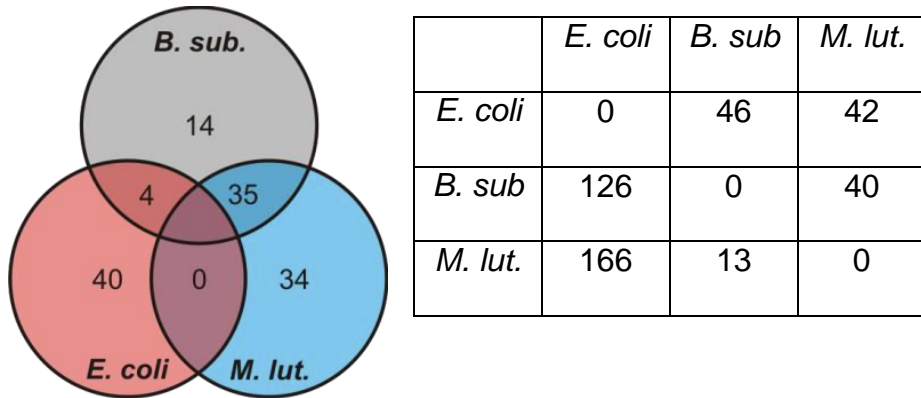
Figure A3.4. Left: Feature specificity diagram comparing *Bacillus subtilis, Escherichia coli, Micrococcusluteus*. Pareto scaled OPLS-DA was used, and features with a correlation coefficient$\geq$ 0.9 were considered specific to a group. There are 963 total features.Groups were permuted in a binary fashion, with two organisms compared against one at a given time. There are 838 shared features. **Right.** Feature specificity matrix comparing *Bacillus subtilis, Escherichia coli, Micrococcusluteus* in a binary fashion. Pareto scaled OPLS-DA was used and a correlation coefficient of $\geq$0.9 was used as a threshold for feature specific to an organism pair. The bottom half of the matrix corresponds to features specific to the organism indicated in the first column compared to the organism in the first row. The top half of the matrix corresponds to features specific to the organism in the first row when compared to the organism in the first column. There are 963 total features.

Structure elucidation of mutaxanthenes

Feature 1 (Fig. 3B, Table S2) was isolated with UV spectrum showing absorption maxima at 225, 252, 279 and 409 nm. The high resolution mass spectrum yielded an apparent m/z of 443.101, [M+H]$^+$. Combining mass with ^{1}H and ^{13}C NMR spectral data (Table S2) determined molecular formula of $C_{22}H_{18}O_{10}$ with 14 degrees of unsaturation. The ^{13}C NMR and HMBC spectra indicated the presence of 22 carbons including one methyl group, one methoxy, two methylene, five methine and thirteen quaternary carbons. The ten olefinic carbons and 5 carbonyls accounted for 10 degrees of unsaturaturation suggesting the presence of four rings. The 2D NMR spectral data allowed to establish partial structures (**I** - **III**) (**Figure 3.3(A)**). The COSY, HSQC and HMBC NMR correlations indicated that the aromatic ring of fragment a istrisubstituted with the hydroxyl group in C7 position. The chemical shifts of carbons C6 and C11 suggested that they are α,β-unsaturated carbonyls in a ring. The HMBC correlations from aromatic proton H10 to carbon C11 and from aromatic proton H8 to carbon C6 allowed to establish the positions of carbons C6 and C11 in the ring and suggested that they are adjacent to the aromatic ring. The structure of fragment a was confirmed by the feeding experiment with the 1,2-^{13}C sodium acetate where the incorporation pattern allowed to unambiguously establish the carbon backbone of **I**. The partial structure **II** (**Figure 3.3(A)**) was determined based on ^{1}H and ^{13}C NMR chemical shifts, HMBC and 1,1-ADEQUATE correlations and confirmed with data from incorporation of labeled 1,2-^{13}C sodium acetate experiment. The HMBC correlations from H12 methylene protons to the

quaternary carbons C11a and C12a indicated the position of C12 in the fragment **II**. The 1,1-ADEQUATE experiment and labeled acetate incorporation pattern further confirmed that C12 is adjacent to C11a and C12a. The chemical shift of methine C1 indicated the presence of neighboring oxygen atom. The HMBC correlations from H1 proton to C17 carbon and from H17 protons to C1 carbon confirmed the presence of the methoxy group attached to the methine C1. The HMBC correlations from proton H1 to carbons C2 and C12a indicated that methine C1 is adjacent to C2 and C12a and this was confirmed by 1,1-ADEQUATE spectral data and labeled acetate incorporation pattern. The chemical shift of methine C4a also indicated the presence of neighboring oxygen. The HMBC correlations from proton C4a to carbons C4 and C12a suggested that they are adjacent and the position of carbon C3 was established based on labeled acetate incorporation pattern which indicated that carbons C2 and C3 are attached. Furthermore the HMBC correlation from proton H1 to carbon C3 allowed assembling another ring within fragment **II**. The crucial HMBC and 1,1-ADEQUATE correlations from protons H12 to carbon C11a and from proton C4a to carbon C5 determined the connectivity between fragments **I** and **II** and allowed to assemble the last ring which turned out to be unusual xanthene scaffold. Finally, the position of carboxylic acid moiety in fragment **II** was established based on HMBC correlations from H12 methylene protons, H4a methine proton and H1 methine proton to C16 carbon. The last partial structure **III** (**Figure 3.3(A)**) was determined based on COSY correlations between methyl C15 and methylene C14 and HMBC from C14 protons to C13 ketone. Furthermore, the

HMBC correlations from C14 methylene protons to C3 quaternary carbon allowed assembling fragment **II** with fragment **III** and as result we proposed the final structure (**Figure 3.3(B)**). Mutaxanthene B (**2**) was assigned to the molecular formula of $C_{23}H_{20}O_{10}$ by HR-MS (*m/z* 457.115, [M + H]$^+$). Comparison of ^{1}H and ^{13}C NMR spectra of compounds **1** and **2** revealed the presence of the additional methoxy group (δ_H 3.96, δ_C 56.9) which showed the HMBC correlations to two olefinic carbons (C7 and C8) in the aromatic ring (**Table A3.3**). The molecular formula of mutaxanthene C (**3**) was established as $C_{21}H_{16}O_{10}$ by HR-MS of *m/z* 429.085, [M + H]$^+$. Comparison of ^{1}H and ^{13}C NMR spectra revealed the absence of methylene C14 and significant downfield shift of C15 methyl suggesting replacement of ethyl group with methyl group. The HMBC correlations to C13 and C3 confirmed the structure of **3** (**Table A3.4**). Mutaxanthene D (**4**) was assigned to the molecular formula of $C_{22}H_{19}NO_9$. The ^{1}H and ^{13}C NMR spectra of **1** and **4** were very similar with the most significant difference in chemical shift from 208.2 for **1** to 182.5 for **2** for carbon C13 indicating the replacement of ketone group with amino group in this position along with equilibrium shift from endocyclicenol as dominant tautomer for compound **1** and ketone as dominant tautomer for compound **4** (**Table A3.5**). The structure of mutaxanthene E (**5**) was established based on molecular formula of $C_{21}H_{17}NO_9$ and comparison of ^{1}H and ^{13}C NMR spectra of **5** to compounds **3** and **4** indicating the presence of amino group in C13 position and methyl group adjacent to C13 carbon (**Table A3.6**).

Table A3.2. NMR spectroscopic data for compound **1** in CD$_3$OD.
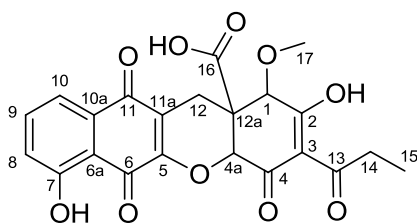
Pos.	^{13}C	^{1}H	HMBC	J_{CC}/Hz
1	83.3	4.12, 1H, br	2,3,4a,12,12a, 16,17	br
2	190.2			48.3
3	109.1			60
4	190.8			br
4a	76.3	5.56, 1H, br	1,4,5,12,12a, 16	br
5	154.3			61.6
6	183.9			61.6
6a	114.6			64
7	162.3			64
8	124.7	7.0, 1H, d, 8.3 Hz	6, 6a, 7, 10	58.2
9	137.8	7.43, 1H, br dd, 8Hz	7, 10a	58.2
10	119.6	7.24, 1H, d, 7.2Hz	6a, 8, 11	62.5
10a	132.5			62.5
11	183.3			56.9
11a	120			56.9
12	23.1	2.38, 1H br d, 3.08, 1H, br d, 19Hz	1,4a,5,11,11a,12a,16	33.3
12a	48			33.3
13	208.2			
14	34.5	2.97, 2H, m	3, 13, 15	35.2
15	8.3	1.05, 3H, br t, 7.1Hz	13, 14	35.2
16	172.1			
17	60.9	3.5, 3H, br s	1	

Table A3.3. NMR spectroscopic data for compound **2** in D_2O.
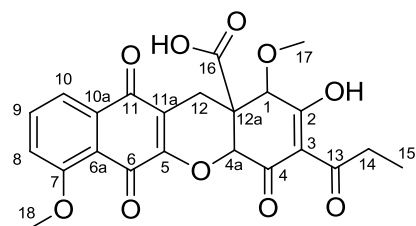
Pos.	^{13}C	^1H	HMBC
1	86.0	3.77, 1H, br	2, 3, 4a, 12, 12a, 16, 17
2	188.6		
3	112.2		
4	189.5		
4a	76.5	5.44, 1H, br	4, 5, 12, 12a, 16
5	154.5		
6	179.1		
6a	116.9		
7	159.6		
8	118.5	7.23, 1H, d,	6, 6a, 7, 10
9	136.4	7.52, 1H, brdd,	7, 10a
10	119.0	7.34, 1H, d,	6a, 8, 11
10a	133.1		
11	184.8		
11a	117.6		
12	22.4	2.26, 1H br d,2.96, 1H, br d,	1, 4a, 5, 11, 11a, 12a, 16
12a	48.2		
13	210.0		
14	35.8	2.55, 2H, m	13, 15
15	8.5	0.89, 3H, br t,	13, 14
16	176.5		
17	59.8	3.43, 3H, br s	1
18	56.2	3.83, 3H, s	7, 8

Table A3.4. NMR spectroscopic data for compound **3** in CD$_3$OD.
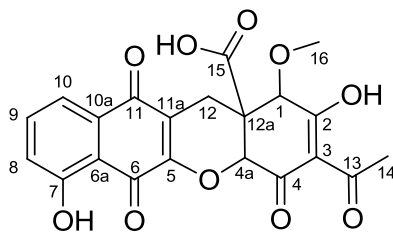
Pos.	^{13}C	^{1}H	HMBC
1	82.9	4.17, 1H, br	
2	-		
3	109.6		
4	-		
4a	76.9	5.55, 1H, br	
5	154.4		
6	178.4		
6a	114.9		
7	162.6		
8	124.5	7.24, 1H, d,	6a, 7, 10
9	137.7	7.65, 1H, brdd,	7, 10a
10	119.4	7.56, 1H, d,	6a, 8,11
10a	132.9		
11	183.4		
11a	119.9		
12	23.0	2.50, 1H br d,3.19, 1H, br d,	1, 4a, 5,6, 11, 11a, 12a, 16
12a	48.1		
13	203.7		
14	27.4	2.56, 3H, s	3, 13
15	172.0		
16	60.7	3.57, 3H, br s	

Table A3.5. NMR spectroscopic data for compound **4** in D_2O.
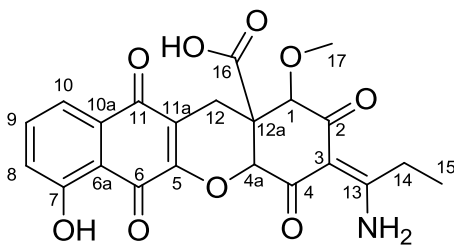
Pos.	^{13}C	^{1}H	HMBC	J_{CC}/Hz
1	85.7	3.82, 1H, s	2, 3, 4a, 12, 12a, 16, 17	45.5
2	192.5			45.5
3	102.3			61.2
4	192.2			61.2
4a	77.2	5.43, 1H, d	1, 4, 5, 12, 12a, 16	
5	153.4			61.0
6	183.1			61.0
6a	113.3			64.5
7	160.0			64.5
8	123.8	7.0, 1H, d, 8.3 Hz	6, 6a, 7, 10	58.4
9	137.1	7.43, 1H, dd, 8Hz	7, 10a	58.4
10	119.2	7.22, 1H, d, 7.2Hz	6a, C8, 11	62.8
10a	131.1			62.8
11	183.9			57.6
11a	119.9			57.6
12	22.2	2.17, 1H dd,2.94, 1H, dd, 19Hz	1, 4a, 5, 11, 11a, 12a, 16	34.4
12a	47.3			34.4
13	182.5			56
14	29.8	2.83, 2H, dq	3, 13, 15	-
15	11.3	1.09, 3H, t, 7.1Hz	13, 14	-
16	175.8			
17	59.9	3.42, 3H, s	1	

Table A3.6. NMR spectroscopic data for compound **5** in D$_2$O.
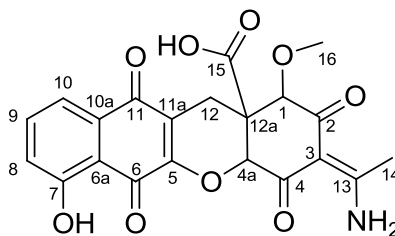
Pos.	^{13}C	^{1}H	HMBC
1	85.3	3.83, 1H, s	2, 3, 4a, 12, 12a, 16, 17
2	192.7		
3	103.3		
4	192.3		
4a	77.4	5.42, 1H, d	1, 4, 5, 12, 12a, 16
5	153.7		
6	183.3		
6a	113.6		
7	160.2		
8	123.8	7.15, 1H, d,	6, 6a, 7, 10
9	137.1	7.56, 1H, dd,	7, 10a
10	119.3	7.43, 1H, d,	6a, 8, 11
10a	131.4		
11	184.6		
11a	120.0		
12	22.3	2.26, 1H dd,2.95, 1H, dd,	1, 4a, 5, 11, 11a, 12a, 16
12a	47.6		
13	177.8		
14	24.2	2.41, 3H, s	13, 3
15	175.9		
16	60.0	3.42, 3H, s	1
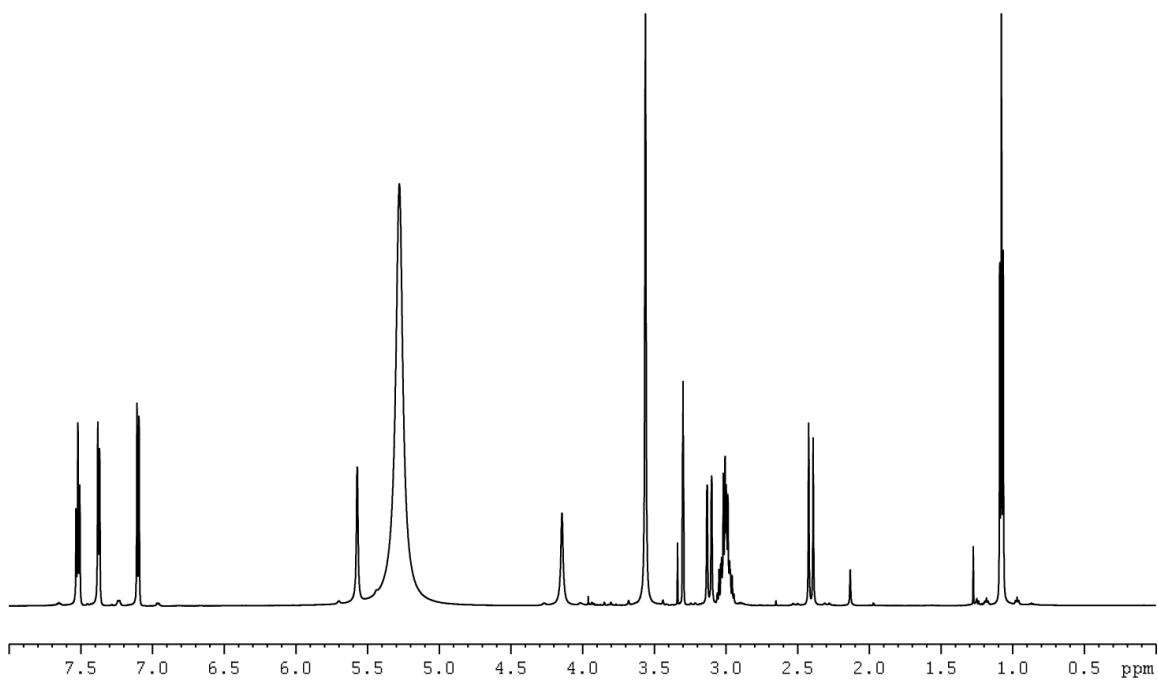
Figure A3.6. ^{1}H proton NMR of mutaxanthene A (1) in CD$_3$OD.

Mutaxanthene A
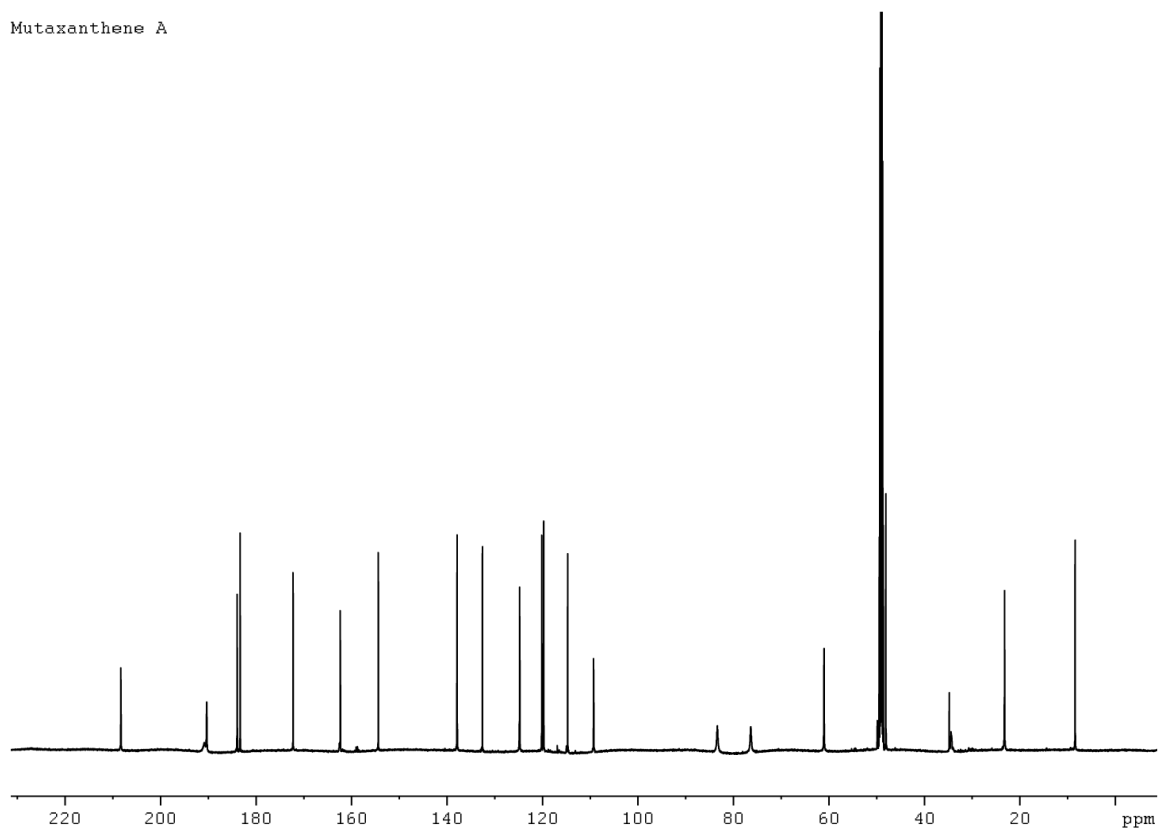
Figure A3.7. ^{13}C carbon NMR of mutaxanthene A (1) in CD$_3$OD.
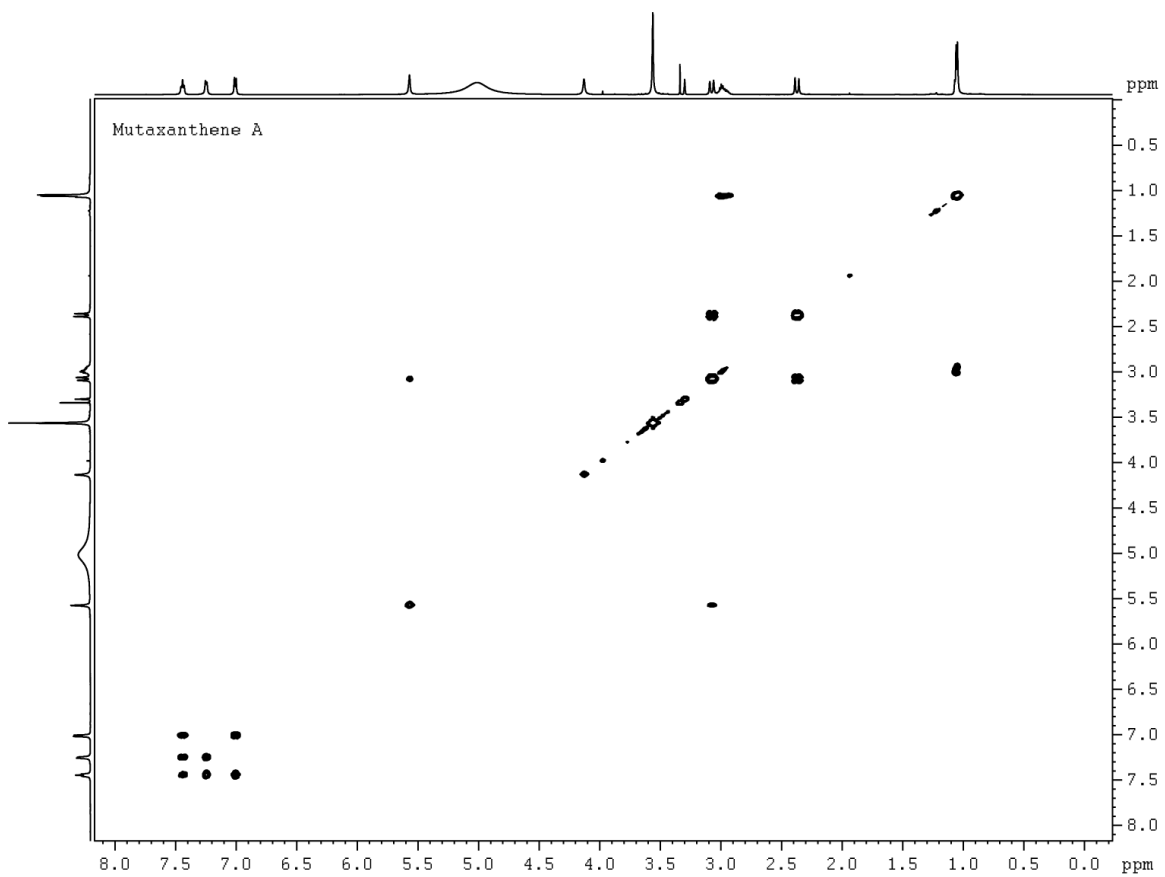
Figure A3.8. 2D COSY NMR of mutaxanthene A (1) in CD$_3$OD.
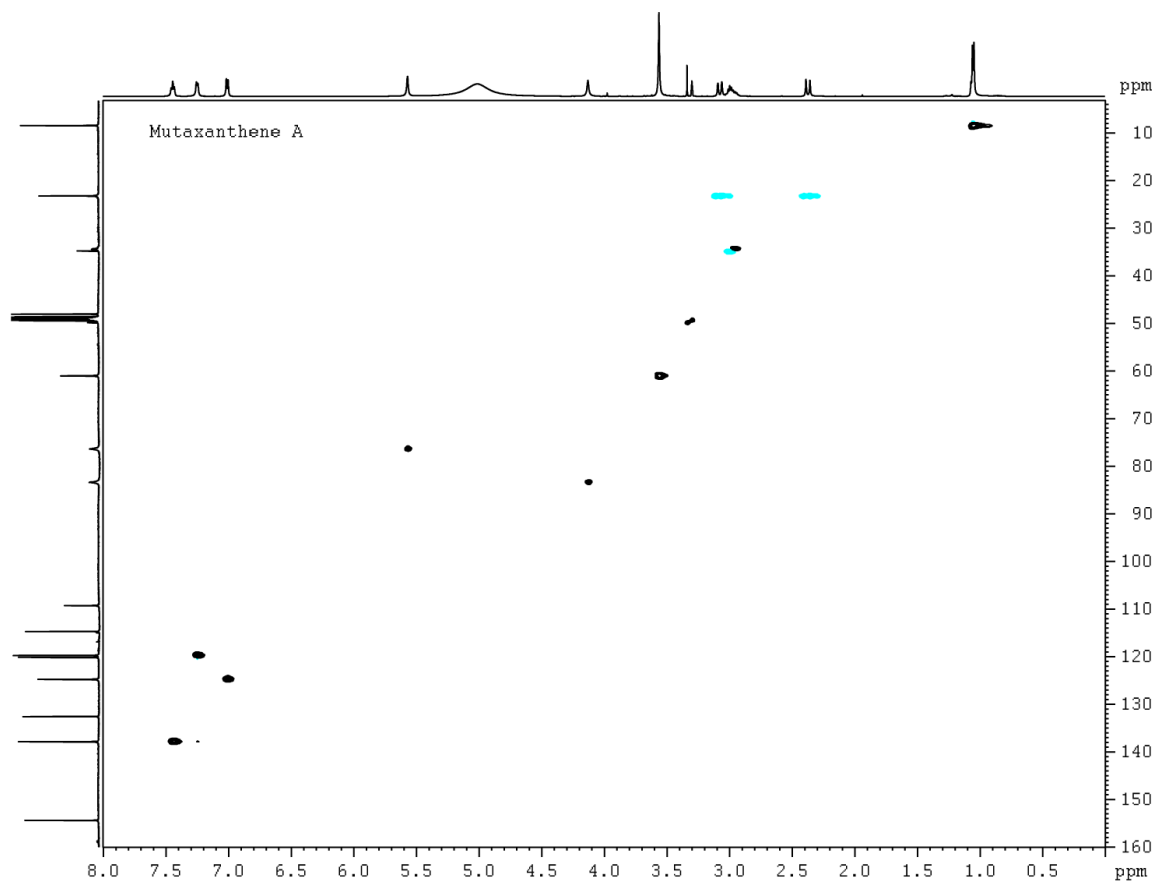
Figure A3.9. 2D HSQC NMR of mutaxanthene A (1) in CD$_3$OD.
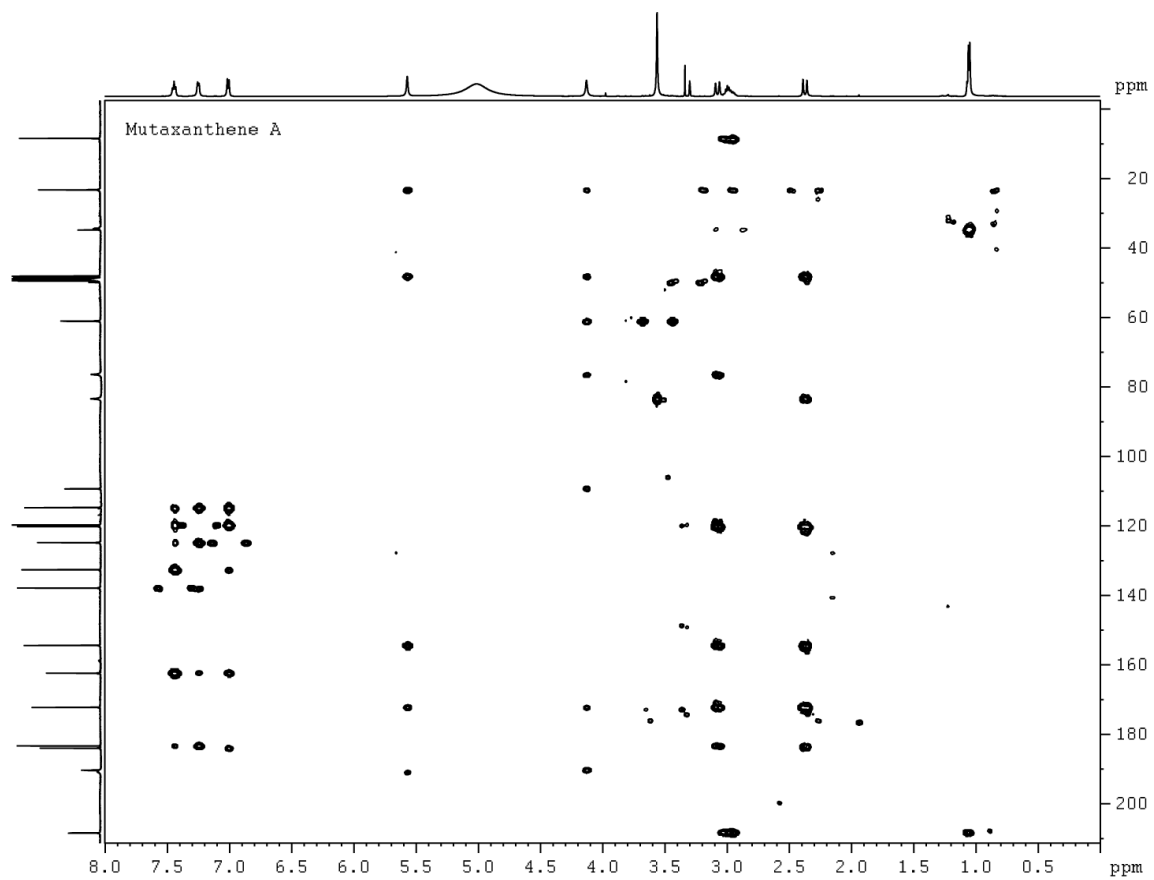
Figure A3.10. 2D HMBC NMR of mutaxanthene A (1) in CD$_3$OD.
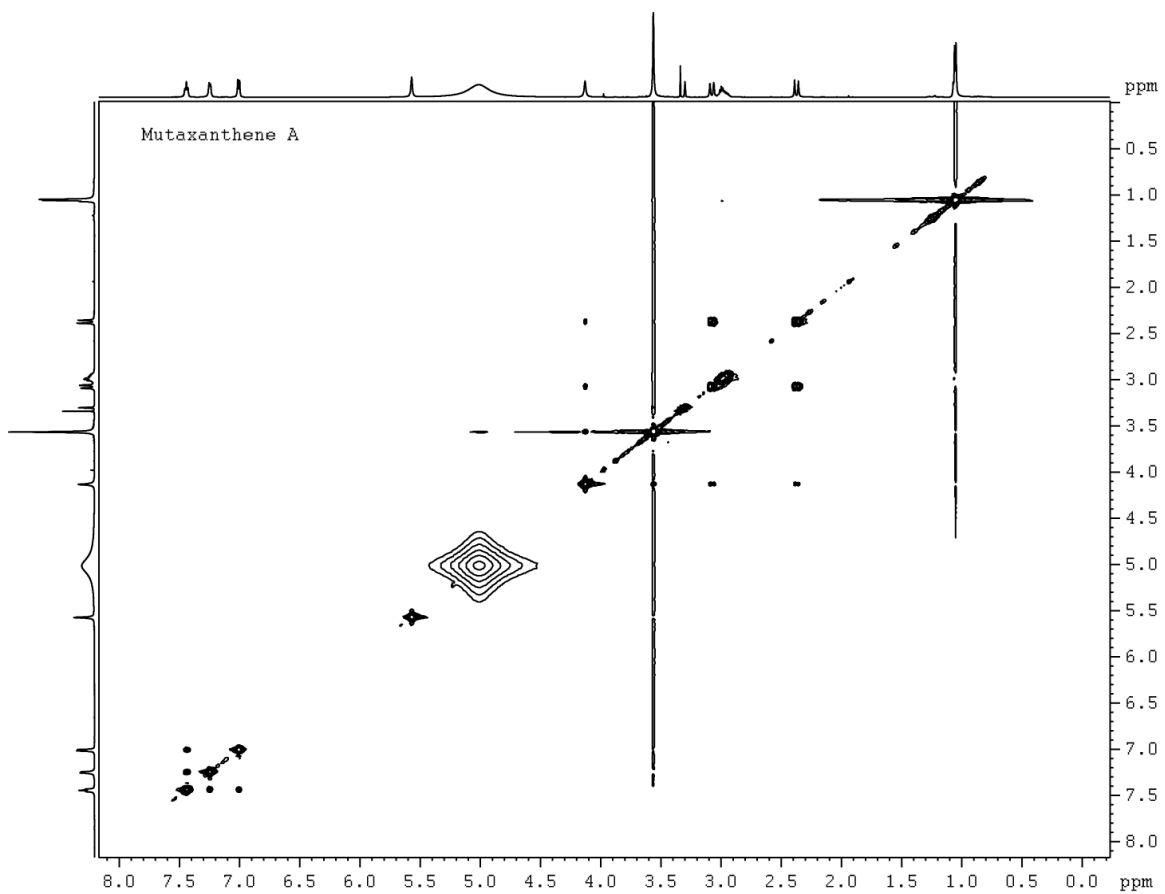
Figure A3.11. 2D NOESY NMR of mutaxanthene A (1) in CD$_3$OD.
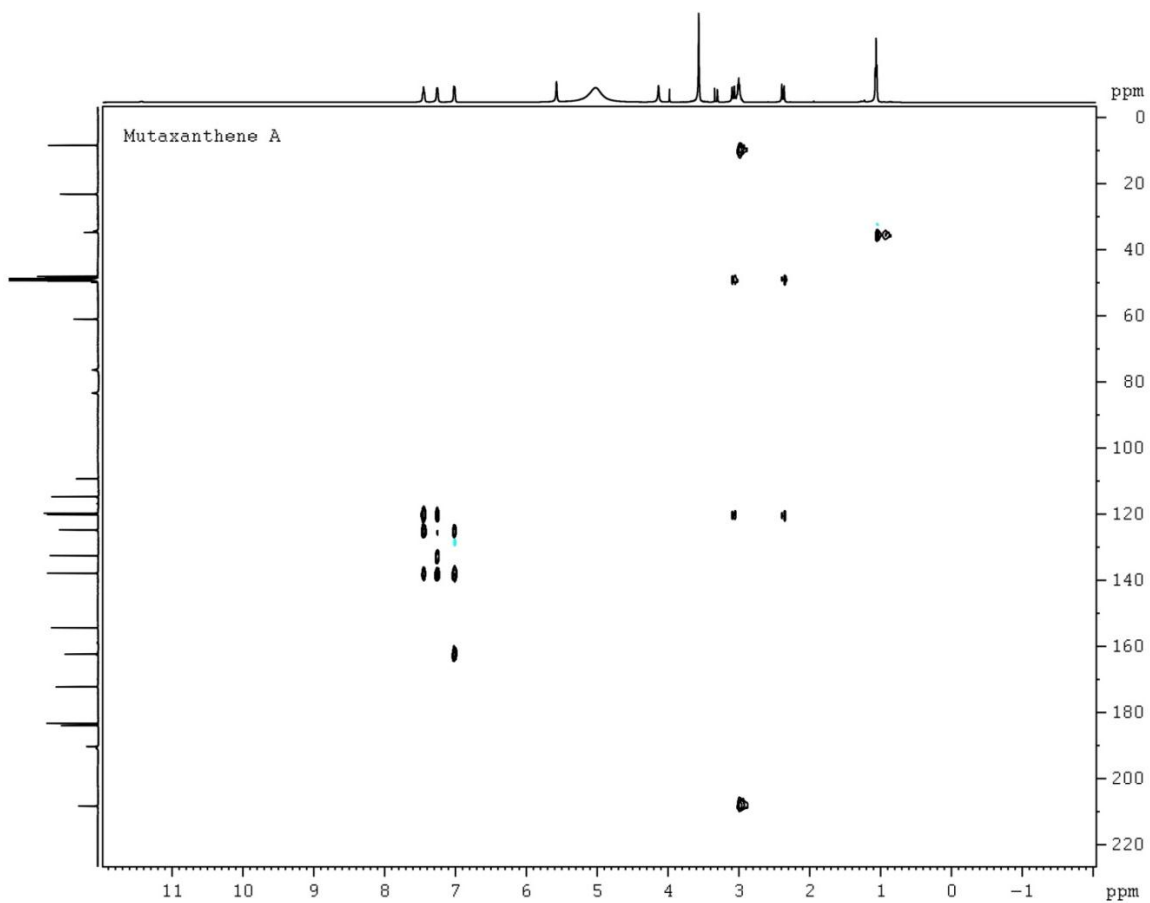
Figure A3.12. 2D 1,1-ADEQUATE NMR of mutaxanthene A (1) in CD$_3$OD.
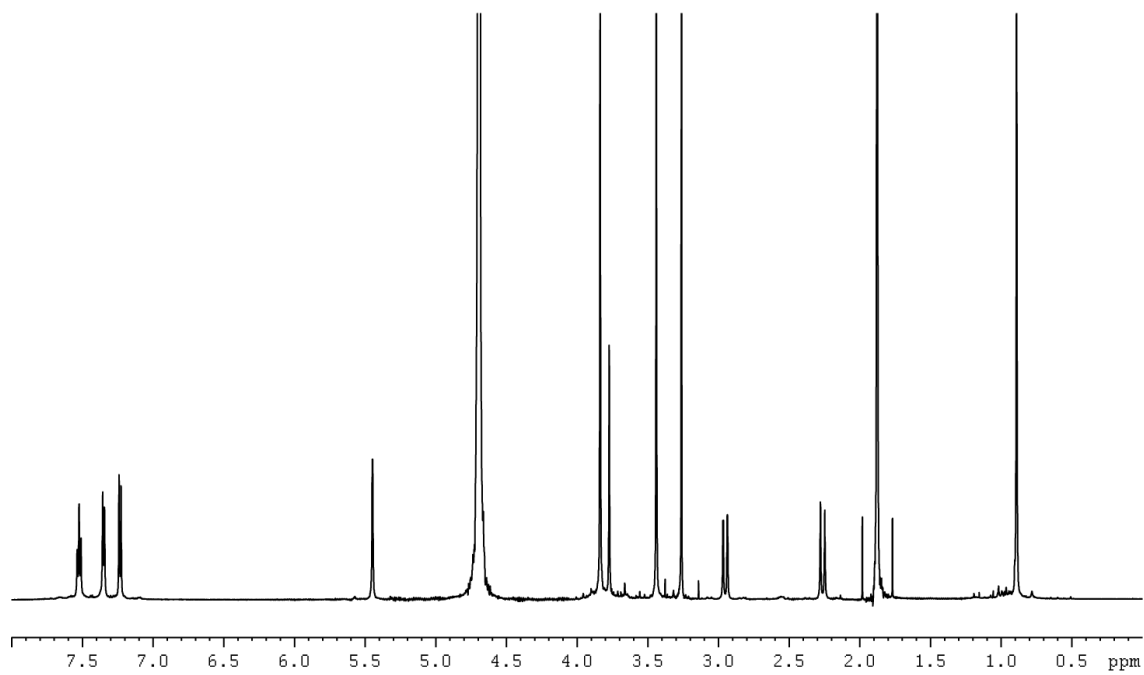
Figure A3.13. ^{1}H proton NMR of mutaxanthene B (2) in D$_2$O.
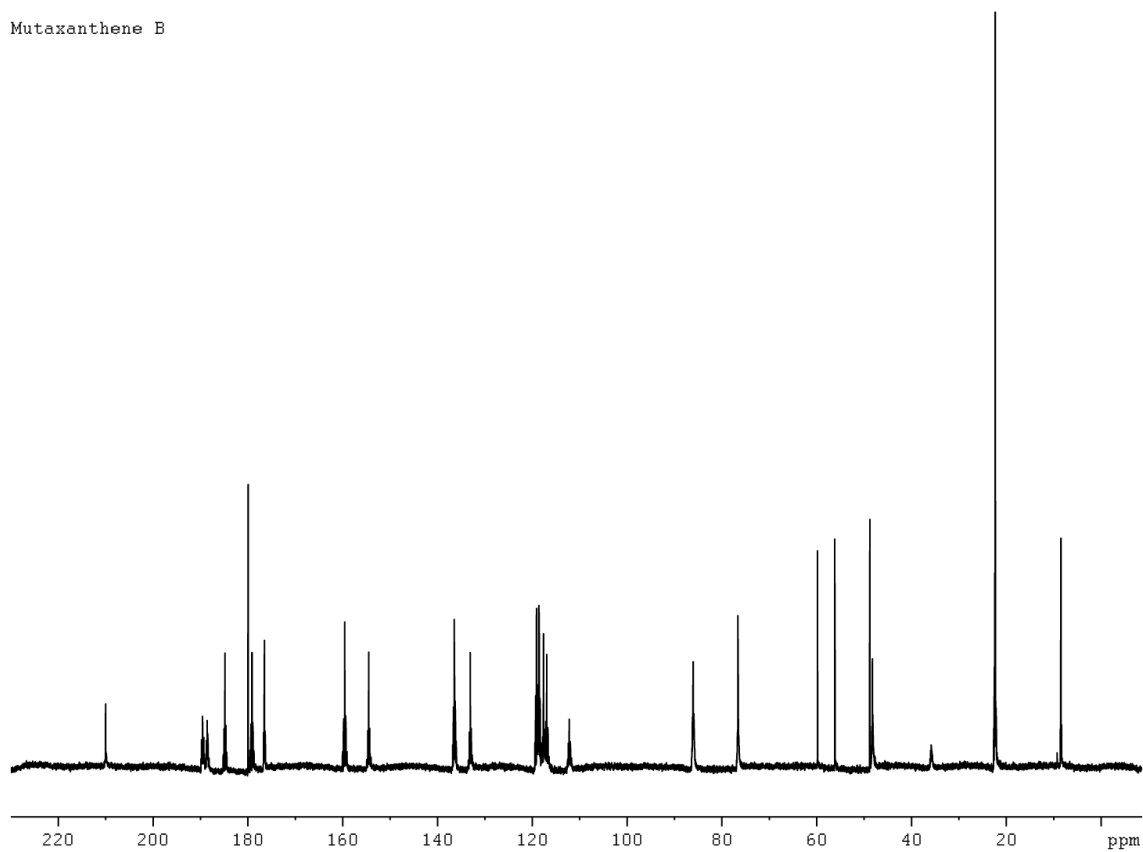
Figure A3.14. ^{13}C carbon NMR of mutaxanthene B (2) in D$_2$O
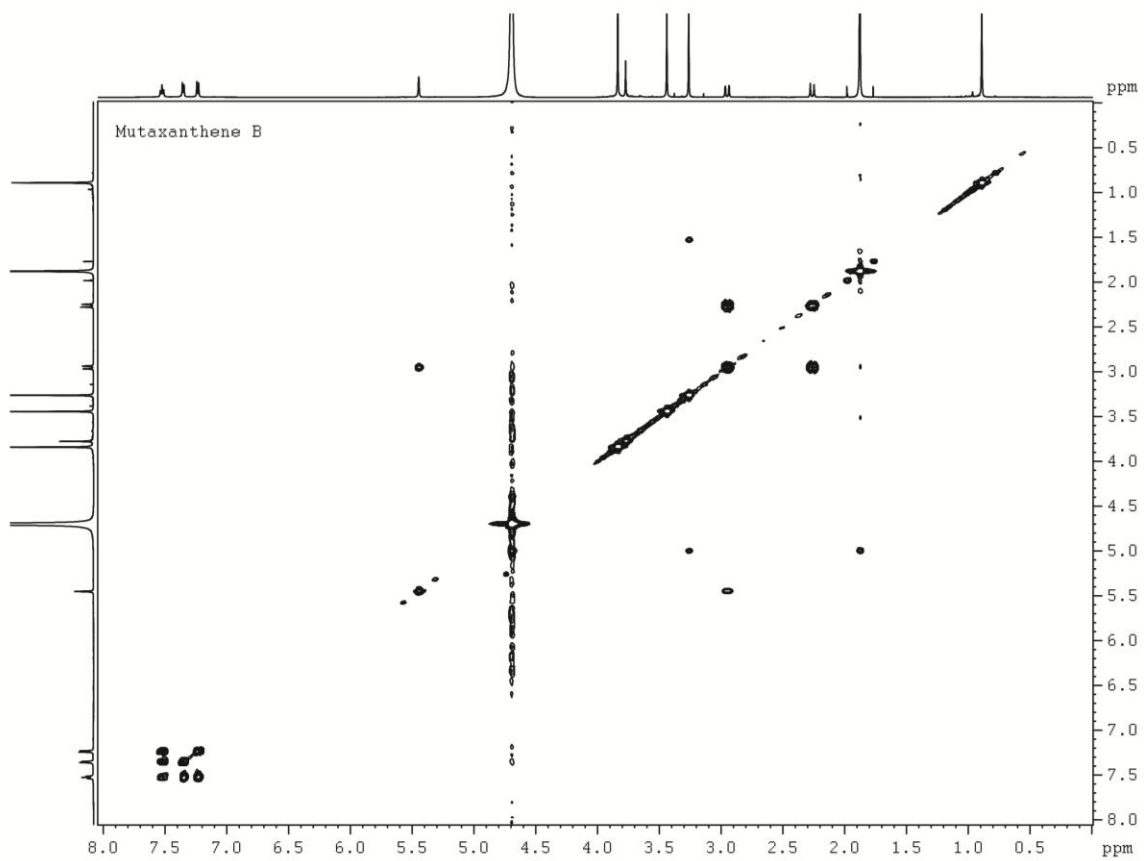
Figure A3.15. 2D COSY NMR of mutaxanthene B (2) in D$_2$O.
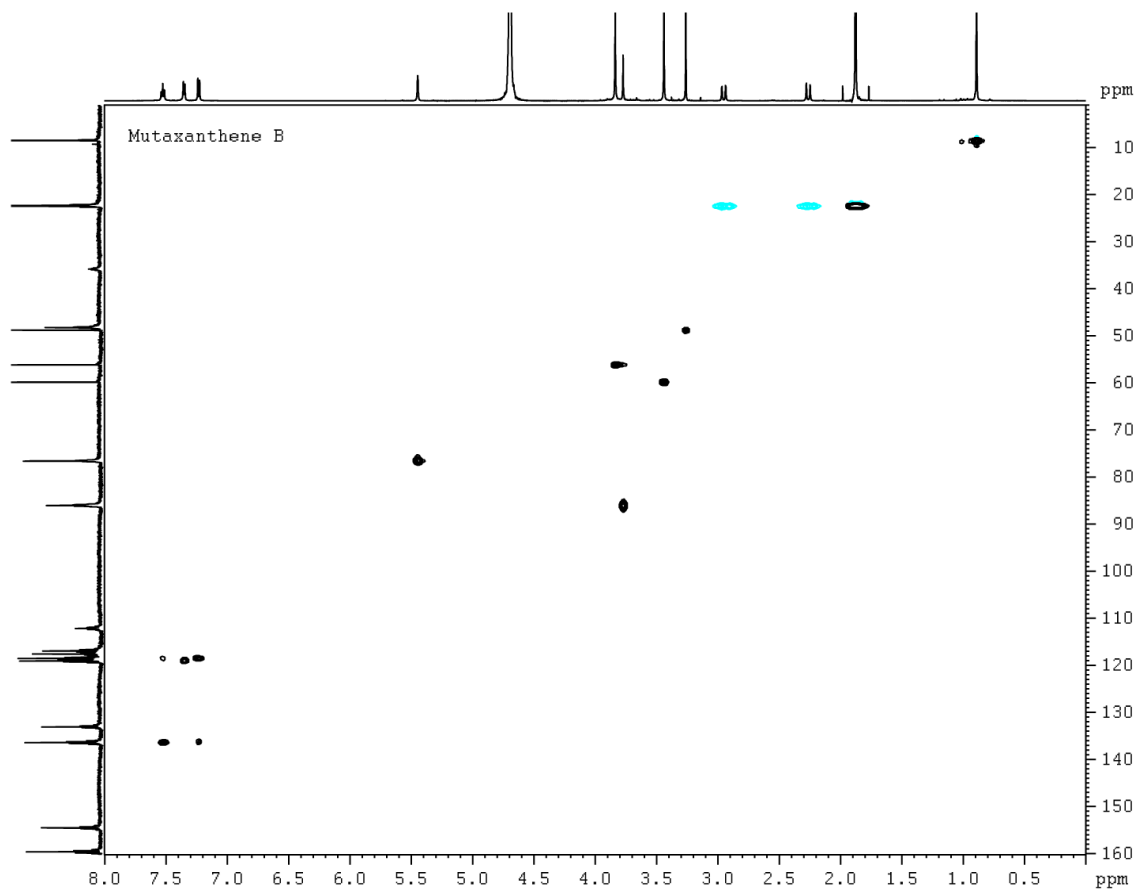
Figure A3.16. 2D HSQC NMR of mutaxanthene B (2) in D$_2$O.
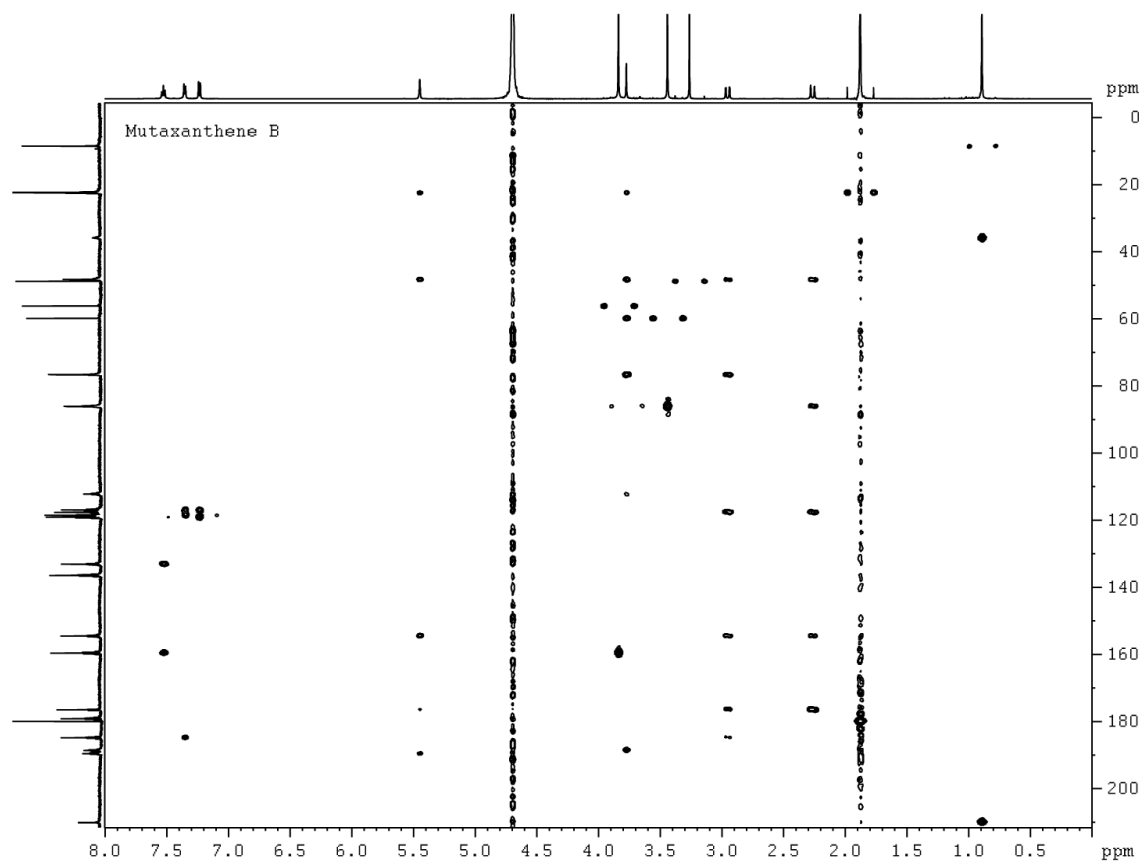
Figure A3.17. 2D HMBC NMR of mutaxanthene B (2) in D₂O.
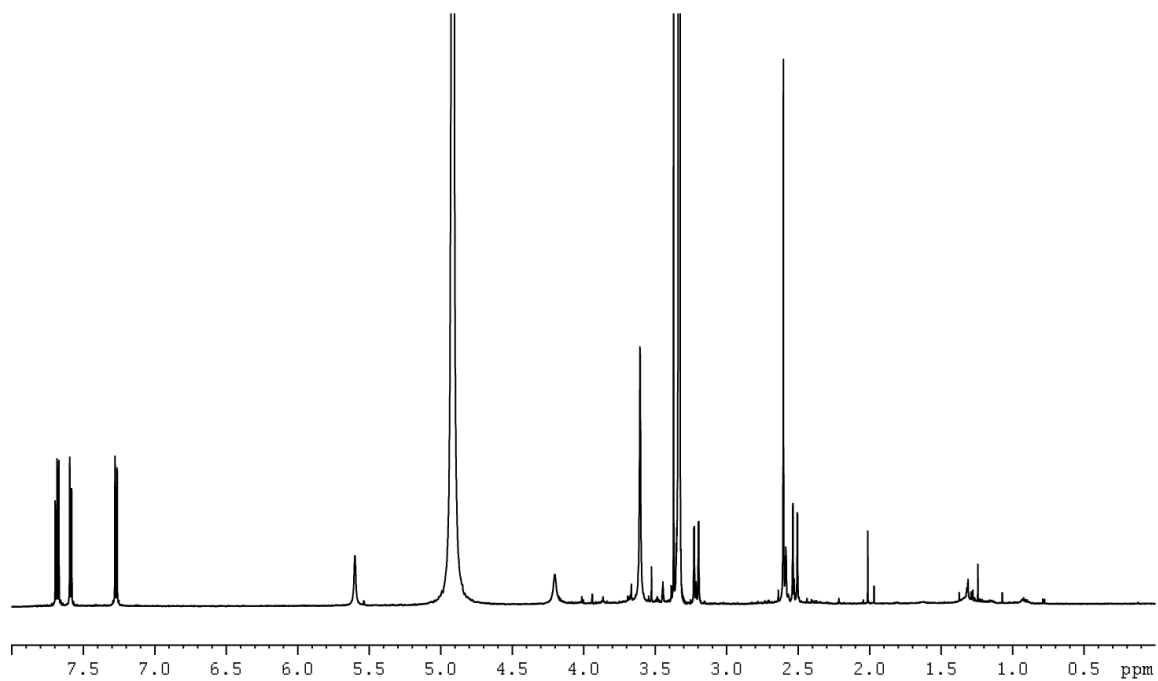
Figure A3.18. ^{1}H proton NMR of mutaxanthene C (3) in CD$_3$OD.
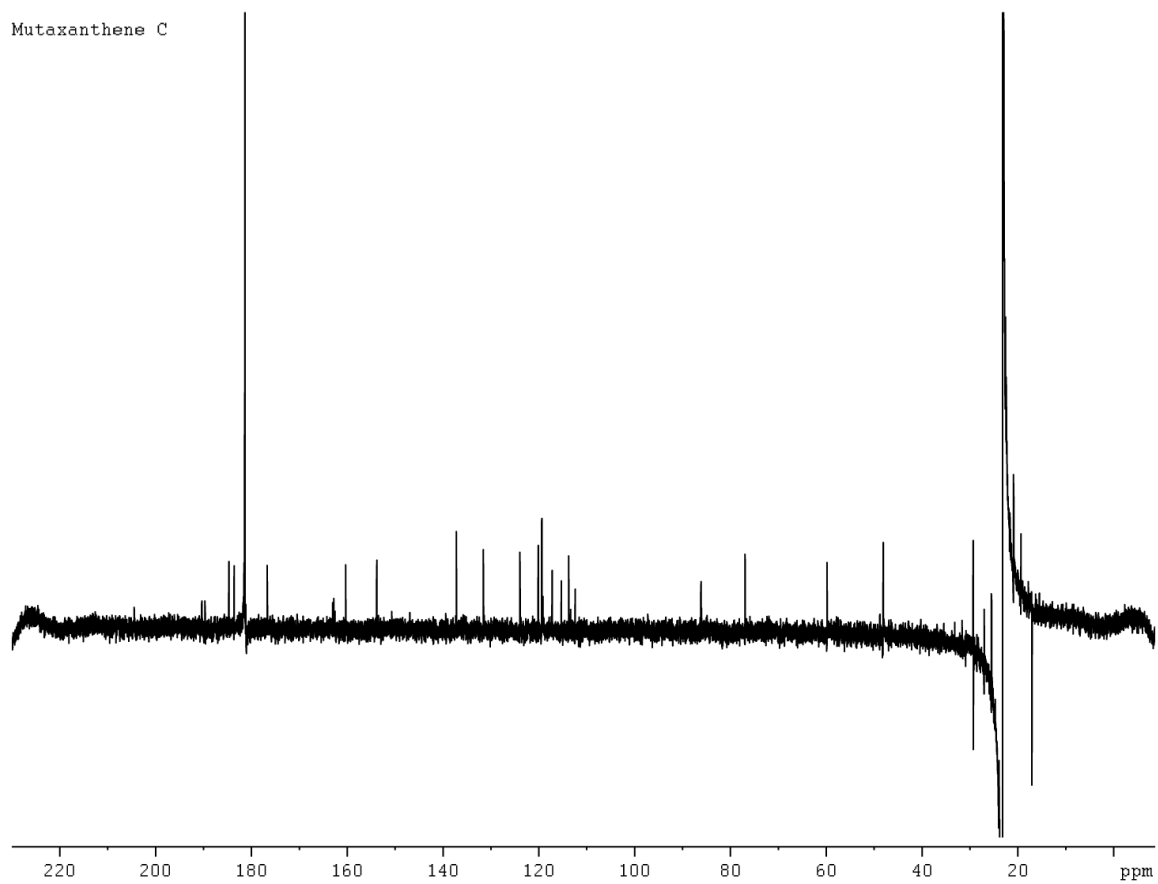
Figure A3.19. ^{13}C proton NMR of mutaxanthene C (2) in D_2O.
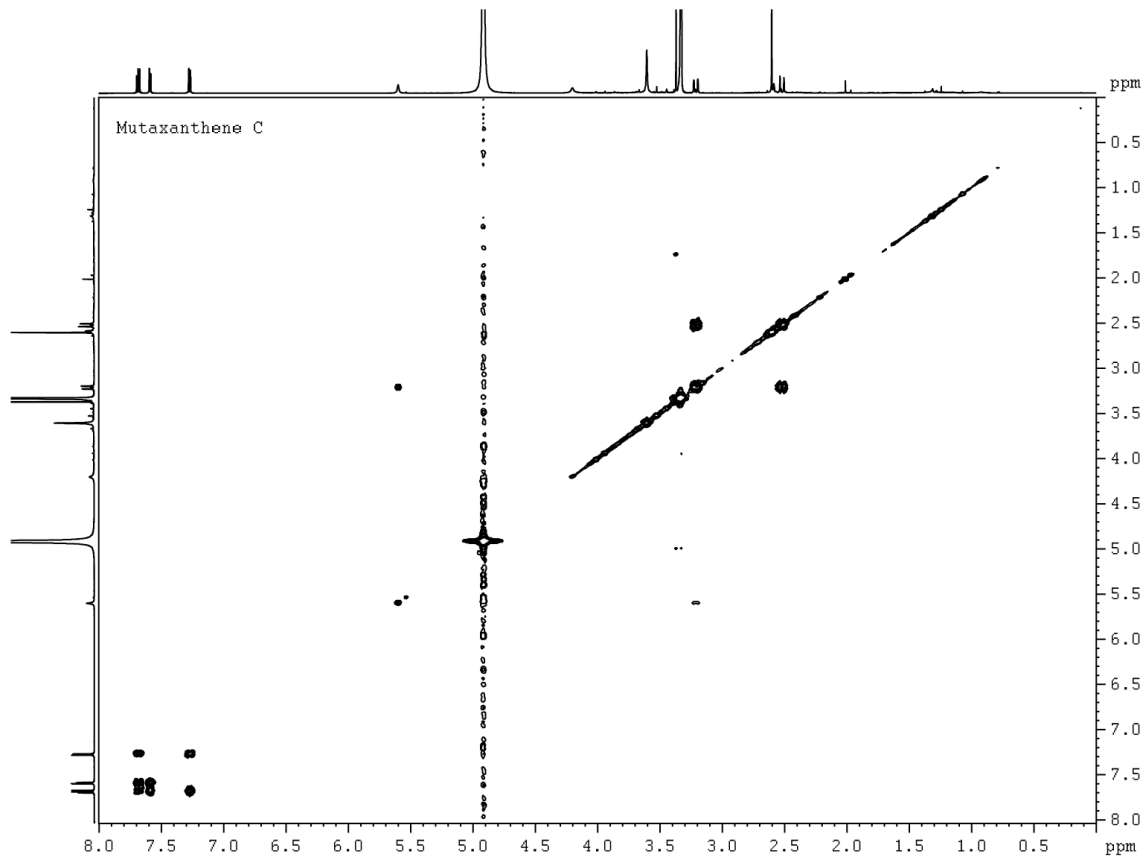
Figure A3.20. 2D COSY NMR of mutaxanthene C (3) in CD₃OD.
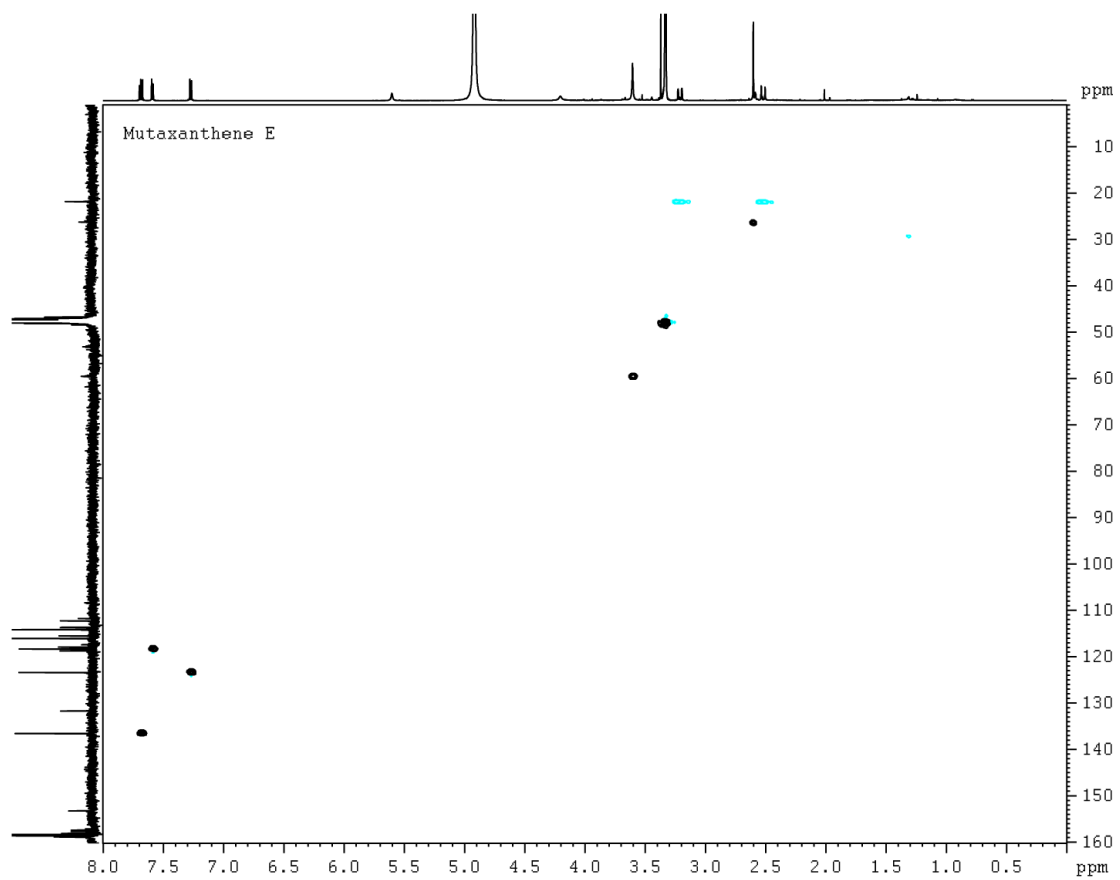
Figure A3.21. 2D HSQC NMR of mutaxanthene C (3) in CD$_3$OD.
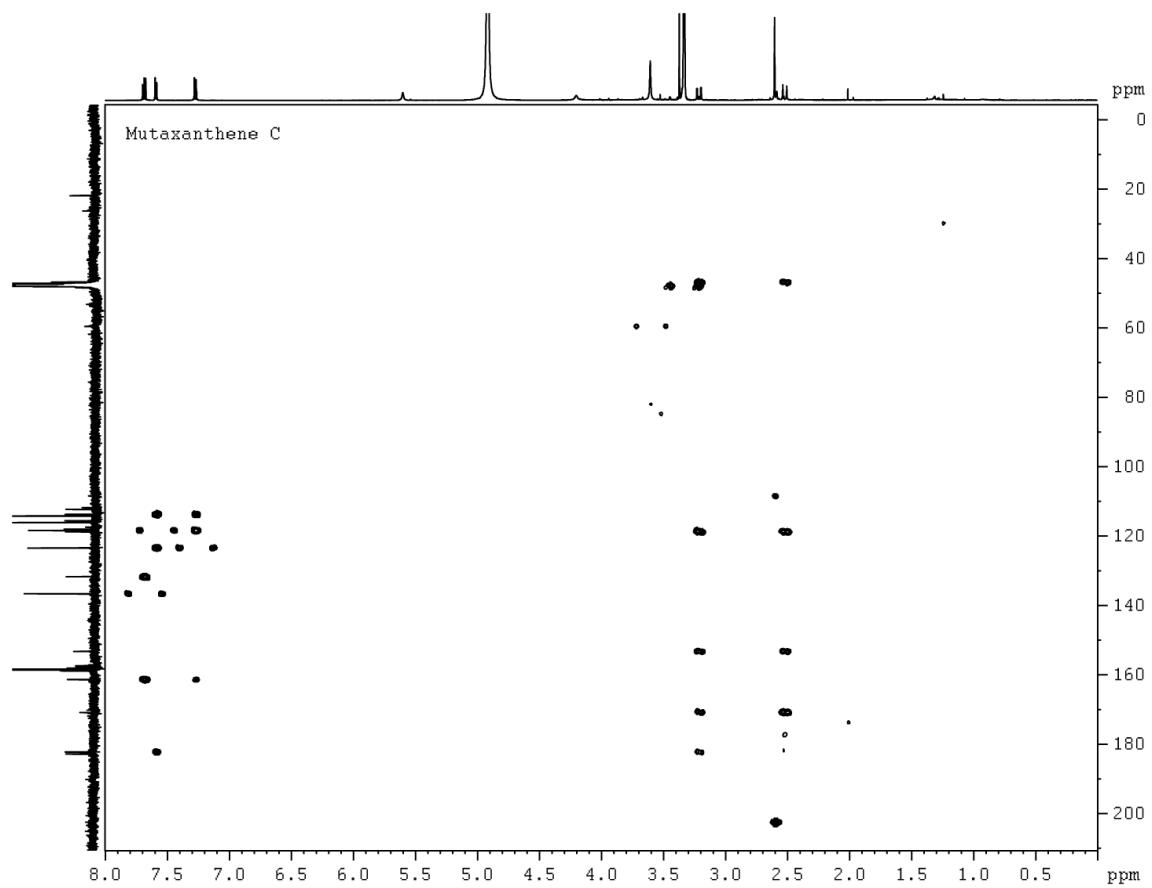
Figure A3.22. 2D HMBC NMR of mutaxanthene C (3) in CD₃OD.

Mutaxanthene D
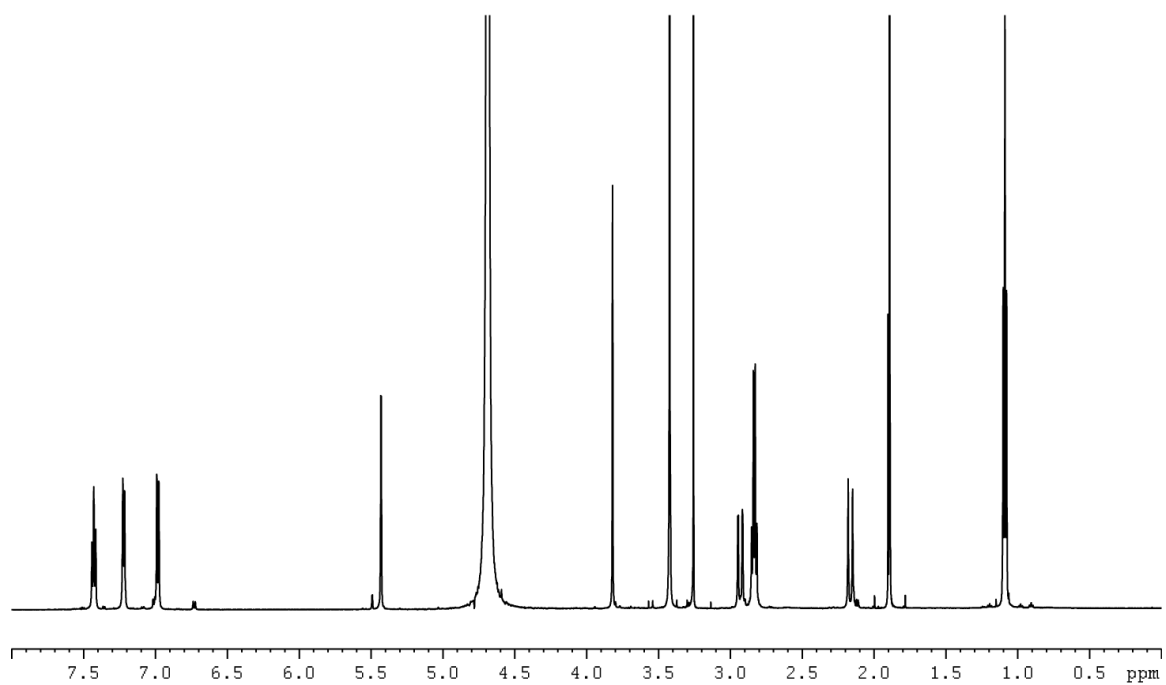
Figure A3.23. ^{1}H proton NMR of mutaxanthene D (4) in D$_2$O.
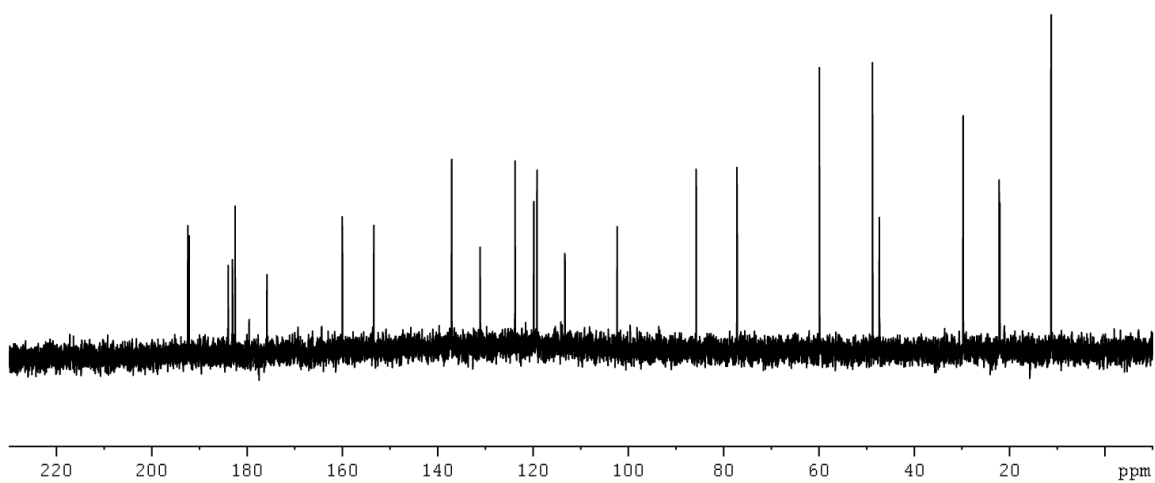
Figure A3.24. ^{13}C proton NMR of mutaxanthene D (4) in D$_2$O.
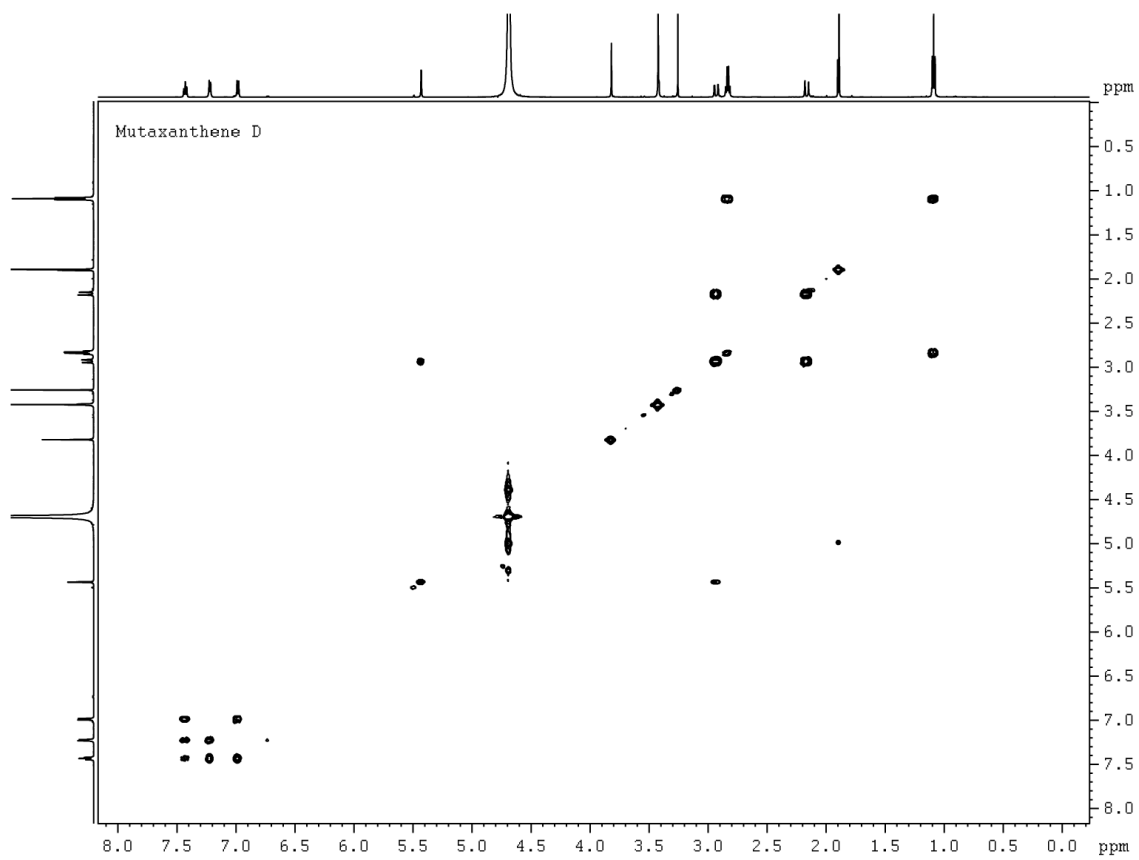
Figure A3.25. 2D COSY NMR of mutaxanthene D (4) in D₂O.
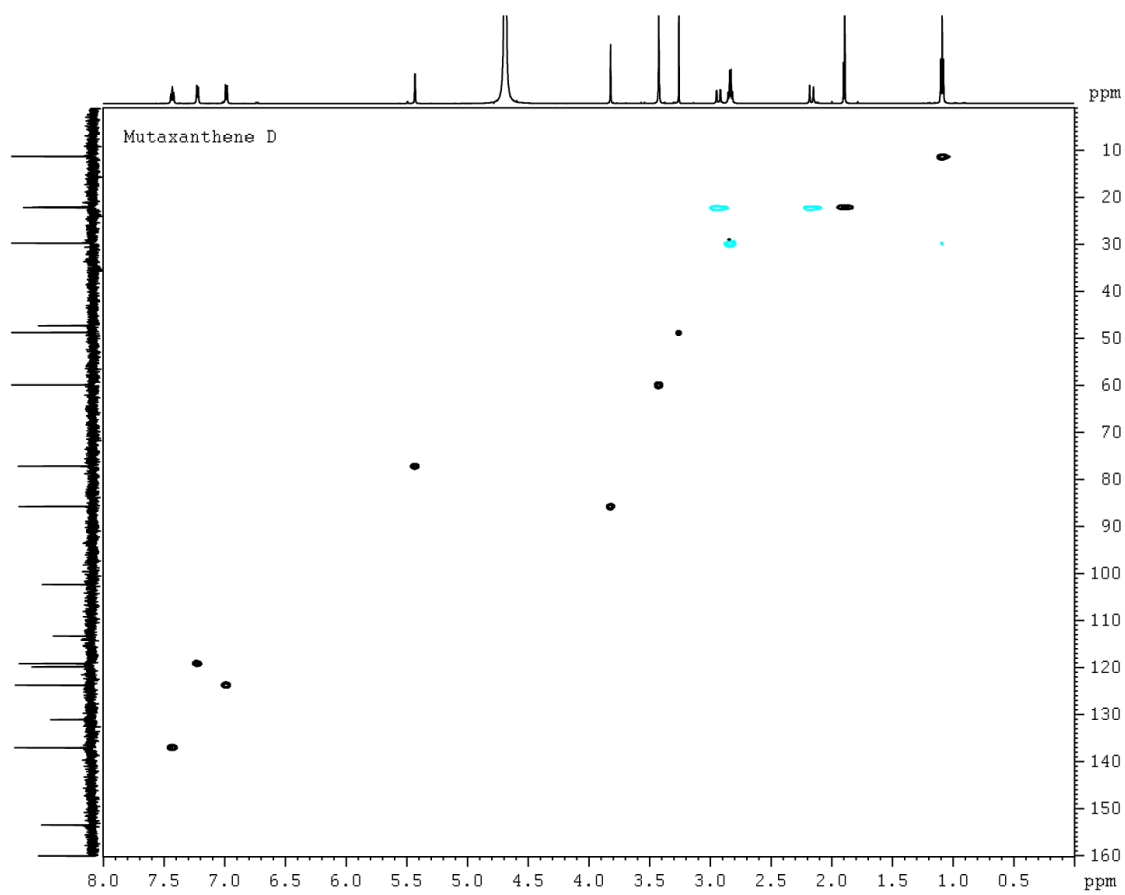
Figure A3.26. 2D HSQC NMR of mutaxanthene D (4) in D$_2$O.
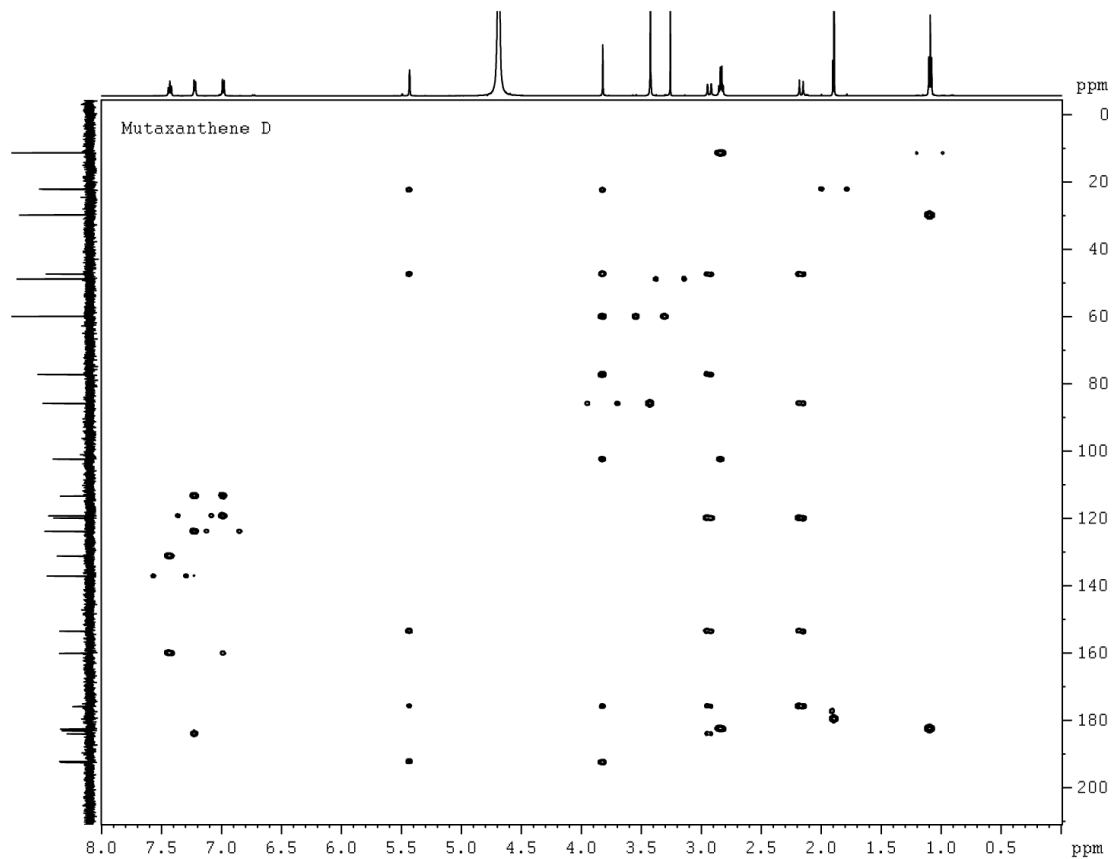
Figure A3.27. 2D HMBC NMR of mutaxanthene D (4) in D$_2$O.
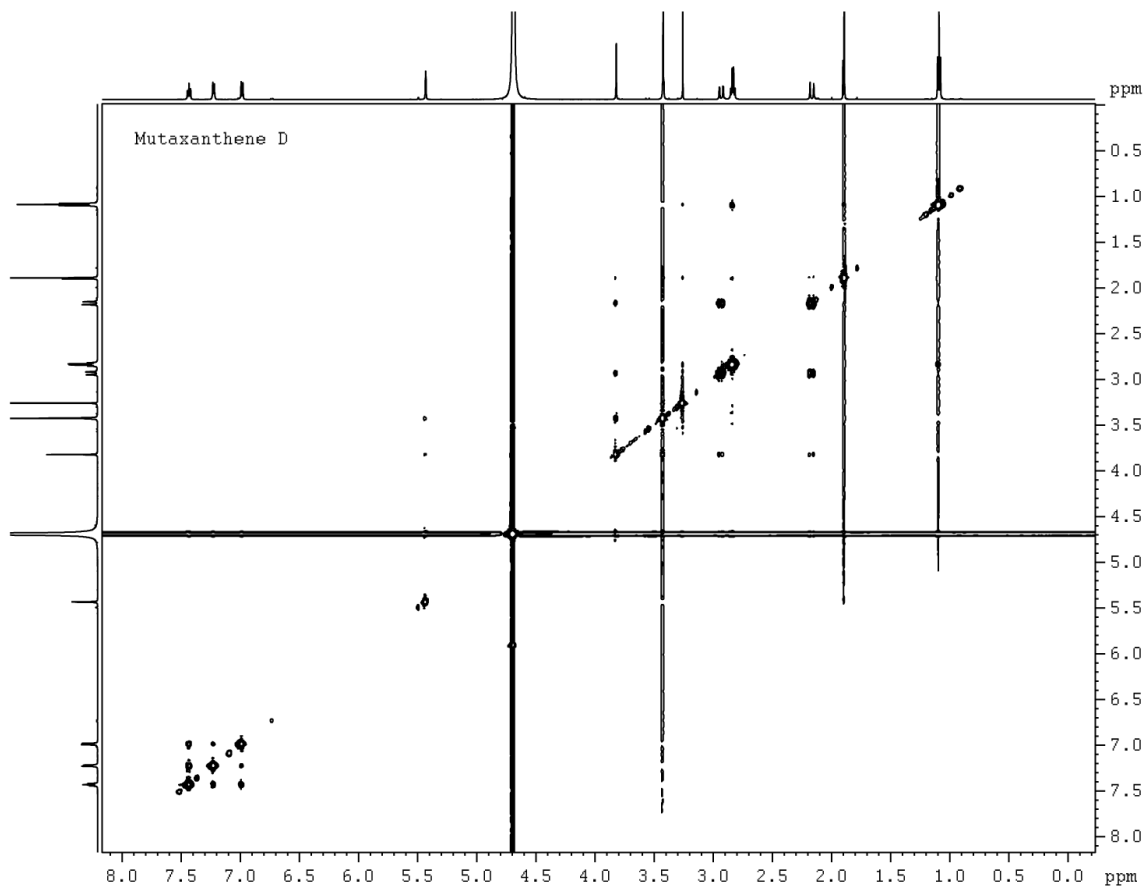
Figure A3.28. 2D NOESY NMR of mutaxanthene D (4) in D$_2$O.
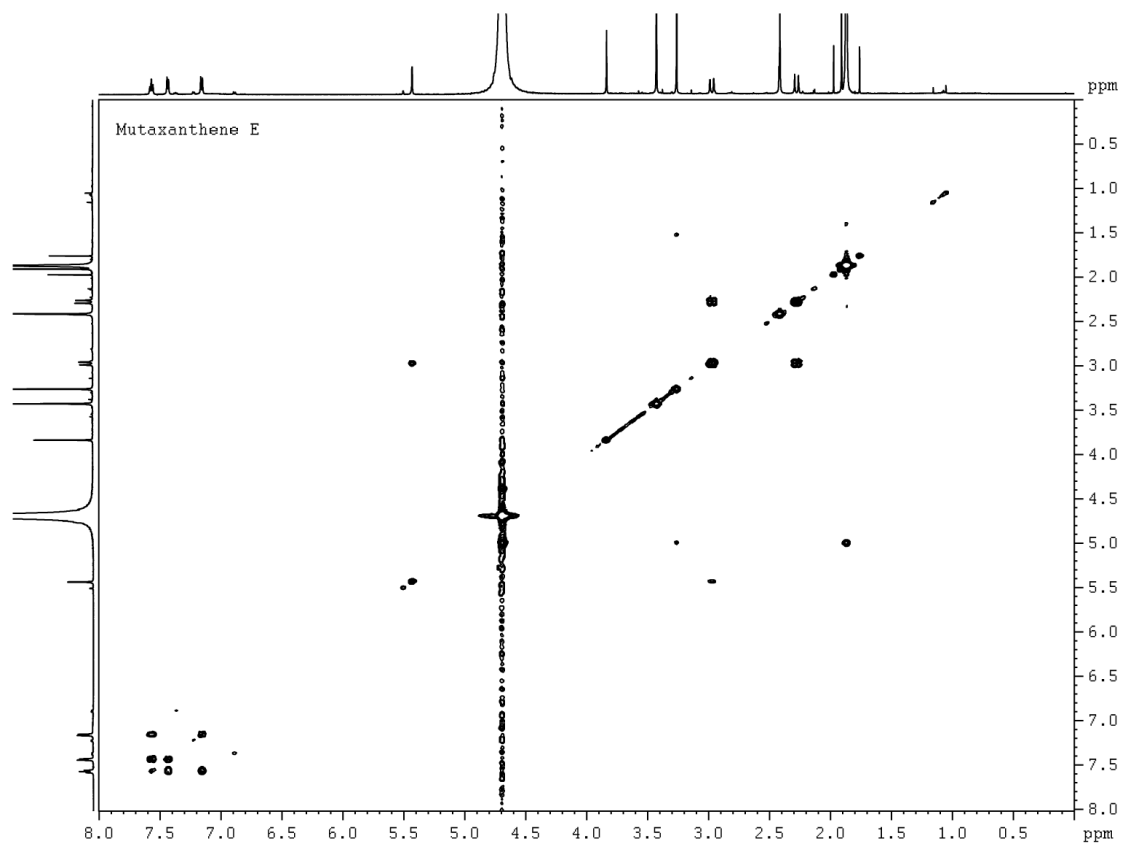
Figure A3.29. 1H proton NMR of mutaxanthene E (5)
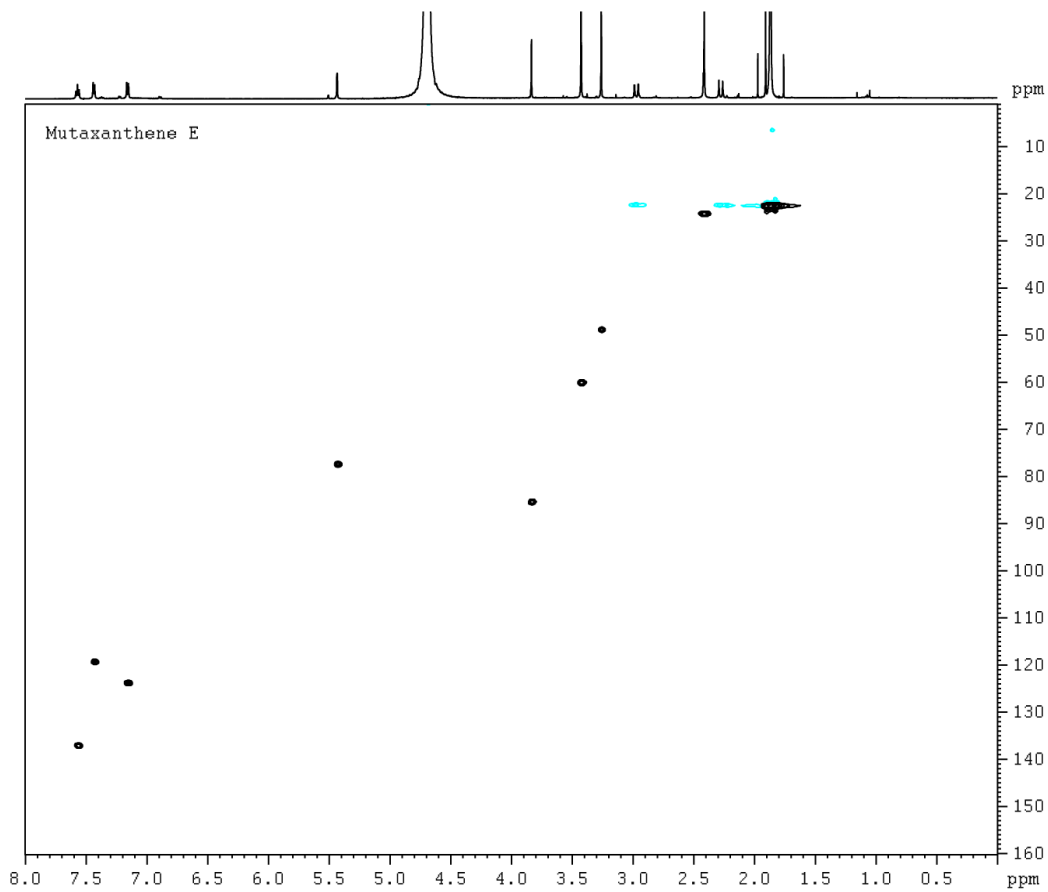
Figure A3.30. 2D COSY NMR of mutaxanthene E (5) in D₂O.
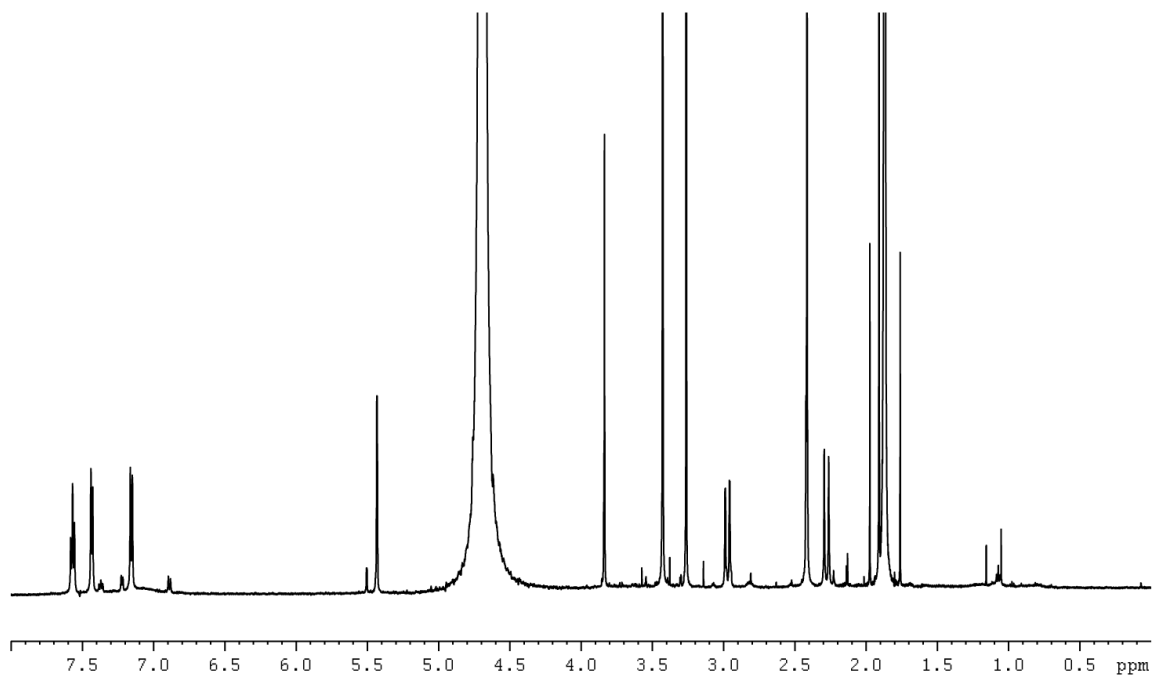
Figure A3.31. 2D HSQC NMR of mutaxanthene E (5) in D$_2$O.
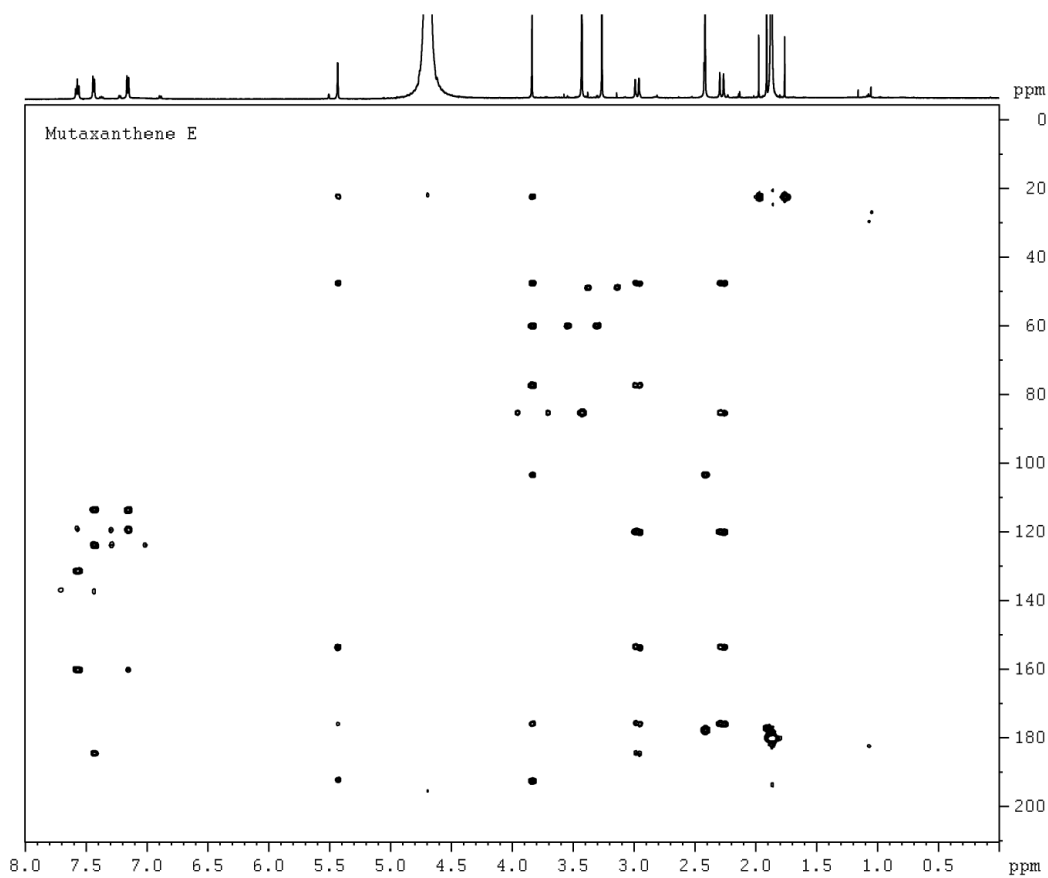
Figure A3.32. 2D HMBC NMR of mutaxanthene E (5) in D$_2$O.
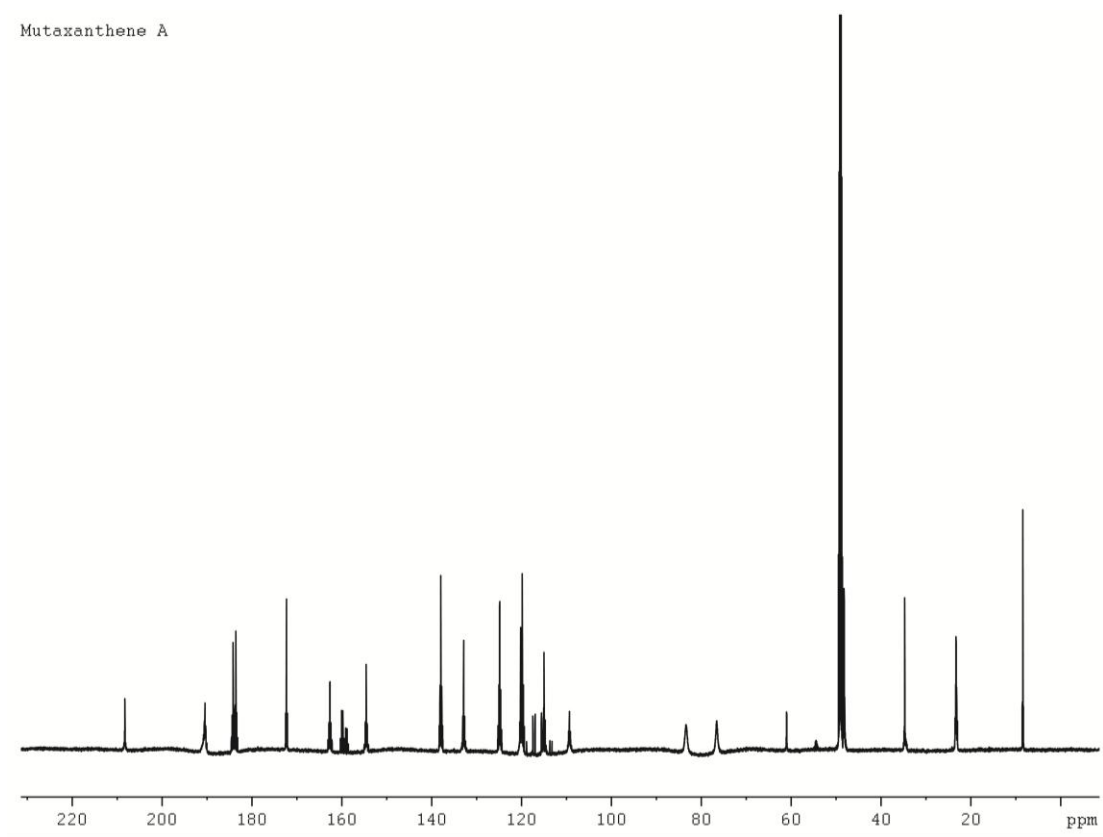
Figure A3.33. ^{13}C proton NMR of mutaxanthene A (4) enriched with 1,2-^{13}C sodium acetate in CD$_3$OD.
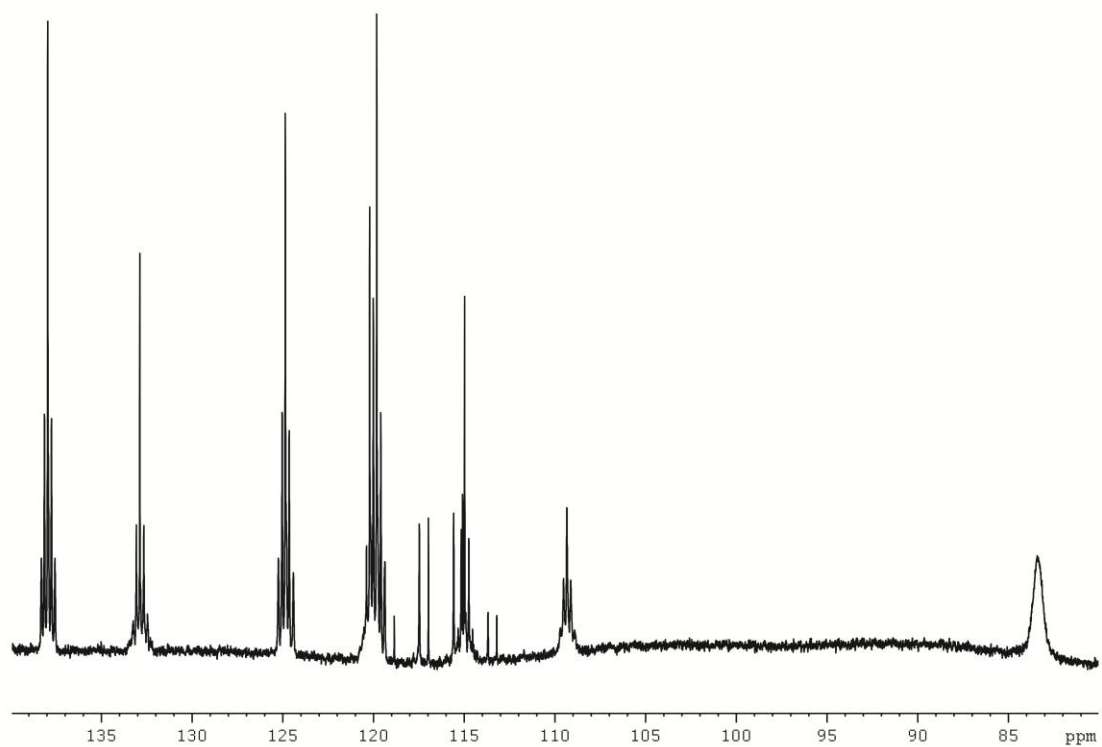
Mutaxanthene A

Figure A3.34. ^{13}C proton NMR of mutaxanthene A (4) enriched with 1,2-^{13}C sodium acetate in CD$_3$OD.
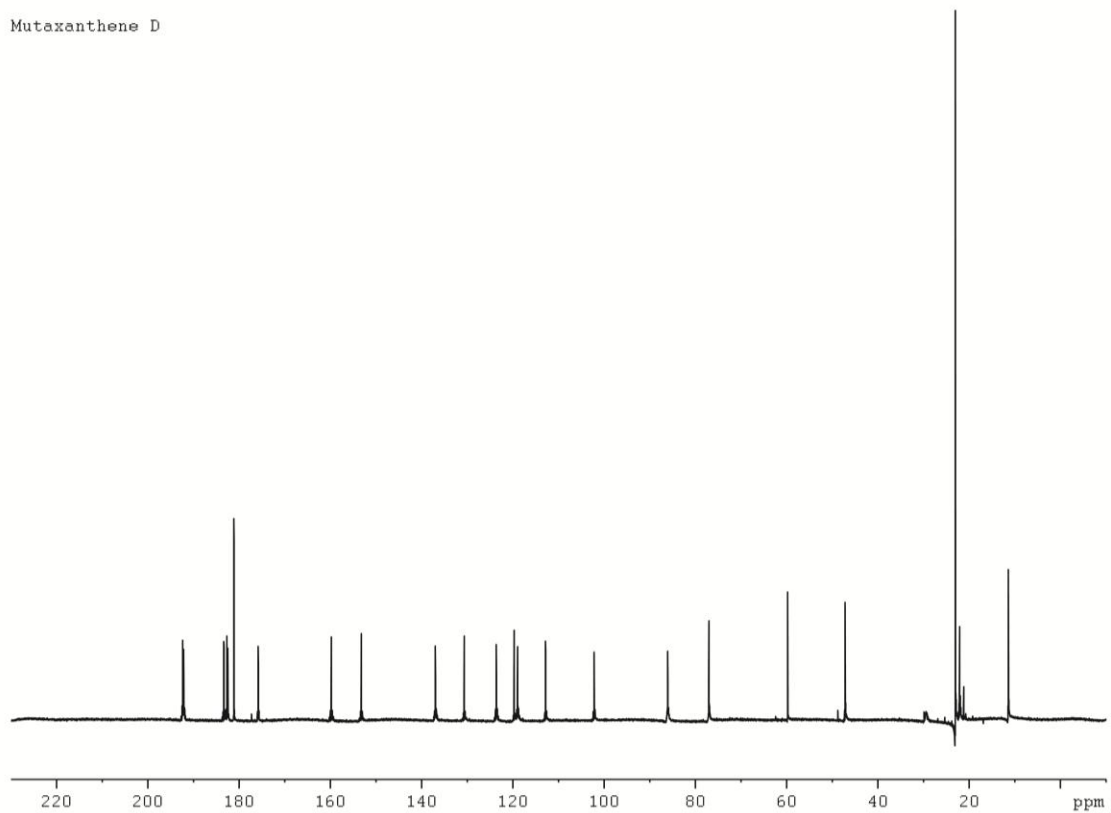
Mutaxanthene D

Figure A3.35. ^{13}C proton NMR of mutaxanthene D (4) enriched with 1,2-^{13}C sodium acetate in CD$_3$OD.
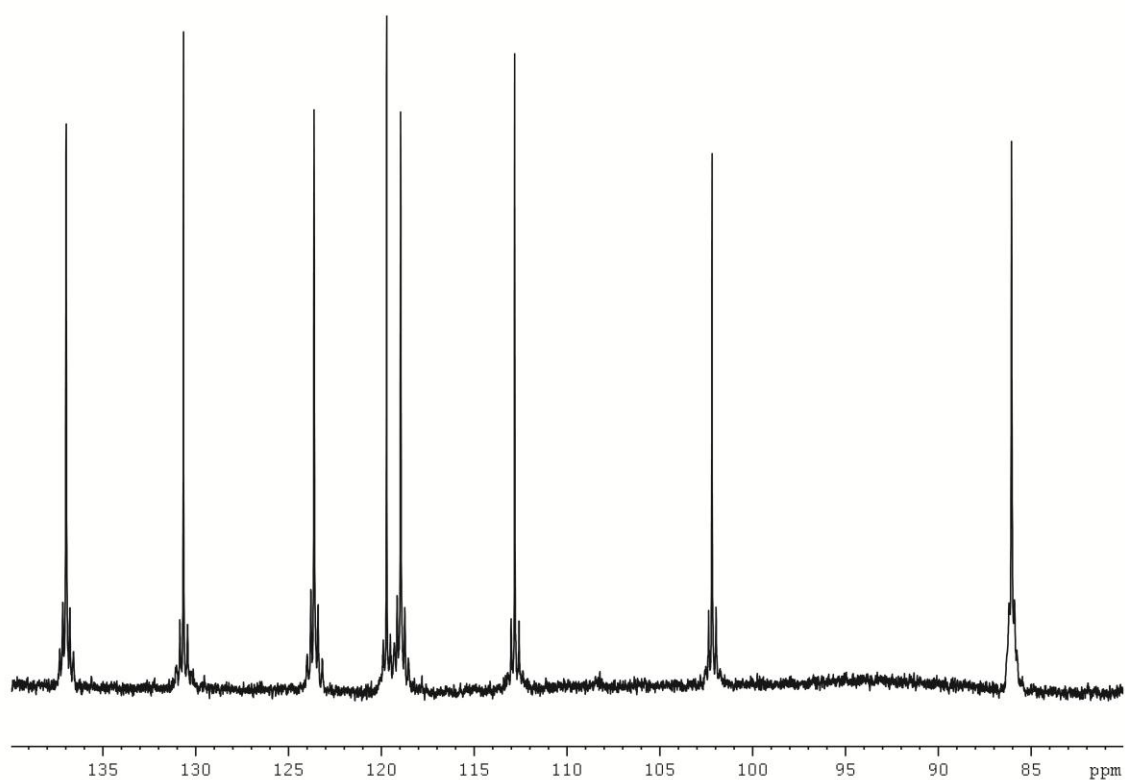
Mutaxanthene D

Figure A3.36. ^{13}C proton NMR of mutaxanthene D (4) enriched with 1,2-^{13}C sodium acetate in CD$_3$OD.

Table A3.7. Deduced functions of ORFs in the mutaxanthene biosynthetic gene cluster
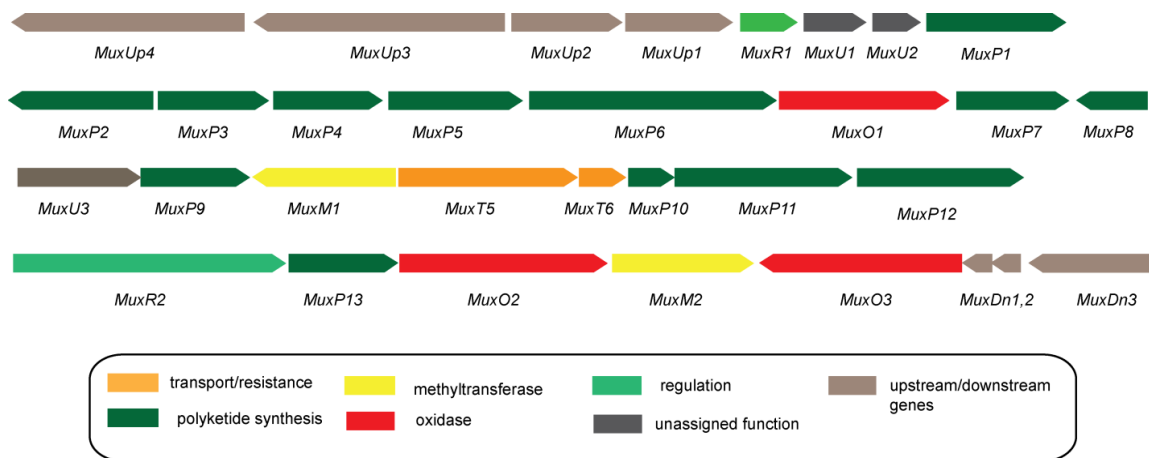
gene	size (aa)	similar protein	GeneBank accession numbers	Identity(%)/ Similarity(%)	proposed function
MuxUp4	-577	SSMG_06347, Streptomyces sp. AA4	ZP_07282307	99/99	ABC transporter
MuxUp3	-627	SSMG_06347, Streptomyces sp. AA4	ZP_07282307.1	99/98	ABC transporter
MuxUp2	254	SSMG_06348, Streptomyces sp. AA4	ZP_07282308	96/98	ABC transporter
MuxUp1	247	SSMG_06349, Streptomyces sp. AA4	ZP_07282309	96/98	ABC transporter
MuxR2	114	SSMG_06351, Streptomyces sp. AA4	ZP_07282311	97/96	PadR fam.transcriptional repressor
MuxU1	128	SSMG_06350	ZP_07282310	94/98	hypothetical protein
MuxU2	91	SSMG_06352	ZP_07282312.1	97/94	hypothetical protein
MuxP1	332	AlkNF, Streptomyces galilaeus	BAB72049	69/55	type II acyl transferase (AT)
MuxP2	-345	CosE, Streptomyces olindensis	ABC00733	56/69	type II ketosynthase (KS) for starter
MuxP3	258	PokC2, Streptomyces diastatochromogenes	ACN64846	78/65	type II polyketide cyclase
MuxP4	250	PokT1, Streptomyces diastatochromogenes	ACN64844.1	64/50	type II ketoreductase (KR)
MuxP5	320	orf6, Streptomyces echinatus	ABL09954	69/57	type II cyclase/dehydratase
MuxP6	618	Sfla_5326,Streptomyces flavogriseus	YP_004926240	60/47	acyl CoA ligase
MuxO1	412	Sfla_5326,Streptomyces flavogriseus	YP_004926243.1	70/55	flavin-dependent oxidase
MuxD1	262	simA6, Streptomyces antibioticus	AF324838_6	86/75	type II ketoreductase
MuxP7	-154	SnoaL_4, uncultured bacterium (expressed)	AEM44306.1	60/51	type II cyclase/dehydratase
MuxU3	288	none	--	--	hypothetical protein
MuxD2	253	Strvi_4376, Streptomyces violaceusniger Tu 4113	YP_004814300	61/42	type II ketoreductase (KR)

MuxM1	-341	phzM, Saccharopolyspora erythraea	YP_001106227	57/43	O-methyltransferase
MuxT4	438	SAV_5944,Streptomyces avermitilis	NP_827121	63/47	transport efflux
MuxT5	84	Sros_2592, Streptosporangium roseum	YP_003338305	72/50	transport efflux
MuxP8	86	ChaC, Streptomyces chartreusis	CAH10163	69/51	type II acyl carrier protein (ACP)
MuxP9	431	ORF32, uncultured bacterium (expressed)	AEM44309	85/74	type II beta-ketoacyl synthase (KS)
MuxP10	402	ORF2, uncultured bacterium (expressed)	AEM44279.1	66/53	type II beta-ketoacyl synthase (KS)
MuxR3	681	RubS. Streptomyces collinus	AAM97369.1	55/41	SARP type transcriptional activator
MuxD3	252	ORF2, uncultured bacterium (expressed)	AEM44279	66/53	type II ketoreductase (KR)
MuxO2	511	ORF20, uncultured bacterium (expressed)	AEM44297	71/61	flavin-dependent oxidase
MuxM2	335	SsfM1, Streptomyces sp. SF2575	ADE34508.1	72/89	O-methyltransferase
MuxO3	-500	ovmOI, Streptomyces antibioticus	CAG14963.1	63/50	flavin-dependent oxidase
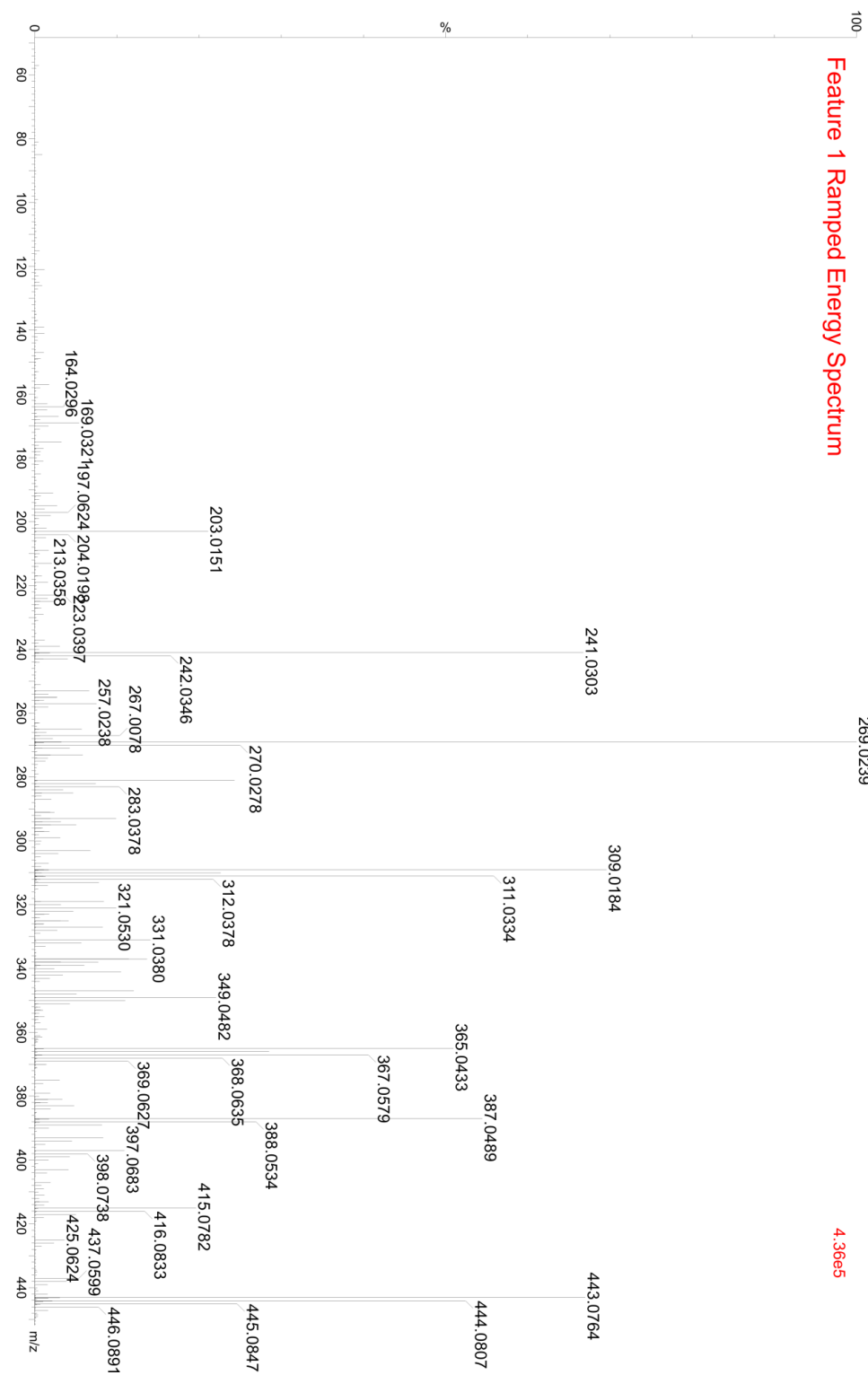
Figure A3.37. Mobility separated ramped energy mass spectrum for feature 1, Mutaxanthene A.
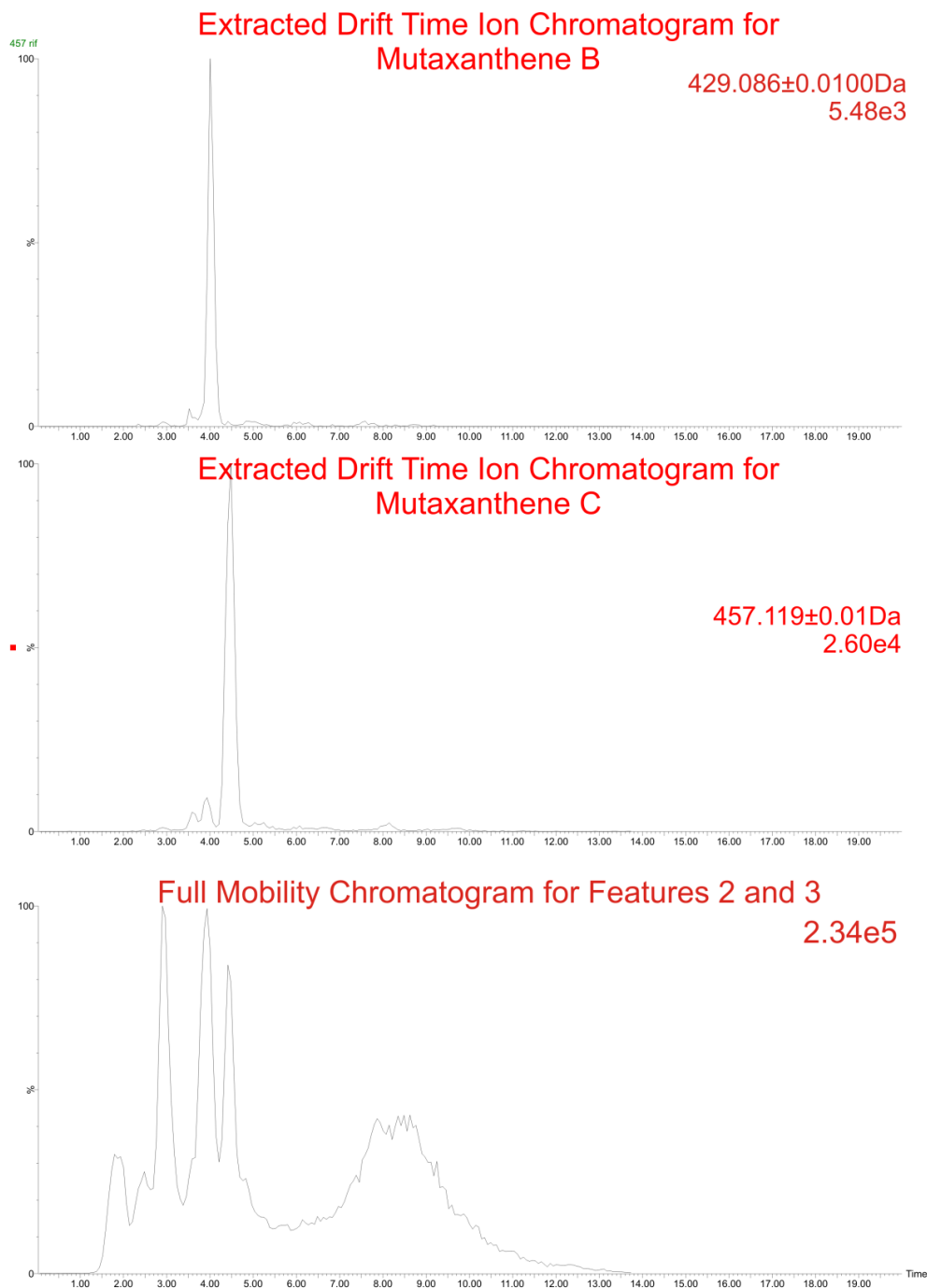
Figure A3.38. Retention time selected drift time chromatograms and extracted drift time ion chromatograms for coeluting mutaxanthenes B and C. Using mobility separation, fragmentation profiles for each were extracted.
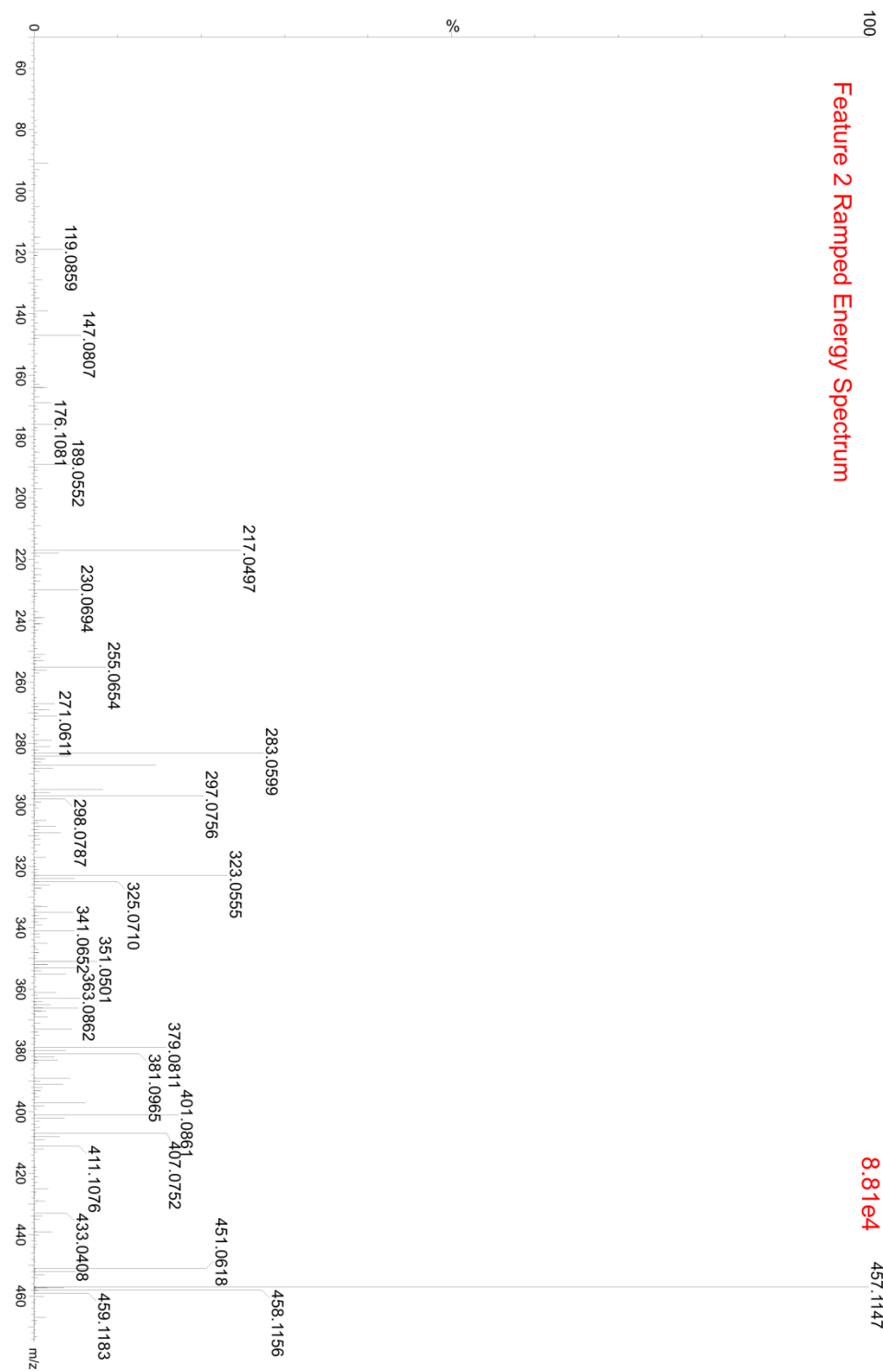
Figure A3.39. Mobility separated ramped energy mass spectrum for feature 2, Mutaxanthene C.
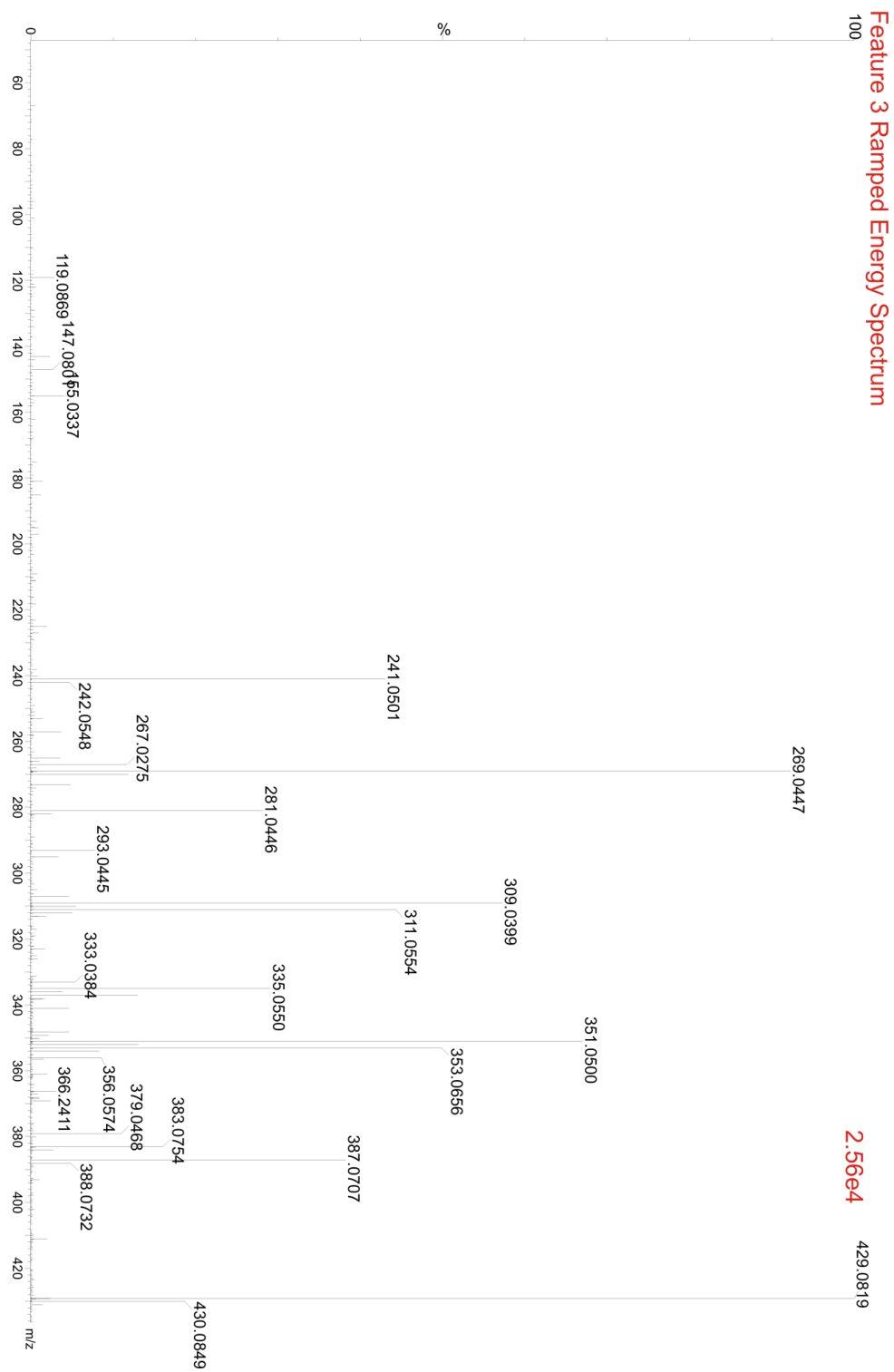
Figure A3.40. Mobility separated ramped energy mass spectrum for feature 3, Mutaxanthene B.
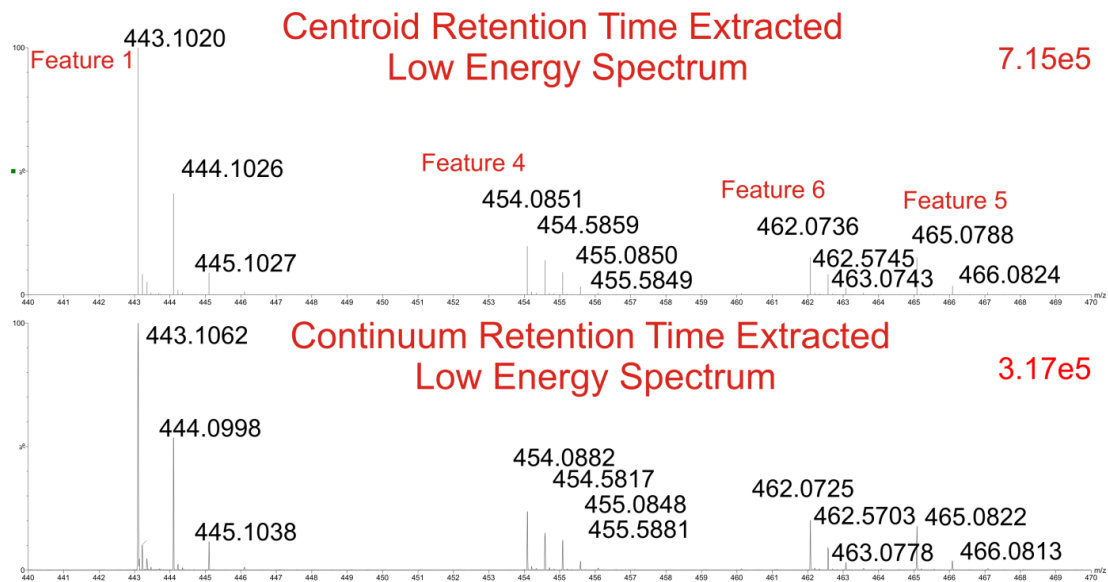
Figure A3.41. Retention time extracted low energy spectra demonstrating Mutaxanthene A adducts.
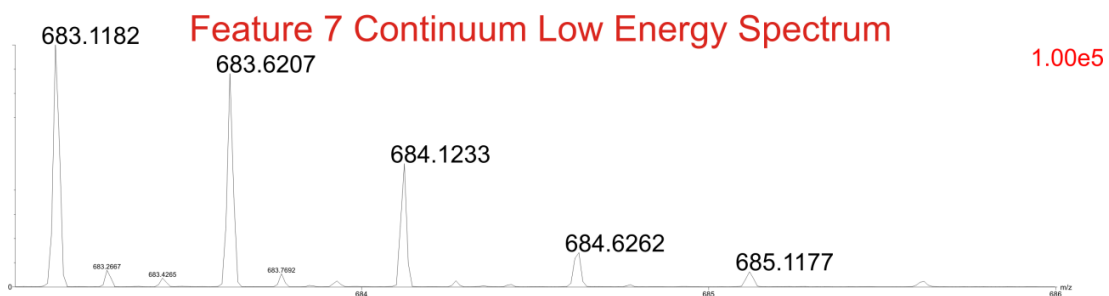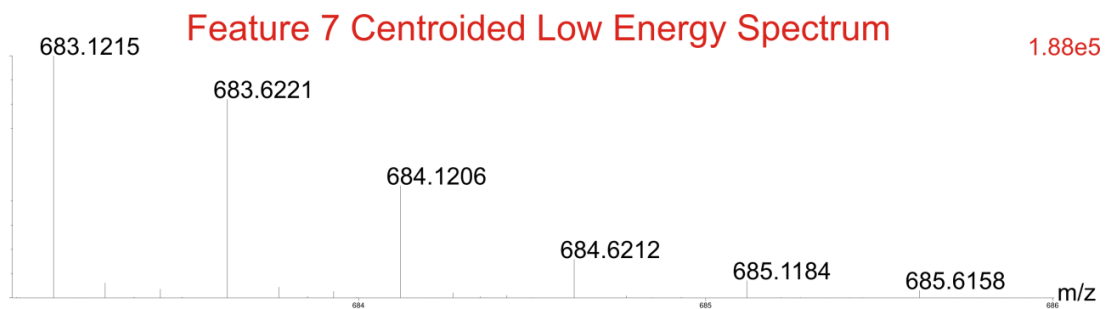
Figure A3.42. Retention time extracted low energy spectra displaying feature 7 isotopic envelope.
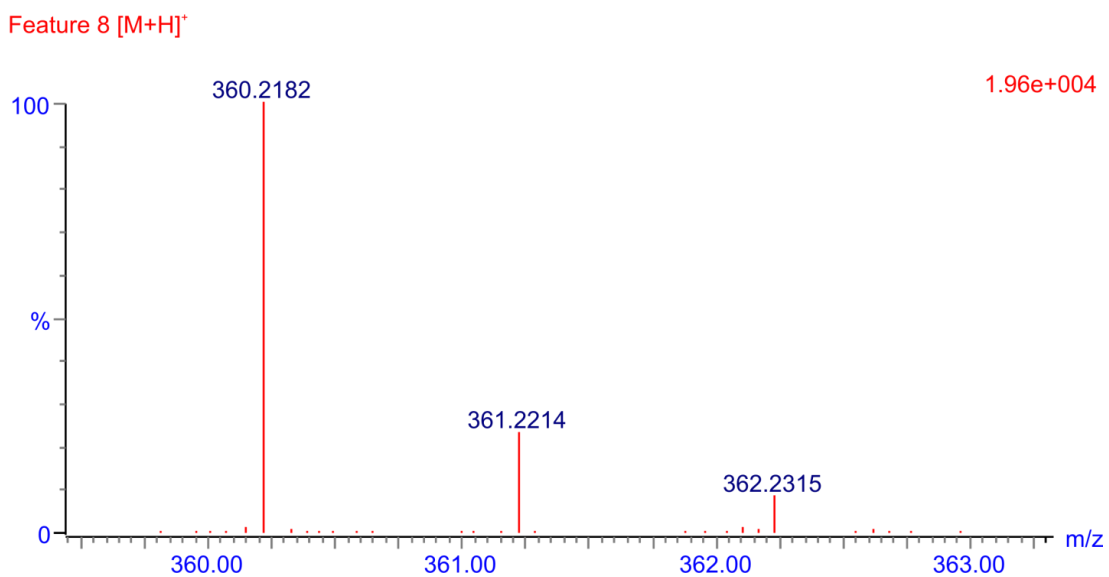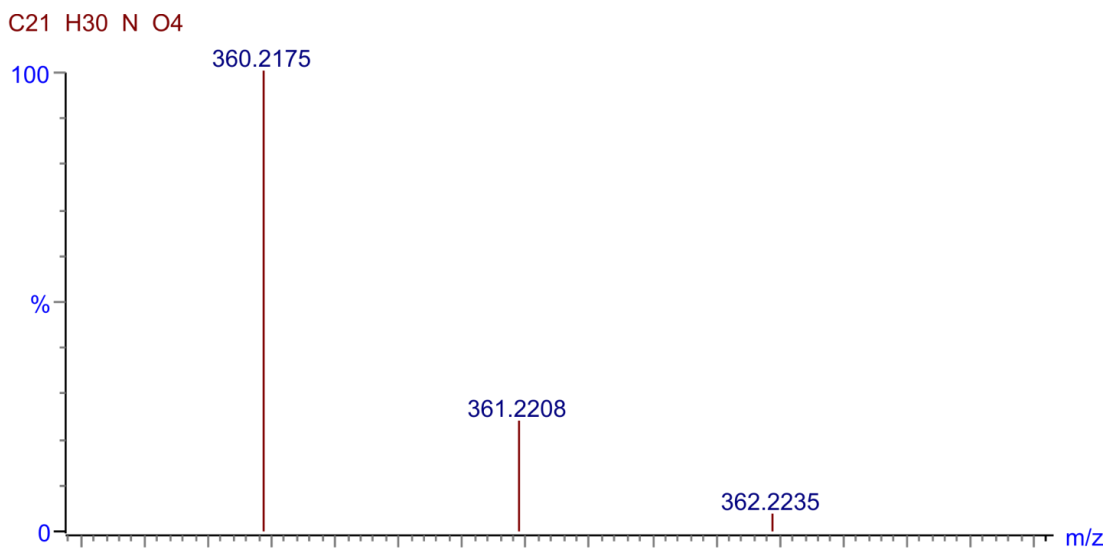
Figure A3.43. (Above) Theoretical isotopic profile for $[C_{21}H_{29}NO_4+H]^+$. (Below) Accurate mass isotopic envelope of feature 8, as specified in Table 3.1.
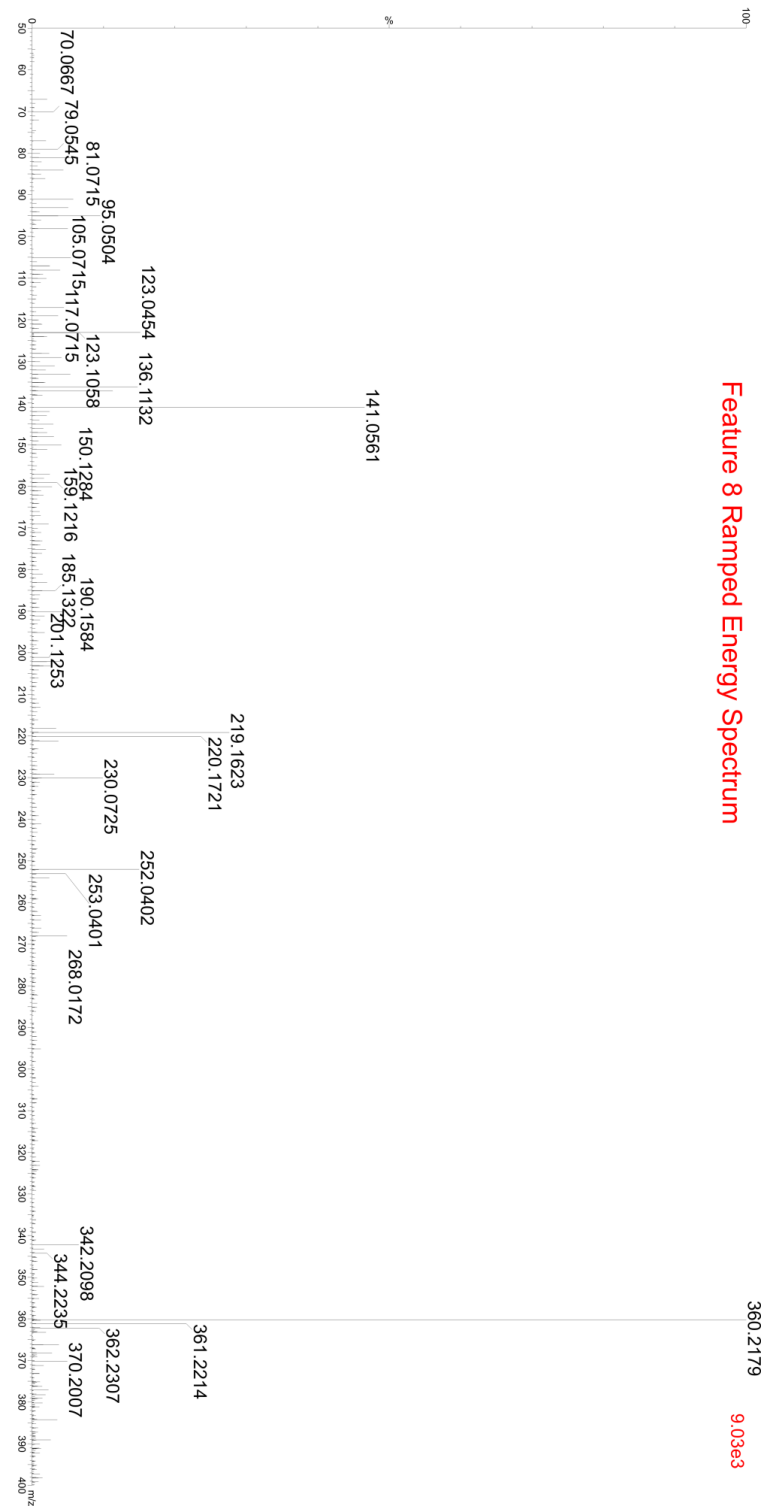
Figure A3.44. Mobility separated ramped energy mass spectrum for feature 8.
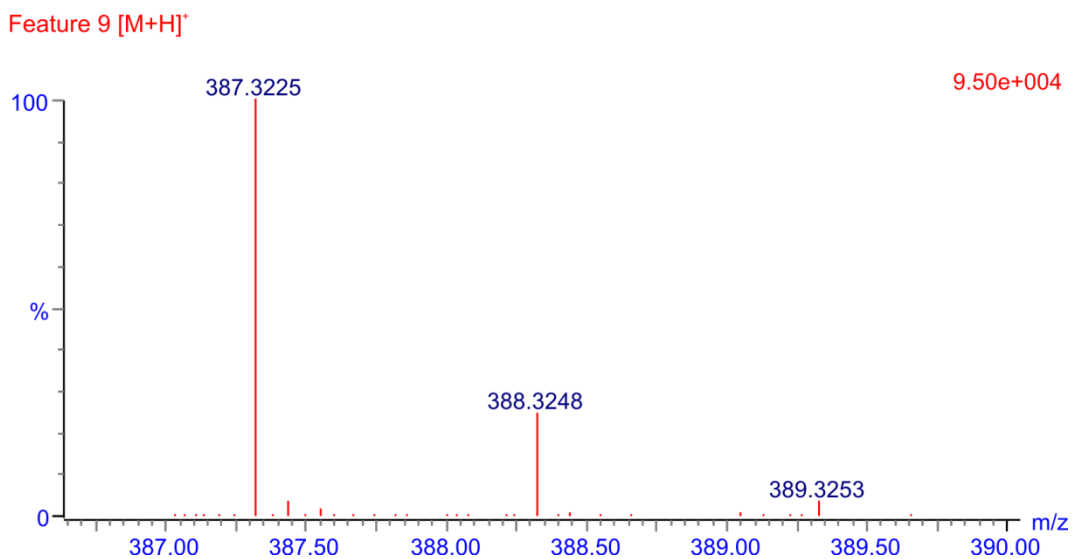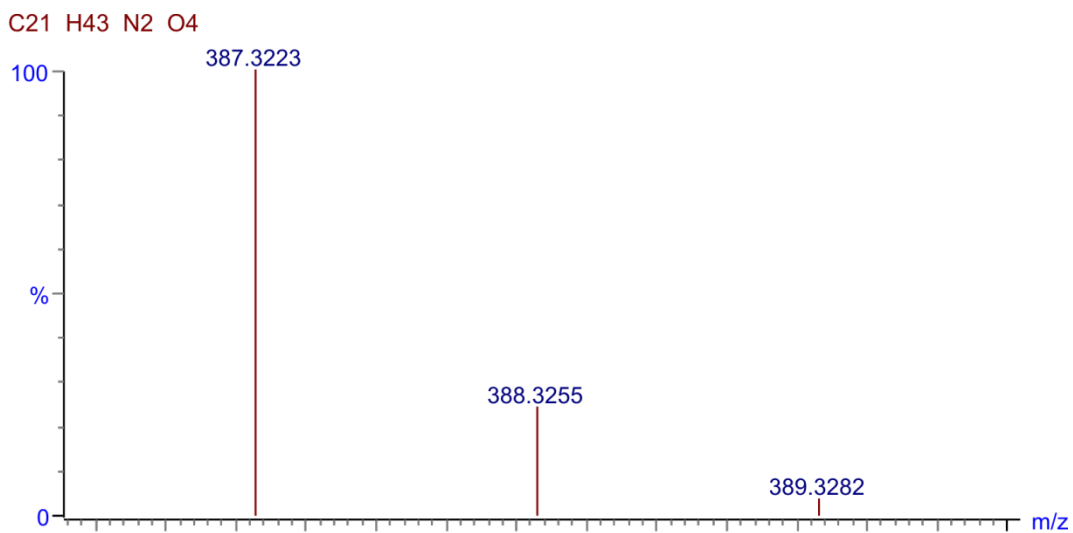
Figure A3.45. (Above) Theoretical isotopic profile for $[C_{21}H_{42}N_2O_4+H]^+$. (Below) Accurate mass isotopic envelope of feature 9, as specified in Table 3.1.
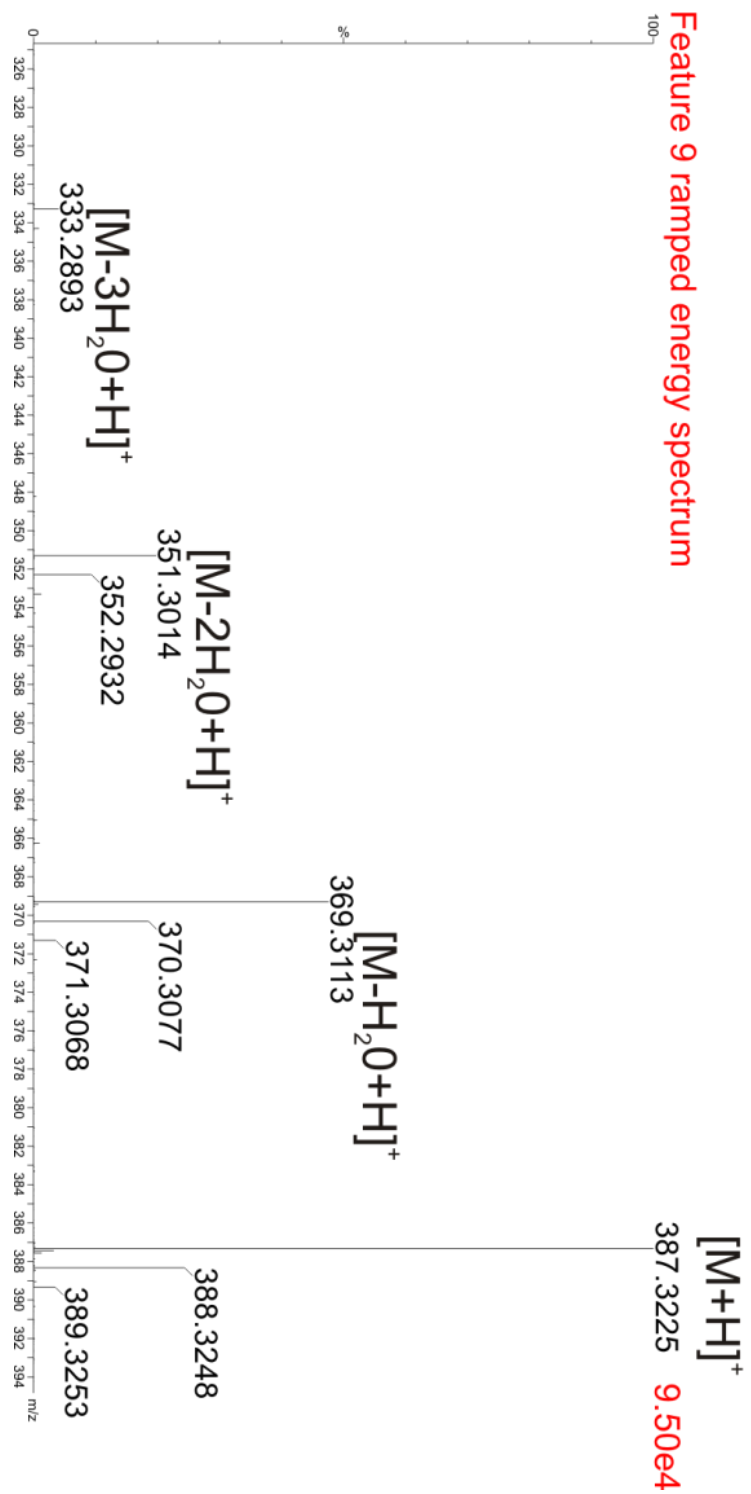
Figure A3.46. Mobility separated ramped energy mass spectrum for feature 9, indicating neutral losses. These neutral losses corroborate the chemical formula determination.
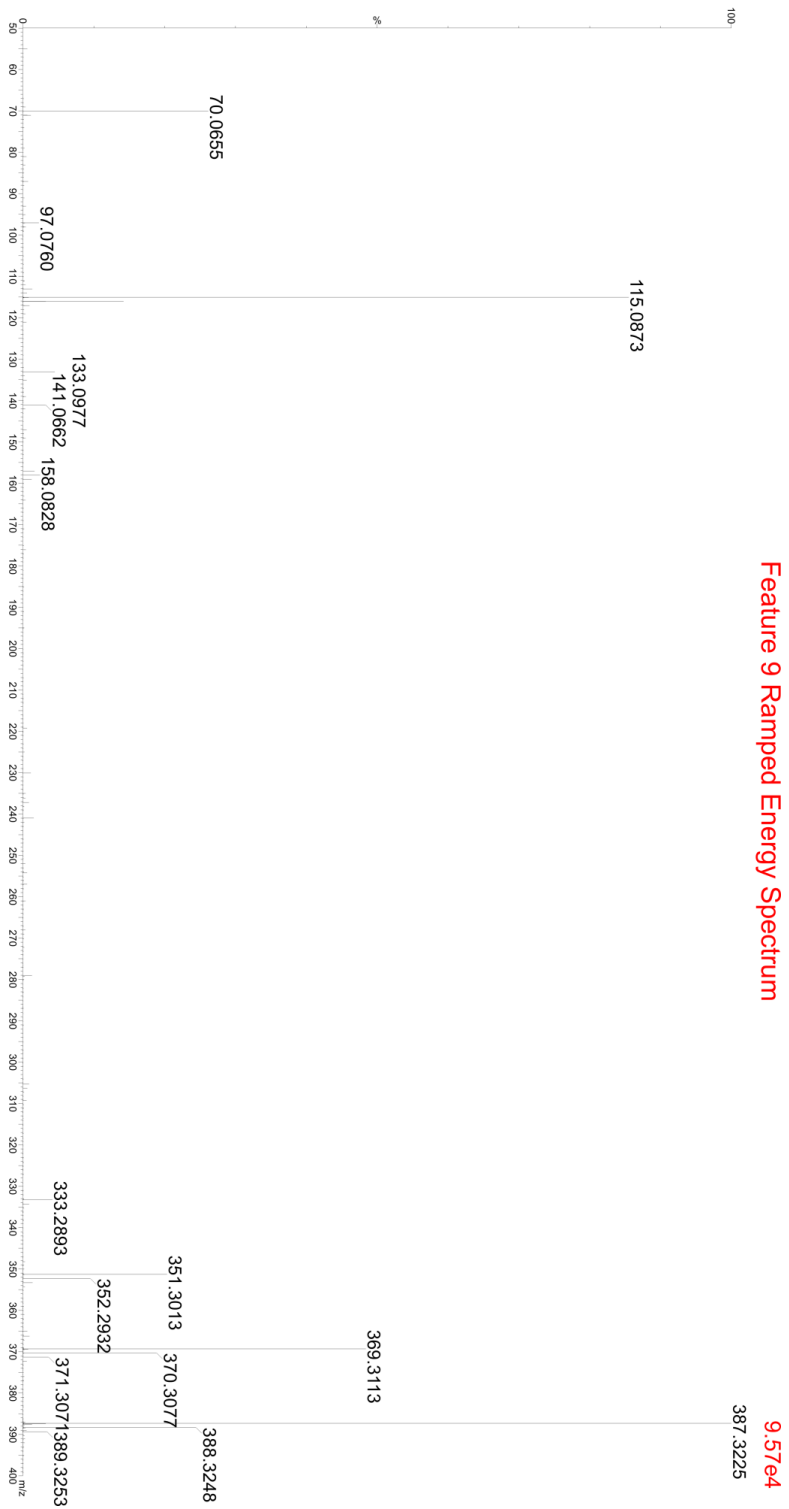
Figure A3.47. Mobility separated ramped energy mass spectrum for feature 9.
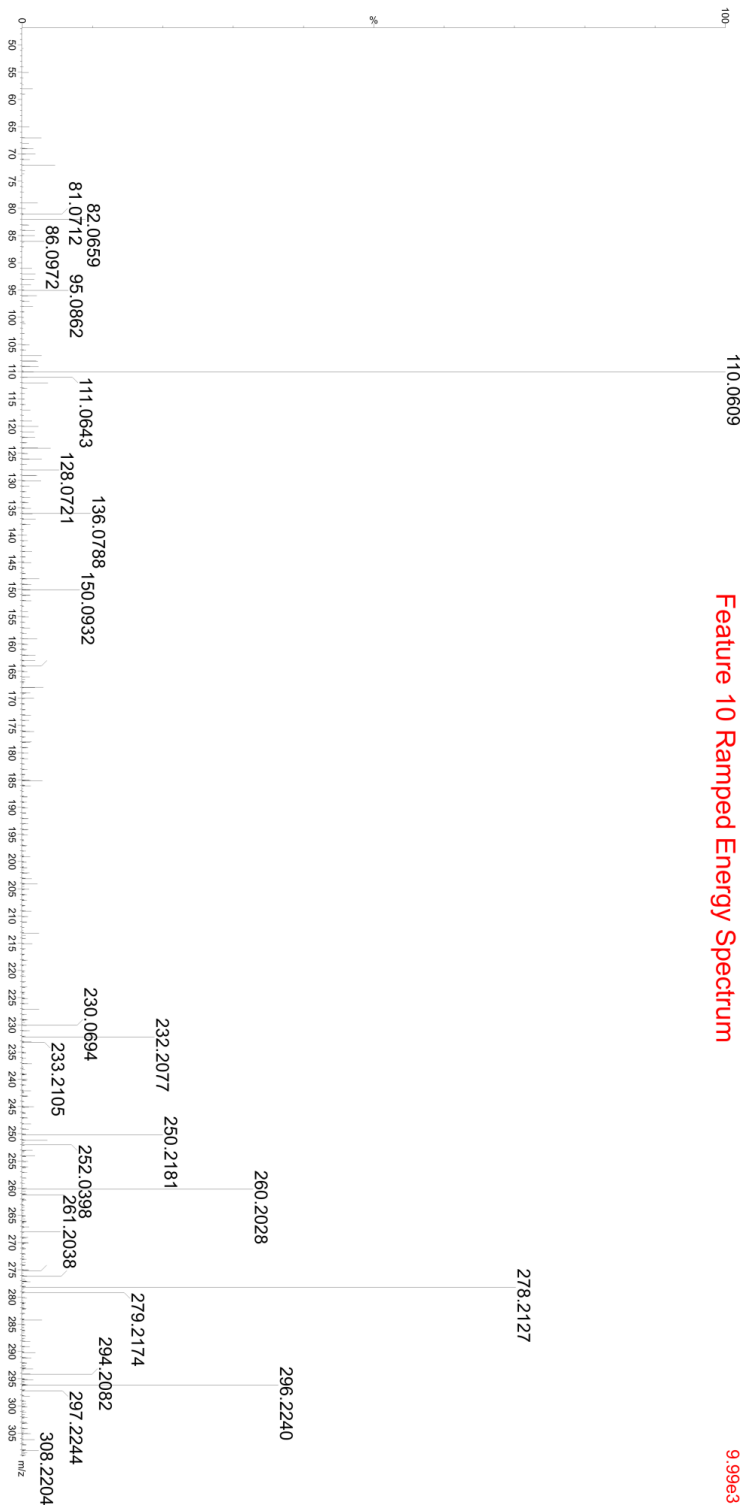
Figure A3.48. Mobility separated ramped energy mass spectrum for feature 10.
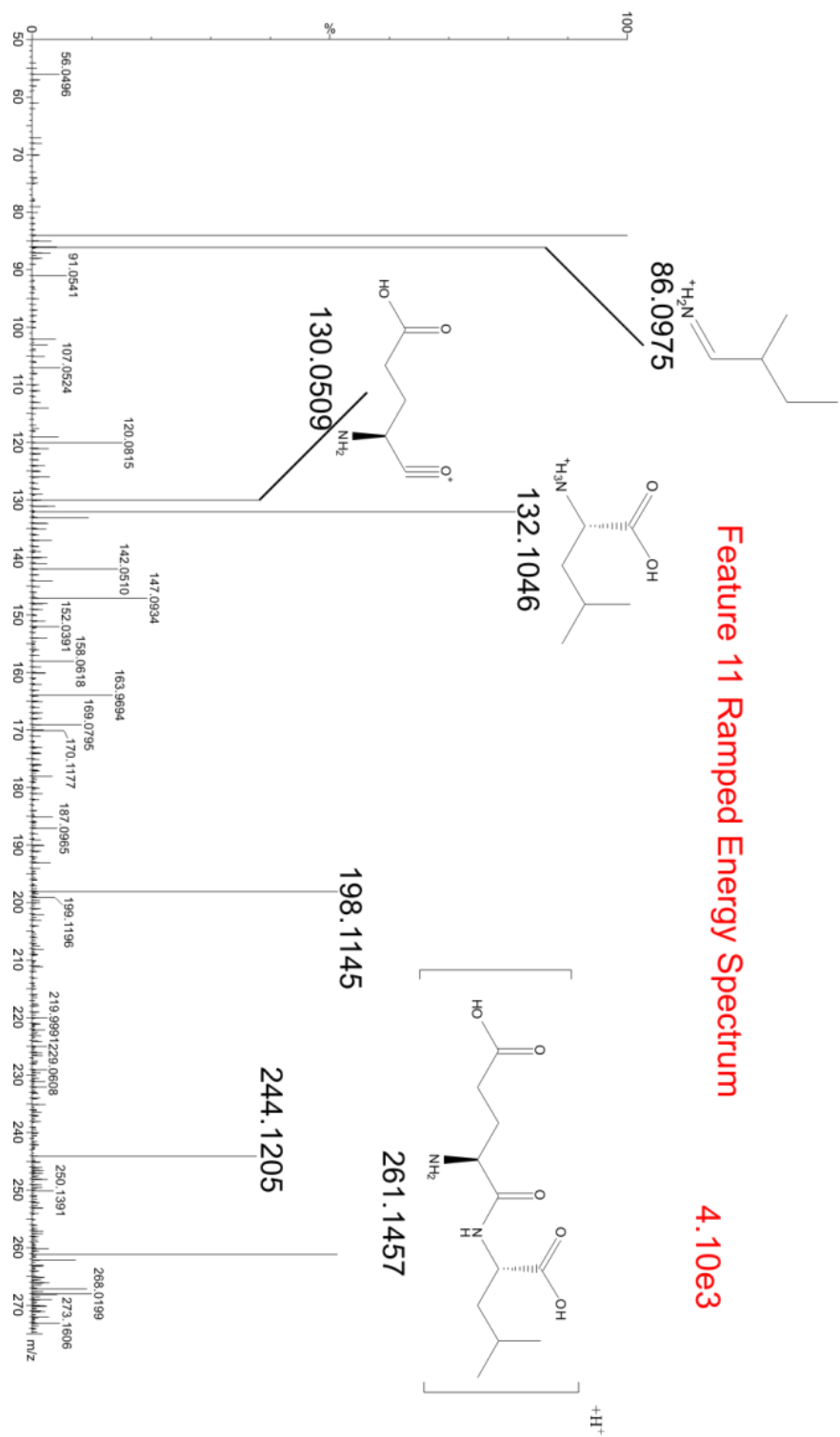
Figure A3.49. Mobility separated ramped energy mass spectrum for feature 11, indicating proposed fragment identities.
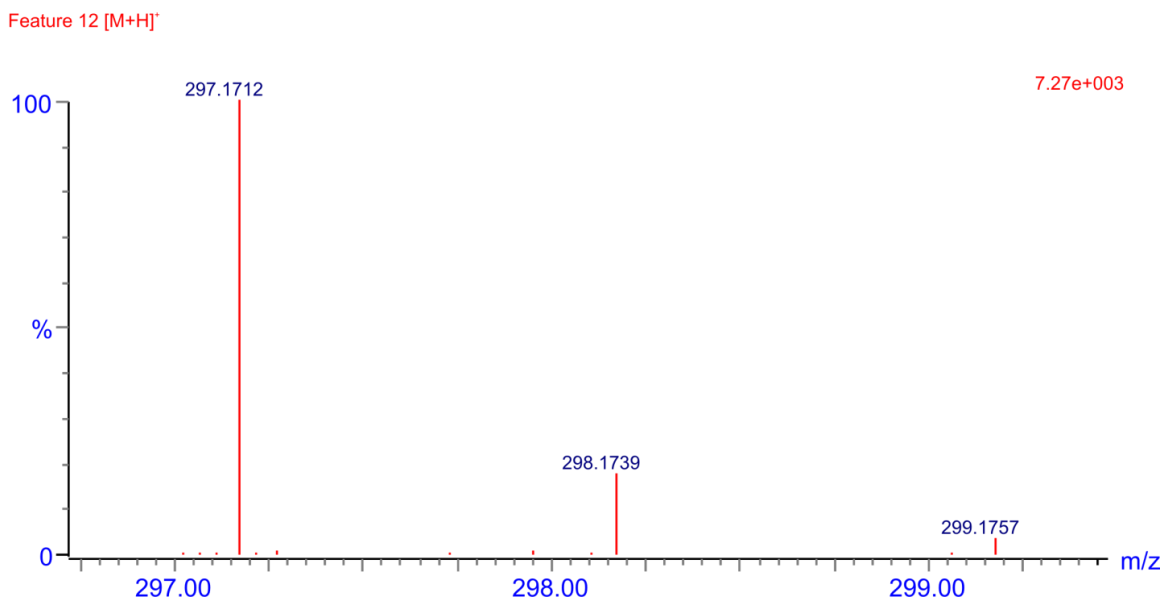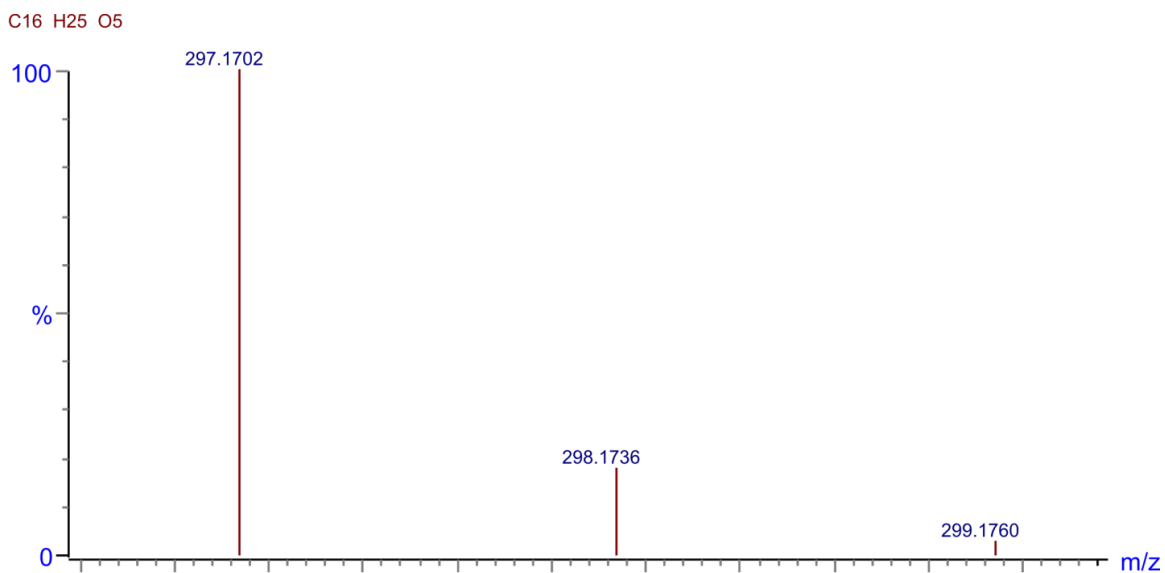
Figure A3.50. (Above) Theoretical isotopic profile for $[C_{16}H_{24}O_5+H]^+$. (Below) Accurate mass isotopic envelope of feature 12, as specified in Table 3.1.
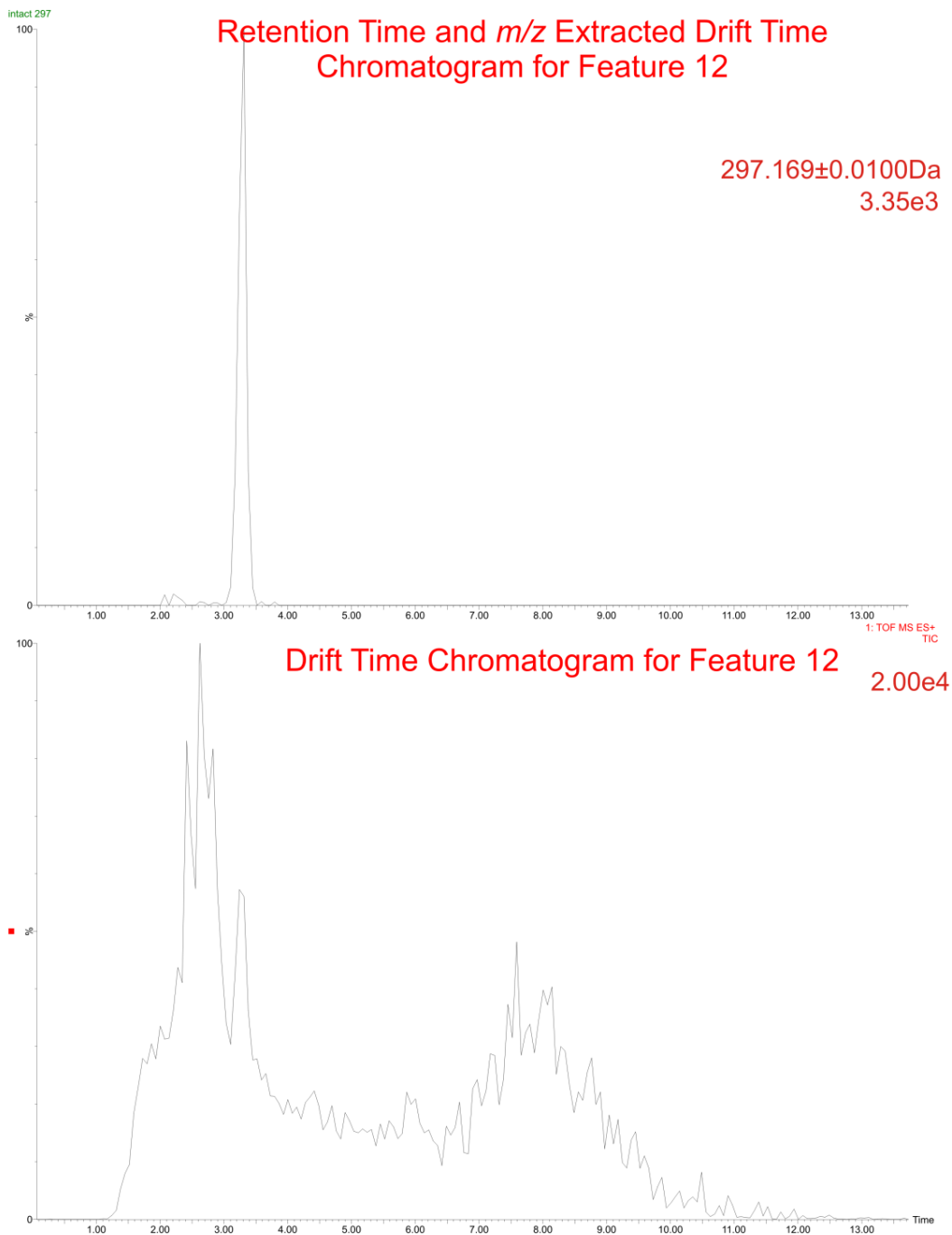
Figure A3.51. Retention time selected drift time chromatograms and extracted drift time ion chromatogram for feature 12. This drift time was used to select the proper drift time for high energy data interrogation.
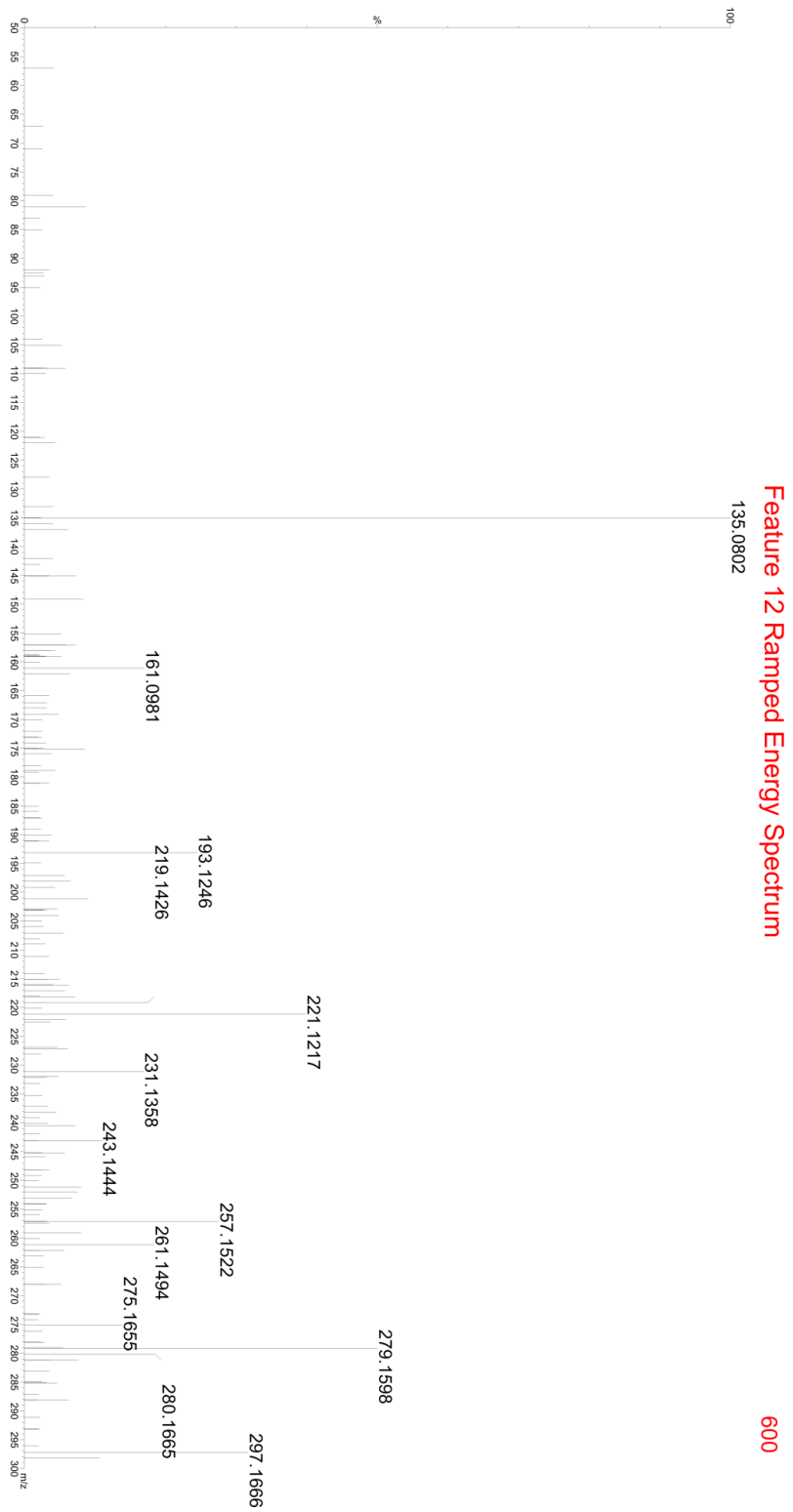
Figure A3.52. Mobility separated ramped energy mass spectrum for feature 12.
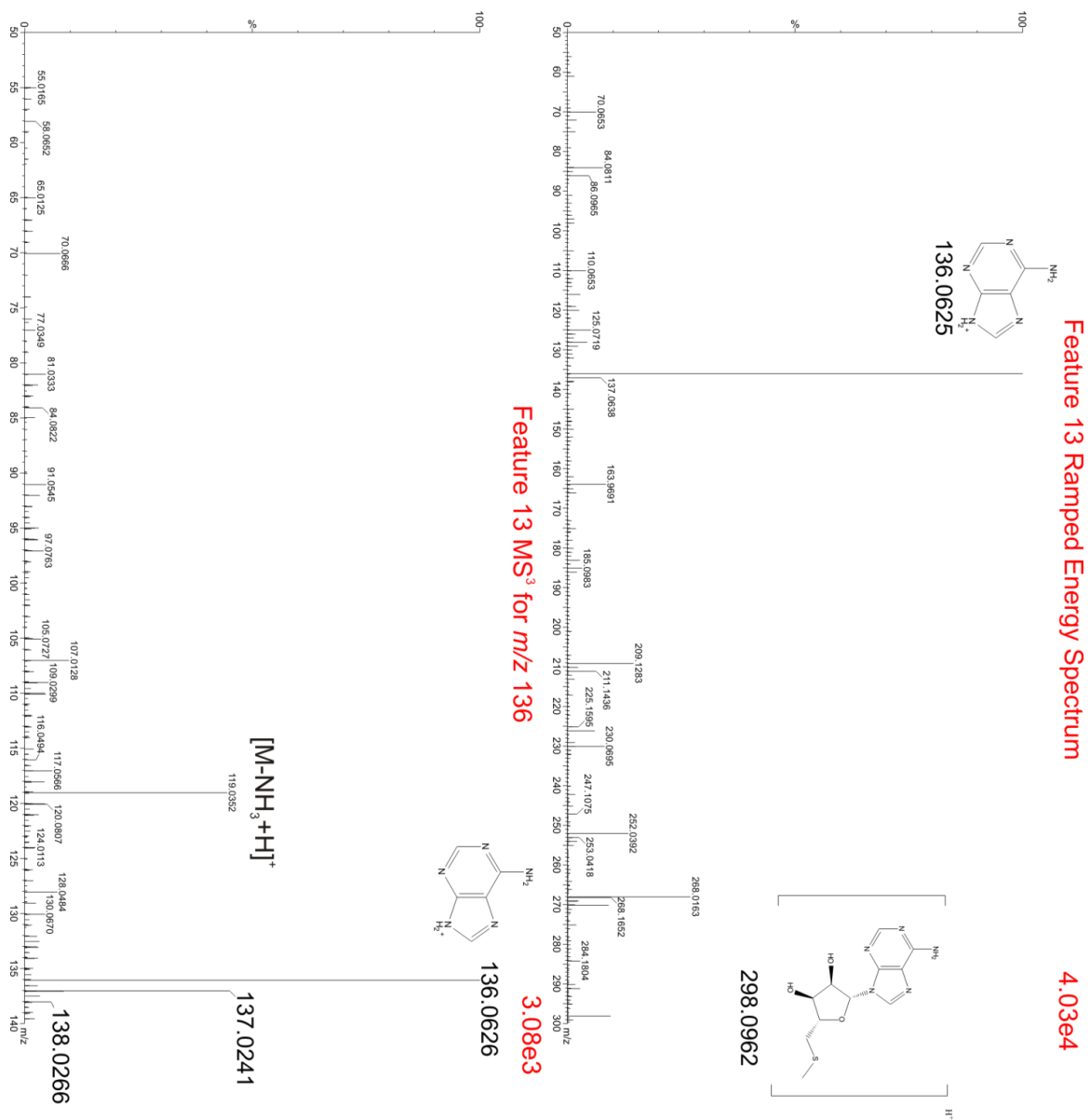
Figure A3.53. (Above) Mobility separated ramped energy mass spectrum for feature 13, indicating proposed fragment identities. (Bottom) Mobility separated MS^3 of product ion 136.0626. These fragments further corroborate identification.
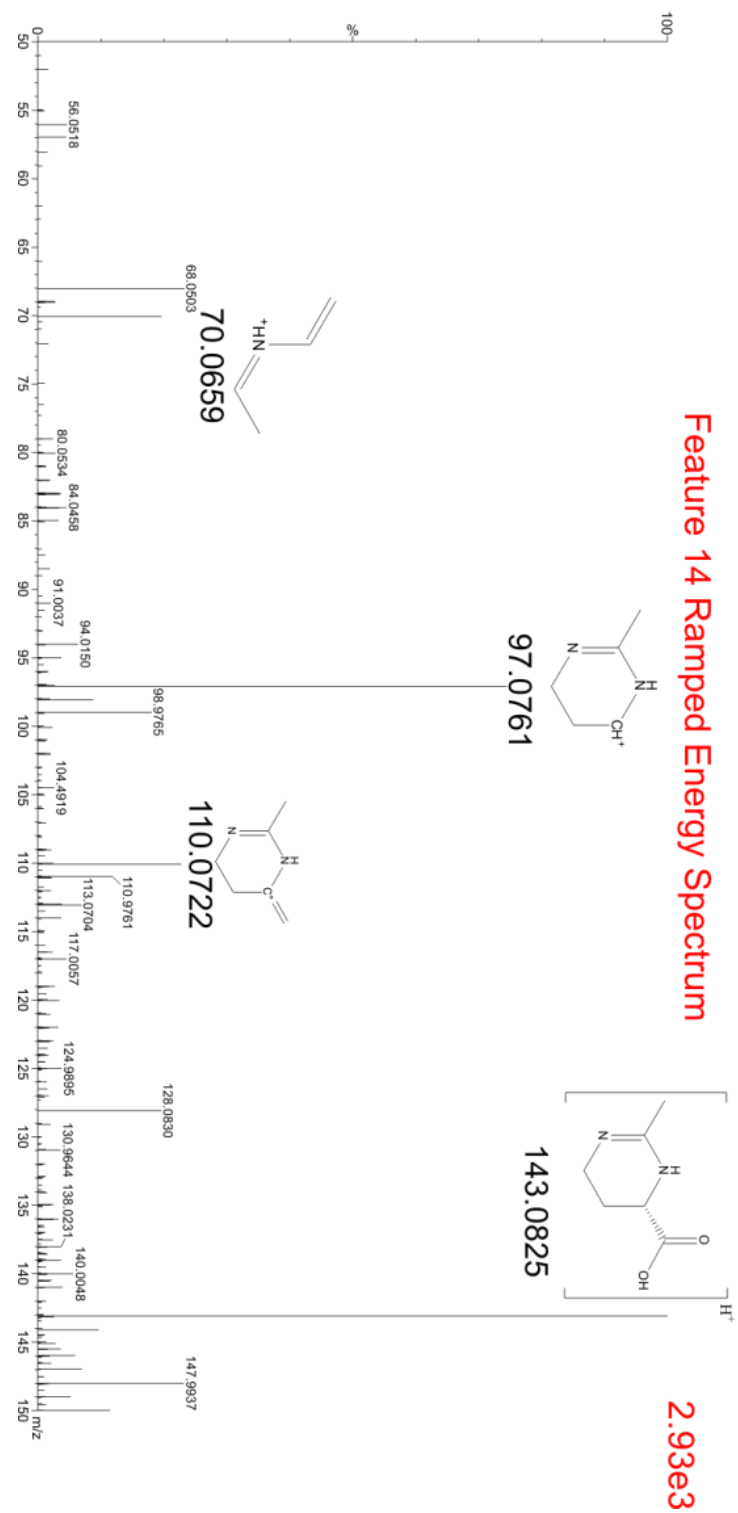
Figure A3.54. (Above) Mobility separated ramped energy mass spectrum for feature 14, indicating proposed fragment identities.
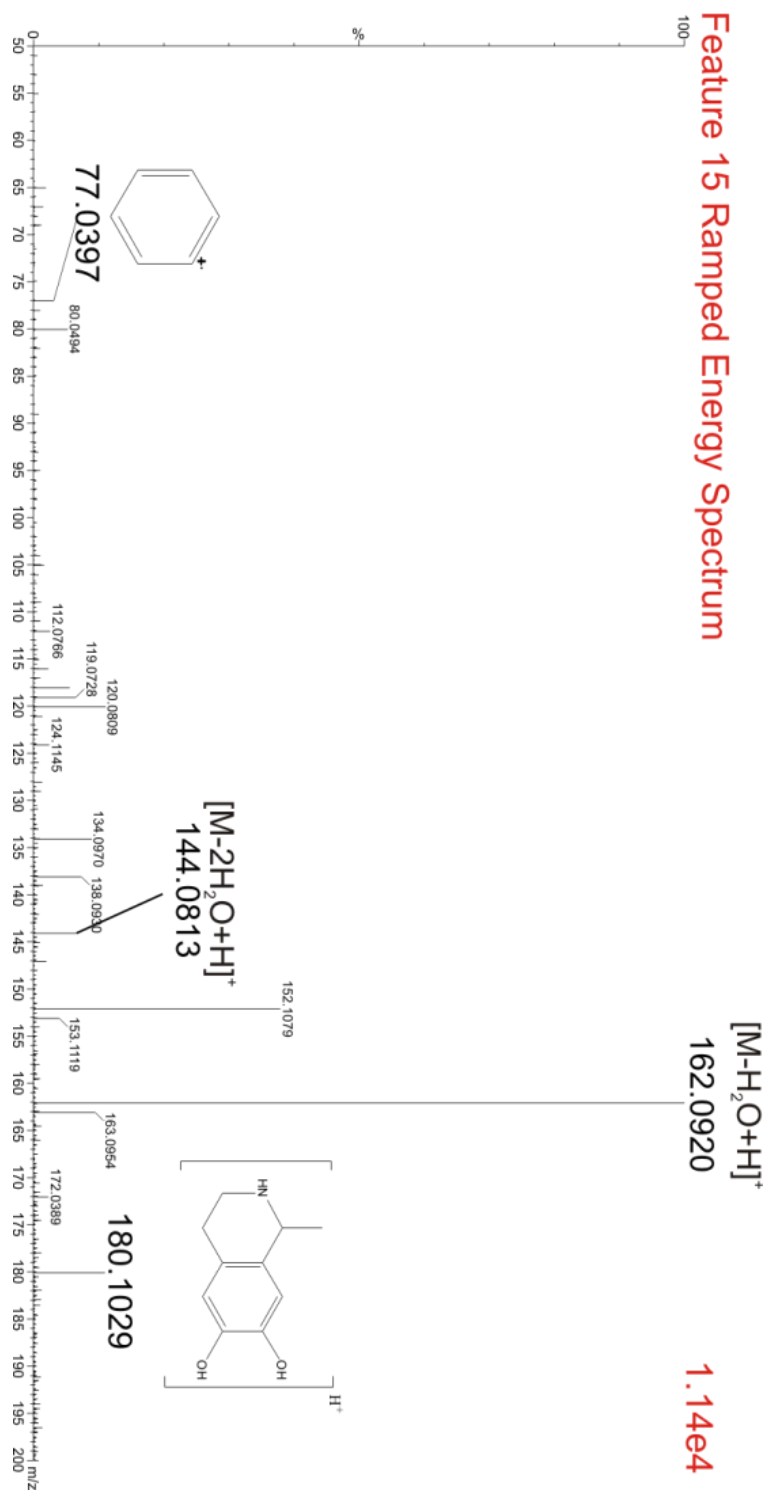
Figure A3.55. (Above) Mobility separated ramped energy mass spectrum for feature 15, indicating proposed fragment identities. Feature 15 is the result of the in-source neutral loss of water.
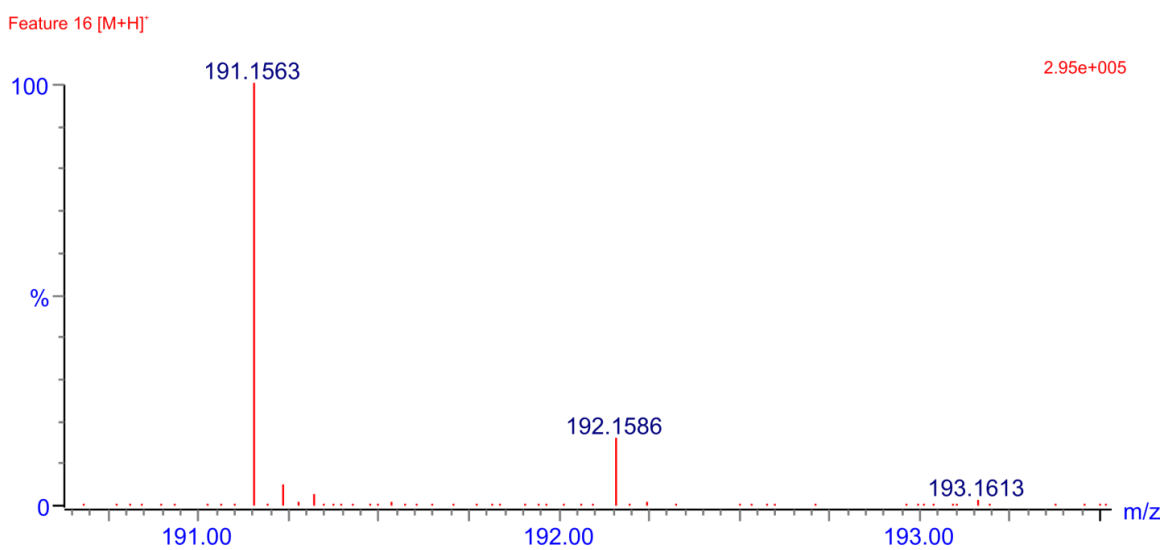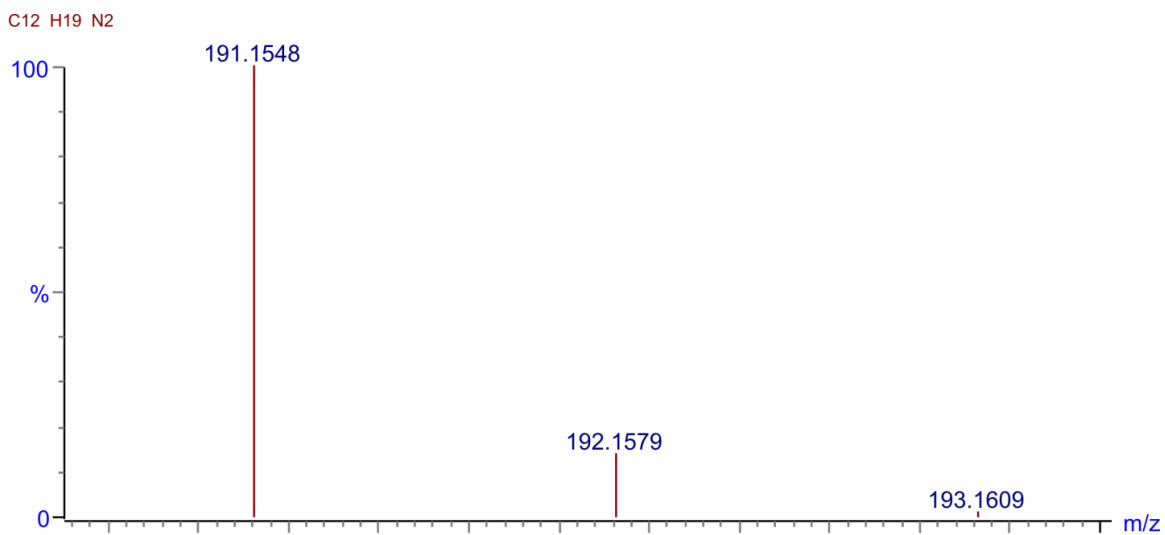
Figure A3.56. (Above) Theoretical isotopic profile for $[C_{12}H_{18}N_2+H]^+$. (Below) Accurate mass isotopic envelope of feature 16, as specified in Table 3.1.
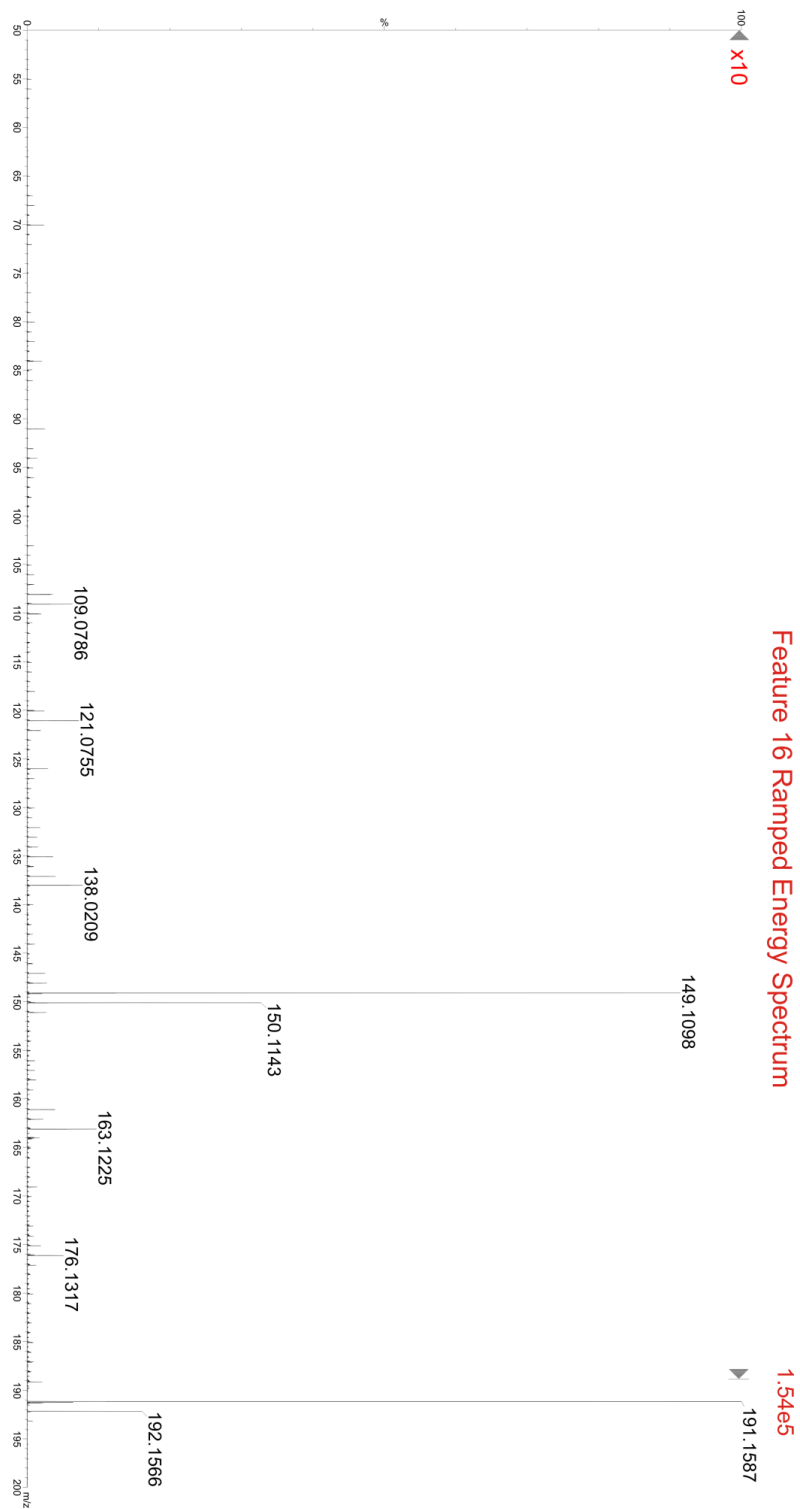
Figure A3.57. Mobility separated ramped energy mass spectrum for feature 16. The region from 50-190Da is magnified 10x.
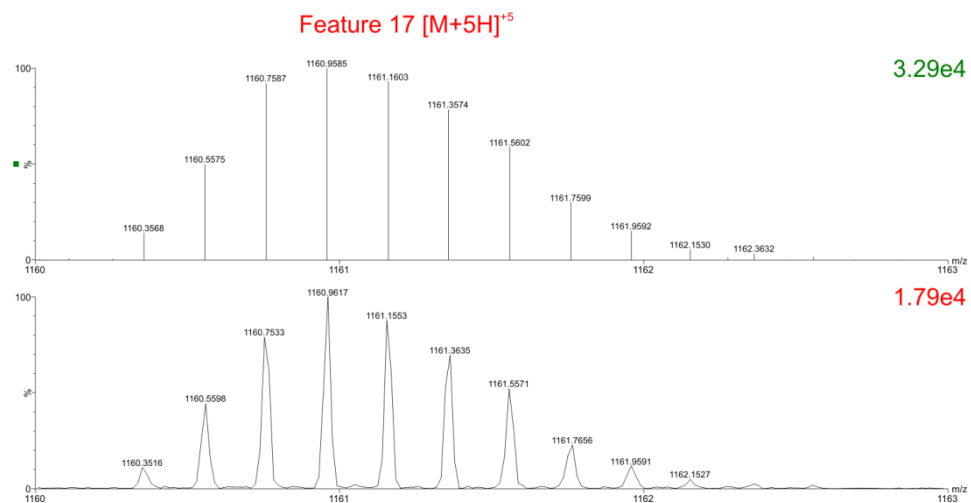
Figure A3.58. (Above) Centroided accurate mass isotopic envelope for feature 17 . (Below) Continuum accurate mass isotopic envelope of feature 17, as specified in Table 3.1.
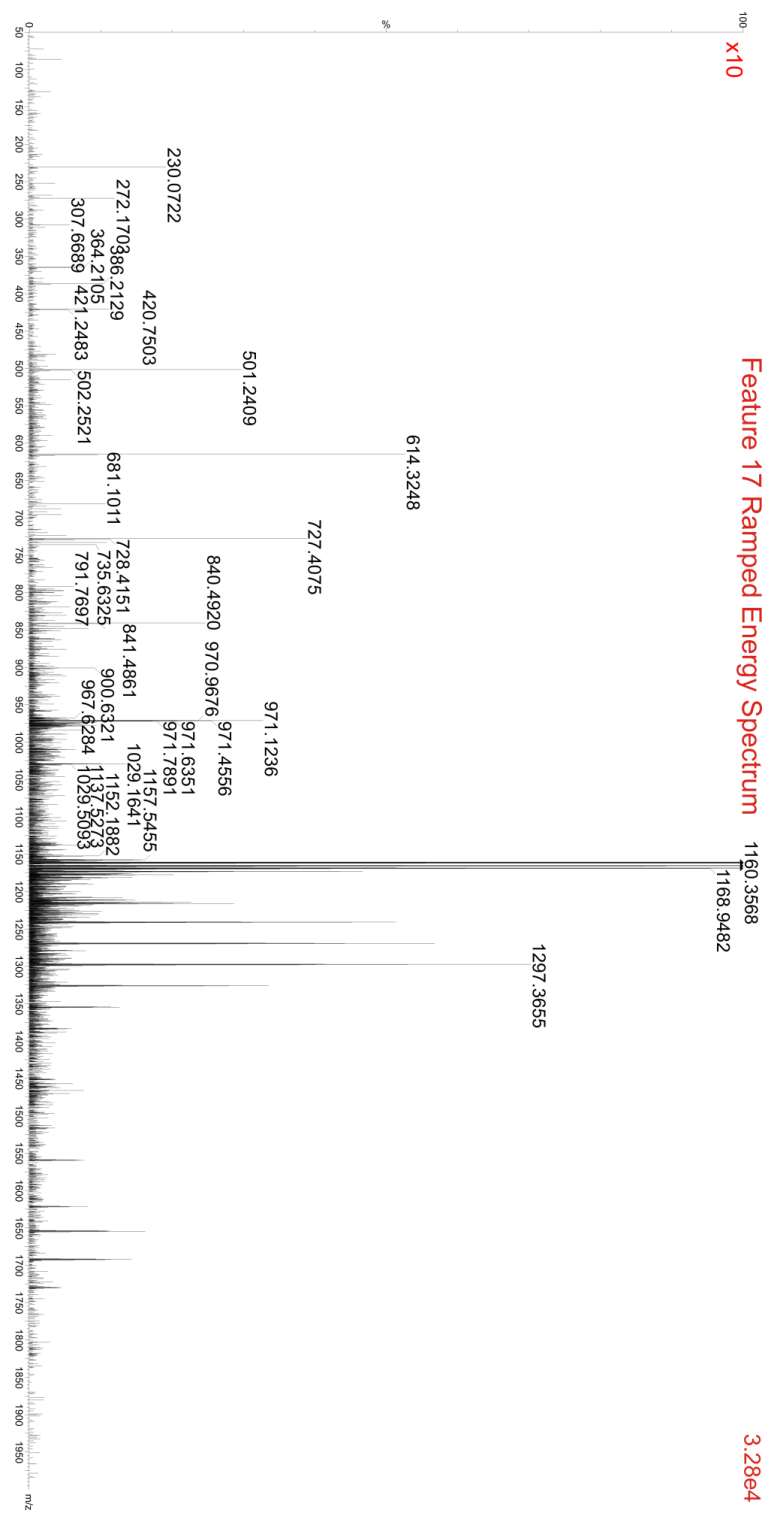
Figure A3.59. Mobility separated ramped energy mass spectrum for feature 17. Spectrum is magnified 10x.
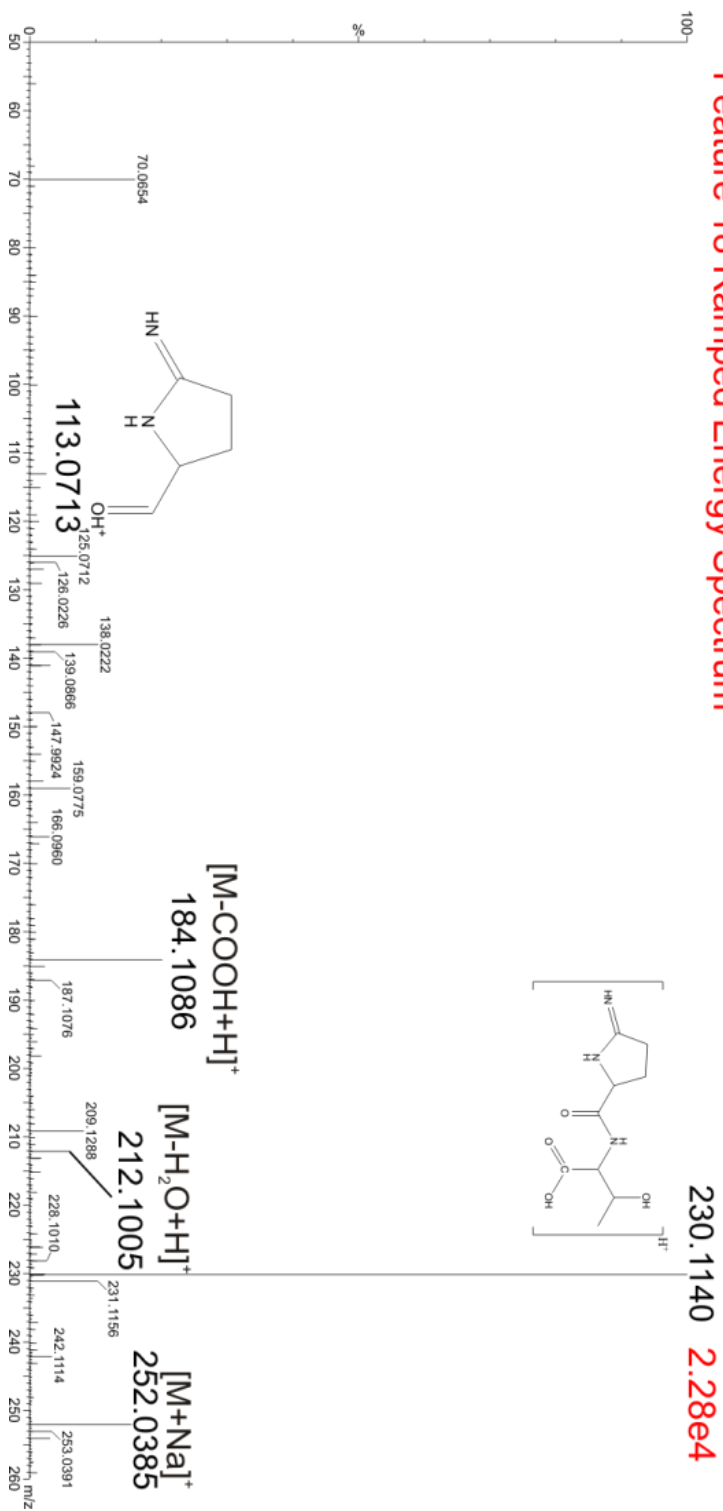
Figure A3.60. (Above) Mobility separated ramped energy mass spectrum for feature 18, indicating proposed fragment identities.
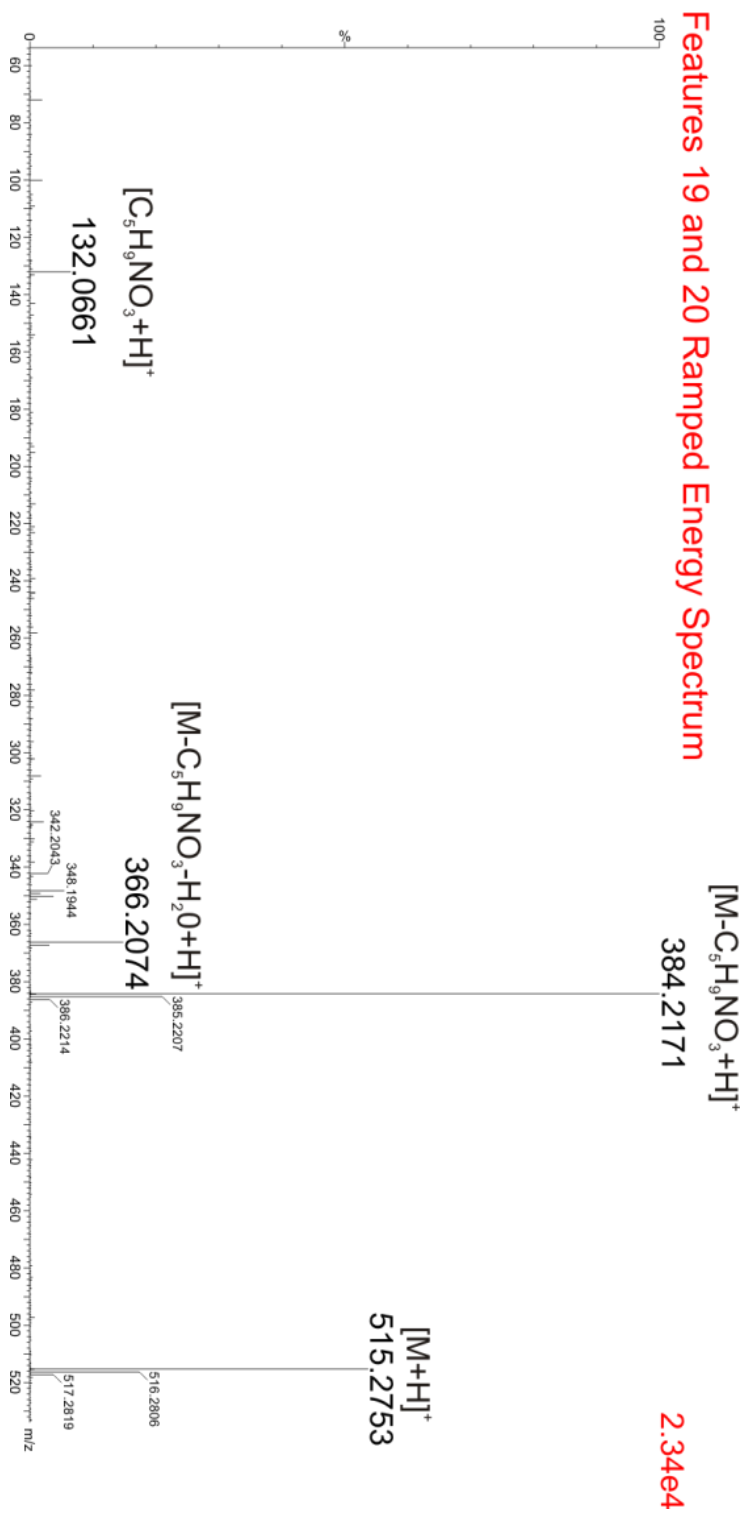
Figure A3.61. (Above) Mobility separated ramped energy mass spectrum for feature 18 and 19, indicating proposed fragment identities.
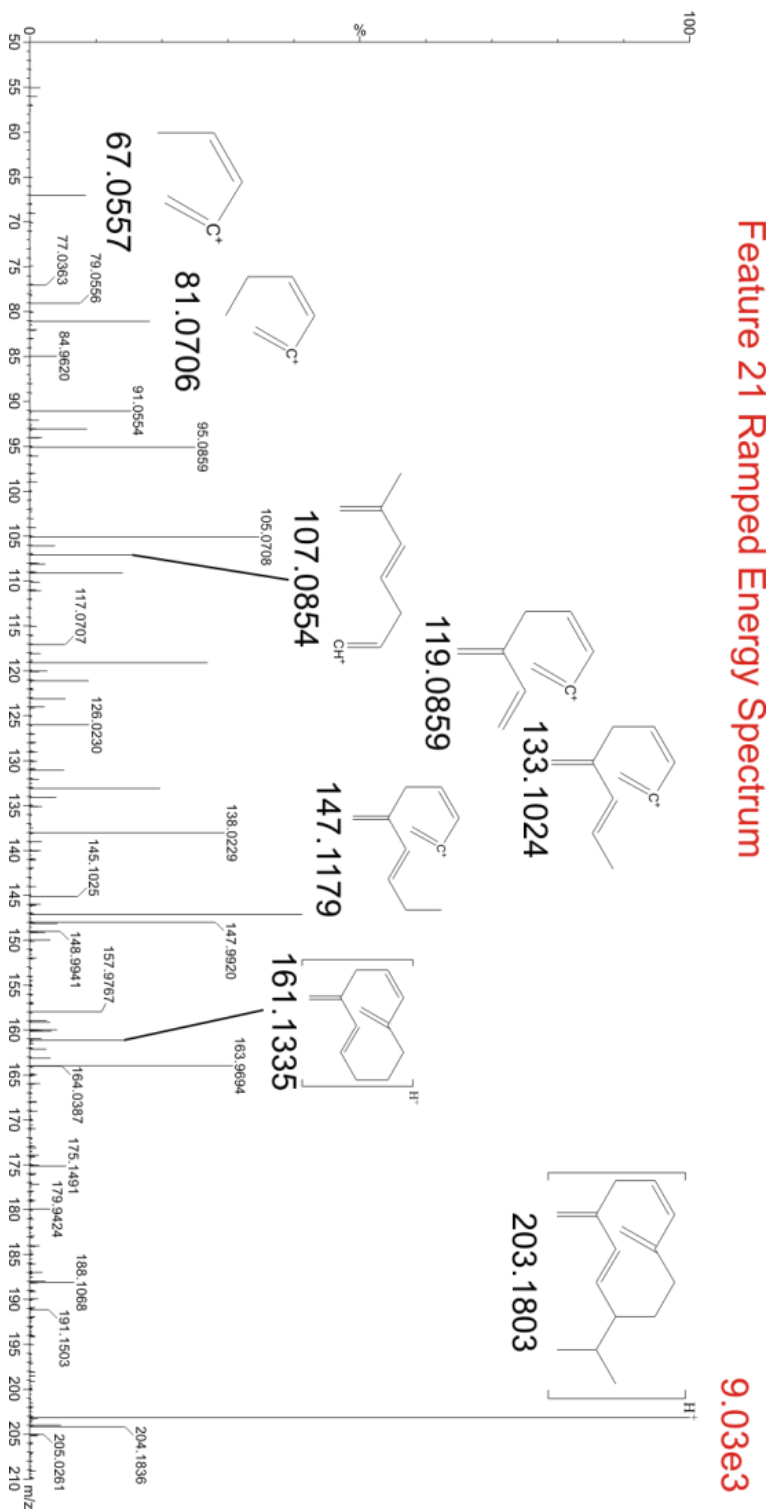
Figure A3.62. Mobility separated ramped energy mass spectrum for feature 21, indicating proposed fragment identities.
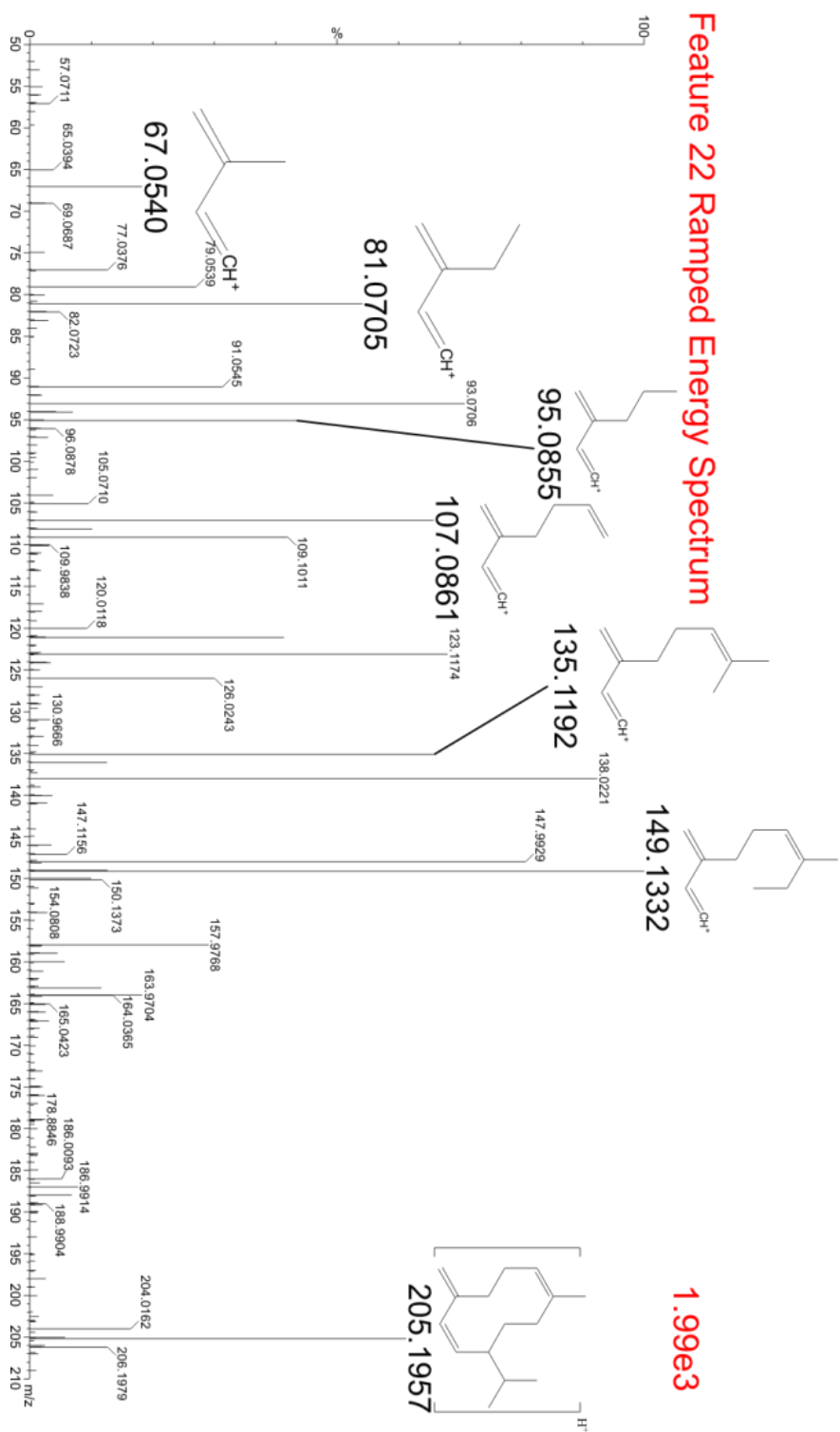
Figure A3.63. Mobility separated ramped energy mass spectrum for feature 22, indicating proposed fragment identities.
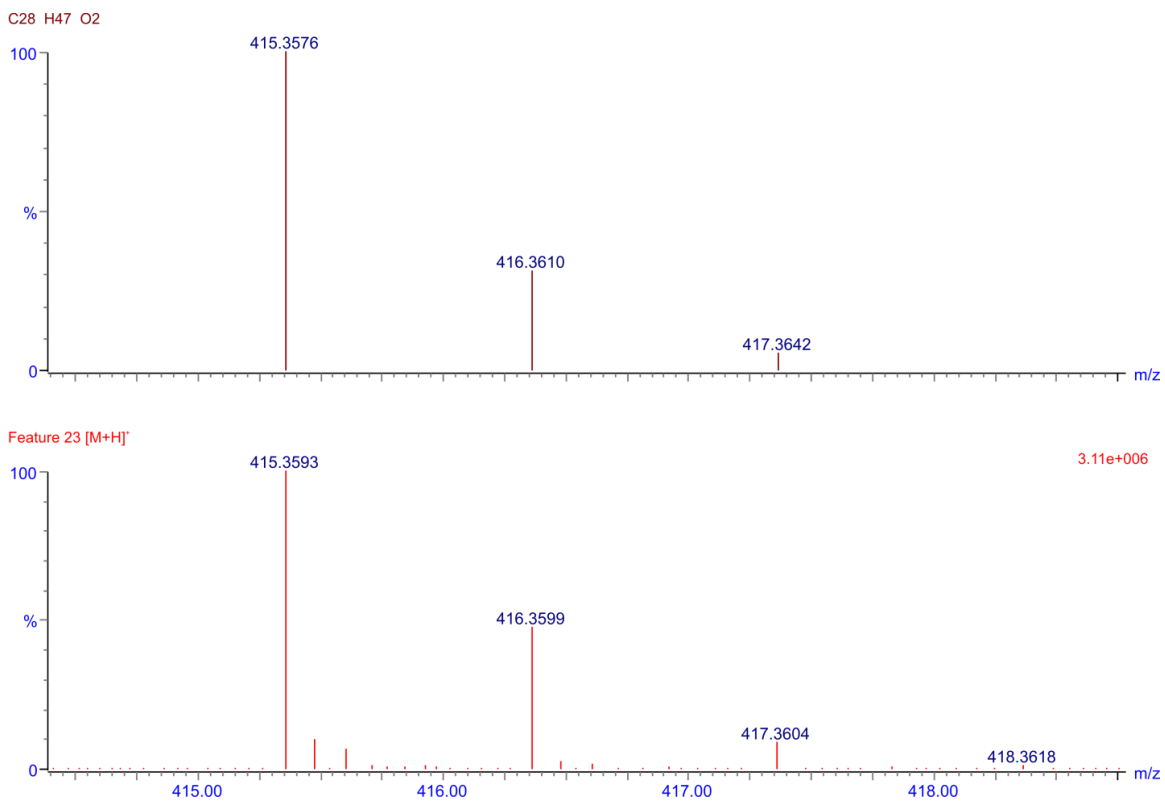
Figure A3.64. (Above) Theoretical isotopic profile for $[C_{28}H_{46}O_2+H]^+$. (Below) Accurate mass isotopic envelope of feature 23, as specified in Table 3.1.

Figure A3.65. Mobility separated ramped energy mass spectrum for feature 23.
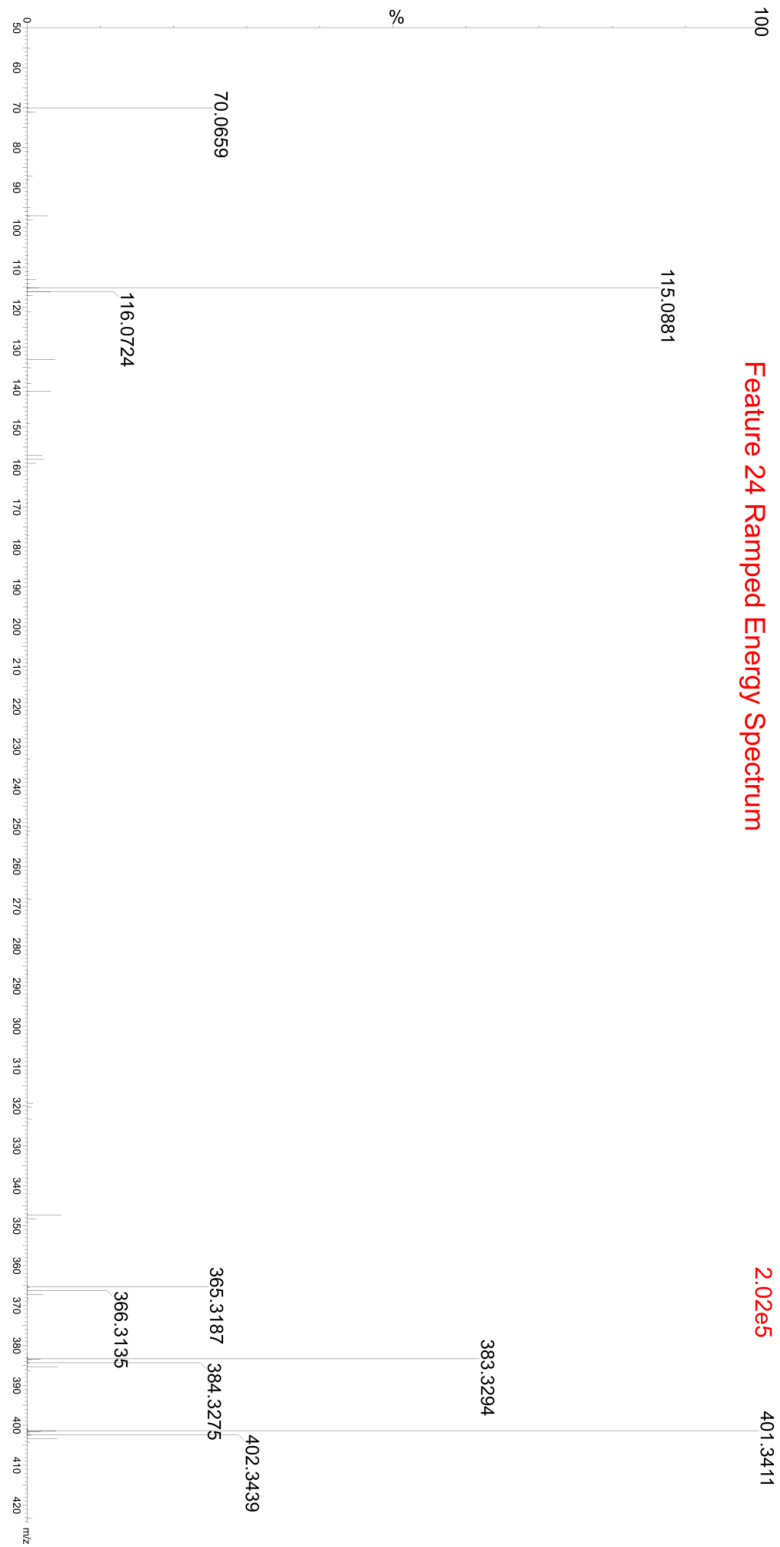
Figure A3.66. Mobility separated ramped energy mass spectrum for feature 24.
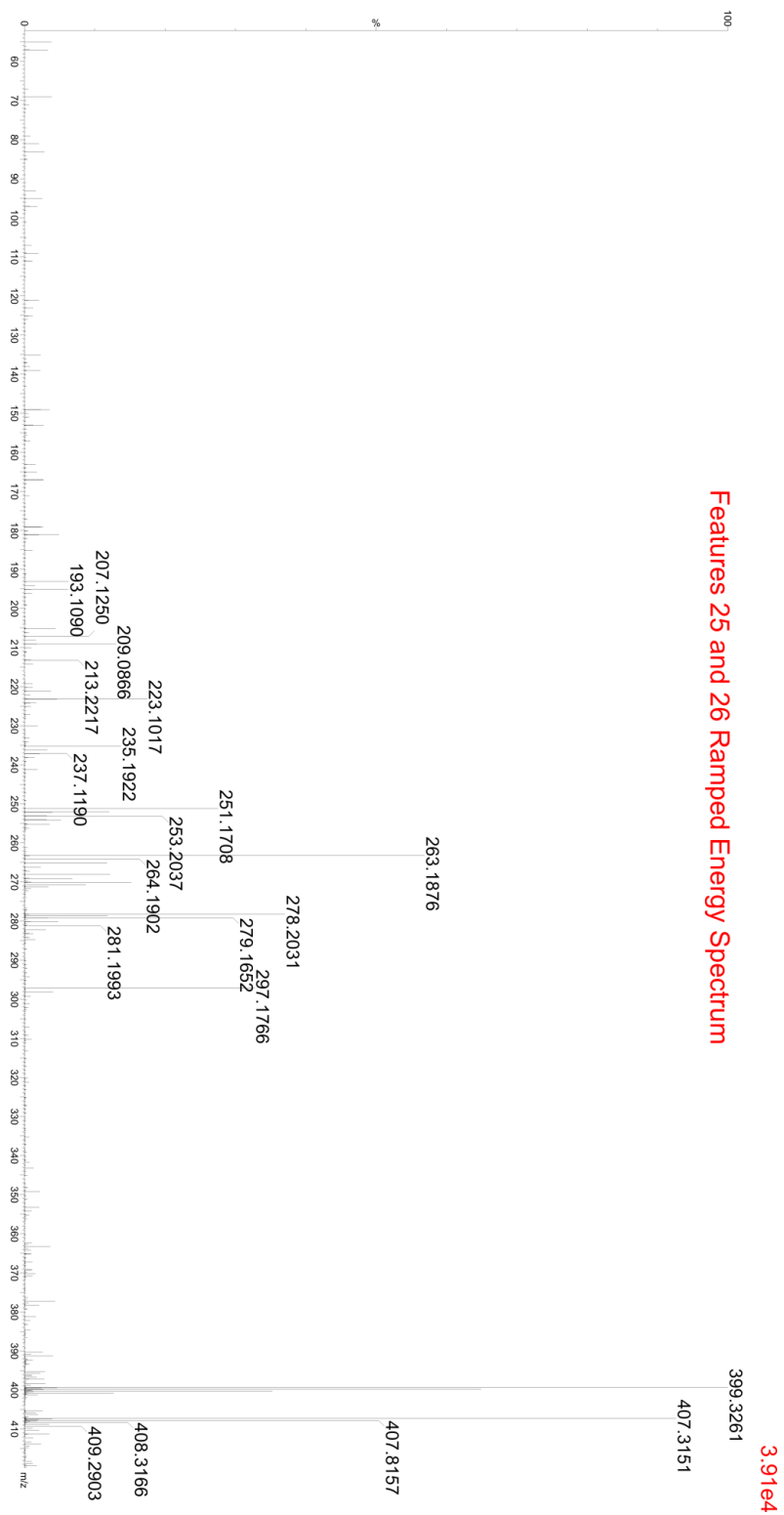
Figure A3.67. Mobility separated ramped energy mass spectrum for feature 25 and 26.
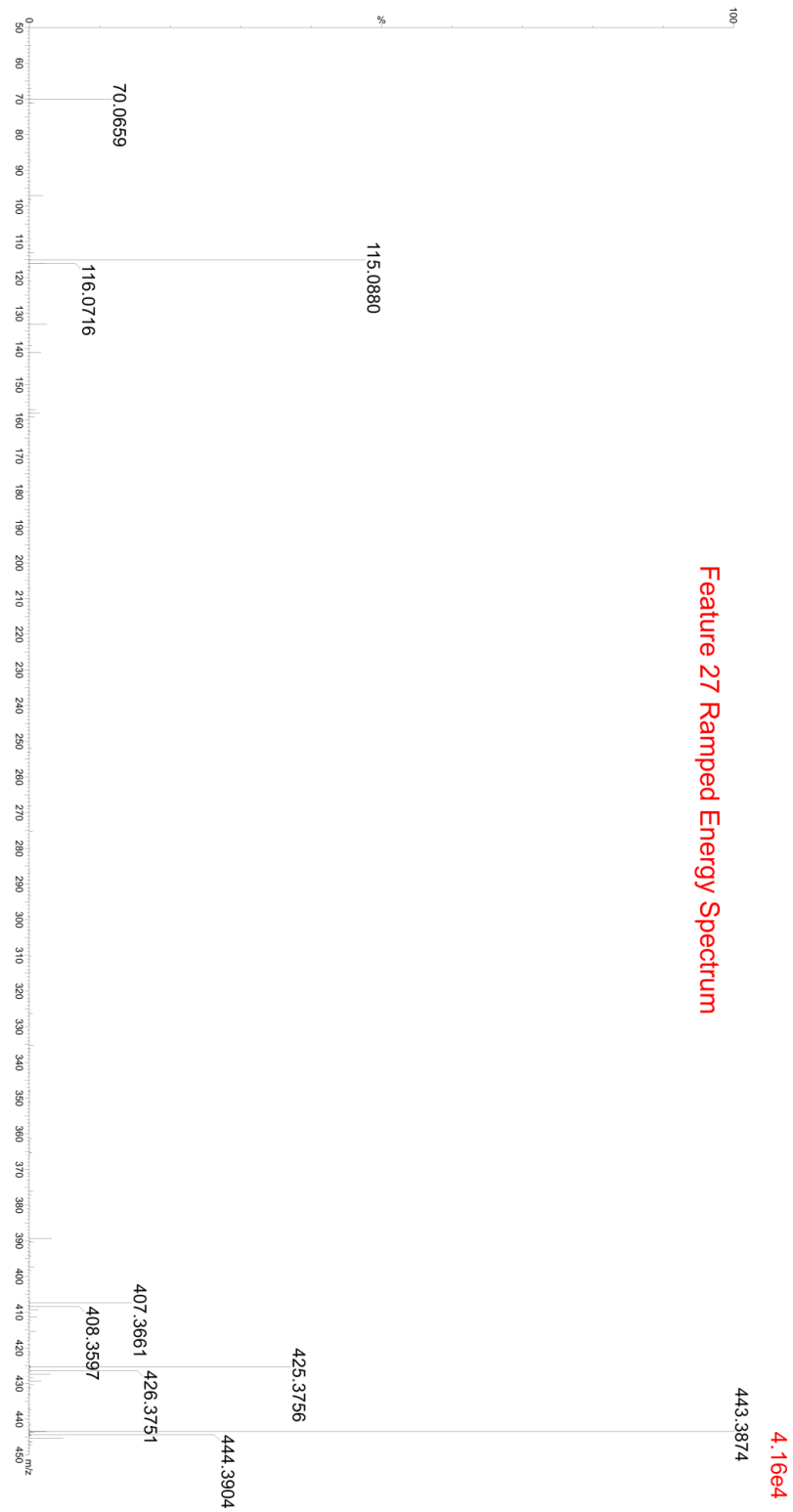
Figure A3.68. Mobility separated ramped energy mass spectrum for feature 27.
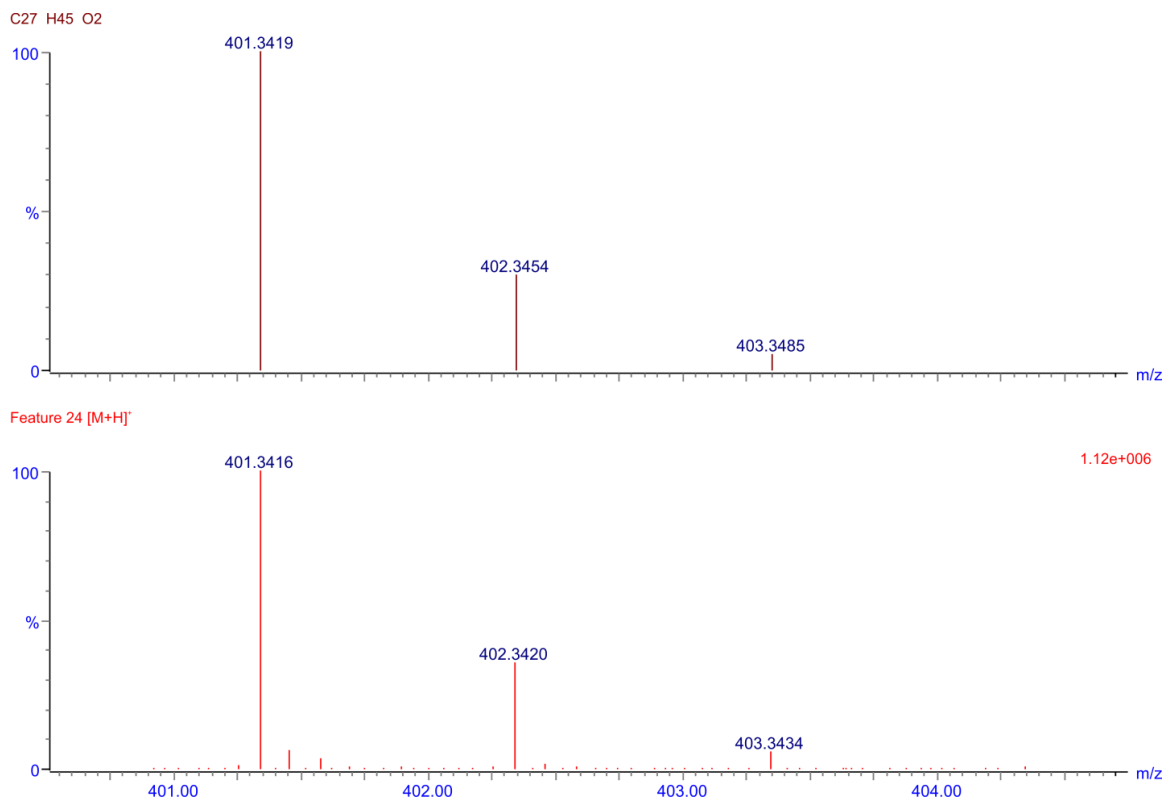
Figure A3.69. (Above) Theoretical isotopic profile for $[C_{27}H_{44}O_2+H]^+$. (Below) Accurate mass isotopic envelope of feature 24, as specified in Table 3.1.

Feature 25 [M+2H]$^{2+}$ 2.79e5

399.3260

399.8258

400.3242

400.8244

401.3249
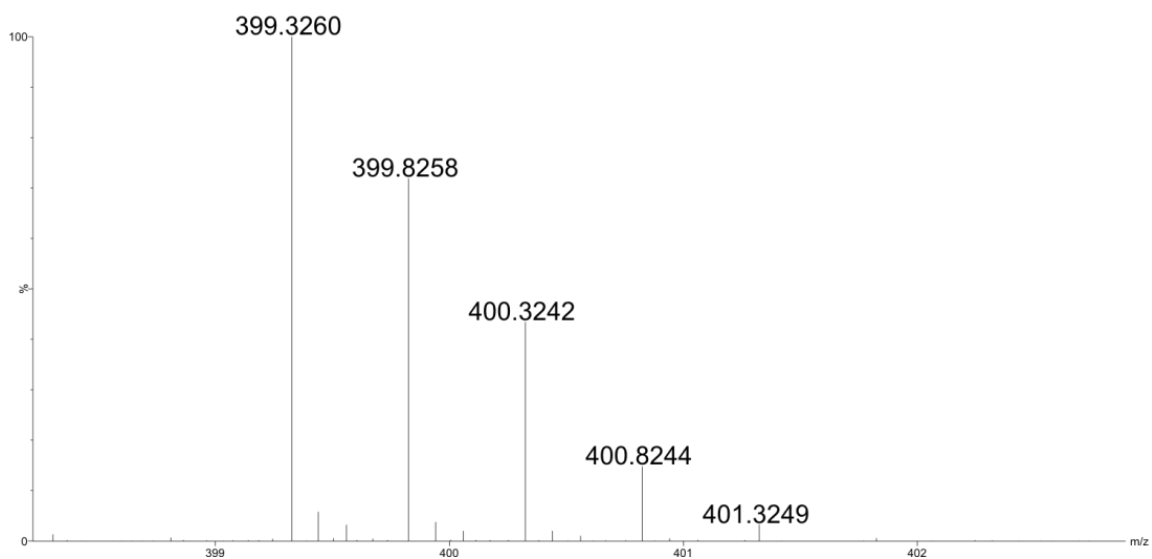
Figure A3.70. Accurate mass isotopic envelope of feature 25, as specified in Table 3.1.
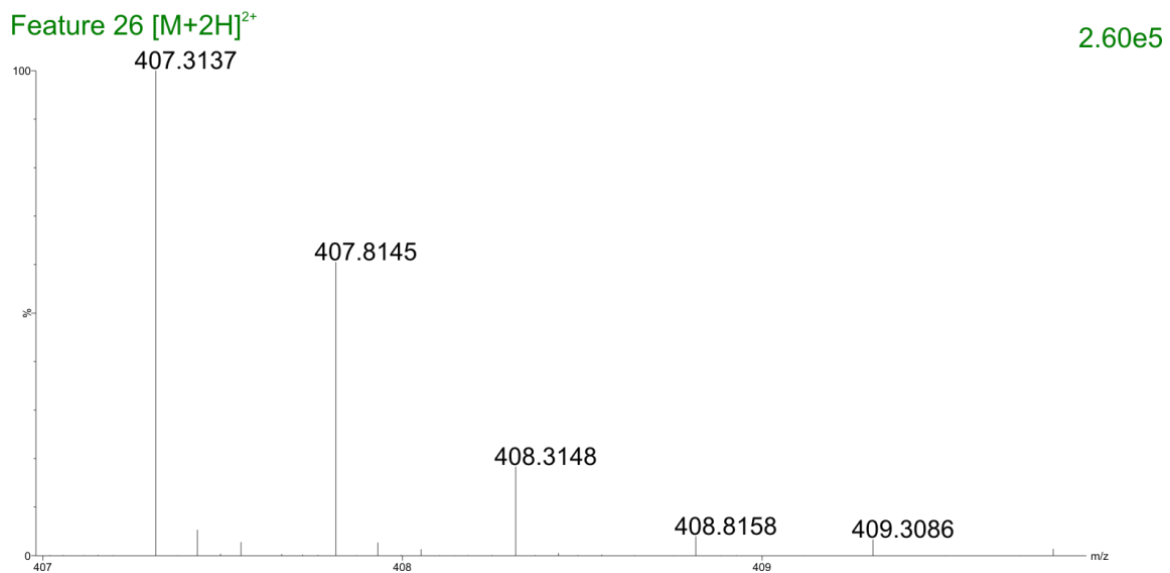
Figure A3.71. Accurate mass isotopic envelope of feature 26, as specified in Table 1.
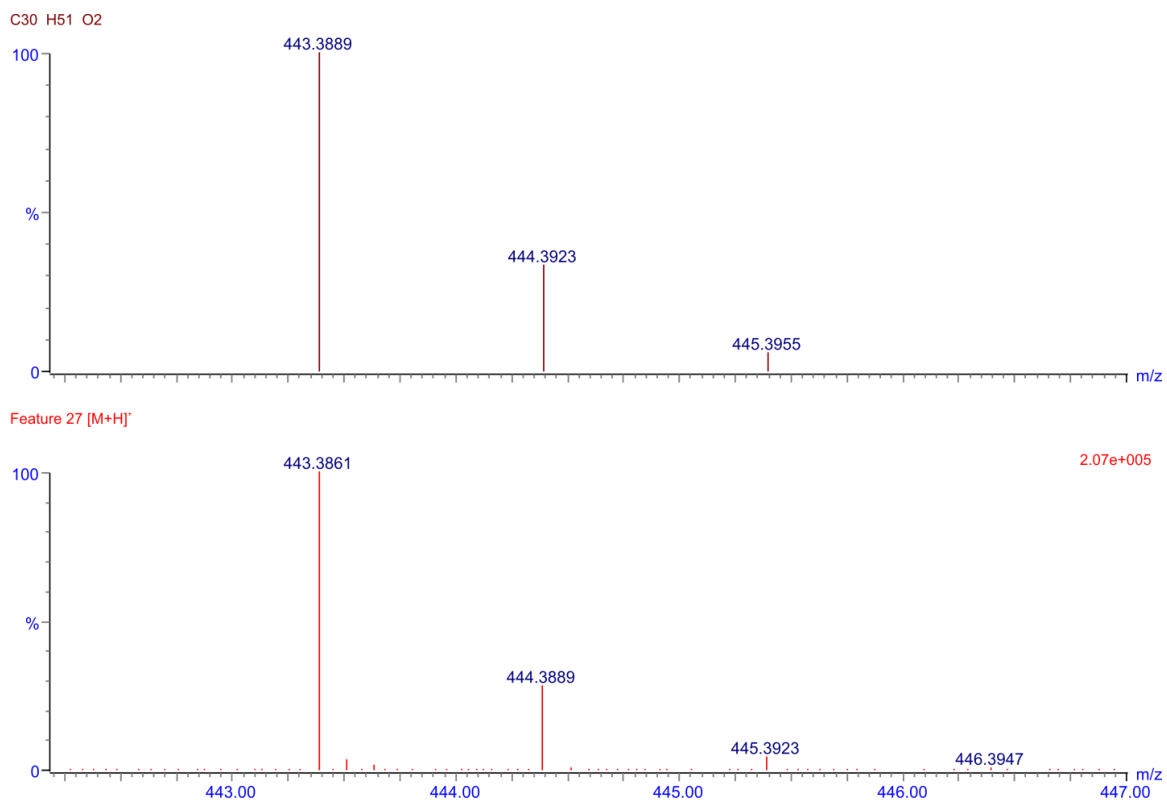
Figure A3.72. (Above) Theoretical isotopic profile for $[C_{30}H_{50}O_2+H]^+$. **(Below)** Accurate mass isotopic envelope of feature 27, as specified in Table 1.

Feature 1 EIC (±0.01Da)

Figure A3.73. Extracted ion chromatograms for feature 1 w/ ±0.01Da tolerance.
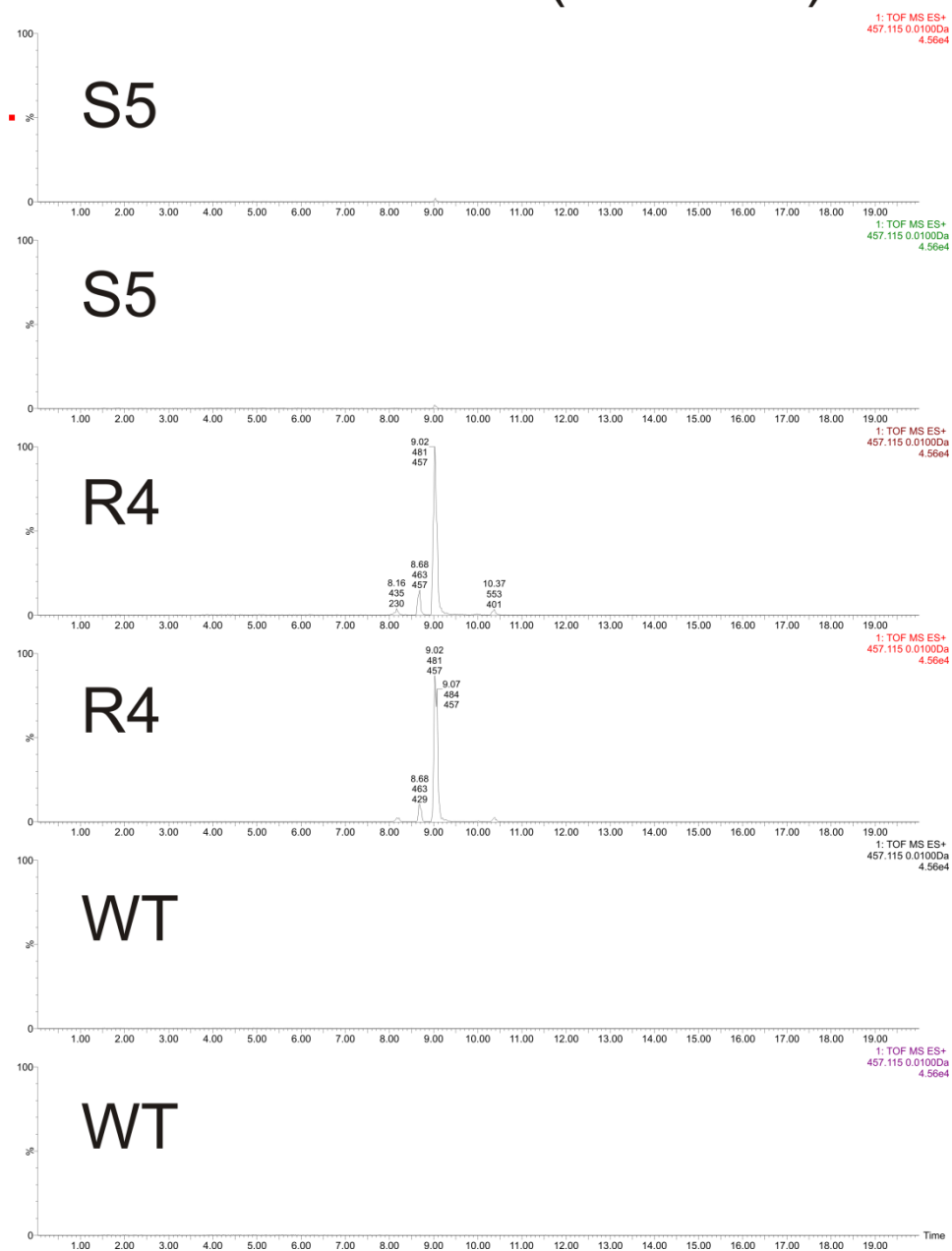
Feature 2 EIC (±0.01Da)

Figure A3.74. Extracted ion chromatograms for feature 2 w/ ±0.01Da tolerance.
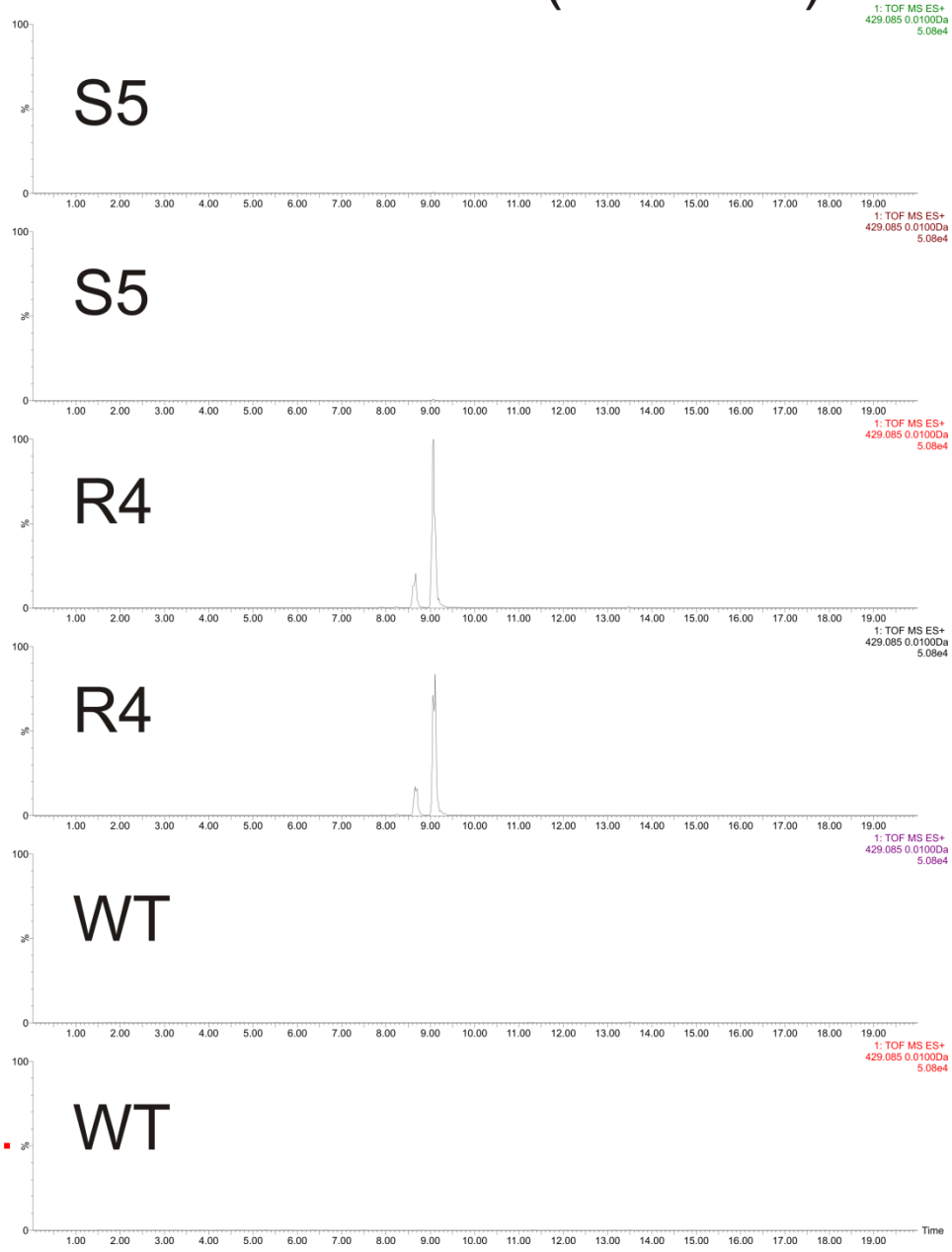
Figure A3.75. Extracted ion chromatograms for feature 3 w/ ±0.01Da tolerance.

Feature 4 EIC (±0.01Da)
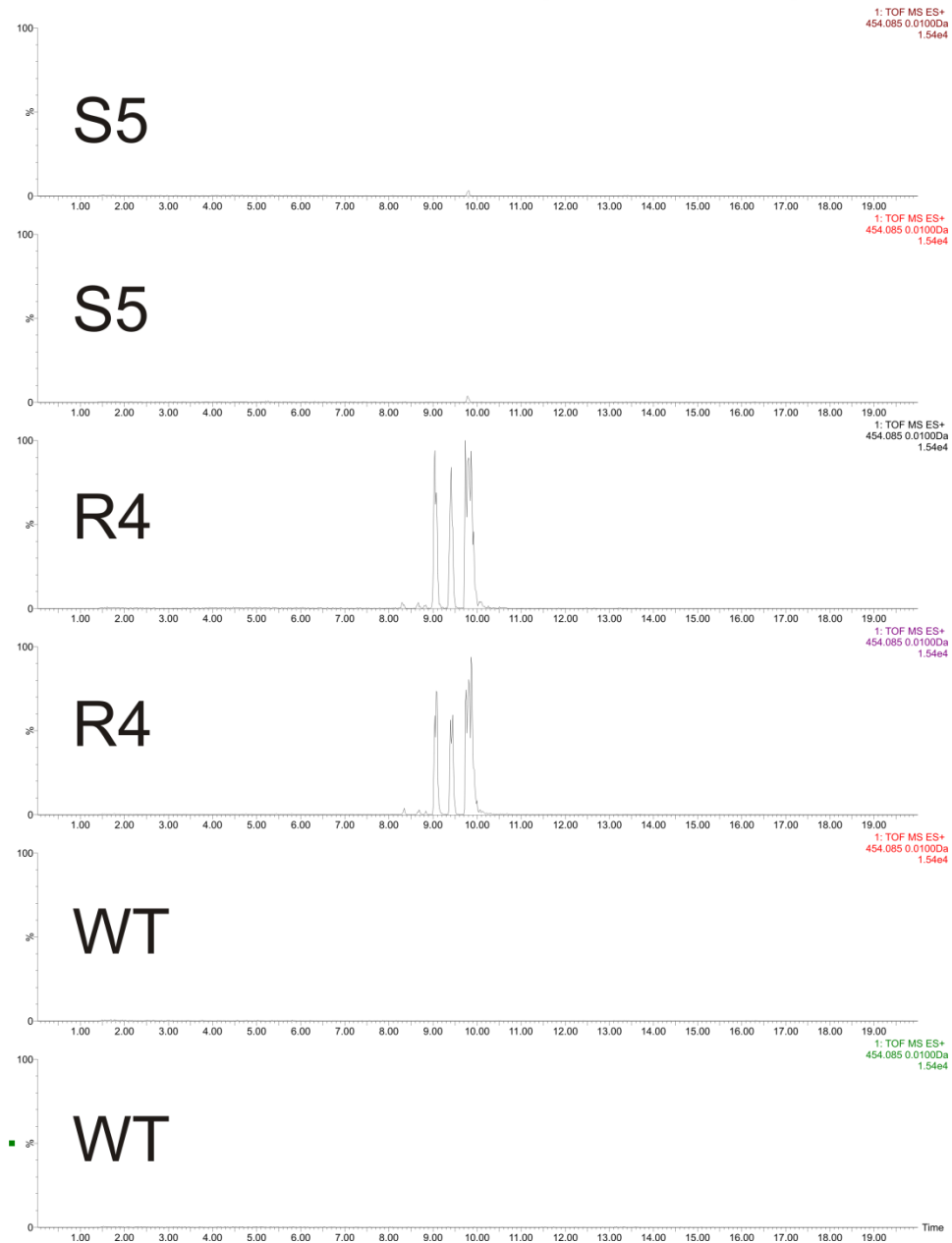
Figure A3.76. Extracted ion chromatograms for feature 4 w/ ±0.01Da tolerance.

Feature 5 EIC (±0.01Da)
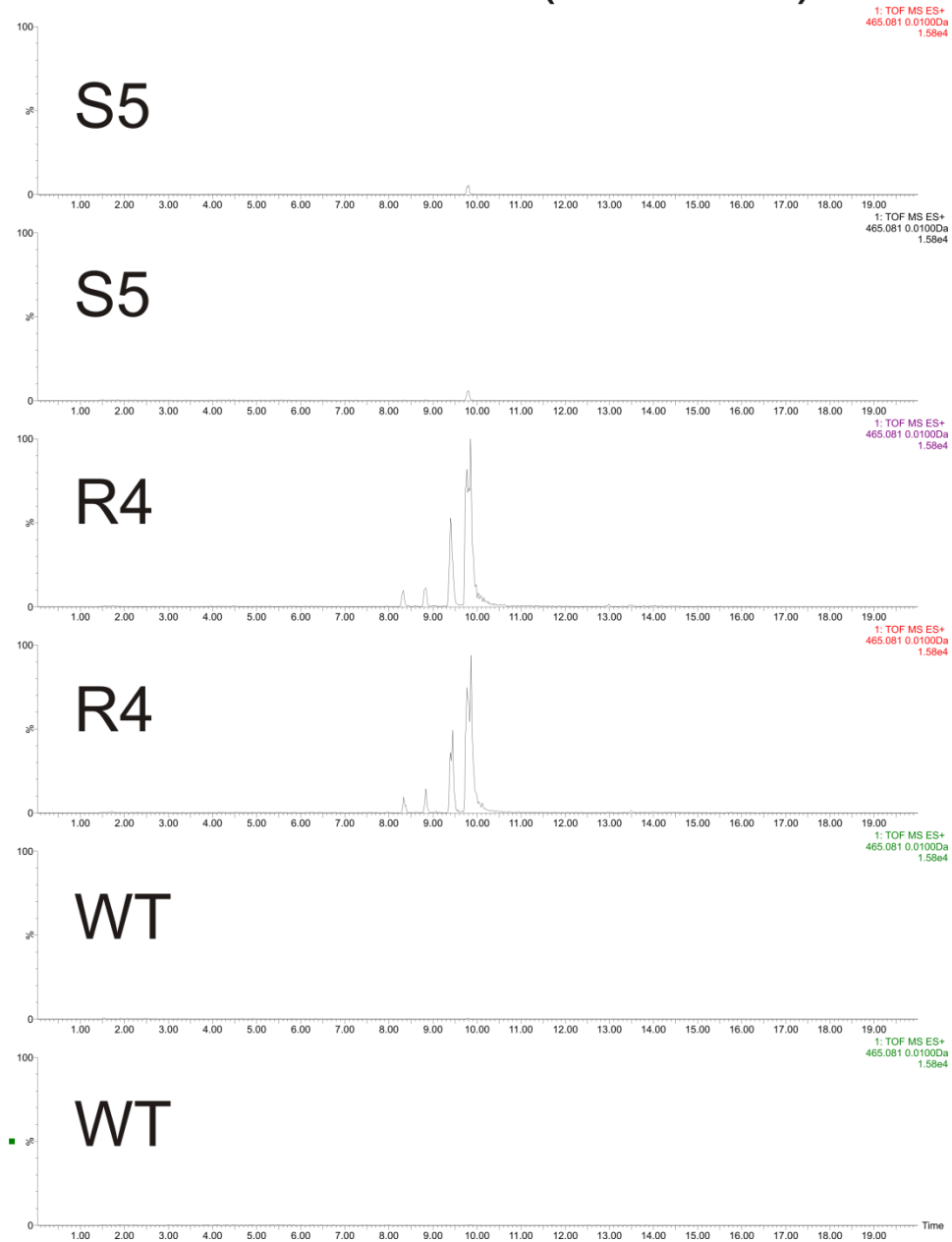
Figure A3.77. Extracted ion chromatograms for feature 5 w/ ±0.01Da tolerance.
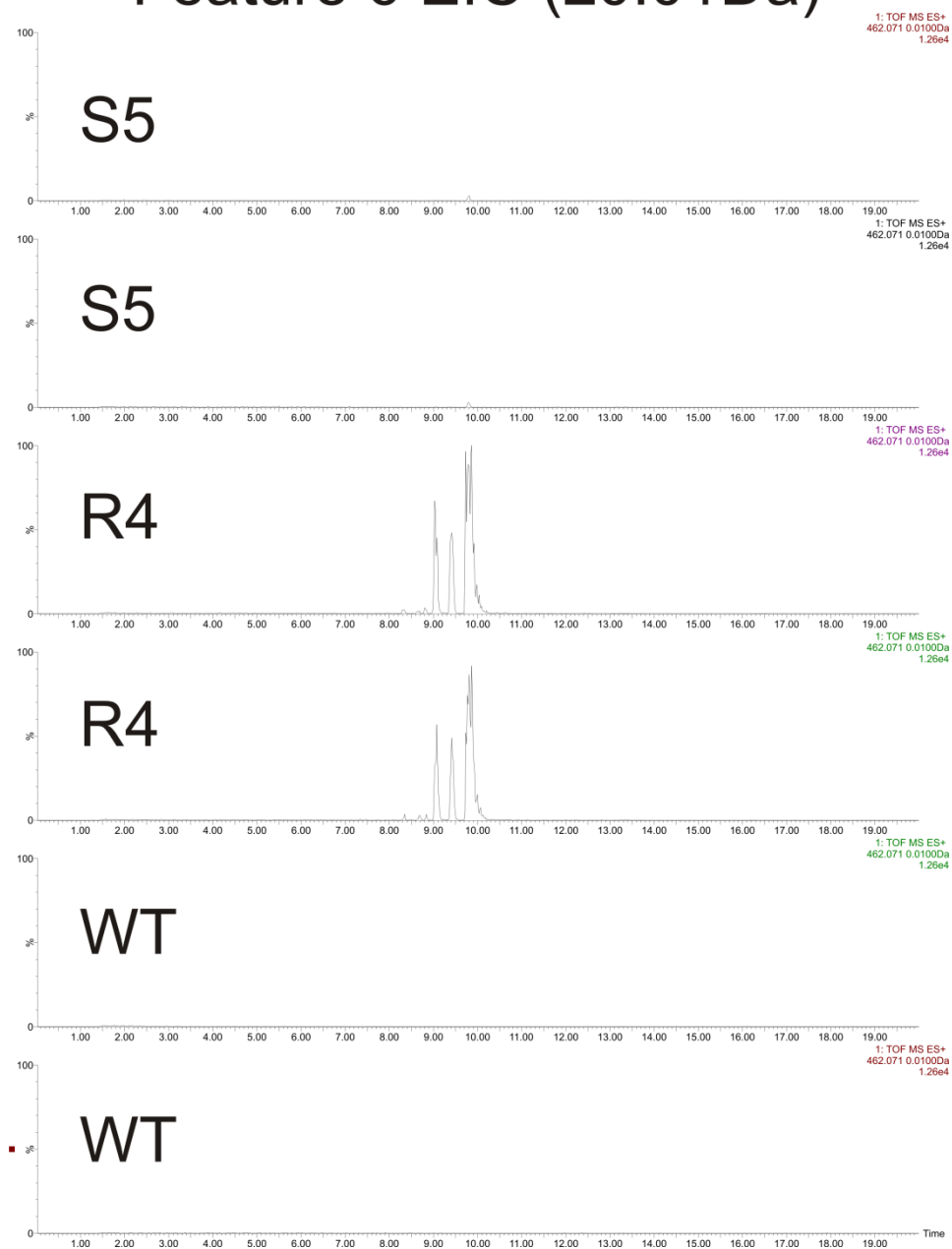
Figure A3.78. Extracted ion chromatograms for feature 6 w/ ±0.01Da tolerance.

Feature 7 EIC (±0.01Da)
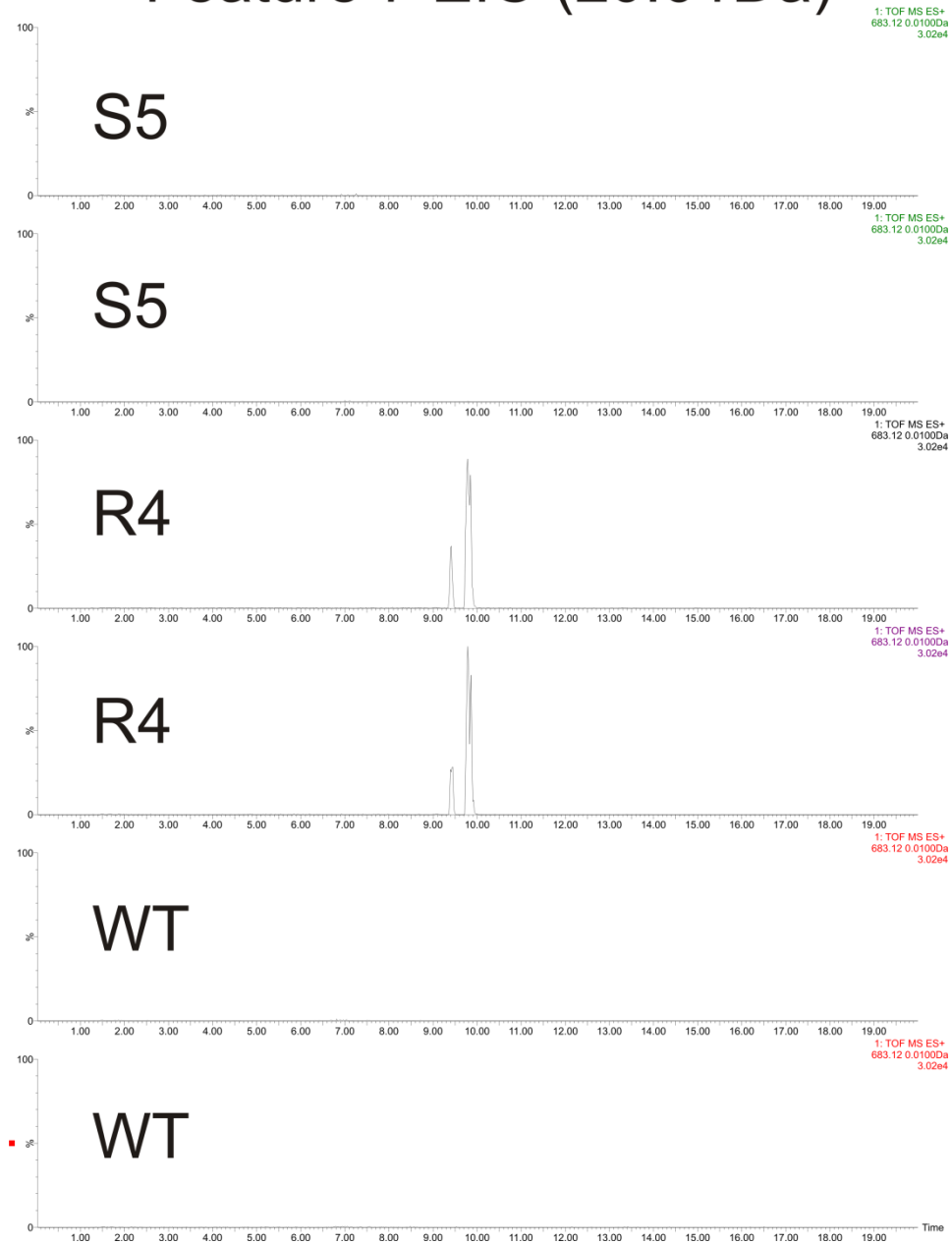
Figure A3.79. Extracted ion chromatograms for feature 7 w/ ±0.01Da tolerance.

Feature 8 EIC (±0.01Da)
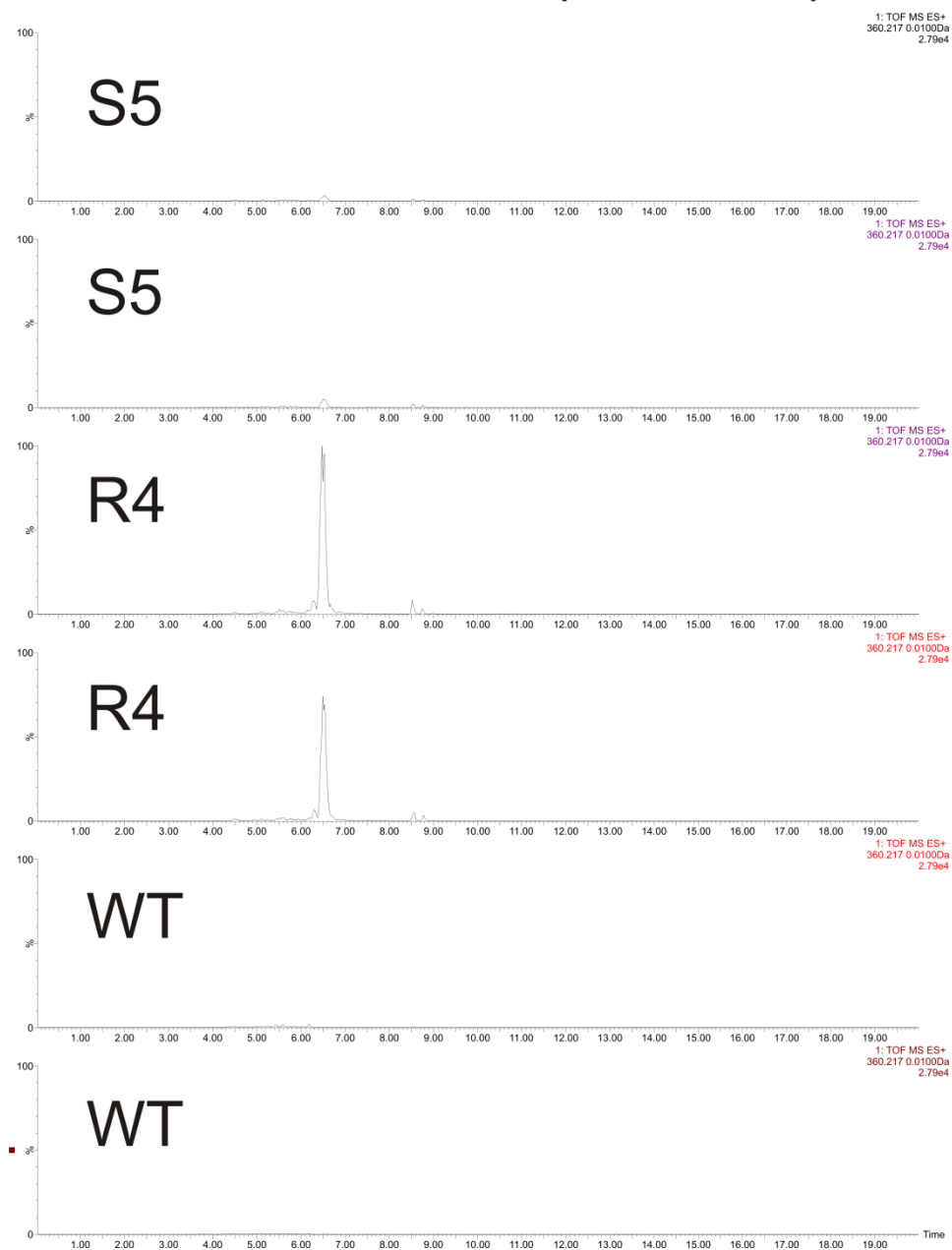
Figure A3.80. Extracted ion chromatograms for feature 8 w/ ±0.01Da tolerance.

Feature 9 EIC (±0.01Da)
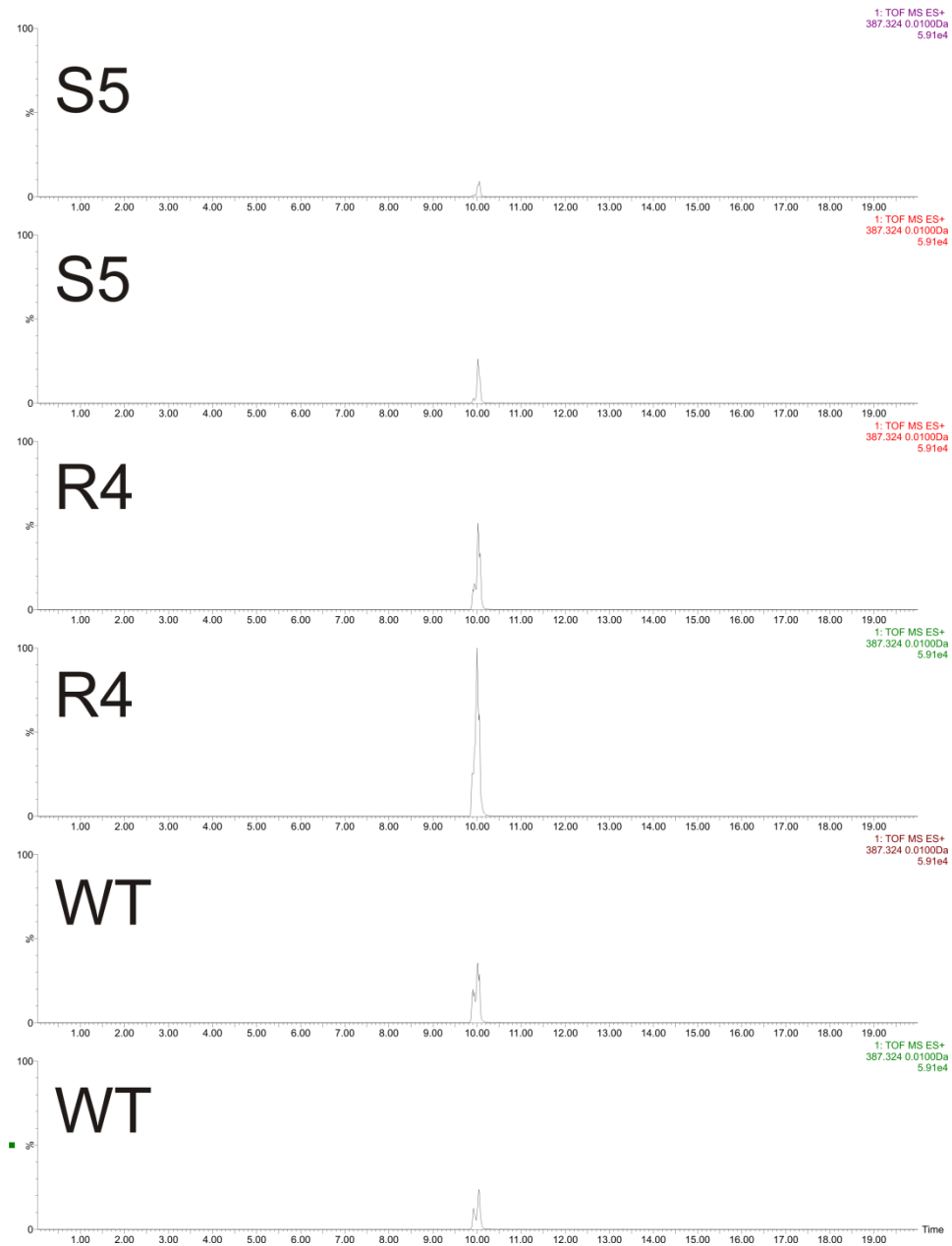
Figure A3.81. Extracted ion chromatograms for feature 9 w/ ±0.01Da tolerance.

Feature 10 EIC (±0.01Da)
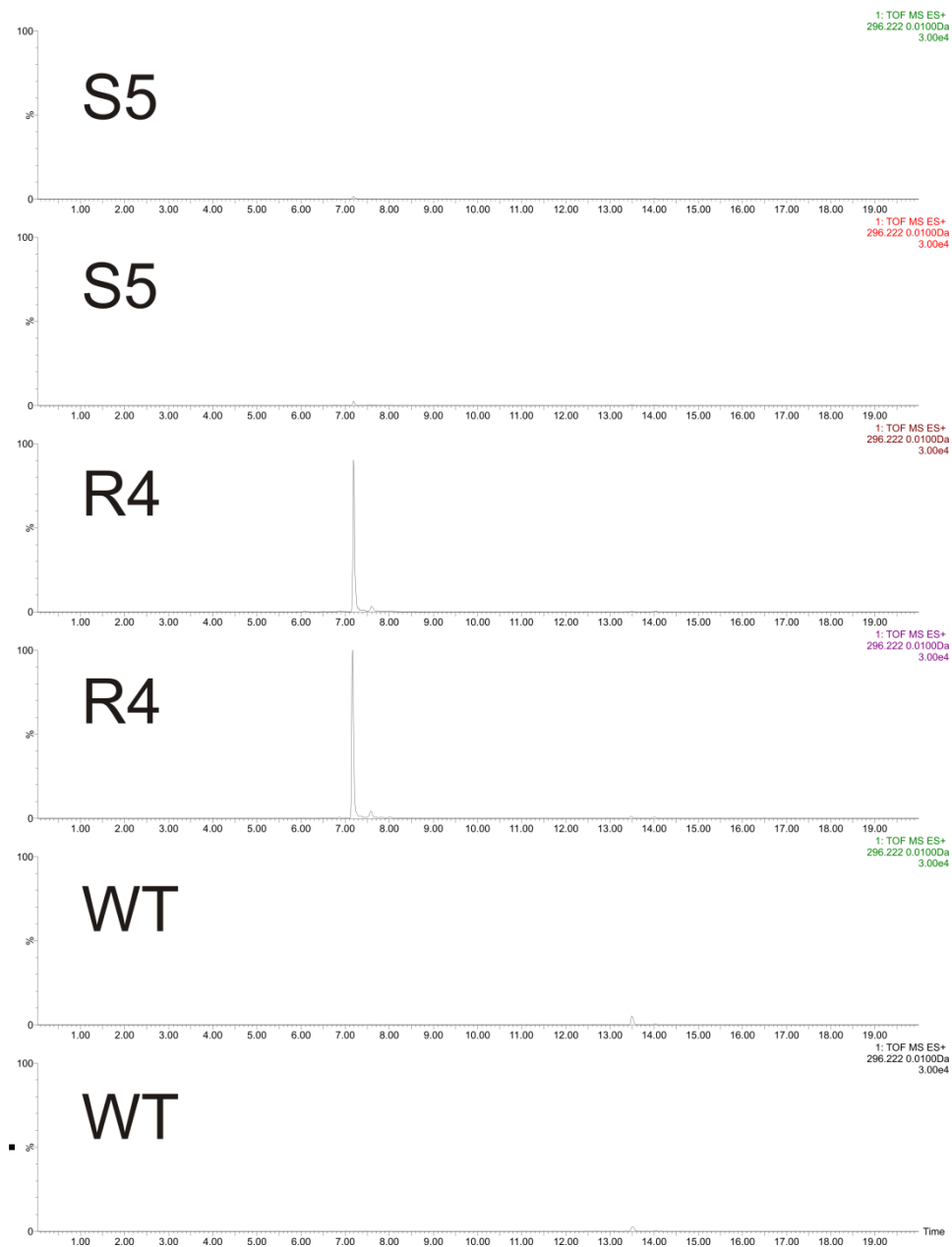
Figure A3.82. Extracted ion chromatograms for feature 10 w/ ±0.01Da tolerance.

Feature 11 EIC (±0.01Da)
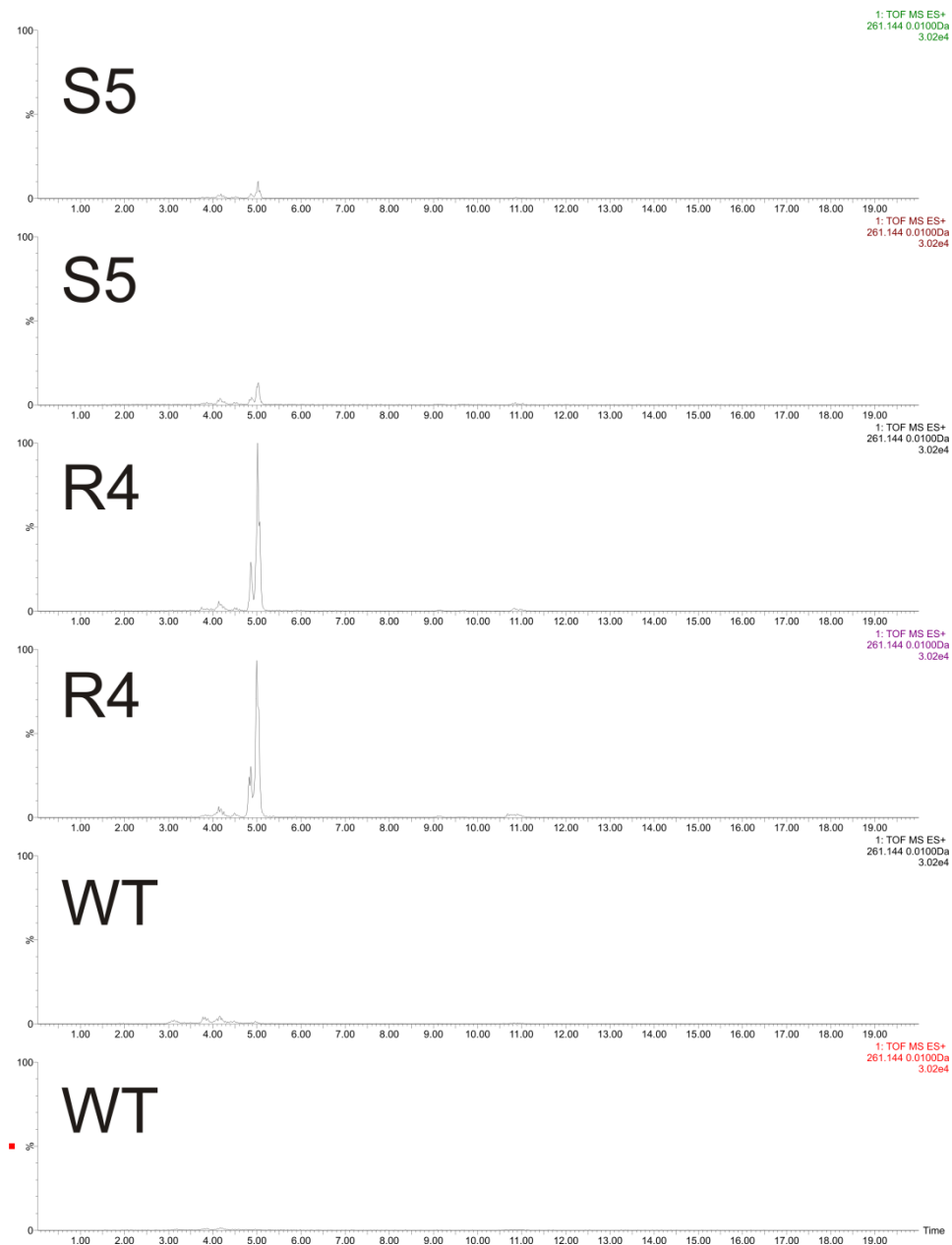
Figure A3.83. Extracted ion chromatograms for feature 11 w/ ±0.01Da tolerance.

Feature 12 EIC (±0.01Da)
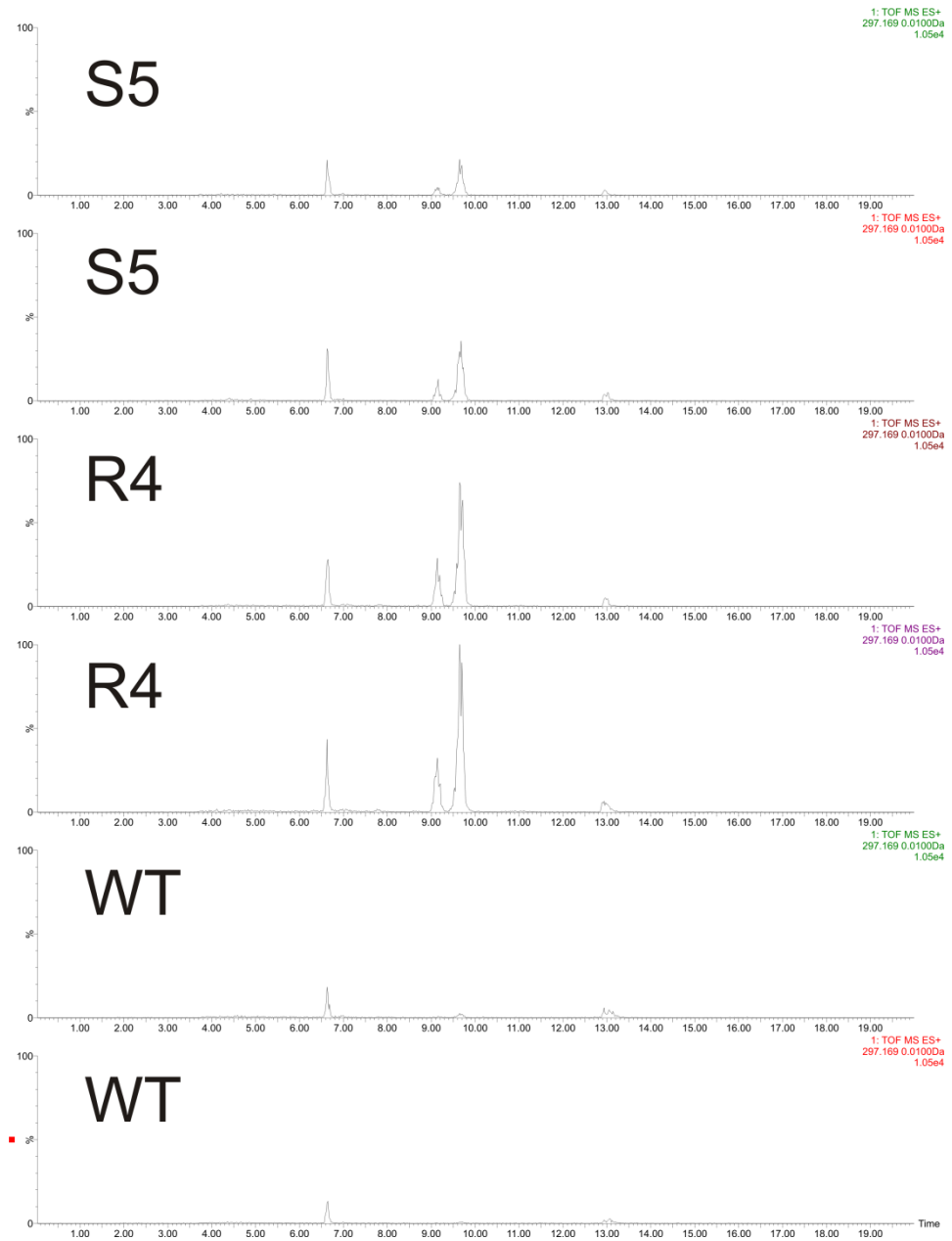
Figure A3.84. Extracted ion chromatograms for feature 12 w/ ±0.01Da tolerance.

Feature 13 EIC (±0.01Da)
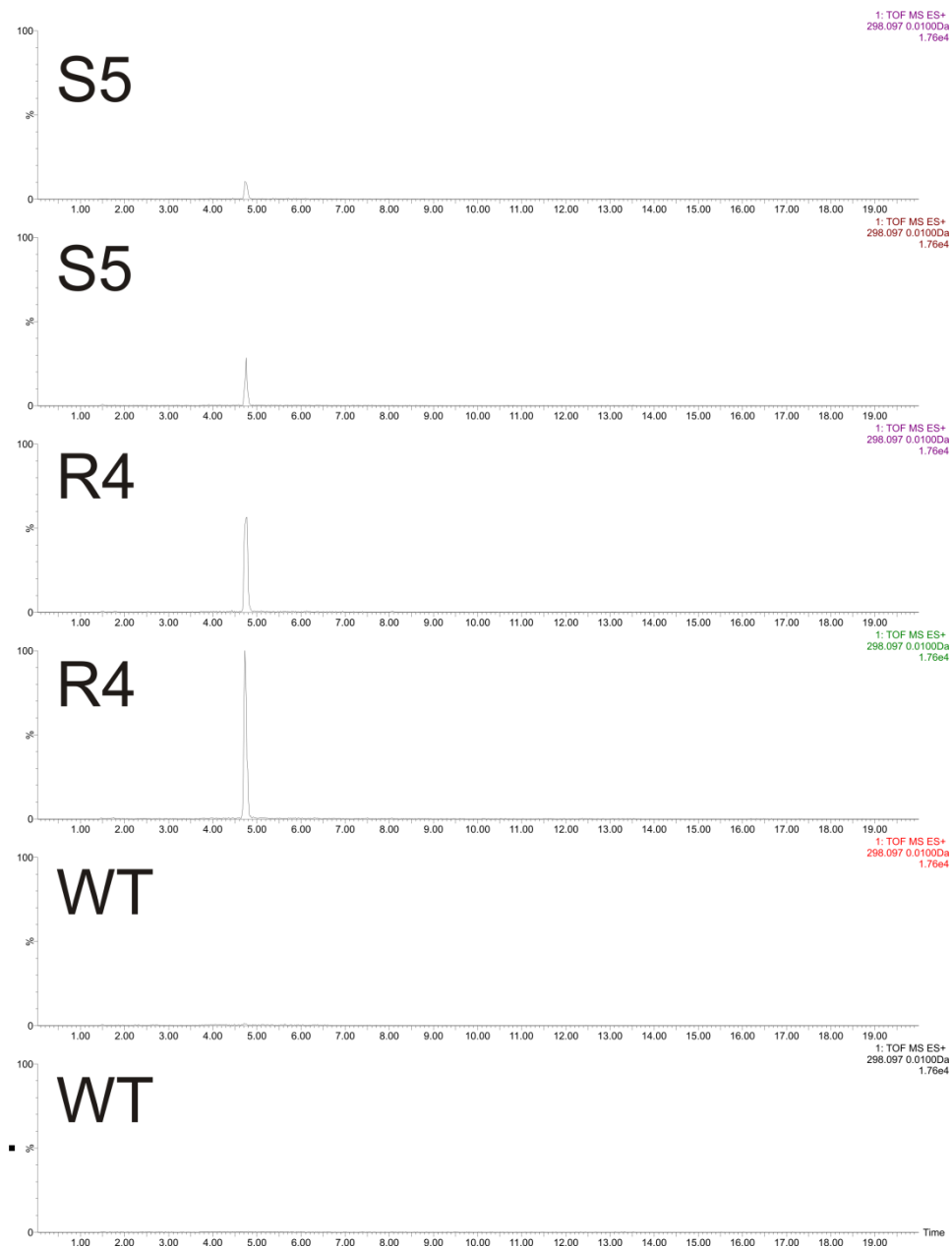
Figure A3.85. Extracted ion chromatograms for feature 13 w/ ±0.01Da tolerance.

Feature 14 EIC (±0.01Da)
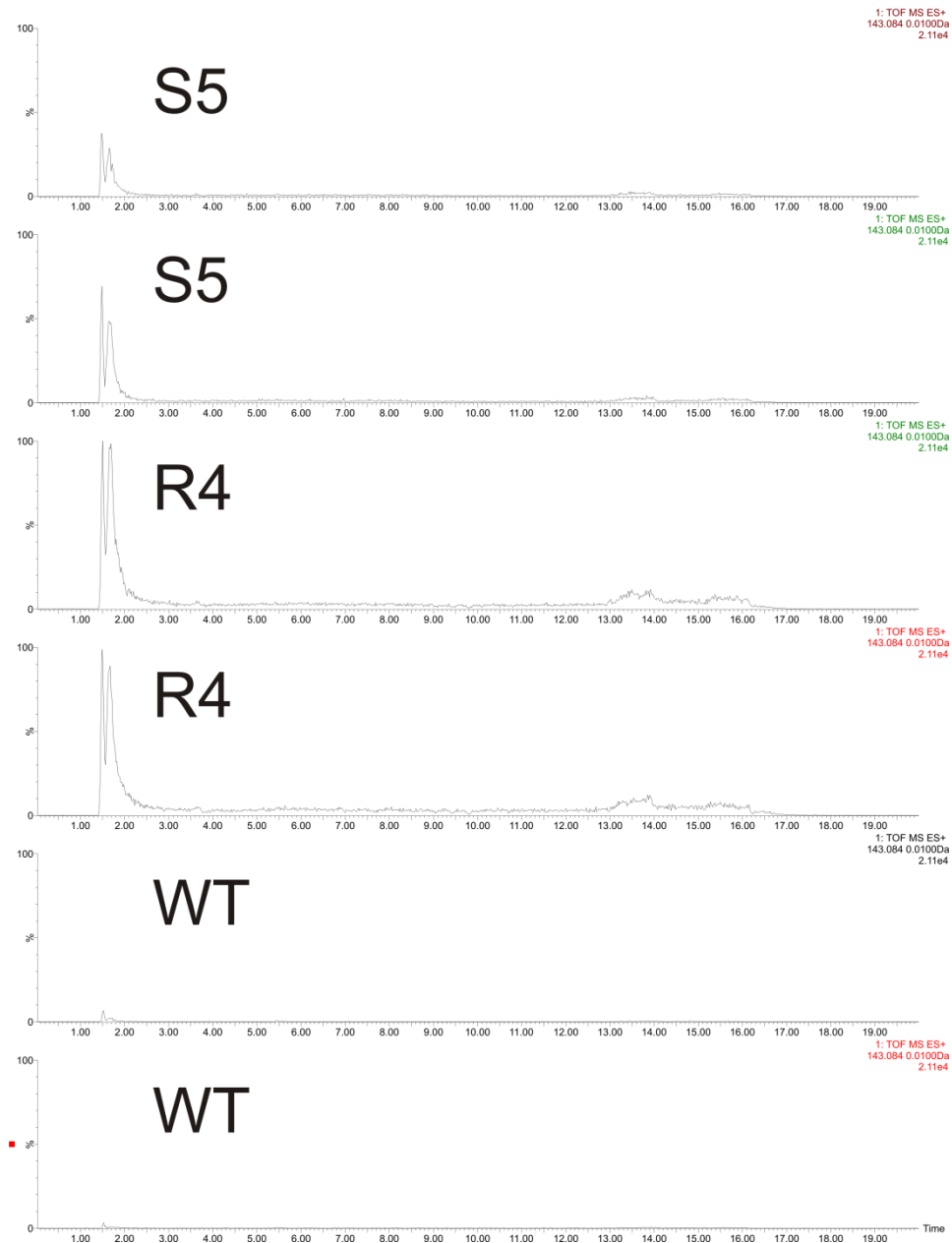
Figure A3.86. Extracted ion chromatograms for feature 14 w/ ±0.01Da tolerance.
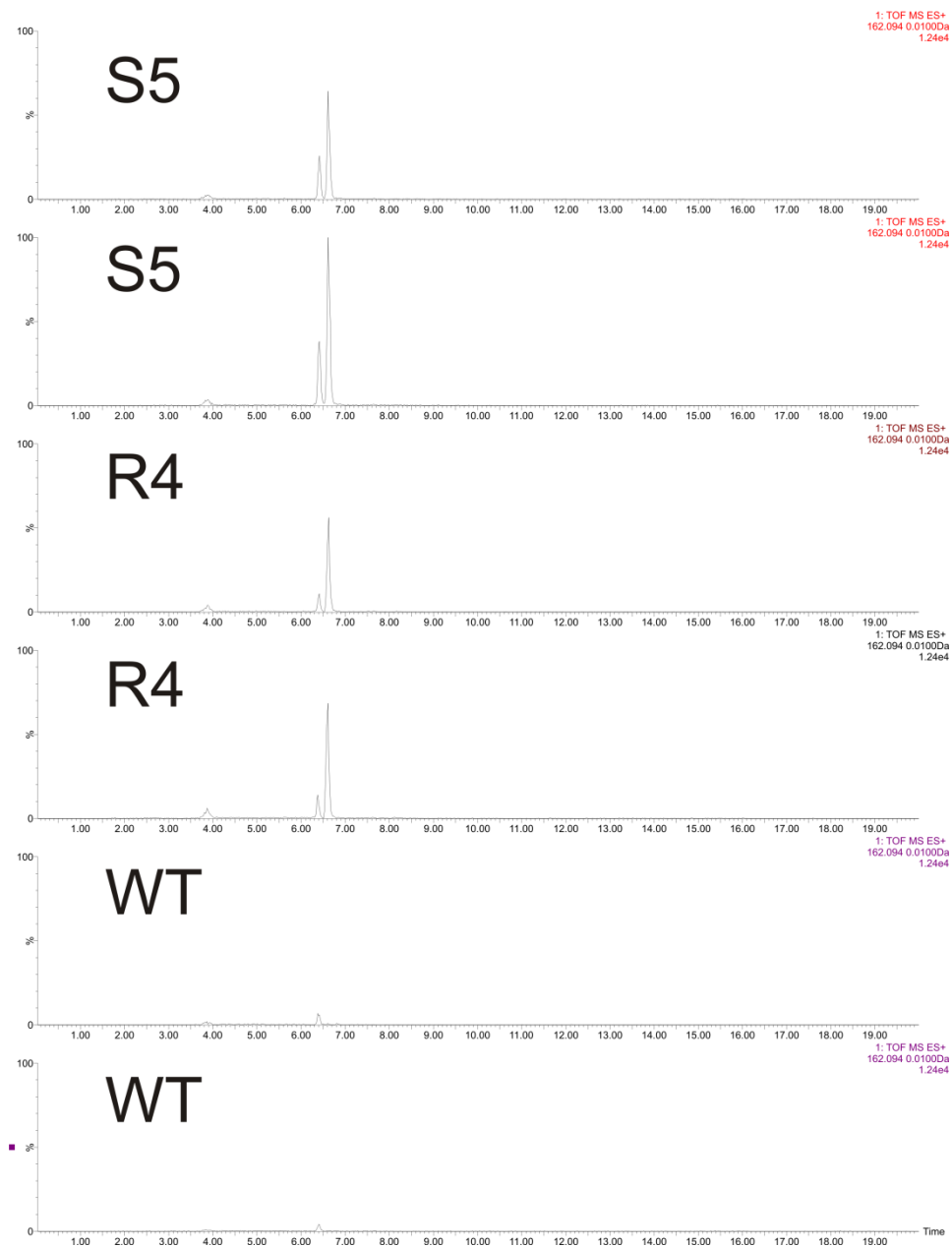
Figure A3.87. Extracted ion chromatograms for feature 15 w/ ±0.01Da tolerance.

Feature 16 EIC (±0.01Da)
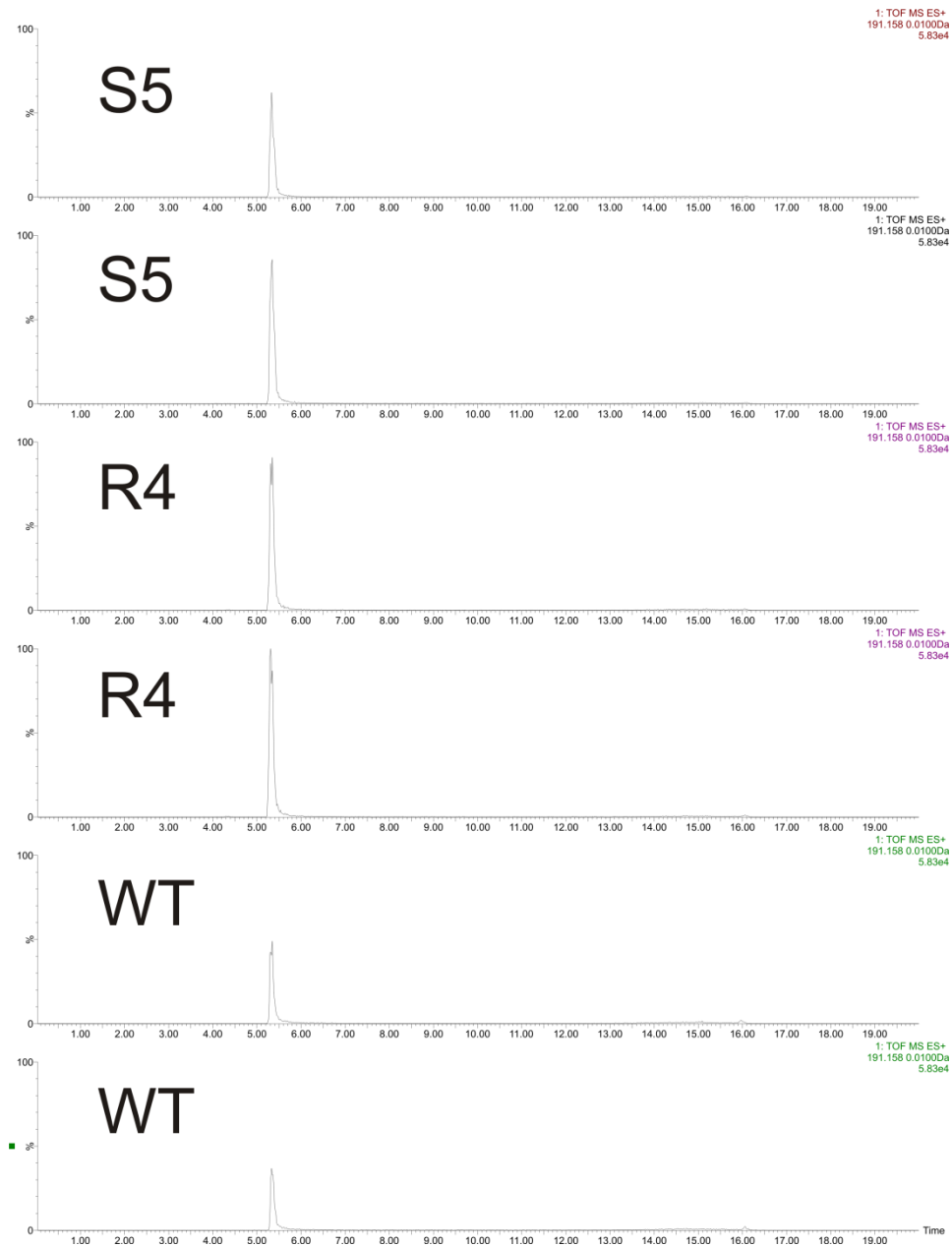
Figure A3.88. Extracted ion chromatograms for feature 16 w/ ±0.01Da tolerance.

Feature 17 EIC (±0.01Da)
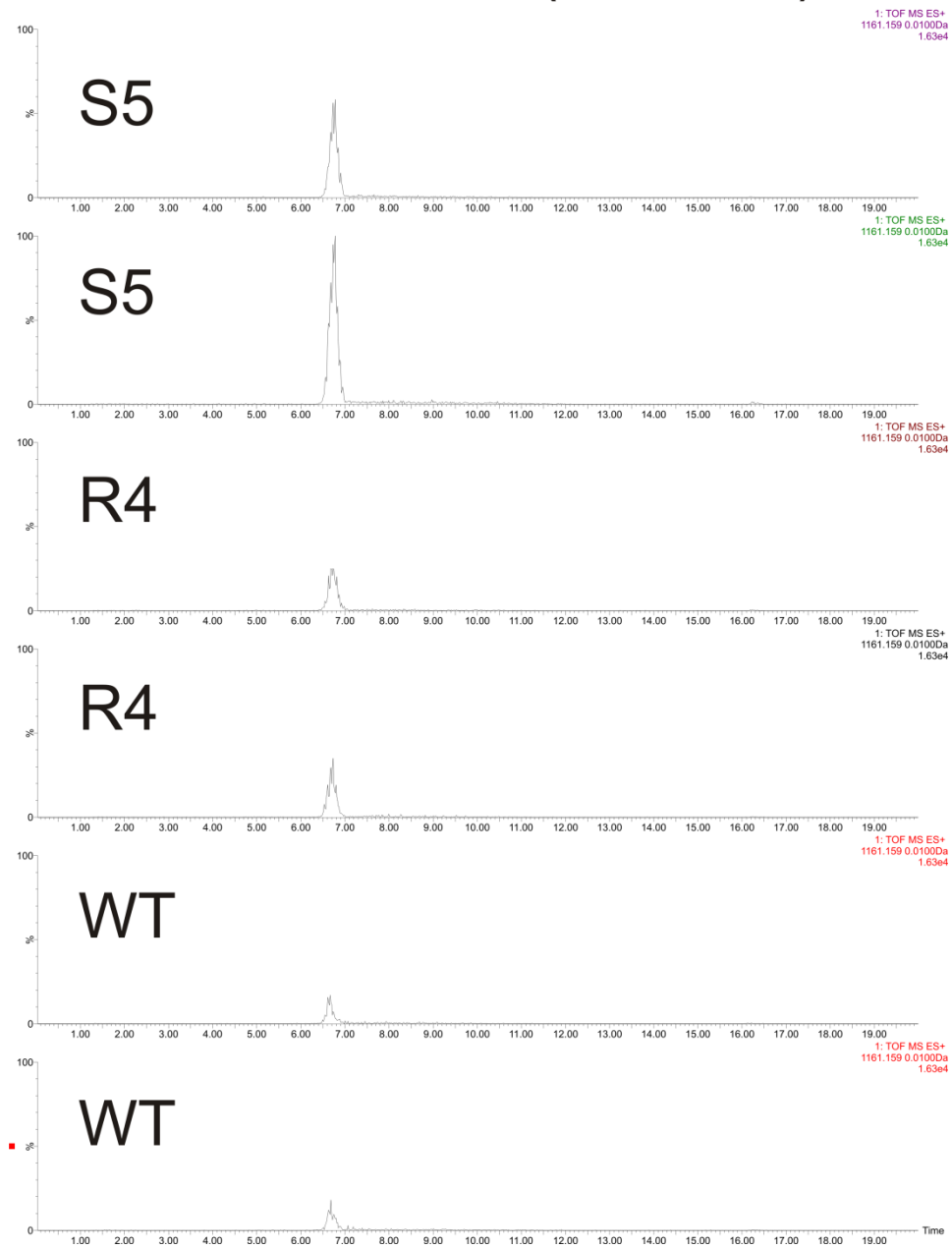
Figure A3.89. Extracted ion chromatograms for feature 17 w/ ±0.01Da tolerance.

Feature 18 EIC (±0.01Da)
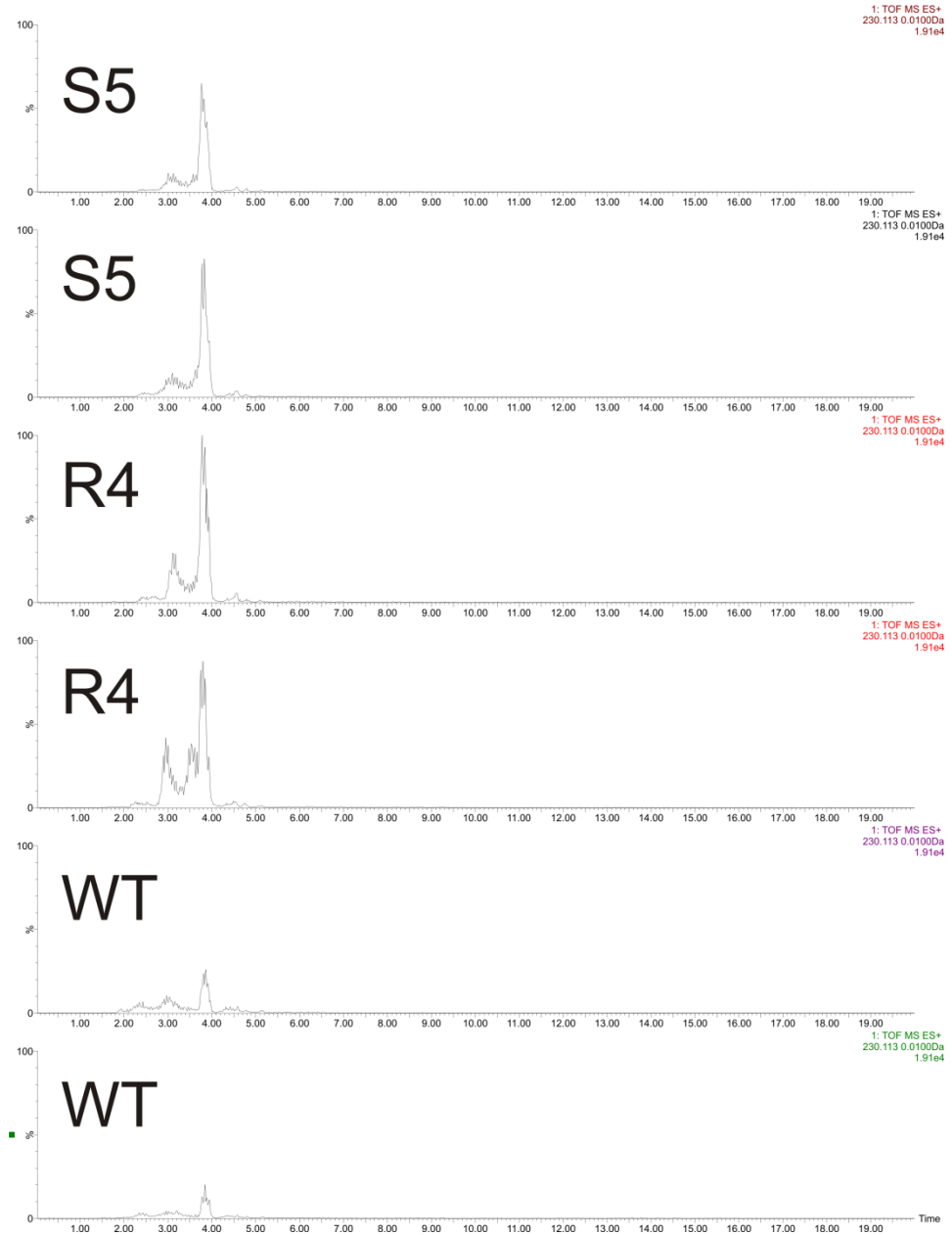
Figure A3.90. Extracted ion chromatograms for feature 18 w/ ±0.01Da tolerance.

Feature 19 EIC (±0.01Da)
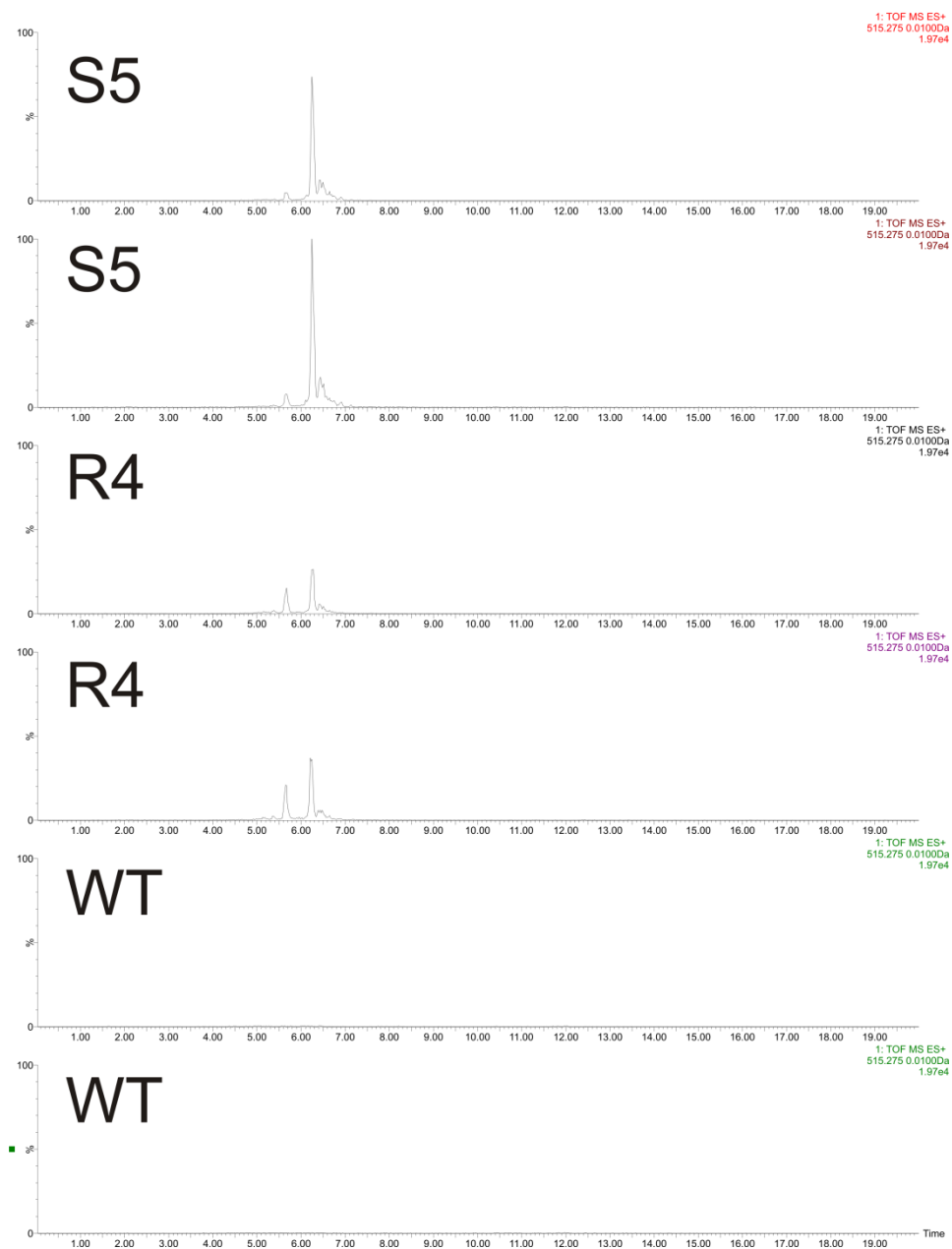
Figure A3.91. Extracted ion chromatograms for feature 19 w/ ±0.01Da tolerance.
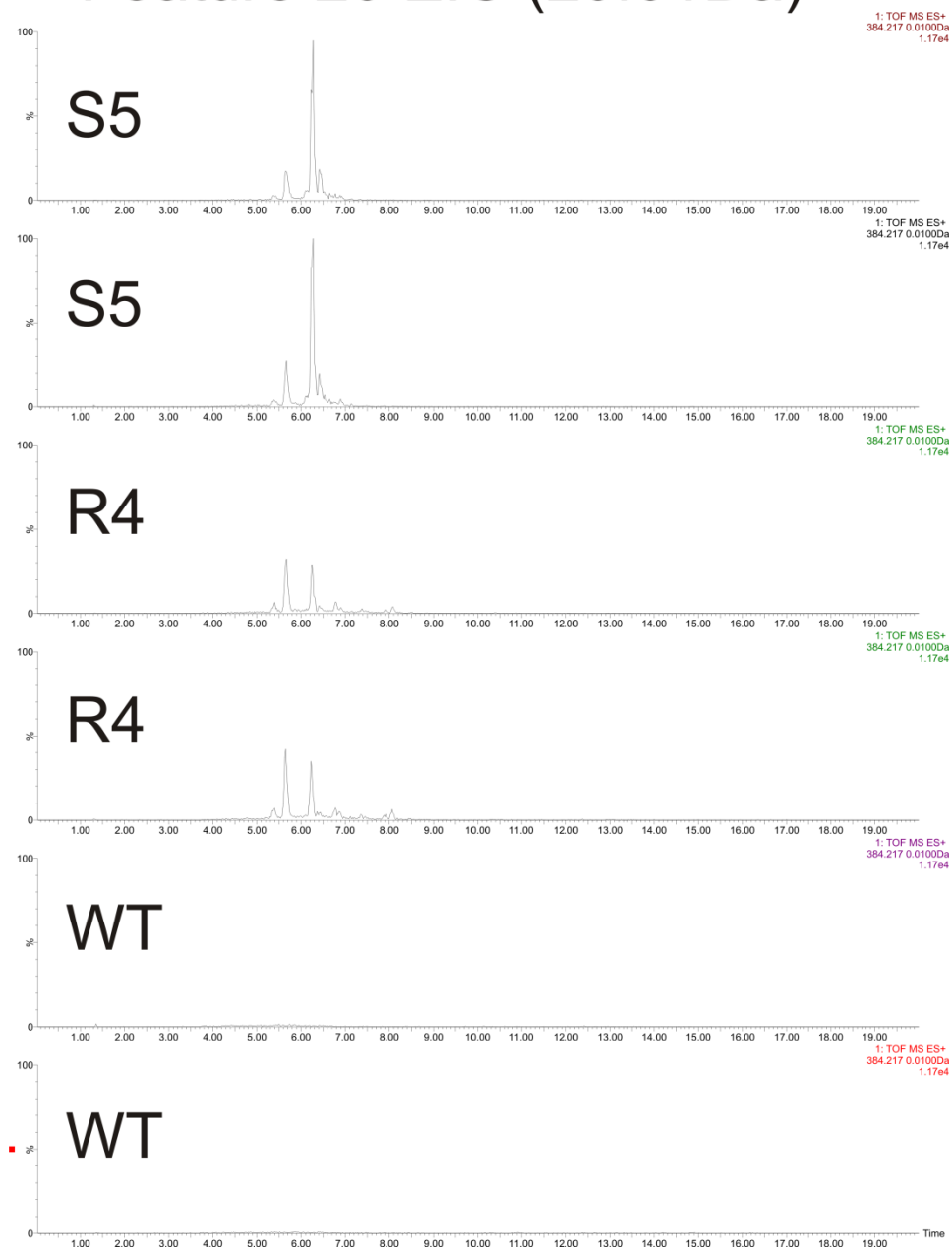
Figure A3.92. Extracted ion chromatograms for feature 20 w/ ±0.01Da tolerance.

Feature 21 EIC (±0.01Da)
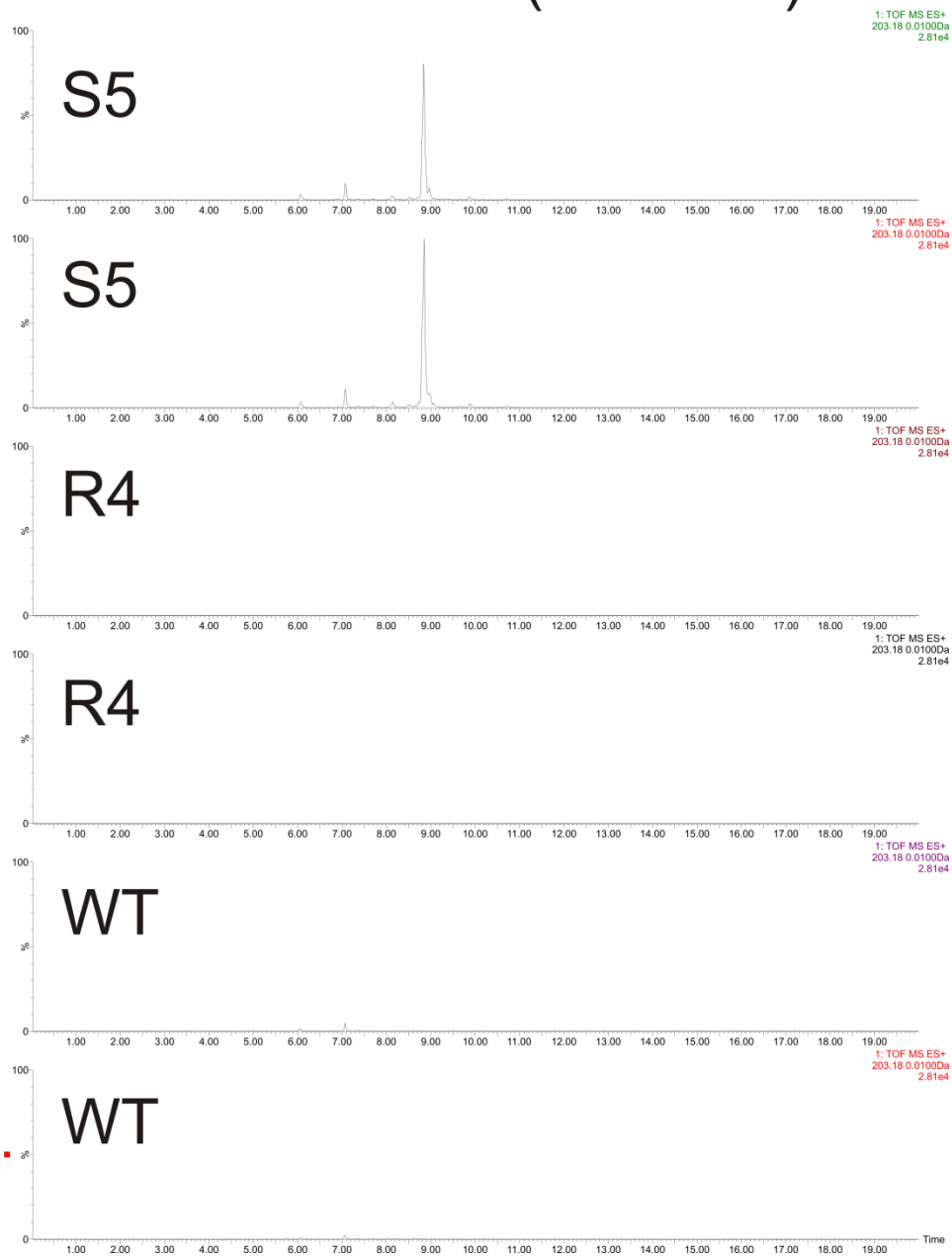
Figure A3.93. Extracted ion chromatograms for feature 21 w/ ±0.01Da tolerance.
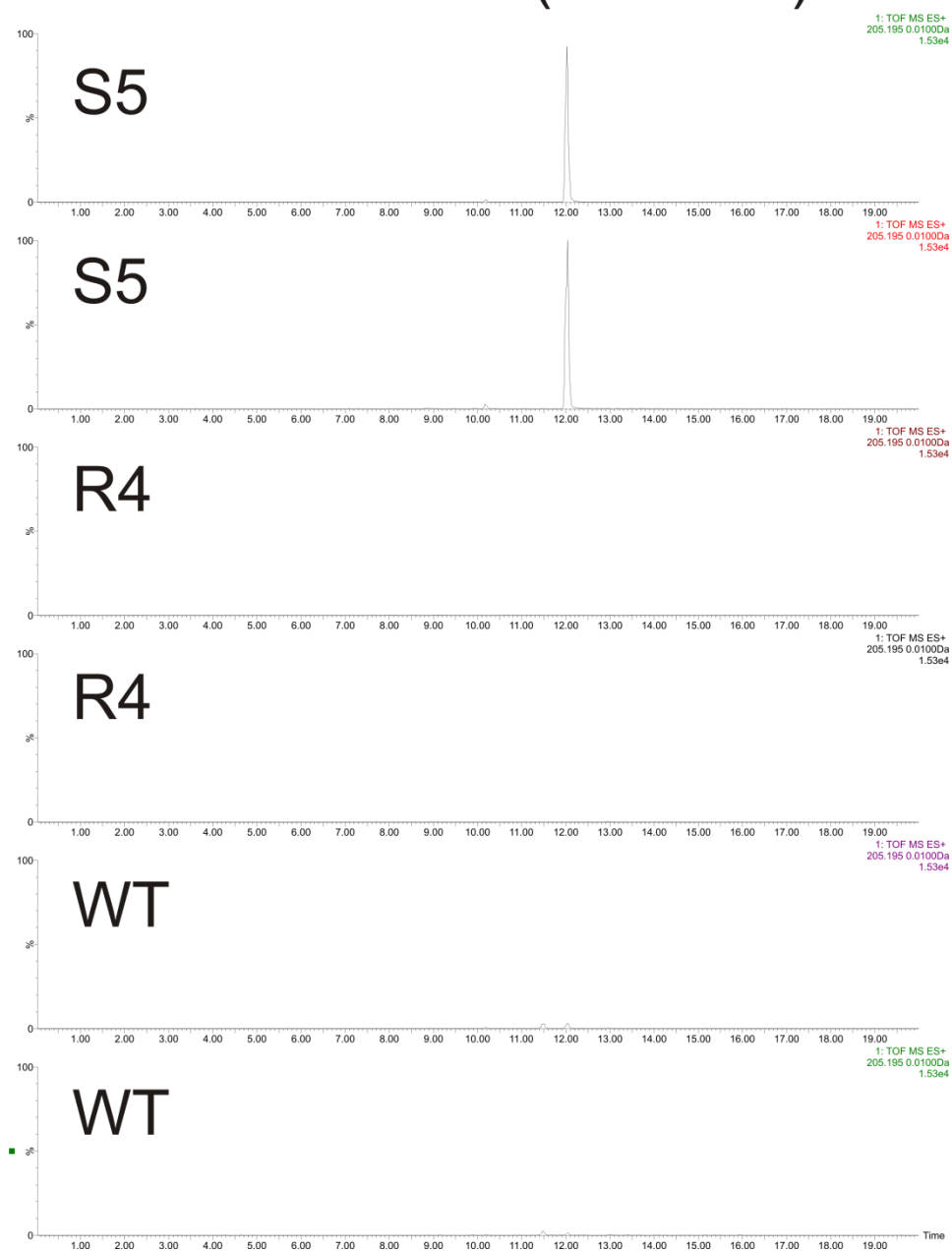
Figure A3.94. Extracted ion chromatograms for feature 22 w/ ±0.01Da tolerance.

Feature 23 EIC (±0.01Da)
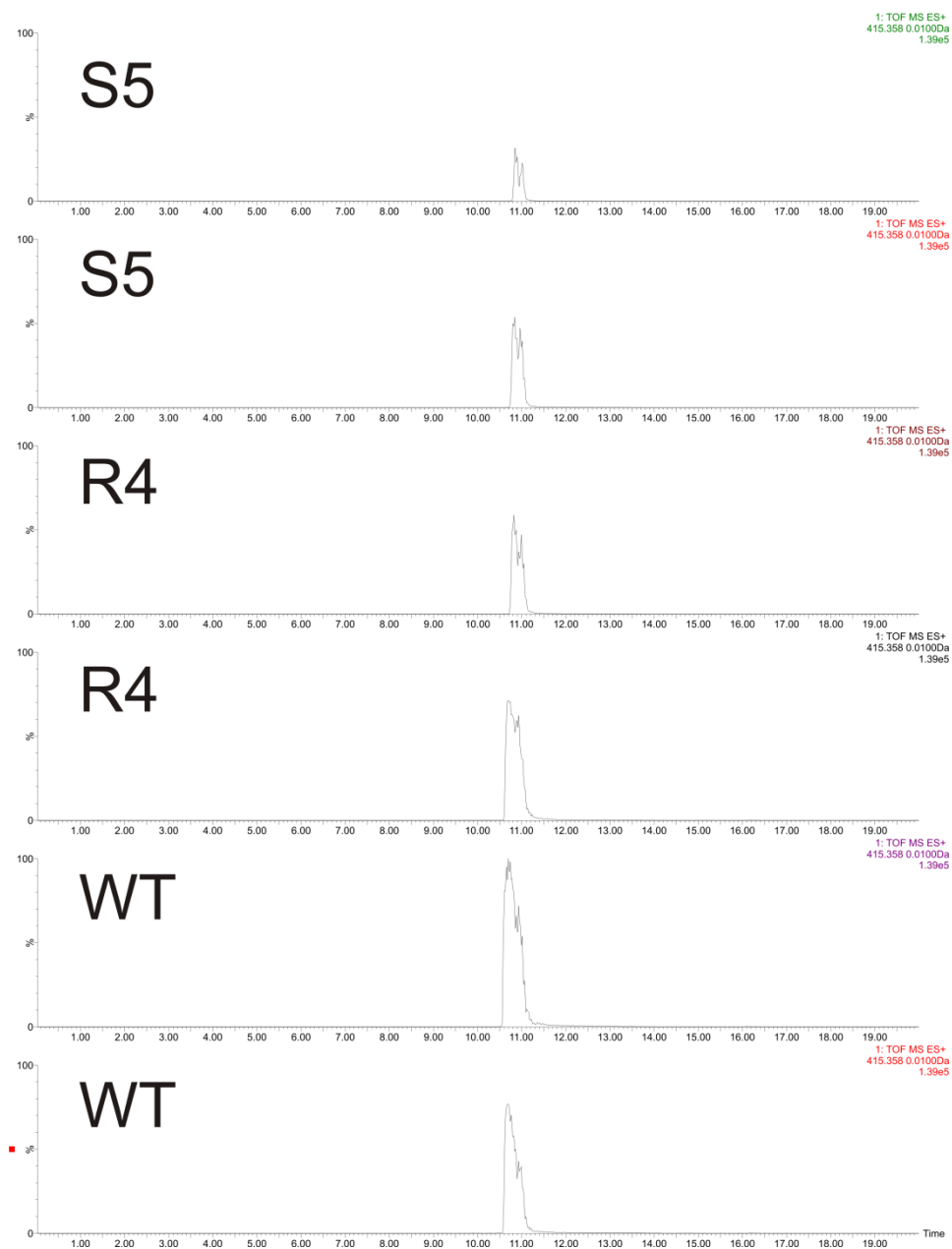
Figure A3.95. Extracted ion chromatograms for feature 23 w/ ±0.01Da tolerance.

Feature 24 EIC (±0.01Da)
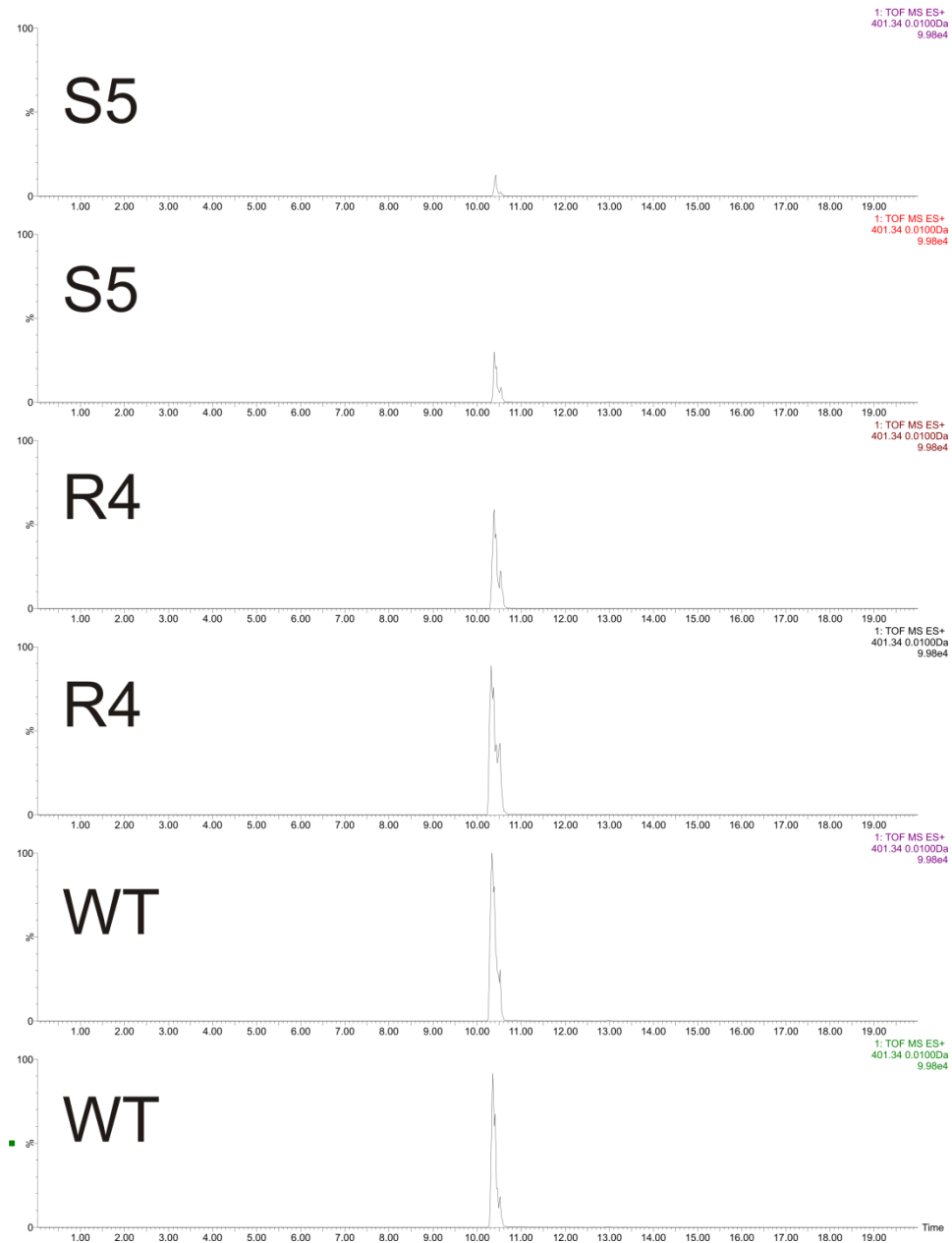
Figure A3.96. Extracted ion chromatograms for feature 24 w/ ±0.01Da tolerance.

Feature 25 EIC (±0.01Da)
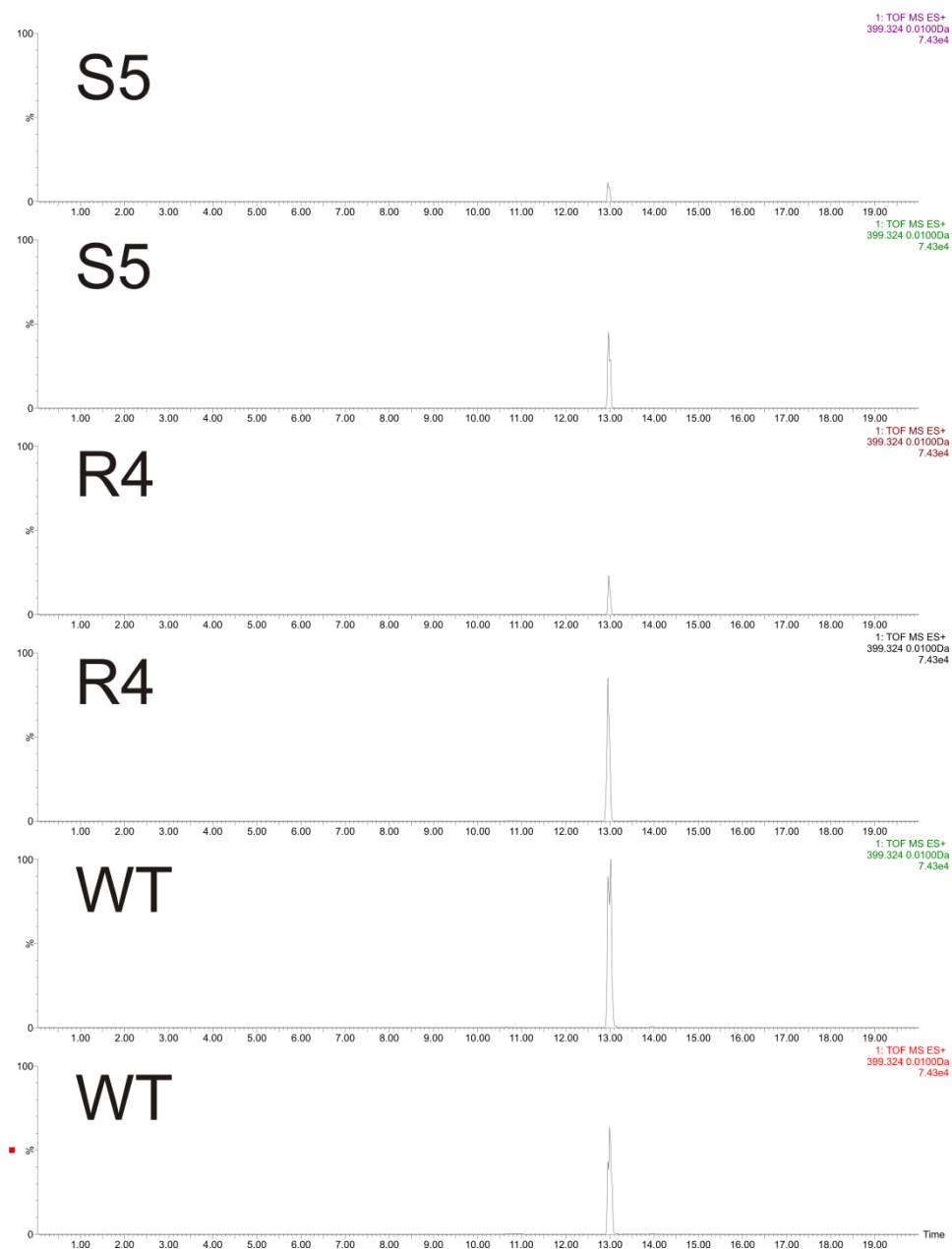
Figure A3.97. Extracted ion chromatograms for feature 25 w/ ±0.01Da tolerance.

Feature 26 EIC (±0.01Da)
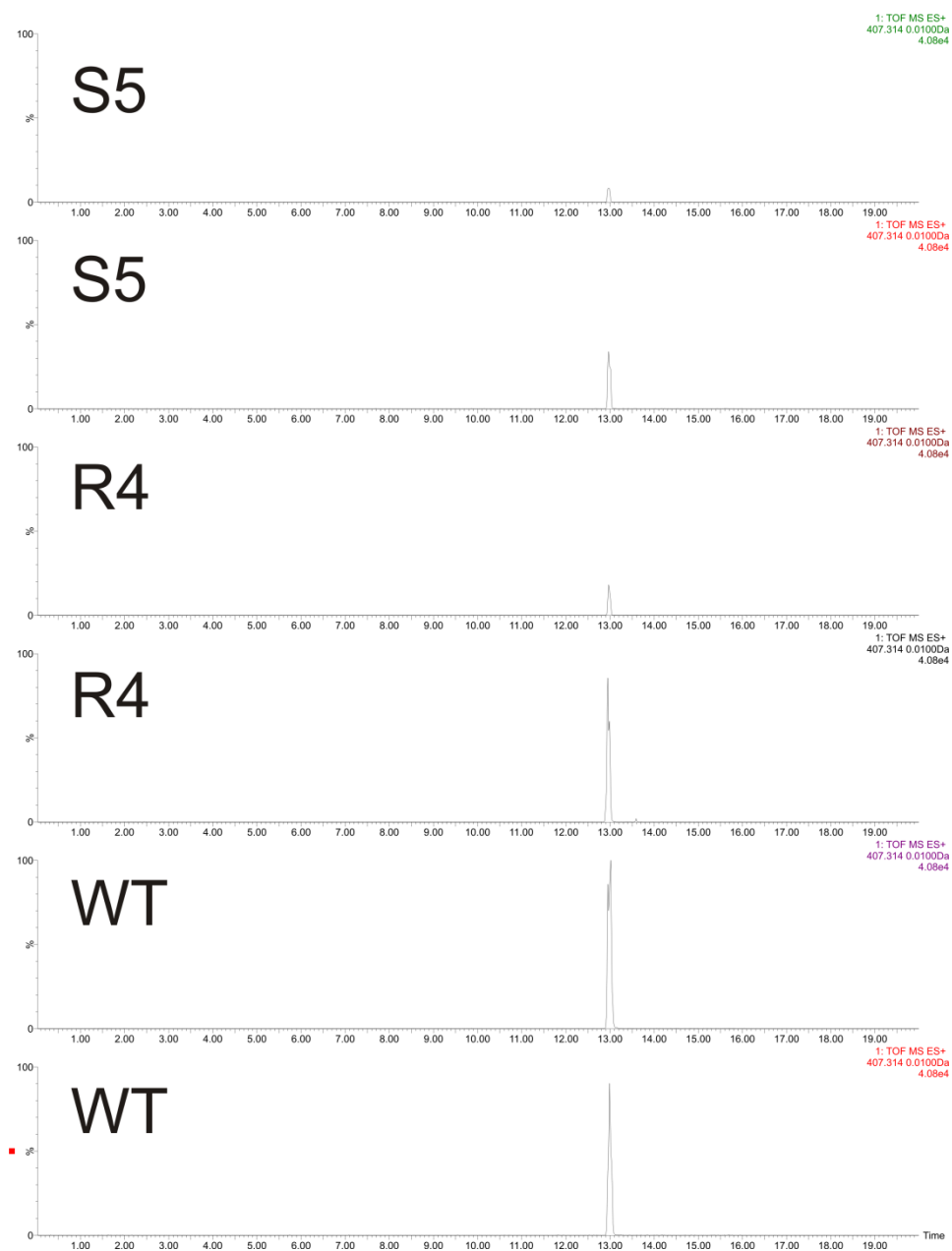
Figure A3.98. Extracted ion chromatograms for feature 26 w/ ±0.01Da tolerance.

Feature 27 EIC (±0.01Da)
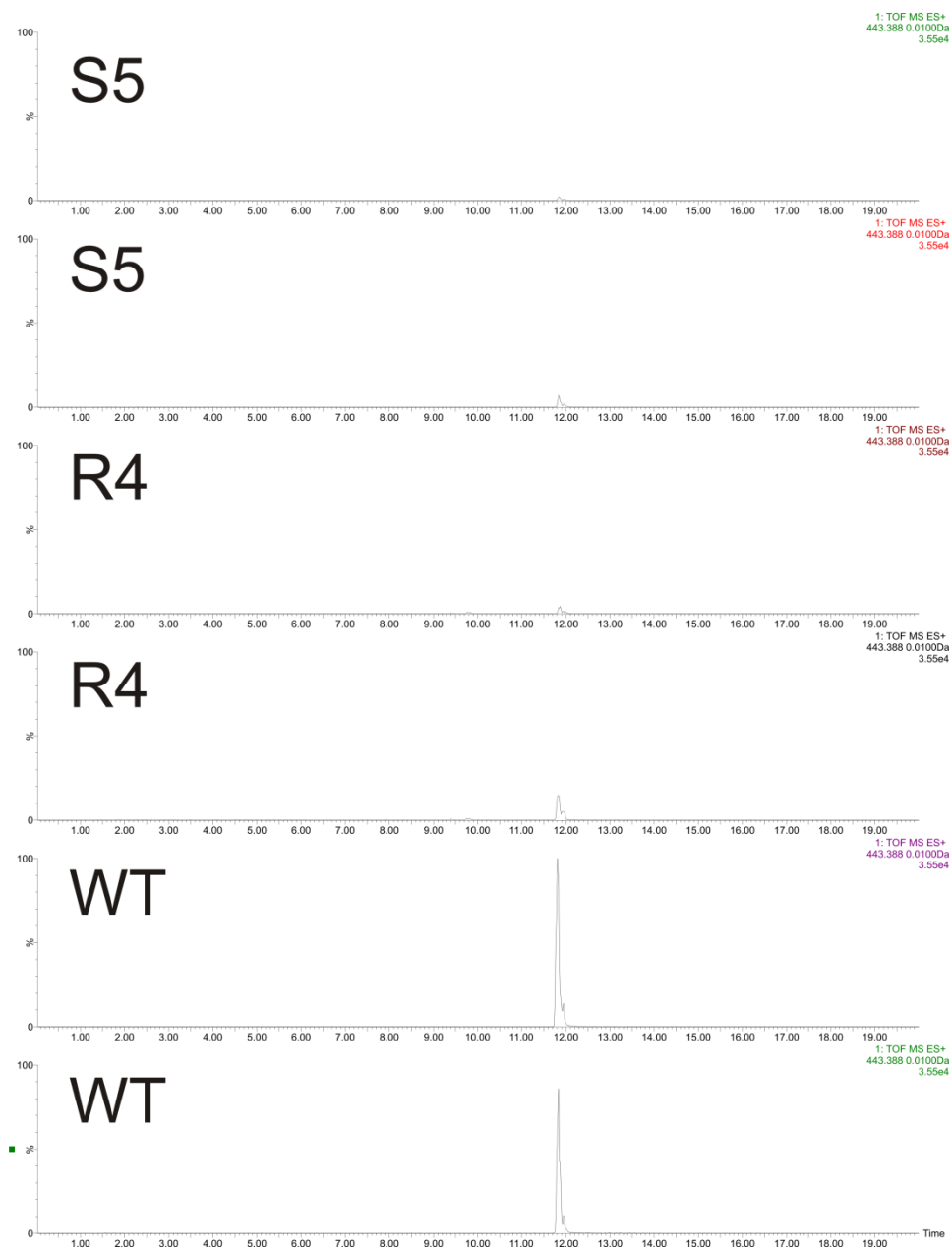
Figure A3.99. Extracted ion chromatograms for feature 27 w/ ±0.01Da tolerance.

Table A3.7. Normalized heat map of features described as unique in **Figure A3.4** when comparing *Bacillus subtilus* and *Micrococcus luteus* to *Escherichia coli* extracts using OPLS-DA and extracting features from the generated S-plot with correlation coefficients ≥0.9. Features are normalized to maximum intensity for that feature.

Feature ID (RT_*m/z*)	B sub	B sub	B sub	E coli	E coli	E coli	M lut	M lut	M lut
1.59_136.0628	0.00	0.04	0.07	0.36	1.00	0.87	0.00	0.06	0.03
1.18_203.0538	0.00	0.22	0.00	1.00	0.71	0.75	0.00	0.01	0.00
8.87_225.1991	0.00	0.00	0.00	0.86	1.00	0.78	0.00	0.00	0.00
8.87_226.1249	0.00	0.00	0.00	1.00	0.95	0.88	0.00	0.00	0.00
6.33_243.0892	0.00	0.16	0.13	0.87	0.78	1.00	0.00	0.00	0.00
3.58_246.1339	0.00	0.00	0.02	0.68	0.79	1.00	0.00	0.02	0.00
1.23_258.1102	0.00	0.00	0.00	0.80	1.00	0.76	0.00	0.01	0.01
3.47_276.1486	0.00	0.00	0.00	0.95	1.00	0.64	0.00	0.00	0.00
1.16_280.0940	0.00	0.00	0.00	0.61	1.00	0.88	0.00	0.00	0.00
7.38_364.1685	0.00	0.00	0.00	1.00	0.79	0.52	0.00	0.01	0.00
8.87_392.1643	0.00	0.00	0.00	0.93	1.00	0.66	0.00	0.00	0.00
2.45_424.1838	0.00	0.00	0.00	0.74	1.00	0.64	0.00	0.00	0.00
3.59_438.1989	0.00	0.00	0.00	1.00	0.66	0.87	0.00	0.00	0.00
10.27_452.2766	0.00	0.00	0.00	0.50	0.81	1.00	0.00	0.00	0.00
2.41_442.1934	0.00	0.00	0.00	1.00	0.50	0.72	0.00	0.00	0.00
3.58_456.2096	0.00	0.00	0.01	1.00	0.69	0.88	0.00	0.00	0.00
10.91_466.2961	0.00	0.00	0.00	0.61	0.62	1.00	0.00	0.00	0.00
3.40_488.1789	0.00	0.00	0.00	1.00	0.40	0.69	0.02	0.00	0.02
11.83_494.3263	0.00	0.00	0.00	0.52	0.62	1.00	0.00	0.00	0.00
5.04_542.3153	0.00	0.00	0.00	1.00	0.91	0.92	0.01	0.00	0.00
3.37_604.2482	0.00	0.00	0.00	0.91	0.58	1.00	0.00	0.00	0.01
3.63_600.2512	0.00	0.00	0.00	0.56	0.57	1.00	0.01	0.00	0.02
1.19_723.1992	0.00	0.00	0.00	0.57	0.98	1.00	0.00	0.00	0.00
1.22_707.2229	0.00	0.00	0.00	1.00	0.80	0.93	0.00	0.00	0.00
14.78_742.5100	0.00	0.00	0.01	0.90	0.60	1.00	0.00	0.08	0.00
11.13_454.2957	0.00	0.00	0.00	0.56	0.91	1.00	0.00	0.00	0.00
10.68_466.2947	0.00	0.00	0.00	0.55	0.56	1.00	0.00	0.00	0.00
1.33_428.1800	0.00	0.01	0.00	0.93	0.82	1.00	0.00	0.00	0.00
7.37_226.1255	0.00	0.00	0.00	0.92	0.94	1.00	0.00	0.00	0.00
1.21_365.1089	0.00	0.00	0.00	0.77	1.00	0.89	0.00	0.00	0.00
4.33_260.1502	0.00	0.00	0.00	1.00	0.60	0.86	0.01	0.14	0.06
1.20_381.0798	0.01	0.00	0.00	1.00	0.83	0.94	0.00	0.00	0.00
1.13_380.0978	0.01	0.01	0.02	0.78	0.92	1.00	0.00	0.00	0.01
4.15_260.1506	0.02	0.00	0.00	1.00	0.51	0.99	0.00	0.01	0.00
3.50_230.1384	0.02	0.07	0.00	0.66	1.00	0.60	0.00	0.03	0.00
1.23_446.1908	0.03	0.00	0.00	0.99	0.85	1.00	0.00	0.00	0.00
4.29_447.2276	0.05	0.00	0.00	1.00	0.40	0.96	0.00	0.00	0.00
3.95_328.1408	0.06	0.09	0.00	0.83	1.00	0.63	0.01	0.07	0.08
5.25_164.0700	0.11	0.18	0.08	0.88	1.00	0.71	0.45	0.14	0.22
5.57_277.1177	0.16	0.12	0.11	0.86	0.98	1.00	0.07	0.01	0.12
6.91_233.0782	0.30	0.27	0.35	1.00	0.98	0.93	0.37	0.45	0.39
1.32_247.1405	0.38	0.77	1.00	0.04	0.00	0.00	0.67	0.77	0.84
5.24_374.2291	0.49	0.89	0.96	0.00	0.00	0.00	1.00	0.72	0.91
6.71_514.3211	0.52	0.77	0.64	0.00	0.00	0.00	1.00	0.65	0.80
5.31_489.2739	0.55	0.60	0.59	0.00	0.00	0.00	0.85	0.89	1.00
5.97_441.3089	0.56	0.52	0.53	0.05	0.05	0.02	1.00	0.81	0.86
6.93_527.2267	0.58	0.76	1.00	0.00	0.00	0.00	0.83	0.78	0.48
3.65_248.1052	0.62	0.76	0.66	0.00	0.00	0.08	0.89	1.00	0.51
7.20_340.2507	0.63	0.73	0.89	0.00	0.00	0.00	0.95	0.97	1.00
8.43_384.2770	0.64	0.47	0.60	0.00	0.00	0.00	0.88	1.00	0.71
8.74_340.2520	0.66	0.52	0.71	0.00	0.00	0.00	0.86	0.76	1.00

8.15_368.2806	0.66	0.47	0.57	0.00	0.00	0.00	0.87	1.00	0.91
5.48_287.1006	0.69	0.72	1.00	0.00	0.00	0.05	0.77	0.69	0.61
7.14_120.0804	0.69	0.84	0.88	0.01	0.01	0.02	1.00	0.88	0.81
8.16_386.2928	0.70	0.70	0.69	0.00	0.00	0.00	0.69	1.00	0.90
1.26_246.1797	0.70	0.99	0.82	0.02	0.00	0.00	0.89	0.99	1.00
7.49_358.2600	0.71	0.66	0.72	0.00	0.00	0.00	0.90	0.96	1.00
6.73_224.1250	0.71	0.83	0.75	0.02	0.00	0.00	1.00	0.67	0.97
5.17_188.0713	0.72	1.00	0.93	0.00	0.04	0.00	0.77	0.85	0.69
6.72_406.2313	0.72	0.80	0.81	0.00	0.00	0.00	0.98	0.81	1.00
1.24_369.1533	0.77	1.00	0.86	0.00	0.00	0.00	0.66	0.71	0.87
7.59_517.3020	0.77	0.77	0.99	0.00	0.00	0.01	1.00	0.91	0.92
7.90_328.2507	0.77	0.54	0.61	0.00	0.00	0.00	0.98	1.00	0.75
1.05_341.1557	0.80	0.90	0.46	0.00	0.00	0.00	0.86	0.75	1.00
6.97_326.2351	0.81	0.64	0.75	0.00	0.01	0.00	0.87	1.00	1.00
1.05_323.1483	0.81	0.81	0.88	0.00	0.00	0.00	0.80	1.00	0.79
1.20_257.1491	0.81	0.44	0.64	0.05	0.04	0.00	0.96	1.00	0.74
7.13_236.1285	0.81	0.78	0.87	0.01	0.00	0.00	0.80	1.00	0.95
7.14_396.2770	0.81	0.69	0.85	0.00	0.00	0.00	0.98	1.00	0.79
7.20_358.2601	0.87	0.65	0.72	0.00	0.00	0.00	0.85	0.92	1.00
7.59_263.1407	0.87	0.64	0.88	0.00	0.00	0.00	1.00	0.89	0.73
6.07_159.0926	0.87	0.56	0.85	0.00	0.01	0.00	0.72	1.00	0.56
6.45_341.1501	0.90	0.63	0.86	0.02	0.02	0.03	0.80	0.99	1.00
6.94_227.1782	0.90	0.84	1.00	0.00	0.00	0.03	0.75	0.72	0.69
6.07_299.1768	0.90	0.83	1.00	0.00	0.00	0.00	0.81	0.62	0.67
6.96_300.1824	0.91	0.63	1.00	0.00	0.00	0.00	0.86	0.89	0.70
4.93_265.1574	0.92	0.66	0.89	0.01	0.00	0.00	0.86	0.80	1.00
5.09_245.1881	0.96	0.77	0.82	0.00	0.00	0.00	0.95	1.00	0.99
6.96_382.2573	0.96	0.78	0.73	0.00	0.00	0.00	0.76	0.96	1.00
6.08_201.1028	0.97	0.97	1.00	0.00	0.00	0.02	1.00	0.76	0.94
6.96_282.1702	0.99	0.70	0.94	0.00	0.00	0.00	0.86	0.99	1.00
7.14_258.1102	1.00	0.62	0.88	0.00	0.00	0.00	0.94	1.00	0.97
6.08_188.0708	1.00	0.80	0.58	0.01	0.02	0.00	0.54	1.00	0.99
3.90_186.0783	1.00	0.70	0.58	0.00	0.02	0.00	0.61	0.92	0.84
3.98_215.1417	1.00	0.60	0.80	0.00	0.00	0.00	0.57	0.88	0.62
5.42_245.1308	1.00	0.74	0.80	0.00	0.00	0.03	0.68	0.68	0.65
4.69_302.2081	1.00	0.95	0.90	0.02	0.00	0.00	0.93	0.87	0.75
6.71_327.0330	1.00	0.72	0.98	0.00	0.01	0.03	0.82	0.87	0.64
6.68_356.1087	1.00	0.86	0.92	0.00	0.00	0.00	0.95	0.92	0.76
6.76_393.1819	1.00	0.67	0.89	0.01	0.01	0.02	0.66	0.73	0.77
5.66_522.2907	1.00	0.62	0.92	0.00	0.00	0.00	0.93	0.98	0.92
5.40_613.3562	1.00	0.58	0.73	0.00	0.00	0.01	0.86	0.81	0.94
6.96_913.9555	1.00	0.81	0.92	0.00	0.00	0.00	0.55	0.91	0.98

Table A3.8. Normalized heat map of features described as unique in **Figure A3.4** when comparing *Bacillus subtilus* and *Escherichia coli* to *Micrococcus luteus* extracts using OPLS-DA and extracting features from the generated S-plot with correlation coefficients ≥0.9. Features are normalized to maximum intensity for that feature.

Feature ID (RT_*m/z*)	B sub	B sub	B sub	E coli	E coli	E coli	M lut	M lut	M lut
3.85_239.1416	0.00	0.09	0.00	0.00	0.00	0.01	1.00	0.59	0.88
5.44_316.2237	0.00	0.20	0.00	0.00	0.00	0.03	0.81	1.00	0.63
1.31_324.1312	0.00	0.10	0.21	0.00	0.00	0.00	0.98	1.00	0.54
5.57_322.1904	0.00	0.19	0.21	0.00	0.00	0.00	0.62	1.00	0.88
5.04_334.1767	0.00	0.00	0.00	0.00	0.00	0.50	1.00	0.80	0.77
5.69_349.7333	0.00	0.08	0.09	0.00	0.00	0.00	1.00	0.78	0.72
5.31_368.1632	0.00	0.00	0.00	0.30	0.00	0.00	0.73	1.00	0.57
9.55_400.1299	0.00	0.00	0.00	0.00	0.00	0.00	0.61	1.00	0.45
5.16_408.2509	0.00	0.00	0.00	0.13	0.00	0.03	0.80	1.00	0.86
5.02_407.2347	0.00	0.00	0.05	0.00	0.00	0.00	0.69	1.00	0.78
6.75_431.2681	0.00	0.00	0.31	0.00	0.00	0.00	0.90	0.96	1.00
5.75_749.3707	0.00	0.24	0.01	0.00	0.00	0.00	1.00	0.97	0.84
5.88_473.2311	0.01	0.03	0.03	0.00	0.00	0.00	0.96	1.00	0.75
5.45_764.4128	0.03	0.00	0.02	0.00	0.00	0.00	0.92	1.00	0.87
6.02_378.2402	0.04	0.36	0.25	0.00	0.00	0.02	1.00	0.73	0.70
5.58_291.6759	0.06	0.30	0.18	0.00	0.00	0.00	1.00	0.83	0.85
5.64_507.2827	0.06	0.00	0.16	0.00	0.00	0.01	0.84	0.81	1.00
10.32_317.2674	0.07	0.03	0.08	0.00	0.00	0.00	1.00	0.97	0.80
5.06_471.2746	0.10	0.04	0.04	0.00	0.00	0.00	1.00	0.47	0.82
5.64_360.2149	0.10	0.20	0.21	0.00	0.00	0.14	0.95	1.00	0.87
10.32_299.2598	0.12	0.05	0.10	0.00	0.00	0.00	1.00	0.63	0.66
5.18_423.2211	0.14	0.16	0.26	0.00	0.09	0.00	1.00	0.60	0.72
4.50_493.2325	0.15	0.28	0.28	0.00	0.13	0.00	1.00	0.82	0.86
5.58_582.3392	0.17	0.00	0.23	0.01	0.00	0.01	1.00	0.69	0.69
6.17_557.3688	0.18	0.10	0.19	0.00	0.00	0.01	1.00	0.80	0.96
6.11_734.3731	0.22	0.15	0.07	0.00	0.00	0.00	0.49	1.00	0.79
4.74_284.1566	0.23	0.38	0.12	0.14	0.19	0.04	0.69	1.00	0.65
5.88_378.2396	0.23	0.00	0.00	0.06	0.00	0.00	0.59	1.00	0.81
6.80_857.4155	0.28	0.00	0.26	0.00	0.00	0.00	0.98	0.86	1.00
8.64_342.2650	0.35	0.00	0.03	0.00	0.00	0.00	0.78	1.00	0.81
6.15_608.3295	0.39	0.35	0.18	0.00	0.00	0.01	1.00	0.87	0.98
6.00_288.0498	0.42	0.17	0.15	0.00	0.00	0.00	0.98	1.00	0.61
6.26_475.2939	0.42	0.09	0.37	0.08	0.00	0.00	0.90	0.90	1.00
5.50_374.2277	0.45	0.36	0.17	0.00	0.00	0.12	1.00	0.75	0.87

Table A3.9. Normalized heat map of features described as unique in **Figure A3.4** when comparing *Bacillus subtilus* to *Micrococcus luteus* and *Escherichia coli* extracts using OPLS-DA and extracting features from the generated S-plot with correlation coefficients ≥0.9. Features are normalized to maximum intensity for that feature.

Feature ID (RT_*m/z*)	B sub	B sub	B sub	E coli	E coli	E coli	M lut	M lut	M lut
4.42_357.1859	0.40	0.32	0.26	1.00	0.67	0.94	0.73	0.84	0.75
2.31_289.1405	0.62	1.00	0.56	0.02	0.00	0.00	0.33	0.12	0.00
3.38_271.1408	0.65	1.00	0.51	0.00	0.00	0.00	0.00	0.00	0.29
4.62_190.0525	0.67	1.00	0.69	0.00	0.00	0.08	0.03	0.24	0.17
5.71_441.7064	0.71	0.62	1.00	0.32	0.00	0.00	0.00	0.18	0.00
2.28_259.1292	0.74	1.00	0.59	0.00	0.00	0.05	0.22	0.00	0.08
4.49_201.1581	0.79	1.00	0.74	0.00	0.00	0.00	0.08	0.14	0.04
5.68_512.3435	0.88	1.00	0.98	0.00	0.00	0.01	0.02	0.15	0.19
8.21_272.1420	0.94	0.77	1.00	0.00	0.00	0.00	0.06	0.01	0.02
1.79_124.0404	1.00	0.85	0.84	0.07	0.10	0.00	0.28	0.50	0.18
8.29_223.1446	1.00	0.82	0.79	0.00	0.00	0.00	0.03	0.00	0.02
1.32_221.1124	1.00	0.69	0.94	0.02	0.00	0.00	0.46	0.00	0.08
6.22_246.1732	1.00	0.80	0.72	0.00	0.00	0.00	0.35	0.31	0.31
4.78_374.2088	1.00	0.88	0.91	0.00	0.00	0.00	0.42	0.43	0.00
4.69_431.2509	1.00	0.98	0.57	0.00	0.03	0.00	0.31	0.35	0.10

Table A3.10. Normalized heat map of features described as unique in **Figure 3.2(B)** and **(C)** when comparing wild type *Nocardiopsis sp. FU40 ΔApoS8* to the R1 rifampicin resistant mutant extract using OPLS-DA and extracting features from the generated S-plot with correlation coefficients ≥0.9. Features are normalized to maximum intensity for that feature.

Feature ID (RT_*m/z*)	WT	WT	R1	R1
12.03_135.1163	0.00	0.11	0.93	1.00
12.03_123.1165	0.00	0.00	1.00	0.99
4.87_118.0679	0.00	0.20	0.64	1.00
1.50_103.5345	0.00	0.00	1.00	0.69
13.61_149.0907	0.00	0.00	1.00	0.97
1.50_165.0624	0.00	0.00	1.00	0.78
6.56_162.0938	0.00	0.00	0.73	1.00
4.31_160.1140	0.00	0.00	0.63	1.00
5.78_170.1204	0.00	0.00	0.80	1.00
7.08_169.0882	0.00	0.06	1.00	0.83
2.44_166.0747	0.00	0.20	0.81	1.00
6.60_180.1017	0.00	0.03	0.76	1.00
5.02_180.1014	0.00	0.00	0.88	1.00
10.70_179.1435	0.00	0.00	0.97	1.00
4.95_177.1399	0.00	0.29	0.67	1.00
4.39_192.1130	0.00	0.21	0.90	1.00
9.12_191.0134	0.00	0.00	0.76	1.00
4.02_198.1143	0.00	0.00	0.71	1.00
8.84_203.1804	0.00	0.00	0.75	1.00
6.22_203.0786	0.00	0.10	1.00	1.00
9.80_203.0277	0.00	0.00	0.70	1.00
7.49_207.0994	0.00	0.07	0.71	1.00
1.30_205.9283	0.00	0.00	1.00	1.00
4.84_205.1323	0.00	0.00	0.68	1.00
9.81_205.1237	0.00	0.00	0.92	1.00
10.22_205.1232	0.00	0.00	0.92	1.00
1.32_211.8786	0.00	0.00	1.00	0.60
9.81_210.0363	0.00	0.00	0.77	1.00
5.35_210.0350	0.00	0.00	0.64	1.00
10.24_222.1533	0.00	0.00	1.00	0.96
9.81_222.1504	0.00	0.00	0.87	1.00
8.84_221.1903	0.00	0.00	0.73	1.00
7.99_225.1125	0.00	0.07	0.95	1.00
5.48_229.0656	0.00	0.00	0.73	1.00
4.61_230.0715	0.00	0.38	1.00	0.94
10.62_236.1643	0.00	0.00	1.00	0.83
5.11_236.1306	0.00	0.25	1.00	0.86
8.54_235.1344	0.00	0.00	0.80	1.00
11.28_233.1548	0.00	0.00	0.95	1.00
9.80_241.0261	0.00	0.00	0.70	1.00
11.75_239.1663	0.00	0.01	1.00	0.90
10.69_238.1826	0.00	0.00	1.00	1.00
5.81_248.1281	0.00	0.32	0.77	1.00
11.16_252.0381	0.00	0.00	1.00	0.60
13.78_251.2405	0.00	0.00	0.48	1.00
11.26_250.1814	0.00	0.00	1.00	0.91
4.56_252.0394	0.00	0.18	0.72	1.00
8.66_252.0394	0.00	0.00	0.47	1.00
7.48_252.0388	0.00	0.00	1.00	0.65
6.82_252.0384	0.00	0.00	1.00	0.57
3.87_257.1146	0.00	0.29	0.97	1.00
12.02_263.1978	0.00	0.09	0.94	1.00
1.78_262.1278	0.00	0.00	1.00	0.73
5.86_262.1048	0.00	0.32	0.66	1.00
10.71_261.1779	0.00	0.01	0.77	1.00
10.68_260.1641	0.00	0.00	0.98	1.00

5.43_268.0192	0.00	0.12	0.61	1.00
5.18_266.1406	0.00	0.33	0.76	1.00
5.27_264.2082	0.00	0.00	0.79	1.00
5.84_281.1328	0.00	0.00	0.63	1.00
9.12_279.1585	0.00	0.00	1.00	0.84
7.18_278.2110	0.00	0.00	0.60	1.00
13.60_278.2028	0.00	0.00	0.93	1.00
7.50_283.1523	0.00	0.04	0.65	1.00
1.73_282.0649	0.00	0.03	1.00	0.92
7.72_281.1420	0.00	0.00	1.00	0.91
7.82_294.2085	0.00	0.00	0.75	1.00
7.15_293.2251	0.00	0.00	0.71	1.00
3.76_299.1387	0.00	0.05	0.68	1.00
4.74_298.0969	0.00	0.08	0.90	1.00
9.60_297.1694	0.00	0.01	0.46	1.00
7.19_296.2224	0.00	0.00	0.82	1.00
3.78_300.1386	0.00	0.33	0.74	1.00
14.29_307.2281	0.00	0.00	1.00	0.82
8.43_314.1381	0.00	0.29	1.00	0.89
7.24_312.2197	0.00	0.00	0.98	1.00
5.82_322.1007	0.00	0.00	0.78	1.00
1.74_322.0446	0.00	0.03	1.00	0.72
14.63_321.2420	0.00	0.00	1.00	0.89
9.13_319.1539	0.00	0.00	1.00	0.68
6.08_324.1828	0.00	0.42	0.79	1.00
10.73_340.1475	0.00	0.19	1.00	1.00
14.63_339.2533	0.00	0.00	1.00	0.90
14.31_347.2205	0.00	0.00	1.00	0.82
5.26_354.0787	0.00	0.16	0.69	1.00
8.24_352.2057	0.00	0.00	1.00	0.84
6.95_350.2147	0.00	0.05	1.00	0.93
8.53_359.2035	0.00	0.25	0.80	1.00
9.80_367.0822	0.00	0.00	0.60	1.00
6.22_366.2068	0.00	0.36	0.76	1.00
14.32_379.2817	0.00	0.00	1.00	0.61
9.80_387.0731	0.00	0.00	0.72	1.00
6.24_384.2171	0.00	0.00	0.75	1.00
13.61_399.3201	0.00	0.00	1.00	0.57
1.49_394.1142	0.00	0.00	1.00	0.58
14.57_393.2988	0.00	0.00	0.76	1.00
13.61_407.3140	0.00	0.00	1.00	0.69
3.75_414.2692	0.00	0.00	0.64	1.00
9.08_429.0845	0.00	0.00	1.00	0.92
14.04_428.3345	0.00	0.07	0.79	1.00
14.04_420.3477	0.00	0.05	0.78	1.00
6.99_443.3240	0.00	0.12	0.66	1.00
9.73_443.1014	0.00	0.00	0.83	1.00
10.02_459.0960	0.00	0.00	0.57	1.00
11.52_456.3791	0.00	0.00	1.00	0.88
9.81_454.0847	0.00	0.00	0.86	1.00
9.78_481.0499	0.00	0.00	1.00	0.98
6.98_499.2793	0.00	0.00	1.00	0.74
4.37_494.2617	0.00	0.00	0.82	1.00
9.09_512.3013	0.00	0.00	0.91	1.00
13.62_510.2556	0.00	0.03	1.00	0.94
12.00_515.2832	0.00	0.00	1.00	1.00
1.76_515.1445	0.00	0.00	0.84	1.00
1.49_527.1567	0.00	0.00	1.00	0.64
10.06_526.3139	0.00	0.00	0.84	1.00
7.20_544.2918	0.00	0.00	1.00	0.66
12.03_565.3746	0.00	0.04	1.00	0.99
1.72_551.1035	0.00	0.00	1.00	0.66
5.52_601.2501	0.00	0.00	0.53	1.00
1.76_588.1814	0.00	0.00	0.54	1.00
9.79_576.6021	0.00	0.00	0.60	1.00
7.01_1221.4414	0.00	0.00	0.67	1.00
7.00_1216.1209	0.00	0.43	0.97	1.00
14.64_361.2361	0.00	0.00	1.00	0.86
7.48_177.0877	0.01	0.00	0.55	1.00
9.79_218.0234	0.01	0.08	0.72	1.00

1.82_228.1004	0.01	0.00	1.00	0.70
1.29_203.9309	0.01	0.00	1.00	0.96
1.75_507.1572	0.02	0.00	0.70	1.00
9.66_279.1583	0.02	0.00	0.72	1.00
9.78_465.0808	0.02	0.06	0.88	1.00
9.81_269.0437	0.03	0.00	0.73	1.00
6.95_368.2220	0.03	0.05	0.97	1.00
13.79_531.4249	0.03	0.10	0.80	1.00
16.15_710.1773	0.03	0.01	1.00	0.90
12.02_205.1953	0.04	0.00	0.94	1.00
5.43_377.1482	0.04	0.00	0.67	1.00
14.31_325.2414	0.04	0.03	1.00	0.81
9.41_281.1770	0.04	0.08	0.81	1.00
9.67_319.1539	0.04	0.06	1.00	0.93
6.24_515.2753	0.04	0.02	0.78	1.00
4.75_136.0625	0.05	0.00	0.68	1.00
13.79_365.2675	0.05	0.06	1.00	0.67
8.60_236.1631	0.05	0.11	0.69	1.00
1.74_150.0789	0.06	0.00	1.00	0.95
8.53_283.1523	0.06	0.13	0.72	1.00
9.14_239.1284	0.06	0.06	1.00	0.73
14.78_323.2583	0.07	0.13	1.00	0.83
1.73_338.0231	0.07	0.00	1.00	0.66
8.53_177.0880	0.07	0.07	0.66	1.00
3.86_150.0940	0.07	0.13	0.61	1.00
6.95_218.1203	0.07	0.15	0.69	1.00
8.53_207.1002	0.07	0.09	0.69	1.00
14.04_295.2283	0.08	0.15	1.00	0.86
1.70_260.1135	0.10	0.00	1.00	0.70
7.42_280.1237	0.11	0.31	0.64	1.00
11.43_466.2973	0.12	0.35	1.00	0.78
6.27_207.0660	0.12	0.22	0.74	1.00
7.89_192.1015	0.13	0.22	0.69	1.00
3.07_230.1126	0.13	0.31	1.00	0.81
6.41_165.0905	0.13	0.09	0.72	1.00
8.29_401.1993	0.14	0.00	0.73	1.00
4.87_329.1844	0.14	0.00	0.72	1.00
4.88_188.0708	0.15	0.26	0.68	1.00
14.41_309.2409	0.16	0.29	1.00	0.85
3.83_198.1623	0.17	0.12	0.62	1.00
3.85_276.1433	0.18	0.10	0.67	1.00
7.42_196.0651	0.18	0.09	0.69	1.00
4.30_310.1305	0.19	0.04	0.73	1.00
9.47_211.0868	0.19	0.33	0.69	1.00
5.27_685.1761	0.20	0.00	0.84	1.00
3.82_230.1126	0.21	0.13	0.61	1.00
13.84_397.2963	0.22	0.00	1.00	0.86
8.08_219.1411	0.22	0.32	0.75	1.00
6.78_176.0714	0.22	0.37	0.69	1.00
16.18_335.9929	0.28	0.00	0.83	1.00
13.50_409.7445	0.30	0.38	0.84	1.00
6.15_485.2027	0.37	0.39	0.67	1.00
12.62_416.2462	0.37	0.45	1.00	0.88
9.69_220.1127	0.40	0.47	0.98	1.00
16.15_481.1090	0.42	0.00	0.89	1.00
14.82_332.2940	0.43	0.28	1.00	0.85
4.29_244.1199	0.45	0.46	0.78	1.00
5.16_210.1137	0.45	0.44	0.70	1.00
12.40_251.2372	0.47	0.00	1.00	0.98
11.97_299.2600	0.49	0.61	1.00	0.91
10.60_346.3091	0.51	1.00	0.00	0.00
10.40_371.3275	0.52	1.00	0.00	0.00
10.70_288.2557	0.52	1.00	0.00	0.00
6.40_439.1986	0.52	0.52	0.90	1.00
9.48_225.1993	0.53	1.00	0.01	0.02
6.81_807.1918	0.54	1.00	0.00	0.00
4.26_669.2631	0.56	1.00	0.00	0.00
11.80_235.1712	0.56	1.00	0.00	0.00
4.09_573.1785	0.58	1.00	0.00	0.00
4.37_663.2850	0.59	1.00	0.00	0.00

5.20_239.1759	0.62	1.00	0.10	0.12
4.64_412.2067	0.62	1.00	0.00	0.14
6.19_181.1351	0.63	1.00	0.05	0.05
1.50_432.0982	0.66	1.00	0.13	0.00
4.27_647.2871	0.67	1.00	0.04	0.00
1.50_448.0831	0.67	1.00	0.14	0.00
11.44_223.2060	0.67	1.00	0.00	0.00
7.62_970.6124	0.70	1.00	0.00	0.00
6.85_824.9348	0.70	1.00	0.00	0.00
16.15_442.8736	0.71	1.00	0.00	0.00
7.07_184.1710	0.72	1.00	0.00	0.00
4.37_150.0945	0.72	1.00	0.00	0.00
3.89_518.1743	0.73	1.00	0.03	0.00
11.18_473.3585	0.75	1.00	0.52	0.41
1.53_143.0837	0.76	1.00	0.00	0.00
12.74_443.3505	0.77	1.00	0.00	0.07
12.98_282.2118	0.82	1.00	0.00	0.14
3.86_242.1126	0.82	0.90	1.00	1.00
9.26_219.1735	0.88	1.00	0.00	0.00
4.50_359.1197	0.89	1.00	0.24	0.28
1.49_594.1582	0.91	1.00	0.66	0.45
15.94_338.3442	0.91	1.00	0.78	0.80
13.48_341.2200	0.91	1.00	0.00	0.00
13.49_295.2258	0.91	1.00	0.14	0.08
1.47_508.0657	0.91	1.00	0.47	0.19
1.50_260.0296	0.92	1.00	0.12	0.06
1.47_748.1127	0.94	1.00	0.66	0.51
12.73_320.2010	0.94	1.00	0.00	0.30
1.48_481.1031	0.96	1.00	0.70	0.43
4.49_225.1597	0.97	1.00	0.20	0.23
13.95_270.2746	1.00	1.00	0.52	0.66
3.99_164.0936	1.00	0.90	0.39	0.60
1.50_230.0720	1.00	0.75	0.52	0.27
9.27_240.2315	1.00	0.88	0.17	0.15
10.39_268.2627	1.00	0.83	0.00	0.00
6.59_273.1670	1.00	0.84	0.00	0.21
13.97_282.2786	1.00	0.85	0.67	0.58
3.80_288.1929	1.00	0.87	0.00	0.00
11.44_291.1951	1.00	0.75	0.00	0.00
11.33_299.2599	1.00	0.77	0.00	0.00
15.49_338.3442	1.00	0.86	0.18	0.00
1.55_385.5441	1.00	0.65	0.22	0.05
1.50_401.0693	1.00	0.93	0.73	0.51
12.86_485.3471	1.00	0.86	0.66	0.44
13.92_641.5490	1.00	0.85	0.00	0.00
4.37_685.2548	1.00	0.86	0.00	0.30
7.66_916.7249	1.00	0.76	0.00	0.00

Table A3.11. Normalized heat map of features described as unique in **Figure 3.2(B)** and **(C)** when comparing wild type *Nocardiopsis sp. FU40 ΔApoS8* to the R2 rifampicin resistant mutant extract using OPLS-DA and extracting features from the generated S-plot with correlation coefficients ≥0.9. Features are normalized to maximum intensity for that feature.

Feature ID (RT_*m/z*)	WT	WT	R2	R2
12.03_135.1163	0.00	0.31	0.69	1.00
12.03_123.1165	0.00	0.00	1.00	0.65
4.87_118.0679	0.00	0.18	1.00	1.00
12.03_149.1327	0.00	0.00	1.00	0.61
13.61_149.0907	0.00	0.00	1.00	0.91
1.50_165.0624	0.00	0.00	1.00	0.98
10.69_163.6058	0.00	0.00	1.00	0.67
6.56_162.0938	0.00	0.00	0.66	1.00
5.78_170.1204	0.00	0.00	1.00	1.00
7.08_169.0882	0.00	0.01	0.62	1.00
6.60_180.1017	0.00	0.03	1.00	0.91
5.02_180.1014	0.00	0.00	1.00	0.86
4.95_177.1399	0.00	0.38	1.00	0.94
4.39_192.1130	0.00	0.26	0.80	1.00
9.26_191.1250	0.00	0.00	1.00	0.74
9.12_191.0134	0.00	0.00	1.00	0.88
6.97_190.1257	0.00	0.00	1.00	0.80
4.14_186.1168	0.00	0.00	0.95	1.00
9.08_196.0187	0.00	0.00	1.00	0.68
8.84_203.1804	0.00	0.00	1.00	0.90
8.12_203.1781	0.00	0.00	1.00	0.94
9.08_203.0278	0.00	0.00	1.00	0.72
9.80_203.0277	0.00	0.00	1.00	0.72
9.42_202.0393	0.00	0.00	0.75	1.00
4.35_209.0956	0.00	0.00	0.82	1.00
5.44_208.0539	0.00	0.01	1.00	0.97
7.49_207.0994	0.00	0.10	1.00	0.75
1.30_205.9283	0.00	0.00	1.00	1.00
4.84_205.1323	0.00	0.00	1.00	0.91
1.32_211.8786	0.00	0.00	1.00	0.98
9.25_211.0284	0.00	0.04	1.00	0.81
8.31_210.0369	0.00	0.00	1.00	0.59
9.81_210.0363	0.00	0.00	1.00	0.76
9.07_210.0305	0.00	0.00	1.00	0.86
9.41_219.0312	0.00	0.00	1.00	0.77
9.03_217.0413	0.00	0.00	1.00	0.82
16.16_223.9875	0.00	0.00	1.00	0.84
8.84_221.1903	0.00	0.00	1.00	0.93
6.51_220.1710	0.00	0.07	0.97	1.00
5.15_226.5984	0.00	0.03	1.00	0.86
7.35_225.1140	0.00	0.00	1.00	0.89
7.99_225.1125	0.00	0.02	1.00	0.94
9.04_225.0298	0.00	0.01	1.00	0.79
9.77_224.0325	0.00	0.00	1.00	0.83
5.48_229.0656	0.00	0.00	0.97	1.00
5.11_227.1386	0.00	0.00	1.00	0.99
9.19_230.0719	0.00	0.00	1.00	0.69
9.82_230.0718	0.00	0.03	0.79	1.00
8.41_230.0715	0.00	0.00	1.00	0.90
10.62_236.1643	0.00	0.00	1.00	0.82
5.11_236.1306	0.00	0.17	1.00	0.92
8.54_235.1344	0.00	0.00	1.00	0.88
9.80_241.0261	0.00	0.00	1.00	0.85
8.82_241.0249	0.00	0.00	0.72	1.00
5.81_248.1281	0.00	0.36	0.99	1.00
9.03_248.0351	0.00	0.00	1.00	0.83
8.44_247.1345	0.00	0.00	0.75	1.00

4.04_247.1287	0.00	0.00	1.00	0.88
7.33_247.0943	0.00	0.11	1.00	0.94
9.07_246.5440	0.00	0.00	1.00	0.83
5.04_244.1219	0.00	0.00	1.00	0.91
11.26_250.1814	0.00	0.00	1.00	0.82
4.94_250.1290	0.00	0.00	1.00	0.93
8.52_250.0297	0.00	0.00	1.00	0.94
4.31_249.0807	0.00	0.00	1.00	0.87
8.16_249.0423	0.00	0.00	1.00	0.80
4.56_252.0394	0.00	0.13	0.90	1.00
6.01_252.0391	0.00	0.00	1.00	0.84
6.82_252.0384	0.00	0.00	1.00	0.82
6.23_258.1449	0.00	0.00	1.00	0.86
6.94_256.2241	0.00	0.00	1.00	0.89
4.75_255.5956	0.00	0.28	1.00	0.83
6.97_254.2139	0.00	0.00	1.00	0.86
9.81_253.5524	0.00	0.01	1.00	0.86
4.75_263.0841	0.00	0.16	1.00	0.81
1.78_262.1278	0.00	0.00	1.00	0.73
9.91_261.5430	0.00	0.00	0.52	1.00
5.01_261.1438	0.00	0.06	1.00	0.94
9.03_260.5527	0.00	0.00	1.00	0.64
8.32_268.0180	0.00	0.00	1.00	0.94
10.77_267.1616	0.00	0.06	0.55	1.00
5.18_266.1406	0.00	0.37	1.00	0.82
5.27_264.2082	0.00	0.00	1.00	0.80
7.49_268.0200	0.00	0.00	1.00	0.68
9.67_268.0195	0.00	0.00	1.00	0.74
7.61_273.1085	0.00	0.00	1.00	0.84
5.84_281.1328	0.00	0.00	1.00	0.97
7.18_278.2110	0.00	0.00	1.00	0.88
6.07_276.1943	0.00	0.00	1.00	0.79
5.71_286.2118	0.00	0.00	1.00	0.83
7.19_284.2219	0.00	0.00	0.86	1.00
12.79_284.1681	0.00	0.05	1.00	0.98
7.50_283.1523	0.00	0.05	1.00	0.92
1.73_282.0649	0.00	0.03	1.00	0.94
7.72_281.1420	0.00	0.00	0.83	1.00
3.93_291.1653	0.00	0.00	1.00	0.83
9.72_290.1445	0.00	0.00	0.99	1.00
7.06_287.2336	0.00	0.00	0.93	1.00
5.22_295.1312	0.00	0.03	0.87	1.00
6.82_294.2084	0.00	0.00	1.00	0.82
7.15_293.2251	0.00	0.00	1.00	0.65
4.87_293.1612	0.00	0.35	1.00	0.91
6.49_292.1923	0.00	0.01	0.96	1.00
3.76_299.1387	0.00	0.00	0.54	1.00
2.95_299.1385	0.00	0.00	1.00	0.90
12.77_298.1902	0.00	0.00	0.95	1.00
4.74_298.0969	0.00	0.06	0.99	1.00
7.19_296.2224	0.00	0.00	1.00	0.92
5.83_303.1558	0.00	0.04	0.65	1.00
7.70_303.1206	0.00	0.04	1.00	0.99
3.78_300.1386	0.00	0.05	1.00	0.78
12.02_309.1921	0.00	0.06	1.00	0.80
6.00_308.2238	0.00	0.00	1.00	0.83
8.43_314.1381	0.00	0.21	1.00	0.60
6.06_312.2197	0.00	0.00	0.92	1.00
6.84_312.2197	0.00	0.00	1.00	0.91
7.24_312.2197	0.00	0.00	1.00	0.81
9.72_312.1580	0.00	0.00	1.00	0.77
10.59_311.1859	0.00	0.00	1.00	0.72
9.79_311.0549	0.00	0.00	1.00	0.92
7.47_310.2026	0.00	0.00	0.84	1.00
5.82_322.1007	0.00	0.00	1.00	0.87
1.74_322.0446	0.00	0.03	1.00	0.96
9.13_319.1539	0.00	0.00	1.00	0.83
6.92_318.2094	0.00	0.00	1.00	0.93
6.00_328.7423	0.00	0.13	1.00	0.93
5.91_328.5999	0.00	0.00	1.00	0.92

6.01_326.2353	0.00	0.00	0.95	1.00
4.97_326.0999	0.00	0.34	1.00	0.77
6.08_324.1828	0.00	0.23	1.00	0.93
6.31_335.7452	0.00	0.00	1.00	0.80
6.62_334.2005	0.00	0.00	1.00	0.80
9.73_334.1684	0.00	0.00	1.00	0.77
8.76_329.1942	0.00	0.19	0.99	1.00
12.72_342.2152	0.00	0.10	1.00	0.86
5.99_338.1374	0.00	0.00	0.88	1.00
9.08_348.2310	0.00	0.00	1.00	0.77
6.22_346.2031	0.00	0.00	0.71	1.00
7.48_345.1875	0.00	0.00	1.00	0.85
7.37_344.2218	0.00	0.00	1.00	0.84
9.69_356.1867	0.00	0.00	1.00	0.85
5.26_354.0787	0.00	0.28	0.97	1.00
8.24_352.2057	0.00	0.00	1.00	0.88
12.66_364.2323	0.00	0.28	1.00	0.74
6.67_362.2335	0.00	0.00	0.97	1.00
6.51_360.2165	0.00	0.00	1.00	0.89
8.53_359.2035	0.00	0.18	1.00	0.87
8.77_368.2219	0.00	0.00	1.00	0.92
7.52_368.2211	0.00	0.00	1.00	0.87
9.80_367.0822	0.00	0.00	1.00	0.96
10.08_366.2455	0.00	0.00	1.00	0.72
9.04_366.2404	0.00	0.00	1.00	0.83
6.22_366.2068	0.00	0.12	0.76	1.00
5.64_366.2063	0.00	0.00	0.91	1.00
8.47_382.2398	0.00	0.00	1.00	0.75
9.68_378.2012	0.00	0.00	1.00	0.72
7.43_374.2181	0.00	0.00	0.61	1.00
7.83_387.1861	0.00	0.00	1.00	0.94
9.80_387.0731	0.00	0.00	1.00	0.86
6.88_386.2329	0.00	0.01	1.00	0.90
6.24_384.2171	0.00	0.00	1.00	0.85
8.63_398.2317	0.00	0.00	1.00	1.00
1.49_394.1142	0.00	0.00	1.00	0.92
12.60_408.2538	0.00	0.15	1.00	0.67
7.68_401.3048	0.00	0.00	1.00	0.86
9.40_418.0851	0.00	0.00	1.00	0.97
8.66_429.0854	0.00	0.00	1.00	0.77
9.08_429.0845	0.00	0.00	1.00	0.82
4.02_423.1940	0.00	0.00	0.98	1.00
1.48_431.0890	0.00	0.45	1.00	0.91
9.07_451.0615	0.00	0.00	1.00	0.97
9.09_448.0576	0.00	0.00	1.00	0.71
6.99_443.3240	0.00	0.08	1.00	0.95
9.73_443.1014	0.00	0.00	1.00	0.87
8.33_443.0954	0.00	0.00	1.00	0.90
6.90_461.2902	0.00	0.00	1.00	0.96
5.90_459.3212	0.00	0.13	1.00	0.76
10.02_459.0960	0.00	0.00	1.00	0.77
9.03_457.1145	0.00	0.00	1.00	0.79
8.67_457.1133	0.00	0.00	1.00	0.95
11.52_456.3791	0.00	0.00	0.70	1.00
6.21_455.1906	0.00	0.19	1.00	0.85
9.81_454.0847	0.00	0.00	1.00	0.88
9.05_454.0819	0.00	0.00	1.00	0.72
5.01_452.1838	0.00	0.00	0.99	1.00
6.42_472.2832	0.00	0.00	0.56	1.00
6.46_471.2466	0.00	0.01	1.00	0.90
10.02_470.0758	0.00	0.00	1.00	0.82
9.02_468.1011	0.00	0.00	1.00	0.83
8.31_465.0807	0.00	0.00	1.00	0.79
8.82_465.0807	0.00	0.00	1.00	0.70
9.79_462.0710	0.00	0.00	1.00	0.81
9.04_462.0699	0.00	0.00	1.00	0.73
9.78_481.0499	0.00	0.00	0.74	1.00
9.02_479.0963	0.00	0.00	1.00	0.88
10.01_478.0692	0.00	0.00	1.00	0.66
4.15_476.2404	0.00	0.00	1.00	0.84

9.02_476.0877	0.00	0.00	1.00	0.79
7.51_499.2782	0.00	0.06	1.00	0.92
9.02_495.0687	0.00	0.00	1.00	0.95
4.37_494.2617	0.00	0.00	0.50	1.00
9.74_493.2809	0.00	0.01	1.00	0.93
5.37_493.1709	0.00	0.00	1.00	0.80
9.79_513.1525	0.00	0.00	1.00	0.62
6.65_512.8485	0.00	0.00	0.95	1.00
5.76_512.6875	0.00	0.00	1.00	1.00
9.09_512.3013	0.00	0.00	1.00	0.82
13.62_510.2556	0.00	0.37	1.00	0.85
5.65_504.2609	0.00	0.00	1.00	0.99
5.64_515.2738	0.00	0.00	1.00	0.91
9.71_537.3041	0.00	0.00	0.95	1.00
10.06_526.3139	0.00	0.00	1.00	0.86
7.21_526.2839	0.00	0.02	0.97	1.00
7.20_544.2918	0.00	0.00	1.00	0.93
7.57_542.3960	0.00	0.15	1.00	0.65
12.03_565.3746	0.00	0.08	0.73	1.00
7.14_560.1805	0.00	0.00	0.75	1.00
6.90_555.3068	0.00	0.00	1.00	0.92
5.52_601.2501	0.00	0.00	1.00	0.87
9.02_590.6205	0.00	0.00	1.00	0.79
9.74_581.3322	0.00	0.00	0.96	1.00
9.79_576.6021	0.00	0.00	0.82	1.00
9.06_576.6005	0.00	0.00	0.97	1.00
1.25_639.8836	0.00	0.00	1.00	0.83
12.72_634.4531	0.00	0.00	1.00	0.73
9.71_625.3598	0.00	0.00	1.00	0.84
9.73_669.3835	0.00	0.00	1.00	0.90
9.02_704.1451	0.00	0.00	1.00	0.61
9.03_696.1548	0.00	0.00	1.00	0.81
9.71_694.1152	0.00	0.00	0.77	1.00
9.03_690.1259	0.00	0.00	1.00	0.54
9.79_683.1204	0.00	0.00	1.00	0.77
9.06_676.1101	0.00	0.00	1.00	0.87
9.74_713.4076	0.00	0.00	0.65	1.00
9.78_885.1896	0.00	0.00	1.00	0.69
9.07_879.1306	0.00	0.00	0.96	1.00
9.02_935.1961	0.00	0.00	1.00	0.77
7.20_920.0962	0.00	0.00	0.77	1.00
7.21_916.0943	0.00	0.00	0.54	1.00
9.80_907.1678	0.00	0.00	1.00	0.88
9.04_907.1662	0.00	0.00	1.00	0.53
7.65_1000.0444	0.00	0.00	0.87	1.00
7.63_942.9948	0.00	0.00	1.00	0.83
7.01_1221.4414	0.00	0.00	0.92	1.00
6.97_357.2762	0.00	0.00	1.00	0.85
9.79_218.0234	0.00	0.01	1.00	0.89
7.07_184.1710	0.00	0.00	1.00	0.83
9.78_465.0808	0.00	0.01	1.00	0.94
8.21_315.2621	0.00	0.01	1.00	0.83
8.21_212.2021	0.00	0.00	1.00	0.84
5.66_384.2168	0.00	0.00	1.00	0.87
9.79_1349.2480	0.01	0.00	1.00	0.88
9.27_343.2981	0.01	0.03	1.00	0.92
8.34_150.0928	0.01	0.09	0.90	1.00
10.70_288.2557	0.01	0.01	1.00	0.74
1.64_174.0879	0.01	0.00	1.00	1.00
6.76_310.2021	0.01	0.00	1.00	1.00
1.82_228.1004	0.01	0.00	1.00	0.82
6.06_294.2084	0.01	0.00	1.00	0.80
6.24_515.2753	0.01	0.00	1.00	0.97
8.74_542.3146	0.01	0.00	0.89	1.00
1.29_203.9309	0.01	0.00	0.96	1.00
1.64_246.1172	0.01	0.00	1.00	0.96
9.71_757.4327	0.01	0.00	0.92	1.00
6.65_282.2073	0.02	0.11	1.00	0.75
7.48_177.0877	0.02	0.00	1.00	0.86
1.75_507.1572	0.02	0.00	1.00	0.62

8.10_301.1534	0.02	0.10	1.00	0.95
8.29_401.1993	0.03	0.00	1.00	0.82
4.82_393.2208	0.03	0.00	1.00	0.74
16.15_710.1773	0.03	0.01	0.61	1.00
1.53_143.0837	0.04	0.05	0.82	1.00
9.27_240.2315	0.04	0.03	1.00	0.81
5.43_377.1482	0.04	0.00	1.00	0.99
12.62_416.2462	0.04	0.05	1.00	0.74
3.22_235.1201	0.05	0.00	0.91	1.00
7.06_325.1861	0.05	0.31	1.00	0.78
9.66_279.1583	0.06	0.00	1.00	0.80
12.02_205.1953	0.07	0.00	1.00	0.62
9.14_239.1284	0.07	0.06	1.00	0.88
1.74_150.0789	0.07	0.00	1.00	0.87
4.75_136.0625	0.07	0.00	0.85	1.00
1.73_338.0231	0.07	0.00	0.97	1.00
6.39_336.2172	0.08	0.06	1.00	0.68
12.57_815.5173	0.08	0.25	1.00	0.86
10.40_371.3275	0.08	0.15	1.00	0.80
12.73_328.1928	0.08	0.00	1.00	0.86
6.72_1450.6973	0.08	0.02	0.72	1.00
8.53_283.1523	0.08	0.18	0.82	1.00
1.70_260.1135	0.08	0.00	1.00	0.97
6.66_264.1980	0.08	0.04	1.00	0.88
6.95_218.1203	0.09	0.19	1.00	0.87
12.66_372.2164	0.10	0.24	1.00	0.80
12.70_350.2054	0.10	0.19	1.00	0.86
16.22_252.0441	0.11	0.19	0.60	1.00
1.77_218.1042	0.11	0.03	1.00	1.00
3.86_150.0940	0.11	0.21	1.00	0.92
7.25_371.1508	0.12	0.00	1.00	0.87
6.71_1160.7578	0.12	0.00	0.81	1.00
12.78_306.1796	0.13	0.22	1.00	0.89
12.63_394.2284	0.13	0.10	1.00	0.73
7.06_221.1900	0.14	0.44	1.00	0.97
7.62_970.6124	0.15	0.21	0.74	1.00
8.53_207.1002	0.15	0.19	0.85	1.00
7.42_280.1237	0.15	0.42	1.00	0.93
12.55_438.2596	0.16	0.26	1.00	0.68
3.80_288.1929	0.17	0.15	1.00	0.93
12.73_320.2010	0.17	0.18	1.00	0.90
12.62_787.4580	0.18	0.31	1.00	0.92
7.06_203.1787	0.19	0.35	1.00	0.91
8.53_177.0880	0.19	0.18	1.00	0.85
10.98_442.3651	0.20	0.16	1.00	0.77
4.88_188.0708	0.20	0.35	1.00	0.92
12.70_699.4109	0.20	0.23	1.00	0.96
6.41_165.0905	0.21	0.14	0.89	1.00
6.06_203.1781	0.21	0.37	1.00	0.92
4.87_329.1844	0.22	0.00	1.00	0.87
16.18_335.9929	0.22	0.00	0.66	1.00
12.78_611.3565	0.22	0.25	1.00	0.98
1.51_393.5330	0.23	0.58	1.00	0.98
5.84_299.0939	0.23	0.11	0.69	1.00
12.61_771.4862	0.24	0.30	1.00	0.83
12.73_655.3845	0.24	0.29	1.00	1.00
4.31_265.0552	0.24	0.00	1.00	0.82
12.67_743.4367	0.24	0.27	1.00	0.95
12.70_683.4373	0.24	0.32	1.00	0.83
5.97_286.6247	0.24	0.04	0.82	1.00
12.79_595.3829	0.25	0.34	1.00	0.84
12.67_727.4605	0.25	0.34	1.00	0.81
2.84_200.1047	0.25	0.00	1.00	0.99
12.74_639.4067	0.26	0.31	1.00	0.84
6.95_368.2220	0.27	0.47	1.00	0.85
12.86_523.3040	0.27	0.18	0.94	1.00
12.80_567.3292	0.27	0.32	0.97	1.00
3.85_276.1433	0.28	0.16	0.98	1.00
1.65_159.0768	0.28	0.00	0.65	1.00
12.86_507.3281	0.28	0.43	1.00	0.74

4.30_310.1305	0.28	0.06	1.00	0.96
4.12_413.1243	0.32	0.58	1.00	0.99
7.91_389.2523	0.33	0.15	1.00	0.93
3.83_198.1623	0.33	0.23	1.00	0.89
7.65_970.5389	0.33	0.00	1.00	0.95
12.82_551.3593	0.34	0.50	0.86	1.00
12.87_262.1528	0.35	0.15	1.00	0.94
6.78_176.0714	0.36	0.62	1.00	0.87
12.70_678.4764	0.37	0.21	1.00	0.72
12.86_502.3745	0.37	0.45	1.00	0.72
12.86_463.2998	0.37	0.49	1.00	0.79
3.76_347.1589	0.38	0.00	1.00	0.75
12.56_441.2657	0.39	0.56	0.84	1.00
6.73_1160.5609	0.39	0.00	0.82	1.00
12.67_722.5060	0.41	0.20	1.00	0.73
5.61_343.2002	0.43	0.10	1.00	0.85
4.29_244.1199	0.47	0.49	0.93	1.00
4.00_320.1711	0.49	0.06	1.00	0.99
14.78_323.2583	0.50	1.00	0.00	0.03
13.49_420.3478	0.51	1.00	0.01	0.00
10.60_346.3091	0.51	1.00	0.00	0.00
13.00_413.3095	0.52	1.00	0.05	0.00
5.16_210.1137	0.52	0.51	0.96	1.00
9.48_225.1993	0.53	1.00	0.01	0.00
6.81_807.1918	0.54	1.00	0.00	0.00
6.15_485.2027	0.55	0.59	1.00	0.88
7.42_196.0651	0.55	0.29	1.00	0.92
4.26_669.2631	0.56	1.00	0.00	0.00
11.80_235.1712	0.56	1.00	0.04	0.00
10.15_739.4618	0.56	1.00	0.03	0.02
14.41_309.2409	0.56	1.00	0.04	0.03
10.53_531.4000	0.57	1.00	0.00	0.00
4.86_372.1909	0.57	0.29	1.00	0.89
12.97_407.3144	0.58	1.00	0.01	0.00
12.98_399.3242	0.58	1.00	0.01	0.00
4.09_573.1785	0.58	1.00	0.00	0.00
3.79_359.1699	0.59	0.29	1.00	0.92
4.64_137.0376	0.59	0.61	1.00	0.87
4.37_663.2850	0.59	1.00	0.05	0.00
13.98_433.3418	0.61	1.00	0.01	0.00
4.64_412.2067	0.62	1.00	0.10	0.08
6.19_181.1351	0.63	1.00	0.00	0.07
10.97_401.2525	0.63	1.00	0.00	0.00
11.58_415.2745	0.65	1.00	0.00	0.00
12.62_273.1378	0.66	1.00	0.00	0.00
12.97_290.7254	0.66	1.00	0.15	0.05
4.27_647.2871	0.67	1.00	0.01	0.06
11.44_223.2060	0.67	1.00	0.00	0.00
8.08_219.1411	0.68	1.00	0.36	0.28
6.40_263.1761	0.70	0.75	1.00	0.88
6.85_824.9348	0.70	1.00	0.19	0.00
4.81_506.2950	0.71	1.00	0.39	0.33
16.15_442.8736	0.71	1.00	0.15	0.06
4.40_158.0302	0.72	0.53	0.99	1.00
4.34_266.1408	0.72	0.56	0.98	1.00
4.37_150.0945	0.72	1.00	0.00	0.00
5.94_213.1018	0.73	0.55	0.97	1.00
3.89_518.1743	0.73	1.00	0.00	0.00
11.18_473.3585	0.75	1.00	0.02	0.02
16.18_214.9181	0.76	1.00	0.43	0.27
12.74_443.3505	0.77	1.00	0.00	0.00
12.97_547.4060	0.77	1.00	0.07	0.00
13.86_425.2896	0.78	1.00	0.22	0.14
5.26_147.0936	0.79	1.00	0.33	0.30
13.50_409.7445	0.80	1.00	0.34	0.09
4.28_227.1066	0.80	1.00	0.59	0.57
11.97_299.2600	0.80	1.00	0.00	0.00
13.50_524.2740	0.81	1.00	0.22	0.15
15.06_413.2647	0.81	1.00	0.27	0.14
4.55_279.1361	0.81	1.00	0.65	0.60

1.50_710.1736	0.81	0.82	0.96	1.00
11.84_443.3878	0.82	1.00	0.09	0.06
11.03_354.1608	0.82	1.00	0.11	0.09
11.28_440.3462	0.82	1.00	0.00	0.00
12.98_282.2118	0.82	1.00	0.00	0.00
13.79_365.2675	0.84	1.00	0.00	0.00
9.69_220.1127	0.87	1.00	0.19	0.44
10.38_401.3397	0.88	1.00	0.18	0.13
9.26_219.1735	0.88	1.00	0.00	0.00
14.79_310.3109	0.90	1.00	0.55	0.67
15.94_338.3442	0.91	1.00	0.44	0.37
13.48_341.2200	0.91	1.00	0.34	0.19
13.49_295.2258	0.91	1.00	0.00	0.00
1.47_508.0657	0.91	1.00	0.76	0.71
1.47_748.1127	0.94	1.00	0.84	0.83
4.58_336.1924	0.95	1.00	0.68	0.54
1.48_481.1031	0.96	1.00	0.73	0.71
4.49_225.1597	0.97	1.00	0.52	0.50
13.95_270.2746	1.00	1.00	0.33	0.27
6.34_150.0787	1.00	0.95	0.88	0.81
10.36_211.6353	1.00	0.89	0.20	0.00
3.82_209.1275	1.00	0.90	0.72	0.65
11.31_225.6512	1.00	0.95	0.17	0.00
11.44_291.1951	1.00	0.75	0.00	0.00
11.33_299.2599	1.00	0.77	0.00	0.00
5.53_306.1782	1.00	0.69	0.37	0.26
12.62_313.2746	1.00	0.83	0.00	0.00
14.31_325.2414	1.00	0.74	0.00	0.08
14.82_332.2940	1.00	0.65	0.00	0.10
15.49_338.3442	1.00	0.86	0.00	0.00
4.26_356.1796	1.00	0.84	0.64	0.56
15.92_360.3229	1.00	0.71	0.26	0.20
13.48_397.3392	1.00	0.75	0.00	0.00
10.78_415.3581	1.00	0.61	0.18	0.15
13.95_411.3586	1.00	0.78	0.00	0.00
13.27_419.3131	1.00	0.81	0.00	0.00
10.77_434.3251	1.00	0.58	0.21	0.00
12.97_555.3910	1.00	0.94	0.19	0.09
13.92_641.5490	1.00	0.85	0.00	0.00
4.37_685.2548	1.00	0.86	0.20	0.23
6.87_807.0837	1.00	0.57	0.00	0.00

Table A3.12. Normalized heat map of features described as unique in **Figure 3.2(B)** and **(C)** when comparing wild type *Nocardiopsis sp. FU40 ΔApoS8* to the R2 rifampicin resistant mutant extract using OPLS-DA and extracting features from the generated S-plot with correlation coefficients ≥0.9. Features are normalized to maximum intensity for that feature.

Feature ID (RT_*m/z*)	WT	WT	R3	R3
12.03_135.1163	0.00	0.13	1.00	0.81
1.52_129.5659	0.00	0.00	1.00	0.65
12.03_123.1165	0.00	0.00	1.00	0.81
4.87_118.0679	0.00	0.13	0.60	1.00
4.95_114.0908	0.00	0.00	0.84	1.00
1.50_165.0624	0.00	0.00	1.00	0.83
6.56_162.0938	0.00	0.00	1.00	0.86
4.31_160.1140	0.00	0.00	1.00	0.88
5.78_170.1204	0.00	0.00	1.00	0.92
7.08_169.0882	0.00	0.02	0.64	1.00
2.44_166.0747	0.00	0.12	1.00	0.85
6.60_180.1017	0.00	0.02	1.00	0.77
4.95_177.1399	0.00	0.43	1.00	0.94
9.12_191.0134	0.00	0.00	1.00	0.78
6.97_190.1257	0.00	0.00	1.00	0.82
4.99_198.1134	0.00	0.00	0.68	1.00
9.08_196.0187	0.00	0.00	1.00	0.99
8.84_203.1804	0.00	0.00	1.00	0.93
9.08_203.0278	0.00	0.00	0.89	1.00
9.80_203.0277	0.00	0.00	1.00	0.82
9.42_202.0393	0.00	0.00	1.00	0.87
4.35_209.0956	0.00	0.00	0.65	1.00
4.54_208.1355	0.00	0.00	0.95	1.00
5.44_208.0539	0.00	0.00	0.95	1.00
7.49_207.0994	0.00	0.07	1.00	0.63
1.30_205.9283	0.00	0.00	1.00	0.75
4.84_205.1323	0.00	0.00	1.00	0.94
8.67_212.0251	0.00	0.00	1.00	0.87
1.32_211.8786	0.00	0.00	1.00	0.84
9.81_210.0363	0.00	0.00	0.85	1.00
9.07_210.0305	0.00	0.00	0.58	1.00
9.41_219.0312	0.00	0.00	0.69	1.00
3.69_218.1136	0.00	0.30	1.00	0.83
8.67_218.0490	0.00	0.00	0.92	1.00
9.03_217.0413	0.00	0.00	1.00	0.99
8.84_221.1903	0.00	0.00	1.00	0.85
6.51_220.1710	0.00	0.03	0.59	1.00
4.58_226.1445	0.00	0.00	0.91	1.00
5.11_226.1427	0.00	0.03	0.67	1.00
9.04_225.0298	0.00	0.01	1.00	0.97
9.77_224.0325	0.00	0.00	0.95	1.00
5.11_227.1386	0.00	0.00	0.91	1.00
9.82_230.0718	0.00	0.04	1.00	1.00
6.24_230.0717	0.00	0.34	1.00	0.88
8.41_230.0715	0.00	0.00	1.00	0.75
5.11_236.1306	0.00	0.12	0.68	1.00
4.89_235.1441	0.00	0.00	1.00	0.98
9.80_241.0261	0.00	0.00	1.00	0.63
5.81_248.1281	0.00	0.25	0.76	1.00
9.03_248.0351	0.00	0.00	1.00	0.51
4.04_247.1287	0.00	0.00	1.00	0.91
5.04_244.1219	0.00	0.00	0.87	1.00
2.62_252.0382	0.00	0.29	0.96	1.00
11.26_250.1814	0.00	0.00	1.00	0.73
14.09_252.0478	0.00	0.00	0.56	1.00
8.66_252.0394	0.00	0.00	0.67	1.00
12.02_263.1978	0.00	0.10	1.00	0.79

1.78_262.1278	0.00	0.00	0.87	1.00
5.86_262.1048	0.00	0.26	0.68	1.00
10.71_261.1779	0.00	0.03	1.00	0.87
5.01_261.1438	0.00	0.03	1.00	0.79
5.43_268.0192	0.00	0.06	1.00	0.52
8.32_268.0180	0.00	0.00	0.97	1.00
10.77_267.1616	0.00	0.12	1.00	0.81
2.47_276.1033	0.00	0.00	0.81	1.00
9.12_279.1585	0.00	0.00	1.00	0.94
7.18_278.2110	0.00	0.00	1.00	0.97
7.19_284.2219	0.00	0.00	0.95	1.00
7.50_283.1523	0.00	0.05	1.00	0.81
9.01_283.1521	0.00	0.13	0.70	1.00
1.73_282.0649	0.00	0.03	0.98	1.00
7.72_281.1420	0.00	0.00	0.95	1.00
5.22_295.1312	0.00	0.02	1.00	0.82
7.82_294.2085	0.00	0.00	1.00	0.80
6.82_294.2084	0.00	0.00	0.68	1.00
7.15_293.2251	0.00	0.00	1.00	0.96
4.87_293.1612	0.00	0.25	0.79	1.00
3.76_299.1387	0.00	0.00	1.00	0.57
4.74_298.0969	0.00	0.07	1.00	0.85
9.60_297.1694	0.00	0.01	1.00	0.84
7.19_296.2224	0.00	0.00	0.97	1.00
3.78_300.1386	0.00	0.03	1.00	0.68
12.02_309.1921	0.00	0.03	1.00	0.66
6.00_308.2238	0.00	0.00	1.00	0.97
6.06_312.2197	0.00	0.00	1.00	0.87
6.84_312.2197	0.00	0.00	0.95	1.00
7.24_312.2197	0.00	0.00	0.96	1.00
9.79_311.0549	0.00	0.00	0.75	1.00
1.74_322.0446	0.00	0.02	0.91	1.00
9.13_319.1539	0.00	0.00	1.00	0.92
6.92_318.2094	0.00	0.00	1.00	0.85
6.00_328.7423	0.00	0.09	1.00	0.56
5.91_328.5999	0.00	0.00	0.62	1.00
7.34_326.2353	0.00	0.00	1.00	0.89
6.01_326.2353	0.00	0.00	1.00	0.87
4.97_326.0999	0.00	0.27	1.00	0.90
12.03_325.1706	0.00	0.00	1.00	0.66
6.08_324.1828	0.00	0.23	0.81	1.00
6.62_334.2005	0.00	0.00	1.00	1.00
8.76_329.1942	0.00	0.09	0.92	1.00
5.84_341.1007	0.00	0.00	0.85	1.00
7.48_345.1875	0.00	0.00	0.89	1.00
7.37_344.2218	0.00	0.00	1.00	0.75
6.06_359.1205	0.00	0.00	0.58	1.00
8.24_352.2057	0.00	0.00	0.71	1.00
4.01_351.5992	0.00	0.00	0.81	1.00
6.67_362.2335	0.00	0.00	0.99	1.00
6.51_360.2165	0.00	0.00	1.00	0.75
8.53_359.2035	0.00	0.12	1.00	0.70
8.77_368.2219	0.00	0.00	1.00	0.66
6.02_368.2219	0.00	0.07	0.95	1.00
7.52_368.2211	0.00	0.00	1.00	0.73
9.80_367.0822	0.00	0.00	1.00	0.99
9.04_366.2404	0.00	0.00	1.00	0.66
5.64_366.2063	0.00	0.00	0.75	1.00
9.80_387.0731	0.00	0.00	0.98	1.00
6.88_386.2329	0.00	0.00	1.00	0.76
6.89_384.2172	0.00	0.00	0.86	1.00
6.24_384.2171	0.00	0.00	0.54	1.00
8.63_398.2317	0.00	0.00	0.97	1.00
1.49_394.1142	0.00	0.00	0.53	1.00
8.66_429.0854	0.00	0.00	0.94	1.00
9.08_429.0845	0.00	0.00	1.00	0.92
9.42_432.0873	0.00	0.00	1.00	1.00
9.07_451.0615	0.00	0.00	1.00	0.69
9.09_448.0576	0.00	0.00	1.00	0.66
6.99_443.3240	0.00	0.06	1.00	0.61

355

9.73_443.1014	0.00	0.00	1.00	0.99
8.33_443.0954	0.00	0.00	1.00	0.82
6.90_461.2902	0.00	0.00	0.96	1.00
5.90_459.3212	0.00	0.09	1.00	0.68
10.02_459.0960	0.00	0.00	1.00	0.76
9.03_457.1145	0.00	0.00	1.00	0.91
8.67_457.1133	0.00	0.00	1.00	0.75
11.52_456.3791	0.00	0.00	1.00	0.50
6.21_455.1906	0.00	0.16	0.99	1.00
9.81_454.0847	0.00	0.00	1.00	0.70
6.46_471.2466	0.00	0.01	1.00	0.67
9.02_468.1011	0.00	0.00	1.00	0.61
9.08_467.0388	0.00	0.00	1.00	0.68
9.79_462.0710	0.00	0.00	1.00	0.67
9.78_481.0499	0.00	0.00	0.57	1.00
9.02_479.0963	0.00	0.00	1.00	0.84
10.01_478.0692	0.00	0.00	1.00	0.76
4.15_476.2404	0.00	0.00	1.00	0.80
9.02_476.0877	0.00	0.00	1.00	0.78
6.98_499.2793	0.00	0.00	1.00	0.62
7.51_499.2782	0.00	0.05	0.81	1.00
9.02_495.0687	0.00	0.00	1.00	0.61
4.37_494.2617	0.00	0.00	0.98	1.00
5.37_493.1709	0.00	0.00	0.71	1.00
9.79_513.1525	0.00	0.00	1.00	0.59
9.09_512.3013	0.00	0.00	1.00	0.54
5.65_504.2609	0.00	0.00	0.83	1.00
5.64_515.2738	0.00	0.01	1.00	0.79
10.06_526.3139	0.00	0.00	1.00	0.57
7.21_526.2839	0.00	0.02	1.00	0.98
5.90_546.1391	0.00	0.00	0.76	1.00
7.20_544.2918	0.00	0.00	1.00	0.69
7.57_542.3960	0.00	0.09	1.00	0.59
9.00_540.1495	0.00	0.00	1.00	0.72
6.63_570.3104	0.00	0.00	1.00	0.84
12.03_565.3746	0.00	0.04	1.00	0.90
6.90_555.3068	0.00	0.00	1.00	0.77
5.52_601.2501	0.00	0.00	0.95	1.00
9.79_576.6021	0.00	0.00	1.00	0.56
1.25_639.8836	0.00	0.00	1.00	0.72
9.07_662.0928	0.00	0.00	1.00	0.90
9.02_704.1451	0.00	0.00	1.00	0.95
9.79_683.1204	0.00	0.00	1.00	0.66
9.06_676.1101	0.00	0.00	1.00	1.00
9.78_885.1896	0.00	0.00	1.00	0.56
7.60_846.3434	0.00	0.00	0.75	1.00
9.02_935.1961	0.00	0.00	1.00	0.55
9.80_907.1678	0.00	0.00	1.00	0.66
7.69_1031.1674	0.00	0.09	0.61	1.00
7.63_942.9948	0.00	0.00	0.57	1.00
7.01_1221.4414	0.00	0.00	1.00	0.76
9.79_218.0234	0.00	0.01	1.00	0.86
9.78_465.0808	0.00	0.01	1.00	0.81
8.74_542.3146	0.00	0.00	0.66	1.00
9.79_1349.2480	0.00	0.00	1.00	0.51
8.34_150.0928	0.00	0.07	1.00	0.93
1.64_174.0879	0.01	0.00	0.88	1.00
9.81_269.0437	0.01	0.00	0.62	1.00
6.76_310.2021	0.01	0.00	1.00	0.84
1.82_228.1004	0.01	0.00	0.88	1.00
5.66_384.2168	0.01	0.00	1.00	0.77
6.06_294.2084	0.01	0.00	0.81	1.00
1.29_203.9309	0.01	0.00	1.00	0.80
1.64_246.1172	0.01	0.00	1.00	0.94
6.24_515.2753	0.01	0.01	0.93	1.00
7.48_177.0877	0.02	0.00	0.94	1.00
8.10_301.1534	0.02	0.07	1.00	0.75
1.53_143.0837	0.03	0.03	0.93	1.00
1.75_507.1572	0.03	0.00	0.68	1.00
3.22_235.1201	0.03	0.00	1.00	0.87

16.15_710.1773	0.03	0.01	0.77	1.00
12.02_205.1953	0.04	0.00	1.00	0.79
5.43_377.1482	0.05	0.00	1.00	0.86
1.73_338.0231	0.05	0.00	0.98	1.00
7.06_325.1861	0.05	0.29	1.00	0.91
8.29_401.1993	0.05	0.00	1.00	0.92
4.37_326.1802	0.05	0.32	0.66	1.00
6.39_336.2172	0.05	0.04	1.00	0.91
9.66_279.1583	0.06	0.00	0.69	1.00
6.66_264.1980	0.06	0.03	0.66	1.00
3.07_230.1126	0.06	0.15	0.85	1.00
1.77_218.1042	0.06	0.02	1.00	0.83
9.67_319.1539	0.07	0.09	0.83	1.00
4.75_136.0625	0.07	0.00	1.00	0.84
8.53_283.1523	0.07	0.14	1.00	0.90
7.62_970.6124	0.07	0.10	0.54	1.00
1.74_150.0789	0.07	0.00	1.00	0.81
1.70_260.1135	0.07	0.00	1.00	0.93
6.95_218.1203	0.08	0.16	1.00	0.83
9.14_239.1284	0.10	0.09	1.00	0.62
16.24_268.0194	0.10	0.20	0.72	1.00
8.53_207.1002	0.10	0.12	0.61	1.00
3.83_292.1654	0.11	0.00	0.56	1.00
6.72_1450.6973	0.12	0.03	1.00	0.69
3.80_288.1929	0.12	0.11	0.88	1.00
3.86_150.0940	0.13	0.23	1.00	0.92
1.65_159.0768	0.13	0.00	0.83	1.00
6.95_368.2220	0.13	0.22	1.00	0.95
7.06_221.1900	0.13	0.39	1.00	0.74
8.53_177.0880	0.13	0.13	1.00	0.98
7.25_371.1508	0.13	0.00	0.58	1.00
10.52_673.3745	0.14	0.22	1.00	0.70
16.22_252.0441	0.14	0.25	0.77	1.00
7.42_280.1237	0.16	0.43	1.00	0.84
1.76_596.1679	0.16	0.00	0.74	1.00
13.77_459.1339	0.16	0.35	0.67	1.00
6.71_1160.7578	0.17	0.00	1.00	0.69
7.06_203.1787	0.17	0.33	1.00	0.91
5.97_286.6247	0.18	0.03	1.00	1.00
3.82_230.1126	0.20	0.12	0.78	1.00
6.41_165.0905	0.21	0.14	1.00	0.85
4.87_329.1844	0.22	0.00	1.00	0.97
4.31_265.0552	0.23	0.00	0.85	1.00
4.88_188.0708	0.23	0.40	0.92	1.00
9.41_281.1770	0.26	0.48	1.00	0.84
3.85_276.1433	0.26	0.15	1.00	0.83
4.30_284.1098	0.27	0.08	0.68	1.00
4.30_310.1305	0.28	0.06	0.94	1.00
4.12_413.1243	0.28	0.50	0.76	1.00
16.18_335.9929	0.28	0.00	1.00	0.67
6.06_203.1781	0.29	0.51	1.00	0.99
5.11_307.1591	0.31	0.00	0.74	1.00
4.81_464.2611	0.34	0.41	1.00	0.92
3.76_347.1589	0.38	0.00	1.00	0.78
6.78_176.0714	0.39	0.66	1.00	0.96
3.80_194.0821	0.43	0.00	0.92	1.00
4.29_244.1199	0.44	0.45	1.00	0.93
4.64_137.0376	0.44	0.45	1.00	0.86
5.61_343.2002	0.49	0.11	1.00	0.96
4.86_372.1909	0.49	0.25	1.00	0.86
12.43_386.2820	0.50	1.00	0.00	0.00
3.79_359.1699	0.51	0.25	1.00	0.93
10.60_346.3091	0.51	1.00	0.00	0.00
9.48_225.1993	0.53	1.00	0.01	0.01
6.81_807.1918	0.54	1.00	0.00	0.00
6.15_485.2027	0.55	0.59	0.86	1.00
4.26_669.2631	0.56	1.00	0.00	0.00
11.80_235.1712	0.56	1.00	0.00	0.00
10.15_739.4618	0.56	1.00	0.03	0.02
14.41_309.2409	0.56	1.00	0.00	0.09

6.27_207.0660	0.57	1.00	0.00	0.00
10.53_531.4000	0.57	1.00	0.00	0.00
12.97_407.3144	0.58	1.00	0.05	0.02
12.98_399.3242	0.58	1.00	0.05	0.02
7.42_196.0651	0.59	0.30	0.97	1.00
4.37_663.2850	0.59	1.00	0.05	0.03
13.98_433.3418	0.61	1.00	0.00	0.00
6.90_166.0720	0.61	1.00	0.00	0.00
4.64_412.2067	0.62	1.00	0.00	0.06
6.19_181.1351	0.63	1.00	0.03	0.00
10.97_401.2525	0.63	1.00	0.00	0.00
11.58_415.2745	0.65	1.00	0.00	0.00
12.62_273.1378	0.66	1.00	0.00	0.00
12.86_507.3281	0.66	1.00	0.20	0.14
12.97_290.7254	0.66	1.00	0.31	0.16
4.27_647.2871	0.67	1.00	0.02	0.01
12.82_551.3593	0.67	1.00	0.21	0.16
11.44_223.2060	0.67	1.00	0.00	0.00
8.08_219.1411	0.68	1.00	0.14	0.17
12.56_441.2657	0.70	1.00	0.28	0.26
6.40_263.1761	0.70	0.75	1.00	0.89
6.85_824.9348	0.70	1.00	0.00	0.00
4.81_506.2950	0.71	1.00	0.12	0.10
16.15_442.8736	0.71	1.00	0.00	0.00
7.07_184.1710	0.72	1.00	0.00	0.00
4.37_150.0945	0.72	1.00	0.00	0.00
12.79_595.3829	0.73	1.00	0.25	0.17
3.89_518.1743	0.73	1.00	0.03	0.00
12.67_727.4605	0.74	1.00	0.33	0.21
11.18_473.3585	0.75	1.00	0.02	0.00
12.70_683.4373	0.77	1.00	0.28	0.21
12.86_463.2998	0.77	1.00	0.07	0.18
12.74_443.3505	0.77	1.00	0.00	0.00
12.97_547.4060	0.77	1.00	0.00	0.04
13.86_425.2896	0.78	1.00	0.27	0.23
1.50_401.0693	0.79	0.73	0.95	1.00
5.26_147.0936	0.79	1.00	0.29	0.30
3.75_267.1417	0.80	1.00	0.58	0.43
12.61_771.4862	0.80	1.00	0.32	0.24
11.97_299.2600	0.80	1.00	0.00	0.00
15.06_413.2647	0.81	1.00	0.27	0.26
12.86_502.3745	0.82	1.00	0.18	0.12
11.84_443.3878	0.82	1.00	0.09	0.04
11.03_354.1608	0.82	1.00	0.05	0.05
11.28_440.3462	0.82	1.00	0.00	0.00
12.98_282.2118	0.82	1.00	0.00	0.00
12.73_655.3845	0.83	1.00	0.00	0.22
12.74_639.4067	0.83	1.00	0.31	0.22
13.79_365.2675	0.84	1.00	0.00	0.00
12.80_567.3292	0.85	1.00	0.30	0.19
12.83_546.4021	0.86	1.00	0.19	0.13
10.38_401.3397	0.88	1.00	0.24	0.16
9.26_219.1735	0.88	1.00	0.00	0.00
12.67_743.4367	0.88	1.00	0.37	0.24
4.50_359.1197	0.89	1.00	0.63	0.50
12.70_699.4109	0.89	1.00	0.20	0.00
5.43_241.1546	0.91	0.93	0.98	1.00
12.78_611.3565	0.91	1.00	0.33	0.07
15.94_338.3442	0.91	1.00	0.41	0.39
13.49_295.2258	0.91	1.00	0.04	0.02
12.73_320.2010	0.94	1.00	0.00	0.20
1.48_481.1031	0.96	1.00	0.88	0.83
4.49_225.1597	0.97	1.00	0.45	0.40
12.89_441.3208	0.99	1.00	0.15	0.13
12.78_590.4295	1.00	1.00	0.20	0.14
13.95_270.2746	1.00	1.00	0.35	0.33
3.99_164.0936	1.00	0.90	0.63	0.69
10.36_211.6353	1.00	0.89	0.25	0.00
3.82_209.1275	1.00	0.90	0.51	0.39
11.31_225.6512	1.00	0.95	0.00	0.00

358

9.27_240.2315	1.00	0.88	0.16	0.16
10.39_268.2627	1.00	0.83	0.00	0.03
6.59_273.1670	1.00	0.84	0.66	0.53
11.44_291.1951	1.00	0.75	0.00	0.00
11.33_299.2599	1.00	0.77	0.00	0.00
12.62_313.2746	1.00	0.83	0.01	0.00
14.31_325.2414	1.00	0.74	0.00	0.00
14.82_332.2940	1.00	0.65	0.16	0.00
15.49_338.3442	1.00	0.86	0.00	0.06
4.26_356.1796	1.00	0.84	0.59	0.52
15.92_360.3229	1.00	0.71	0.32	0.13
13.48_397.3392	1.00	0.75	0.00	0.00
10.78_415.3581	1.00	0.61	0.22	0.15
13.95_411.3586	1.00	0.78	0.00	0.00
13.27_419.3131	1.00	0.81	0.00	0.00
10.77_434.3251	1.00	0.58	0.18	0.00
12.86_485.3471	1.00	0.86	0.13	0.09
12.86_523.3040	1.00	0.66	0.25	0.24
12.81_529.3766	1.00	0.77	0.13	0.12
12.97_555.3910	1.00	0.94	0.00	0.12
12.79_573.4039	1.00	0.73	0.11	0.15
12.75_617.4294	1.00	0.84	0.16	0.15
13.92_641.5490	1.00	0.85	0.00	0.00
4.37_685.2548	1.00	0.86	0.00	0.00
12.67_705.4810	1.00	0.93	0.25	0.15
6.87_807.0837	1.00	0.57	0.00	0.00

Table A3.13. Normalized heat map of features described as unique in **Figure 3.2(B)** and **(C)** when comparing wild type *Nocardiopsis sp. FU40 ΔApoS8* to the R4 rifampicin resistant mutant extract using OPLS-DA and extracting features from the generated S-plot with correlation coefficients ≥0.9. Features are normalized to maximum intensity for that feature.

Feature ID (RT_*m/z*)	WT	WT	R4	R4
1.51_137.5554	0.00	0.00	1.00	0.52
1.52_129.5659	0.00	0.00	1.00	0.52
1.50_103.5345	0.00	0.00	0.50	1.00
13.61_149.0907	0.00	0.00	1.00	0.75
6.56_162.0938	0.00	0.00	0.80	1.00
4.31_160.1140	0.00	0.00	0.67	1.00
5.78_170.1204	0.00	0.00	0.64	1.00
6.60_180.1017	0.00	0.03	0.58	1.00
5.02_180.1014	0.00	0.00	0.58	1.00
9.12_191.0134	0.00	0.00	0.60	1.00
4.14_186.1168	0.00	0.00	0.93	1.00
9.08_196.0187	0.00	0.00	0.79	1.00
8.68_204.0325	0.00	0.00	0.72	1.00
9.08_203.0278	0.00	0.00	0.76	1.00
9.42_202.0393	0.00	0.00	0.68	1.00
1.42_201.0074	0.00	0.00	0.79	1.00
4.35_209.0956	0.00	0.00	0.51	1.00
4.54_208.1355	0.00	0.00	0.90	1.00
5.44_208.0539	0.00	0.00	0.78	1.00
7.49_207.0994	0.00	0.11	0.55	1.00
1.30_205.9283	0.00	0.00	0.53	1.00
4.84_205.1323	0.00	0.00	0.86	1.00
8.67_212.0251	0.00	0.00	0.63	1.00
1.49_211.0584	0.00	0.19	0.65	1.00
9.25_211.0284	0.00	0.01	1.00	0.92
8.31_210.0369	0.00	0.00	0.81	1.00
9.81_210.0363	0.00	0.00	1.00	0.66
9.07_210.0305	0.00	0.00	0.77	1.00
9.41_219.0312	0.00	0.00	1.00	0.86
8.67_218.0490	0.00	0.00	0.82	1.00
9.03_217.0413	0.00	0.00	0.70	1.00
2.51_216.0981	0.00	0.02	0.49	1.00
16.16_223.9875	0.00	0.00	0.90	1.00
6.51_220.1710	0.00	0.04	1.00	0.99
4.58_226.1445	0.00	0.00	1.00	0.82
5.11_226.1427	0.00	0.02	0.53	1.00
8.67_226.0395	0.00	0.00	0.61	1.00
9.04_225.0298	0.00	0.01	0.74	1.00
9.77_224.0325	0.00	0.00	0.63	1.00
5.11_227.1386	0.00	0.00	0.56	1.00
9.19_230.0719	0.00	0.00	1.00	0.54
9.82_230.0718	0.00	0.03	0.91	1.00
8.41_230.0715	0.00	0.00	0.96	1.00
10.62_236.1643	0.00	0.00	1.00	0.76
5.11_236.1306	0.00	0.18	0.96	1.00
4.89_235.1441	0.00	0.00	0.93	1.00
8.54_235.1344	0.00	0.00	0.60	1.00
9.80_241.0261	0.00	0.00	1.00	0.78
8.82_241.0249	0.00	0.00	1.00	0.94
4.13_237.1268	0.00	0.35	1.00	0.96
5.81_248.1281	0.00	0.35	1.00	0.99
9.03_248.0351	0.00	0.00	0.80	1.00

4.04_247.1287	0.00	0.00	0.50	1.00
9.07_246.5440	0.00	0.00	0.71	1.00
5.63_245.1880	0.00	0.00	1.00	0.83
5.04_244.1219	0.00	0.00	0.85	1.00
4.70_243.1326	0.00	0.00	0.55	1.00
8.52_250.0297	0.00	0.00	0.76	1.00
4.31_249.0807	0.00	0.00	0.72	1.00
8.08_252.0397	0.00	0.00	1.00	0.84
4.56_252.0394	0.00	0.16	1.00	0.63
8.66_252.0394	0.00	0.00	1.00	0.58
6.82_252.0384	0.00	0.00	0.83	1.00
6.23_258.1449	0.00	0.00	1.00	0.75
9.81_253.5524	0.00	0.02	0.91	1.00
1.78_262.1278	0.00	0.00	0.75	1.00
5.86_262.1048	0.00	0.41	0.85	1.00
9.91_261.5430	0.00	0.00	1.00	0.65
5.01_261.1438	0.00	0.08	0.80	1.00
9.03_260.5527	0.00	0.00	0.72	1.00
8.32_268.0180	0.00	0.00	1.00	0.55
10.77_267.1616	0.00	0.02	1.00	1.00
5.27_264.2082	0.00	0.00	0.79	1.00
9.67_268.0195	0.00	0.00	1.00	0.94
2.47_276.1033	0.00	0.00	0.83	1.00
9.12_279.1585	0.00	0.00	0.56	1.00
7.18_278.2110	0.00	0.00	0.62	1.00
6.07_276.1943	0.00	0.00	0.57	1.00
5.71_286.2118	0.00	0.00	0.84	1.00
7.19_284.2219	0.00	0.00	0.63	1.00
12.79_284.1681	0.00	0.22	1.00	0.68
7.50_283.1523	0.00	0.06	0.78	1.00
1.73_282.0649	0.00	0.03	0.61	1.00
5.22_295.1312	0.00	0.05	0.70	1.00
7.48_294.2085	0.00	0.00	1.00	0.58
7.82_294.2085	0.00	0.00	0.56	1.00
6.82_294.2084	0.00	0.00	0.63	1.00
7.15_293.2251	0.00	0.00	0.92	1.00
4.87_293.1612	0.00	0.39	1.00	0.83
6.49_292.1923	0.00	0.01	0.80	1.00
3.76_299.1387	0.00	0.08	0.64	1.00
7.73_298.2024	0.00	0.00	0.60	1.00
4.74_298.0969	0.00	0.05	0.68	1.00
9.60_297.1694	0.00	0.01	0.61	1.00
7.19_296.2224	0.00	0.00	0.58	1.00
6.00_308.2238	0.00	0.00	0.64	1.00
6.92_313.1550	0.00	0.00	0.55	1.00
6.06_312.2197	0.00	0.00	0.84	1.00
6.84_312.2197	0.00	0.00	0.52	1.00
7.24_312.2197	0.00	0.00	0.62	1.00
10.59_311.1859	0.00	0.00	0.65	1.00
9.79_311.0549	0.00	0.00	0.57	1.00
7.47_310.2026	0.00	0.00	1.00	0.56
5.82_322.1007	0.00	0.00	0.89	1.00
1.74_322.0446	0.00	0.03	0.90	1.00
3.86_320.0995	0.00	0.00	0.64	1.00
9.13_319.1539	0.00	0.00	0.60	1.00
6.92_318.2094	0.00	0.00	0.76	1.00
5.91_328.5999	0.00	0.00	0.65	1.00
7.34_326.2353	0.00	0.00	0.58	1.00
6.01_326.2353	0.00	0.00	0.79	1.00
4.97_326.0999	0.00	0.23	0.83	1.00
6.08_324.1828	0.00	0.09	0.64	1.00
6.31_335.7452	0.00	0.00	1.00	0.52
6.62_334.2005	0.00	0.00	0.50	1.00
5.84_341.1007	0.00	0.00	0.59	1.00
5.99_338.1374	0.00	0.00	1.00	0.77

6.22_346.2031	0.00	0.00	1.00	0.86
7.48_345.1875	0.00	0.00	0.84	1.00
7.37_344.2218	0.00	0.00	0.66	1.00
5.26_354.0787	0.00	0.32	1.00	0.94
8.24_352.2057	0.00	0.00	0.54	1.00
6.67_362.2335	0.00	0.00	1.00	0.86
6.51_360.2165	0.00	0.00	1.00	0.81
8.53_359.2035	0.00	0.11	0.90	1.00
8.77_368.2219	0.00	0.00	0.73	1.00
6.02_368.2219	0.00	0.04	0.72	1.00
7.52_368.2211	0.00	0.00	0.90	1.00
9.80_367.0822	0.00	0.00	0.66	1.00
5.64_366.2063	0.00	0.00	0.71	1.00
8.47_382.2398	0.00	0.00	0.89	1.00
7.30_389.1593	0.00	0.00	1.00	0.89
9.80_387.0731	0.00	0.00	0.56	1.00
6.88_386.2329	0.00	0.00	0.66	1.00
6.24_384.2171	0.00	0.00	0.70	1.00
8.63_398.2317	0.00	0.00	0.65	1.00
1.49_394.1142	0.00	0.00	0.61	1.00
9.40_418.0851	0.00	0.00	0.59	1.00
8.66_429.0854	0.00	0.00	0.56	1.00
9.08_429.0845	0.00	0.00	0.57	1.00
4.02_423.1940	0.00	0.00	0.61	1.00
9.15_440.0708	0.00	0.00	0.59	1.00
9.42_432.0873	0.00	0.00	0.65	1.00
1.48_431.0890	0.00	0.41	0.98	1.00
9.09_448.0576	0.00	0.00	0.61	1.00
9.73_443.1014	0.00	0.00	0.82	1.00
8.33_443.0954	0.00	0.00	0.93	1.00
8.80_443.0945	0.00	0.00	0.61	1.00
6.90_461.2902	0.00	0.00	0.90	1.00
10.02_459.0960	0.00	0.00	0.58	1.00
9.03_457.1145	0.00	0.00	0.60	1.00
8.67_457.1133	0.00	0.00	0.66	1.00
6.21_455.1906	0.00	0.16	0.86	1.00
9.81_454.0847	0.00	0.00	0.78	1.00
9.05_454.0819	0.00	0.00	0.57	1.00
6.42_472.2832	0.00	0.00	0.75	1.00
6.46_471.2466	0.00	0.01	0.64	1.00
10.02_470.0758	0.00	0.00	0.62	1.00
9.02_468.1011	0.00	0.00	0.58	1.00
9.08_467.0388	0.00	0.00	0.79	1.00
8.31_465.0807	0.00	0.00	0.70	1.00
8.82_465.0807	0.00	0.00	0.67	1.00
9.79_462.0710	0.00	0.00	0.72	1.00
9.04_462.0699	0.00	0.00	0.61	1.00
7.03_483.0939	0.00	0.00	0.72	1.00
9.78_481.0499	0.00	0.00	1.00	0.75
9.02_479.0963	0.00	0.00	0.62	1.00
10.01_478.0692	0.00	0.00	0.53	1.00
4.15_476.2404	0.00	0.00	0.56	1.00
9.02_476.0877	0.00	0.00	0.55	1.00
7.06_475.1057	0.00	0.00	0.61	1.00
9.02_495.0687	0.00	0.00	0.70	1.00
4.37_494.2617	0.00	0.00	0.68	1.00
5.37_493.1709	0.00	0.00	1.00	0.69
9.79_513.1525	0.00	0.00	0.48	1.00
5.64_515.2738	0.00	0.01	0.65	1.00
1.76_515.1445	0.00	0.00	0.74	1.00
10.06_526.3139	0.00	0.00	1.00	0.54
7.21_526.2839	0.00	0.06	0.58	1.00
7.20_544.2918	0.00	0.00	0.61	1.00
9.00_540.1495	0.00	0.00	0.63	1.00
6.63_570.3104	0.00	0.00	0.91	1.00

9.67_563.3802	0.00	0.00	0.59	1.00
9.08_562.5875	0.00	0.00	0.62	1.00
7.14_560.1805	0.00	0.00	0.64	1.00
6.90_555.3068	0.00	0.00	0.53	1.00
1.72_551.1035	0.00	0.00	0.96	1.00
5.52_601.2501	0.00	0.00	0.73	1.00
9.02_590.6205	0.00	0.00	0.63	1.00
9.79_576.6021	0.00	0.00	1.00	0.60
9.06_576.6005	0.00	0.00	0.60	1.00
1.25_639.8836	0.00	0.00	0.63	1.00
9.07_662.0928	0.00	0.00	0.48	1.00
9.02_704.1451	0.00	0.00	0.54	1.00
9.03_696.1548	0.00	0.00	0.49	1.00
9.71_694.1152	0.00	0.00	0.66	1.00
9.03_690.1259	0.00	0.00	0.54	1.00
9.79_683.1204	0.00	0.00	1.00	0.68
9.06_676.1101	0.00	0.00	0.53	1.00
9.41_675.1324	0.00	0.00	0.54	1.00
9.78_885.1896	0.00	0.00	0.47	1.00
9.07_879.1306	0.00	0.00	0.69	1.00
7.69_868.6024	0.00	0.00	1.00	0.57
9.02_935.1961	0.00	0.00	0.53	1.00
7.21_916.0943	0.00	0.00	1.00	0.78
9.80_907.1678	0.00	0.00	0.82	1.00
9.04_907.1662	0.00	0.00	0.51	1.00
9.41_904.1590	0.00	0.00	0.53	1.00
7.67_1031.2480	0.00	0.14	0.97	1.00
7.69_1031.1674	0.00	0.10	1.00	0.91
7.67_1031.0798	0.00	0.00	0.91	1.00
7.69_1000.1273	0.00	0.00	0.49	1.00
7.65_1000.0444	0.00	0.00	0.92	1.00
7.63_942.9948	0.00	0.00	1.00	0.90
7.01_1221.4414	0.00	0.00	0.55	1.00
9.41_1125.2062	0.00	0.00	0.48	1.00
9.78_465.0808	0.00	0.00	0.87	1.00
9.79_1349.2480	0.00	0.00	0.51	1.00
6.06_294.2084	0.00	0.00	0.59	1.00
9.81_269.0437	0.00	0.00	0.61	1.00
8.34_150.0928	0.00	0.07	0.56	1.00
6.65_282.2073	0.01	0.04	0.76	1.00
6.76_310.2021	0.01	0.00	1.00	0.90
8.74_542.3146	0.01	0.00	1.00	0.73
1.75_507.1572	0.01	0.00	0.69	1.00
1.29_203.9309	0.01	0.00	0.50	1.00
5.66_384.2168	0.01	0.00	0.71	1.00
1.64_246.1172	0.02	0.00	0.74	1.00
7.48_177.0877	0.02	0.00	0.60	1.00
1.64_174.0879	0.02	0.01	1.00	0.56
6.66_264.1980	0.03	0.01	0.63	1.00
8.10_301.1534	0.03	0.11	0.90	1.00
5.43_377.1482	0.03	0.00	0.68	1.00
16.15_710.1773	0.04	0.01	0.70	1.00
9.14_239.1284	0.04	0.04	0.59	1.00
6.24_515.2753	0.04	0.02	0.84	1.00
9.66_279.1583	0.05	0.00	0.65	1.00
9.67_319.1539	0.05	0.06	0.64	1.00
1.74_150.0789	0.05	0.00	0.59	1.00
3.22_235.1201	0.05	0.00	1.00	0.67
6.95_368.2220	0.05	0.09	1.00	0.59
8.53_283.1523	0.05	0.12	0.85	1.00
8.29_401.1993	0.06	0.00	0.56	1.00
3.07_230.1126	0.06	0.14	0.82	1.00
4.75_136.0625	0.06	0.00	0.78	1.00
1.73_338.0231	0.06	0.00	0.84	1.00
1.70_260.1135	0.08	0.00	0.75	1.00

8.53_207.1002	0.09	0.11	0.81	1.00
6.95_218.1203	0.09	0.18	0.63	1.00
8.53_177.0880	0.09	0.09	0.84	1.00
7.25_371.1508	0.09	0.00	0.67	1.00
9.41_281.1770	0.10	0.19	0.65	1.00
10.52_673.3745	0.12	0.19	0.63	1.00
10.18_621.4210	0.13	0.00	0.59	1.00
3.86_150.0940	0.14	0.25	0.68	1.00
3.83_198.1623	0.14	0.10	0.57	1.00
1.77_218.1042	0.14	0.03	0.70	1.00
3.80_288.1929	0.15	0.13	1.00	0.77
6.41_165.0905	0.17	0.11	0.78	1.00
3.86_338.1113	0.19	0.00	0.65	1.00
4.31_265.0552	0.19	0.00	0.80	1.00
1.65_159.0768	0.21	0.00	1.00	0.65
1.73_288.1454	0.21	0.00	0.85	1.00
5.97_286.6247	0.22	0.04	1.00	0.66
4.30_478.1379	0.22	0.05	0.76	1.00
3.85_276.1433	0.22	0.13	0.58	1.00
4.87_329.1844	0.23	0.00	0.80	1.00
7.91_389.2523	0.23	0.10	0.63	1.00
7.89_192.1015	0.23	0.40	0.74	1.00
6.72_1450.6973	0.25	0.06	0.68	1.00
3.76_347.1589	0.28	0.00	0.76	1.00
16.18_335.9929	0.29	0.00	0.69	1.00
1.60_229.1318	0.29	0.06	0.78	1.00
4.30_310.1305	0.29	0.06	0.71	1.00
5.97_278.6345	0.30	0.08	1.00	0.95
9.11_505.3321	0.33	0.00	0.70	1.00
9.47_211.0868	0.34	0.59	1.00	0.98
3.82_230.1126	0.34	0.22	1.00	0.80
4.00_320.1711	0.43	0.05	0.99	1.00
5.11_307.1591	0.44	0.00	1.00	0.92
4.81_464.2611	0.44	0.52	1.00	0.80
4.86_372.1909	0.49	0.25	0.81	1.00
10.60_346.3091	0.51	1.00	0.00	0.00
10.40_371.3275	0.52	1.00	0.00	0.00
10.70_288.2557	0.52	1.00	0.00	0.00
4.64_137.0376	0.53	0.55	0.84	1.00
9.48_225.1993	0.53	1.00	0.01	0.02
7.06_203.1787	0.53	1.00	0.01	0.00
4.26_669.2631	0.56	1.00	0.00	0.00
11.80_235.1712	0.56	1.00	0.00	0.04
10.15_739.4618	0.56	1.00	0.06	0.05
14.41_309.2409	0.56	1.00	0.14	0.13
10.53_531.4000	0.57	1.00	0.00	0.00
12.97_407.3144	0.58	1.00	0.20	0.09
12.98_399.3242	0.58	1.00	0.19	0.09
4.09_573.1785	0.58	1.00	0.00	0.00
4.37_663.2850	0.59	1.00	0.01	0.00
5.45_144.0814	0.60	1.00	0.13	0.21
13.98_433.3418	0.61	1.00	0.02	0.01
4.64_412.2067	0.62	1.00	0.08	0.10
6.19_181.1351	0.63	1.00	0.09	0.11
10.97_401.2525	0.63	1.00	0.00	0.00
11.58_415.2745	0.65	1.00	0.00	0.00
12.62_273.1378	0.66	1.00	0.00	0.00
12.86_507.3281	0.66	1.00	0.37	0.22
4.27_647.2871	0.67	1.00	0.00	0.01
12.82_551.3593	0.67	1.00	0.38	0.32
11.44_223.2060	0.67	1.00	0.00	0.00
8.08_219.1411	0.68	1.00	0.00	0.00
12.56_441.2657	0.70	1.00	0.24	0.35
6.85_824.9348	0.70	1.00	0.00	0.00
4.81_506.2950	0.71	1.00	0.24	0.26

16.15_442.8736	0.71	1.00	0.00	0.00
7.07_184.1710	0.72	1.00	0.00	0.00
4.37_150.0945	0.72	1.00	0.00	0.00
12.79_595.3829	0.73	1.00	0.46	0.37
12.67_727.4605	0.74	1.00	0.22	0.33
11.18_473.3585	0.75	1.00	0.04	0.01
4.34_266.1408	0.75	0.59	0.98	1.00
12.70_683.4373	0.77	1.00	0.48	0.36
12.86_463.2998	0.77	1.00	0.48	0.31
12.74_443.3505	0.77	1.00	0.00	0.00
12.97_547.4060	0.77	1.00	0.38	0.19
13.86_425.2896	0.78	1.00	0.30	0.28
5.26_147.0936	0.79	1.00	0.25	0.37
12.61_771.4862	0.80	1.00	0.47	0.38
11.97_299.2600	0.80	1.00	0.00	0.00
12.86_502.3745	0.82	1.00	0.34	0.33
11.84_443.3878	0.82	1.00	0.09	0.05
11.03_354.1608	0.82	1.00	0.00	0.04
11.28_440.3462	0.82	1.00	0.00	0.00
12.98_282.2118	0.82	1.00	0.14	0.03
12.73_655.3845	0.83	1.00	0.56	0.44
12.74_639.4067	0.83	1.00	0.51	0.39
13.79_365.2675	0.84	1.00	0.05	0.00
12.80_567.3292	0.85	1.00	0.55	0.36
12.83_546.4021	0.86	1.00	0.00	0.24
5.16_237.1592	0.87	1.00	0.21	0.29
10.38_401.3397	0.88	1.00	0.50	0.32
9.26_219.1735	0.88	1.00	0.00	0.00
12.67_743.4367	0.88	1.00	0.54	0.53
4.50_359.1197	0.89	1.00	0.00	0.00
14.79_310.3109	0.90	1.00	0.51	0.53
12.78_611.3565	0.91	1.00	0.63	0.53
15.94_338.3442	0.91	1.00	0.32	0.34
13.49_295.2258	0.91	1.00	0.08	0.03
1.47_508.0657	0.91	1.00	0.60	0.39
1.50_260.0296	0.92	1.00	0.58	0.26
1.47_748.1127	0.94	1.00	0.76	0.59
4.29_244.1199	0.97	1.00	0.42	0.49
4.49_225.1597	0.97	1.00	0.49	0.50
12.89_441.3208	0.99	1.00	0.40	0.25
12.78_590.4295	1.00	1.00	0.40	0.33
13.95_270.2746	1.00	1.00	0.31	0.41
3.99_164.0936	1.00	0.90	0.41	0.45
10.36_211.6353	1.00	0.89	0.60	0.50
11.31_225.6512	1.00	0.95	0.26	0.18
9.27_240.2315	1.00	0.88	0.00	0.11
4.59_251.1399	1.00	0.99	0.81	0.84
10.39_268.2627	1.00	0.83	0.00	0.00
11.44_291.1951	1.00	0.75	0.00	0.00
11.33_299.2599	1.00	0.77	0.00	0.00
12.62_313.2746	1.00	0.83	0.00	0.00
14.31_325.2414	1.00	0.74	0.00	0.00
14.82_332.2940	1.00	0.65	0.00	0.20
4.25_343.1235	1.00	0.70	0.01	0.00
15.49_338.3442	1.00	0.86	0.00	0.03
4.42_351.1212	1.00	0.79	0.09	0.14
4.39_362.1069	1.00	0.88	0.00	0.08
15.92_360.3229	1.00	0.71	0.22	0.13
13.48_397.3392	1.00	0.75	0.00	0.01
10.78_415.3581	1.00	0.61	0.36	0.19
13.95_411.3586	1.00	0.78	0.00	0.00
13.27_419.3131	1.00	0.81	0.00	0.00
12.86_485.3471	1.00	0.86	0.31	0.23
1.45_519.0543	1.00	0.72	0.41	0.18
12.81_529.3766	1.00	0.77	0.31	0.19

12.97_555.3910	1.00	0.94	0.56	0.33
12.79_573.4039	1.00	0.73	0.29	0.21
12.75_617.4294	1.00	0.84	0.00	0.25
13.92_641.5490	1.00	0.85	0.00	0.00
4.37_685.2548	1.00	0.86	0.00	0.00
12.67_705.4810	1.00	0.93	0.15	0.26
6.87_807.0837	1.00	0.57	0.08	0.00

Table A3.14. Normalized heat map of features described as unique in **Figure 3.2(B)** and **(C)** when comparing wild type *Nocardiopsis sp. FU40 ΔApoS8* to the R5 rifampicin resistant mutant extract using OPLS-DA and extracting features from the generated S-plot with correlation coefficients ≥0.9. Features are normalized to maximum intensity for that feature.

Feature ID (RT_*m/z*)	WT	WT	R5	R5
12.03_135.1163	0.00	0.07	1.00	0.65
12.03_123.1165	0.00	0.00	1.00	0.99
1.50_103.5345	0.00	0.00	1.00	0.70
6.56_162.0938	0.00	0.00	1.00	0.88
16.16_174.0876	0.00	0.00	0.70	1.00
5.78_170.1204	0.00	0.00	1.00	0.77
7.08_169.0882	0.00	0.02	1.00	0.84
6.60_180.1017	0.00	0.01	0.84	1.00
5.02_180.1014	0.00	0.00	1.00	0.74
4.95_177.1399	0.00	0.21	0.98	1.00
4.39_192.1130	0.00	0.14	1.00	0.80
9.12_191.0134	0.00	0.00	0.93	1.00
4.14_186.1168	0.00	0.00	1.00	0.54
9.08_196.0187	0.00	0.00	1.00	0.74
8.84_203.1804	0.00	0.00	1.00	0.91
8.12_203.1781	0.00	0.00	0.96	1.00
9.08_203.0278	0.00	0.00	0.99	1.00
9.80_203.0277	0.00	0.00	1.00	0.84
9.42_202.0393	0.00	0.00	1.00	0.83
5.44_208.0539	0.00	0.01	0.66	1.00
7.49_207.0994	0.00	0.05	1.00	0.74
1.30_205.9283	0.00	0.00	1.00	0.91
4.84_205.1323	0.00	0.00	1.00	0.96
1.32_211.8786	0.00	0.00	0.81	1.00
1.49_211.0584	0.00	0.15	0.98	1.00
9.81_210.0363	0.00	0.00	1.00	0.85
9.07_210.0305	0.00	0.00	1.00	0.67
9.41_219.0312	0.00	0.00	0.67	1.00
3.69_218.1136	0.00	0.32	1.00	0.78
8.84_221.1903	0.00	0.00	1.00	0.98
7.35_225.1140	0.00	0.00	0.67	1.00
7.99_225.1125	0.00	0.03	1.00	0.60
7.49_230.0712	0.00	0.00	0.82	1.00
5.48_229.0656	0.00	0.00	1.00	0.91
9.82_230.0718	0.00	0.09	1.00	0.74
5.11_236.1306	0.00	0.13	1.00	0.67
4.89_235.1441	0.00	0.00	1.00	0.71
8.54_235.1344	0.00	0.00	0.83	1.00
4.13_237.1268	0.00	0.17	1.00	0.82
7.33_247.0943	0.00	0.25	1.00	0.90
5.04_244.1219	0.00	0.00	1.00	0.62
4.31_249.0807	0.00	0.00	0.96	1.00
8.08_252.0397	0.00	0.00	1.00	0.86
4.56_252.0394	0.00	0.21	0.86	1.00
6.01_252.0391	0.00	0.00	1.00	0.87
5.12_252.0389	0.00	0.00	0.90	1.00
7.48_252.0388	0.00	0.00	1.00	0.91
6.23_258.1449	0.00	0.00	1.00	0.57
12.02_263.1978	0.00	0.03	1.00	0.93
1.78_262.1278	0.00	0.00	0.63	1.00
5.86_262.1048	0.00	0.17	1.00	0.77
5.01_261.1438	0.00	0.03	0.85	1.00
7.18_278.2110	0.00	0.00	1.00	0.75
6.07_276.1943	0.00	0.00	0.85	1.00
7.50_283.1523	0.00	0.03	0.83	1.00
7.72_281.1420	0.00	0.00	0.90	1.00

5.22_295.1312	0.00	0.01	0.56	1.00
7.48_294.2085	0.00	0.00	0.58	1.00
7.82_294.2085	0.00	0.00	1.00	1.00
1.50_294.0959	0.00	0.44	1.00	0.85
7.15_293.2251	0.00	0.00	1.00	0.51
4.87_293.1612	0.00	0.19	0.73	1.00
7.73_298.2024	0.00	0.00	0.75	1.00
7.19_296.2224	0.00	0.00	1.00	0.93
5.83_303.1558	0.00	0.01	1.00	0.88
7.70_303.1206	0.00	0.09	1.00	0.65
3.78_300.1386	0.00	0.03	1.00	0.51
12.02_309.1921	0.00	0.01	0.89	1.00
6.00_308.2238	0.00	0.00	1.00	0.86
6.84_312.2197	0.00	0.00	1.00	0.97
7.24_312.2197	0.00	0.00	1.00	0.93
7.47_310.2026	0.00	0.00	0.99	1.00
1.74_322.0446	0.00	0.03	0.56	1.00
6.92_318.2094	0.00	0.00	0.58	1.00
7.34_326.2353	0.00	0.00	0.84	1.00
6.01_326.2353	0.00	0.00	0.99	1.00
12.03_325.1706	0.00	0.00	1.00	0.93
6.08_324.1828	0.00	0.31	0.99	1.00
5.99_338.1374	0.00	0.00	0.92	1.00
6.07_337.1394	0.00	0.03	0.55	1.00
10.06_348.2310	0.00	0.00	0.79	1.00
5.19_344.6196	0.00	0.23	0.89	1.00
6.06_359.1205	0.00	0.00	0.98	1.00
5.26_354.0787	0.00	0.13	0.78	1.00
8.24_352.2057	0.00	0.00	0.92	1.00
4.01_351.5992	0.00	0.00	0.64	1.00
6.51_360.2165	0.00	0.00	0.56	1.00
8.77_368.2219	0.00	0.00	0.60	1.00
7.52_368.2211	0.00	0.00	1.00	0.74
7.83_387.1861	0.00	0.00	1.00	0.55
6.88_386.2329	0.00	0.02	0.60	1.00
6.89_384.2172	0.00	0.01	1.00	0.84
6.24_384.2171	0.00	0.00	1.00	0.64
1.49_394.1142	0.00	0.00	1.00	0.99
3.74_416.1928	0.00	0.01	1.00	0.70
3.75_414.2692	0.00	0.00	1.00	0.76
8.66_429.0854	0.00	0.00	0.93	1.00
9.08_429.0845	0.00	0.00	0.52	1.00
9.07_451.0615	0.00	0.00	1.00	0.76
9.09_448.0576	0.00	0.00	1.00	0.77
9.73_443.1014	0.00	0.00	0.77	1.00
8.33_443.0954	0.00	0.00	0.81	1.00
5.90_459.3212	0.00	0.02	0.69	1.00
9.03_457.1145	0.00	0.01	0.76	1.00
8.67_457.1133	0.00	0.00	1.00	0.97
11.52_456.3791	0.00	0.00	0.86	1.00
6.21_455.1906	0.00	0.11	1.00	0.75
9.81_454.0847	0.00	0.00	0.67	1.00
9.05_454.0819	0.00	0.00	0.79	1.00
6.42_472.2832	0.00	0.00	1.00	0.67
9.08_467.0388	0.00	0.00	0.94	1.00
8.82_465.0807	0.00	0.00	1.00	0.90
9.79_462.0710	0.00	0.00	0.79	1.00
9.04_462.0699	0.00	0.00	1.00	0.86
9.78_481.0499	0.00	0.00	1.00	1.00
4.15_476.2404	0.00	0.00	1.00	0.57
7.51_499.2782	0.00	0.02	0.93	1.00
5.37_493.1709	0.00	0.00	1.00	0.81
6.65_512.8485	0.00	0.00	1.00	0.82
5.65_504.2609	0.00	0.00	1.00	0.90
5.64_515.2738	0.00	0.03	1.00	1.00
1.76_515.1445	0.00	0.00	1.00	0.96
10.06_526.3139	0.00	0.00	0.60	1.00
7.21_526.2839	0.00	0.06	1.00	0.82
6.79_549.3505	0.00	0.00	1.00	0.52
7.20_544.2918	0.00	0.00	0.56	1.00

7.57_542.3960	0.00	0.01	1.00	0.67
6.63_570.3104	0.00	0.00	1.00	0.87
12.03_565.3746	0.00	0.00	1.00	0.87
9.67_563.3802	0.00	0.00	1.00	0.88
6.90_555.3068	0.00	0.00	0.84	1.00
5.52_601.2501	0.00	0.00	1.00	0.77
9.79_576.6021	0.00	0.00	0.51	1.00
9.06_576.6005	0.00	0.00	0.51	1.00
1.25_639.8836	0.00	0.00	1.00	0.75
6.02_637.3187	0.00	0.00	1.00	0.97
5.79_646.1977	0.00	0.00	0.82	1.00
9.79_683.1204	0.00	0.00	0.81	1.00
9.80_907.1678	0.00	0.00	0.84	1.00
7.01_1221.4414	0.00	0.00	0.65	1.00
7.00_1216.1209	0.00	0.37	0.79	1.00
9.79_218.0234	0.00	0.02	0.98	1.00
8.34_150.0928	0.00	0.04	0.66	1.00
9.78_465.0808	0.00	0.01	1.00	0.94
6.76_310.2021	0.01	0.00	1.00	0.98
7.48_177.0877	0.01	0.00	1.00	0.72
8.10_301.1534	0.01	0.03	1.00	0.87
1.75_507.1572	0.01	0.00	0.61	1.00
1.82_228.1004	0.01	0.00	0.88	1.00
6.06_294.2084	0.02	0.00	1.00	0.70
6.24_515.2753	0.02	0.01	0.83	1.00
8.74_542.3146	0.02	0.00	0.73	1.00
7.06_325.1861	0.02	0.14	1.00	0.86
6.65_282.2073	0.03	0.15	1.00	0.69
5.43_377.1482	0.03	0.00	1.00	0.87
8.29_401.1993	0.03	0.00	0.83	1.00
1.64_174.0879	0.03	0.02	0.97	1.00
4.75_136.0625	0.03	0.00	1.00	0.69
9.66_279.1583	0.04	0.00	1.00	0.61
1.53_143.0837	0.04	0.05	1.00	0.81
5.66_384.2168	0.04	0.00	1.00	0.86
6.95_218.1203	0.04	0.09	0.92	1.00
3.22_235.1201	0.05	0.00	1.00	0.97
1.73_338.0231	0.05	0.00	1.00	0.76
7.06_221.1900	0.06	0.17	0.71	1.00
7.42_280.1237	0.06	0.16	0.65	1.00
8.53_283.1523	0.06	0.13	0.91	1.00
3.86_150.0940	0.06	0.11	1.00	0.97
6.66_264.1980	0.06	0.03	1.00	0.75
8.53_177.0880	0.06	0.06	1.00	0.58
7.80_291.1290	0.06	0.23	1.00	0.93
10.52_673.3745	0.07	0.10	0.94	1.00
8.53_207.1002	0.07	0.08	1.00	0.70
3.75_289.1389	0.07	0.31	1.00	0.93
9.67_319.1539	0.07	0.10	0.74	1.00
1.77_218.1042	0.07	0.02	1.00	0.92
3.83_198.1623	0.08	0.06	0.84	1.00
4.88_188.0708	0.08	0.14	1.00	0.91
7.06_203.1787	0.08	0.15	1.00	0.89
4.37_326.1802	0.08	0.50	1.00	0.91
6.72_1450.6973	0.09	0.02	1.00	0.94
6.06_203.1781	0.10	0.18	1.00	0.98
4.30_310.1305	0.11	0.02	1.00	0.55
4.87_329.1844	0.12	0.00	1.00	0.85
6.41_165.0905	0.14	0.09	1.00	0.83
9.47_211.0868	0.15	0.25	1.00	0.91
9.14_239.1284	0.16	0.15	1.00	0.77
5.27_685.1761	0.17	0.00	1.00	0.82
5.83_325.1311	0.17	0.00	1.00	0.98
4.26_450.2439	0.19	0.01	0.78	1.00
1.65_159.0768	0.19	0.00	0.78	1.00
7.89_192.1015	0.20	0.35	1.00	0.96
16.18_335.9929	0.22	0.00	0.93	1.00
4.30_284.1098	0.24	0.07	1.00	0.94
5.20_239.1759	0.24	0.39	1.00	0.97
3.85_258.1333	0.24	0.00	1.00	0.62

4.86_372.1909	0.25	0.13	1.00	0.74
6.60_152.1087	0.25	0.46	1.00	0.93
4.63_149.1104	0.26	0.41	1.00	0.94
5.34_191.1575	0.26	0.37	1.00	0.71
5.19_249.1604	0.27	0.43	1.00	0.87
1.73_288.1454	0.27	0.00	1.00	0.81
4.00_320.1711	0.28	0.03	1.00	0.79
3.80_194.0821	0.29	0.00	1.00	0.95
9.41_281.1770	0.29	0.54	0.95	1.00
7.15_504.8508	0.30	0.59	1.00	0.91
16.22_252.0441	0.30	0.53	1.00	0.96
6.74_1160.9454	0.31	0.26	0.83	1.00
4.34_266.1408	0.31	0.24	1.00	0.72
5.00_152.1079	0.33	0.50	1.00	0.84
6.78_176.0714	0.33	0.56	1.00	0.97
6.62_297.1617	0.33	0.59	1.00	0.88
5.16_237.1592	0.33	0.38	1.00	0.79
16.15_365.1085	0.34	0.00	1.00	0.82
3.82_230.1126	0.34	0.21	1.00	0.74
8.22_220.1332	0.34	0.49	0.95	1.00
4.53_236.1764	0.34	0.44	1.00	0.95
5.78_164.0706	0.34	0.46	0.98	1.00
4.77_179.0472	0.34	0.62	1.00	1.00
4.64_137.0376	0.35	0.36	0.95	1.00
4.40_158.0302	0.36	0.27	1.00	0.94
5.71_249.1598	0.38	0.52	1.00	0.89
6.15_485.2027	0.38	0.41	1.00	0.84
5.81_605.2195	0.39	0.55	1.00	0.88
4.70_221.1315	0.39	0.58	0.99	1.00
3.81_136.0628	0.40	0.64	1.00	0.86
4.16_256.1718	0.40	0.55	1.00	0.87
4.66_304.1776	0.42	0.62	1.00	0.90
5.16_210.1137	0.43	0.42	1.00	0.82
16.17_188.9130	0.43	0.00	1.00	0.88
16.18_204.8884	0.44	0.00	0.99	1.00
4.67_270.1917	0.44	0.60	1.00	0.97
3.94_254.1629	0.45	0.17	1.00	0.90
6.34_469.2088	0.49	0.63	1.00	0.87
4.39_362.1069	0.49	0.43	0.99	1.00
6.23_251.1781	0.49	0.54	1.00	0.87
12.43_386.2820	0.50	1.00	0.00	0.00
14.78_323.2583	0.50	1.00	0.00	0.00
13.49_420.3478	0.51	1.00	0.00	0.00
10.60_346.3091	0.51	1.00	0.00	0.00
13.00_413.3095	0.52	1.00	0.00	0.00
10.40_371.3275	0.52	1.00	0.00	0.03
10.70_288.2557	0.52	1.00	0.00	0.00
9.48_225.1993	0.53	1.00	0.00	0.02
6.81_807.1918	0.54	1.00	0.00	0.00
13.53_339.2529	0.55	1.00	0.00	0.00
4.26_669.2631	0.56	1.00	0.00	0.13
11.80_235.1712	0.56	1.00	0.06	0.07
10.15_739.4618	0.56	1.00	0.06	0.04
14.41_309.2409	0.56	1.00	0.00	0.00
12.99_526.2341	0.56	1.00	0.00	0.06
10.53_531.4000	0.57	1.00	0.00	0.00
4.81_415.2090	0.57	0.40	1.00	0.89
12.97_407.3144	0.58	1.00	0.00	0.00
6.02_274.1066	0.58	0.40	1.00	0.86
12.98_399.3242	0.58	1.00	0.00	0.00
4.09_573.1785	0.58	1.00	0.00	0.00
12.98_510.2581	0.59	1.00	0.00	0.11
4.37_663.2850	0.59	1.00	0.00	0.20
4.59_251.1399	0.60	0.60	1.00	0.90
13.98_433.3418	0.61	1.00	0.00	0.00
6.90_166.0720	0.61	1.00	0.00	0.00
4.64_412.2067	0.62	1.00	0.00	0.16
6.19_181.1351	0.63	1.00	0.00	0.07
10.97_401.2525	0.63	1.00	0.08	0.08
16.14_274.0340	0.63	0.45	1.00	0.97

370

11.58_415.2745	0.65	1.00	0.00	0.00
12.62_273.1378	0.66	1.00	0.00	0.00
12.86_507.3281	0.66	1.00	0.21	0.02
12.97_290.7254	0.66	1.00	0.00	0.00
4.27_647.2871	0.67	1.00	0.00	0.14
11.44_223.2060	0.67	1.00	0.00	0.00
8.08_219.1411	0.68	1.00	0.22	0.18
4.44_178.1088	0.70	0.60	0.99	1.00
6.85_824.9348	0.70	1.00	0.00	0.00
4.37_150.0945	0.72	1.00	0.00	0.00
3.89_518.1743	0.73	1.00	0.00	0.00
11.18_473.3585	0.75	1.00	0.00	0.03
12.86_463.2998	0.77	1.00	0.00	0.08
12.74_443.3505	0.77	1.00	0.00	0.01
12.97_547.4060	0.77	1.00	0.00	0.00
13.86_425.2896	0.78	1.00	0.48	0.46
13.50_409.7445	0.80	1.00	0.00	0.04
4.28_227.1066	0.80	1.00	0.41	0.47
12.61_771.4862	0.80	1.00	0.00	0.37
11.97_299.2600	0.80	1.00	0.03	0.00
13.50_524.2740	0.81	1.00	0.01	0.10
15.06_413.2647	0.81	1.00	0.42	0.42
12.86_502.3745	0.82	1.00	0.36	0.00
11.84_443.3878	0.82	1.00	0.06	0.06
11.03_354.1608	0.82	1.00	0.00	0.03
11.28_440.3462	0.82	1.00	0.00	0.00
12.98_282.2118	0.82	1.00	0.00	0.00
13.79_365.2675	0.84	1.00	0.00	0.00
12.80_567.3292	0.85	1.00	0.00	0.00
10.38_401.3397	0.88	1.00	0.29	0.27
14.79_310.3109	0.90	1.00	0.18	0.00
12.78_611.3565	0.91	1.00	0.21	0.57
13.48_341.2200	0.91	1.00	0.00	0.20
13.49_295.2258	0.91	1.00	0.00	0.00
1.50_260.0296	0.92	1.00	0.30	0.47
4.49_225.1597	0.97	1.00	0.51	0.49
12.89_441.3208	0.99	1.00	0.46	0.31
12.78_590.4295	1.00	1.00	0.25	0.00
3.99_164.0936	1.00	0.90	0.58	0.61
10.36_211.6353	1.00	0.89	0.00	0.34
11.31_225.6512	1.00	0.95	0.00	0.00
5.40_230.0720	1.00	0.81	0.58	0.47
9.27_240.2315	1.00	0.88	0.25	0.00
10.39_268.2627	1.00	0.83	0.00	0.00
12.97_278.2028	1.00	0.62	0.00	0.04
11.44_291.1951	1.00	0.75	0.00	0.00
11.33_299.2599	1.00	0.77	0.00	0.00
12.62_313.2746	1.00	0.83	0.00	0.00
14.31_325.2414	1.00	0.74	0.00	0.00
14.82_332.2940	1.00	0.65	0.27	0.10
15.49_338.3442	1.00	0.86	0.00	0.03
15.92_360.3229	1.00	0.71	0.37	0.20
13.48_397.3392	1.00	0.75	0.00	0.00
10.78_415.3581	1.00	0.61	0.20	0.19
13.95_411.3586	1.00	0.78	0.00	0.00
13.27_419.3131	1.00	0.81	0.00	0.00
10.77_434.3251	1.00	0.58	0.00	0.16
10.98_442.3651	1.00	0.78	0.00	0.00
12.86_485.3471	1.00	0.86	0.19	0.41
12.81_529.3766	1.00	0.77	0.00	0.31
12.97_555.3910	1.00	0.94	0.00	0.00
12.75_617.4294	1.00	0.84	0.20	0.41
13.92_641.5490	1.00	0.85	0.00	0.00
12.67_705.4810	1.00	0.93	0.15	0.50
6.87_807.0837	1.00	0.57	0.19	0.00

Table A3.15. Normalized heat map of features described as unique in **Figure 3.2(B)** and **(C)** when comparing wild type *Nocardiopsis sp. FU40 ΔApoS8* to the S1 streptomycin resistant mutant extract using OPLS-DA and extracting features from the generated S-plot with correlation coefficients ≥0.9. Features are normalized to maximum intensity for that feature.

Feature ID (RT_*m/z*)	WT	WT	S1	S1
12.03_135.1163	0.00	0.04	0.67	1.00
12.03_123.1165	0.00	0.00	0.66	1.00
4.95_114.0908	0.00	0.00	0.50	1.00
1.50_103.5345	0.00	0.00	0.76	1.00
12.03_149.1327	0.00	0.00	0.66	1.00
13.61_149.0907	0.00	0.00	0.87	1.00
6.56_162.0938	0.00	0.00	1.00	0.94
5.78_170.1204	0.00	0.00	0.73	1.00
4.29_169.0959	0.00	0.00	1.00	0.76
2.44_166.0747	0.00	0.13	0.99	1.00
6.60_180.1017	0.00	0.03	0.85	1.00
9.12_191.0134	0.00	0.00	0.60	1.00
4.14_186.1168	0.00	0.00	1.00	0.79
4.02_198.1143	0.00	0.00	0.72	1.00
8.84_203.1804	0.00	0.00	0.69	1.00
6.22_203.0786	0.00	0.03	0.84	1.00
7.49_207.0994	0.00	0.08	0.88	1.00
1.30_205.9283	0.00	0.00	0.73	1.00
4.84_205.1323	0.00	0.00	0.53	1.00
10.22_205.1232	0.00	0.00	0.91	1.00
1.32_211.8786	0.00	0.00	0.85	1.00
9.81_210.0363	0.00	0.00	0.51	1.00
9.03_217.0413	0.00	0.00	1.00	0.82
16.16_223.9875	0.00	0.00	0.92	1.00
10.24_222.1533	0.00	0.06	0.72	1.00
8.84_221.1903	0.00	0.00	0.78	1.00
5.48_229.0656	0.00	0.00	0.78	1.00
5.11_236.1306	0.00	0.14	0.83	1.00
8.54_235.1344	0.00	0.00	0.81	1.00
11.28_233.1548	0.00	0.01	0.51	1.00
11.16_252.0381	0.00	0.00	0.52	1.00
13.78_251.2405	0.00	0.00	0.96	1.00
11.26_250.1814	0.00	0.00	0.78	1.00
8.08_252.0397	0.00	0.00	1.00	0.65
4.56_252.0394	0.00	0.17	0.90	1.00
5.12_252.0389	0.00	0.00	0.91	1.00
7.48_252.0388	0.00	0.00	0.98	1.00
12.02_263.1978	0.00	0.03	0.71	1.00
5.86_262.1048	0.00	0.37	0.81	1.00
10.71_261.1779	0.00	0.01	0.72	1.00
11.95_266.1298	0.00	0.00	0.66	1.00
5.27_264.2082	0.00	0.00	1.00	0.99
7.50_283.1523	0.00	0.06	0.95	1.00
9.01_283.1521	0.00	0.09	0.88	1.00
1.73_282.0649	0.00	0.03	0.80	1.00
7.15_293.2251	0.00	0.00	0.75	1.00
4.87_293.1612	0.00	0.33	0.74	1.00
6.49_292.1923	0.00	0.14	1.00	0.82
3.78_300.1386	0.00	0.42	0.90	1.00
12.02_309.1921	0.00	0.01	0.61	1.00
14.29_307.2281	0.00	0.00	0.89	1.00
1.74_322.0446	0.00	0.03	0.45	1.00
14.63_321.2420	0.00	0.00	1.00	0.91
12.03_325.1706	0.00	0.00	0.66	1.00
13.85_333.2427	0.00	0.00	1.00	0.79
10.73_340.1475	0.00	0.10	0.81	1.00

14.63_339.2533	0.00	0.00	1.00	0.75
15.50_349.2615	0.00	0.00	1.00	0.89
14.31_347.2205	0.00	0.00	0.78	1.00
7.48_345.1875	0.00	0.00	1.00	0.94
4.01_351.5992	0.00	0.00	1.00	0.79
6.95_350.2147	0.00	0.02	1.00	1.00
12.59_361.1697	0.00	0.15	1.00	0.92
6.51_360.2165	0.00	0.00	0.52	1.00
7.52_368.2211	0.00	0.00	0.58	1.00
9.80_367.0822	0.00	0.00	0.51	1.00
14.32_379.2817	0.00	0.00	1.00	0.80
7.43_374.2181	0.00	0.00	0.76	1.00
6.24_384.2171	0.00	0.00	0.66	1.00
13.61_399.3201	0.00	0.00	1.00	0.94
1.49_394.1142	0.00	0.00	0.48	1.00
14.57_393.2988	0.00	0.00	1.00	0.89
14.04_420.3477	0.00	0.07	0.68	1.00
8.04_432.2606	0.00	0.00	1.00	0.83
9.03_457.1145	0.00	0.15	0.53	1.00
11.52_456.3791	0.00	0.00	0.46	1.00
6.21_455.1906	0.00	0.17	0.88	1.00
11.66_454.2954	0.00	0.23	1.00	0.89
9.81_454.0847	0.00	0.00	0.43	1.00
9.79_462.0710	0.00	0.00	0.51	1.00
9.78_481.0499	0.00	0.00	0.49	1.00
7.51_499.2782	0.00	0.06	0.86	1.00
4.37_494.2617	0.00	0.00	0.75	1.00
8.58_490.2972	0.00	0.00	0.67	1.00
12.00_515.2832	0.00	0.00	0.84	1.00
1.76_515.1445	0.00	0.00	0.63	1.00
9.11_548.3433	0.00	0.06	0.65	1.00
12.03_565.3746	0.00	0.00	0.77	1.00
6.90_555.3068	0.00	0.00	0.91	1.00
12.03_549.4012	0.00	0.00	0.74	1.00
9.02_549.3610	0.00	0.02	1.00	0.81
5.52_601.2501	0.00	0.00	0.82	1.00
7.20_920.0962	0.00	0.00	1.00	0.74
7.21_916.0943	0.00	0.00	1.00	0.92
7.01_1221.4414	0.00	0.00	1.00	0.93
8.34_150.0928	0.00	0.06	0.69	1.00
14.64_361.2361	0.01	0.00	1.00	0.90
7.48_177.0877	0.01	0.00	0.82	1.00
6.95_368.2220	0.01	0.02	0.86	1.00
8.10_301.1534	0.01	0.05	0.53	1.00
8.54_447.2904	0.02	0.13	0.57	1.00
3.22_235.1201	0.02	0.00	0.84	1.00
12.02_205.1953	0.02	0.00	0.72	1.00
10.18_621.4210	0.02	0.00	0.53	1.00
1.29_203.9309	0.02	0.00	0.65	1.00
13.79_365.2675	0.02	0.02	1.00	0.93
14.31_335.2563	0.03	0.00	1.00	0.60
11.43_466.2973	0.03	0.08	0.95	1.00
6.92_332.1986	0.03	0.01	1.00	0.97
6.24_515.2753	0.03	0.01	1.00	0.83
1.75_507.1572	0.04	0.00	0.92	1.00
9.11_505.3321	0.05	0.00	0.63	1.00
8.52_491.3179	0.06	0.00	0.63	1.00
1.74_150.0789	0.06	0.00	0.64	1.00
3.07_230.1126	0.06	0.15	0.84	1.00
13.79_531.4249	0.06	0.19	0.69	1.00
9.78_465.0808	0.06	0.18	0.55	1.00
1.73_338.0231	0.06	0.00	1.00	0.95
8.53_177.0880	0.07	0.06	0.73	1.00
10.52_673.3745	0.07	0.11	0.49	1.00
12.39_279.1366	0.07	0.19	0.99	1.00
3.86_150.0940	0.08	0.14	0.60	1.00
8.53_283.1523	0.08	0.17	1.00	0.96
8.53_207.1002	0.08	0.10	0.84	1.00
5.97_286.6247	0.09	0.01	0.94	1.00
7.95_433.2783	0.09	0.24	0.65	1.00

11.73_360.1653	0.10	0.23	0.78	1.00
6.95_218.1203	0.10	0.21	0.61	1.00
14.78_323.2583	0.11	0.21	1.00	0.83
11.33_299.2599	0.11	0.08	0.97	1.00
5.43_377.1482	0.11	0.00	0.63	1.00
12.40_251.2372	0.11	0.00	0.94	1.00
11.73_352.1729	0.11	0.48	1.00	1.00
11.97_299.2600	0.11	0.14	0.67	1.00
13.53_339.2529	0.12	0.21	1.00	0.85
1.82_228.1004	0.13	0.01	0.57	1.00
7.42_280.1237	0.13	0.36	0.64	1.00
7.89_192.1015	0.13	0.23	0.88	1.00
5.97_278.6345	0.14	0.03	1.00	0.88
6.41_165.0905	0.15	0.10	0.89	1.00
14.31_325.2414	0.16	0.12	1.00	0.87
7.91_389.2523	0.17	0.08	0.64	1.00
14.04_295.2283	0.17	0.32	1.00	0.95
4.87_329.1844	0.18	0.00	0.68	1.00
12.39_401.2333	0.19	0.47	1.00	0.96
12.62_313.2746	0.19	0.16	0.89	1.00
4.31_265.0552	0.20	0.00	0.73	1.00
7.06_203.1787	0.21	0.38	0.66	1.00
12.62_273.1378	0.21	0.32	0.83	1.00
6.06_203.1781	0.22	0.39	0.71	1.00
6.87_807.0837	0.22	0.13	1.00	0.80
9.69_220.1127	0.23	0.26	0.73	1.00
4.30_310.1305	0.23	0.05	0.75	1.00
4.75_136.0625	0.24	0.00	1.00	0.85
1.73_288.1454	0.24	0.00	0.71	1.00
3.82_230.1126	0.25	0.15	0.71	1.00
3.83_198.1623	0.25	0.18	0.77	1.00
14.41_309.2409	0.26	0.46	1.00	0.94
3.85_276.1433	0.28	0.16	0.76	1.00
5.96_534.2942	0.32	0.07	1.00	0.95
16.18_335.9929	0.33	0.00	0.68	1.00
4.88_188.0708	0.34	0.58	0.80	1.00
5.61_343.2002	0.35	0.08	0.67	1.00
13.84_397.2963	0.38	0.00	1.00	0.82
12.70_699.4109	0.39	0.43	0.78	1.00
12.62_787.4580	0.39	0.66	0.91	1.00
14.79_310.3109	0.41	0.46	1.00	0.78
12.78_611.3565	0.43	0.47	0.73	1.00
3.80_194.0821	0.43	0.00	0.97	1.00
12.86_523.3040	0.43	0.29	0.94	1.00
12.63_394.2284	0.47	0.36	1.00	0.93
12.67_743.4367	0.48	0.54	0.81	1.00
12.73_655.3845	0.48	0.58	0.85	1.00
13.50_409.7445	0.48	0.60	0.84	1.00
12.74_639.4067	0.48	0.58	0.77	1.00
15.06_413.2647	0.49	0.60	1.00	0.85
12.61_771.4862	0.49	0.62	0.80	1.00
6.15_485.2027	0.50	0.53	0.75	1.00
12.86_463.2998	0.50	0.66	1.00	0.99
10.60_346.3091	0.51	1.00	0.00	0.00
9.48_225.1993	0.53	1.00	0.02	0.02
5.18_364.0987	0.54	1.00	0.07	0.07
12.78_590.4295	0.55	0.56	0.90	1.00
4.26_669.2631	0.56	1.00	0.00	0.00
11.80_235.1712	0.56	1.00	0.00	0.05
3.80_119.0369	0.56	1.00	0.11	0.00
12.83_546.4021	0.58	0.67	0.85	1.00
1.28_188.9112	0.59	1.00	0.24	0.00
4.37_663.2850	0.59	1.00	0.01	0.00
13.92_641.5490	0.61	0.52	1.00	0.83
12.70_678.4764	0.61	0.35	0.93	1.00
6.90_166.0720	0.61	1.00	0.00	0.00
4.64_412.2067	0.62	1.00	0.00	0.11
5.19_249.1604	0.63	1.00	0.20	0.27
6.19_181.1351	0.63	1.00	0.03	0.00
6.39_336.2172	0.66	0.54	1.00	0.89

4.27_647.2871	0.67	1.00	0.00	0.00
11.44_223.2060	0.67	1.00	0.00	0.00
8.08_219.1411	0.68	1.00	0.00	0.10
1.28_172.9358	0.69	1.00	0.28	0.39
7.62_970.6124	0.70	1.00	0.10	0.00
4.81_506.2950	0.71	1.00	0.29	0.33
4.37_150.0945	0.72	1.00	0.00	0.00
3.89_518.1743	0.73	1.00	0.00	0.02
11.18_473.3585	0.75	1.00	0.29	0.35
12.89_441.3208	0.75	0.76	0.92	1.00
12.74_443.3505	0.77	1.00	0.00	0.03
4.28_227.1066	0.80	1.00	0.35	0.50
4.55_279.1361	0.81	1.00	0.47	0.53
11.28_440.3462	0.82	1.00	0.55	0.36
12.98_282.2118	0.82	1.00	0.21	0.15
4.27_302.2070	0.86	1.00	0.70	0.59
5.16_237.1592	0.87	1.00	0.36	0.32
9.26_219.1735	0.88	1.00	0.00	0.00
4.50_359.1197	0.89	1.00	0.00	0.00
10.84_227.1557	0.90	1.00	0.15	0.00
13.49_295.2258	0.91	1.00	0.22	0.18
1.47_508.0657	0.91	1.00	0.40	0.00
1.50_260.0296	0.92	1.00	0.05	0.14
1.47_748.1127	0.94	1.00	0.61	0.76
4.58_336.1924	0.95	1.00	0.76	0.57
1.48_481.1031	0.96	1.00	0.62	0.69
4.29_244.1199	0.97	1.00	0.28	0.00
4.49_225.1597	0.97	1.00	0.12	0.18
1.50_710.1736	0.99	1.00	0.73	0.82
13.95_270.2746	1.00	1.00	0.34	0.39
4.44_178.1088	1.00	0.86	0.33	0.50
3.80_288.1929	1.00	0.87	0.00	0.00
11.44_291.1951	1.00	0.75	0.00	0.00
4.25_343.1235	1.00	0.70	0.08	0.00
15.49_338.3442	1.00	0.86	0.00	0.00
4.26_356.1796	1.00	0.84	0.42	0.58
4.42_351.1212	1.00	0.79	0.18	0.20
4.39_362.1069	1.00	0.88	0.18	0.00
1.55_385.5441	1.00	0.65	0.12	0.00
13.95_411.3586	1.00	0.78	0.60	0.53
10.98_442.3651	1.00	0.78	0.12	0.33
4.37_685.2548	1.00	0.86	0.00	0.00
7.66_916.7249	1.00	0.76	0.00	0.00
7.00_916.3325	1.00	0.59	0.07	0.17
7.00_913.0933	1.00	0.71	0.00	0.10

Table A3.16. Normalized heat map of features described as unique in **Figure 3.2(B)** and **(C)** when comparing wild type *Nocardiopsis sp. FU40 ΔApoS8* to the S2 streptomycin resistant mutant extract using OPLS-DA and extracting features from the generated S-plot with correlation coefficients ≥0.9. Features are normalized to maximum intensity for that feature.

Feature ID (RT_*m/z*)	WT	WT	S2	S2
12.03_135.1163	0.00	0.07	1.00	0.69
12.03_123.1165	0.00	0.00	1.00	0.72
1.50_103.5345	0.00	0.00	1.00	0.81
12.03_149.1327	0.00	0.00	1.00	0.70
13.61_149.0907	0.00	0.00	0.76	1.00
1.50_165.0624	0.00	0.00	1.00	0.85
6.56_162.0938	0.00	0.00	0.58	1.00
2.01_158.0950	0.00	0.30	1.00	0.88
5.78_170.1204	0.00	0.00	1.00	0.91
4.29_169.0959	0.00	0.00	0.66	1.00
6.60_180.1017	0.00	0.02	0.99	1.00
5.02_180.1014	0.00	0.00	0.91	1.00
10.70_179.1435	0.00	0.00	1.00	0.66
4.95_177.1399	0.00	0.28	1.00	0.96
4.39_192.1130	0.00	0.30	1.00	0.94
9.12_191.0134	0.00	0.00	1.00	0.84
4.02_198.1143	0.00	0.00	0.95	1.00
4.99_198.1134	0.00	0.00	0.76	1.00
9.08_196.0187	0.00	0.00	0.55	1.00
8.84_203.1804	0.00	0.00	1.00	0.82
8.12_203.1781	0.00	0.00	1.00	0.78
9.08_203.0278	0.00	0.00	1.00	0.72
9.80_203.0277	0.00	0.00	1.00	0.86
4.35_209.0956	0.00	0.00	1.00	0.91
5.44_208.0539	0.00	0.00	1.00	0.80
7.49_207.0994	0.00	0.12	1.00	0.85
1.30_205.9283	0.00	0.00	1.00	0.96
4.84_205.1323	0.00	0.00	1.00	0.98
1.32_211.8786	0.00	0.00	1.00	0.91
1.49_211.0584	0.00	0.24	1.00	0.85
9.81_210.0363	0.00	0.00	1.00	0.77
9.41_219.0312	0.00	0.00	1.00	0.70
9.03_217.0413	0.00	0.00	1.00	0.90
1.85_216.1242	0.00	0.05	0.98	1.00
16.16_223.9875	0.00	0.00	0.63	1.00
10.24_222.1533	0.00	0.08	1.00	0.70
9.81_222.1504	0.00	0.05	1.00	0.80
8.84_221.1903	0.00	0.00	1.00	0.79
9.04_225.0298	0.00	0.04	1.00	0.86
9.77_224.0325	0.00	0.00	1.00	0.80
5.48_229.0656	0.00	0.00	1.00	0.94
9.19_230.0719	0.00	0.00	1.00	0.98
9.82_230.0718	0.00	0.05	0.84	1.00
8.41_230.0715	0.00	0.00	1.00	0.63
10.62_236.1643	0.00	0.00	0.93	1.00
5.11_236.1306	0.00	0.13	0.79	1.00
8.54_235.1344	0.00	0.00	1.00	0.69
9.80_241.0261	0.00	0.00	1.00	0.91
10.69_238.1826	0.00	0.00	1.00	0.65
4.13_237.1268	0.00	0.31	1.00	0.81
5.81_248.1281	0.00	0.27	1.00	0.85
9.03_248.0351	0.00	0.00	0.80	1.00
8.44_247.1345	0.00	0.00	1.00	0.95
4.04_247.1287	0.00	0.00	0.74	1.00
9.07_246.5440	0.00	0.00	1.00	0.75
5.04_244.1219	0.00	0.00	1.00	0.94
4.31_249.0807	0.00	0.00	1.00	0.87
8.08_252.0397	0.00	0.00	0.91	1.00

9.63_252.0395	0.00	0.00	0.88	1.00
8.66_252.0394	0.00	0.00	1.00	0.55
5.12_252.0389	0.00	0.00	0.55	1.00
7.48_252.0388	0.00	0.00	0.79	1.00
6.23_258.1449	0.00	0.00	1.00	0.69
3.87_257.1146	0.00	0.30	1.00	0.95
9.81_253.5524	0.00	0.03	1.00	0.97
12.02_263.1978	0.00	0.08	1.00	0.84
1.78_262.1278	0.00	0.00	0.96	1.00
5.86_262.1048	0.00	0.27	0.97	1.00
5.01_261.1438	0.00	0.06	0.77	1.00
9.03_260.5527	0.00	0.00	0.94	1.00
10.52_268.0194	0.00	0.21	0.89	1.00
5.43_268.0192	0.00	0.06	0.96	1.00
6.28_268.0191	0.00	0.10	1.00	0.96
8.32_268.0180	0.00	0.00	1.00	0.55
5.18_266.1406	0.00	0.27	1.00	0.91
5.27_264.2082	0.00	0.00	1.00	0.88
7.49_268.0200	0.00	0.00	0.51	1.00
4.60_268.0196	0.00	0.00	1.00	0.82
11.39_268.0195	0.00	0.00	0.93	1.00
5.84_281.1328	0.00	0.00	0.91	1.00
9.12_279.1585	0.00	0.00	1.00	0.67
7.18_278.2110	0.00	0.00	1.00	0.80
6.07_276.1943	0.00	0.00	1.00	0.97
4.52_276.1726	0.00	0.00	0.97	1.00
5.71_286.2118	0.00	0.00	1.00	0.70
7.19_284.2219	0.00	0.00	1.00	0.68
7.50_283.1523	0.00	0.05	1.00	0.74
1.73_282.0649	0.00	0.02	1.00	0.87
7.72_281.1420	0.00	0.00	1.00	0.80
5.22_295.1312	0.00	0.04	1.00	0.81
7.82_294.2085	0.00	0.00	1.00	0.84
6.82_294.2084	0.00	0.00	1.00	0.56
3.86_294.1559	0.00	0.40	1.00	0.86
7.15_293.2251	0.00	0.00	1.00	0.67
4.87_293.1612	0.00	0.22	0.87	1.00
6.49_292.1923	0.00	0.03	0.65	1.00
3.76_299.1387	0.00	0.00	1.00	0.71
7.73_298.2024	0.00	0.00	1.00	0.87
4.74_298.0969	0.00	0.06	1.00	0.84
9.60_297.1694	0.00	0.00	1.00	0.64
7.19_296.2224	0.00	0.00	1.00	0.89
5.83_303.1558	0.00	0.01	0.95	1.00
3.78_300.1386	0.00	0.04	1.00	0.81
12.02_309.1921	0.00	0.02	1.00	0.90
6.00_308.2238	0.00	0.00	1.00	0.92
6.06_312.2197	0.00	0.00	0.99	1.00
6.84_312.2197	0.00	0.00	1.00	0.78
7.24_312.2197	0.00	0.00	1.00	0.70
10.59_311.1859	0.00	0.00	1.00	0.67
7.47_310.2026	0.00	0.00	0.97	1.00
5.82_322.1007	0.00	0.00	1.00	0.89
1.74_322.0446	0.00	0.02	1.00	0.91
14.63_321.2420	0.00	0.00	0.64	1.00
9.13_319.1539	0.00	0.00	1.00	0.71
6.92_318.2094	0.00	0.00	0.94	1.00
6.00_328.7423	0.00	0.24	1.00	0.83
7.34_326.2353	0.00	0.00	1.00	0.84
12.03_325.1706	0.00	0.00	1.00	0.92
6.08_324.1828	0.00	0.30	1.00	0.84
6.31_335.7452	0.00	0.00	1.00	0.82
6.62_334.2005	0.00	0.00	0.51	1.00
8.76_329.1942	0.00	0.10	1.00	0.76
5.84_341.1007	0.00	0.00	1.00	0.86
14.63_339.2533	0.00	0.00	1.00	0.89
7.48_345.1875	0.00	0.00	1.00	0.78
5.26_354.0787	0.00	0.16	0.98	1.00
8.24_352.2057	0.00	0.00	1.00	0.96
4.01_351.5992	0.00	0.00	1.00	0.87

6.95_350.2147	0.00	0.10	1.00	0.72
6.51_360.2165	0.00	0.00	1.00	0.82
8.53_359.2035	0.00	0.09	1.00	0.74
7.52_368.2211	0.00	0.00	0.92	1.00
9.80_367.0822	0.00	0.00	1.00	0.84
10.08_366.2455	0.00	0.00	1.00	0.73
6.22_366.2068	0.00	0.15	1.00	0.92
5.64_366.2063	0.00	0.00	0.75	1.00
7.83_387.1861	0.00	0.00	1.00	0.96
9.80_387.0731	0.00	0.00	1.00	0.77
6.88_386.2329	0.00	0.03	0.95	1.00
6.24_384.2171	0.00	0.00	1.00	0.96
8.63_398.2317	0.00	0.00	1.00	0.69
9.08_429.0845	0.00	0.00	1.00	0.75
7.98_431.2698	0.00	0.05	1.00	0.80
9.07_451.0615	0.00	0.00	1.00	0.78
6.99_443.3240	0.00	0.06	1.00	0.92
9.73_443.1014	0.00	0.00	1.00	0.83
6.90_461.2902	0.00	0.00	0.88	1.00
5.90_459.3212	0.00	0.14	1.00	0.88
10.02_459.0960	0.00	0.00	1.00	0.67
9.03_457.1145	0.00	0.01	1.00	0.77
11.52_456.3791	0.00	0.00	1.00	0.64
6.21_455.1906	0.00	0.15	1.00	0.82
9.81_454.0847	0.00	0.00	1.00	0.73
9.79_462.0710	0.00	0.00	1.00	0.67
9.78_481.0499	0.00	0.00	1.00	0.79
9.02_479.0963	0.00	0.00	1.00	0.87
4.15_476.2404	0.00	0.00	1.00	0.74
6.98_499.2793	0.00	0.00	1.00	0.75
7.51_499.2782	0.00	0.04	1.00	0.91
9.02_495.0687	0.00	0.00	1.00	0.78
5.37_493.1709	0.00	0.00	1.00	0.85
9.09_512.3013	0.00	0.00	1.00	0.78
13.62_510.2556	0.00	0.28	1.00	0.73
5.65_504.2609	0.00	0.00	1.00	0.98
5.64_515.2738	0.00	0.01	1.00	0.74
6.62_515.2737	0.00	0.00	0.86	1.00
1.76_515.1445	0.00	0.00	0.92	1.00
10.06_526.3139	0.00	0.00	1.00	0.65
7.21_526.2839	0.00	0.03	0.97	1.00
6.79_549.3505	0.00	0.00	1.00	0.60
7.20_544.2918	0.00	0.00	1.00	0.85
7.57_542.3960	0.00	0.20	1.00	0.78
12.03_565.3746	0.00	0.02	1.00	0.85
7.14_560.1805	0.00	0.00	0.76	1.00
6.90_555.3068	0.00	0.00	1.00	0.82
1.72_551.1035	0.00	0.00	1.00	0.87
12.03_549.4012	0.00	0.00	1.00	0.84
5.52_601.2501	0.00	0.00	0.60	1.00
1.25_639.8836	0.00	0.00	1.00	0.61
6.02_637.3187	0.00	0.00	1.00	0.84
9.79_683.1204	0.00	0.00	1.00	0.51
7.60_846.3434	0.00	0.00	1.00	0.91
7.20_920.0962	0.00	0.00	0.89	1.00
7.21_916.0943	0.00	0.00	0.86	1.00
9.80_907.1678	0.00	0.00	1.00	0.79
7.67_1031.2480	0.00	0.22	1.00	0.77
7.69_1031.1674	0.00	0.27	1.00	0.93
7.67_1031.0798	0.00	0.00	1.00	0.59
7.63_970.6960	0.00	0.00	1.00	0.53
7.01_1221.4414	0.00	0.00	1.00	0.93
7.00_1216.1209	0.00	0.36	1.00	0.85
7.70_1064.5448	0.00	0.13	0.60	1.00
8.34_150.0928	0.00	0.03	1.00	0.86
9.79_218.0234	0.00	0.02	0.96	1.00
1.64_174.0879	0.00	0.00	0.59	1.00
9.78_465.0808	0.01	0.02	1.00	0.61
6.76_310.2021	0.01	0.00	0.99	1.00
6.24_515.2753	0.01	0.00	1.00	0.79

1.82_228.1004	0.01	0.00	0.89	1.00
1.29_203.9309	0.01	0.00	1.00	0.90
8.10_301.1534	0.01	0.04	1.00	0.77
5.66_384.2168	0.01	0.00	1.00	0.96
1.64_246.1172	0.01	0.00	0.93	1.00
3.22_235.1201	0.01	0.00	0.84	1.00
9.81_269.0437	0.02	0.00	1.00	0.73
6.06_294.2084	0.02	0.00	1.00	0.78
7.48_177.0877	0.02	0.00	1.00	0.89
9.66_279.1583	0.02	0.00	1.00	0.69
8.74_542.3146	0.02	0.00	0.90	1.00
12.02_205.1953	0.02	0.00	1.00	0.71
9.14_239.1284	0.03	0.02	1.00	0.75
5.43_377.1482	0.03	0.00	1.00	0.74
9.67_319.1539	0.03	0.05	0.64	1.00
1.73_338.0231	0.04	0.00	1.00	0.99
7.06_325.1861	0.04	0.23	1.00	1.00
8.53_283.1523	0.04	0.09	0.88	1.00
1.74_150.0789	0.04	0.00	1.00	0.77
6.95_218.1203	0.05	0.10	1.00	0.90
6.95_368.2220	0.05	0.09	1.00	0.76
3.07_230.1126	0.05	0.12	0.96	1.00
10.52_673.3745	0.06	0.10	1.00	0.69
1.70_260.1135	0.06	0.00	0.91	1.00
7.42_280.1237	0.07	0.19	1.00	0.88
4.75_136.0625	0.07	0.00	0.80	1.00
10.98_442.3651	0.07	0.05	1.00	0.65
4.61_247.1287	0.07	0.00	0.81	1.00
3.83_198.1623	0.07	0.05	1.00	0.89
3.86_150.0940	0.07	0.13	1.00	0.90
1.76_596.1679	0.07	0.00	0.64	1.00
4.37_326.1802	0.07	0.44	0.97	1.00
8.53_207.1002	0.07	0.09	0.97	1.00
5.97_286.6247	0.08	0.01	0.84	1.00
8.53_177.0880	0.08	0.07	1.00	0.95
7.80_291.1290	0.08	0.30	1.00	0.91
14.64_361.2361	0.09	0.00	0.95	1.00
5.84_299.0939	0.11	0.05	0.99	1.00
7.25_371.1508	0.11	0.00	0.89	1.00
5.83_325.1311	0.12	0.00	0.92	1.00
9.41_281.1770	0.13	0.24	1.00	0.77
7.06_221.1900	0.13	0.40	1.00	0.79
6.41_165.0905	0.14	0.09	1.00	0.72
1.65_159.0768	0.16	0.00	0.75	1.00
9.79_1349.2480	0.16	0.00	0.89	1.00
4.87_329.1844	0.17	0.00	1.00	0.86
4.30_310.1305	0.17	0.04	1.00	0.86
3.85_276.1433	0.17	0.10	1.00	0.86
6.71_1160.7578	0.17	0.00	1.00	0.77
7.06_203.1787	0.17	0.32	1.00	0.90
6.06_203.1781	0.18	0.32	1.00	0.79
1.78_217.1296	0.18	0.37	0.78	1.00
9.47_211.0868	0.18	0.32	1.00	0.72
1.73_288.1454	0.20	0.00	1.00	0.86
4.31_265.0552	0.20	0.00	1.00	0.92
4.81_464.2611	0.21	0.25	1.00	0.82
8.29_401.1993	0.21	0.00	1.00	0.92
3.82_230.1126	0.22	0.14	0.93	1.00
4.30_478.1379	0.23	0.05	1.00	0.89
5.81_222.1598	0.24	0.46	1.00	0.85
16.18_335.9929	0.24	0.00	1.00	0.83
4.12_413.1243	0.25	0.45	1.00	0.89
7.42_196.0651	0.25	0.13	1.00	0.87
4.09_573.1785	0.27	0.46	1.00	0.90
6.39_336.2172	0.28	0.23	1.00	0.95
4.88_188.0708	0.29	0.50	0.99	1.00
12.62_416.2462	0.30	0.36	1.00	0.90
4.26_450.2439	0.30	0.01	1.00	0.92
4.86_372.1909	0.30	0.16	1.00	0.91
6.27_207.0660	0.32	0.57	1.00	1.00

4.64_137.0376	0.33	0.34	1.00	0.98
5.27_685.1761	0.33	0.00	1.00	0.89
3.80_194.0821	0.34	0.00	0.77	1.00
5.96_534.2942	0.35	0.08	1.00	0.90
16.15_459.1339	0.35	0.00	0.74	1.00
5.81_605.2195	0.36	0.51	1.00	0.81
4.63_149.1104	0.38	0.61	1.00	0.89
6.78_176.0714	0.38	0.65	1.00	0.93
5.16_210.1137	0.40	0.39	1.00	0.83
8.22_220.1332	0.40	0.59	1.00	0.81
5.34_191.1575	0.44	0.63	1.00	0.90
4.32_308.1712	0.46	0.16	1.00	0.89
4.34_266.1408	0.46	0.36	0.90	1.00
12.43_386.2820	0.50	1.00	0.00	0.00
13.49_420.3478	0.51	1.00	0.03	0.04
10.60_346.3091	0.51	1.00	0.00	0.00
3.93_438.1964	0.51	0.19	1.00	0.89
13.00_413.3095	0.52	1.00	0.06	0.04
10.40_371.3275	0.52	1.00	0.00	0.00
6.40_263.1761	0.53	0.57	1.00	0.92
9.48_225.1993	0.53	1.00	0.02	0.01
6.81_807.1918	0.54	1.00	0.00	0.00
4.40_158.0302	0.54	0.40	1.00	0.88
13.53_339.2529	0.55	1.00	0.00	0.00
4.26_669.2631	0.56	1.00	0.00	0.00
11.80_235.1712	0.56	1.00	0.07	0.00
10.15_739.4618	0.56	1.00	0.01	0.02
14.41_309.2409	0.56	1.00	0.05	0.17
6.15_485.2027	0.57	0.61	1.00	0.81
10.53_531.4000	0.57	1.00	0.00	0.00
1.94_252.0411	0.57	0.43	0.95	1.00
12.97_407.3144	0.58	1.00	0.04	0.03
12.98_399.3242	0.58	1.00	0.05	0.03
4.37_663.2850	0.59	1.00	0.00	0.00
4.29_244.1199	0.61	0.63	1.00	0.87
13.98_433.3418	0.61	1.00	0.00	0.00
6.90_166.0720	0.61	1.00	0.00	0.00
5.20_239.1759	0.62	1.00	0.23	0.19
4.64_412.2067	0.62	1.00	0.13	0.12
3.86_242.1126	0.63	0.68	0.91	1.00
6.19_181.1351	0.63	1.00	0.06	0.06
10.97_401.2525	0.63	1.00	0.12	0.04
3.87_166.0522	0.65	0.38	0.96	1.00
6.40_439.1986	0.65	0.65	1.00	0.84
11.58_415.2745	0.65	1.00	0.02	0.00
12.62_273.1378	0.66	1.00	0.00	0.00
12.86_507.3281	0.66	1.00	0.29	0.25
12.97_290.7254	0.66	1.00	0.31	0.24
4.27_647.2871	0.67	1.00	0.01	0.01
12.82_551.3593	0.67	1.00	0.37	0.26
11.44_223.2060	0.67	1.00	0.00	0.00
5.72_240.1231	0.68	0.47	0.88	1.00
6.85_824.9348	0.70	1.00	0.00	0.00
4.81_506.2950	0.71	1.00	0.10	0.00
16.15_442.8736	0.71	1.00	0.00	0.00
4.50_359.1197	0.71	0.79	0.97	1.00
7.07_184.1710	0.72	1.00	0.00	0.00
4.37_150.0945	0.72	1.00	0.00	0.00
12.79_595.3829	0.73	1.00	0.43	0.35
3.89_518.1743	0.73	1.00	0.05	0.00
12.67_727.4605	0.74	1.00	0.45	0.40
4.81_415.2090	0.74	0.52	1.00	0.95
11.18_473.3585	0.75	1.00	0.00	0.01
3.75_245.1607	0.75	1.00	0.13	0.15
6.23_251.1781	0.76	0.84	1.00	0.94
5.43_241.1546	0.76	0.78	0.98	1.00
12.70_683.4373	0.77	1.00	0.52	0.40
12.86_463.2998	0.77	1.00	0.00	0.23
12.74_443.3505	0.77	1.00	0.01	0.02
6.34_150.0787	0.77	0.73	0.91	1.00

12.97_547.4060	0.77	1.00	0.10	0.13
13.86_425.2896	0.78	1.00	0.32	0.26
5.26_147.0936	0.79	1.00	0.38	0.32
11.97_299.2600	0.80	1.00	0.00	0.00
13.50_524.2740	0.81	1.00	0.54	0.42
15.06_413.2647	0.81	1.00	0.09	0.34
12.86_502.3745	0.82	1.00	0.52	0.35
11.84_443.3878	0.82	1.00	0.21	0.13
11.03_354.1608	0.82	1.00	0.10	0.10
11.28_440.3462	0.82	1.00	0.00	0.00
12.98_282.2118	0.82	1.00	0.00	0.04
12.73_655.3845	0.83	1.00	0.22	0.42
12.74_639.4067	0.83	1.00	0.46	0.40
13.79_365.2675	0.84	1.00	0.00	0.00
12.80_567.3292	0.85	1.00	0.00	0.37
12.83_546.4021	0.86	1.00	0.46	0.30
10.38_401.3397	0.88	1.00	0.29	0.21
9.26_219.1735	0.88	1.00	0.00	0.00
12.67_743.4367	0.88	1.00	0.59	0.51
12.70_699.4109	0.89	1.00	0.34	0.24
14.79_310.3109	0.90	1.00	0.67	0.66
12.78_611.3565	0.91	1.00	0.19	0.49
15.94_338.3442	0.91	1.00	0.59	0.48
13.49_295.2258	0.91	1.00	0.01	0.00
1.47_508.0657	0.91	1.00	0.44	0.17
12.73_320.2010	0.94	1.00	0.13	0.00
4.49_225.1597	0.97	1.00	0.36	0.32
12.89_441.3208	0.99	1.00	0.38	0.19
12.78_590.4295	1.00	1.00	0.58	0.46
10.36_211.6353	1.00	0.89	0.31	0.00
3.82_209.1275	1.00	0.90	0.62	0.56
11.31_225.6512	1.00	0.95	0.38	0.31
9.27_240.2315	1.00	0.88	0.10	0.00
10.39_268.2627	1.00	0.83	0.00	0.00
6.59_273.1670	1.00	0.84	0.62	0.67
11.44_291.1951	1.00	0.75	0.00	0.00
11.33_299.2599	1.00	0.77	0.00	0.00
12.62_313.2746	1.00	0.83	0.00	0.00
14.82_332.2940	1.00	0.65	0.21	0.23
4.25_343.1235	1.00	0.70	0.34	0.08
15.49_338.3442	1.00	0.86	0.00	0.00
15.92_360.3229	1.00	0.71	0.09	0.32
13.48_397.3392	1.00	0.75	0.00	0.00
10.78_415.3581	1.00	0.61	0.11	0.22
13.95_411.3586	1.00	0.78	0.01	0.02
13.27_419.3131	1.00	0.81	0.00	0.00
12.86_485.3471	1.00	0.86	0.32	0.24
12.81_529.3766	1.00	0.77	0.35	0.14
12.97_555.3910	1.00	0.94	0.00	0.23
12.79_573.4039	1.00	0.73	0.34	0.24
12.75_617.4294	1.00	0.84	0.39	0.25
13.92_641.5490	1.00	0.85	0.00	0.00
4.37_685.2548	1.00	0.86	0.00	0.00
12.67_705.4810	1.00	0.93	0.57	0.33
6.87_807.0837	1.00	0.57	0.11	0.00

Table A3.17. Normalized heat map of features described as unique in **Figure 3.2(B)** and **(C)** when comparing wild type *Nocardiopsis sp. FU40 ΔApoS8* to the S3 streptomycin resistant mutant extract using OPLS-DA and extracting features from the generated S-plot with correlation coefficients ≥0.9. Features are normalized to maximum intensity for that feature.

Feature ID (RT_*m/z*)	WT	WT	S3	S3
12.03_135.1163	0.00	0.05	0.98	1.00
12.03_123.1165	0.00	0.00	0.93	1.00
4.87_118.0679	0.00	0.14	0.81	1.00
12.03_149.1327	0.00	0.00	0.98	1.00
6.56_162.0938	0.00	0.00	0.88	1.00
2.01_158.0950	0.00	0.27	1.00	0.67
5.78_170.1204	0.00	0.00	1.00	0.97
7.08_169.0882	0.00	0.01	1.00	0.70
2.44_166.0747	0.00	0.10	0.94	1.00
6.60_180.1017	0.00	0.02	1.00	0.98
5.02_180.1014	0.00	0.00	0.66	1.00
4.95_177.1399	0.00	0.31	0.92	1.00
4.39_192.1130	0.00	0.16	1.00	0.98
9.12_191.0134	0.00	0.00	0.83	1.00
4.14_186.1168	0.00	0.00	1.00	0.60
4.02_198.1143	0.00	0.00	1.00	0.96
4.99_198.1134	0.00	0.00	1.00	0.97
9.08_196.0187	0.00	0.00	1.00	0.97
8.84_203.1804	0.00	0.00	0.96	1.00
8.12_203.1781	0.00	0.00	0.97	1.00
9.08_203.0278	0.00	0.00	1.00	0.98
9.80_203.0277	0.00	0.00	0.95	1.00
1.42_201.0074	0.00	0.00	0.99	1.00
4.35_209.0956	0.00	0.00	0.86	1.00
4.54_208.1355	0.00	0.00	0.72	1.00
5.44_208.0539	0.00	0.00	1.00	0.76
7.49_207.0994	0.00	0.08	1.00	0.83
1.30_205.9283	0.00	0.00	1.00	0.94
4.84_205.1323	0.00	0.00	0.92	1.00
9.81_205.1237	0.00	0.00	1.00	1.00
10.22_205.1232	0.00	0.00	1.00	0.51
1.32_211.8786	0.00	0.00	0.80	1.00
1.49_211.0584	0.00	0.18	0.74	1.00
9.81_210.0363	0.00	0.00	0.94	1.00
9.07_210.0305	0.00	0.00	0.76	1.00
9.41_219.0312	0.00	0.00	0.99	1.00
3.69_218.1136	0.00	0.39	1.00	0.78
9.03_217.0413	0.00	0.00	1.00	1.00
8.84_221.1903	0.00	0.00	1.00	0.98
6.51_220.1710	0.00	0.13	1.00	0.86
5.15_226.5984	0.00	0.08	1.00	0.85
7.35_225.1140	0.00	0.00	1.00	0.73
7.99_225.1125	0.00	0.02	1.00	0.97
9.04_225.0298	0.00	0.02	0.93	1.00
9.77_224.0325	0.00	0.00	1.00	0.92
5.48_229.0656	0.00	0.00	0.97	1.00
4.02_228.1701	0.00	0.00	0.91	1.00
9.82_230.0718	0.00	0.04	1.00	0.58
8.41_230.0715	0.00	0.00	1.00	0.50
5.11_236.1306	0.00	0.16	0.98	1.00
8.54_235.1344	0.00	0.00	1.00	0.92
9.80_241.0261	0.00	0.00	1.00	0.99
8.82_241.0249	0.00	0.00	1.00	0.85
10.69_238.1826	0.00	0.00	1.00	0.74
5.81_248.1281	0.00	0.23	1.00	0.85
9.03_248.0351	0.00	0.00	1.00	0.90
4.04_247.1287	0.00	0.00	1.00	0.99

7.33_247.0943	0.00	0.18	0.96	1.00
9.07_246.5440	0.00	0.00	1.00	0.72
5.04_244.1219	0.00	0.00	0.84	1.00
4.31_249.0807	0.00	0.00	1.00	0.94
4.56_252.0394	0.00	0.11	1.00	0.57
6.01_252.0391	0.00	0.00	0.63	1.00
7.48_252.0388	0.00	0.00	0.92	1.00
3.87_257.1146	0.00	0.33	0.88	1.00
9.81_253.5524	0.00	0.03	0.89	1.00
12.02_263.1978	0.00	0.03	0.87	1.00
1.78_262.1278	0.00	0.00	1.00	0.89
5.86_262.1048	0.00	0.27	1.00	0.82
10.71_261.1779	0.00	0.01	0.79	1.00
5.01_261.1438	0.00	0.03	0.99	1.00
9.03_260.5527	0.00	0.00	1.00	0.75
10.68_260.1641	0.00	0.00	0.98	1.00
6.81_268.0194	0.00	0.00	1.00	0.67
5.18_266.1406	0.00	0.25	0.71	1.00
5.27_264.2082	0.00	0.00	1.00	0.83
9.67_268.0195	0.00	0.00	0.87	1.00
5.84_281.1328	0.00	0.00	1.00	0.78
7.18_278.2110	0.00	0.00	0.93	1.00
6.07_276.1943	0.00	0.00	0.64	1.00
5.71_286.2118	0.00	0.00	1.00	0.93
9.01_283.1521	0.00	0.07	0.97	1.00
1.73_282.0649	0.00	0.02	0.91	1.00
7.72_281.1420	0.00	0.00	1.00	0.72
5.10_288.1525	0.00	0.05	0.97	1.00
5.22_295.1312	0.00	0.01	1.00	0.86
7.82_294.2085	0.00	0.00	0.89	1.00
4.87_293.1612	0.00	0.29	0.69	1.00
6.49_292.1923	0.00	0.02	1.00	0.68
3.76_299.1387	0.00	0.00	0.70	1.00
2.95_299.1385	0.00	0.00	0.87	1.00
4.74_298.0969	0.00	0.08	1.00	0.91
9.60_297.1694	0.00	0.01	1.00	1.00
7.19_296.2224	0.00	0.00	0.83	1.00
5.83_303.1558	0.00	0.01	1.00	0.98
7.70_303.1206	0.00	0.05	1.00	0.73
12.02_309.1921	0.00	0.01	0.91	1.00
3.90_307.1446	0.00	0.00	0.93	1.00
6.84_312.2197	0.00	0.00	0.85	1.00
10.59_311.1859	0.00	0.00	0.51	1.00
9.79_311.0549	0.00	0.00	0.82	1.00
7.47_310.2026	0.00	0.00	0.81	1.00
1.74_322.0446	0.00	0.02	0.94	1.00
9.13_319.1539	0.00	0.00	0.82	1.00
6.92_318.2094	0.00	0.00	1.00	0.98
6.00_328.7423	0.00	0.09	1.00	0.83
5.91_328.5999	0.00	0.00	0.60	1.00
7.34_326.2353	0.00	0.00	0.84	1.00
6.01_326.2353	0.00	0.00	0.99	1.00
4.97_326.0999	0.00	0.15	0.94	1.00
12.03_325.1706	0.00	0.00	0.99	1.00
6.31_335.7452	0.00	0.00	1.00	0.77
5.84_341.1007	0.00	0.00	0.99	1.00
6.07_337.1394	0.00	0.03	0.91	1.00
10.06_348.2310	0.00	0.00	1.00	0.76
7.48_345.1875	0.00	0.00	0.73	1.00
5.19_344.6196	0.00	0.04	1.00	0.77
7.37_344.2218	0.00	0.00	0.93	1.00
6.06_359.1205	0.00	0.00	1.00	0.82
4.84_357.1855	0.00	0.16	1.00	0.72
5.26_354.0787	0.00	0.16	1.00	0.97
8.24_352.2057	0.00	0.00	0.60	1.00
6.67_362.2335	0.00	0.00	0.62	1.00
6.51_360.2165	0.00	0.00	0.89	1.00
8.53_359.2035	0.00	0.09	1.00	0.90
8.77_368.2219	0.00	0.00	1.00	0.67
7.52_368.2211	0.00	0.00	0.98	1.00

9.80_367.0822	0.00	0.00	0.75	1.00
5.64_366.2063	0.00	0.00	0.90	1.00
7.43_374.2181	0.00	0.00	0.95	1.00
7.83_387.1861	0.00	0.00	0.93	1.00
9.80_387.0731	0.00	0.00	0.74	1.00
6.89_384.2172	0.00	0.01	1.00	0.92
6.24_384.2171	0.00	0.00	0.93	1.00
8.63_398.2317	0.00	0.00	1.00	0.84
1.49_394.1142	0.00	0.00	1.00	0.97
9.40_418.0851	0.00	0.00	0.88	1.00
3.74_416.1928	0.00	0.04	0.77	1.00
8.66_429.0854	0.00	0.00	0.91	1.00
9.08_429.0845	0.00	0.00	0.97	1.00
8.04_432.2606	0.00	0.00	1.00	0.95
1.48_431.0890	0.00	0.37	1.00	0.90
9.07_451.0615	0.00	0.00	0.86	1.00
6.99_443.3240	0.00	0.08	0.84	1.00
9.73_443.1014	0.00	0.00	0.96	1.00
8.33_443.0954	0.00	0.00	1.00	0.99
8.80_443.0945	0.00	0.00	0.88	1.00
6.90_461.2902	0.00	0.00	1.00	0.96
5.90_459.3212	0.00	0.03	1.00	0.95
10.02_459.0960	0.00	0.00	1.00	0.98
9.03_457.1145	0.00	0.01	0.92	1.00
8.67_457.1133	0.00	0.00	0.94	1.00
11.52_456.3791	0.00	0.00	1.00	0.93
6.21_455.1906	0.00	0.15	0.85	1.00
9.81_454.0847	0.00	0.00	0.86	1.00
9.05_454.0819	0.00	0.00	0.97	1.00
6.42_472.2832	0.00	0.00	1.00	0.99
6.46_471.2466	0.00	0.03	1.00	0.83
9.02_468.1011	0.00	0.00	0.91	1.00
8.82_465.0807	0.00	0.00	0.68	1.00
9.79_462.0710	0.00	0.00	0.98	1.00
9.78_481.0499	0.00	0.00	0.92	1.00
4.15_476.2404	0.00	0.00	1.00	0.83
9.02_476.0877	0.00	0.00	1.00	0.85
7.51_499.2782	0.00	0.06	1.00	0.94
9.02_495.0687	0.00	0.00	1.00	0.99
4.37_494.2617	0.00	0.00	0.98	1.00
5.37_493.1709	0.00	0.00	0.91	1.00
1.49_491.1254	0.00	0.17	1.00	0.74
8.58_490.2972	0.00	0.00	0.89	1.00
9.79_513.1525	0.00	0.00	0.94	1.00
6.65_512.8485	0.00	0.00	1.00	0.95
9.09_512.3013	0.00	0.00	0.90	1.00
5.65_504.2609	0.00	0.00	1.00	0.55
5.64_515.2738	0.00	0.02	1.00	0.90
1.76_515.1445	0.00	0.00	0.74	1.00
10.06_526.3139	0.00	0.00	0.69	1.00
7.21_526.2839	0.00	0.08	1.00	1.00
6.79_549.3505	0.00	0.00	1.00	0.90
9.11_548.3433	0.00	0.02	0.83	1.00
7.20_544.2918	0.00	0.00	1.00	0.71
7.57_542.3960	0.00	0.34	0.86	1.00
12.03_565.3746	0.00	0.00	0.94	1.00
9.67_563.3802	0.00	0.00	0.86	1.00
6.90_555.3068	0.00	0.00	1.00	0.95
12.03_549.4012	0.00	0.00	1.00	0.93
9.02_549.3610	0.00	0.01	0.84	1.00
5.52_601.2501	0.00	0.00	1.00	0.97
9.79_576.6021	0.00	0.00	1.00	0.96
9.06_576.6005	0.00	0.00	1.00	0.87
1.25_639.8836	0.00	0.00	1.00	0.94
9.79_683.1204	0.00	0.00	1.00	0.92
9.78_885.1896	0.00	0.00	0.66	1.00
7.69_868.6024	0.00	0.00	1.00	0.84
7.60_846.3434	0.00	0.00	1.00	0.50
7.20_920.0962	0.00	0.00	1.00	0.94
9.80_907.1678	0.00	0.00	0.83	1.00

7.69_1031.1674	0.00	0.20	1.00	0.90
7.65_1000.0444	0.00	0.00	0.89	1.00
7.63_970.6960	0.00	0.00	0.61	1.00
7.63_942.9948	0.00	0.00	0.74	1.00
7.01_1221.4414	0.00	0.00	1.00	0.56
7.00_1216.1209	0.00	0.29	1.00	0.68
9.79_218.0234	0.00	0.02	0.79	1.00
8.34_150.0928	0.00	0.04	0.96	1.00
9.78_465.0808	0.00	0.01	1.00	0.99
6.76_310.2021	0.00	0.00	1.00	0.93
1.64_174.0879	0.01	0.00	1.00	0.96
10.18_621.4210	0.01	0.00	0.87	1.00
8.54_447.2904	0.01	0.05	0.90	1.00
1.82_228.1004	0.01	0.00	1.00	0.93
9.81_269.0437	0.01	0.00	0.81	1.00
1.29_203.9309	0.01	0.00	0.92	1.00
1.64_246.1172	0.01	0.00	0.98	1.00
8.10_301.1534	0.01	0.05	1.00	0.98
7.48_177.0877	0.02	0.00	1.00	0.83
12.02_205.1953	0.02	0.00	0.96	1.00
8.74_542.3146	0.02	0.00	1.00	0.68
9.11_505.3321	0.02	0.00	0.91	1.00
3.22_235.1201	0.02	0.00	1.00	0.97
9.79_1349.2480	0.02	0.00	0.88	1.00
5.66_384.2168	0.02	0.00	1.00	0.89
8.52_491.3179	0.02	0.00	0.86	1.00
6.24_515.2753	0.02	0.01	1.00	0.79
4.82_393.2208	0.02	0.00	1.00	0.79
6.06_294.2084	0.02	0.00	0.89	1.00
8.29_401.1993	0.02	0.00	0.89	1.00
7.06_325.1861	0.02	0.14	1.00	0.99
10.18_223.2085	0.03	0.21	1.00	1.00
1.73_338.0231	0.04	0.00	1.00	0.98
6.65_282.2073	0.04	0.24	0.85	1.00
7.95_433.2783	0.04	0.10	0.90	1.00
5.43_377.1482	0.04	0.00	0.94	1.00
3.07_230.1126	0.05	0.12	1.00	0.79
16.15_710.1773	0.05	0.01	1.00	0.97
1.74_150.0789	0.05	0.00	0.87	1.00
1.70_260.1135	0.05	0.00	0.92	1.00
9.66_279.1583	0.06	0.00	0.85	1.00
6.95_218.1203	0.06	0.12	0.96	1.00
8.53_283.1523	0.06	0.14	0.91	1.00
7.06_221.1900	0.07	0.20	1.00	0.99
5.84_299.0939	0.07	0.03	1.00	0.95
8.53_207.1002	0.07	0.09	0.86	1.00
4.37_326.1802	0.07	0.42	1.00	0.93
8.53_177.0880	0.07	0.07	0.81	1.00
6.71_1160.7578	0.07	0.00	1.00	0.97
3.86_150.0940	0.08	0.14	0.97	1.00
5.83_325.1311	0.08	0.00	1.00	0.92
7.06_203.1787	0.08	0.15	0.98	1.00
9.67_319.1539	0.09	0.12	1.00	0.64
4.75_136.0625	0.09	0.00	0.92	1.00
3.83_198.1623	0.10	0.07	0.94	1.00
7.42_280.1237	0.11	0.29	0.92	1.00
5.97_286.6247	0.11	0.02	1.00	0.82
6.06_203.1781	0.11	0.19	0.86	1.00
3.80_288.1929	0.11	0.10	0.95	1.00
7.91_389.2523	0.12	0.05	0.86	1.00
1.65_159.0768	0.12	0.00	0.96	1.00
9.14_239.1284	0.12	0.11	0.89	1.00
1.73_288.1454	0.14	0.00	1.00	0.56
5.97_278.6345	0.14	0.04	1.00	0.88
5.11_231.1676	0.14	0.51	0.95	1.00
4.88_188.0708	0.15	0.26	0.80	1.00
6.39_336.2172	0.16	0.13	1.00	0.85
6.41_165.0905	0.17	0.11	0.94	1.00
3.85_276.1433	0.19	0.11	0.93	1.00
4.30_310.1305	0.19	0.04	0.95	1.00

6.66_264.1980	0.19	0.08	1.00	0.84
3.82_230.1126	0.20	0.12	0.86	1.00
4.87_329.1844	0.20	0.00	0.89	1.00
4.31_265.0552	0.20	0.00	1.00	0.82
4.64_137.0376	0.21	0.22	1.00	0.97
4.30_478.1379	0.22	0.05	1.00	0.75
7.25_371.1508	0.22	0.00	1.00	0.88
4.12_413.1243	0.24	0.43	1.00	0.82
4.77_179.0472	0.28	0.51	0.90	1.00
7.64_999.9779	0.28	0.00	0.74	1.00
5.27_685.1761	0.29	0.00	1.00	0.91
4.81_464.2611	0.29	0.34	0.99	1.00
16.18_335.9929	0.30	0.00	1.00	0.84
4.86_372.1909	0.30	0.15	1.00	0.91
7.42_196.0651	0.33	0.17	0.85	1.00
9.41_281.1770	0.34	0.65	0.93	1.00
9.47_211.0868	0.34	0.60	0.93	1.00
5.11_307.1591	0.35	0.00	0.97	1.00
5.61_343.2002	0.37	0.08	0.90	1.00
3.80_194.0821	0.38	0.00	0.91	1.00
4.63_149.1104	0.40	0.65	0.88	1.00
12.62_416.2462	0.42	0.52	1.00	0.94
5.16_210.1137	0.44	0.44	0.96	1.00
3.85_258.1333	0.45	0.00	1.00	0.98
4.34_266.1408	0.46	0.36	0.98	1.00
5.34_191.1575	0.48	0.68	0.90	1.00
7.29_331.2114	0.50	0.72	0.94	1.00
12.43_386.2820	0.50	1.00	0.00	0.00
4.32_308.1712	0.50	0.18	1.00	0.91
14.78_323.2583	0.50	1.00	0.00	0.00
13.49_420.3478	0.51	1.00	0.00	0.00
10.60_346.3091	0.51	1.00	0.00	0.00
3.94_180.0961	0.51	0.23	0.88	1.00
13.00_413.3095	0.52	1.00	0.00	0.00
10.40_371.3275	0.52	1.00	0.04	0.00
9.48_225.1993	0.53	1.00	0.01	0.01
14.04_295.2283	0.54	1.00	0.00	0.00
6.81_807.1918	0.54	1.00	0.00	0.00
3.86_242.1126	0.55	0.60	0.90	1.00
13.53_339.2529	0.55	1.00	0.00	0.00
4.26_669.2631	0.56	1.00	0.00	0.00
11.80_235.1712	0.56	1.00	0.00	0.00
10.15_739.4618	0.56	1.00	0.00	0.00
14.41_309.2409	0.56	1.00	0.00	0.00
12.99_526.2341	0.56	1.00	0.08	0.03
10.53_531.4000	0.57	1.00	0.00	0.00
4.29_244.1199	0.57	0.59	1.00	0.98
4.40_158.0302	0.57	0.42	0.92	1.00
12.97_407.3144	0.58	1.00	0.00	0.00
12.98_399.3242	0.58	1.00	0.00	0.00
12.98_510.2581	0.59	1.00	0.12	0.00
6.40_263.1761	0.59	0.63	0.89	1.00
4.37_663.2850	0.59	1.00	0.00	0.00
13.98_433.3418	0.61	1.00	0.00	0.00
6.90_166.0720	0.61	1.00	0.00	0.00
5.72_240.1231	0.62	0.43	1.00	0.88
4.64_412.2067	0.62	1.00	0.11	0.05
6.19_181.1351	0.63	1.00	0.00	0.00
4.39_362.1069	0.63	0.55	1.00	0.89
10.97_401.2525	0.63	1.00	0.00	0.00
4.50_359.1197	0.64	0.72	1.00	0.99
6.15_485.2027	0.65	0.69	0.91	1.00
11.58_415.2745	0.65	1.00	0.00	0.00
12.62_273.1378	0.66	1.00	0.00	0.00
12.86_507.3281	0.66	1.00	0.29	0.26
12.97_290.7254	0.66	1.00	0.05	0.00
4.27_647.2871	0.67	1.00	0.04	0.00
12.82_551.3593	0.67	1.00	0.23	0.23
1.49_594.1582	0.67	0.74	1.00	0.92
11.44_223.2060	0.67	1.00	0.00	0.00

1.50_401.0693	0.67	0.62	1.00	0.90
6.40_439.1986	0.68	0.69	0.94	1.00
12.56_441.2657	0.70	1.00	0.37	0.29
4.59_251.1399	0.70	0.70	1.00	0.86
6.85_824.9348	0.70	1.00	0.00	0.00
16.15_442.8736	0.71	1.00	0.00	0.00
7.07_184.1710	0.72	1.00	0.00	0.00
4.37_150.0945	0.72	1.00	0.00	0.00
12.79_595.3829	0.73	1.00	0.32	0.31
13.98_292.2624	0.73	1.00	0.22	0.21
3.89_518.1743	0.73	1.00	0.00	0.05
12.67_727.4605	0.74	1.00	0.37	0.34
11.18_473.3585	0.75	1.00	0.01	0.01
6.23_251.1781	0.75	0.82	0.94	1.00
12.70_683.4373	0.77	1.00	0.38	0.38
12.86_463.2998	0.77	1.00	0.31	0.00
12.74_443.3505	0.77	1.00	0.00	0.00
10.84_227.1557	0.77	0.85	1.00	0.99
12.97_547.4060	0.77	1.00	0.13	0.08
13.86_425.2896	0.78	1.00	0.17	0.23
5.26_147.0936	0.79	1.00	0.28	0.35
13.50_409.7445	0.80	1.00	0.06	0.00
12.61_771.4862	0.80	1.00	0.38	0.00
11.97_299.2600	0.80	1.00	0.00	0.00
13.50_524.2740	0.81	1.00	0.10	0.04
15.06_413.2647	0.81	1.00	0.19	0.19
12.86_502.3745	0.82	1.00	0.28	0.00
11.84_443.3878	0.82	1.00	0.03	0.00
11.03_354.1608	0.82	1.00	0.00	0.02
11.28_440.3462	0.82	1.00	0.00	0.00
12.98_282.2118	0.82	1.00	0.00	0.00
12.73_655.3845	0.83	1.00	0.53	0.47
12.74_639.4067	0.83	1.00	0.44	0.40
13.79_365.2675	0.84	1.00	0.00	0.00
12.80_567.3292	0.85	1.00	0.45	0.00
12.83_546.4021	0.86	1.00	0.28	0.12
10.38_401.3397	0.88	1.00	0.18	0.19
12.67_743.4367	0.88	1.00	0.53	0.47
12.70_699.4109	0.89	1.00	0.61	0.62
14.79_310.3109	0.90	1.00	0.57	0.67
12.78_611.3565	0.91	1.00	0.53	0.41
15.94_338.3442	0.91	1.00	0.41	0.48
13.48_341.2200	0.91	1.00	0.17	0.00
13.49_295.2258	0.91	1.00	0.00	0.00
1.47_508.0657	0.91	1.00	0.73	0.79
12.73_320.2010	0.94	1.00	0.52	0.24
4.49_225.1597	0.97	1.00	0.26	0.27
12.89_441.3208	0.99	1.00	0.18	0.20
12.78_590.4295	1.00	1.00	0.38	0.36
13.95_270.2746	1.00	1.00	0.40	0.47
10.36_211.6353	1.00	0.89	0.22	0.26
3.82_209.1275	1.00	0.90	0.55	0.58
11.31_225.6512	1.00	0.95	0.00	0.00
9.27_240.2315	1.00	0.88	0.00	0.00
10.39_268.2627	1.00	0.83	0.00	0.00
12.97_278.2028	1.00	0.62	0.09	0.02
11.44_291.1951	1.00	0.75	0.00	0.00
11.33_299.2599	1.00	0.77	0.00	0.00
12.62_313.2746	1.00	0.83	0.00	0.00
14.31_325.2414	1.00	0.74	0.00	0.00
14.82_332.2940	1.00	0.65	0.11	0.00
15.49_338.3442	1.00	0.86	0.00	0.23
15.92_360.3229	1.00	0.71	0.26	0.32
13.48_397.3392	1.00	0.75	0.00	0.00
10.78_415.3581	1.00	0.61	0.14	0.15
13.95_411.3586	1.00	0.78	0.00	0.00
13.27_419.3131	1.00	0.81	0.00	0.00
10.77_434.3251	1.00	0.58	0.00	0.00
12.86_485.3471	1.00	0.86	0.14	0.29
12.81_529.3766	1.00	0.77	0.39	0.00

12.97_555.3910	1.00	0.94	0.14	0.00
12.79_573.4039	1.00	0.73	0.21	0.24
12.75_617.4294	1.00	0.84	0.10	0.27
13.92_641.5490	1.00	0.85	0.00	0.00
4.37_685.2548	1.00	0.86	0.42	0.21
6.87_807.0837	1.00	0.57	0.00	0.00

Table A3.18. Normalized heat map of features described as unique in **Figure 3.2(B)** and **(C)** when comparing wild type *Nocardiopsis sp. FU40 ΔApoS8* to the S4 streptomycin resistant mutant extract using OPLS-DA and extracting features from the generated S-plot with correlation coefficients ≥0.9. Features are normalized to maximum intensity for that feature.

Feature ID (RT_*m/z*)	WT	WT	S4	S4
1.50_165.0624	0.00	0.00	1.00	1.00
6.56_162.0938	0.00	0.00	0.63	1.00
5.78_170.1204	0.00	0.00	0.55	1.00
5.02_180.1014	0.00	0.00	0.73	1.00
4.95_177.1399	0.00	0.17	0.57	1.00
4.14_186.1168	0.00	0.00	1.00	0.70
4.02_198.1143	0.00	0.00	0.81	1.00
9.08_196.0187	0.00	0.00	0.85	1.00
9.80_203.0277	0.00	0.00	0.57	1.00
7.49_207.0994	0.00	0.05	0.62	1.00
4.84_205.1323	0.00	0.00	0.63	1.00
5.48_229.0656	0.00	0.00	0.51	1.00
4.61_230.0715	0.00	0.18	0.90	1.00
4.27_237.0717	0.00	0.26	1.00	0.73
9.80_241.0261	0.00	0.00	1.00	0.67
5.81_248.1281	0.00	0.15	0.83	1.00
5.04_244.1219	0.00	0.00	1.00	0.60
13.78_251.2405	0.00	0.00	0.96	1.00
4.31_249.0807	0.00	0.00	0.78	1.00
8.08_252.0397	0.00	0.00	0.67	1.00
6.01_252.0391	0.00	0.00	0.93	1.00
1.78_262.1278	0.00	0.00	0.87	1.00
5.01_261.1438	0.00	0.17	0.72	1.00
5.18_266.1406	0.00	0.19	1.00	0.90
11.95_266.1298	0.00	0.00	0.74	1.00
7.50_283.1523	0.00	0.03	0.63	1.00
1.73_282.0649	0.00	0.01	0.67	1.00
4.87_293.1612	0.00	0.11	1.00	0.86
4.74_298.0969	0.00	0.15	1.00	0.99
6.00_308.2238	0.00	0.00	1.00	0.90
5.82_322.1007	0.00	0.00	1.00	0.69
1.74_322.0446	0.00	0.01	0.99	1.00
8.76_329.1942	0.00	0.14	1.00	1.00
10.73_340.1475	0.00	0.10	0.65	1.00
14.63_339.2533	0.00	0.00	1.00	0.84
6.07_337.1394	0.00	0.13	0.86	1.00
5.19_344.6196	0.00	0.07	1.00	0.85
5.26_354.0787	0.00	0.14	1.00	0.98
4.01_351.5992	0.00	0.00	0.59	1.00
8.53_359.2035	0.00	0.10	0.54	1.00
5.64_366.2063	0.00	0.00	1.00	0.72
1.49_394.1142	0.00	0.00	0.78	1.00
14.04_420.3477	0.00	0.23	1.00	0.79
11.52_456.3791	0.00	0.00	1.00	0.97
6.21_455.1906	0.00	0.09	0.55	1.00
6.98_499.2793	0.00	0.00	0.78	1.00
5.64_515.2738	0.00	0.02	0.68	1.00
1.49_527.1567	0.00	0.00	1.00	0.53
5.52_601.2501	0.00	0.00	0.57	1.00
1.25_639.8836	0.00	0.00	0.78	1.00
12.72_634.4531	0.00	0.00	1.00	0.79
7.21_916.0943	0.00	0.00	0.69	1.00
3.22_235.1201	0.01	0.00	1.00	0.79
16.15_710.1773	0.02	0.00	0.84	1.00
1.73_338.0231	0.02	0.00	0.93	1.00
1.74_150.0789	0.03	0.00	0.67	1.00

3.86_150.0940	0.04	0.07	0.64	1.00
5.43_377.1482	0.04	0.00	0.57	1.00
6.24_515.2753	0.05	0.02	0.69	1.00
1.82_228.1004	0.05	0.01	1.00	0.68
1.70_260.1135	0.05	0.00	1.00	0.98
4.87_329.1844	0.07	0.00	0.55	1.00
11.79_304.1184	0.08	0.42	0.97	1.00
6.41_165.0905	0.08	0.05	0.87	1.00
11.43_466.2973	0.09	0.27	0.98	1.00
4.30_310.1305	0.10	0.02	0.65	1.00
6.89_843.7588	0.11	0.00	1.00	0.69
15.37_230.0721	0.11	0.37	1.00	0.84
16.24_268.0194	0.11	0.22	1.00	0.94
3.83_198.1623	0.12	0.09	0.63	1.00
16.22_252.0441	0.13	0.23	1.00	0.71
4.30_478.1379	0.14	0.03	0.79	1.00
5.27_685.1761	0.17	0.00	0.60	1.00
4.12_413.1243	0.18	0.31	0.99	1.00
4.34_266.1408	0.21	0.16	1.00	0.65
5.16_210.1137	0.22	0.21	0.63	1.00
3.85_276.1433	0.22	0.13	1.00	0.99
3.80_194.0821	0.23	0.00	1.00	0.91
4.26_450.2439	0.24	0.01	0.78	1.00
13.79_365.2675	0.25	0.29	1.00	0.85
4.38_242.1131	0.26	0.47	1.00	0.76
5.61_343.2002	0.26	0.06	0.84	1.00
16.15_365.1085	0.28	0.00	0.67	1.00
12.73_328.1928	0.28	0.00	0.76	1.00
3.85_258.1333	0.28	0.00	0.69	1.00
5.71_249.1598	0.29	0.40	0.83	1.00
4.32_308.1712	0.29	0.10	1.00	0.79
4.88_188.0708	0.29	0.50	0.78	1.00
4.70_221.1315	0.31	0.45	0.74	1.00
1.50_423.1007	0.33	0.49	1.00	0.76
4.86_372.1909	0.35	0.18	0.71	1.00
4.59_251.1399	0.38	0.37	1.00	0.91
3.82_209.1275	0.38	0.34	0.91	1.00
6.10_320.1966	0.40	0.00	0.77	1.00
6.34_150.0787	0.41	0.39	0.71	1.00
4.60_303.1563	0.43	0.30	1.00	0.71
6.02_274.1066	0.44	0.31	0.85	1.00
12.43_386.2820	0.50	1.00	0.00	0.00
13.97_282.2786	0.50	0.43	0.75	1.00
13.49_420.3478	0.51	1.00	0.04	0.02
10.60_346.3091	0.51	1.00	0.00	0.00
3.86_242.1126	0.51	0.56	0.78	1.00
10.70_288.2557	0.52	1.00	0.00	0.00
3.94_180.0961	0.53	0.24	0.94	1.00
9.48_225.1993	0.53	1.00	0.01	0.00
13.53_339.2529	0.55	1.00	0.00	0.00
4.26_669.2631	0.56	1.00	0.00	0.01
11.80_235.1712	0.56	1.00	0.02	0.10
3.80_119.0369	0.56	1.00	0.14	0.00
10.15_739.4618	0.56	1.00	0.03	0.04
10.53_531.4000	0.57	1.00	0.00	0.00
6.95_368.2220	0.57	1.00	0.00	0.00
12.97_407.3144	0.58	1.00	0.13	0.08
12.98_399.3242	0.58	1.00	0.13	0.08
4.09_573.1785	0.58	1.00	0.00	0.00
4.37_663.2850	0.59	1.00	0.00	0.00
3.79_359.1699	0.60	0.30	1.00	0.89
13.98_433.3418	0.61	1.00	0.00	0.02
6.90_166.0720	0.61	1.00	0.00	0.00
4.64_412.2067	0.62	1.00	0.22	0.25
6.19_181.1351	0.63	1.00	0.00	0.00
11.58_415.2745	0.65	1.00	0.06	0.12
4.27_647.2871	0.67	1.00	0.05	0.09
11.44_223.2060	0.67	1.00	0.00	0.00
1.48_497.0811	0.68	0.39	1.00	0.99
8.08_219.1411	0.68	1.00	0.00	0.00

7.62_970.6124	0.70	1.00	0.00	0.00
4.81_506.2950	0.71	1.00	0.00	0.00
16.15_442.8736	0.71	1.00	0.00	0.00
7.07_184.1710	0.72	1.00	0.38	0.28
4.37_150.0945	0.72	1.00	0.00	0.01
3.89_518.1743	0.73	1.00	0.05	0.01
11.18_473.3585	0.75	1.00	0.03	0.02
12.74_443.3505	0.77	1.00	0.00	0.00
12.97_547.4060	0.77	1.00	0.34	0.23
15.06_413.2647	0.81	1.00	0.59	0.55
11.84_443.3878	0.82	1.00	0.04	0.04
11.03_354.1608	0.82	1.00	0.00	0.00
11.28_440.3462	0.82	1.00	0.00	0.00
12.98_282.2118	0.82	1.00	0.07	0.00
5.16_237.1592	0.87	1.00	0.00	0.00
10.38_401.3397	0.88	1.00	0.18	0.23
9.26_219.1735	0.88	1.00	0.00	0.00
13.49_295.2258	0.91	1.00	0.00	0.00
4.49_225.1597	0.97	1.00	0.18	0.14
5.94_213.1018	1.00	0.76	0.00	0.00
10.36_211.6353	1.00	0.89	0.06	0.01
11.31_225.6512	1.00	0.95	0.00	0.00
9.27_240.2315	1.00	0.88	0.16	0.50
10.39_268.2627	1.00	0.83	0.00	0.07
6.59_273.1670	1.00	0.84	0.46	0.23
11.44_291.1951	1.00	0.75	0.00	0.00
12.62_313.2746	1.00	0.83	0.43	0.46
6.39_336.2172	1.00	0.82	0.00	0.00
14.82_332.2940	1.00	0.65	0.08	0.00
15.49_338.3442	1.00	0.86	0.10	0.00
13.48_397.3392	1.00	0.75	0.00	0.00
10.78_415.3581	1.00	0.61	0.24	0.18
13.95_411.3586	1.00	0.78	0.06	0.08
13.27_419.3131	1.00	0.81	0.00	0.00
10.77_434.3251	1.00	0.58	0.00	0.00
10.98_442.3651	1.00	0.78	0.16	0.14
12.97_555.3910	1.00	0.94	0.52	0.61
13.92_641.5490	1.00	0.85	0.00	0.00
4.37_685.2548	1.00	0.86	0.10	0.00
7.66_916.7249	1.00	0.76	0.00	0.26
7.00_916.3325	1.00	0.59	0.00	0.00

Table A3.19. Normalized heat map of features described as unique in **Figure 3.2(B)** and **(C)** when comparing wild type *Nocardiopsis sp. FU40 ΔApoS8* to the S5 streptomycin resistant mutant extract using OPLS-DA and extracting features from the generated S-plot with correlation coefficients ≥0.9. Features are normalized to maximum intensity for that feature.

Feature ID (RT_*m/z*)	WT	WT	S5	S5
12.03_135.1163	0.00	0.04	0.79	1.00
12.03_123.1165	0.00	0.00	0.84	1.00
4.95_114.0908	0.00	0.00	0.96	1.00
1.50_103.5345	0.00	0.00	0.92	1.00
12.03_149.1327	0.00	0.00	0.88	1.00
1.50_165.0624	0.00	0.00	1.00	0.96
6.56_162.0938	0.00	0.00	0.82	1.00
16.16_174.0876	0.00	0.00	0.60	1.00
5.78_170.1204	0.00	0.00	0.97	1.00
2.44_166.0747	0.00	0.24	1.00	0.91
6.60_180.1017	0.00	0.01	0.89	1.00
5.02_180.1014	0.00	0.00	0.90	1.00
4.95_177.1399	0.00	0.27	0.99	1.00
9.26_191.1250	0.00	0.00	0.89	1.00
9.12_191.0134	0.00	0.00	0.88	1.00
4.14_186.1168	0.00	0.00	0.81	1.00
4.02_198.1143	0.00	0.00	1.00	0.61
8.84_203.1804	0.00	0.00	0.85	1.00
8.12_203.1781	0.00	0.00	0.96	1.00
6.22_203.0786	0.00	0.02	1.00	0.92
9.80_203.0277	0.00	0.00	0.93	1.00
7.49_207.0994	0.00	0.06	0.86	1.00
1.30_205.9283	0.00	0.00	1.00	0.89
4.84_205.1323	0.00	0.00	1.00	0.89
1.32_211.8786	0.00	0.00	1.00	0.92
1.49_211.0584	0.00	0.25	1.00	0.88
9.81_210.0363	0.00	0.00	1.00	0.65
9.41_219.0312	0.00	0.00	1.00	0.77
8.84_221.1903	0.00	0.00	0.98	1.00
4.61_230.0715	0.00	0.25	1.00	0.81
10.62_236.1643	0.00	0.00	1.00	0.97
5.11_236.1306	0.00	0.11	0.88	1.00
8.54_235.1344	0.00	0.00	0.96	1.00
7.38_246.1513	0.00	0.00	0.62	1.00
2.62_252.0382	0.00	0.47	0.96	1.00
4.31_249.0807	0.00	0.00	0.73	1.00
10.50_252.0400	0.00	0.11	0.52	1.00
8.08_252.0397	0.00	0.00	1.00	0.97
4.56_252.0394	0.00	0.09	0.81	1.00
6.01_252.0391	0.00	0.00	0.56	1.00
7.48_252.0388	0.00	0.00	0.82	1.00
3.58_252.0387	0.00	0.35	1.00	1.00
3.87_257.1146	0.00	0.34	0.72	1.00
9.81_253.5524	0.00	0.12	1.00	0.57
12.02_263.1978	0.00	0.03	0.93	1.00
1.78_262.1278	0.00	0.00	0.74	1.00
5.86_262.1048	0.00	0.22	0.91	1.00
10.71_261.1779	0.00	0.01	0.90	1.00
5.01_261.1438	0.00	0.16	1.00	0.98
9.03_260.5527	0.00	0.00	1.00	0.76
6.81_268.0194	0.00	0.00	0.64	1.00
6.28_268.0191	0.00	0.13	1.00	0.72
10.77_267.1616	0.00	0.05	0.99	1.00
5.18_266.1406	0.00	0.28	1.00	0.89
5.27_264.2082	0.00	0.00	0.97	1.00
4.60_268.0196	0.00	0.00	0.83	1.00

9.12_279.1585	0.00	0.00	0.54	1.00
7.18_278.2110	0.00	0.00	0.79	1.00
6.07_276.1943	0.00	0.00	1.00	0.74
7.50_283.1523	0.00	0.03	0.93	1.00
1.73_282.0649	0.00	0.01	0.74	1.00
7.72_281.1420	0.00	0.00	1.00	0.98
3.86_294.1559	0.00	0.44	0.98	1.00
7.15_293.2251	0.00	0.00	0.69	1.00
4.87_293.1612	0.00	0.19	1.00	0.61
6.49_292.1923	0.00	0.03	0.89	1.00
3.76_299.1387	0.00	0.04	0.68	1.00
7.73_298.2024	0.00	0.00	0.88	1.00
4.74_298.0969	0.00	0.09	1.00	0.92
9.60_297.1694	0.00	0.01	1.00	1.00
7.19_296.2224	0.00	0.00	0.85	1.00
12.02_309.1921	0.00	0.01	0.90	1.00
6.00_308.2238	0.00	0.00	1.00	0.57
6.06_312.2197	0.00	0.00	1.00	0.83
7.24_312.2197	0.00	0.00	0.97	1.00
10.59_311.1859	0.00	0.00	0.80	1.00
5.82_322.1007	0.00	0.00	1.00	0.99
1.74_322.0446	0.00	0.01	0.78	1.00
9.13_319.1539	0.00	0.00	0.91	1.00
6.92_318.2094	0.00	0.00	1.00	0.94
12.03_325.1706	0.00	0.00	0.84	1.00
8.76_329.1942	0.00	0.09	0.81	1.00
10.73_340.1475	0.00	0.14	1.00	0.71
5.99_338.1374	0.00	0.00	1.00	0.97
6.22_346.2031	0.00	0.00	0.95	1.00
7.48_345.1875	0.00	0.00	1.00	0.72
7.37_344.2218	0.00	0.00	0.73	1.00
5.26_354.0787	0.00	0.18	0.81	1.00
4.01_351.5992	0.00	0.00	1.00	0.57
6.67_362.2335	0.00	0.00	1.00	0.74
6.51_360.2165	0.00	0.00	0.96	1.00
8.53_359.2035	0.00	0.13	1.00	0.80
7.52_368.2211	0.00	0.00	0.71	1.00
9.80_367.0822	0.00	0.00	1.00	1.00
7.83_387.1861	0.00	0.00	1.00	1.00
9.80_387.0731	0.00	0.00	0.59	1.00
6.24_384.2171	0.00	0.00	0.71	1.00
1.49_394.1142	0.00	0.00	0.69	1.00
9.08_429.0845	0.00	0.00	1.00	0.88
4.02_423.1940	0.00	0.00	0.75	1.00
7.98_431.2698	0.00	0.06	0.90	1.00
1.48_431.0890	0.00	0.30	0.88	1.00
9.07_451.0615	0.00	0.00	0.68	1.00
6.99_443.3240	0.00	0.23	0.87	1.00
9.73_443.1014	0.00	0.00	1.00	0.95
10.02_459.0960	0.00	0.00	0.87	1.00
9.03_457.1145	0.00	0.02	0.69	1.00
6.21_455.1906	0.00	0.09	0.66	1.00
6.46_471.2466	0.00	0.03	0.93	1.00
9.79_462.0710	0.00	0.00	0.89	1.00
9.78_481.0499	0.00	0.00	0.92	1.00
9.02_479.0963	0.00	0.00	0.83	1.00
7.51_499.2782	0.00	0.02	1.00	0.97
4.37_494.2617	0.00	0.00	0.78	1.00
1.49_527.1567	0.00	0.00	0.55	1.00
7.21_526.2839	0.00	0.15	0.70	1.00
7.20_544.2918	0.00	0.00	1.00	0.80
12.03_549.4012	0.00	0.00	0.87	1.00
5.52_601.2501	0.00	0.00	0.86	1.00
5.18_599.2879	0.00	0.00	1.00	0.78
1.76_588.1814	0.00	0.00	0.69	1.00
1.25_639.8836	0.00	0.00	1.00	0.77
9.79_683.1204	0.00	0.00	1.00	0.63
9.80_907.1678	0.00	0.00	1.00	1.00
7.62_891.8938	0.00	0.00	1.00	0.76
8.34_150.0928	0.00	0.05	1.00	0.94

9.79_218.0234	0.01	0.05	0.92	1.00
6.24_515.2753	0.01	0.00	0.77	1.00
1.29_203.9309	0.01	0.00	1.00	0.72
7.48_177.0877	0.01	0.00	0.69	1.00
8.10_301.1534	0.01	0.03	0.81	1.00
5.66_384.2168	0.01	0.00	0.81	1.00
12.02_205.1953	0.01	0.00	0.84	1.00
9.78_465.0808	0.02	0.04	0.81	1.00
6.76_310.2021	0.02	0.00	0.93	1.00
8.29_401.1993	0.02	0.00	0.93	1.00
6.06_294.2084	0.02	0.00	0.75	1.00
3.22_235.1201	0.03	0.00	1.00	0.84
16.15_710.1773	0.03	0.01	1.00	0.97
9.66_279.1583	0.03	0.00	0.73	1.00
1.73_338.0231	0.04	0.00	0.82	1.00
1.74_150.0789	0.04	0.00	1.00	0.99
10.18_223.2085	0.04	0.25	1.00	0.79
3.07_230.1126	0.05	0.11	0.79	1.00
5.97_286.6247	0.05	0.01	0.92	1.00
8.53_283.1523	0.05	0.10	0.92	1.00
4.37_326.1802	0.05	0.29	0.77	1.00
6.95_218.1203	0.05	0.10	0.89	1.00
9.14_239.1284	0.05	0.05	1.00	0.70
7.42_280.1237	0.06	0.16	0.95	1.00
8.53_177.0880	0.06	0.06	0.72	1.00
3.86_150.0940	0.06	0.11	0.92	1.00
10.52_673.3745	0.06	0.09	0.87	1.00
8.53_207.1002	0.06	0.07	0.84	1.00
5.43_377.1482	0.06	0.00	0.86	1.00
5.97_278.6345	0.06	0.02	1.00	0.96
4.75_136.0625	0.07	0.00	0.66	1.00
1.53_143.0837	0.08	0.10	0.93	1.00
6.72_1450.6973	0.08	0.02	1.00	0.92
6.41_165.0905	0.09	0.06	0.83	1.00
1.77_218.1042	0.09	0.02	0.92	1.00
7.89_192.1015	0.10	0.17	0.80	1.00
7.42_196.0651	0.10	0.05	0.58	1.00
7.06_221.1900	0.12	0.36	1.00	0.97
15.37_230.0721	0.12	0.40	0.82	1.00
4.30_478.1379	0.13	0.03	0.66	1.00
9.47_211.0868	0.13	0.23	0.82	1.00
3.83_198.1623	0.13	0.09	0.86	1.00
4.87_329.1844	0.13	0.00	0.95	1.00
3.82_230.1126	0.14	0.09	0.81	1.00
6.06_203.1781	0.15	0.26	0.83	1.00
7.06_203.1787	0.15	0.28	0.88	1.00
4.30_310.1305	0.15	0.03	0.80	1.00
3.85_276.1433	0.16	0.09	0.78	1.00
6.73_1161.1593	0.16	0.04	0.85	1.00
5.96_534.2942	0.16	0.04	0.97	1.00
6.78_176.0714	0.17	0.28	0.81	1.00
6.71_1160.7578	0.17	0.00	1.00	0.86
9.41_281.1770	0.19	0.36	0.99	1.00
6.73_1160.5609	0.20	0.00	1.00	1.00
1.60_229.1318	0.21	0.04	0.91	1.00
5.27_685.1761	0.22	0.00	0.72	1.00
4.88_188.0708	0.23	0.39	0.94	1.00
5.61_343.2002	0.23	0.05	0.84	1.00
4.81_464.2611	0.24	0.29	0.94	1.00
3.80_194.0821	0.26	0.00	0.66	1.00
9.11_505.3321	0.27	0.00	0.93	1.00
16.22_252.0441	0.28	0.50	0.80	1.00
5.81_605.2195	0.28	0.40	0.77	1.00
16.18_335.9929	0.28	0.00	0.95	1.00
4.32_308.1712	0.29	0.11	0.73	1.00
4.26_450.2439	0.31	0.02	0.69	1.00
6.60_152.1087	0.31	0.58	0.95	1.00
6.74_1160.9454	0.32	0.26	1.00	0.79
4.63_149.1104	0.32	0.51	0.98	1.00
5.34_191.1575	0.32	0.46	0.91	1.00

4.86_372.1909	0.32	0.17	0.79	1.00
4.00_320.1711	0.33	0.04	0.80	1.00
5.16_210.1137	0.33	0.33	0.91	1.00
6.10_320.1966	0.33	0.00	0.70	1.00
1.49_365.1079	0.35	0.48	0.78	1.00
16.15_481.1090	0.35	0.00	0.73	1.00
6.15_485.2027	0.36	0.38	0.68	1.00
7.25_371.1508	0.36	0.00	1.00	0.98
6.40_263.1761	0.36	0.38	0.81	1.00
3.85_258.1333	0.36	0.00	0.73	1.00
4.53_236.1764	0.37	0.48	0.94	1.00
7.29_331.2114	0.38	0.55	0.91	1.00
5.78_164.0706	0.39	0.52	1.00	0.96
8.22_220.1332	0.39	0.57	0.94	1.00
3.75_267.1417	0.40	0.50	0.78	1.00
9.69_220.1127	0.41	0.48	1.00	0.98
5.71_249.1598	0.41	0.57	0.84	1.00
4.40_158.0302	0.42	0.31	1.00	0.98
5.20_239.1759	0.42	0.69	0.98	1.00
4.67_270.1917	0.43	0.59	0.81	1.00
3.79_359.1699	0.45	0.22	0.72	1.00
4.34_266.1408	0.45	0.35	0.75	1.00
3.94_254.1629	0.45	0.17	0.91	1.00
4.70_221.1315	0.45	0.67	0.96	1.00
4.16_256.1718	0.46	0.62	0.88	1.00
12.73_328.1928	0.46	0.00	0.98	1.00
6.40_439.1986	0.47	0.47	0.81	1.00
8.66_655.2795	0.48	1.00	0.00	0.00
6.23_251.1781	0.49	0.54	0.87	1.00
3.93_438.1964	0.49	0.18	0.91	1.00
1.48_610.1314	0.50	0.23	0.82	1.00
10.60_346.3091	0.51	1.00	0.00	0.00
3.86_242.1126	0.51	0.56	0.83	1.00
10.40_371.3275	0.52	1.00	0.02	0.02
9.48_225.1993	0.53	1.00	0.02	0.02
1.50_401.0693	0.54	0.50	1.00	0.98
4.26_669.2631	0.56	1.00	0.00	0.08
11.80_235.1712	0.56	1.00	0.00	0.09
10.15_739.4618	0.56	1.00	0.11	0.07
5.72_240.1231	0.56	0.39	0.89	1.00
10.53_531.4000	0.57	1.00	0.00	0.00
4.37_663.2850	0.59	1.00	0.00	0.00
12.63_394.2284	0.59	0.45	1.00	0.87
6.59_273.1670	0.60	0.51	0.84	1.00
13.48_341.2200	0.60	0.66	1.00	0.86
13.98_433.3418	0.61	1.00	0.05	0.00
5.43_241.1546	0.61	0.63	0.93	1.00
4.64_412.2067	0.62	1.00	0.15	0.20
6.19_181.1351	0.63	1.00	0.08	0.10
10.97_401.2525	0.63	1.00	0.08	0.21
4.64_137.0376	0.64	0.67	0.83	1.00
3.99_164.0936	0.65	0.59	0.89	1.00
11.58_415.2745	0.65	1.00	0.07	0.02
12.62_273.1378	0.66	1.00	0.00	0.00
4.27_647.2871	0.67	1.00	0.09	0.00
11.44_223.2060	0.67	1.00	0.00	0.00
8.08_219.1411	0.68	1.00	0.30	0.24
6.85_824.9348	0.70	1.00	0.00	0.23
16.15_442.8736	0.71	1.00	0.00	0.00
7.07_184.1710	0.72	1.00	0.00	0.00
4.37_150.0945	0.72	1.00	0.00	0.00
3.89_518.1743	0.73	1.00	0.06	0.00
11.18_473.3585	0.75	1.00	0.08	0.04
12.74_443.3505	0.77	1.00	0.01	0.00
1.50_230.0720	0.77	0.58	1.00	0.98
11.97_299.2600	0.80	1.00	0.31	0.21
15.06_413.2647	0.81	1.00	0.42	0.57
11.84_443.3878	0.82	1.00	0.11	0.06
11.03_354.1608	0.82	1.00	0.09	0.25
11.28_440.3462	0.82	1.00	0.00	0.00

12.98_282.2118	0.82	1.00	0.15	0.10
5.16_237.1592	0.87	1.00	0.66	0.73
10.38_401.3397	0.88	1.00	0.27	0.16
9.26_219.1735	0.88	1.00	0.00	0.00
4.50_359.1197	0.89	1.00	0.00	0.00
15.94_338.3442	0.91	1.00	0.74	0.68
13.49_295.2258	0.91	1.00	0.06	0.00
1.47_508.0657	0.91	1.00	0.37	0.00
4.49_225.1597	0.97	1.00	0.54	0.56
12.89_441.3208	0.99	1.00	0.49	0.58
10.36_211.6353	1.00	0.89	0.03	0.00
11.31_225.6512	1.00	0.95	0.00	0.00
9.27_240.2315	1.00	0.88	0.00	0.00
10.39_268.2627	1.00	0.83	0.00	0.00
11.44_291.1951	1.00	0.75	0.00	0.00
12.62_313.2746	1.00	0.83	0.12	0.11
14.31_325.2414	1.00	0.74	0.00	0.00
15.49_338.3442	1.00	0.86	0.00	0.00
13.48_397.3392	1.00	0.75	0.00	0.00
13.95_411.3586	1.00	0.78	0.06	0.00
13.27_419.3131	1.00	0.81	0.00	0.00
10.98_442.3651	1.00	0.78	0.00	0.29
12.97_555.3910	1.00	0.94	0.77	0.59
12.75_617.4294	1.00	0.84	0.36	0.00
13.92_641.5490	1.00	0.85	0.00	0.00
4.37_685.2548	1.00	0.86	0.12	0.23
7.00_916.3325	1.00	0.59	0.00	0.00

Table A3.20. Normalized heat map of features described as unique in **Figure 3.2(B)** and **(C)** when comparing wild type *Nocardiopsis sp. FU40 ΔApoS8* to the S6 streptomycin resistant mutant extract using OPLS-DA and extracting features from the generated S-plot with correlation coefficients ≥0.9. Features are normalized to maximum intensity for that feature.

Feature ID (RT_*m/z*)	WT	WT	S6	S6
12.03_135.1163	0.00	0.04	0.52	1.00
12.03_123.1165	0.00	0.00	0.83	1.00
1.50_103.5345	0.00	0.00	0.90	1.00
12.03_149.1327	0.00	0.00	0.77	1.00
13.61_149.0907	0.00	0.00	1.00	0.65
1.50_165.0624	0.00	0.00	0.96	1.00
6.56_162.0938	0.00	0.00	0.91	1.00
4.31_160.1140	0.00	0.00	0.71	1.00
16.16_174.0876	0.00	0.00	0.77	1.00
5.78_170.1204	0.00	0.00	0.84	1.00
7.08_169.0882	0.00	0.05	0.72	1.00
6.60_180.1017	0.00	0.02	1.00	0.97
5.02_180.1014	0.00	0.00	0.73	1.00
10.70_179.1435	0.00	0.00	1.00	0.89
4.95_177.1399	0.00	0.17	0.64	1.00
4.39_192.1130	0.00	0.27	0.80	1.00
9.12_191.0134	0.00	0.00	0.86	1.00
4.14_186.1168	0.00	0.00	0.86	1.00
4.02_198.1143	0.00	0.00	0.97	1.00
9.08_196.0187	0.00	0.00	0.64	1.00
8.84_203.1804	0.00	0.00	0.95	1.00
8.12_203.1781	0.00	0.00	0.91	1.00
6.22_203.0786	0.00	0.08	1.00	0.92
9.08_203.0278	0.00	0.00	0.77	1.00
9.80_203.0277	0.00	0.00	0.61	1.00
9.42_202.0393	0.00	0.00	0.61	1.00
5.44_208.0539	0.00	0.01	0.91	1.00
7.49_207.0994	0.00	0.07	0.89	1.00
1.30_205.9283	0.00	0.00	0.96	1.00
4.84_205.1323	0.00	0.00	0.62	1.00
10.22_205.1232	0.00	0.00	0.61	1.00
8.67_212.0251	0.00	0.00	1.00	0.81
1.32_211.8786	0.00	0.00	0.94	1.00
1.49_211.0584	0.00	0.14	0.92	1.00
9.81_210.0363	0.00	0.00	0.60	1.00
5.35_210.0350	0.00	0.00	0.84	1.00
9.41_219.0312	0.00	0.00	0.93	1.00
10.24_222.1533	0.00	0.14	1.00	0.98
8.84_221.1903	0.00	0.00	1.00	0.94
6.51_220.1710	0.00	0.04	1.00	0.60
8.67_226.0395	0.00	0.00	1.00	0.94
7.99_225.1125	0.00	0.09	0.76	1.00
9.04_225.0298	0.00	0.02	0.56	1.00
9.77_224.0325	0.00	0.00	0.95	1.00
5.48_229.0656	0.00	0.00	0.95	1.00
9.82_230.0718	0.00	0.05	1.00	0.75
5.11_236.1306	0.00	0.11	0.76	1.00
9.80_241.0261	0.00	0.00	1.00	0.83
8.82_241.0249	0.00	0.00	0.97	1.00
5.04_244.1219	0.00	0.00	0.71	1.00
11.26_250.1814	0.00	0.00	1.00	0.69
8.08_252.0397	0.00	0.00	1.00	0.69
9.63_252.0395	0.00	0.00	0.48	1.00
6.01_252.0391	0.00	0.00	0.79	1.00
5.12_252.0389	0.00	0.00	1.00	0.84
7.48_252.0388	0.00	0.00	0.62	1.00
3.87_257.1146	0.00	0.30	0.82	1.00

12.02_263.1978	0.00	0.03	0.77	1.00
1.78_262.1278	0.00	0.00	0.86	1.00
5.86_262.1048	0.00	0.22	0.90	1.00
10.71_261.1779	0.00	0.00	0.71	1.00
5.01_261.1438	0.00	0.12	0.78	1.00
10.77_267.1616	0.00	0.21	0.58	1.00
5.18_266.1406	0.00	0.18	0.78	1.00
5.27_264.2082	0.00	0.00	1.00	0.78
7.18_278.2110	0.00	0.00	0.83	1.00
6.07_276.1943	0.00	0.00	0.83	1.00
12.79_284.1681	0.00	0.20	0.88	1.00
7.50_283.1523	0.00	0.05	1.00	0.82
1.73_282.0649	0.00	0.01	0.63	1.00
7.82_294.2085	0.00	0.00	1.00	1.00
4.87_293.1612	0.00	0.21	0.98	1.00
6.49_292.1923	0.00	0.03	1.00	0.96
4.74_298.0969	0.00	0.07	1.00	0.84
9.60_297.1694	0.00	0.05	0.66	1.00
7.19_296.2224	0.00	0.00	0.94	1.00
3.78_300.1386	0.00	0.10	0.69	1.00
12.02_309.1921	0.00	0.01	0.99	1.00
6.00_308.2238	0.00	0.00	0.80	1.00
6.06_312.2197	0.00	0.00	1.00	0.91
6.84_312.2197	0.00	0.00	0.91	1.00
7.24_312.2197	0.00	0.00	1.00	0.78
5.82_322.1007	0.00	0.00	1.00	0.98
6.92_318.2094	0.00	0.00	1.00	0.76
7.34_326.2353	0.00	0.00	1.00	0.82
6.01_326.2353	0.00	0.00	0.80	1.00
12.03_325.1706	0.00	0.00	0.78	1.00
8.76_329.1942	0.00	0.06	0.98	1.00
5.84_341.1007	0.00	0.00	1.00	0.70
5.19_344.6196	0.00	0.18	0.77	1.00
7.37_344.2218	0.00	0.00	0.98	1.00
5.26_354.0787	0.00	0.13	1.00	0.83
8.24_352.2057	0.00	0.00	0.91	1.00
4.01_351.5992	0.00	0.00	1.00	1.00
6.67_362.2335	0.00	0.00	0.67	1.00
6.51_360.2165	0.00	0.00	1.00	0.75
9.80_367.0822	0.00	0.00	0.61	1.00
9.80_387.0731	0.00	0.00	0.64	1.00
6.88_386.2329	0.00	0.01	1.00	0.82
6.89_384.2172	0.00	0.00	0.57	1.00
6.24_384.2171	0.00	0.00	0.92	1.00
8.63_398.2317	0.00	0.00	0.87	1.00
1.49_394.1142	0.00	0.00	0.83	1.00
3.74_416.1928	0.00	0.07	0.72	1.00
9.08_429.0845	0.00	0.00	1.00	0.92
4.02_423.1940	0.00	0.00	0.55	1.00
9.07_451.0615	0.00	0.00	0.78	1.00
6.99_443.3240	0.00	0.15	1.00	0.61
9.73_443.1014	0.00	0.00	1.00	0.99
8.80_443.0945	0.00	0.00	0.95	1.00
10.02_459.0960	0.00	0.00	1.00	0.93
9.03_457.1145	0.00	0.01	1.00	0.98
6.21_455.1906	0.00	0.10	0.95	1.00
9.81_454.0847	0.00	0.00	0.80	1.00
9.05_454.0819	0.00	0.00	1.00	0.98
6.46_471.2466	0.00	0.01	0.76	1.00
8.82_465.0807	0.00	0.00	0.84	1.00
9.79_462.0710	0.00	0.00	0.68	1.00
9.04_462.0699	0.00	0.00	0.59	1.00
9.78_481.0499	0.00	0.00	0.87	1.00
9.02_479.0963	0.00	0.00	0.79	1.00
7.37_478.2069	0.00	0.12	0.69	1.00
4.15_476.2404	0.00	0.00	1.00	0.96
7.51_499.2782	0.00	0.05	1.00	0.83
8.58_490.2972	0.00	0.00	1.00	0.76
9.79_513.1525	0.00	0.00	0.79	1.00
5.64_515.2738	0.00	0.01	0.57	1.00

6.62_515.2737	0.00	0.00	1.00	0.61
1.76_515.1445	0.00	0.00	0.60	1.00
7.21_526.2839	0.00	0.02	1.00	0.95
7.20_544.2918	0.00	0.00	1.00	0.68
6.63_570.3104	0.00	0.00	0.95	1.00
12.03_565.3746	0.00	0.00	0.96	1.00
9.67_563.3802	0.00	0.00	0.86	1.00
6.90_555.3068	0.00	0.00	0.84	1.00
1.72_551.1035	0.00	0.00	0.72	1.00
12.03_549.4012	0.00	0.00	1.00	0.86
9.02_590.6205	0.00	0.00	0.87	1.00
9.79_576.6021	0.00	0.00	0.77	1.00
1.25_639.8836	0.00	0.00	0.63	1.00
12.72_634.4531	0.00	0.00	1.00	0.53
9.79_683.1204	0.00	0.00	0.84	1.00
7.20_920.0962	0.00	0.00	1.00	0.83
9.80_907.1678	0.00	0.00	1.00	1.00
7.01_1221.4414	0.00	0.00	0.91	1.00
9.79_218.0234	0.00	0.01	0.64	1.00
8.34_150.0928	0.00	0.03	0.85	1.00
9.78_465.0808	0.00	0.01	0.78	1.00
9.81_269.0437	0.00	0.00	0.57	1.00
6.76_310.2021	0.00	0.00	0.99	1.00
6.24_515.2753	0.01	0.00	1.00	0.78
8.10_301.1534	0.01	0.03	1.00	0.92
5.66_384.2168	0.01	0.00	0.95	1.00
1.29_203.9309	0.01	0.00	0.99	1.00
7.48_177.0877	0.01	0.00	0.81	1.00
8.74_542.3146	0.01	0.00	1.00	0.77
12.02_205.1953	0.01	0.00	0.89	1.00
3.22_235.1201	0.02	0.00	0.59	1.00
6.65_282.2073	0.02	0.11	1.00	0.97
16.15_710.1773	0.02	0.01	1.00	0.63
5.43_377.1482	0.02	0.00	0.85	1.00
8.54_447.2904	0.02	0.21	1.00	1.00
1.74_150.0789	0.03	0.00	0.69	1.00
8.53_177.0880	0.03	0.03	0.81	1.00
4.75_136.0625	0.03	0.00	0.83	1.00
8.53_283.1523	0.03	0.07	1.00	0.92
6.95_218.1203	0.03	0.07	0.71	1.00
8.53_207.1002	0.04	0.04	0.97	1.00
9.79_1349.2480	0.04	0.00	0.82	1.00
7.06_325.1861	0.04	0.21	1.00	0.95
1.73_338.0231	0.04	0.00	1.00	0.98
3.86_150.0940	0.04	0.08	0.83	1.00
10.52_673.3745	0.05	0.08	0.97	1.00
3.07_230.1126	0.06	0.14	1.00	0.79
1.70_260.1135	0.06	0.00	0.83	1.00
1.82_228.1004	0.06	0.01	0.92	1.00
10.18_223.2085	0.06	0.39	1.00	0.81
1.53_143.0837	0.07	0.09	0.75	1.00
7.42_196.0651	0.07	0.04	0.55	1.00
4.82_393.2208	0.07	0.00	1.00	0.93
6.66_264.1980	0.08	0.03	0.99	1.00
6.41_165.0905	0.08	0.06	0.80	1.00
7.42_280.1237	0.09	0.26	1.00	0.96
4.87_329.1844	0.10	0.00	0.91	1.00
5.27_685.1761	0.10	0.00	0.77	1.00
6.78_176.0714	0.11	0.18	0.79	1.00
7.06_221.1900	0.11	0.34	0.90	1.00
7.89_192.1015	0.11	0.20	0.74	1.00
5.97_286.6247	0.12	0.02	0.83	1.00
4.30_310.1305	0.12	0.03	0.95	1.00
7.06_203.1787	0.12	0.23	0.87	1.00
5.97_278.6345	0.12	0.03	0.61	1.00
6.06_203.1781	0.13	0.22	0.92	1.00
1.77_218.1042	0.13	0.03	0.92	1.00
9.47_211.0868	0.13	0.23	0.78	1.00
16.18_335.9929	0.14	0.00	1.00	0.75
5.81_605.2195	0.14	0.20	0.97	1.00

3.82_230.1126	0.16	0.10	1.00	0.92
4.63_149.1104	0.21	0.35	0.81	1.00
4.88_188.0708	0.22	0.37	1.00	1.00
7.29_331.2114	0.22	0.32	0.81	1.00
4.31_265.0552	0.22	0.00	0.66	1.00
1.60_229.1318	0.23	0.05	0.90	1.00
8.29_401.1993	0.24	0.00	0.86	1.00
1.73_288.1454	0.24	0.00	1.00	0.94
5.81_222.1598	0.25	0.48	0.91	1.00
6.60_152.1087	0.26	0.47	0.83	1.00
4.64_137.0376	0.26	0.27	0.75	1.00
16.15_365.1085	0.28	0.00	1.00	0.86
6.15_485.2027	0.29	0.31	0.98	1.00
4.77_179.0472	0.29	0.54	0.96	1.00
6.34_150.0787	0.31	0.29	0.81	1.00
4.34_266.1408	0.31	0.24	0.72	1.00
16.18_204.8884	0.32	0.00	1.00	0.98
8.22_220.1332	0.33	0.49	0.84	1.00
5.78_164.0706	0.34	0.46	0.95	1.00
6.62_297.1617	0.34	0.61	0.90	1.00
5.71_249.1598	0.35	0.49	0.88	1.00
4.40_158.0302	0.36	0.26	0.83	1.00
4.70_268.1679	0.36	0.65	1.00	0.99
3.80_288.1929	0.37	0.32	1.00	0.77
4.67_270.1917	0.38	0.52	0.97	1.00
4.16_256.1718	0.38	0.51	0.99	1.00
4.00_320.1711	0.38	0.04	1.00	0.73
3.94_254.1629	0.39	0.15	1.00	0.94
6.34_469.2088	0.39	0.51	1.00	0.92
5.16_210.1137	0.41	0.40	0.80	1.00
16.17_188.9130	0.42	0.00	1.00	1.00
6.23_251.1781	0.42	0.46	0.81	1.00
6.40_263.1761	0.43	0.46	0.91	1.00
3.75_267.1417	0.44	0.55	0.98	1.00
6.10_320.1966	0.44	0.00	0.94	1.00
3.82_209.1275	0.44	0.40	0.78	1.00
4.66_304.1776	0.45	0.67	1.00	0.97
6.40_439.1986	0.46	0.46	1.00	1.00
11.27_448.3444	0.48	1.00	0.00	0.00
12.43_386.2820	0.50	1.00	0.00	0.00
3.75_245.1607	0.50	0.67	1.00	0.91
16.14_274.0340	0.51	0.36	1.00	0.77
10.60_346.3091	0.51	1.00	0.00	0.00
10.40_371.3275	0.52	1.00	0.00	0.00
10.70_288.2557	0.52	1.00	0.00	0.00
3.86_242.1126	0.52	0.57	0.82	1.00
9.48_225.1993	0.53	1.00	0.00	0.02
3.94_180.0961	0.54	0.24	0.90	1.00
6.74_1160.9454	0.54	0.45	0.89	1.00
3.79_359.1699	0.55	0.27	0.90	1.00
13.53_339.2529	0.55	1.00	0.00	0.00
7.22_541.3491	0.56	1.00	0.00	0.10
4.26_669.2631	0.56	1.00	0.00	0.00
11.80_235.1712	0.56	1.00	0.06	0.07
10.15_739.4618	0.56	1.00	0.08	0.07
14.41_309.2409	0.56	1.00	0.22	0.09
5.95_273.1788	0.56	1.00	0.23	0.00
10.53_531.4000	0.57	1.00	0.00	0.00
4.59_251.1399	0.57	0.57	0.85	1.00
12.97_407.3144	0.58	1.00	0.24	0.02
5.72_240.1231	0.58	0.40	0.95	1.00
6.02_274.1066	0.58	0.40	0.86	1.00
12.98_399.3242	0.58	1.00	0.22	0.02
4.37_663.2850	0.59	1.00	0.00	0.00
13.98_433.3418	0.61	1.00	0.04	0.00
6.90_166.0720	0.61	1.00	0.00	0.00
5.20_239.1759	0.62	1.00	0.25	0.31
9.69_220.1127	0.62	0.72	0.88	1.00
4.64_412.2067	0.62	1.00	0.07	0.20
6.19_181.1351	0.63	1.00	0.06	0.11

10.97_401.2525	0.63	1.00	0.00	0.09
11.58_415.2745	0.65	1.00	0.00	0.03
12.62_273.1378	0.66	1.00	0.00	0.00
4.27_647.2871	0.67	1.00	0.00	0.07
1.50_448.0831	0.67	1.00	0.19	0.00
11.44_223.2060	0.67	1.00	0.00	0.00
1.50_423.1007	0.67	1.00	0.00	0.20
8.08_219.1411	0.68	1.00	0.00	0.00
4.81_415.2090	0.69	0.48	0.91	1.00
16.15_442.8736	0.71	1.00	0.00	0.00
7.07_184.1710	0.72	1.00	0.00	0.00
4.37_150.0945	0.72	1.00	0.00	0.00
3.89_518.1743	0.73	1.00	0.00	0.02
11.18_473.3585	0.75	1.00	0.04	0.02
12.86_463.2998	0.77	1.00	0.31	0.33
12.74_443.3505	0.77	1.00	0.00	0.00
12.97_547.4060	0.77	1.00	0.46	0.06
13.86_425.2896	0.78	1.00	0.55	0.40
11.97_299.2600	0.80	1.00	0.05	0.00
15.06_413.2647	0.81	1.00	0.53	0.42
11.84_443.3878	0.82	1.00	0.14	0.07
11.03_354.1608	0.82	1.00	0.06	0.05
11.28_440.3462	0.82	1.00	0.00	0.00
12.98_282.2118	0.82	1.00	0.00	0.00
13.79_365.2675	0.84	1.00	0.00	0.00
4.81_464.2611	0.84	1.00	0.48	0.21
12.83_546.4021	0.86	1.00	0.71	0.59
10.38_401.3397	0.88	1.00	0.41	0.26
9.26_219.1735	0.88	1.00	0.00	0.00
10.84_227.1557	0.90	1.00	0.62	0.43
15.94_338.3442	0.91	1.00	0.58	0.52
13.49_295.2258	0.91	1.00	0.05	0.01
1.47_508.0657	0.91	1.00	0.53	0.67
1.50_260.0296	0.92	1.00	0.28	0.12
12.73_320.2010	0.94	1.00	0.00	0.37
4.49_225.1597	0.97	1.00	0.22	0.24
5.43_241.1546	0.98	1.00	0.00	0.00
12.89_441.3208	0.99	1.00	0.65	0.48
3.99_164.0936	1.00	0.90	0.67	0.59
1.64_174.0879	1.00	0.59	0.00	0.00
5.94_213.1018	1.00	0.76	0.00	0.00
10.36_211.6353	1.00	0.89	0.00	0.00
11.31_225.6512	1.00	0.95	0.03	0.00
9.27_240.2315	1.00	0.88	0.00	0.30
10.39_268.2627	1.00	0.83	0.00	0.00
11.44_291.1951	1.00	0.75	0.00	0.00
11.33_299.2599	1.00	0.77	0.00	0.00
12.62_313.2746	1.00	0.83	0.00	0.00
14.31_325.2414	1.00	0.74	0.00	0.24
4.25_343.1235	1.00	0.70	0.00	0.00
15.49_338.3442	1.00	0.86	0.00	0.00
13.48_397.3392	1.00	0.75	0.03	0.00
13.95_411.3586	1.00	0.78	0.06	0.00
13.27_419.3131	1.00	0.81	0.00	0.00
10.77_434.3251	1.00	0.58	0.00	0.00
12.86_485.3471	1.00	0.86	0.57	0.49
1.61_539.0459	1.00	0.57	0.00	0.00
13.92_641.5490	1.00	0.85	0.00	0.00
4.37_685.2548	1.00	0.86	0.00	0.00
7.66_916.7249	1.00	0.76	0.00	0.25

Table A3.21. Normalized heat map of features described as unique in **Figure 3.3(A)** when comparing wild type *Nocardiopsis sp. FU40 ΔApoS8* and S5 streptomycin resistant mutant to the R4 rifampicin resistant mutant extract using OPLS-DA and extracting features from the generated S-plot with correlation coefficients ≥0.9. Features are normalized to maximum intensity for that feature.

Feature ID (RT_*m/z*)	WT	WT	R4	R4	S5	S5
1.51_137.5554	0.00	0.00	1.00	0.52	0.00	0.00
1.52_129.5659	0.00	0.00	1.00	0.52	0.00	0.00
4.95_114.0908	0.00	0.00	0.45	1.00	0.12	0.13
4.31_160.1140	0.00	0.00	0.67	1.00	0.00	0.00
9.08_196.0187	0.00	0.00	0.79	1.00	0.00	0.00
8.68_204.0325	0.00	0.00	0.72	1.00	0.00	0.00
9.08_203.0278	0.00	0.00	0.76	1.00	0.00	0.05
9.42_202.0393	0.00	0.00	0.68	1.00	0.00	0.00
1.42_201.0074	0.00	0.00	0.79	1.00	0.00	0.00
4.54_208.1355	0.00	0.00	0.90	1.00	0.02	0.00
8.67_212.0251	0.00	0.00	0.63	1.00	0.00	0.01
9.25_211.0284	0.00	0.01	1.00	0.92	0.00	0.00
8.31_210.0369	0.00	0.00	0.81	1.00	0.00	0.00
9.81_210.0363	0.00	0.00	1.00	0.66	0.23	0.15
9.07_210.0305	0.00	0.00	0.77	1.00	0.00	0.00
9.41_219.0312	0.00	0.00	1.00	0.86	0.04	0.03
8.67_218.0490	0.00	0.00	0.82	1.00	0.00	0.00
9.03_217.0413	0.00	0.00	0.70	1.00	0.05	0.02
2.51_216.0981	0.00	0.02	0.49	1.00	0.05	0.08
16.16_223.9875	0.00	0.00	0.90	1.00	0.00	0.00
6.51_220.1710	0.00	0.04	1.00	0.99	0.00	0.00
4.58_226.1445	0.00	0.00	1.00	0.82	0.00	0.00
5.11_226.1427	0.00	0.02	0.53	1.00	0.00	0.00
8.67_226.0395	0.00	0.00	0.61	1.00	0.15	0.00
9.04_225.0298	0.00	0.01	0.74	1.00	0.04	0.00
9.77_224.0325	0.00	0.00	0.63	1.00	0.32	0.09
5.11_227.1386	0.00	0.00	0.56	1.00	0.00	0.00
9.19_230.0719	0.00	0.00	1.00	0.54	0.00	0.00
9.82_230.0718	0.00	0.03	0.91	1.00	0.16	0.50
4.89_235.1441	0.00	0.00	0.93	1.00	0.00	0.00
9.80_241.0261	0.00	0.00	1.00	0.78	0.00	0.09
8.82_241.0249	0.00	0.00	1.00	0.94	0.00	0.00
9.03_248.0351	0.00	0.00	0.80	1.00	0.00	0.00
4.04_247.1287	0.00	0.00	0.50	1.00	0.00	0.05
9.07_246.5440	0.00	0.00	0.71	1.00	0.03	0.01
5.63_245.1880	0.00	0.00	1.00	0.83	0.00	0.00
5.04_244.1219	0.00	0.00	0.85	1.00	0.13	0.00
4.70_243.1326	0.00	0.00	0.55	1.00	0.00	0.10
8.52_250.0297	0.00	0.00	0.76	1.00	0.00	0.00
9.81_253.5524	0.00	0.02	0.91	1.00	0.13	0.07
9.91_261.5430	0.00	0.00	1.00	0.65	0.00	0.00
9.03_260.5527	0.00	0.00	0.72	1.00	0.05	0.04
10.77_267.1616	0.00	0.02	1.00	1.00	0.31	0.32
9.67_268.0195	0.00	0.00	1.00	0.94	0.49	0.00
7.18_278.2110	0.00	0.00	0.62	1.00	0.05	0.06
6.07_276.1943	0.00	0.00	0.57	1.00	0.19	0.14
5.71_286.2118	0.00	0.00	0.84	1.00	0.08	0.32
7.19_284.2219	0.00	0.00	0.63	1.00	0.00	0.08
5.22_295.1312	0.00	0.05	0.70	1.00	0.10	0.00
7.48_294.2085	0.00	0.00	1.00	0.58	0.00	0.03
7.82_294.2085	0.00	0.00	0.56	1.00	0.00	0.08
6.82_294.2084	0.00	0.00	0.63	1.00	0.18	0.00
7.73_298.2024	0.00	0.00	0.60	1.00	0.09	0.10
7.19_296.2224	0.00	0.00	0.58	1.00	0.05	0.06
6.00_308.2238	0.00	0.00	0.64	1.00	0.07	0.04
6.92_313.1550	0.00	0.00	0.55	1.00	0.09	0.00
6.06_312.2197	0.00	0.00	0.84	1.00	0.10	0.09

6.84_312.2197	0.00	0.00	0.52	1.00	0.06	0.00
9.79_311.0549	0.00	0.00	0.57	1.00	0.00	0.22
3.86_320.0995	0.00	0.00	0.64	1.00	0.00	0.01
6.92_318.2094	0.00	0.00	0.76	1.00	0.11	0.10
5.91_328.5999	0.00	0.00	0.65	1.00	0.06	0.00
7.34_326.2353	0.00	0.00	0.58	1.00	0.03	0.06
6.01_326.2353	0.00	0.00	0.79	1.00	0.12	0.03
4.97_326.0999	0.00	0.23	0.83	1.00	0.00	0.00
6.08_324.1828	0.00	0.09	0.64	1.00	0.08	0.21
6.62_334.2005	0.00	0.00	0.50	1.00	0.00	0.00
5.84_341.1007	0.00	0.00	0.59	1.00	0.00	0.00
6.22_346.2031	0.00	0.00	1.00	0.86	0.26	0.27
7.37_344.2218	0.00	0.00	0.66	1.00	0.03	0.04
8.24_352.2057	0.00	0.00	0.54	1.00	0.07	0.00
6.67_362.2335	0.00	0.00	1.00	0.86	0.07	0.05
6.51_360.2165	0.00	0.00	1.00	0.81	0.20	0.21
8.77_368.2219	0.00	0.00	0.73	1.00	0.09	0.00
6.02_368.2219	0.00	0.04	0.72	1.00	0.00	0.00
9.80_367.0822	0.00	0.00	0.66	1.00	0.13	0.13
5.64_366.2063	0.00	0.00	0.71	1.00	0.00	0.00
8.47_382.2398	0.00	0.00	0.89	1.00	0.05	0.00
7.30_389.1593	0.00	0.00	1.00	0.89	0.16	0.00
9.80_387.0731	0.00	0.00	0.56	1.00	0.08	0.13
6.88_386.2329	0.00	0.00	0.66	1.00	0.11	0.00
8.63_398.2317	0.00	0.00	0.65	1.00	0.00	0.00
9.40_418.0851	0.00	0.00	0.59	1.00	0.00	0.00
8.66_429.0854	0.00	0.00	0.56	1.00	0.00	0.00
9.08_429.0845	0.00	0.00	0.57	1.00	0.02	0.02
9.15_440.0708	0.00	0.00	0.59	1.00	0.00	0.00
9.42_432.0873	0.00	0.00	0.65	1.00	0.00	0.00
9.09_448.0576	0.00	0.00	0.61	1.00	0.00	0.00
9.73_443.1014	0.00	0.00	0.82	1.00	0.06	0.06
8.33_443.0954	0.00	0.00	0.93	1.00	0.03	0.00
8.80_443.0945	0.00	0.00	0.61	1.00	0.00	0.00
6.90_461.2902	0.00	0.00	0.90	1.00	0.29	0.00
10.02_459.0960	0.00	0.00	0.58	1.00	0.07	0.09
9.03_457.1145	0.00	0.00	0.60	1.00	0.03	0.04
8.67_457.1133	0.00	0.00	0.66	1.00	0.00	0.00
3.92_456.2075	0.00	0.32	0.61	1.00	0.00	0.00
9.81_454.0847	0.00	0.00	0.78	1.00	0.00	0.03
9.05_454.0819	0.00	0.00	0.57	1.00	0.00	0.00
6.42_472.2832	0.00	0.00	0.75	1.00	0.00	0.02
6.46_471.2466	0.00	0.01	0.64	1.00	0.19	0.21
10.02_470.0758	0.00	0.00	0.62	1.00	0.00	0.00
9.02_468.1011	0.00	0.00	0.58	1.00	0.00	0.00
9.08_467.0388	0.00	0.00	0.79	1.00	0.00	0.00
8.31_465.0807	0.00	0.00	0.70	1.00	0.00	0.00
8.82_465.0807	0.00	0.00	0.67	1.00	0.00	0.00
9.79_462.0710	0.00	0.00	0.72	1.00	0.03	0.03
9.04_462.0699	0.00	0.00	0.61	1.00	0.00	0.00
7.03_483.0939	0.00	0.00	0.72	1.00	0.00	0.00
9.78_481.0499	0.00	0.00	1.00	0.75	0.07	0.08
9.02_479.0963	0.00	0.00	0.62	1.00	0.04	0.04
10.01_478.0692	0.00	0.00	0.53	1.00	0.00	0.00
4.15_476.2404	0.00	0.00	0.56	1.00	0.00	0.03
9.02_476.0877	0.00	0.00	0.55	1.00	0.00	0.00
7.06_475.1057	0.00	0.00	0.61	1.00	0.00	0.01
9.02_495.0687	0.00	0.00	0.70	1.00	0.00	0.03
5.37_493.1709	0.00	0.00	1.00	0.69	0.00	0.14
9.79_513.1525	0.00	0.00	0.48	1.00	0.00	0.00
1.76_515.1445	0.00	0.00	0.74	1.00	0.00	0.00
10.06_526.3139	0.00	0.00	1.00	0.54	0.02	0.00
7.20_544.2918	0.00	0.00	0.61	1.00	0.20	0.16
9.00_540.1495	0.00	0.00	0.63	1.00	0.00	0.00
6.63_570.3104	0.00	0.00	0.91	1.00	0.00	0.00
9.08_562.5875	0.00	0.00	0.62	1.00	0.00	0.00
7.14_560.1805	0.00	0.00	0.64	1.00	0.13	0.00
9.02_590.6205	0.00	0.00	0.63	1.00	0.00	0.00
9.79_576.6021	0.00	0.00	1.00	0.60	0.03	0.00
9.06_576.6005	0.00	0.00	0.60	1.00	0.00	0.00

9.07_662.0928	0.00	0.00	0.48	1.00	0.00	0.00
9.02_704.1451	0.00	0.00	0.54	1.00	0.00	0.00
9.03_696.1548	0.00	0.00	0.49	1.00	0.00	0.00
9.71_694.1152	0.00	0.00	0.66	1.00	0.00	0.00
9.03_690.1259	0.00	0.00	0.54	1.00	0.00	0.00
9.79_683.1204	0.00	0.00	1.00	0.68	0.00	0.00
9.06_676.1101	0.00	0.00	0.53	1.00	0.00	0.00
9.41_675.1324	0.00	0.00	0.54	1.00	0.00	0.00
9.78_885.1896	0.00	0.00	0.47	1.00	0.00	0.00
9.07_879.1306	0.00	0.00	0.69	1.00	0.00	0.00
9.02_935.1961	0.00	0.00	0.53	1.00	0.00	0.00
7.21_916.0943	0.00	0.00	1.00	0.78	0.13	0.00
9.80_907.1678	0.00	0.00	0.82	1.00	0.01	0.01
9.04_907.1662	0.00	0.00	0.51	1.00	0.02	0.00
9.41_904.1590	0.00	0.00	0.53	1.00	0.00	0.00
7.67_1031.2480	0.00	0.14	0.97	1.00	0.47	0.00
7.69_1031.1674	0.00	0.10	1.00	0.91	0.13	0.22
7.67_1031.0798	0.00	0.00	0.91	1.00	0.00	0.00
7.69_1000.1273	0.00	0.00	0.49	1.00	0.00	0.07
7.63_942.9948	0.00	0.00	1.00	0.90	0.00	0.00
7.01_1221.4414	0.00	0.00	0.55	1.00	0.00	0.00
9.41_1125.2062	0.00	0.00	0.48	1.00	0.00	0.00
9.78_465.0808	0.00	0.00	0.87	1.00	0.09	0.11
9.79_1349.2480	0.00	0.00	0.51	1.00	0.00	0.00
6.06_294.2084	0.00	0.00	0.59	1.00	0.11	0.14
9.81_269.0437	0.00	0.00	0.61	1.00	0.17	0.00
6.65_282.2073	0.01	0.04	0.76	1.00	0.00	0.14
8.74_542.3146	0.01	0.00	1.00	0.73	0.00	0.00
1.64_246.1172	0.02	0.00	0.74	1.00	0.19	0.00
1.64_174.0879	0.02	0.01	1.00	0.56	0.12	0.01
6.66_264.1980	0.03	0.01	0.63	1.00	0.00	0.02
1.70_260.1135	0.08	0.00	0.75	1.00	0.49	0.00
7.25_371.1508	0.09	0.00	0.67	1.00	0.26	0.25
10.18_621.4210	0.13	0.00	0.59	1.00	0.00	0.00
3.80_288.1929	0.15	0.13	1.00	0.77	0.13	0.00
3.86_338.1113	0.19	0.00	0.65	1.00	0.00	0.18
7.91_389.2523	0.23	0.10	0.63	1.00	0.34	0.00
4.39_362.1069	0.62	0.54	0.00	0.05	0.64	1.00
12.61_771.4862	0.68	0.85	0.40	0.33	0.86	1.00
12.67_727.4605	0.69	0.94	0.21	0.30	0.86	1.00
12.79_595.3829	0.73	1.00	0.46	0.37	0.79	0.83
12.70_683.4373	0.77	1.00	0.48	0.36	0.89	0.90
12.78_590.4295	0.78	0.78	0.32	0.26	0.79	1.00
12.73_655.3845	0.83	1.00	0.56	0.44	0.82	1.00
12.80_567.3292	0.85	1.00	0.55	0.36	0.75	0.92
14.79_310.3109	0.85	0.95	0.48	0.50	0.72	1.00
12.83_546.4021	0.86	1.00	0.00	0.24	0.76	0.84
5.16_237.1592	0.87	1.00	0.21	0.29	0.66	0.73
15.94_338.3442	0.91	1.00	0.32	0.34	0.74	0.68
11.33_299.2599	1.00	0.77	0.00	0.00	0.69	0.51
4.42_351.1212	1.00	0.79	0.09	0.14	0.79	0.66
15.92_360.3229	1.00	0.71	0.22	0.13	0.66	0.88

Table A3.22. Normalized heat map of features described as unique in **Figure 3.3(A)** when comparing wild type *Nocardiopsis sp. FU40 ΔApoS8* and R4 rifampicin resistant mutant to the S5 streptomycin resistant mutant extract using OPLS-DA and extracting features from the generated S-plot with correlation coefficients ≥0.9. Features are normalized to maximum intensity for that feature.

Feature ID (RT_*m/z*)	WT	WT	R4	R4	S5	S5
12.03_135.1163	0.00	0.04	0.00	0.00	0.79	1.00
12.03_123.1165	0.00	0.00	0.00	0.00	0.84	1.00
12.03_149.1327	0.00	0.00	0.00	0.00	0.88	1.00
6.56_162.0938	0.00	0.00	0.28	0.35	0.82	1.00
16.16_174.0876	0.00	0.00	0.00	0.00	0.60	1.00
6.60_180.1017	0.00	0.01	0.23	0.40	0.89	1.00
8.84_203.1804	0.00	0.00	0.00	0.00	0.85	1.00
8.12_203.1781	0.00	0.00	0.00	0.00	0.96	1.00
6.22_203.0786	0.00	0.02	0.00	0.00	1.00	0.92
7.49_207.0994	0.00	0.06	0.28	0.52	0.86	1.00
8.84_221.1903	0.00	0.00	0.00	0.00	0.98	1.00
10.62_236.1643	0.00	0.00	0.39	0.30	1.00	0.97
8.54_235.1344	0.00	0.00	0.30	0.51	0.96	1.00
7.38_246.1513	0.00	0.00	0.00	0.00	0.62	1.00
3.58_252.0387	0.00	0.35	0.11	0.52	1.00	1.00
12.02_263.1978	0.00	0.03	0.00	0.00	0.93	1.00
10.71_261.1779	0.00	0.01	0.00	0.00	0.90	1.00
6.28_268.0191	0.00	0.13	0.17	0.16	1.00	0.72
5.27_264.2082	0.00	0.00	0.36	0.46	0.97	1.00
4.60_268.0196	0.00	0.00	0.44	0.18	0.83	1.00
7.15_293.2251	0.00	0.00	0.27	0.29	0.69	1.00
12.02_309.1921	0.00	0.01	0.00	0.00	0.90	1.00
12.03_325.1706	0.00	0.00	0.00	0.00	0.84	1.00
10.73_340.1475	0.00	0.14	0.00	0.00	1.00	0.71
5.99_338.1374	0.00	0.00	0.30	0.24	1.00	0.97
4.01_351.5992	0.00	0.00	0.00	0.00	1.00	0.57
7.52_368.2211	0.00	0.00	0.31	0.34	0.71	1.00
7.83_387.1861	0.00	0.00	0.50	0.00	1.00	1.00
6.24_384.2171	0.00	0.00	0.07	0.11	0.71	1.00
7.98_431.2698	0.00	0.06	0.00	0.11	0.90	1.00
6.99_443.3240	0.00	0.23	0.00	0.00	0.87	1.00
7.51_499.2782	0.00	0.02	0.07	0.49	1.00	0.97
4.37_494.2617	0.00	0.00	0.06	0.09	0.78	1.00
7.57_542.3960	0.00	0.42	0.00	0.00	0.79	1.00
12.03_549.4012	0.00	0.00	0.00	0.00	0.87	1.00
5.18_599.2879	0.00	0.00	0.00	0.00	1.00	0.78
6.02_637.3187	0.00	0.00	0.00	0.00	0.38	1.00
6.24_515.2753	0.01	0.00	0.15	0.18	0.77	1.00
8.10_301.1534	0.01	0.03	0.28	0.31	0.81	1.00
12.02_205.1953	0.01	0.00	0.00	0.00	0.84	1.00
8.29_401.1993	0.02	0.00	0.20	0.36	0.93	1.00
10.18_223.2085	0.04	0.25	0.00	0.00	1.00	0.79
5.97_286.6247	0.05	0.01	0.21	0.14	0.92	1.00
7.42_280.1237	0.06	0.16	0.21	0.37	0.95	1.00
3.86_150.0940	0.06	0.11	0.29	0.43	0.92	1.00
10.52_673.3745	0.06	0.09	0.32	0.51	0.87	1.00
5.97_278.6345	0.06	0.02	0.21	0.20	1.00	0.96
6.72_1450.6973	0.08	0.02	0.22	0.32	1.00	0.92
7.89_192.1015	0.10	0.17	0.31	0.42	0.80	1.00
7.42_196.0651	0.10	0.05	0.11	0.19	0.58	1.00
7.06_221.1900	0.12	0.36	0.01	0.00	1.00	0.97
15.37_230.0721	0.12	0.40	0.20	0.45	0.82	1.00
9.47_211.0868	0.13	0.23	0.39	0.38	0.82	1.00
3.82_230.1126	0.14	0.09	0.41	0.33	0.81	1.00
6.06_203.1781	0.15	0.26	0.00	0.13	0.83	1.00
7.06_203.1787	0.15	0.28	0.00	0.00	0.88	1.00

6.73_1161.1593	0.16	0.04	0.12	0.07	0.85	1.00
5.96_534.2942	0.16	0.04	0.16	0.16	0.97	1.00
6.71_1160.7578	0.17	0.00	0.31	0.00	1.00	0.86
6.73_1160.5609	0.20	0.00	0.05	0.17	1.00	1.00
5.61_343.2002	0.23	0.05	0.22	0.32	0.84	1.00
4.81_464.2611	0.24	0.29	0.55	0.44	0.94	1.00
5.81_605.2195	0.28	0.40	0.38	0.62	0.77	1.00
4.32_308.1712	0.29	0.11	0.32	0.50	0.73	1.00
6.74_1160.9454	0.32	0.26	0.22	0.14	1.00	0.79
4.63_149.1104	0.32	0.51	0.38	0.66	0.98	1.00
5.34_191.1575	0.32	0.46	0.31	0.56	0.91	1.00
1.49_365.1079	0.35	0.48	0.31	0.35	0.78	1.00
6.40_263.1761	0.36	0.38	0.37	0.56	0.81	1.00
13.98_292.2624	0.36	0.49	0.29	0.40	0.66	1.00
4.53_236.1764	0.37	0.48	0.36	0.57	0.94	1.00
5.78_164.0706	0.39	0.52	0.39	0.60	1.00	0.96
8.22_220.1332	0.39	0.57	0.44	0.73	0.94	1.00
3.75_267.1417	0.40	0.50	0.35	0.62	0.78	1.00
9.69_220.1127	0.41	0.48	0.29	0.00	1.00	0.98
5.71_249.1598	0.41	0.57	0.38	0.61	0.84	1.00
4.67_270.1917	0.43	0.59	0.44	0.57	0.81	1.00
4.70_221.1315	0.45	0.67	0.43	0.63	0.96	1.00
6.23_251.1781	0.49	0.54	0.37	0.61	0.87	1.00
1.50_401.0693	0.54	0.50	0.60	0.33	1.00	0.98
5.72_240.1231	0.56	0.39	0.47	0.51	0.89	1.00
6.59_273.1670	0.60	0.51	0.53	0.67	0.84	1.00
5.43_241.1546	0.61	0.63	0.59	0.79	0.93	1.00
7.00_916.3325	1.00	0.59	0.55	0.66	0.00	0.00

Table A3.23. Normalized heat map of features described as unique in **Figure 3.3(A)** when comparing wild type *Nocardiopsis sp. FU40 ΔApoS8* to the R4 rifampicin resistant and S5 streptomycin resistant mutant extracts using OPLS-DA and extracting features from the generated S-plot with correlation coefficients ≥0.9. Features are normalized to maximum intensity for that feature.

Feature ID (RT_*m/z*)	WT	WT	R4	R4	S5	S5
1.50_103.5345	0.00	0.00	0.50	1.00	0.83	0.90
4.14_186.1168	0.00	0.00	0.76	0.81	0.81	1.00
4.84_205.1323	0.00	0.00	0.74	0.86	1.00	0.89
1.32_211.8786	0.00	0.00	0.42	0.94	1.00	0.92
1.49_211.0584	0.00	0.19	0.65	1.00	0.77	0.68
5.11_236.1306	0.00	0.11	0.59	0.61	0.88	1.00
8.08_252.0397	0.00	0.00	0.72	0.60	1.00	0.97
1.78_262.1278	0.00	0.00	0.61	0.81	0.74	1.00
9.60_297.1694	0.00	0.01	0.61	1.00	0.71	0.71
5.82_322.1007	0.00	0.00	0.87	0.97	1.00	0.99
9.13_319.1539	0.00	0.00	0.60	1.00	0.63	0.70
7.48_345.1875	0.00	0.00	0.77	0.91	1.00	0.72
8.53_359.2035	0.00	0.11	0.90	1.00	0.78	0.62
1.49_394.1142	0.00	0.00	0.61	1.00	0.63	0.92
4.02_423.1940	0.00	0.00	0.53	0.86	0.75	1.00
1.48_431.0890	0.00	0.30	0.72	0.73	0.88	1.00
5.52_601.2501	0.00	0.00	0.53	0.73	0.86	1.00
1.25_639.8836	0.00	0.00	0.48	0.77	1.00	0.77
5.66_384.2168	0.01	0.00	0.45	0.64	0.81	1.00
16.15_710.1773	0.03	0.01	0.60	0.86	1.00	0.97
9.66_279.1583	0.03	0.00	0.46	0.71	0.73	1.00
5.43_377.1482	0.03	0.00	0.68	1.00	0.50	0.58
1.73_338.0231	0.04	0.00	0.50	0.59	0.82	1.00
9.14_239.1284	0.04	0.04	0.59	1.00	0.80	0.56
1.74_150.0789	0.04	0.00	0.47	0.80	0.91	0.99
3.07_230.1126	0.05	0.11	0.65	0.79	0.79	1.00
8.53_283.1523	0.05	0.10	0.73	0.86	0.92	1.00
8.53_177.0880	0.06	0.06	0.53	0.63	0.72	1.00
4.75_136.0625	0.06	0.00	0.78	1.00	0.56	0.85
8.53_207.1002	0.06	0.07	0.56	0.69	0.84	1.00
3.83_198.1623	0.13	0.09	0.54	0.95	0.86	1.00
1.73_288.1454	0.16	0.00	0.62	0.73	1.00	0.56
1.60_229.1318	0.21	0.04	0.54	0.70	0.91	1.00
9.11_505.3321	0.27	0.00	0.59	0.84	0.93	1.00
16.18_335.9929	0.28	0.00	0.67	0.98	0.95	1.00
4.00_320.1711	0.33	0.04	0.76	0.77	0.80	1.00
12.11_316.2860	0.41	1.00	0.00	0.01	0.00	0.00
11.78_354.1615	0.44	1.00	0.00	0.00	0.00	0.00
11.49_251.2052	0.45	1.00	0.00	0.00	0.00	0.00
11.27_448.3444	0.48	1.00	0.09	0.00	0.00	0.00
12.43_386.2820	0.50	1.00	0.15	0.00	0.18	0.00
10.60_346.3091	0.51	1.00	0.00	0.00	0.00	0.00
10.40_371.3275	0.52	1.00	0.00	0.00	0.02	0.02
10.70_288.2557	0.52	1.00	0.00	0.00	0.00	0.20
9.48_225.1993	0.53	1.00	0.01	0.02	0.02	0.02
4.26_669.2631	0.56	1.00	0.00	0.00	0.00	0.08
11.80_235.1712	0.56	1.00	0.00	0.04	0.00	0.09
10.15_739.4618	0.56	1.00	0.06	0.05	0.11	0.07
14.41_309.2409	0.56	1.00	0.14	0.13	0.32	0.23
10.53_531.4000	0.57	1.00	0.00	0.00	0.00	0.00
12.97_407.3144	0.58	1.00	0.20	0.09	0.30	0.12
12.98_399.3242	0.58	1.00	0.19	0.09	0.31	0.12
4.37_663.2850	0.59	1.00	0.01	0.00	0.00	0.00
13.98_433.3418	0.61	1.00	0.02	0.01	0.05	0.00
4.64_412.2067	0.62	1.00	0.08	0.10	0.15	0.20
6.19_181.1351	0.63	1.00	0.09	0.11	0.08	0.10

10.97_401.2525	0.63	1.00	0.00	0.00	0.08	0.21
11.58_415.2745	0.65	1.00	0.00	0.00	0.07	0.02
12.62_273.1378	0.66	1.00	0.00	0.00	0.00	0.00
4.27_647.2871	0.67	1.00	0.00	0.01	0.09	0.00
11.44_223.2060	0.67	1.00	0.00	0.00	0.00	0.00
8.08_219.1411	0.68	1.00	0.00	0.00	0.30	0.24
6.85_824.9348	0.70	1.00	0.00	0.00	0.00	0.23
16.15_442.8736	0.71	1.00	0.00	0.00	0.00	0.00
7.07_184.1710	0.72	1.00	0.00	0.00	0.00	0.00
4.37_150.0945	0.72	1.00	0.00	0.00	0.00	0.00
11.18_473.3585	0.75	1.00	0.04	0.01	0.08	0.04
12.74_443.3505	0.77	1.00	0.00	0.00	0.01	0.00
11.97_299.2600	0.80	1.00	0.00	0.00	0.31	0.21
11.84_443.3878	0.82	1.00	0.09	0.05	0.11	0.06
11.03_354.1608	0.82	1.00	0.00	0.04	0.09	0.25
11.28_440.3462	0.82	1.00	0.00	0.00	0.00	0.00
12.98_282.2118	0.82	1.00	0.14	0.03	0.15	0.10
10.38_401.3397	0.88	1.00	0.50	0.32	0.27	0.16
9.26_219.1735	0.88	1.00	0.00	0.00	0.00	0.00
4.50_359.1197	0.89	1.00	0.00	0.00	0.00	0.00
13.49_295.2258	0.91	1.00	0.08	0.03	0.06	0.00
4.49_225.1597	0.97	1.00	0.49	0.50	0.54	0.56
12.89_441.3208	0.99	1.00	0.40	0.25	0.49	0.58
11.31_225.6512	1.00	0.95	0.26	0.18	0.00	0.00
9.27_240.2315	1.00	0.88	0.00	0.11	0.00	0.00
10.39_268.2627	1.00	0.83	0.00	0.00	0.00	0.00
11.44_291.1951	1.00	0.75	0.00	0.00	0.00	0.00
12.62_313.2746	1.00	0.83	0.00	0.00	0.12	0.11
14.31_325.2414	1.00	0.74	0.00	0.00	0.00	0.00
15.49_338.3442	1.00	0.86	0.00	0.03	0.00	0.00
13.48_397.3392	1.00	0.75	0.00	0.01	0.00	0.00
13.95_411.3586	1.00	0.78	0.00	0.00	0.06	0.00
13.27_419.3131	1.00	0.81	0.00	0.00	0.00	0.00
12.75_617.4294	1.00	0.84	0.00	0.25	0.36	0.00
13.92_641.5490	1.00	0.85	0.00	0.00	0.00	0.00
4.37_685.2548	1.00	0.86	0.00	0.00	0.12	0.23

APPENDIX 4

SUPPORTING INFORMATION FOR CHAPTER 4
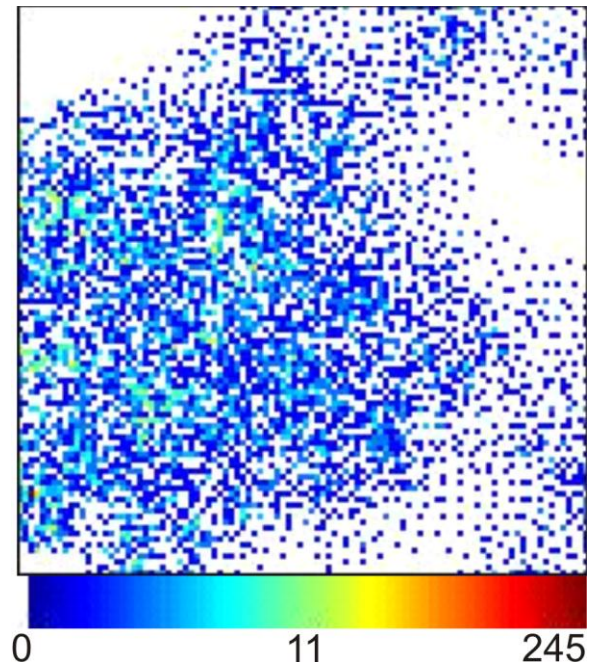
Figure A4.1. Density map for **Figure 4.2(B).** Color indicates the density of features per node. These features are then summed to determine the node intensity.
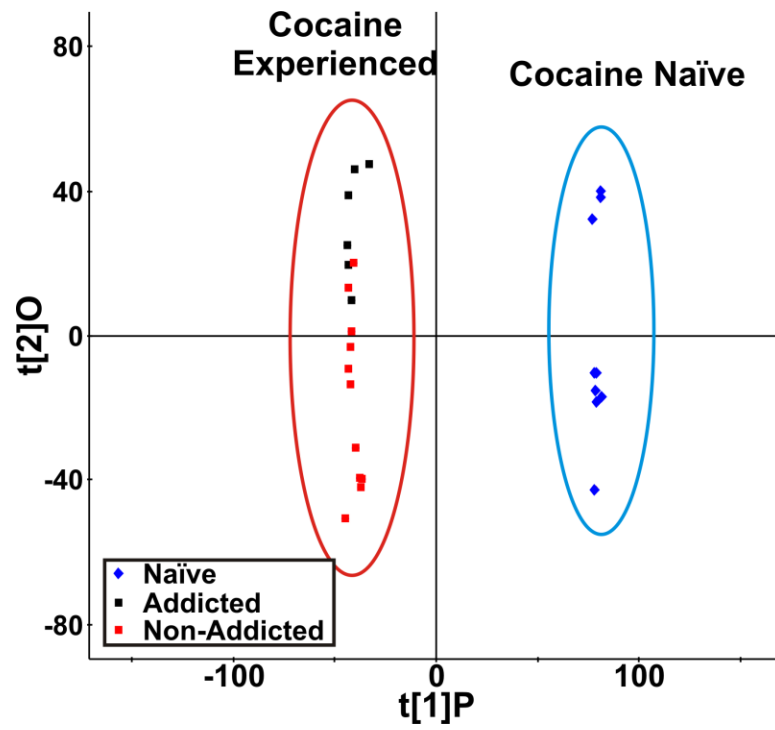
Figure A4.2. Orthogonal partial least square-discriminant analysis comparing cocaine experienced (-1) to cocaine naïve (+1) rat sera profiles.

Table A4.1. Region "a" statistical summary.

Blue	Non-addicted averages	Addicted averages	Naïve averages	Experienced averages
	6200.54	8959.59	3002.5	6200.54
	10163.6	7979.64	2892.6	10163.6
	8724.59	11042.4	2606.9	8724.59
	7838.07	8700.31	2218.3	7838.07
	9355.55	8140.3	2057.7	9355.55
	5919.37	8945.93	2298.2	5919.37
	8781.63		2461	8781.63
	5323.97		2551.5	5323.97
	6343.24		2704.5	6343.24
	6202.28			6202.28
				8959.59
				7979.64
				11042.4
				8700.31
				8140.3
				8945.93

Kruskal-Wallace One-way ANOVA					
SUMMARY					
Groups	*Count*	*Sum*	*Average*	*Variance*	
Column 1	10	74852.9	7485.286	2859614	
Column 2	6	53768.1	8961.355	1207373	
Column 3	9	22793.3	2532.586	96271.43	
Column 4	16	128621	8038.812	2662921	
ANOVA					
H=22.02	df=3		Non-addicted	Addicted	Naïve	Experienced
p<0.0001	Mean Ranks for Sample		22.7	30.2	5	25.5

***Post hoc* test: Bonferroni-Holm**

Group 1	Group 2	Critical	P	Significant?
Addicted average	Naïve average	0.008333	3.25E-10	**Yes**
Naïve average	Experienced average	0.01	8.69E-10	**Yes**
Non-addicted average	Naïve average	0.0125	1.28E-07	**Yes**
Non-addicted average	Addicted average	0.016667	0.078596	No
Addicted average	Experienced average	0.025	0.218321	No
Non-addicted average	Experienced average	0.05	0.414697	No

Test for Equal Variance

F	DFn	DFd	P	
6.716522861	3	37	0.000987	FAIL-equal variance cannot be assumed

Table A4.2. Region "b" statistical summary.

Gray	Non-addicted averages	Addicted averages	Naïve averages	Experienced averages
	2170.11	1016.38	245.32	2170.11
	2101.32	692.3	327.03	2101.32
	1542.41	782.36	331.68	1542.41
	843.41	879.43	400.34	843.41
	748.87	879.85	338.84	748.87
	814.03	1082.14	439.14	814.03
	737.19		401.79	737.19
	704.62		476.22	704.62
	593.51		515.46	593.51
	620.41			620.41
				1016.38
				692.3
				782.36
				879.43
				879.85
				1082.14

ANOVA: Single Factor

SUMMARY						
Groups	*Count*	*Sum*	*Average*	*Variance*		
Column 1	10	10875.9	1087.588	376374.2		
Column 2	6	5332.46	888.7433	20753.32		
Column 3	9	3475.82	386.2022	7077.63		
Column 4	16	16208.3	1013.021	242627.1		
ANOVA						
Source of Variation	*SS*	*df*	*MS*	*F*	*P-value*	*F crit*
Between Groups	2908170	3	969389.9	4.990485	0.00525	4.3595
Within Groups	7187162	37	194247.6			
Total	10095332	40				

Post hoc test: Bonferroni-Holm

Group 1	Group 2	Critical	P	Significant?
Addicted average	Naïve average	0.008333	1.02E-06	Yes
Naïve average	Experienced average	0.01	0.001037	Yes
Non-addicted average	Naïve average	0.0125	0.003471	Yes
Non-addicted average	Addicted average	0.016667	0.453466	No
Addicted average	Experienced average	0.025	0.555188	No
Non-addicted average	Experienced average	0.05	0.735433	No

Test for Equal Variance

F	DFn	DFd	P	
2.31283416	3	37	0.091936	PASS - equal variance may be assumed (p > 0.05).

Table A4.3. Region "c" statistical summary.

Green	Non-addicted averages	Addicted averages	Naïve averages	Experienced averages
	1878.46	2836.05	504.97	1878.46
	1469.38	3042.55	448.33	1469.38
	1993.71	2200.57	345.58	1993.71
	2543.64	1483.77	251.39	2543.64
	1045.84	1382.98	293.38	1045.84
	8985.16	726.63	296.93	8985.16
	6632.13		263.09	6632.13
	7836.09		405.93	7836.09
	7118.23		333.42	7118.23
	6014.89			6014.89
				2836.05
				3042.55
				2200.57
				1483.77
				1382.98
				726.63

Kruskal-Wallace one-way ANOVA				
SUMMARY				

Groups	*Count*	*Sum*	*Average*	*Variance*
Column 1	10	45517.5	4551.753	9223617
Column 2	6	11672.6	1945.425	815385.2
Column 3	9	3143.02	349.2244	7550.15
Column 4	16	57190.1	3574.38	7504202

ANOVA					
H=21.83	df=3	Non-addicted	Addicted	Naïve	Experienced
p<0.0001	Mean Ranks for Sample	28.1	21.2	5	25.5

Post hoc test: Bonferroni-Holm				
Group 1	**Group 2**	**Critical**	**P**	**Significant?**
Addicted average	Naïve average	0.008333	0.000128	Yes
Naïve average	Experienced average	0.01	0.000688	Yes
Non-addicted average	Naïve average	0.0125	0.001938	Yes
Non-addicted average	Addicted average	0.016667	0.062533	No
Addicted average	Experienced average	0.025	0.174181	No
Non-addicted average	Experienced average	0.05	0.404085	No

Test for Equal Variance				
F	**DFn**	**DFd**	**P**	
11.32572354	3	37	2.05E-05	FAIL-equal variance cannot be assumed

Table A4.4. Region "d" statistical summary.

Purple	Non-addicted averages	Addicted averages	Naïve averages	Experienced averages
	1961.77	1068.04	564.75	1961.77
	1714.38	1373.17	459.78	1714.38
	1701.73	1044.29	582.72	1701.73
	1803.42	1004.43	388.91	1803.42
	3796.06	1516.42	345.29	3796.06
	964.43	1350.24	536.04	964.43
	841.67		772.68	841.67
	1642.09		675.7	1642.09
	1295.13		673.84	1295.13
	1657.07			1657.07
				1068.04
				1373.17
				1044.29
				1004.43
				1516.42
				1350.24

ANOVA: Single Factor

SUMMARY						
Groups	*Count*	*Sum*	*Average*	*Variance*		
Column 1	10	17377.8	1737.775	656170.8		
Column 2	6	7356.59	1226.098	45700.29		
Column 3	9	4999.71	555.5233	19740.94		
Column 4	16	24734.3	1545.896	474389.1		

ANOVA						
Source of Variation	*SS*	*df*	*MS*	*F*	*P-value*	*F crit*
Between Groups	7871591	3	2623864	7.240781	0.00061	4.3595
Within Groups	13407803	37	362373.1			
Total	21279394	40				

Post hoc test: Bonferroni-Holm

Group 1	Group 2	Critical	P	Significant?
Addicted average	Naïve average	0.008333	5.35E-06	**Yes**
Naïve average	Experienced average	0.01	0.00032	**Yes**
Non-addicted average	Naïve average	0.0125	0.000476	**Yes**
Non-addicted average	Addicted average	0.016667	0.156613	No
Addicted average	Experienced average	0.025	0.283378	No
Non-addicted average	Experienced average	0.05	0.524272	No

Test for Equal Variance

F	DFn	DFd	P	
2.801616821	3	37	0.053266	PASS - equal variance may be assumed (p > 0.05).

Table A4.5. Region "e" statistical summary.

Red	Non-addicted averages	Addicted averages	Naïve averages	Experienced averages
	411.94	655.04	174.65	411.94
	386.85	238.99	176.65	386.85
	1046.58	487.88	209.55	1046.58
	889.8	897.8	155.11	889.8
	1555.52	652.19	151.64	1555.52
	494.63	1134.66	158.86	494.63
	581.41		384.33	581.41
	878.57		344.2	878.57
	417.64		345.88	417.64
	723.63			723.63
				655.04
				238.99
				487.88
				897.8
				652.19
				1134.66

ANOVA: Single Factor						
SUMMARY						
Groups	*Count*	*Sum*	*Average*	*Variance*		
Column 1	10	7386.57	738.657	135840.8		
Column 2	6	4066.56	677.76	97383.75		
Column 3	9	2100.87	233.43	9164.929		
Column 4	16	11453.1	715.8206	114892.8		

ANOVA						
H=18.9	df=3		Non-addicted	Addicted	Naïve	Experienced
p<0.0001	Mean Ranks for Sample		25.5	25	5.7	25.3

Post hoc test: Bonferroni-Holm				
Group 1	**Group 2**	**Critical**	**P**	**Significant?**
Addicted average	Naïve average	0.008333	0.000395	Yes
Naïve average	Experienced average	0.01	0.000963	Yes
Non-addicted average	Naïve average	0.0125	0.001348	Yes
Non-addicted average	Addicted average	0.016667	0.740765	No
Addicted average	Experienced average	0.025	0.813415	No
Non-addicted average	Experienced average	0.05	0.872901	No

Test for Equal Variance				
F	**DFn**	**DFd**	**P**	
5.963301904	3	37	0.002013	FAIL - equal variance cannot be assumed.

Table A4.6. Region "f" statistical summary.

White	Non-addicted averages	Addicted averages	Naïve averages	Experienced averages
	1950.42	1520.41	470.8	1950.42
	786.35	2827.55	511.69	786.35
	915.45	2014.75	446.62	915.45
	1068.64	2372.6	359.06	1068.64
	2538.34	3169.89	414.26	2538.34
	1199.5	2626.97	294.02	1199.5
	694.17		408.2	694.17
	1263.33		300.77	1263.33
	1087.39		318.73	1087.39
	728.13			728.13
				1520.41
				2827.55
				2014.75
				2372.6
				3169.89
				2626.97

Kruskal-Wallis One-way ANOVA

SUMMARY

Groups	Count	Sum	Average	Variance		
Column 1	10	12231.7	1223.172	345940.3		
Column 2	6	14532.2	2422.028	349396.1		
Column 3	9	3524.15	391.5722	6081.414		
Column 4	16	26763.9	1672.743	683343.6		

ANOVA

H=25.6	df=3	Non-addicted	Addicted	Naïve	Experienced
p<0.0001	Mean Ranks for Sample	20.3	34.2	5	25.5

Post hoc test: Bonferroni-Holm

Group 1	Group 2	Critical	P	Significant?
Addicted average	Naïve average	0.008333	1.18E-07	Yes
Naïve average	Experienced average	0.01	0.000128	Yes
Non-addicted average	Naïve average	0.0125	0.000606	Yes
Non-addicted average	Addicted average	0.016667	0.00148	Yes
Addicted average	Experienced average	0.025	0.05688	No
Non-addicted average	Experienced average	0.05	0.148061	No

Test for Equal Variance

F	DFn	DFd	P	
10.23623293	3	37	4.79E-05	FAIL - equal variance cannot be assumed.

Table S4.7. Features within region extracted from the S-plot in **Figure 4.4(B)**. Included are the retention time, mass, loadings and correlation coefficients, averages for each group, factor of change with uncertainty, in addition to the regional location in the MEDI heat map in **Figure 4.4(C).**

Retention Time	Mass	p[1]P	p(corr)[1]P	Experienced Average	Naïve Average	Factor of Change	Uncertainty	Region
11.76	130.066	-0.077	-0.730	60.693	4.294	14.1	5.121	blue
12.87	614.174	-0.046	-0.584	25.551	0.000	-3.4E+07	10000	green
12.83	616.179	-0.186	-0.689	354.740	0.000	10000	10000	blue
13.22	158.154	-0.056	-0.576	51.840	13.964	3.7	0.709	blue
10.19	162.056	-0.051	-0.739	26.495	1.509	17.6	12.02	purple
9.92	182.192	-0.198	-0.811	475.820	139.393	3.4	0.274	blue
10.82	185.116	-0.066	-0.633	64.801	17.044	3.8	0.653	blue
10.46	186.223	-0.031	-0.577	16.783	5.390	3.1	0.819	red
11.78	190.086	-0.059	-0.720	35.808	1.642	21.8	14.47	blue
9.09	201.072	-0.057	-0.670	47.493	13.496	3.5	0.548	grey
1.2	203.054	-0.049	-0.636	31.450	4.884	6.4	1.842	white
9.98	211.143	-0.056	-0.583	39.752	2.159	18.4	8.956	blue
9.6	215.125	-0.078	-0.615	96.993	29.218	3.3	0.497	blue
11.94	223.066	-0.042	-0.628	25.111	5.240	4.8	1.275	white
12.62	225.110	-0.065	-0.591	54.029	3.078	17.6	7.917	green
9.85	229.069	-0.084	-0.549	139.021	49.404	2.8	0.44	blue
10.53	229.142	-0.182	-0.709	418.809	97.261	4.3	0.527	blue
10.77	243.104	-0.065	-0.643	46.404	0.571	81.3	89.034	blue
10.85	257.136	-0.055	-0.602	48.442	14.323	3.4	0.556	blue
12.63	261.109	-0.100	-0.575	165.129	44.117	3.7	0.613	blue
9.55	269.129	-0.050	-0.704	35.318	9.933	3.6	0.595	purple
10.34	273.168	-0.069	-0.577	97.670	39.432	2.5	0.327	blue
9.09	279.688	-0.044	-0.571	33.130	10.547	3.1	0.667	blue
9.22	305.159	-0.032	-0.555	16.740	3.643	4.6	1.467	green
10.19	308.091	-0.049	-0.659	27.579	2.347	11.8	5.586	blue
9.49	338.087	-0.053	-0.598	32.848	0.000	-2.4E+07	10000	blue
9.74	340.104	-0.049	-0.630	29.279	2.385	12.3	6.83	blue
10.55	361.138	-0.049	-0.609	54.713	27.654	2	0.225	blue
9.48	371.227	-0.052	-0.606	41.785	10.601	3.9	0.875	purple
10.71	383.113	-0.042	-0.556	21.828	0.000	10000	10000	white
10.58	392.138	-0.046	-0.594	30.563	5.803	5.3	1.534	green
9.54	399.625	-0.037	-0.610	15.955	0.000	10000	10000	red
9.6	406.164	-0.046	-0.600	27.037	1.929	14	7.712	green
12.18	430.296	-0.067	-0.712	44.363	0.000	-4.2E+07	10000	green
9.96	431.090	-0.046	-0.728	19.933	0.000	-4E+07	10000	green
9.58	432.280	-0.048	-0.680	33.715	10.099	3.3	0.601	gray
12.18	448.306	-0.050	-0.626	29.513	1.137	26	20.871	green

12.19	466.318	-0.067	-0.556	58.968	2.487	23.7	11.808	green
14.09	500.277	-0.063	-0.577	48.380	1.157	41.8	33.792	blue
9.72	520.313	-0.069	-0.854	51.818	12.795	4	0.548	blue
14.11	542.327	-0.045	-0.582	24.440	0.000	-3.2E+07	10000	white
9.86	547.334	-0.031	-0.558	18.339	6.459	2.8	0.559	purple
9.93	608.387	-0.034	-0.680	18.797	7.236	2.6	0.481	purple

REFERENCES

(1)   Dunn, W. B.; Ellis, D. I., *TrAC Trends in Analytical Chemistry* **2005,** *24*, 285-294.
(2)   Fernie, A. R.; Trethewey, R. N.; Krotzky, A. J.; Willmitzer, L., *Nat Rev Mol Cell Biol* **2004,** *5*, 763-769.
(3)   Baillie, T. A.; Cayen, M. N.; Fouda, H.; Gerson, R. J.; Green, J. D.; Grossman, S. J.; Klunk, L. J.; LeBlanc, B.; Perkins, D. G.; Shipley, L. A., *Toxicology and Applied Pharmacology* **2002,** *182*, 188-196.
(4)   Halket, J. M.; Waterman, D.; Przyborowska, A. M.; Patel, R. K. P.; Fraser, P. D.; Bramley, P. M., *J. Exp. Bot.* **2005,** *56*, 219-243.
(5)   Cox, K. A.; Clarke, N.; Rindgen, D., *Encyclopedia of Pharmaceutical Technology: Third Edition* **2006**, 2262 - 2268.
(6)   Bohrer, B. C.; Merenbloom, S. I.; Koeniger, S. L.; Hilderbrand, A. E.; Clemmer, D. E., *Annual Review of Analytical Chemistry* **2008,** *1*, 293-327.
(7)   Wyttenbach, T.; Bowers, M. T., *Topics in Current Chemistry* **2003,** *225*, 207-232.
(8)   Clemmer, D. E.; Jarrold, M. F., *Journal of Mass Spectrometry* **1997,** *32*, 577-592.
(9)   McLean, J. A.; Ruotolo, B. T.; Gillig, K. J.; Russell, D. H., *International Journal of Mass Spectrometry* **2005,** *240*, 301-315.
(10)   Ruotolo, B. T.; Gillig, K. J.; Stone, E. G.; Russell, D. H., *Journal of Chromatography B* **2002,** *782*, 385-392.
(11)   Collins, D. C.; Lee, M. L., *Analytical and Bioanalytical Chemistry* **2002,** *372*, 66-73.
(12)   Cohen, M. J.; Karasek, F. W., *Journal of Chromatographic Science* **1970,** *8*, 330-337.
(13)   Herbert H. Hill, J., *Chromatography: A Century of Discovery 1900-2000: The Bridge to the Sciences/Technology*, Gehre, C. W.; Wixom, R. L.; Bayer, E., Eds. Elsevier: New York, 2001; pp 226-230.
(14)   Pringle, S. D.; Giles, K.; Wildgoose, J. L.; Williams, J. P.; Slade, S. E.; Thalassinos, K.; Bateman, R. H.; Bowers, M. T.; Scrivens, J. H., *International Journal of Mass Spectrometry* **2007,** *261*, 1-12.
(15)   Guevremont, R., *Canadian Journal of Analytical Sciences and Spectroscopy* **2004,** *49*, 105-113.
(16)   Krylov, E. V.; Nazarov, E. G.; Miller, R. A., *International Journal of Mass Spectrometry* **2007,** *266*, 76-85.
(17)   de la Mora, J. F.; de Juan, L.; Eichler, T.; Rosell, J., *TrAC Trends in Analytical Chemistry* **1998,** *17*, 328-339.
(18)   Kaufman, S. L., *Journal of Aerosol Science* **1998,** *29*, 537-552.
(19)   Srebalus, C. A.; Li, J.; Marshall, W. S.; Clemmer, D. E., *Analytical Chemistry* **1999,** *71*, 3918-3927.
(20)   Merenbloom, S. I.; Glaskin, R. S.; Henson, Z. B.; Clemmer, D. E., *Analytical Chemistry* **2009,** *81*, 1482-1487.
(21)   Tung, L. S.; Barr, W. L.; Lowder, R. S.; Post, R. F., *Journal of Applied Physics* **1996,** *80*, 3646-3655.
(22)   Shvartsburg, A. A.; Danielson, W. F.; Smith, R. D., *Analytical Chemistry* **2010,** *82*, 2456-2462.
(23)   Santos, J. P.; Hontan, E.; Ramiro, E.; Alonso, M., *Atmos. Chem. Phys.* **2009,** *9*, 2419-2429.
(24)   Eiceman, G. A.; Stone, J. A., *Analytical Chemistry* **2004,** *76*, 390A-397A.
(25)   Mason, E. A.; McDaniel, E. W., John Wiley & Sons: New York, 1988; p 560.
(26)   Mesleh, M. F.; Hunter, J. M.; Shvartsburg, A. A.; Schatz, G. C.; Jarrold, M. F., *Journal of Physical Chemistry* **1996,** *100*, 16082-16086.
(27)   Shersby-Harvie, R. B. R., *Proceedings of the Physical Society* **1948,** *61*, 255.
(28)   Tyndall, A. M.; Starr, L. H.; Powell, C. F., *Proceedings of the Royal Society of London. Series A, Containing Papers of a Mathematical and Physical Character* **1928,** *121*, 172-184.
(29)   Stevenson, P. C.; Thomas, R. A.; Lane, S., *Nuclear Instruments and Methods* **1970,** *89*, 177-187.

(30) Kolakowski, B. M.; Mester, Z., *The Analyst* **2007,** *132*, 842-864.
(31) Barnett, D. A.; Ells, B.; Guevremont, R.; Purves, R. W., *Journal of the American Society for Mass Spectrometry* **1999,** *10*, 1279-1284.
(32) Shvartsburg, A. A.; Tang, K.; Smith, R. D., 2008; *Vol. 492,* pp 417-445.
(33) Viehland, L. A.; Guevremont, R.; Purves, R. W.; Barnett, D. A., *International Journal of Mass Spectrometry* **2000,** *197*, 123-130.
(34) Zimmermann, S.; Abel, N.; Baether, W.; Barth, S., *Sensors and Actuators B: Chemical* **2007,** *125*, 428-434.
(35) de la Mora, J. F.; de Juan, L.; Liedtke, K.; Schmidt-Ott, A., *Journal of Aerosol Science* **2003,** *34*, 79-98.
(36) Harden, C. S.; Shoff, D. B.; Ewing, R. G. 6th International Workshop on Ion Mobility Spectrometry, Bastei, Germany, 1997; Bastei, Germany, 1997; p 306.
(37) Creaser, C. S.; Griffiths, J. R.; Bramwell, C. J.; Noreen, S.; Hill, C. A.; Thomas, C. L. P., *Analyst* **2004,** *129*, 984-994.
(38) Valentine, S. J.; Counterman, A. E.; Clemmer, D. E., *Journal of the American Society for Mass Spectrometry* **1999,** *10*, 1188-1211.
(39) McDaniel, E. W.; Martin, D. W.; Barnes, W. S., *Review of Scientific Instruments* **1962,** *33*, 2-7.
(40) Bloomfield, C. H.; Hasted, J. B., *Discussions of the Faraday Society* **1964,** *37*, 176-184.
(41) Kanu, A. B.; Dwivedi, P.; Tam, M.; Matz, L.; Hill, H. H., Jr., *Journal of Mass Spectrometry* **2008,** *43*, 1-22.
(42) Covey, T. R.; Thomson, B. A.; Schneider, B. B., *Mass Spectrometry Reviews* **2009,** *28*, 870-897.
(43) McKnight, L. G.; McAfee, K. B.; Sipler, D. P., *Physical Review* **1967,** *164*, 62.
(44) Canterbury, J. D.; Yi, X.; Hoopmann, M. R.; MacCoss, M. J., *Analytical Chemistry* **2008,** *80*, 6888-6897.
(45) Kaneko, Y.; Megill, L. R.; Hasted, J. B., *The Journal of Chemical Physics* **1966,** *45*, 3741-3751.
(46) Hilton, G. R.; Jackson, A. T.; Thalassinos, K.; Scrivens, J. H., *Analytical Chemistry* **2008,** *80*, 9720-9725.
(47) Rose, D. J.; Opiteck, G. J., *Analytical Chemistry* **1994,** *66*, 2529-2536.
(48) O'Farrell, P. H., *J Biol Chem* **1975,** *250*, 4007-21.
(49) Klose, J., *Humangenetik* **1975,** *26*, 231-43.
(50) Ruotolo, B. T.; Gillig, K. J.; Stone, E. G.; Russell, D. H., *Journal of Chromatography B-Analytical Technologies in the Biomedical and Life Sciences* **2002,** *782*, 385-392.
(51) Wyttenbach, T.; Bowers, M. T., *Modern Mass Spectrometry* **2003,** *225*, 207-232.
(52) Giddings, J. C., *Analytical Chemistry* **1984,** *56*, 1258-&.
(53) Shen, Y. F.; Zhang, R.; Moore, R. J.; Kim, J.; Metz, T. O.; Hixson, K. K.; Zhao, R.; Livesay, E. A.; Udseth, H. R.; Smith, R. D., *Analytical Chemistry* **2005,** *77*, 3090-3100.
(54) Welthagen, W.; Shellie, R.; Spranger, J.; Ristow, M.; Zimmermann, R.; Fiehn, O., *Metabolomics* **2005,** *1*, 65-73.
(55) Dunn, W. B.; Knowles, J. D.; Broadhurst, D.; Williams, R.; Ashworth, J. J.; Cameron, M.; Kell, D. B., *Analytical Chemistry* **2006,** *79*, 464-476.
(56) Soga, T.; Ohashi, Y.; Ueno, Y.; Naraoka, H.; Tomita, M.; Nishioka, T., *Journal of Proteome Research* **2003,** *2*, 488-494.
(57) Shigeru, S.; Tomoyoshi, S.; Takaaki, N.; Masaru, T., *The Plant Journal* **2004,** *40*, 151-163.
(58) Imperato, A.; Di Chiara, G., *J. Neurosci.* **1984,** *4*, 966-977.
(59) Bayer, E.; Grom, E.; Kaltenegger, B.; Uhmann, R., *Analytical Chemistry* **1976,** *48*, 1106-1109.
(60) Soga, T.; Heiger, D. N., *Analytical Chemistry* **2000,** *72*, 1236-1241.
(61) Monton, M. R. N.; Soga, T., *Journal of Chromatography A* **2007,** *1168*, 237-246.
(62) Camilleri, P., CRC Press: Boca Raton, FL, 1998.
(63) Krupcík, J.; Garaj, J.; Cellár, P.; Guiochon, G., *Journal of Chromatography A* **1984,** *312*, 1-10.
(64) Lan, K.; Jorgenson, J. W., *Analytical Chemistry* **1999,** *71*, 709-714.

(65)   Snyder, L. R.; Kirkland, J. J.; Dolan, J. W., John Wiley & Sons: Hoboken, NJ, 2009; p 912.

(66)   van Asten, A. C.; Stegeman, G.; Kok, W. T.; Tijssen, R.; Poppe, H., *Analytical Chemistry* **1994,** *66*, 3073-3080.

(67)   Martin, M.; Jaulmes, A., *Separation Science and Technology* **1981,** *16*, 691 - 724.

(68)   Hoaglund, C. S.; Valentine, S. J.; Sporleder, C. R.; Reilly, J. P.; Clemmer, D. E., *Analytical Chemistry* **1998,** *70*, 2236-2242.

(69)   Liu, X.; Plasencia, M.; Ragg, S.; Valentine, S. J.; Clemmer, D. E., *Briefings in Functional Genomics and Proteomics* **2004,** *3*, 177-186.

(70)   Li, J.; Purves, R. W.; Richards, J. C., *Anal Chem* **2004,** *76*, 4676-83.

(71)   Griffin, G. W.; Dzidic, I.; Carroll, D. I.; Stillwell, R. N.; Horning, E. C., *Analytical Chemistry* **1973,** *45*, 1204-1209.

(72)   Dwivedi, P.; Schultz, A. J.; Jr, H. H. H., *International Journal of Mass Spectrometry In Press, Corrected Proof*.

(73)   Kaplan, K.; Dwivedi, P.; Davidson, S.; Yang, Q.; Tso, P.; Siems, W.; Hill, H. H., *Analytical Chemistry* **2009,** *81*, 7944-7953.

(74)   Dwivedi, P.; Wu, P.; Klopsch, S. J.; Puzon, G. J.; Xun, L.; Hill, H. H., *Metabolomics* **2008,** *4*, 63-80.

(75)   Nielsen, J.; Jewett, M., *Metabolomics*, 2007; pp 1-10.

(76)   McLean, J. A., *Journal of the American Society for Mass Spectrometry* **2009,** *20*, 1775-1781.

(77)   Fenn, L. S.; Kliman, M.; Mahsut, A.; Zhao, S. R.; McLean, J. A., *Analytical and Bioanalytical Chemistry* **2009,** *394*, 235-244.

(78)   Want, E. J.; Cravatt, B. F.; Siuzdak, G., *ChemBioChem* **2005,** *6*, 1941-1951.

(79)   Fenselau, C.; Smith, P. B. W., *Xenobiotica: The fate and safety evaluation of foreign compounds in biological systems* **1992,** *22*, 1207 - 1219.

(80)   Spangler, G. E., *International Journal of Ion Mobility Spectrometry* **2002,** *5*, 135-159.

(81)   Ruotolo, B. T.; Benesch, J. L. P.; Sandercock, A. M.; Hyung, S.-J.; Robinson, C. V., *Nat. Protocols* **2008,** *3*, 1139-1152.

(82)   Saba, J.; Bonneil, E.; PomieÌ€s, C.; Eng, K.; Thibault, P., *Journal of Proteome Research* **2009,** *8*, 3355-3366.

(83)   Domon, B.; Costello, C. E., *Glycoconjugate Journal* **1988,** *5*, 397-409.

(84)   McLean, J. A.; Fenn, L. S.; Enders, J. R., Springer: Hatfield, Hertfordshire, UK, 2010; *Vol. 656*, p 363.

(85)   Bateman, K. P.; Castro-Perez, J.; Wrona, M.; Shockcor, J. P.; Yu, K.; Oballa, R.; Nicoll-Griffith, D. A., *Rapid Communications in Mass Spectrometry* **2007,** *21*, 1485-1496.

(86)   Kessler, H., *Angewandte Chemie International Edition in English* **1982,** *21*, 512-523.

(87)   Wilkinson, B.; Micklefield, J., *Nat Chem Biol* **2007,** *3*, 379-386.

(88)   Challis, G. L., *Journal of Medicinal Chemistry* **2008,** *51*, 2618-2628.

(89)   Mason, E. A.; McDaniel, E. W., John Wiley & Sons, Inc.: New York, 1988.

(90)   Tao, L.; McLean, J. R.; McLean, J. A.; Russell, D. H., *Journal of the American Society for Mass Spectrometry* **2007,** *18*, 1232-1238.

(91)   Ruotolo, B. T.; Tate, C. C.; Russell, D. H., *Journal of the American Society for Mass Spectrometry* **2004,** *15*, 870-878.

(92)   Sundarapandian, S.; May, J. C.; McLean, J. A., *Analytical Chemistry* **2010,** *82*, 3247-3254.

(93)   Frisch, M.; Trucks, G.; Schlegel, H.; Scuseria, G.; Robb, M.; Cheeseman, J.; Montgomery, J. J.; Vreven, T.; Kudin, K.; Burant, J.; Millam, J.; Iyengar, S.; Tomasi, J.; Barone, V.; Mennucci, B.; Cossi, M.; Scalmani, G.; Rega, N.; Petersson, G.; Nakatsuji, H.; Hada, M.; Ehara, M.; Toyota, K.; Fukuda, R.; Hasegawa, J.; Ishida, M.; Nakajima, T.; Honda, Y.; Kitao, O.; Nakai, H.; Klene, M.; Li, X.; Knox, J.; Hratchian, H.; Cross, J.; Bakken, V.; Adamo, C.; Jaramillo, J.; Gomperts, R.; Stratmann, R.; Yazyev, O.; Austin, A.; Cammi, R.; Pomelli, C.; Ochterski, J.; Ayala, P.; Morokuma, K.; Voth, G.; Salvador, P.; Dannenberg, J.; Zakrzewski, V.; Dapprich, S.; Daniels, A.; Strain, M.; Farkas, O.; Malick, D.; Rabuck, A.; Raghavachari, K.; Foresman, J.; Ortiz, J.; Cui, Q.; Baboul, A.; Clifford, S.; Cioslowski, J.; Stefanov, B.; Liu, G.; Liashenko, A.; Piskorz, P.; Komaromi, I.; Martin, R.;

Fox, D.; Keith, T.; Al-Laham, M.; Peng, C.; Nanayakkara, A.; Challacombe, M.; Gill, P.; Johnson, B.; Chen, W.; Wong, M.; Gonzalez, C.; Pople, J. Wallingford CT 2004.

(94) Case, D. A.; Darden, T. A.; Cheatham, I., T.E.; Simmerling, C. L.; Wang, J.; Duke, R. E.; Luo, R.; Walker, R. C.; Zhang, W.; Merz, K. M.; Roberts, B.; Wang, B.; Hayik, S.; Roitberg, A.; Seabra, G.; Kolossvai, I.; Wong, K. F.; Paesani, F.; Vanicek, J.; Liu, J.; Wu, X.; Brozell, S. R.; Steinbrecher, T.; Gohlke, H.; Cai, Q.; Ye, X.; Wang, J.; Hsieh, M.-J.; Cui, G.; Roe, D. R.; Mathews, D. H.; Seetin, M. G.; Sagui, C.; Babin, V.; Luchko, T.; Gusarov, S.; Kovalenko, A.; Kollman, P. A. 2010.

(95) Wang, J.; Wolf, R. M.; Caldwell, J. W.; Kollman, P. A.; Case, D. A., *Journal of Computational Chemistry* **2004,** *25*, 1157-1174.

(96) Hornak, V.; Okur, A.; Rizzo, R. C.; Simmerling, C., 2006; Vol. 103, pp 915-920.

(97) Hornak, V.; Abel, R.; Okur, A.; Strockbine, B.; Roitberg, A.; Simmerling, C., *Proteins: Structure, Function, and Bioinformatics* **2006,** *65*, 712-725.

(98) Shvartsburg, A. A.; Jarrold, M. F., *Chemical Physics Letters* **1996,** *261*, 86-91.

(99) 10; Chemical Computing Group: 2010.

(100) Wyttenbach, T.; vonHelden, G.; Bowers, M. T., *Journal of the American Chemical Society* **1996,** *118*, 8355-8364.

(101) Valentine, S. J.; Counterman, A. E.; Hoaglund-Hyzer, C. S.; Clemmer, D. E., *Journal of Physical Chemistry B* **1999,** *103*, 1203-1207.

(102) Heaton, A. L.; Moision, R. M.; Armentrout, P. B., *The Journal of Physical Chemistry A* **2008,** *112*, 3319-3327.

(103) Cerda, B. A.; Hoyau, S.; Ohanessian, G.; Wesdemiotis, C., *Journal of the American Chemical Society* **1998,** *120*, 2437-2448.

(104) Frechet, D.; Guitton, J. D.; Herman, F.; Faucher, D.; Helynck, G.; Monegier du Sorbier, B.; Ridoux, J. P.; James-Surcouf, E.; Vuilhorgne, M., *Biochemistry* **1994,** *33*, 42-50.

(105) Constantine, K. L.; Friedrichs, M. S.; Detlefsen, D.; Nishio, M.; Tsunakawa, M.; Furumai, T.; Ohkuma, H.; Oki, T.; Hill, S.; Bruccoleri, R. E.; Lin, P.-F.; Mueller, L., *Journal of Biomolecular NMR* **1995,** *5*, 271-286.

(106) Detlefsen, D. J.; Hill, S. E.; Volk, K. J.; Klohr, S. E.; Tsunakawa, M.; Furumai, T.; Lin, P. F.; Nishio, M.; Kawano, K.; Oki, T.; Lee, M. S., *The Journal of Antibiotics* **1995,** *48*.

(107) Bush, M. F.; Hall, Z.; Giles, K.; Hoyes, J.; Robinson, C. V.; Ruotolo, B. T., *Analytical Chemistry* **2010,** *82*, 9557-9565.

(108) Barton, H. A.; Jurado, V., *Microbe-American* **2007,** *2*, 132.

(109) Lurdes, M. d.; Dapkevicius, N. E., Springer: 2013; *Vol. 1*, p 35-45.

(110) Hill, C. A., *Journal of Cave and Karst Studies* **2000,** *62*, 60-71.

(111) Polyak, V. J.; McIntosh, W. C.; Guven, N.; Provencio, P., *Science* **1998,** *279*, 1919-1922.

(112) Polyak, V. J.; Provencio, P. P., *Journal of Cave and Karst Studies* **2000,** *62*, 72-74.

(113) DuChene, H. R.; Cunningham, K. I., Land, L.; Love, D. L.; Lueth, V. W.; Raatz, W.; Boston, P., Eds. New

Mexico Geological Society, Socorro, NM, **2006**; pp 211-218.

(114) Davis, D. G., *Journal of Cave and Karst Studies* **2000,** *62*, 147-157.

(115) Johnston, M. D.; Muench, B. A.; Banks, E. D.; Barton, H. A., *Journal of Cave and Karst Studies* **2012,** *74*, 278–291.

(116) Barton, H. A.; Taylor, N. M.; Kreate, M. P.; Springer, A. C.; Oehrle, S. A.; Bertog, J. L., *International Journal of Speleology* **2007,** *36*, 93-104.

(117) Northup, D. E.; Barns, S. M.; Yu, L. E.; Spilde, M. N.; Schelble, R. T.; Dano, K. E.; Crossey, L. J.; Connolly, C. A.; Boston, P. J.; Natvig, D. O.; Dahm, C. N., *Environ Microbiol* **2003,** *5*, 1071-1086.

(118) Bhullar, K.; Waglechner, N.; Pawlowski, A.; Koteva, K.; Banks, E. D.; Johnston, M. D.; Barton, H. A.; Wright, G. D., *PLoS One* **2012,** *7*.

(119) Goodwin, C. R.; Fenn, L. S.; Derewacz, D. K.; Bachmann, B. O.; McLean, J. A., *Journal of Natural Products* **2012,** *75*, 48-53.

(120) Sundarapandian, S.; May, J. C.; McLean, J. A., *Analytical Chemistry* **2011,** *82*, 3247-3254.

(121) Fenn, L.; McLean, J., *Analytical and Bioanalytical Chemistry* **2008,** *391*, 905-909.

(122)	Griffith, B. R.; Langenhan, J. M.; Thorson, J. S., *Current Opinion in Biotechnology* **2005,** *16*, 622-630.
(123)	Neumann, C. S.; Fujimori, D. G.; Walsh, C. T., *Chemistry & Biology* **2008,** *15*, 99-109.
(124)	Clardy, J.; Walsh, C., *Nature* **2004,** *432*, 829-837.
(125)	Rohr, J.; Thiericke, R., *Nat. Prod. Rep.* **1992,** *9*, 103-137.
(126)	Newton, G. L.; Bewley, C. A.; Dwyer, T. J.; Horn, R.; Aharonowitz, Y.; Cohen, G.; Davies, J.; Faulkner, D. J.; Fahey, R. C., *Eur. J. Biochem.* **1995,** *230*, 821-825.
(127)	Sakuda, S.; Zhou, Z. Y.; Yamada, Y., *Biosci Biotech Bioch* **1994,** *58*, 1347-1348.
(128)	Steenkamp, D. J.; Spies, H. S. C., *Eur. J. Biochem.* **1994,** *223*, 43-50.
(129)	Nicholas, G. M.; Kovac, P.; Bewley, C. A., *J. Am. Chem. Soc.* **2002,** *124*, 3492-3493.
(130)	Newton, G. L.; Av-Gay, Y.; Fahey, R. C., *Biochemistry* **2000,** *39*, 10739-10746.
(131)	Forsberg, K. J.; Reyes, A.; Wang, B.; Selleck, E. M.; Sommer, M. O.; Dantas, G., *Science* **2012,** *337*, 1107-11.
(132)	Bhullar, K.; Waglechner, N.; Pawlowski, A.; Koteva, K.; Banks, E. D.; Johnston, M. D.; Barton, H. A.; Wright, G. D., *PLoS One* **2012,** *7*, e34953.
(133)	Galas, D. J.; Branscomb, E. W., *Nature* **1976,** *262*, 617-619.
(134)	Jin, D. J.; Gross, C. A., *Journal of Molecular Biology* **1988,** *202*, 45-58.
(135)	Campbell, E. A.; Korzheva, N.; Mustaev, A.; Murakami, K.; Nair, S.; Goldfarb, A.; Darst, S. A., *Cell* **2001,** *104*, 901-12.
(136)	Sandalakis, V.; Psaroulaki, A.; De Bock, P.-J.; Christidou, A.; Gevaert, K.; Tsiotis, G.; Tselentis, Y., *Journal of Proteome Research* **2012,** *11*, 2374-2385.
(137)	Neri, A.; Mignogna, G.; Fazio, C.; Giorgi, A.; Schinina, M.; Stefanelli, P., **2010,** *10*, 246.
(138)	Hosaka, T.; Xu, J.; Ochi, K., *Molecular Microbiology* **2006,** *61*, 883-897.
(139)	Hu, H.; Zhang, Q.; Ochi, K., *J Bacteriol* **2002,** *184*, 3984-91.
(140)	Wang, G.; Hosaka, T.; Ochi, K., *Appl Environ Microb* **2008,** *74*, 2834-40.
(141)	Hosaka, T.; Ohnishi-Kameyama, M.; Muramatsu, H.; Murakami, K.; Tsurumi, Y.; Kodani, S.; Yoshida, M.; Fujie, A.; Ochi, K., *Nat Biotechnol* **2009,** *27*, 462-464.
(142)	Gomez-Escribano, J. P.; Song, L. J.; Fox, D. J.; Yeo, V.; Bibb, M. J.; Challis, G. L., *Chem Sci* **2012,** *3*, 2716-2720.
(143)	Weckwerth, W.; Morgenthal, K., *Drug Discovery Today* **2005,** *10*, 1551-1558.
(144)	Wiklund, S.; Johansson, E.; Sjostrom, L.; Mellerowicz, E. J.; Edlund, U.; Shockcor, J. P.; Gottfries, J.; Moritz, T.; Trygg, J., *Analytical Chemistry* **2007,** *80*, 115-122.
(145)	Daniel, P. T.; Koert, U.; Schuppan, J., *Angew Chem Int Ed Engl* **2006,** *45*, 872-93.
(146)	Du, Y.; Derewacz, D. K.; Deguire, S. M.; Teske, J.; Ravel, J.; Sulikowski, G. A.; Bachmann, B. O., *Tetrahedron* **2011,** *67*, 6568-6575.
(147)	van den Berg, R.; Hoefsloot, H.; Westerhuis, J.; Smilde, A.; van der Werf, M., *BMC Genomics* **2006,** *7*, 142.
(148)	Bjorkman, J.; Nagaev, I.; Berg, O. G.; Hughes, D.; Andersson, D. I., *Science* **2000,** *287*, 1479-82.
(149)	Brandis, G.; Wrande, M.; Liljas, L.; Hughes, D., *Mol Microbiol* **2012,** *85*, 142-51.
(150)	Fenn, L. S.; Kliman, M.; Mahsut, A.; Zhao, S. R.; McLean, J. A., *Anal Bioanal Chem* **2009,** *394*, 235-44.
(151)	Bylesjö, M.; Rantalainen, M.; Cloarec, O.; Nicholson, J. K.; Holmes, E.; Trygg, J., *Journal of Chemometrics* **2006,** *20*, 341-351.
(152)	Daum, M.; Peintner, I.; Linnenbrink, A.; Frerich, A.; Weber, M.; Paululat, T.; Bechthold, A., *Chembiochem* **2009,** *10*, 1073-83.
(153)	Lombo, F.; Menendez, N.; Salas, J. A.; Mendez, C., *Appl Microbiol Biotechnol* **2006,** *73*, 1-14.
(154)	Beam, M. P.; Bosserman, M. A.; Noinaj, N.; Wehenkel, M.; Rohr, J., *Biochemistry* **2009,** *48*, 4476-87.
(155)	Xiang, L.; Kalaitzis, J. A.; Moore, B. S., *Proc Natl Acad Sci U S A* **2004,** *101*, 15609-14.
(156)	Wright, J. L. C.; Hu, T.; McLachlan, J. L.; Needham, J.; Walter, J. A., *J Am Chem Soc* **1996,** *118*, 8757-8758.
(157)	Aubry-Damon, H.; Galimand, M.; Gerbaud, G.; Courvalin, P., *Antimicrobial Agents and Chemotherapy* **2002,** *46*, 1571-1573.
(158)	Maness, M. J.; Sparling, P. F., *The Journal of Infectious Diseases* **1973,** *128*, 321-330.

(159) Pozzi, G.; Meloni, M.; Iona, E.; Orru, G.; Thoresen, O. F.; Ricci, M. L.; Oggioni, M. R.; Fattorini, L.; Orefici, G., *Journal of Clinical Microbiology* **1999,** *37*, 1197-1199.

(160) Rochfort, S., *Journal of Natural Products* **2005,** *68*, 1813-1820.

(161) Goodacre, R.; Vaidyanathan, S.; Dunn, W. B.; Harrigan, G. G.; Kell, D. B., *Trends in Biotechnology* **2004,** *22*, 245-252.

(162) Nordstrom, A.; O'Maille, G.; Qin, C.; Siuzdak, G., *Analytical Chemistry* **2006,** *78*, 3289-3295.

(163) Smith, C. A.; Elizabeth, J.; O'Maille, G.; Abagyan, R.; Siuzdak, G., *Analytical Chemistry* **2006,** *78*, 779-787.

(164) Eichler, G. S.; Huang, S.; Ingber, D. E., *Bioinformatics* **2003,** *19*, 2321-2322.

(165) Patterson, A. D.; Li, H.; Eichler, G. S.; Krausz, K. W.; Weinstein, J. N.; Fornace Jr, A. J.; Gonzalez, F. J.; Jeffrey, R., *Analytical Chemistry* **2008,** *80*, 665-674.

(166) Tyburski, J. B.; Patterson, A. D.; Krausz, K. W.; Slavik, J.; Fornace Jr, A. J.; Gonzalez, F. J.; Idle, J. R., *Radiation Research* **2008,** *170*, 1-14.

(167) Schramm-Sapyta, N. L.; Olsen, C. M.; Winder, D. G., *Neuropsychopharmacology* **2005,** *31*, 1444-1451.

(168) Wishart, D. S.; Knox, C.; Guo, A. C.; Eisner, R.; Young, N.; Gautam, B.; Hau, D. D.; Psychogios, N.; Dong, E.; Bouatra, S., *Nucleic Acids Research* **2009,** *37*, D603-D610.

(169) Wishart, D. S.; Tzur, D.; Knox, C.; Eisner, R.; Guo, A. C.; Young, N.; Cheng, D.; Jewell, K.; Arndt, D.; Sawhney, S., *Nucleic Acids Research* **2007,** *35*, D521-D526.

(170) Smith, C. A.; Maille, G. O.; Want, E. J.; Qin, C.; Trauger, S. A.; Brandon, T. R.; Custodio, D. E.; Abagyan, R.; Siuzdak, G., *Therapeutic Drug Monitoring* **2005,** *27*, 747.

(171) Sud, M.; Fahy, E.; Cotter, D.; Brown, A.; Dennis, E. A.; Glass, C. K.; Merrill Jr, A. H.; Murphy, R. C.; Raetz, C. R. H.; Russell, D. W., *Nucleic Acids Research* **2007,** *35*, D527-D532.

(172) Novakova, L.; Vlckova, H., *Analytica Chimica Acta* **2009,** *656*, 8-35.

(173) Alvarez-Sanchez, B.; Priego-Capote, F.; Luque de Castro, M. D., *TrAC Trends in Analytical Chemistry* **2010,** *29*, 111-119.

(174) Ogata, H.; Goto, S.; Sato, K.; Fujibuchi, W.; Bono, H.; Kanehisa, M., *Nucleic Acids Research* **1999,** *27*, 29-34.

(175) Kanehisa, M.; Goto, S.; Hattori, M.; Aoki-Kinoshita, K. F.; Itoh, M.; Kawashima, S.; Katayama, T.; Araki, M.; Hirakawa, M., *Nucleic Acids Research* **2006,** *34*, D354-D357.

(176) Wiklund, S.; Johansson, E.; Sjstrm, L.; Mellerowicz, E. J.; Edlund, U.; Shockcor, J. P.; Gottfries, J.; Moritz, T.; Trygg, J., *Analytical Chemistry* **2008,** *80*, 115-122.

(177) Lovenberg, W.; Bruckwick, E. A.; Hanbauer, I., *Proceedings of the National Academy of Sciences* **1975,** *72*, 2955.

(178) McDougle Cj, B. J. E. M. R. T.; et al., *Archives of General Psychiatry* **1994,** *51*, 713-719.

(179) Rockhold, R. W.; Oden, G.; Ho, I. K.; Andrew, M.; Farley, J. M., *Brain Research Bulletin* **1991,** *27*, 721-723.

(180) Garg, U. C.; Turndorf, H.; Bansinath, M., *Neuroscience* **1993,** *57*, 467-472.

(181) Niwa, T.; Takeda, N.; Maeda, K.; Shibata, M.; Tatematsu, A., *Clinica Chimica Acta* **1988,** *173*, 127-138.

(182) Costigan, M. G.; Yaqoob, M.; Lindup, W. E., *Nephrology Dialysis Transplantation* **1996,** *11*, 803-807.

(183) Okuda, S.; Nishiyama, N.; Saito, H.; Katsuki, H., *Journal of Neurochemistry* **1998,** *70*, 299-307.

(184) Fallstrom, S.-P.; Lindblad, B.; Steen, G., *Acta Pædiatrica* **1981,** *70*, 315-320.

(185) Evans, A. H.; Lees, A. J., *Current Opinion in Neurology* **2004,** *17*, 393.

(186) Faraj, B. A.; Camp, V. M.; Kutner, M., *Alcoholism: Clinical and Experimental Research* **1991,** *15*, 86-89.

(187) Alberts, B., *Science* **2012,** *337*, 1583-1583.

(188) Rios, J. L.; Recio, M. C.; Villar, A., *Journal of Etnopharmacology* **1988,** *23*, 127-149.

(189) Scherlach, K.; Hertweck, C., *Organic & Biomolecular Chemistry* **2009,** *7*, 1753-1760.

(190) Onaka, H.; Mori, Y.; Igarashi, Y.; Furumai, T., *Applied and Environmental Microbiology* **2011,** *77*, 400-406.

(191)   Bentley, S. D.; Chater, K. F.; Cerdeno-Tarraga, A. M.; Challis, G. L.; Thomson, N. R.; James, K. D.; Harris, D. E.; Quail, M. A.; Kieser, H.; Harper, D., *Nature* **2002**, *417*, 141-147.

(192)   Krieger, C. J.; Zhang, P.; Mueller, L. A.; Wang, A.; Paley, S.; Arnaud, M.; Pick, J.; Rhee, S. Y.; Karp, P. D., *Nucleic Acids* **2004,** *32*, D438-D442.

(193)   Caspi, R.; Foerster, H.; Fulcher, C. A.; Kaipa, P.; Krummenacker, M.; Latendresse, M.; Paley, S.; Rhee, S. Y.; Shearer, A. G.; Tissier, C., *Nucleic Acids* **2008,** *36*, D623-D631.

(194)   Wolf, S.; Schmidt, S.; Muller-Hannemann, M.; Neumann, S., 2010; Vol. 11, p 148.

(195)   Mortelmans, L.; Nuyts, J.; Pamel, G.; Maegdenbergh, V.; Roo, M.; Suetens, P., *European Journal of Nuclear Medicine and Molecular Imaging* **1986,** *12*, 284-290.

(196)   Gehlenborg, N.; O'Donoghue, S. I.; Baliga, N. S.; Goesmann, A.; Hibbs, M. A.; Kitano, H.; Kohlbacher, O.; Neuweger, H.; Schneider, R.; Tenenbaum, D., *Nature* **2010,** *7*, S56-S68.

(197)   Ridenour, W. B.; Kliman, M.; McLean, J. A.; Caprioli, R. M., *Analytical Chemistry* **2010,** *82*, 1881-1889.

(198)   Frisch, M. J.; Trucks, G. W.; Schlegel, H. B.; Scuseria, G. E.; Robb, M. A.; Cheeseman, J. R.; Montgomery Jr, J. A.; Vreven, T.; Kudin, K. N.; Burant, J. C., *Inc., Wallingford, CT* **2004,** *5*.

(199)   Case, D. A.; Darden, T. A.; Cheatham, I., T. E.; Simmerling, C. L.; Wang, J.; Duke, R. E.; Luo, R.; C., W. R.; Zhang, W.; Merz, K. M.; Roberts, B.; Wang, B.; Hayik, S.; Roitberg, A.; Seabra, G.; Kolossvary, I.; Wong, K. F.; Paesani, F.; Vanicek, J.; Wu, X.; Brozell, S. R.; Steinbrecher, T.; BGohlke, H.; Cai, Q.; Ye, X.; Wang, J.; Hsieh, M. J.; Cui, G.; Roe, D. H.; Mathews, D. H.; Seetin, M. G.; Saqui, C.; Babin, V.; Luchko, T.; Gusarov, S.; Kovalenko, A.; Kollman, P. A. University of California: San Francisco, 2010.

(200)   Hornak, V.; Okur, A.; Rizzo, R. C.; Simmerling, C., *Proceedings of the National Academy of Sciences* **2006,** *103*, 915.

(201)   2010.09; Chemical Computing Group, Inc.

Curriculum Vitae
Cody R. Goodwin

4302 Idaho Avenue   Cody.R.Goodwin@vanderbilt.edu
Nashville, TN 37209   Cody.R.Goodwin@gmail.com
Work Phone: 615-343-4563   Home Phone: 850-585-8002

EDUCATION

Vanderbilt University, Nashville, TN (2008-present) Doctoral Candidate, Chemistry (3.91 GPA)

University of Central Florida, Orlando, FL (2005-2008) Bachelor of Science, Chemistry (3.85 GPA)

Okaloosa-Walton College, Niceville, FL (2003-2005) Associate of Arts (3.91 GPA)

Niceville Senior High School, Niceville, FL (1999-2003) High School Diploma (4.79 weighted/4.0 unweighted GPA)

LEADERSHIP, TEACHING, AND RESEARCH EXPERIENCE

Graduate Research Coordinator Systems Biology and Bioengineering Undergraduate Research Experience, Vanderbilt University, 2010-present
Research Assistant, Department of Chemistry, Vanderbilt University, 2008-present
Teaching Assistant, Chemistry for Non-Science Majors, Vanderbilt University, 2009
Teaching Assistant, Analytical Chemistry, Vanderbilt University, 2009
Teaching Assistant, General Chemistry, Vanderbilt University, 2008
Teaching Assistant, General Chemistry, University of Central Florida, 2008
Research Assistant, Department of Chemistry, University of Central Florida, 2006-2008

FELLOWSHIPS AND AWARDS

2013   ***St. Jude Graduate Student Symposium Invitee***, St. Jude Children's Research Hospital
2012   ***MSACL Young Investigator Award,*** Mass Spectrometry Applications to the Clinical Lab
2008   ***Mitchum Warren Fellowship,*** Vanderbilt University
2008   ***Outstanding Undergraduate Seminar Award,*** University of Central Florida
2008   ***American Institute of Chemists Outstanding Undergraduate Student Award,*** University of Central Florida
2003   ***Florida Bright Futures Gold Seal Award,*** Florida Department of Education
2003   ***Presidential Scholarship,*** Okaloosa Walton College

PUBLICATIONS / BOOK CHAPTERS

D. K. Derewacz*, **C. R. Goodwin***, C. R. McNees, J. A. McLean, B. O. Bachmann. Antimicrobial drug resistance affects broad changes in metabolomic phenotype in addition to secondary metabolism. *Submitted to the Proceedings of the National Academy of Sciences* (IN PRESS)

J. P. Wikswo, F. E. Block, D. E. Cliffel, **C. R. Goodwin**, C. C. Marasco, D. A. Markov, D. L. McLean, J. A. McLean, J. R. McKenzie, R. S. Reiserer, P. C. Samson, D. K. Schaffer, K. T. Seale, S. D. Sherrod. Engineering Challenges for Instrumenting and Controlling Integrated Organ-on-Chip Systems. *Submitted to the Transactions on Biomolecular Engineering.* (ACCEPTED)

M. Shi, D. Majumdar, Y. Gao, B. Brewer, **C. R. Goodwin**, J. A. McLean, D. Li, D. J. Webb. Glia Co-culture with Neurons in Microfluidic Platforms Promotes the Formation and Stabilization of Synaptic Contacts. *Submitted to Small*

C. R. Goodwin, S. Sherrod, C. C. Marasco, N. M. Smith, B. O. Bachmann, N. Schramm-Sapyta, J. P. Wikswo, J. A. McLean. Phenotypic mapping of metabolic profiles using self-organizing maps. For s*ubmission to PLOS ONE.*

C. R. Goodwin, L. S. Fenn, Dagmara K. Derewacz, B. O. Bachmann, J. A. McLean. Structural Mass Spectrometry: Rapid Methods for Separation and Analysis of Peptide Natural Products. *Journal of Natural Products.* **2012**, *67* (*35*): 48-53

J. May, **C. R. Goodwin**, J. A. McLean. "Gas-Phase Ion Mobility-Mass Spectrometry and Tandem IM-MS Strategies for Metabolism Studies and Metabolomics," in the *Encyclopedia of Drug Metabolism & Drug Interactions,* D. C. Muddiman, Ed., J. Wiley & Sons (to be published **2012**) (IN PRESS).

J. R. Enders, **C. R. Goodwin,** Christina C. Marasco, K. T. Seale, J. P. Wikswo, and J. A. McLean. Advanced structural mass spectrometry for systems biology: Pulling the needles from haystacks, *Current Trends in Mass Spectrometry*, 2011, July: 18-23.

PUBLICATIONS IN PREPARATION

D. K. Derewacz, **C. R. Goodwin**, J. A. McLean, H. A. Barton, B. O. Bachmann. Lechacyclines, new angucyclines and their mycothiol adducts from a deep hypogean streptomycetes. *In preparation for Organic Letters.*

C. R. Goodwin, K. Y. Fong, D. W. Wright, J. A. McLean. Antimalarial mode of action is indicated by metabolic profile. *In preparation for MedChemComm.*

C. R. Goodwin, C. R. McNees, D. K. Derewacz, B. O. Bachmann, J. A. McLean. Mixed fermentation alters secondary metabolite production. *In preparation for JACS*

C. C. Marasco, **C. R. Goodwin**, K. T. Seale, D. Winder, N. Schramm-Sapyta, J. A. McLean, J. P. Wikswo. Systems Level View of Cocaine Addiction: the Interconnect of Immune and Nervous Systems. *In preparation for Experimental Biology and Medicine*.

PRESENTATIONS

C. R. Goodwin, D. K. Derewacz, B. O. Bachmann, J. A. McLean. *Shedding Light on Hypogean Natural Products through Multi-dimensional Separations*, 2013 29th International Symposium on MicroScale Bioseparations, Charlottesvilla, VA (March 2013) (ORAL Accepted)

S. M. Stow, **C. R. Goodwin**, M. Kliman, B. O. Bachmann, J. A. McLean, *Using Distance Geometry with Ion Mobility-Mass Spectrometry Data to Study the Conformational Space of Natural Products,* 2012 Sanibel Conference, St. Pete Beach, FL (January 2012).

N. M. Lareau, L. S. Fenn, **C. R. Goodwin**, J. C. May, B. O. Bachmann, J. A. McLean. *Characterization of Carbohydrates and Carbohydrate Natural Products by LC-Ion Mobility-Mass Spectrometry,* 2012 Sanibel Conference, St. Pete Beach, FL (January 2012).

C. R. Goodwin, C. C. Marasco, J. R. Enders, K. T. Seale, J. P. Wikswo, N. L. Schramm-Sapyta, J. A. McLean. *Analyses of rat and rat leukocyte metabolomic response to cocaine stimulation using multi-dimensional separations methods*, 4th Annual Mass Spectrometry Applications to the Clinical Lab, San Diego, CA (January 2012).

J. R. Enders, C. C. Marasco, **C. R. Goodwin**, J. C. May, K. T. Seale, J. P. Wikswo, J. A. McLean, *Development of a platform for online analysis of the metabolic footprint*, 4th Annual Mass Spectrometry Applications to the Clinical Lab, San Diego, CA (January 2012).

J. R. Enders, C. C. Marasco, **C. R. Goodwin**, J. C. May, K. T. Seale, J. P. Wikswo & J. A. McLean, *A microfluidic-ion mobility-mass spectrometry platform for presymptomatic diagnoses of CBW agent exposure*, 2011 Chemical and Biological Defense Science and Technology Conference, Las Vegas, NV (November 2011).

C. C. Marasco, **C. R. Goodwin**, A. Garza, J. R. Enders, K. T. Seale, J. P. Wikswo, N. L. Schramm-Sapyta, J. A. McLean, *Metabolomic investigation of a cocaine-suppressed immune response to toxin*, 2011 Chemical and Biological Defense Science and Technology Conference, Las Vegas, NV (November 2011).

A. Garza, C. C. Marasco, **C. R. Goodwin**, J. R. Enders, K. T. Seale, J. A. McLean, J. P. Wikswo, *Leukocyte metabolic profiling and non-translational motion quantization for dual indication of multiple toxin response*, 2011 Chemical and Biological Defense Science and Technology Conference, Las Vegas, NV (November 2011).

R. Harvey, C. C. Marasco, **C. R. Goodwin**, J. R. Enders, K. T. Seale, J. A. McLean, J. P. Wikswo, *Quantitation of single cell calcium signaling during T-cell activation*, 2011 Chemical and Biological Defense Science and Technology Conference, Las Vegas, NV (November 2011).

C. R. Goodwin, Analyses of Rat and Rat Leukocyte Metabolomic Response to Cocaine Stimulation using Muti-dimensional Separations Methods, MSACL, San Diego, CA (January 16, 2012). POSTER

C. R. Goodwin, Structural Mass Spectrometry for Characterizing Complex Biological Systems, Aegis Sciences Symposium, Vanderbilt University, Nashville, TN (November 7, 201 1). INVITED ORAL

C. R. Goodwin, C. C. Marasco, J.R. Enders, J. P. Wikswo, N. Schramm-Sapyta, J. A. McLean, Analysis of Rat Leukocyte Metabolomic Response to Cocaine Stimulation using Ion Mobility-

Mass Spectrometry, 5th Annual Conference on Cellular Information Processing, Santa Fe, NM (August 10-14, 2011). POSTER

J. R. Enders; C. C. Marasco; **C. R. Goodwin**; J. May; K. T. Seale; J. P. Wikswo; J. A. Mclean, Development of a Platform for Online Acquisition of Empirical Systems Biology Data, 5th Annual Conference on Cellular Information Processing, Santa Fe, NM (August 10-14, 2011). POSTER

Alexandra Garza, Christina Marasco, **C. R. Goodwin**, J. Enders, K. Seale, J. A. McLean, J. P. Wikswo, Leukocyte Metabolic Profiling and Motion Quantization for Dual Indication of Toxin Response, 5th Annual Conference on Cellular Information Processing, Santa Fe, NM (August 10-14, 2011). POSTER

C. R. Goodwin, L. S. Fenn, R. McNees, N. M. Lareau, B. O. Bachmann, J. A. McLean. Ion Mobility-Mass Spectrometry Driven Natural Product Discovery. 4th Annual q-bio Conference on Cellular Information Processing, Santa Fe, NM. August 2010 POSTER

C. R. Goodwin, C. R. McNees, D. K. Derewacz, L. S. Fenn, B. O. Bachmann, J. A. McLean. Development of Ion Mobility-Mass Spectrometry Based Methods for Natural Product Prioritization. 59th Annual American Society for Mass Spectrometry conference, Denver, CO. (May 2011). POSTER

J. R. Enders, **C. R. Goodwin**, C. C. Marasco, J. May, K. Seale, J. Wikswo, J. McLean. Temporal Analysis of Biological Fluid for the Analysis of Cellular Signaling and Response Using Ion Mobility-mass Spectrometry Analyses . Chemical and Biological Defense Science & Technology conference, Orlando, FL (November 2010). POSTER

C. R. Goodwin, L. S. Fenn, C. R. McNees, B. O. Bachmann, J. A. McLean. Ion Mobility-Mass Spectrometry Driven Natural Product Discovery. Quantitative Understanding in Biology (q-bio) Annual Conference, Santa Fe, NM (August 2010). POSTER

J. R. Enders, C. C. Marasco, **C. R. Goodwin**, K. T. Seale, J. P. Wikswo, J. A. McLean. Characterizing the Saccharomyces cerevisiae respiratory oscillation exometabolome by ion mobility-mass spectrometry. Quantitative Understanding in Biology (q-bio) Annual Conference, Santa Fe, NM (August 2010). POSTER

C. R. Goodwin, L. S. Fenn, B. O Bachmann, J. A. McLean, New Avenues in Natural Product Discovery using Ion Mobility-Mass Spectrometry, 58th American Society for Mass Spectrometry Annual Conference, Salt Lake City, UT (May 2010). POSTER

N. Arinze, M.Kliman, L. S. Fenn, S.Sundarapandian, **C. R. Goodwin**, J. A. McLean, A critical comparison of positively and negatively charged peptide ion structures using ion mobility-mass spectrometry, 58th American Society for Mass Spectrometry Annual Conference, Salt Lake City, UT (May 2010). POSTER

C. R. Goodwin, Michal Kliman, L. S. Fenn, B. O. Bachmann, J. A. McLean Structural Determination of Cyclic Peptide Natural Products Using IM-MS and MD. 36th Annual Federation of Analytical Chemistry and Spectroscopy Societies conference, Louisville, KY (October 2009). POSTER

L. S. Fenn, **C. R. Goodwin**, J. A. McLean, Structural Characterization of Natural Products from Complex Biological Mixtures using Ion Mobility-Mass Spectrometry, 36th Annual Federation of Analytical Chemistry and Spectroscopy Societies conference, Louisville, KY (October 2009). ORAL

C.R. Goodwin, M. Kliman, L. S. Fenn, B. O. Bachmann, J. A. McLean. Structural Characterization of Cyclic Peptide Natural Products Using Ion Mobility-Mass Spectrometry. Vanderbilt Institute of Chemical Biology Retreat (August 2009). POSTER

L.S. Fenn, **C. R. Goodwin**, B.O. Bachmann, J.A. McLean, Structural characterization of natural products from complex biological mixtures using ion mobility-mass spectrometry, to be presented at 36th Annual Federation of Analytical Chemistry and Spectroscopy Societies conference, Louisville, KY (October 2009). POSTER AND ORAL

M. Kliman, J. R. Enders, **C. R. Goodwin**, J. A. McLean. Dynamic Laser Patterning for Biomolecular Imaging MALDI – Mass Spectrometry. Vanderbilt Institute for Chemical Biology 2009 Retreat, Nashville, TN, United States (August 2009). POSTER

C. R. Goodwin, A. P. Gies, L. S. Fenn, J. A. McLean, D. M. Hercules. MALDI-IM-TOF-MS and CID Fragmentation Studies of Polyurethanes. 60th Southeast Regional Meeting of the American Chemical Society, Nashville, TN, United States (November 2008). POSTER